General Disclaimer

One or more of the Following Statements may affect this Document

- This document has been reproduced from the best copy furnished by the organizational source. It is being released in the interest of making available as much information as possible.

- This document may contain data, which exceeds the sheet parameters. It was furnished in this condition by the organizational source and is the best copy available.

- This document may contain tone-on-tone or color graphs, charts and/or pictures, which have been reproduced in black and white.

- This document is paginated as submitted by the original source.

- Portions of this document are not fully legible due to the historical nature of some of the material. However, it is the best reproduction available from the original submission.

Produced by the NASA Center for Aerospace Information (CASI)

11791

MSC 00192

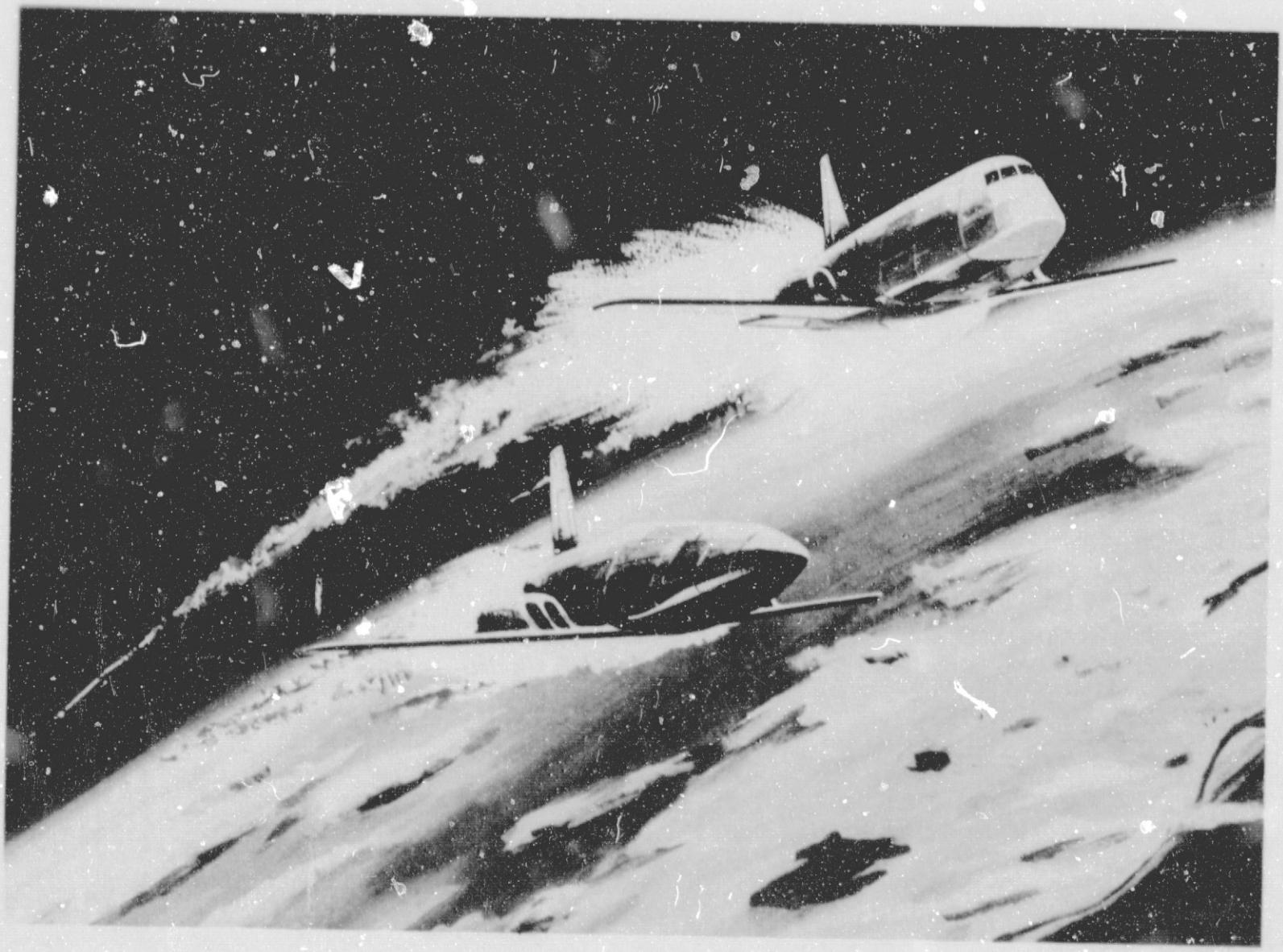

Study of Integral Launch and Reentry Vehicle System

FINAL REPORT

SD 69-573-3

Volume III • Technical Report — Second Phase
Environment and Performance

FACILITY FORM 602
N70-31834 (ACCESSION NUMBER)
521 (PAGES)
CR-102103 (NASA CR OR TMX OR AD NUMBER)
(THRU) 1 (CODE) 31 (CATEGORY)

Space Division
North American Rockwell

SD 69-573-3

MSC 00192

FINAL REPORT

STUDY OF

INTEGRAL LAUNCH AND REENTRY VEHICLE SYSTEM

(Contract NAS9-9205)

VOLUME III

TECHNICAL REPORT - SECOND PHASE ENVIRONMENT AND PERFORMANCE

DECEMBER 1969

APPROVED:

G.F. Fraser
Study Manager

Space Division
North American Rockwell

Space Division
North American Rockwell

PRECEDING PAGE BLANK NOT FILMED.

FOREWORD

This report is submitted to the NASA Manned Spacecraft Center, Houston, Texas, in accordance with Contract NAS9-9205. The report is submitted by the Space Division of North American Rockwell. It presents results of the Study of Integral Launch and Reentry Vehicle System.

Acknowledgement is given to NASA MSC for the aerodynamic and aerothermodynamic test data provided in support of the study. The NASA MSC contracting officer's representative directing the study was R. H. Bradley.

This is Volume III of a five-volume report. It summarizes environment and performance studies of a two-stage, reusable, logistics shuttle vehicle concept investigated during the second phase of the program.

The major contributors to this volume were:

Study Manager:	G. F. Fraser
Project Engineer:	W. E. Bornemann
Aerodynamics:	D. C. Olsen T. Surber H. Parrell
Thermal Environment:	H. Mason
Flight Mechanics:	R. A. Wilson J. S. Prigge, Jr. E. F. Knotts J. K. Dew
Flight Control:	D. A. Engels L. A. Schmidt E. W. Woosley P. P. Shipley
Structural Loads:	R. E. Gatto S. S. Li G. A. Curney

The volumes of the complete final report are as follows:

Study of Integral Launch and Reentry Vehicle

Volume	Title	SD Report No.
I	Summary Report	SD 69-573-1
II	Technology Development Requirements	SD 69-573-2
III	Technical Report - Second Phase Environment and Performance	SD 68-573-3
IV	Technical Report - Second Phase Design and Subsystems Analysis	SD 69-573-4
V	Technical Report - Second Phase Operations and Resources	SD 69-573-5

CONTENTS

Section		Page
1.0	INTRODUCTION	1-1
2.0	SUMMARY	2-1
	2.1 Flight Profile and Vehicle Optimization	2-1
	2.2 Aerodynamics and Design Improvements	2-3
	2.3 Control Concepts	2-7
	2.4 Abort	2-8
	2.5 Thermal Environment	2-8
	2.6 Lateral Ranging Effects and Potential	2-10
	2.7 Approach and Landing	2-10
	2.8 Design Loads	2-12
3.0	OBJECTIVES	3-1
4.0	MISSION AND DESIGN REQUIREMENTS	4-1
5.0	SCOPE	5-1
6.0	APPROACH AND STUDY SCHEDULE	6-1
	6.1 Concept Sizing and Performance Analysis	6-1
	6.2 Design Improvement Concepts and Sensitivity Analysis	6-1
	6.3 Conceptual Design	6-2
	6.4 Resource Plans	6-2
	6.5 Technology	6-6
7.0	PERFORMANCE	7-1
	7.1 Mission Characteristics	7-1
	7.2 Aerodynamics	7-8
	7.3 Flight Mechanics	7-94
	7.4 Thermal Environment	7-219
	7.5 Control Analyses	7-256
8.0	DESIGN ENVIRONMENTS	8-1
	8.1 Summary	8-1
	8.2 12,500-Pound-Baseline Design Environment	8-2
	8.3 50,000-Pound-Payload Baseline	8-41

Section		Page
9.0	CONCLUSIONS	9-1
10.0	REFERENCES	10-1

ILLUSTRATIONS

Figure		Page
2.1-1	Flight Profile	2-2
2.1-2	Baseline Vehicle Configuration, 50,000-Pound Payload Class	2-4
2.1-3	Payload Capability (50,000-Pound Payload System Alternate Orbits)	2-5
2.2-1	Booster and Orbiter Aerodynamic Configuration Characteristics	2-6
2.5-1	Thermal Environment	2-9
2.6-1	Orbiter Lateral Range Potential	2-11
5.0-1	Baseline Vehicle Concept for Phase 2 of Study	5-2
6.0-1	Phase 2 Study Logic	6-3
6.0-2	Phase 2 Study Schedule	6-5
7.1-1	Flight Profile	7-2
7.1-2	Performance Summary	7-7
7.2-1	Configuration Fundamentals	7-12
7.2-2	Effect of Reynolds Number on Fuselage Side Force	7-13
7.2-3	Baseline Configuration of 12,500-Pound Payload Class	7-15
7.2-4	Zero Lift Drag During Boost	7-17
7.2-5	Lift Characteristics, 12,500-Pound Payload Class	7-18
7.2-6	Drag Characteristics, 12,500-Pound Payload Class	7-19
7.2-7	Pitching Moment Characteristics for Composite Configuration, 12,500-Pound Payload Class	7-20
7.2-8	Normal Force and Pitching Moment Characteristics, Booster for 12,500-Pound Payload	7-22
7.2-9	Lift and Drag Characteristics, Booster for 12,500-Pound Payload	7-23
7.2-10	Orbiter Trim Characteristics	7-25
7.2-11	Orbiter Aerodynamics	7-26
7.2-12	Orbiter Hypersonic Lateral - Directional Characteristics, 12,500-Pound Payload Class	7-27
7.2-13	Drag of External Payload	7-28
7.2-14	Tail Size for Subsonic Trim	7-29
7.2-15	Effect of Mach Number on Pitching Moment Characteristics	7-31
7.2-16	Drag of Infinite Circular Cylinder	7-32
7.2-17	Effect of Corner Radius on Subsonic Cross Flow Drag Coefficient	7-34

Figure		Page
7.2-18	Effect of Corner Radius on Wing Body Pitching Moment	7-35
7.2-19	Estimated Subsonic Tail Size for 10 Percent Static Margin at Cruise	7-36
7.2-20	Orbiter Configuration, 50,000-Pound Payload Class	7-37
7.2-21	Orbiter Configuration Incorporating Body Corner Radius	7-39
7.2-22	Effect of Body Corner Radius on Horizontal Tail Size	7-41
7.2-23	Effect of Body Corner Radius on Orbiter Hypersonic Aerodynamics	7-43
7.2-24	Hypersonic Lateral/Directional Characteristics	7-45
7.2-25	Effect of Body Shaping or Hypersonic Lateral/ Directional Characteristics	7-49
7.2-26	Effect of Horizontal Tail Dihedral on Hypersonic Lateral/Directional Characteristics	7-50
7.2-27	Effect of Wing Sweep on Leading Edge Drag	7-52
7.2-28	Aspect Ratio Wave Drag Correction	7-53
7.2-29	Effect of Sweep on Drag Divergence Mach Number	7-54
7.2-30	Wind Tunnel Model, 0.02 Scale Orbiter, 12,500-Pound Payload Class	7-57
7.2-31	Longitudinal Pitching Moment Characteristics, B, W, H_5	7-63
7.2-32	Elevator to Trim at 60-Degree Angle of Attack	7-64
7.2-33	Center of Pressure Component Buildup	7-65
7.2-34	Fuselage Normal Force Variation With Angle of Attack	7-68
7.2-35	Effect of Fuselage Normal Force on Horizontal Tail Size Required for 50,000-Pound-Payload Orbiter	7-69
7.2-36	Effect of Body Nose Shape on Longitudinal Characteristics	7-71
7.2-37	Orbiter-Booster Mated Configuration	7-73
7.2-38	Drag Versus Mach Number, 50,000-Pound-Payload Class Composite Configuration	7-75
7.2-39	Lift Characteristics, 50,000-Pound-Payload Class Composite Configuration	7-76
7.2-40	Pitching Moment Characteristics for 50,000-Pound-Payload Class Composite Configuration	7-77
7.2-41	Orbiter Aerodynamic Configuration 50,000-Pound-Payload Class	7-79
7.2-42	Orbiter Longitudinal Aerodynamic Characteristics, 50,000-Pound-Payload Class	7-80
7.2-43	Horizontal Tail Size for 50,000-Pound-Payload Orbiter	7-81

Figure		Page
7.2-44	Lateral-Directional Characteristics	7-82
7.2-45	Launch Vehicle Configuration Concept	7-85
7.2-46	Booster Aerodynamic Configuration, 50,000-Pound-Payload Class	7-87
7.2-47	Booster Aerodynamics, 50,000-Pound-Payload Orbiter	7-88
7.2-48	Effect of Body Center of Gravity Location on Booster Tail Size	7-89
7.2-49	Effect of Wing Location on Booster Tail Size	7-91
7.2-50	Horizontal Tail Size for 50,000-Pound-Payload Booster	7-92
7.3-1	Vehicle Gross Weight Versus Stage Mixture Ratio	7-99
7.3-2	Vehicle Gross Weight Versus Stage Thrust-to-Weight Ratio	7-99
7.3-3	Ascent Trajectory Profile, 12,000-Pound-Payload Class, 45 by 200 Nautical-Mile Orbit	7-105
7.3-4	Ascent Trajectory Profile, 25,000-Pound-Payload Class, 45 by 100 Nautical-Mile Orbit	7-106
7.3-5	Effect of Inclination Angle on Payload	7-108
7.3-6	Zero Lift Drag Coefficient, Vehicle With 25,000-Pound Payload (15-Foot Diameter by 30-Foot Length)	7-109
7.3-7	Payload Variation for Change in On-Orbit ΔV	7-110
7.3-8	Payload Sensitivities for 50,000-Pound-Payload Class	7-114
7.3-9	Gross Weight Sensitivities for 50,000-Pound-Payload Class	7-115
7.3-10	Ascent Trajectory Profile, Lifting and Nonlifting Flight Modes, 50,000-Pound Payload	7-119
7.3-11	Angle of Attack History for Lifting Ascent	7-120
7.3-12	Wind Profile and Angle of Attack History	7-121
7.3-13	Nominal Ascent Trajectory Profile, 50,000-Pound Payload, 50 by 200 Nautical Mile Orbit.	7-123
7.3-14	Ascent Performance - One Engine Out (50 by 100-Nautical Mile Injection of 50,000-Pound-Payload Class	7-126
7.3-15	Stage Mass Data (3 Million- and 3.5 Million-Pound Gross Weight Vehicles)	7-128
7.3-16	Payload Versus On-Orbit Maneuver Capability	7-132
7.3-17	Stage Propellant Versus Burnout Weight	7-133
7.3-18	Payload Capability (50,000-Pound-Payload System Alternate Orbits)	7-135
7.3-19	ILRV Mission Minimum Duration Rendezvous Profile	7-140
7.3-20	ILRV Mission Rendezvous Profile Arbitrary Phase Angle	7-141

Figure		Page
7.3-21	Time to Rendezvous versus Phase Angle Difference at Insertion	7-143
7.3-22	360-Degree Descent Phase Window Definition	7-146
7.3-23	Lateral Range Requirements for Direct Return to ETR From 270-Nautical Mile Orbit	7-147
7.3-24	Tradeoff of Descent Phasing Time and ΔV for Various Phase Window Increases	7-151
7.3-25	Return Site Phasing = 50, 000-Pound-Payload Orbiter, Cross Range = 190 Nautical Miles	7-152
7.3-26	Effect of Wing Loading and Angle of Attack on Aerodynamic Characteristics of Orbiter	7-157
7.3-27	Effect of Wing Loading and Angle of Attack on Entry Performance of Orbiter	7-158
7.3-28	Effect of Wing Loading and Angle of Attack on Entry Environment of Orbiter	7-159
7.3-29	Effect of Angle of Attack on Aerodynamic Characteristics of Baseline Orbiter	7-160
7.3-30	Effect of Angle of Attack on Entry Performance and Environment of Baseline Orbiter	7-161
7.3-31	Lateral Range Capability With Subsonic Cruise	7-164
7.3-32	Orbiter Lateral Range Capability at Reduced Angle of Attack, 50, 000-Pound-Payload Orbiter	7-166
7.3-33	Effect of Injection Altitude on Entry Performance and Environment of Booster	7-167
7.3-34	Effect of Injection Altitude and Normal Load Factor Limit on Turnaround Performance and Environment of Booster	7-170
7.3-35	Effect of Injection Altitude and Normal Load Factor Limit on Turnaround Performance and Environment of Booster	7-171
7.3-36	Effect of Injection Altitude on Turnaround Performance and Environment of Booster With Normal Load Factor Limited to 4.0	7-172
7.3-37	Orbiter Entry Profile, 50, 000-Pound-Payload Orbiter	7-174
7.3-38	Time History of Design Entry Trajectory of 50, 000-Pound-Payload Orbiter	7-177
7.3-39	Booster Descent Profile	7-180
7.3-40	Time History of Design Turnaround Trajectory of 50, 000-Pound-Payload Booster	7-182
7.3-41	Estimated Optimum Cruise Booster	7-186
7.3-42	P&W JT3D-7 Engine Performance	7-188
7.3-43	Thrust and Drag Characteristics for Booster Cruise	7-189
7.3-44	Booster Cruise Optimization, 12, 500-Pound-Payload Class Systems	7-190

Figure		Page
7.3-45	Go-Around Fuel Requirements	7-191
7.3-46	Landing Flap Effectiveness, Single Slotted Flap	7-192
7.3-47	Payload Sensitivity to Go-Around Capability, 50,000-Pound Payload-Class Orbiter	7-194
7.3-48	Conditions for Booster Level Flight Cruise	7-197
7.3-49	Booster Flyback Propulsion System Selection	7-198
7.3-50	Effect of Fuel Load on Range	7-199
7.3-51	Landing Characteristics, 50,000-Pound-Payload System	7-202
7.3-52	Effect of Landing Weight on Go-Around Fuel Requirements, One Go-Around	7-204
7.3-53	Flight Profile Low Altitude Abort, 50,000-Pound-Payload Orbiter	7-207
7.3-54	Prestaging Abort Performance, 50,000-Pound-Payload Orbiter	7-208
7.3-55	Maximum g Loads During Nonthrusting Poststaging Abort, 50,000-Pound-Payload Class Orbiter	7-211
7.3-56	Abort g Loads With Angle-of-Attack Modulation, 50,000-Pound-Payload Class Orbiter	7-213
7.3-57	Angle-of-Attack Modulation Required for Restricting Maximum Load Factor, 50,000-Pound Payload Class Orbiter	7-214
7.3-58	Variation of Abort Range With Maximum g Load, 50,000-Pound Payload Class Orbiter	7-215
7.3-59	Splashdown Points Following Nonthrusting Poststaging Aborts, 50,000-Pound Payload Class Orbiter	7-216
7.3-60	Stagnation Heating Rate During an Abort	7-217
7.4-1	Stagnation Point and Leading Edge Heating Approximations, 12,500-Pound-Payload Orbiter	7-223
7.4-2	Effect of Corner Radius on Underbody Heating	7-224
7.4-3	Heating Distribution to Sides and Top of Fuselage	7-226
7.4-4	Correlation of Fuselage and Wing Heating Models	7-227
7.4-5	ILRV Fuselage Data Correlation (α = 45 Degrees)	7-229
7.4-6	ILRV Fuselage Data Correlation (α = 15 Degrees)	7-230
7.4-7	Entry Heating Environments, Underside of Wing—12,500-Pound Configuration	7-232
7.4-8	Orbiter Entry Environments, Underside of Body—12,500-Pound Configuration	7-233
7.4-9	ILRV Temperature Concentrations, 12,500-Pound Configuration	7-234
7.4-10	Ascent Heating at Orbiter Burnout	7-235

Figure		Page
7.4-11	Ascent Heating, One-Foot Radius Sphere	7-238
7.4-12	Reference Stagnation Point Heating, One-Foot Radius Sphere	7-239
7.4-13	ILRV Temperature Concentrations, 12,500-Pound Configuration	7-242
7.4-14	Thermal Environment Summary, 50,000-Pound Payload Case	7-243
7.4-15	Stagnation Heating to a 1-Foot Radius Sphere During 50,000-Pound Class Booster Flyback	7-244
7.4-16	Booster Fuselage Heating History During Flyback	7-246
7.4-17	Booster Wing Heating History During Flyback	7-247
7.4-18	Booster Maximum Temperature Distribution During Flyback	7-248
7.4-19	Stagnation Heating to a 1-Foot Radius Sphere During 50,000-Pound Class Orbiter Entry	7-249
7.4-20	History of Entry Heating on Fuselage of 50,000-Pound Class Orbiter	7-250
7.4-21	History of Entry Heating on Wing of 50,000-Pound Class Orbiter	7-251
7.4-22	Reference Heating Rates and Loads	7-252
7.4-23	Orbiter Entry Heating Environments, 50,000-Pound Configuration Payload	7-253
7.4-24	Orbiter Entry Heating Loads, 50,000-Pound Payload Class	7-255
7.5-1	Ascent Control Concepts, 12,500-Pound Payload Class System	7-258
7.5-2	Boost Flight Path Control System, 50,000-Pound Payload Class Vehicle	7-261
7.5-3	Ascent Control Simulation for 50,000-Pound Payload Class	7-263
7.5-4	Booster Interference on Orbiter	7-266
7.5-5	Separation Concept for 50,000-Pound Payload	7-268
7.5-6	Booster-Centered Relative Motion, No Orbiter Thrust	7-269
7.5-7	Booster-Centered Relative Motion, With Orbiter Thrust	7-270
7.5-8	Orbiter Translation Due to Main Engine Thrust	7-271
7.5-9	Pitching Moments at Booster-Orbiter Separation	7-273
7.5-10	Orbiter Entry Control Simulation	7-275
7.5-11	Entry Control System Block Diagram	7-277
7.5-12	Roll and Yaw Phase Plane	7-278
7.5-13	Orbiter Entry Simulation Time History, Stable C_{η_B}	7-27[illegible]
7.5-14	Orbiter Entry Simulation Time History, Neutrally Stable C_{η_B}	7-280
7.5-15	Orbiter Entry Simulation Time History, Unstable C_{η_B}	7-281

Figure		Page
7.5-16	Orbiter Entry Simulation Including Final Roll Maneuver	7-283
7.5-17	Pitch-Down Control System	7-288
7.5-18	Pitch-Down Maneuver Time Histories: Elevator Deflection, Pitch Moment, Angle of Attack	7-289
7.5-19	Pitch-Down Maneuver Time Histories: Altitude, Velocity, Dynamic Pressure	7-290
8.2-1	Ascent Design Trajectory Parameters (12,500-Pound Class Baseline)	8-3
8.2-2	Orbiter Design Trajectory (12,500-Pound Class Baseline)	8-4
8.2-3	Normal Airload Distribution During Launch, Maximum q Alpha	8-7
8.2-4	Effect of Angle of Attack on Airload Distribution During Launch, Maximum q Case	8-8
8.2-5	Axial Load Distribution During Launch, Maximum q Alpha	8-9
8.2-6	Normal Load Distribution During Orbiter Entry	8-10
8.2-7	Normal Load Distribution During Booster Entry	8-11
8.2-8	Axial Load Distribution During Orbiter Entry	8-12
8.2-9	Axial Load Distribution During Booster Entry	8-13
8.2-10	Load Distribution During Orbiter Landing with Flaps Deflected	8-14
8.2-11	Structural Loading Conditions	8-16
8.2-12	Booster Fuselage Bending Moments, 12,500-Pound Payload Class	8-19
8.2-13	Booster Prelaunch Loads	8-20
8.2-14	Booster Limit Net Loads During Maximum q Alpha.	8-23
8.2-15	Booster Axial Load at Maximum Acceleration (End First Stage Boost)	8-24
8.2-16	Booster Limit Net Loads at Maximum Acceleration	8-25
8.2-17	Booster Limit Net Loads During Entry	8-26
8.2-18	Booster Limit Net Loads During Subsonic Pitch-Down Maneuver	8-27
8.2-19	Booster Limit Net Loads During Landing	8-28
8.2-20	Orbiter Fuselage Bending Moments	8-29
8.2-21	Orbiter Limit Net Loads During Maximum q Alpha	8-31
8.2-22	Orbiter Axial Load at Maximum Acceleration (End First Stage Boost)	8-32
8.2-23	Orbiter Limit Shear and Moment Loads, Maximum Acceleration	8-33
8.2-24	Orbiter Limit Net Loads, Second Stage End Boost	8-34

Figure		Page
8.2-25	Orbiter Limit Net Loads During Entry	8-35
8.2-26	Orbiter Net Loads During Subsonic Pitch-Down Maneuver	8-36
8.2-27	Orbiter Limit Loads During Landing	8-37
8.2-28	Wing Limit Loads, 12,500-Pound-Payload Class	8-39
8.2-29	Booster/Orbiter Attachment Loads, 12,500-Pound-Payload Class	8-40
8.3-1	Nominal Ascent Trajectory Profile - 50,000-Pound-Payload Class, 50-by-100 Nautical Mile Orbit	8-44
8.3-2	Thermal Environment Summary of 50,000-Pound-Payload Class	8-46
8.3-3	Normal Airload Distribution During Launch for Maximum q Alpha	8-47
8.3-4	Axial Load Distribution During Launch for Maximum q Alpha	8-48
8.3-5	Booster and Orbiter Distributed Airload During Pitch-Down	8-49
8.3-6	Booster and Orbiter Subsonic Wind and Tail Load	8-50
8.3-7	Orbiter Normal Load Distribution During Entry, 50,000-Pound-Payload Class	8-51
8.3-8	Booster Normal Load Distribution During Entry, 50,000-Pound-Payload Class	8-52
8.3-9	Loads Stations and Sign Conventions, 50,000-Pound-Payload System	8-54
8.3-10	Prelaunch Loads	8-59
8.3-11	Booster Loads for Maximum q Alpha (Axial Load at Aft Attachment)	8-63
8.3-12	Booster Limit Loads for Maximum q Alpha (Axial Load at Forward Attachment)	8-64
8.3-13	Orbiter Loads at Maximum q Alpha (Axial Loads at Aft Attachment)	8-65
8.3-14	Orbiter Loads at Maximum q Alpha (Axial Load at Forward Attachment)	8-66
8.3-15	Booster Loads for Maximum Acceleration (Axial Load at Aft Attachment)	8-68
8.3-16	Booster Loads for Maximum Acceleration (Axial Load at Forward Attachment)	8-69
8.3-17	Orbiter Loads for Maximum Acceleration (Axial Load at Aft Attachment)	8-70
8.3-18	Orbiter Loads at Maximum Acceleration (Axial Load at Forward Attachment)	8-71
8.3-19	Booster Limit Loads During Entry	8-72
8.3-20	Orbiter Limit Loads During Entry	8-73

Figure		Page
8.3-21	Booster Limit Loads During Transition to Cruise Maneuver	8-74
8.3-22	Orbiter Limit Loads During Transition to Cruise Maneuver	8-75
8.3-23	Booster Limit Loads During Landing	8-76
8.3-24	Orbiter Limit Loads During Landing	8-78

PRECEDING PAGE BLANK NOT FILMED.

TABLES

Table		Page
2.8-1	Structural Design Loads	2-13
7.1-1	Design Flight Profiles	7-4
7.1-2	On-Orbit Maneuver Budget	7-5
7.1-3	Overall Vehicle Characteristics, Concept-Sizing Phase	7-6
7.2-1	Body-Corner Radius Weight and Temperature Trade	7-46
7.3-1	Characteristics of 7,700-Pound Payload Vehicle (12,500-Pound Class)	7-100
7.3-2	Characteristics of 25,000-Pound Payload Vehicle (15- by 30-Foot Cargo Bay)	7-100
7.3-3	Characteristics of 25,000-Pound Payload Vehicle (15- by 60-Foot Cargo Bay)	7-102
7.3-4	Characteristics of 50,000-Pound Payload Vehicle (15- by 60-Foot Cargo Bay)	7-103
7.3-5	Characteristics of 50,000-Pound Payload Vehicle 22- by 60-Foot Cargo Bay	7-104
	Characteristics of 50,000-Pound Payload Vehicle (60- by 100-Nautical Mile Orbit, 15- by 60-Foot Cargo Bay)	7-112
7.3-7	Performance Sensitivities (Vehicle Delivering 50,000-Pound Payload)	7-113
7.3-8	Injection Orbit Performance Effects (50,000-Pound Payload)	7-117
7.3-9	Vehicle Conditions at Booster Burnout	7-118
7.3-10	Characteristics of 50,000-Pound Payload Baseline Vehicle (50- by 100-Nautical Mile Orbit)	7-124
7.3-11	Vehicle Characteristics Summary	7-129
7.3-12	Vehicle Characteristics With Optimized Engine Sizes	7-130
7.3-13	Final Vehicle Characteristics, 50,000-Pound Payload Configuration (15- by 60-Foot Cargo Bay, 50- by 100-Nautical Mile Orbit)	7-134
7.3-14	Characteristics of 25,000-Pound Payload Configuration (15- by 60-Foot Cargo Bay, 50- by 100-Nautical Mile Orbit)	7-136
7.3-15	Characteristics of 25,000-Pound Payload Configuration (12- by 48-Foot Cargo Bay, 50- by 100-Nautical Mile Orbit)	7-137
7.3-16	ILRV Rendezvous Maximum-Duration Timeline, Maximum Duration Constrained to 24-Hour Design Requirement	7-144

Table		Page
7.3-17	Initial and Final Conditions for Orbiter Entry Trajectories	7-154
7.3-18	Summary of Design Entry Trajectories	7-155
7.3-19	Initial and Final Conditions for Booster Turnaround Trajectories	7-168
7.3-20	Aerodynamic Characteristics of Booster	7-169
7.3-21	Flight Conditions at Significant Points During Entry of Orbiter	7-176
7.3-22	Flight Conditions at Significant Points During Turnaround of Booster	7-181
7.3-23	Comparison of Booster Cruise-Back Engine and Fuel Weights	7-201
7.3-24	Landing Lift-Drag Budget	7-203
7.4-1	Maximum Ascent Heating Environments on Fuselage Centerline	7-237
7.4-2	Ascent Interference Heating Factors	7-238
7.4-3	Trajectory Matrix	7-240
7.4-4	Maximum Permissible Pitch-Down Velocity and Angle of Attack for Obtaining Baseline Temperatures on Wing Leading Edges	7-241
7.5-1	Summary of Results of Ascent Control Simulation, 50,000-Pound Payload Class Vehicle	7-262
7.5-2	Orbiter Entry Stability Simulation Results	7-282
7.5-3	Effects of C_{ℓ_β} Variations on Orbiter Entry	7-286
7.5-4	RCS Requirements Summary	7-292
7.5-5	Forcing Functions for RCS Propellant Consumption	7-294
8.2-1	Thermal Environment Summary (12,500-Pound Payload Class)	8-5
8.2-2	Structural Design Loads Summary (12,500-Pound Payload Class)	8-17
8.3-1	Flight Conditions at Significant Points During Turnaround of Booster	8-42
8.3-2	Flight Conditions at Significant Points During Entry of Orbiter	8-43
8.3-3	Structural Design Loads Summary, 50,000-Pound-Payload Class	8-55
8.3-4	Aerodynamic Surface Limit Loads at the Root (50,000-Pound-Payload Class)	8-56
8.3-5	Aerodynamic Surface Limit Loads at the One-Third Panel Length From Root	8-56
8.3-6	Limit Attachment Loads, Axial Load at Forward Attachment	8-57
8.3-7	Limit Attachment Loads, Axial Load at Aft Attachment	8-58

NOMENCLATURE

Symbol	Description	Units
A	characteristic area	ft^2
AR	wing aspect ratio	
b_o	body width	in.
MAC	mean aerodynamic chord	in.
b	wing span	in.
C_A	axial force coefficient	
C_D	drag force coefficient	
C_{D_o}	zero lift-drag force coefficient	
C_{D_π}	drag coefficient based on cross section area	
C_{D_C}	cross flow drag coefficient based on planform area	
C_L	lift force coefficient	
C_{L_α}	lift coefficient slope, $dC_L/d\alpha$	1/degree
C_N	normal force coefficient	
C_m	pitching moment coefficient	
C_{m_α}	pitching moment coefficient slope, $dC_m/d\alpha$	1/degree
C_{y_β}	side force coefficient slope, $dC_y/d\beta$	1/degree
C_{ℓ_β}	rolling moment coefficient slope, $dC_\ell/d\beta$	1/degree
C_n	yawing moment coefficient slope, $d C_n/d\beta$	1/degree
$d C_n/dx$	normal force coefficient load distribution	1/in.

Symbol	Description	Units
d C_A/dx	axial force coefficient load distribution	1/in.
ℓ_t	tail length	in.
h	altitude	ft
L	body length	in.
M	Mach number	
n_R	resultant load factor	
n_z	normal load factor	
Re	Reynolds number	
r	radius	in.
W	weight	lb
S	wing area	ft^2
V	velocity	ft/sec
$\dot{q}$	heating rate	$Btu/ft^2/sec$
Q	heat load	Btu/ft^2
L/D	lift-to-drag ratio	
Λ	sweep	degrees
λ	taper ratio	
Δ	incremental change	
α	angle of attack	degrees
Γ	dihedral angle	degrees
β	sideslip angle	degrees
ϵ	incidence angle	degrees

Symbol	Description	Units
W/S	wing loading	lb/ft^2
W/C_LS	lift loading parameter	lb/ft^2

SUBSCRIPTS

B	body
cg	center of gravity
cp	center of pressure
E	elevator
EXP	exposed
FRL	fuselage reference line
F	flap
H	horizontal
LE	leading edge
PLAN	planform area
REF	reference
W	wing
V	vertical

1.0 INTRODUCTION

Future space exploration will be constrained within a limited budget and will benefit from the development of an economical logistic system. NASA, therefore, is directing investigations of reusable logistic vehicles that offer potential major operational cost reductions compared with costs of current systems. Among these investigations is the Study of Integral Launch and Reentry Vehicle Systems performed by the Space Division of North American Rockwell Corporation for the NASA Manned Spacecraft Center, Houston, Texas, in accordance with Contract NAS9-9205. This document contains results of design, performance, and resource studies accomplished during the second phase of the program. These study results were presented in the final oral review at NASA MSC on 5 November 1969.

The contract was negotiated on 31 January 1969, and activity began on 3 March 1969. The study schedule reflects eight months of technical activity and a subsequent reporting period. The major objective of the study was to define logistic systems that achieve an order-of-magnitude reduction in recurring costs and that advance inherent safety. The program was divided into two phases: the first phase was two months in duration and encompassed comparison of logistic vehicle concepts using expendable boosters. The second phase encompassed investigations of a two-stage reusable vehicle conceived by NASA MSC. In the study, vehicles were configured to deliver 10,000-, 25,000-, and 50,000-pound payloads to a 270-nautical-mile, 55-degree-inclination orbit. Vehicles to deliver 25,000- and 50,000-pound payloads were designed to provide the following cargo bay sizes:

Payload (lb)	Cargo Bay Sizes (ft)
25,000	15 x 30
25,000	15 x 30
25,000	12 x 48
50,000	15 x 60
50,000	22 x 60

Emphasis was placed upon the vehicle designed to deliver the 50,000-pound payload with 15-foot-diameter by 60-foot-length cargo bay. The system has two reusable stages with fixed low-sweep wings and similar aerodynamic shapes. The propulsion system uses LO_2/LH_2 propellants with high-chamber-pressure bell or aerospike engines. The vehicle is

configured for vertical takeoff with the orbiter mounted forward on the booster and the booster and orbiter engines operated sequentially. The forward orbiter location provides a forward center of gravity during the ascent phase of the mission and thus achieves an aerodynamically stable configuration. This arrangement minimizes the thrust-vector control requirement, angle of attack, and aerodynamic loads. Because a major requirement of the logistic vehicle is to minimize operational costs, it becomes necessary to provide a reusable thermal protection system. This objective makes it desirable to limit temperatures experienced on the vehicle during reentry. The approach adopted in the vehicle study was to minimize vehicle heating rate upon reentry by reentering at a high angle of attack with high-lift coefficient and low-lift loading. This reentry mode combined with the large planform area results in a low heating rate and low total heat load.

The booster element of the specified vehicle must cruise back to a land-landing site after separation from the orbiter. For this purpose, turbojets are used for the cruise phase of the mission. The subject vehicle configuration achieves a high subsonic lift-to-drag ratio (L/D) to provide efficient cruise capability and low landing speeds.

The study indicated the feasibility of the two-stage reusable fixed-wing concept. Further design and development of the system and technology advancement are required in certain areas. Areas of development that are critical to establishment of a low-weight reusable system are the external structure and the external and internal thermal protection systems.

Current programs encompass development of a high-chamber-pressure bell engine and an aerodynamic-spike-nozzle engine. The program to develop the main propulsion system must be continued to facilitate development of the subject logistic vehicle. Further development also will be necessary for the oxygen/hydrogen reaction control system. Another major area for technology advancement is demonstration of the reusability of the logistic vehicle with minimum maintenance.

2.0 SUMMARY

Presented in this volume are results of the environment and performance studies. They were conducted to define the characteristics of a reusable, two-stage, space shuttle vehicle conceived by NASA MSC. The studies were directed toward:

1. Definition of the mission profile, flight modes and trajectories, and performance capability
2. Establishment of the optimum propellant distribution between orbiter and booster vehicles to minimize gross weight
3. Development of the aerodynamic configuration to provide desired performance, stability, and control characteristics
4. Identification of design improvements
5. Evaluation of ascent and entry control concepts
6. Definition of thermal environment
7. Evaluation of lateral ranging capability of the orbiter
8. Establishment of approach and landing characteristics
9. Definition of design loads

Significant results are summarized in the following sections.

2.1 FLIGHT PROFILE AND VEHICLE OPTIMIZATION

Flight analyses were performed to establish the optimum propellant distribution between orbiter and booster vehicle to minimize system gross weight. Eleven engines were selected for the booster to provide an optimum vehicle design. This was based on the use of two main engines on the orbiter and the same basic engine design on the two vehicle stages.

The flight profile for the selected vehicle is shown in Figure 2.1-1. The two-stage vehicle is launched vertically. Staging occurs at an altitude of 230,000 feet with a velocity of 10,800 fps. Separation is achieved by the

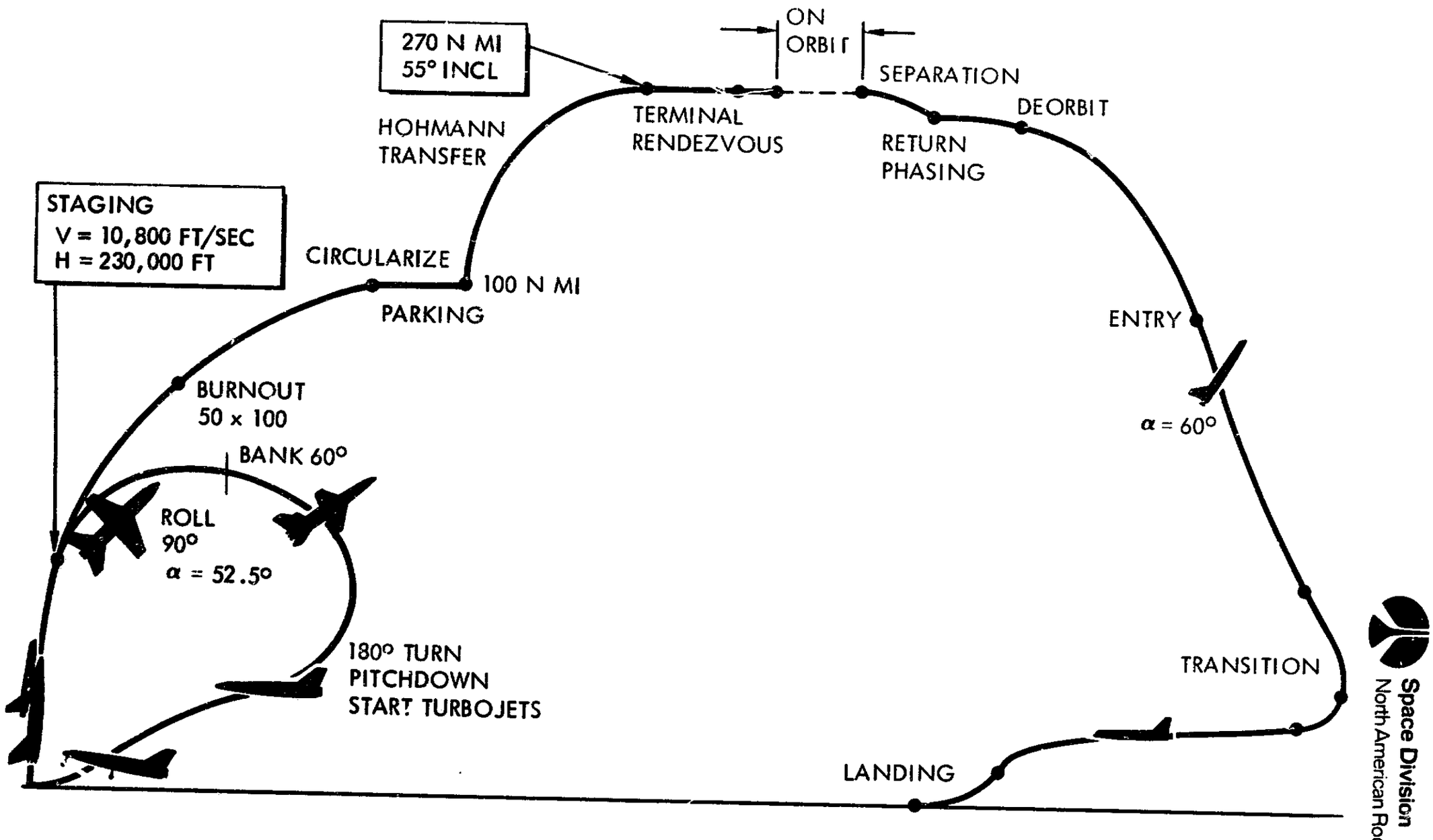

Figure 2.1-1. Flight Profile

use of rockets installed in the orbiter. They displace the vehicle laterally while the attitude of both stages is held constant with the reaction control system. After staging, the booster element rolls with an angle of attack of 52.5 degrees to minimize travel down range. Thus propellant required to cruise back to the landing site is minimized. The orbiter vehicle, after staging, is injected into an orbit of 50 by 100 nautical miles. Then it coasts to an altitude of 100 nautical miles, where the orbit is circularized. A Hohmann transfer is then used to place the orbiter vehicle in a rendezvous orbit of 270 nautical miles and 55 degrees inclination. The orbiter vehicle may remain with the space station from 5 to 30 days. After the orbiter is separated from the space station, a phasing operation is performed to provide a reentry orbit compatible with location of the landing site. It is noted that the minimum orbital maneuvering velocity required to accomplish the mission is less than the specified design requirement. The orbiter vehicle reenters at a 60-degree angle of attack and maintains this attitude until the vehicle achieves subsonic velocities. After reentry, the orbiter vehicle is pitched over to a glide attitude of approximately 5 degrees to return to the landing site.

The general arrangement of the baseline configuration, sized for a 50,000-pound payload, is illustrated in Figure 2.1-2. Performance capability is summarized in Figure 2.1-3.

2.2 AERODYNAMICS AND DESIGN IMPROVEMENTS

Aerodynamic characteristics of the orbiter and booster vehicles were based on an analysis and wind tunnel tests conducted by NASA. Because the center of gravity is forward during boost, the tandem launch configuration is statically stable from lift-off throughout regions of flight where high aerodynamic loads can be developed. This results in low thrust vector deflection angles, a low angle of attack, and low aerodynamic loads.

The flight mode selected for entry and recovery of both stages is similar. Entry is performed at a high angle of attack and maintained until the vehicle decelerates to a low subsonic velocity. Then transition to horizontal flight is performed. Test data confirm that the vehicle is stable and trimmable at the high angle of attack at supersonic, transonic, and subsonic speeds. The horizontal tail has been sized to provide a 7-percent static stability margin during subsonic cruise. Test data confirm that elevator effectiveness is sufficient for transition from a high to a low angle of attack.

Aerodynamic characteristics of the booster and orbiter configurations are summarized in Figure 2.2-1. Both vehicles employ a flat bottom on the fuselage. It is cambered to aid in pitch trim and stability at high angles of

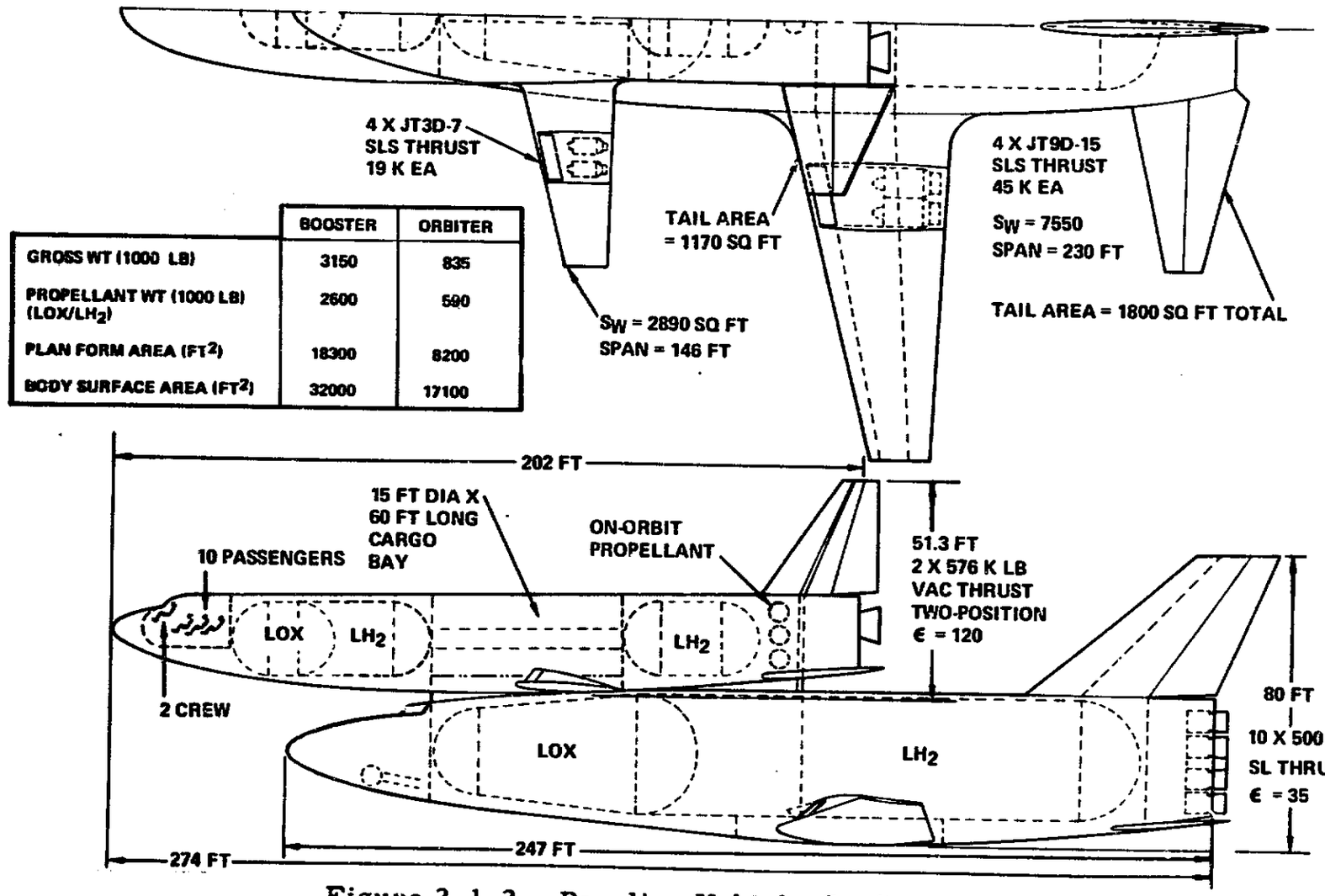

	BOOSTER	ORBITER
GROSS WT (1000 LB)	3150	835
PROPELLANT WT (1000 LB) (LOX/LH_2)	2600	590
PLAN FORM AREA (FT^2)	18300	8200
BODY SURFACE AREA (FT^2)	32000	17100

Figure 2.1-2. Baseline Vehicle Configuration, 50,000-Pound Payload Class

Space Division
North American Rockwell

- KSC LAUNCH
- 50 X 100 N MI INJECTION
- MAX G 3

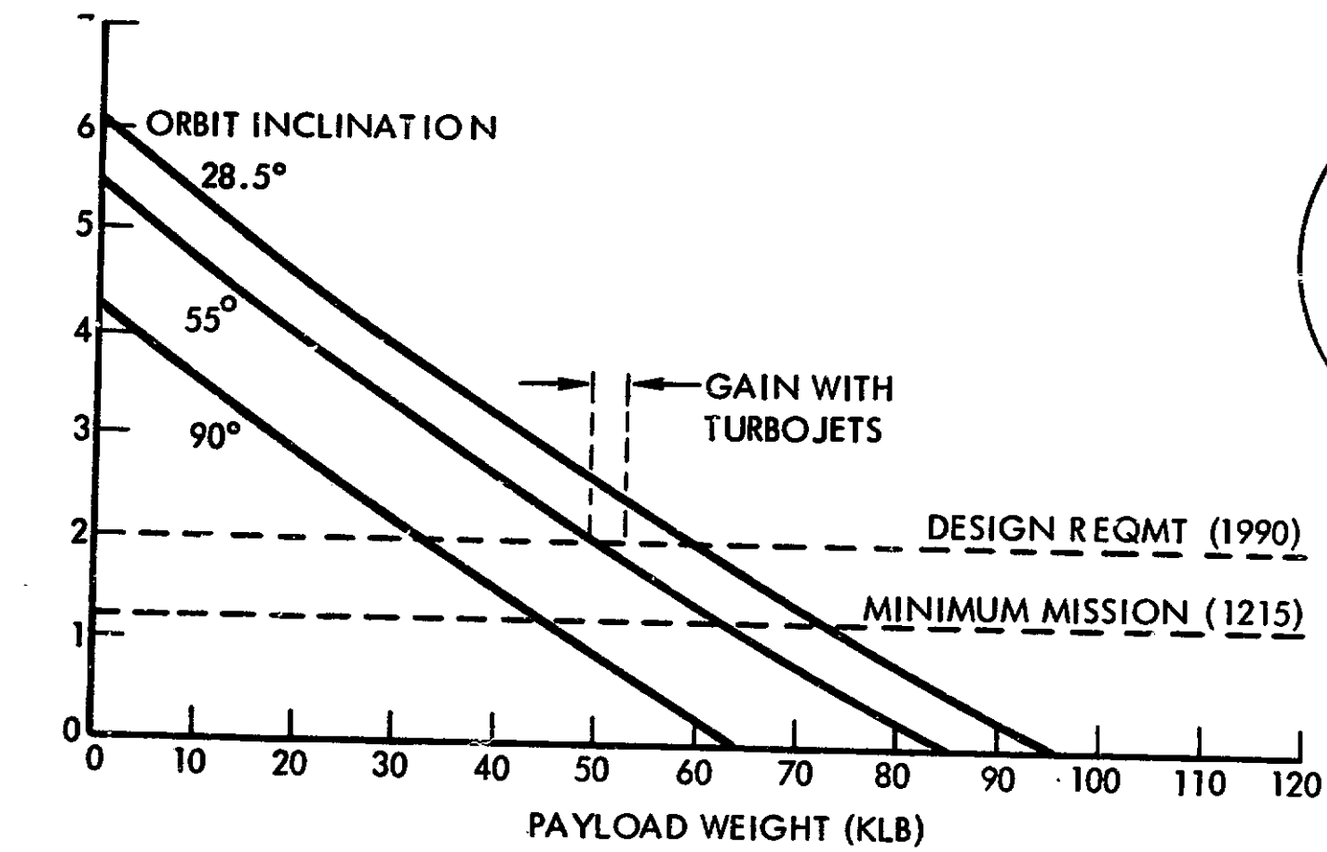

MAXIMUM PAYLOAD (LB)	
28.5° INCL	60,000
55° INCL	50,000
90° INCL	32,700

Figure 2.1-3. Payload Capability, 50,000-Pound Payload System Alternate Orbits

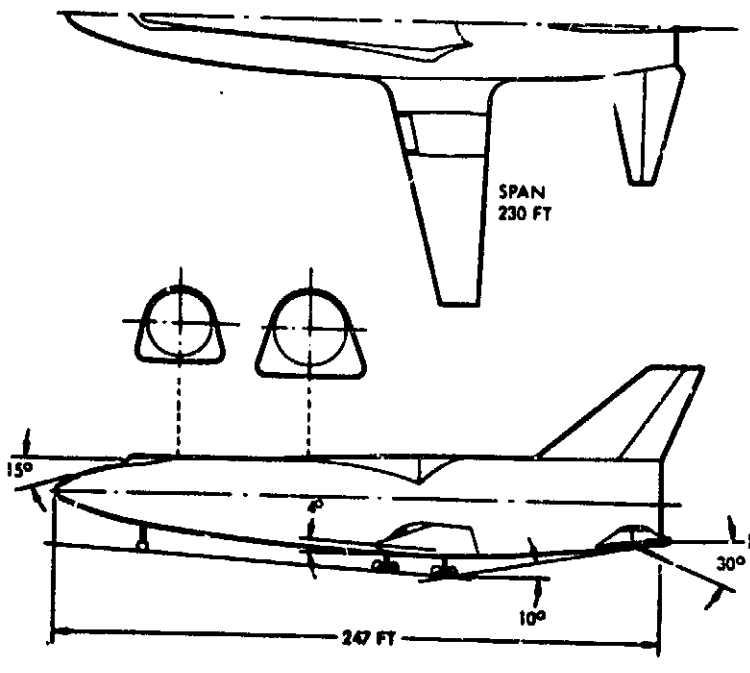

ITEM		
WING		
AREA (TOTAL)	FT^2	7550
ASPECT RATIO		7.0
TAPER RATIO		0.32
AIRFOIL		0014-64 ROOT 0012-64 TIP
M.A.C.	FT	36
HORIZONTAL SURFACE		
AREA (EXPOSED)	FT^2	1800
ASPECT RATIO		4.5
TAPER RATIO		0.3
ELEVATOR AREA	FT^2	120
VERTICAL SURFACE		
AREA (EXPOSED)	FT^2	1408
ASPECT RATIO		1.05
TAPER RATIO		0.43
RUDDER AREA	FT^2	470
AERODYNAMIC PERF		
PLANFORM AREA	FT^2	18350
PLANFORM LOADING	PSF	29
HYPERSONIC L/D		0.69
ENTRY LIFT LDG W/C_LS	PSF	27
SUBSONIC WING LDG	PSF	63
TOUCHDOWN SPEED	KNOTS	112

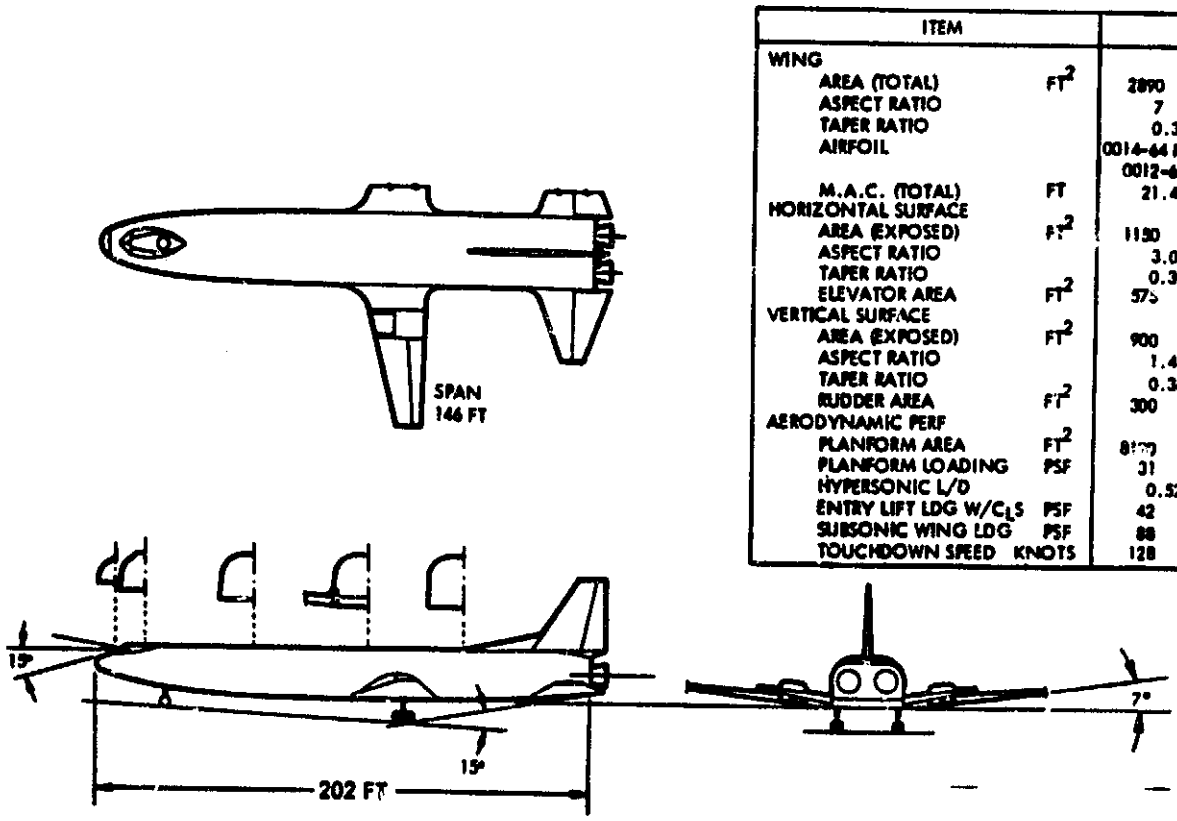

ITEM		
WING		
AREA (TOTAL)	FT^2	2890
ASPECT RATIO		7
TAPER RATIO		0.33
AIRFOIL		0014-64 ROOT 0012-64 TIP
M.A.C. (TOTAL)	FT	21.4
HORIZONTAL SURFACE		
AREA (EXPOSED)	FT^2	1150
ASPECT RATIO		3.0
TAPER RATIO		0.39
ELEVATOR AREA	FT^2	575
VERTICAL SURFACE		
AREA (EXPOSED)	FT^2	900
ASPECT RATIO		1.4
TAPER RATIO		0.36
RUDDER AREA	FT^2	300
AERODYNAMIC PERF		
PLANFORM AREA	FT^2	8[illegible]0
PLANFORM LOADING	PSF	31
HYPERSONIC L/D		0.52
ENTRY LIFT LDG W/C_LS	PSF	42
SUBSONIC WING LDG	PSF	88
TOUCHDOWN SPEED	KNOTS	128

Figure 2.2-1. Booster and Orbiter Aerodynamic Configuration Characteristics

attack. The flat bottom and sharp corners also promote separation around the sides of the body. This results in low temperatures on the sides and upper surface during entry.

Lateral and directional stability is provided by body shaping. Directional stability is essentially neutral at the high angle of attack during entry. Roll stability is provided by wing dihedral.

Orbiter hypersonic L/D is 0.53 during entry at a 60-degree angle of attack and 7.3 during subsonic glide. The booster entry is performed at a 52.5-degree angle of attack at maximum lift coefficient to permit lift modulation and prevent excessive load factors during the flyback maneuver. L/D at entry is 0.69 and 8.4 during subsonic cruise.

Design improvement investigations indicated that:

1. Use of a radius on the lower body will allow reduced horizontal tail size. Additional effort is required to evaluate impact on thermal protection system and vehicle weight.

2. Directional stability can be improved by use of twin verticals or by use of dihedral on the horizontal surface.

3. Incorporating roll-out of the body sides aft of the center of gravity is effective in improving directional stability.

4. Increased wing sweep and reduced aspect ratio should be investigated to improve flyback performance.

5. Because of the extreme aft location of the center of gravity on the booster (greater than 60 percent of the body length), the horizontal tail size becomes excessive. Moving the wing aft reduces the tail size. Use of a canard configuration should also be investigated to minimize aerodynamic surface size.

2.3 CONTROL CONCEPTS

The vehicle is controlled through main engine thrust vector control (TVC) during the ascent phase of the mission, by use of the reaction control system (RCS) for orbital maneuvers and entry, and by aerodynamic surfaces during subsonic flight.

To establish vehicle loading environment, it is necessary to establish the vehicle control characteristics. In the study, the vehicle was analyzed for the ascent phase of the mission with wind and gust profile based upon a 99-percent probability of nonoccurrence.

With a programmed flight path angle control mode, and a 7-degree main engine gimbal limit, the vehicle is subjected to maximum $q\alpha$ of 2970 psf degrees.

A 6-degree-of-freedom control simulation was performed for vehicle reentry. It showed that a control system authority of 0.5 deg/sec^2 acceleration is adequate. A simulation of the transition to cruise maneuver confirmed that pitch-over was smooth and well damped, with use of an elevator command incorporating gain scheduling.

2.4 ABORT

The impact of potential system failures was analyzed. The analysis indicated that failure of a single engine on either the booster or the orbiter will not prevent completion of the primary mission. A system failure requiring premature staging will necessitate action to limit reentry loads on the orbiter and propellant dumping. For low-altitude mission termination, the orbiter with two engines operating will remain at low altitude. For high-altitude mission termination, the orbiter engines (one or two) may be used to shape the trajectory and prevent excessive reentry loads. Failure of two orbiter engines, however, may cause excessive reentry loads and possibly make a water landing necessary. Propellant dumping will be required to minimize loads in event of failure of both orbiter engines.

2.5 THERMAL ENVIRONMENT

For thermal protection system requirements to be established, it was necessary to establish a thermal environment. During ascent, the vehicle is subjected to areas of interference heating on the upper surface of the body. For the upper surface of the orbiter, the critical design temperature is experienced during boost. A temperature of 500 F is reached and is in excess of that experienced during entry.

The most severe thermal environment condition for the under surface of the vehicle occurs during reentry. Figure 2.5-1 illustrates the radiation equilibrium temperatures for the orbiter and booster. For reentry, the temperature is illustrated for two locations on the body and for a number of locations on the wing. The temperature is defined as a function of body station or percentage distance across the wing chord. The temperatures are based on vehicle reentry with a lift loading (W/C_LS) of 50 psf.

As shown in the figure, the orbiter experiences temperatures below 1500 F on 90 percent of the body. This thermal environment is based upon reentry at a 60-degree angle of attack. It should be noted, however, that the equilibrium temperatures on wing leading edges during reentry are significantly greater than temperatures experienced generally on the body.

REENTRY

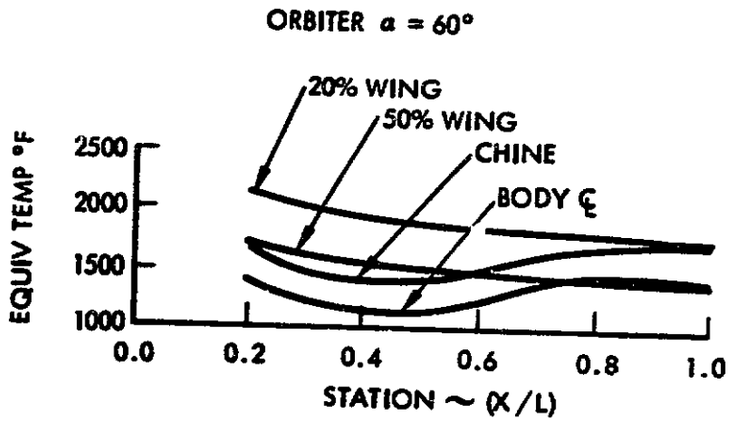

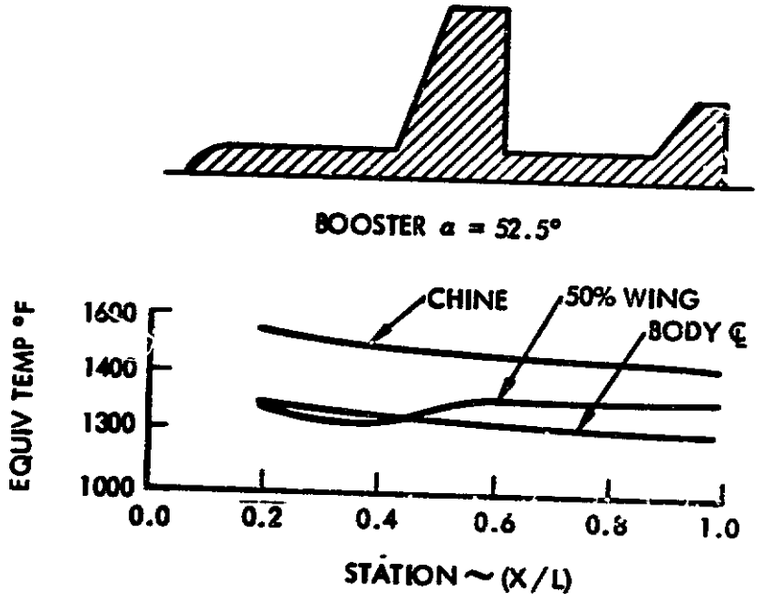

SUMMARY

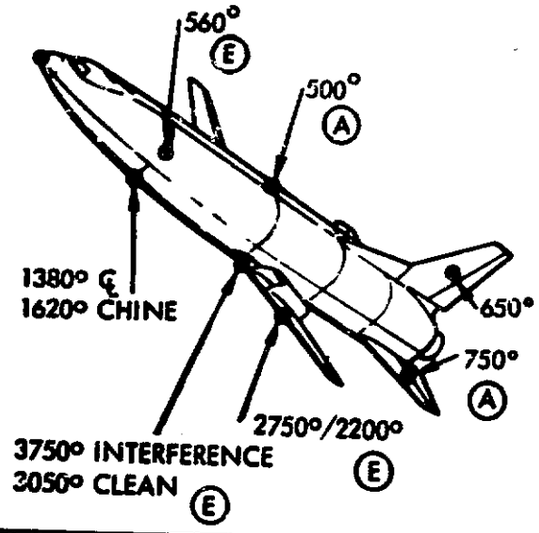

LOCATION	CRITICAL FLIGHT CONDITIONS	RADIATION EQUILIBRIUM TEMPERATURE (°F)	
		BOOSTER	ORBITER
FUSELAGE			
NOSE	ENTRY	1275	1860
LOWER SURFACE 20%	ENTRY	1380	1420
LOWER SURFACE 80%	ENTRY	1220	1450
CHINE	ENTRY	1530	1620
SIDE	ENTRY	540	560
UPPER SURFACE	ASCENT	500	500
WING			
L.E. (NO INTERFERENCE)	ENTRY	2200	3000
LOWER SURFACE 20%	ENTRY	1400	1700
UPPER SURFACE 20%	ASCENT	650	700
HORIZONTAL SURFACE			
L.E.	ENTRY	2020	3450
LOWER SURFACE	ENTRY	1390	1500
UPPER SURFACE	ASCENT	600-650	700
VERTICAL SURFACE			
L.E.	ASCENT	1730	2320
SIDE	ASCENT	600-650	650

Figure 2.5-1. Thermal Environment

Radiation equilibrium temperatures on the wing leading edges are 2800 F to 3200 F without interference effects. Flow interference effects at 20 percent wing span could significantly increase leading edge temperatures.

As illustrated in the figure, temperatures experienced by the booster during reentry are significantly lower than those experienced by the orbiter and are less than 1400 F on 90 percent of the vehicle.

2.6 LATERAL RANGING EFFECTS AND POTENTIAL

In view of the desire to establish vehicle potential for increased lateral range, investigations were performed to establish the impact of reentering at lower angles of attack. Figure 2.6-1 illustrates orbiter body and wing temperatures and heat load experienced during entry at various angles of attack. As illustrated, the vehicle can achieve approximately 1240 nautical miles of lateral ranging capability at a 20-degree angle of attack without exceeding the temperature limitations of the proposed densified quartz material, except for wing leading edges. The increased heat load, however, with the greater lateral ranging, will require an increase of approximately 22,000 pounds in thermal protection system weight.

The lateral ranging capability of the vehicle can also be increased to 1500 nautical miles by cruising with the turbojet engines, offloading payload, and adding turbojet fuel.

2.7 APPROACH AND LANDING

To limit logistics vehicle weight, it becomes extremely important to optimize booster cruise and orbiter landing system weights. Booster descent and turnaround studies were conducted to minimize flyback range. A range of 310 miles was established for the 50,000-pound-payload-class system by developing a banked entry flight mode. This was a 24-percent reduction in range over a straight-in entry. Optimization of the booster flyback propulsion system resulted in selection of a system employing 4 JT9D-15 turbojets and flying at 0.38 Mach number. The lowest weight system was the one that used the fewest engines and cruised at an off-optimum Mach number. The saving in engine weight was greater than the increased fuel required for cruise at off-optimum conditions.

The baseline orbiter vehicle, in accordance with study requirements, is configured to provide go-around capability in event of a landing wave-off. Four JT3D-7 turbojets are used in the 50,000-pound-payload orbiter. Total engine and fuel weight is 20,240 pounds, with 82 percent of that weight due to the engines themselves. Deletion of the climb-out capability by eliminating two engines would reduce system weight by 10,120 pounds. Use of high

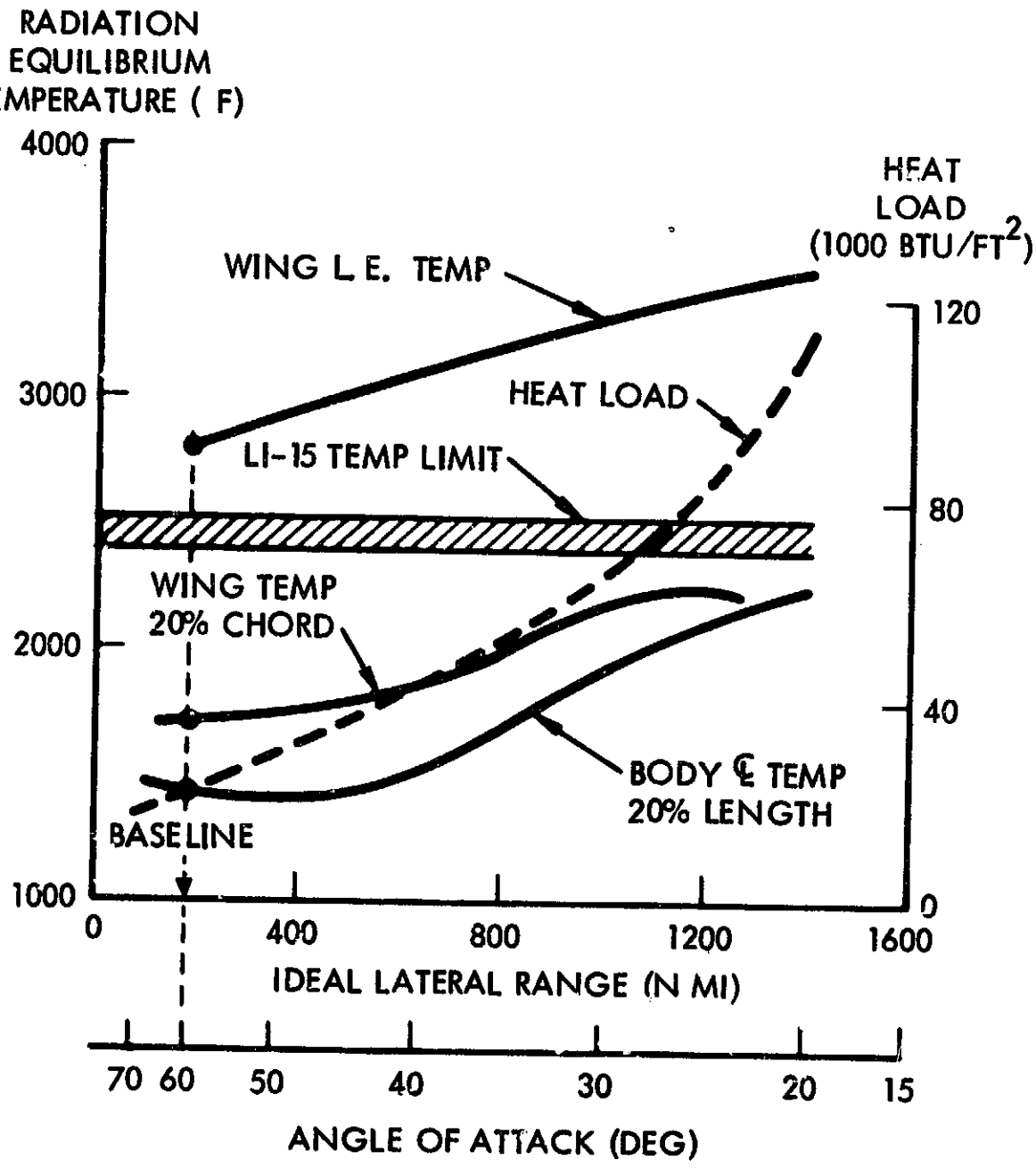

Figure 2.6-1. Orbiter Lateral Range Potential

thrust-to-weight ratio turbojets should be investigated. It was estimated that a 9740-pound weight saving could be realized.

Landing speeds for the booster and orbiter are compatible with present transport aircraft. Nominal touchdown speeds are 113 knots for the booster and 128 knots for the orbiter.

2.8 DESIGN LOADS

Design structural loads were defined for the following flight conditions:

1. Prelaunch, with 99.9 percentile ETR ground winds
2. Maximum $q\alpha$, 2940 psf-deg, with 95 percentile ETR winds aloft
3. Maximum accleration, 3.0 g's for both stages
4. Booster entry, 4.0 g's maximum
5. Orbiter entry, 2.1 g's maximum
6. Transition to cruise maneuver, 2.5 g's
7. Landing - 10 fps sink speed, 1.4 gear load factor, 1.2 body load dynamic factor

Maximum body loads are summarized in Table 2.8-1 for the 50,000-pound-payload-class system.

Table 2.8-1. Structural Design Loads Summary, 50,000-Pound-Payload System

	Load Station (Inches from booster tail with orbiter attached)	Limit Loads			
		Condition	Axial x 10^{-3} (lb)	Shear x 10^{-3} (lb)	Moment x 10^{-6} (in.-lb)
Booster	2870 (fwd attach)	Max q α	-1865	525	250
	2000 (LOX tank aft bulkhead)	Max q α	-4292	-207	-150
		Max accel	-3872	117	430
	1430 (aft attach)	Max q α	-4736	-311	-1,10
		Max accel	-4010	459	357
	1350 (main gear)	Landing	-185	500	-430
	100 (hold-down)	Prelaunch	-3985	-340	520 (Tilt) 740 (No Tilt)
Orbiter	2870 (fwd attach)	Max q α	848	484	215
		Max accel	-1552	254	488
	2320 (main gear)	Max accel	875	270	344
		Landing	-195	-340	-96
	1430 (aft attach)	Max q α	140	-284	-29
		Max accel	80	334	-0.63

3.0 OBJECTIVES

This design study to investigate low-cost space transportation systems is based on the following program objectives:

1. Derive conceptual designs and perform resources analyses to identify the development, manufacturing, procurement, testing, RDT&E, and operations requirements for logistics space vehicle systems to support earth-orbital programs in the post-1974 period. In the major design approaches, attempt to achieve order-of-magnitude reduction in the recurring costs of the total logistic support operational system and to achieve significant advances in the inherent safety of the space vehicle system.

2. Establish requirements for research and technology development; and discuss the potential benefits in terms of systems sensitivities, development risks, etc.

Objectives of the second phase of the study, which is reported in this document, are as follows:

1. Establish sizes and weights of an advanced logistic vehicle concept defined by NASA MSC for payload classes of 10,000, 25,000, and 50,000 pounds.

2. Determine the impact of candidate design improvement concepts for the NASA MSC vehicle.

3. Select vehicle(s) and payload size(s) for conceptual design analysis.

4. Prepare conceptual design definitions of the selected advanced logistic vehicle(s).

5. Define a development approach, and identify technology requirements for the new logistic system.

6. Develop resource plans and cost estimates.

4.0 MISSION AND DESIGN REQUIREMENTS

The following requirements, which are applicable to the shuttle system after it becomes operational, were used during the second phase of the study.

1.	Mission orbit	270-nm, 55-degree inclination.
2.	Launch site	Cape Kennedy.
3.	Payload, up and down	Payload delivered by vehicle with eight 250,000-pound nominal vacuum thrust engines on booster. 25,000-pound payload size, 15-foot diameter by 30-foot length. 25,000-pound payload size, 15-foot diameter by 60-foot length. 25,000-pound payload size, 12-foot diameter by 48-foot length. 50,000-pound payload size, 15-foot diameter by 60-foot length. 50,000-pound payload size, 22-foot diameter by 60-foot length. The payload weight includes ten passengers with provisions and cargo; the payload sizes provide only for cargo. Additional volume will be provided for ten passengers. The weight of two crew members in the orbiter vehicle will be included in the weight of the shuttle vehicle system.
4.	Mission duration	Shuttle vehicle: 30 days on orbit; 7 days active life of systems.

5.	Orbital operations	2,000-foot-per-second velocity capability in excess of that required by the vehicle to obtain a 45- by 100-nm orbit will be provided by the shuttle vehicle.
6.	Launch rate	24 to 50 per year.
7.	Ground mission operations	Conducted from a central facility.
8.	Cargo	Cargo will be self-contained and will provide protective devices or provisions.
9.	Environment	System will be limited to commercial V_n limits; maximum eyeballs-in acceleration for crew will be 3 g; crew and passengers will have shirt-sleeve environment.
10.	Launch and refurbishment sites	Refurbishment site will be the same as launch site.
11.	Communication	Continuous space-to-ground communication will be available; communication will provide for two-day self-validating data transmission.
12.	System failures	System will fail operational after first failure and fail safe after second failure.
13.	Toggle switches	Avoid.
14.	Mission termination and abort	Satisfactory crew and passenger egress shall be made for abort during launch. When necessary, provisions will be made for abort during launch.
15.	Checkout	Shuttle vehicle primary preflight and in-flight checkout systems will be on board the vehicle.

16. Guidance and Navigation	Guidance and navigation functions will be performed on board.
17. Vehicle operation	The vehicle will have a two-man flight crew. It is desirable that it can be flown by a single crewman.
18. Boost stage	The boost stage will be reusable and may be unmanned.
19. Docking	Hard docking is required. Shuttle vehicle atmosphere will be the same as that of the space station base during cargo transfer. Crew transfer will be by IVA. Automatic approach and docking capability will be provided.
20. Orbital insertion	A three-axis translation system is required.
21. Deorbit and reentry	Return opportunity to primary landing site shall be at least once every 24 hours.
22. Landing and go-around	The shuttle vehicle will be capable of go-around with one engine out and more than one landing attempt. Landing visibility will be comparable to that of high-performance aircraft. Zero-zero capability and automatic landing capability should be provided.
23. Self-ferrying	Capability for self-ferry flights between airports will be provided.
24. Onboard provisions	Onboard provisions will be available to ensure postlanding safety.
25. Refurbishment	Minimimum turn-around.
26. Engines	Engines to be considered include high-pressure bell engine and aerospike engine (alternate).

27. Reentry	Vehicles will provide high angle of attack on reentry; RCS will be used.
28. Aerodynamic surfaces for reentry	Aerodynamic surfaces will be fixed for hypersonic velocities.
29. Stability	During boost, vehicle center of gravity will be forward of center of pressure; engine failure will not result in critical design loads.
30. Ranging	Vehicle ranging capability and options to increase lateral ranging will be identified.
31. Margins	A 10-percent weight contingency will be allowed. Performance reserve will be 3/4-percent of the vehicle characteristic velocity with the associated propellant allowance in the terminal stage.

5.0 SCOPE

The basic NASA vehicle concept to be studied is illustrated in Figure 5.0-1. This concept is configured for a crew of two (in orbiter) and the following payloads (which include ten passengers):

1. Payload delivered by vehicle with eight 250,000-pound nominal vacuum thrust engines on booster.

2. 25,000-pound payload, cargo size 15-foot diameter by 30-foot length.

3. 25,000-pound payload, cargo size 15-foot diameter by 60-foot length.

4. 25,000-pound payload, cargo size 12-foot diameter by 48-foot length.

5. 50,000-pound payload, cargo size 15-foot diameter by 60-foot length.

6. 50,000-pound payload, cargo size 22-foot diameter by 60-foot length.

The payload weight includes ten passengers with provisions and cargo; the payload sizes provide only for cargo. Additional volume will be provided for ten passengers. The weight of two crew members in the orbiter vehicle will be included in the weight of the shuttle vehicle system.

Improvement concepts will be investigated, but the following features are mandatory:

1. High angle of attack (approximately 60 degrees) to minimize heating (RCS will be used for control).

2. Fixed wings possibly with adjustable tips; wing shapes may be changed.

3. Fixed turbojets (no swing-out).

Figure 5.0-1. Baseline Vehicle Concept for Phase 2 of Study

4. No window covers.

5. A flat undersurface and a general cross section shape defined by NASA.

6. Vertical takeoff.

7. Two stages (reusable).

8. Propellant to be LO_2/LH_2.

9. High-pressure pump-fed bell or aerospike engines.

10. No ablative-cooled or transpiration-cooled thermal protection system.

11. Horizontal landing.

6.0 APPROACH AND STUDY SCHEDULE

The logic used in the second phase of the study is illustrated in Figure 6.0-1. The study established sizes and weights of the NASA MSC space shuttle vehicle concept for payloads specified in Section 5.0. Design improvement concepts were evaluated, and vehicle sensitivity to design variables was assessed. Conceptual design definitions of selected vehicles were provided. Resource plans and estimated system nonrecurring and recurring costs were defined. Technology advancement requirements were identified. Vehicle sizing studies and investigations of improvement concepts were performed during the six-week period after formal initiation of the second phase of the study. Data were then submitted to NASA MSC, where selection was made of the vehicle payload sizes and vehicle configurations for conceptual design. Conceptual design data and resource plans were generated for a selected vehicle during the last three months of the second study phase. The schedule for the study activity is presented in Figure 6.0-2.

6.1 CONCEPT SIZING AND PERFORMANCE ANALYSIS

Shuttle vehicle sizes and weights defined by NASA MSC were reviewed to establish system weight-scaling equations. Mandatory features of the shuttle vehicle are defined in Section 5.0. Aerodynamic characteristics of basic NASA MSC concept were investigated to confirm projected environment and performance. Flight trajectory analyses were performed to establish the optimum propellant distribution between the booster and orbiter vehicles to deliver the previously specified payloads. Wing and body sizes were established for the desired wing loading and heat rate on reentry. Methods of increasing vehicle lateral ranging capability were identified, and the impact on vehicle payload return capability or system weight was established.

Design, performance, and program implications for internal and external cargo provisions were identified. Weights and preliminary relative costs were also estimated.

6.2 DESIGN IMPROVEMENT CONCEPTS AND SENSITIVITY ANALYSIS

To establish design features that should be incorporated in the shuttle vehicle, candidate improvement concepts were evaluated to determine their impact on vehicle weight, performance, cost, safety, and technology requirements. Vehicle sensitivity analyses were performed to establish the impact of design criteria, engine performance deviations, system weight growth, and more stringent environments (such as reentry thermal load).

6.3 CONCEPTUAL DESIGN

Based on vehicle sizing and design improvement studies, vehicle configurations selected by NASA MSC were subjected to conceptual design analysis.

Aerodynamic characteristics of the vehicle elements for boost, reentry, flyback, and landing were established; and trajectories were computed for these mission phases. Control requirements and structural and thermal environments were calculated and used in the derivation of of major structure and thermal protection system weights.

System flight characteristics and control requirements for all mission phases were determined and rigid body loads analysis performed to compute structural loads during boost, reentry, and flyback maneuvers.

The effects of aerodynamic characteristics and the approach and landing methods, including manned and unmanned automatic landing, were assessed to establish the desirable approach and landing system.

Subsystem trade studies were performed, and conceptual designs were developed to facilitate estimation of vehicle weights. Preliminary definitions were prepared for vehicle subsystems, and the subsystems were analyzed to determine checkout procedures.

6.4 RESOURCE PLANS

Program requirements for the shuttle vehicle were analyzed to provide direction for design studies.

The possible application of aircraft development and testing approaches to the shuttle vehicle was examined to determine the impact on system development time and cost.

For selected vehicles, a test plan was developed and operations analyses were performed to define procedures and equipment requirements for prelaunch, launch, orbital operations, recovery, transportation, and servicing. Resource plans were developed, and system costs were estimated to Level 5.

6.5 TECHNOLOGY

Technology requirements were identified, and the potential impact of the technology program on the system performance, cost, and schedule was described.

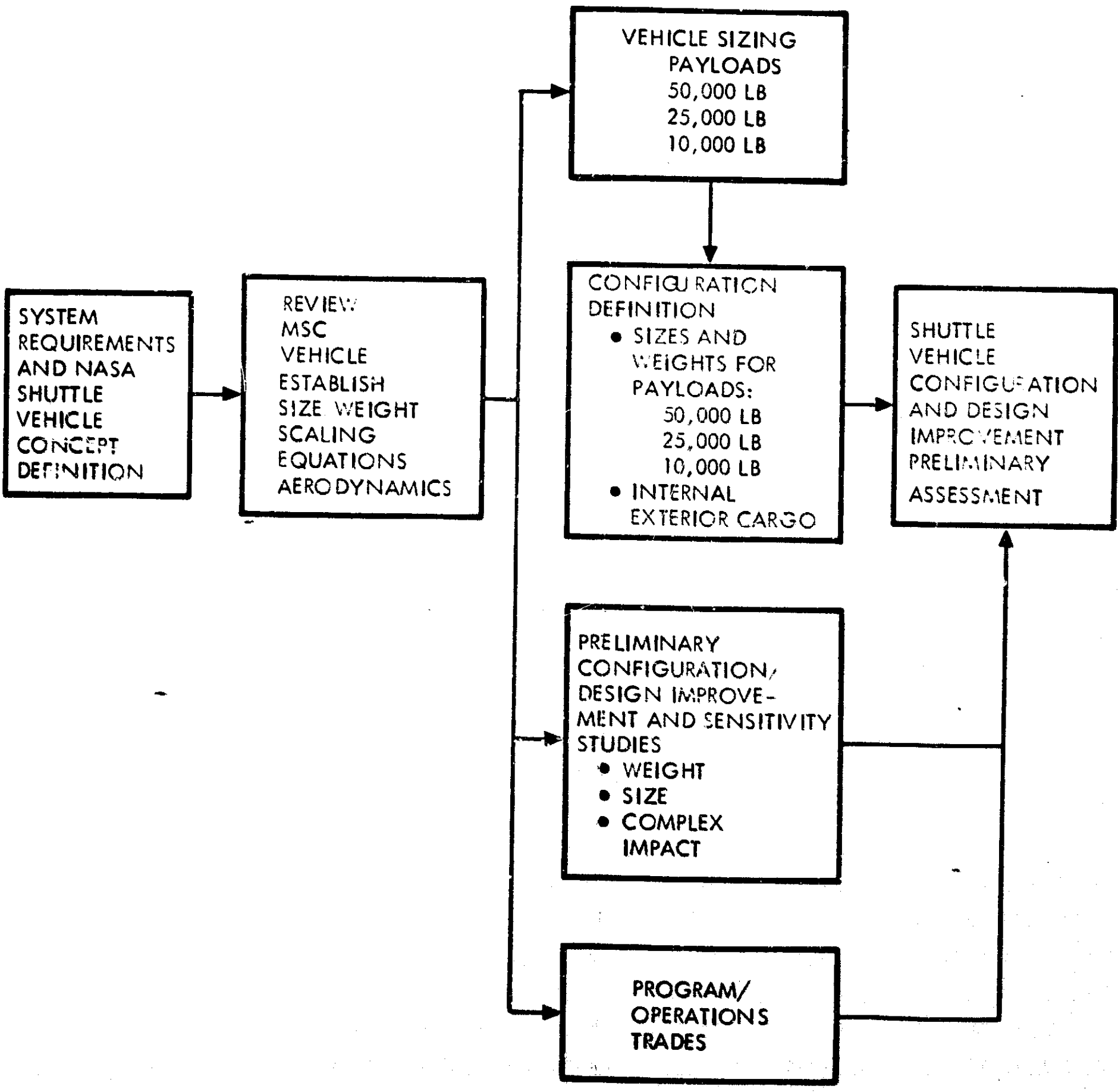

FOLDOUT FRAME 1

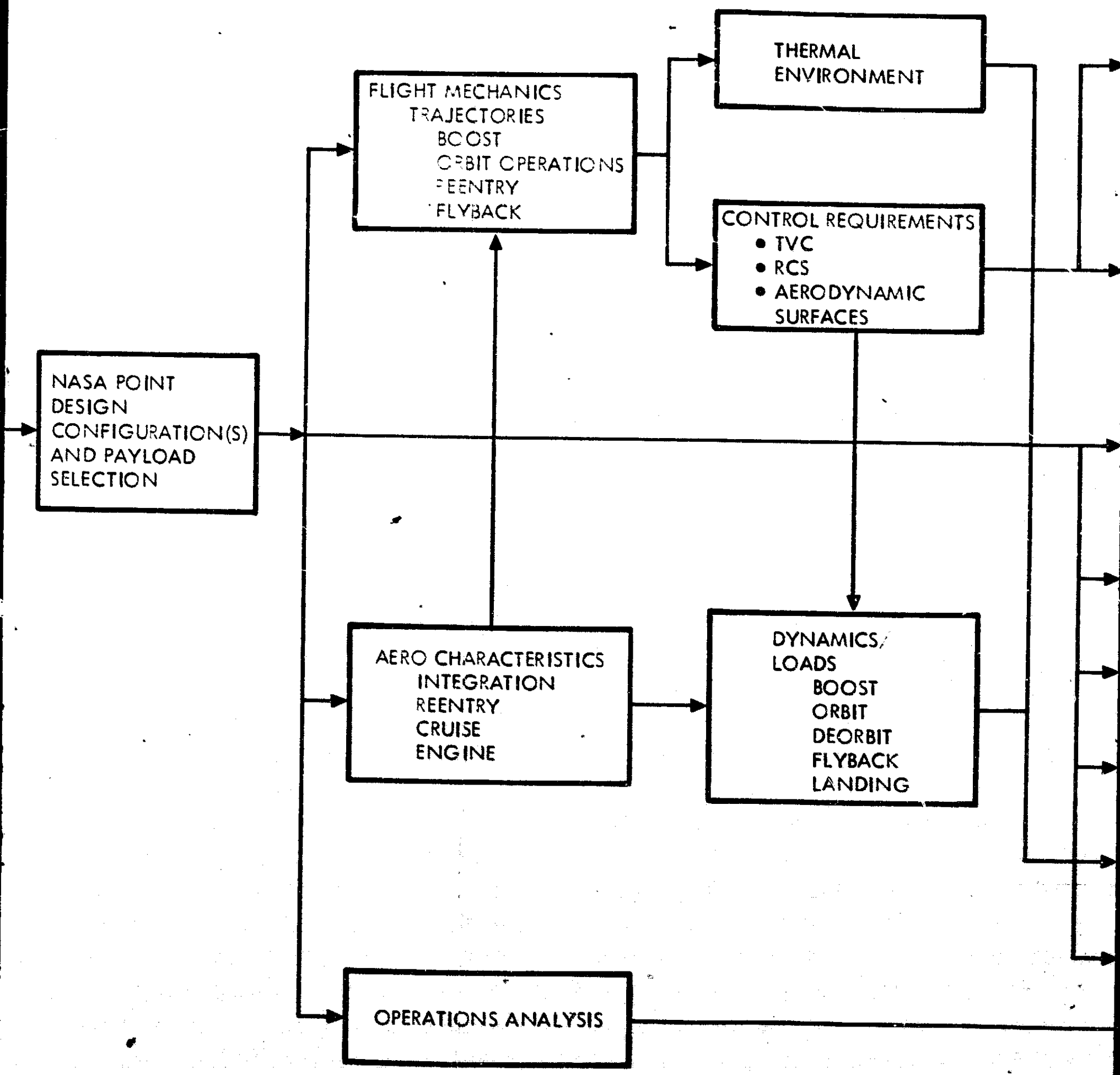

FOLDOUT FRAME 2

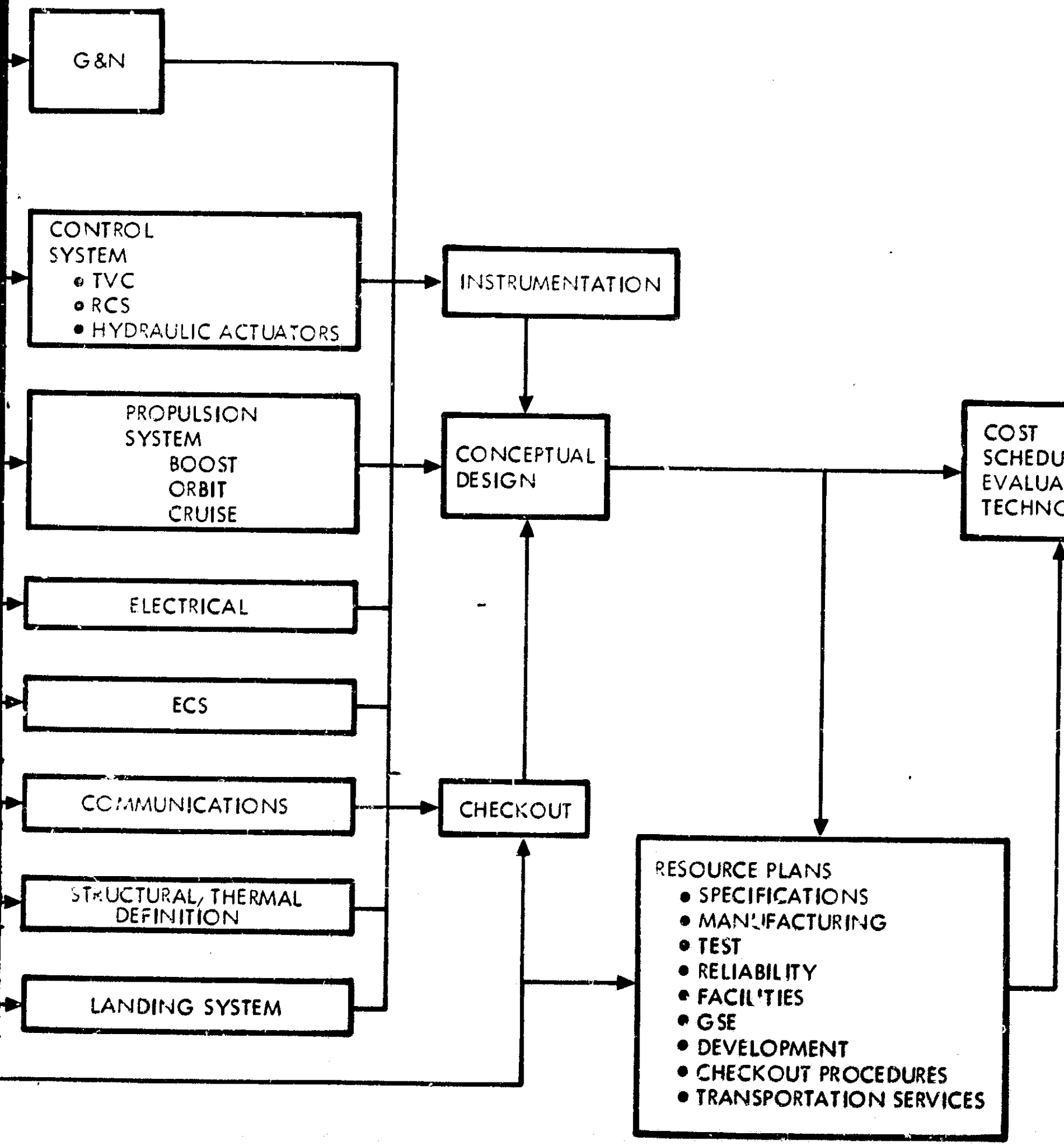

Figure 6.0-1. Phase 2 Study Logic

FOLDOUT FRAME 3

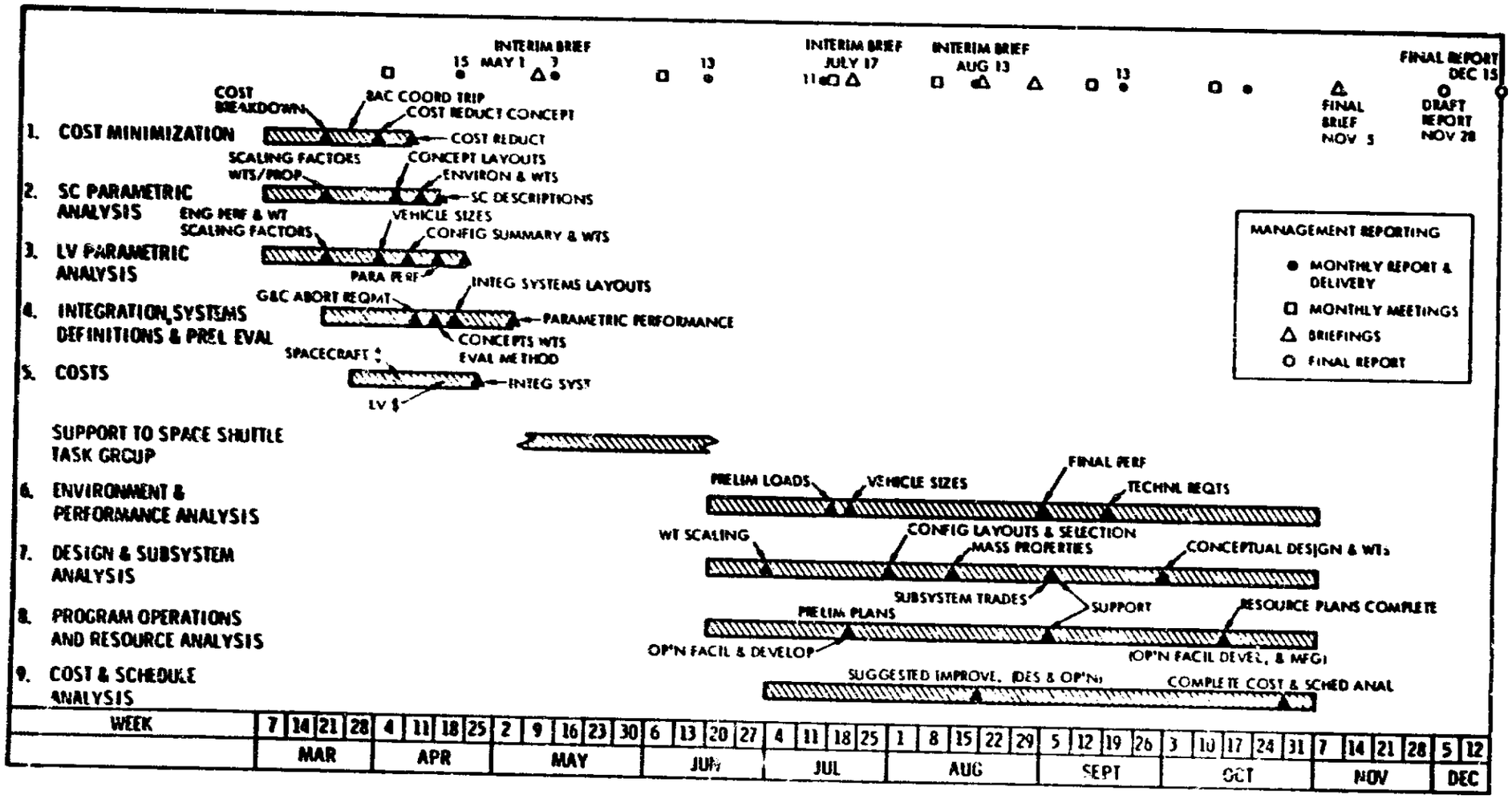

Figure 6.0-2. Phase 2 Study Schedule

Space Division
North American Rockwell

7.0 PERFORMANCE

7.1 MISSION CHARACTERISTICS

This section describes the design flight profile and on-orbit maneuver requirements for use in sizing vehicle systems and summarizes the payload delivery capability for range of vehicle sizes.

7.1.1 Mission Profile

Mission and design requirements were provided by NASA and are summarized in Section 4.0 of this report. The ILRV mission is to ferry crew and cargo to and from a space station located in a low earth orbit, nominally at 270 nautical miles altitude and 55 degrees inclination. Boost is into an orbit of 50 by 100 nautical miles. Selection of the injection condition was based on an evaluation of ascent heating, booster flyback range and propellant requirements, and impact on stage weight and size. The trajectories flown were optimized to minimize launch gross weight. It was considered desirable to keep the peak heat environment on the wing leading edges at or below that experienced during entry if it could be done without major penalty in performance or stage size. This would require an injection altitude of 50 by 100 nautical miles or greater. The effect of injection conditions on stage weight was found to be small over the range of 45-by-100 to 80-by-100 nautical miles. Launch gross weight increased less than two percent for a fixed booster flyback range. Flyback range increased with injection altitude. To minimize weight penalties, the injection altitude was selected on the basis of minimum acceptable heating.

The flight profile is illustrated in Figure 7.1-1. It consists of four phases: ascent, space operations, orbiter descent, and booster descent. The shuttle is launched from the ETR. Staging occurs at 230,000 feet altitude at a velocity of 10,850 fps. Orbiter ignition occurs 7 seconds after separation, and the vehicle is injected into an orbit of 50 by 100 nautical miles, coasts to apogee, and transfers to a parking orbit for rendezvous phasing and docking. Maximum total ascent time is 24 hours. The orbiter is required to be at the space station a maximum of 30 days, with 7 days of active life for orbiter systems.

After the staging, the booster is pitched to angle of attack of 52-1/2 degrees and rolled to a 90-degree bank. Entry is initiated at maximum lift coefficient; the bank angle is reduced to 60 degrees; and the booster performs a banked turn during entry to minimize the flyback range.

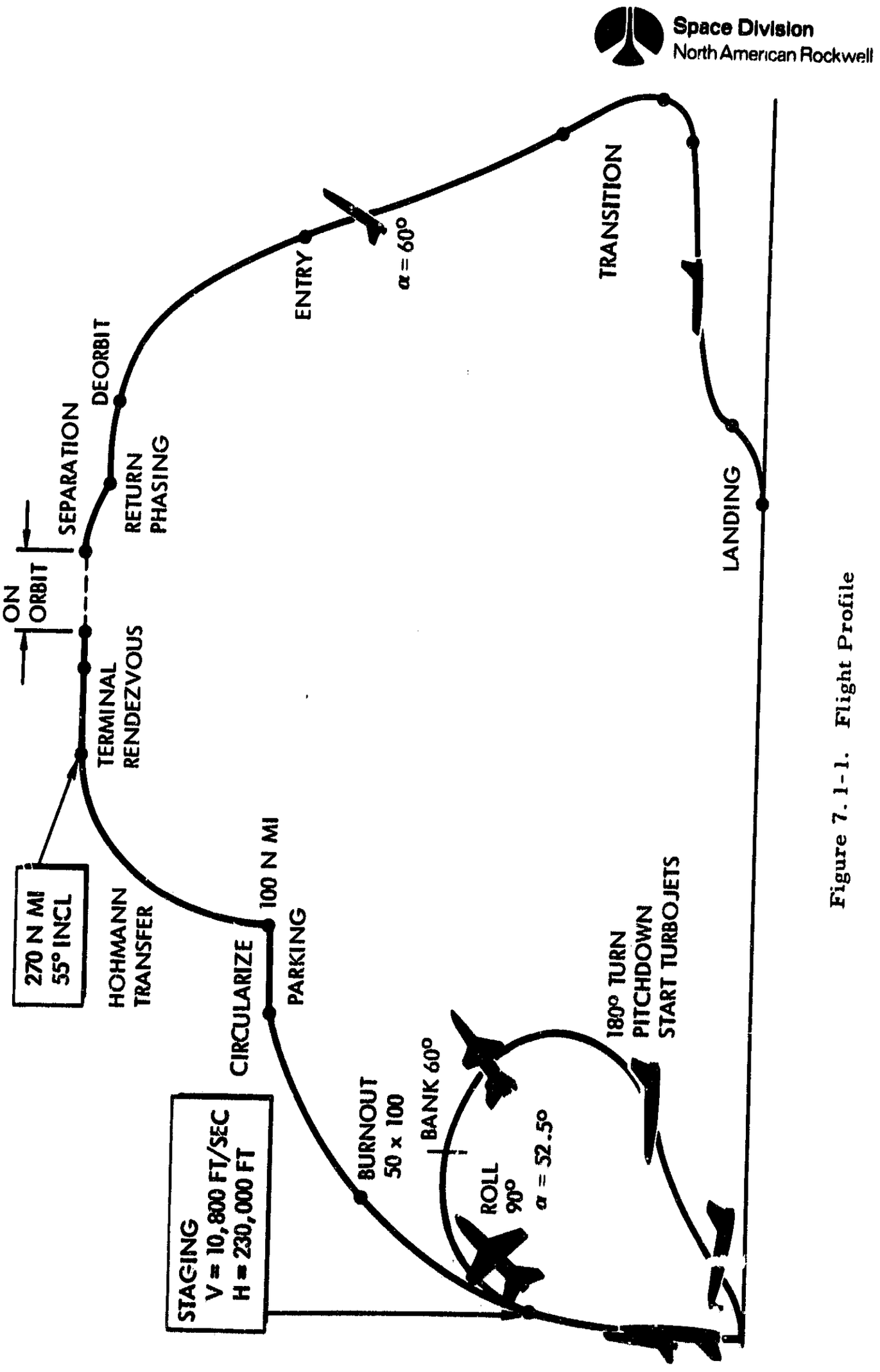

Figure 7.1-1. Flight Profile

The load factor during entry was constrained to 4.0. This is reached at 156,000 feet, where angle-of-attack modulation begins to prevent the load factor from exceeding the design value. The minimum angle of attack reached is 33 degrees. The maximum dynamic pressure is 189 psf. The turn is completed at 78,000 feet at subsonic speed. Pitch-down is commanded, and the vehicle glides at maximum L/D to 22,000 feet. There the turbo jets are ignited for cruise back to the launch site. Total cruise-back range is 310 miles, about 98 miles fewer than would be obtained with a non-banked, straight-in entry. Booster landing speed is 113 knots.

After orbital operations have been completed, the orbiter separates from the space station. Maximum orbiter descent time is 24 hours for return to the primary landing site after the decision is made to deorbit. Launch and primary landing sites are both at the ETR. For return at least once every 24 hours to be possible, for the most adverse phasing between the space station and ETR recovery site requires the equivalent of approximately 335 nautical miles of cross-range capability for the orbiter. For a nominal entry, the orbiter has a cross range of approximately 190 nautical miles. The deficiency in cross range is obtained through orbital phasing prior to entry into the atmosphere. For worst-case phasing, the orbiter transfers to an orbit of 270 by 100 nautical miles and waits for 9 orbits (13.69 hours) before the final deorbit burn is performed. Entry is performed at 60 degrees angle of attack. Ranging is accomplished by roll modulation about the velocity vector. Pitch-down to subsonic glide is performed at approximately 40,000 feet altitude. The turbojets are ignited before the final approach and operated at reduced power setting to provide go-around in event of a wave-off during landing. Landing speed is 128 knots.

Major events occurring during each phase of the flight profile are listed in Table 7.1-1, together with flight times and maneuver requirements for a minimum and maximum duration flight. The minimum-duration flight corresponds to a space station position in orbit that permits direct transfer to and from the station without use of a phasing orbit during ascent or descent. The maximum duration mission corresponds to a station in the most adverse position for rendezvous and return phasing.

7.1.2 On-Orbit Maneuver Requirements

The on-orbit maneuver budget is listed in Table 7.1-2. Both the design and minimum requirements are given for completing the supply mission after injection into the orbit of 50 by 100 nautical miles. Systems were sized according to the design requirement. Reserves and contingency allowances were deleted to arrive at the minimum ΔV requirement.

Table 7.1-1. Design Flight Profiles

Mission Phase	Events	Minimum Duration Mission		Maximum Duration Mission		Remarks
		Time Between Events	ΔV (fps)	Time Between Events	ΔV (fps)	
Ascent Phase						
1. Launch, booster stage	• Lift-off • First-stage boost • First-stage shutdown • Separation • Booster begins descent phase	273 sec	15,400	223 sec	15,400	Launch from ETR into 55-degree inclination orbit. Maximum q 418 psf at 0.92 Mach number and 29,000 feet. Separation occurs at 230,000 feet altitude, 10,800 fps, 5 psf dynamic pressure.
2. Launch, orbiter stage	• Orbiter ignition • Inject into 50- x 100-nm orbit, orbiter stage inclination	7 sec 195 sec	15,076	7 sec 194 sec	15,076	Total ascent time, including 6 seconds for orbiter ignition, is 423 seconds. Orbiter has 225 fps additional propellant reserve.
	Total boost	0.07 hr	30,476	0.07 hr	30,476	
3. Rendezvous	• Orbiter coasts to 100 nm • Circularize at 100 nm • Coast to adjust phase angle • Corrective combination maneuver • Transfer to orbit 10 miles below station	0.73 hr 0.74 hr 0.75 hr 0.77 hr	90 142 279 137	0.73 hr 19.85 hr 0.75 hr 0.77 hr	90 142 479 137	Coelliptic sequencing rendezvous with terminal phase braking occurring in daylight. coelliptic orbit is 10 nm below target orbit. 200 fps ΔV allowed for contingencies and plane change at corrective combination maneuver.
4. Terminal rendezvous and docking	• Perform terminal rendezvous and docking maneuvers • Orbiter attached to space station, and docking mechanism secured	1.33	142	1.33	142	Two-impulse terminal rendezvous maneuvers, thrust and braking applied alternately during docking, 698 fps ΔV for rendezvous, 93 fps allowed for docking.
	Total ascent orbital phase	4.32	790	23.43	990	
	Total ascent phase	4.39	31,266	23.50	31,466	
5. Space station operations				30 days		7 days active systems 30 days maximum staytime
Orbiter Descent Phase						
6. Return phasing	• Separation from space station • Transfer to phasing orbit • Coast until properly phased for deorbit	0	--	13.69	370	For worst case phasing, transfer to 270- by 100-nm elliptic orbit wait for 9 orbits. ΔV required is 295 fps. maximum duration mission includes 75 fps contingency.
7. Deorbit and coast	• Attain retrograde attitude • Retrofire • Attain entry altitude • Coast to 400,000-foot altitude	0.40	425	0.40	130	Entry attitude is 50-degree bank and 60-degree angle of attack Deorbit for phasing orbit for maximum duration mission.
8. Entry and recovery	• Entry into atmosphere • Glide and maneuver to acquire landing site at completion of entry phase • Descend to initiate pitch down maneuver	0.30	--	0.30	--	Orbiter stabilized by RCS, lift modulation by roll control. Entry phase complete at 128,000-foot altitude and 3000-fps velocity.
9. Transition	• Pitch down to cruise attitude • Start turbojets • Descend to landing site	0.05		0.05		Nominal pitch down is at 0.4 Mach number at 40,000-foot altitude.
10. Landing	• High key acquisition • Approach flare • Touchdown	0.20	--	0.20	--	Vehicle has fuel for two go-around maneuvers at 200 knots (12 minutes). Landing speed is 128 knots.
	Total orbit descent phase	0.95	425	14.64	500	
Booster Descent Phase						
1. Separation	• Stabilize booster during separation of orbiter					Altitude = 330,000 feet q = 5 psf
2. Power-off Descent	• Roll to 90-degree bank, pitch to 52.5-degree angle of attack, coast to apogee	0.07		0.07		Apogee at 268,000 feet.
	• Enter at 90-degree bank and hold until g's are 0.5					0.5 g's reached at 221,000 feet at 9,760 fps.
	• Roll to 60-degree bank, hold constant bank angle until heading is 180-degrees.					180-degree heading reached at 78,400-foot altitude at 720 fps. Angle of attack modulated during the turn so that max g's did not exceed 4.0.
3. Transition and cruise	• Pitch down to cruise attitude • Start turbojets • Cruise to landing site	0.81		0.81		Pitch down to cruise angle of attack completed at Mach 0.9 at 55,000-foot altitude. Glide to Mach 0.38 at 22,000-foot altitude and start turbojets.
4. Landing	• High key acquisition • Approach flare • Touchdown	0.20		0.20		Vehicle has fuel for two go-around maneuvers at 200 knots (17 minutes). Landing speed is 113 knots.

Table 7.1-2. On-Orbit Maneuver Budget

Maneuver	Velocity Increment (fps)	
	Minimum Requirement	Design Requirement
Inject 50- by 100-nm orbit		
Circularize at 100-nm	90	90
Transfer to 260-nm phasing orbit	558	558
Terminal rendezvous orbit and docking	142	142
Launch dispersion and plane change		200
Deorbit from 270-nm	425	500
Contingencies		500
Total	1215	1990

7.1.3 Performance Capability

During the first portion of the Phase II study, vehicle gross weights were established for the payload sizes specified by NASA. The space shuttle concept used as a basis for vehicle sizing and definition of performance capability was defined by NASA MSC. The vehicle was configured to contain a payload of 12,500 pounds and provide 2000 cubic feet for cargo. The basic aerodynamic shape and weight-to-planform area relationships for this vehicle were maintained for initial sizing of vehicles configured to deliver 25,000 and 50,000 pounds of payload to a 55-degree-inclination orbit at 270 nautical miles altitude. Sizing and weight scaling for these vehicles is discussed in Volume IV. Table 7.1-3 summarizes the vehicle characteristics for the specified range of payload sizes.

After the concepts were sized, NASA MSC selected a shuttle vehicle for detail analysis. This vehicle, termed the 50,000-pound payload class baseline in this volume, has a cargo bay 15 feet in diameter by 60 feet. The configuration is illustrated in Figure 2.1-2. Final vehicle sizing was based on detailed design and subsystem studies described in Volume IV. These studies indicated that the gross weight of the 50,000-pound payload vehicle will be 4.5 million pounds.

Table 7.1-3. Overall Vehicle Characteristics, Concept Sizing Phase

Payload (1000 lb)	Cargo Bay Size Dia by Length (ft x ft)	Total Vehicle		Booster		Orbiter	
		Weight (1000 lb)	Length (ft)	Weight (1000 lb)	Length (ft)	Weight (1000 lb)	Length (ft)
7.7	9 x 35	1664	206	1279	192	385	132
25	15 x 30	2576	246	2107	207	469	152
25	15 x 60	2730	261	2204	235	526	177
50	15 x 60	3480	289	2739	256	741	183
50	22 x 60	4007	299	3267	268	740	192

Performance capability is summarized in Figure 7.1-2. The figure illustrates the payload delivery capabilities for various gross weight systems to an orbit of 270 nautical miles inclined at 55 degrees. The selected system employs sequential firing of the booster and orbiter and is indicated by a large square symbol. Size and performance of the selected system included a 10-percent weight contingency. If the payload requirement is reduced to 25,000 pounds, gross weight can be reduced by approximately 0.75 million pounds. It is noted that if a 10-percent increase is incurred in excess of the 10-percent weight contingency, the gross weight will increase by more than 0.5 million pounds to maintain a 50,000-pound payload delivery capability. The use of a simultaneous booster and orbiter firing at lift-off would significantly degrade payload.

The study has clearly shown that system feasibility is contingent upon limitation of system weights. The baseline vehicle is configured to provide a 50,000-payload delivery capability, allowing 1990 fps ΔV for on-orbit maneuvers. Without contingencies, the maneuvering ΔV allowance could be reduced to 1215 fps and facilitate a reduction of approximately 200,000 pounds in vehicle gross weight. A number of options exist to improve vehicle performance and reduce gross weight. The use of (1) high thrust-to-weight turbojets in the orbiter, (2) hydrogen fuel in the booster turbojets, and (3) booster turbojet during ascent will reduce vehicle gross weight by approximately 0.75 million pounds for the system with 50,000-pound-payload delivery capability. These are discussed in more detail in subsequent sections of this report.

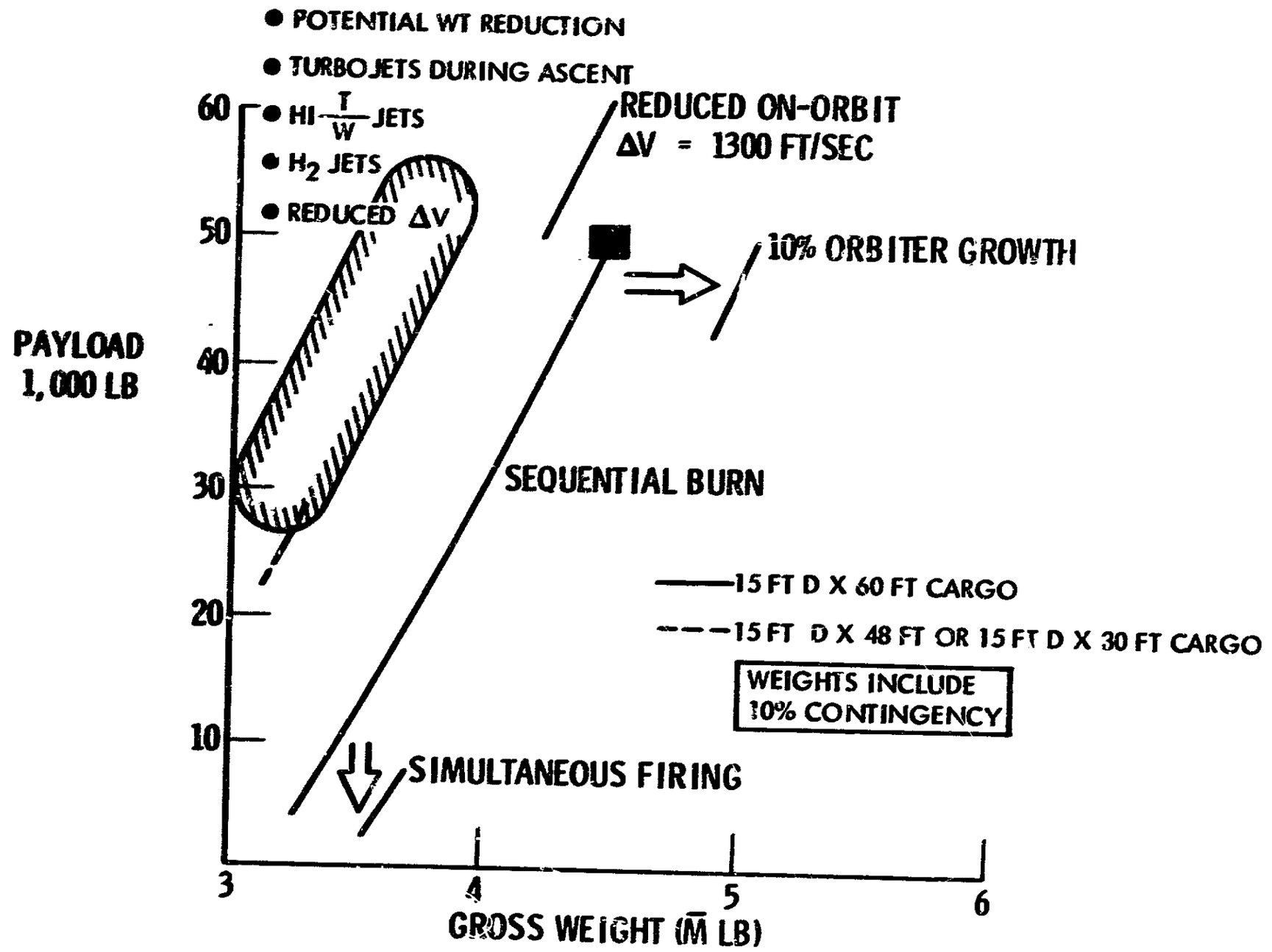

Figure 7.1-2. Performance Summary

7.2 AERODYNAMICS

7.2.1 Summary

The aerodynamic analyses that were performed during Phase II of the contract are described in this section. The objectives of these analyses were to define configuration design requirements and to determine shuttle aerodynamic performance, stability and control, and air loads. Ground rules for the aerodynamic studies were:

1. Vehicles trimmed to a specified high angle of attack during entry and to remain trimmed at this angle of attack until a low subsonic Mach number is attained.

2. Control surfaces are fixed during the high heating portion of entry.

3. Vehicles to be neutrally directionally stable, longitudinally stable, and to have positive effective dihedral during entry.

4. Orbiter vehicle to have go-around capability, and booster to have cruise capability following entry; both vehicles to have ferry capability.

5. Launch combination to be statically stable.

Significant results of the aerodynamic analyses were:

1. The orbiter and booster vehicles are stable and trimmable at the high entry angles of attack at supersonic, transonic, and subsonic speeds.

2. The vehicles are stable and trimmable at subsonic cruise attitude.

3. Sufficient elevator control effectiveness exists to perform the transition from high to low angle of attack at subsonic conditions.

4. Orbiter hypersonic L/D at 60 degrees angle of attack is 0.53 during entry. Subsonic maximum L/D is 7.3.

5. Booster hypersonic L/D at 52.5 degrees angle of attack is 0.69 during entry, and 8.4 maximum during subsonic cruise.

6. Directional stability is essentially neutral during entry, and is stable at reduced Mach numbers.

7. Horizontal tail size can be reduced by body shaping.

8. Moving the wing 1/4 mean aerodynamic chord aft of the center of gravity is effective in reducing horizontal tail size.

9. Nominal orbiter center of gravity during entry is at 58 percent of the body length. A forward travel of 2 feet can be tolerated and still trim at 60 degrees angle of attack. The aft travel limit is 1-1/2 feet set by static margin limits for subsonic cruise.

10. Adequate booster center of gravity control is provided by locating the cruise-back propellant forward in the body, giving an entry center of gravity at 60 percent and a landing center of gravity at 65 percent of the body length.

7.2.2 Configuration Fundamentals

The ILRV configuration functions as a rocket, a reentry spacecraft, and a subsonic airplane. Figure 7.2-1 illustrates some of the fundamental requirements imposed on the configuration as a result of the wide spectrum of altitude and velocity over which it will fly. Features of the general arrangement are shown on the right side of the chart, and fundamentals of the basic configuration are on the left. Because of the forward center-of-gravity location during boost, the tandem launch configuration is statically stable from liftoff and throughout regions of flight when high aerodynamic loads can be developed. This results in low thrust vector deflection angles, low angle of attack, and low aerodynamic loads. Sequential firing was selected on the basis of payload advantage. An investigation of vehicle sizes and performance characteristics for a 3.5-million-pound gross weight system indicated that a payload gain of 9,600 pounds would be obtained over a vehicle using simultaneous booster and orbiter ignition at liftoff. This was a 43 percent improvement.

The high-angle-of-attack entry mode is a concept proven on the Apollo and Gemini programs, and it presents advantages in terms of control and aerodynamic heating. The vehicle is self trimming at a high angle of attack and employs RCS for stabilization and ranging control. In the case of the orbiter, lift is modulated for cross-range control by coordinated roll about the velocity vector in a manner similar to Apollo. The booster entry is flown in a similar manner; however, some pitch modulation may be desirable to minimize loads during descent from staging. The peak heating rate experienced during entry is dependent upon the lift-loading parameter W/C_LS. Minimizing W/C_LS implies entry at maximum lift coefficient. This allows deceleration to occur at high altitude, resulting in reduced maximum heating rate and temperatures experienced during entry. Entry at an angle of attack greater than that corresponding to maximum lift coefficient results in a slight penalty in peak heating rate while reducing the flight time and total heat load into the vehicle. This permits minimizing weight of the thermal protection system. Maximum lift coefficient occurs at approximately 52-1/2 degree angle of attack for the orbiter configuration. Entry is at 60 degrees, resulting in about 4 percent saving in insulation weight at an insignificant change in peak heat rate and temperature.

Transition to low angle of attack occurs at about 0.4 Mach and is accomplished by deflecting the elevator. Subsonically, the orbiter and booster configurations have two stable trim points: one at the high entry angle of attack, the other at a low angle of attack allowing flight at maximum L/D. The elevator is sized to pitch the vehicle down to the subsonic cruise attitude near 5-degree angle of attack. During subsonic flight, about

90 percent of the lift comes from the wing, while during entry the wing contributes only about 22 percent of the lift. Consequently, selection of wing planform is dominated by subsonic cruise and landing considerations. The high-aspect-ratio, low-sweep wing is a low-weight design and permits low landing velocities. The booster touches down at 113 knots, the orbiter at 128.

Fundamentals of the basic configuration are shown on the left side of Figure 7.2-1. Configuration geometry is heavily influenced by stability and heating considerations. A low lift loading is required so that heating environment during entry will be low. Low lift loading implies high lift at hypersonic speeds. The majority of the hypersonic lift comes from the body. The flat bottom of the fuselage promotes high lift, and negative camber on the bottom aids in pitch trim and stability at high angle of attack. The flat bottom and sharp corners also promote separation around the sides of the body, resulting in low temperatures on the sides and upper surfaces.

Roll stability is provided by wing dihedral. Directional stability is essentially neutral at the high angle of attack during entry. The center vertical fin is in a separated area and is ineffective. Stability is provided by sloping the fuselage sides. Forward of the center of gravity, the sides are sloped inward so that at high angle of attack in hypersonic flow they will be essentially hidden from the airstream and contribute very little directional destabilizing moment. Aft of the center of gravity, the fuselage sides are vertical and contribute a small amount of directional stability. The complete fuselage, therefore, provides essentially neutral stability at high angle of attack hypersonically. At subsonic conditions, sloping the sides in this manner may result in the entire fuselage contributing to the vehicle directional stability at high angles of attack, as indicated by results obtained by Polhamas (Reference 7.2-1) shown in Figure 7.2-2.

Wing location was selected to minimize effects of the wing on the pitch characteristics of the configuration. If the location were such that the wing normal force acted forward of the center of gravity, it would be necessary to increase the size of the horizontal required to pitch down from the high entry angle of attack to the subsonic cruise attitude. Locating the wing further aft would reduce the size of the horizontal needed for pitch-down and subsequent stability during cruise. However, more of the horizontal would have to be deflected out of the airstream to trim hypersonically. The total wing mean aerodynamic chord (MAC) is therefore located slightly aft but near the center of gravity.

The high-aspect-ratio wing promotes efficient subsonic cruise. The low sweep provides low touchdown velocity and low weight; however, it may also create the mechanism for transonic wing flutter (wing aerodynamic

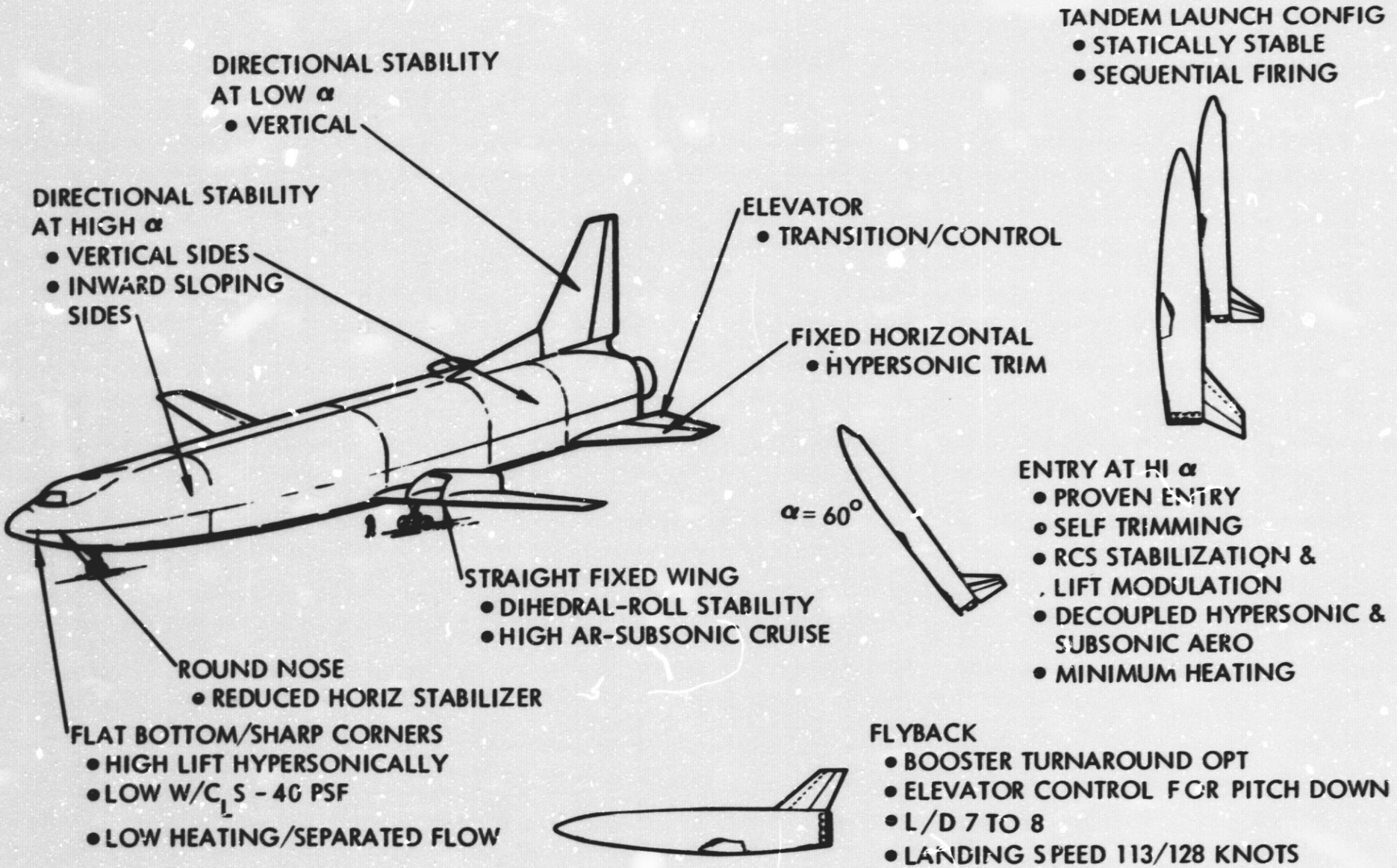

Figure 7.2-1 Configuration Fundamentals

NOTE: DATA OBTAINED FROM NASA TR R-29, "EFFECT OF FLOW INCIDENCE AND REYNOLDS NO. ON LOW SPEED AERODYNAMIC CHARACTERISTICS OF SEVERAL NONCIRCULAR CYLINDERS WITH APPLICATIONS TO DIRECTIONAL STABILITY AND SPINNING" BY E. POLHAMUS, 1959.

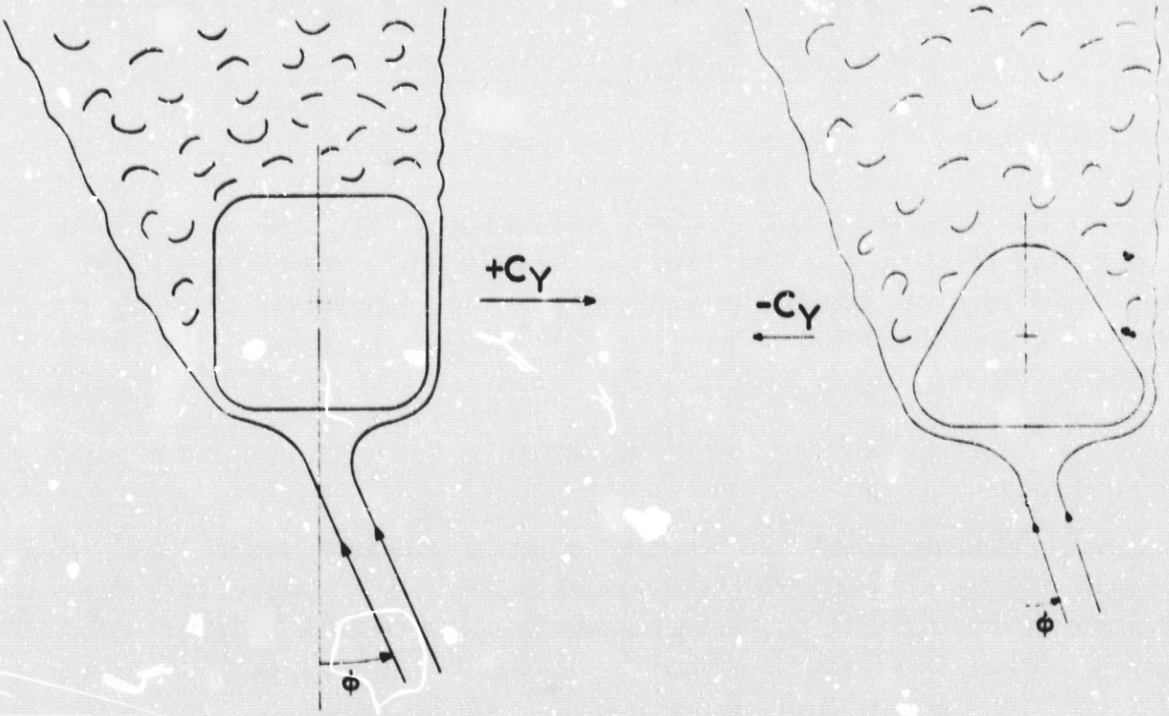

A. SUBCRITICAL REYNOLDS NUMBER

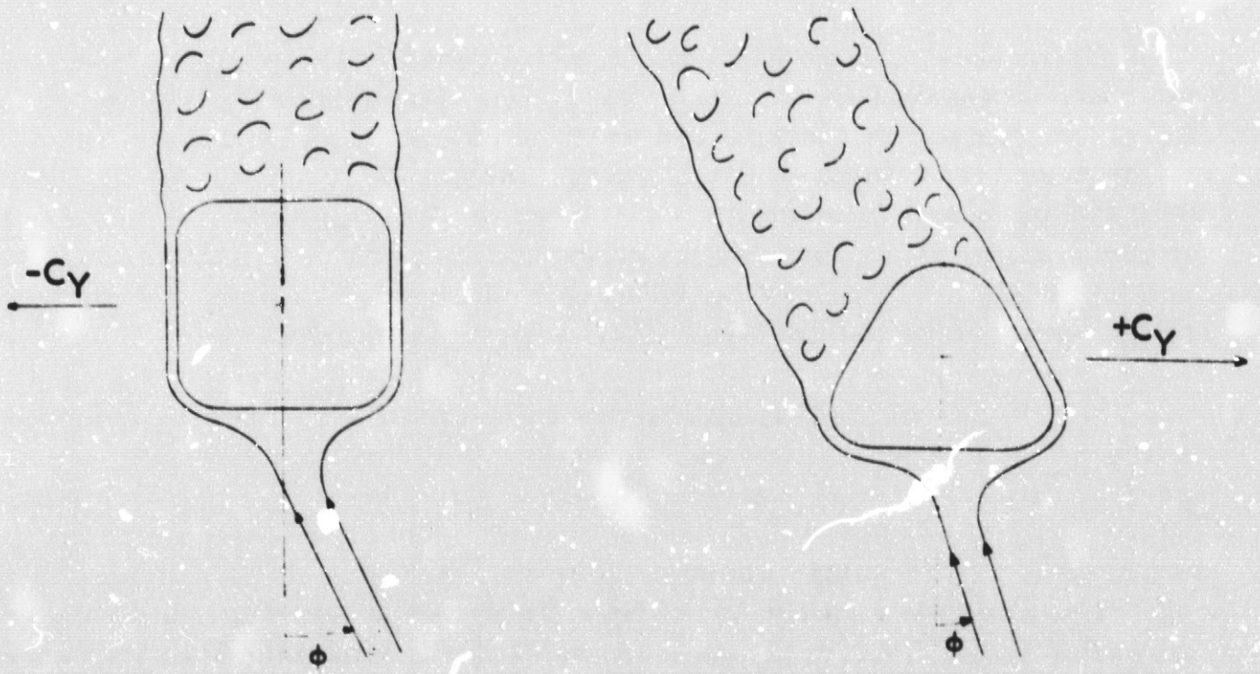

B. SUPERCRITICAL REYNOLDS NUMBER

Figure 7.2-2. Effect of Reynolds Number on Fuselage Side Force

center forward of the wing center of gravity) during boost and a decreased drag divergence Mach number which may be deleterious to cruise range. Tradeoff studies in these parameters are described in Section 7.2.5.

7.2.3 Base-Line Vehicle (12,500-Pound Payload)

The 12,500-pound-payload class vehicle is illustrated in Figure 7.2-3. Aerodynamic performance characteristics and air loads were determined for the orbiter, booster, and composite configuration. Air load data are presented in Section 8.0 of this report. Inviscid, longitudinal, and lateral-directional hypersonic characteristics were estimated by utilizing an NR-developed Newtonian flow program. The program includes the effects of Newtonian shadowing of one vehicle component by another and applies a pressure coefficient of 70 percent vacuum ($C_p = \frac{-1}{M_\infty^2}$) on leeward surfaces. The program evaluates and sums forces and moments for the individual flats, leading edges, and complex body shapes. Good agreement has been found between the results of this program, other analytical hypersonic estimating techniques (shock expansion theory), and experimental data when applied in past studies of hypersonic configurations.

Composite Configuration

Estimates of zero-lift drag for the composite configuration during boost are presented in Figure 7.2-4. The data shown represent drag characteristics with the booster vehicle rocket engines burning (no aspiration) and orbiter stage engines not burning. Major drag items subsonically were the base and friction drags. At supersonic speeds the wave drag of the blunt nose, thick low sweep wings and empennage, and interference drag were high. There is considerable uncertainty in the interference drag; estimates were based on Titan III-C experimental data.

Estimates of the lift characteristics for the composite configuration during boost are presented in Figure 7.2-5. For subsonic and supersonic speeds, data from the Datcom (USAF), Reference 7.2-1, and NACA Report 1307 (Reference 7.2-3) were used. The NR Newtonian flow program was used for hypersonic speeds. The interference due to influence of the orbiter wing vortex on the local flow field on the booster wing was estimated to be less than 7 percent. At transonic conditions the data show an abrupt drop in lift curve slope caused by the wing thickness ratio. This effect is desirable in terms of decreasing the load in the transonic range.

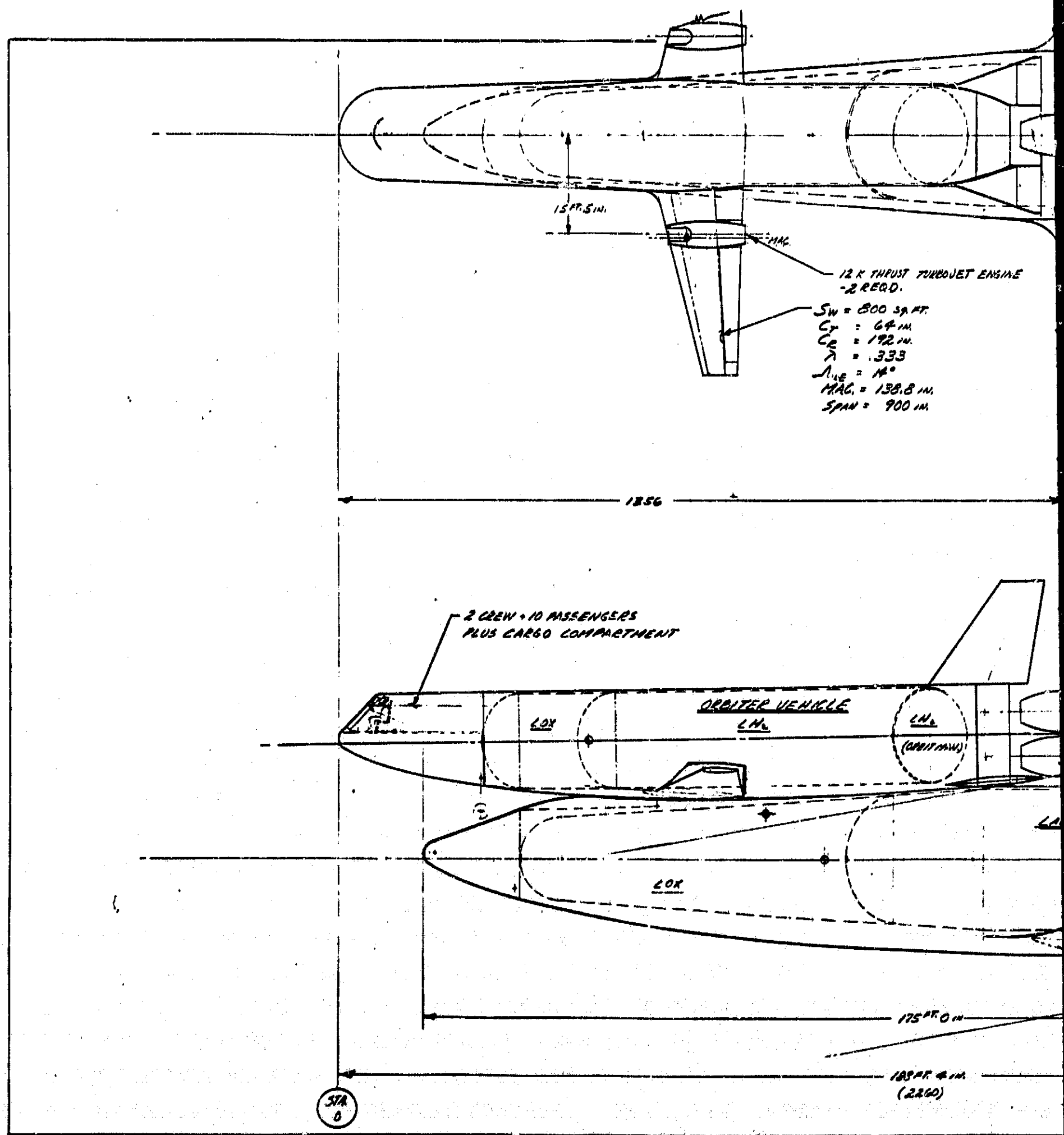

FOLDOUT FRAME 1

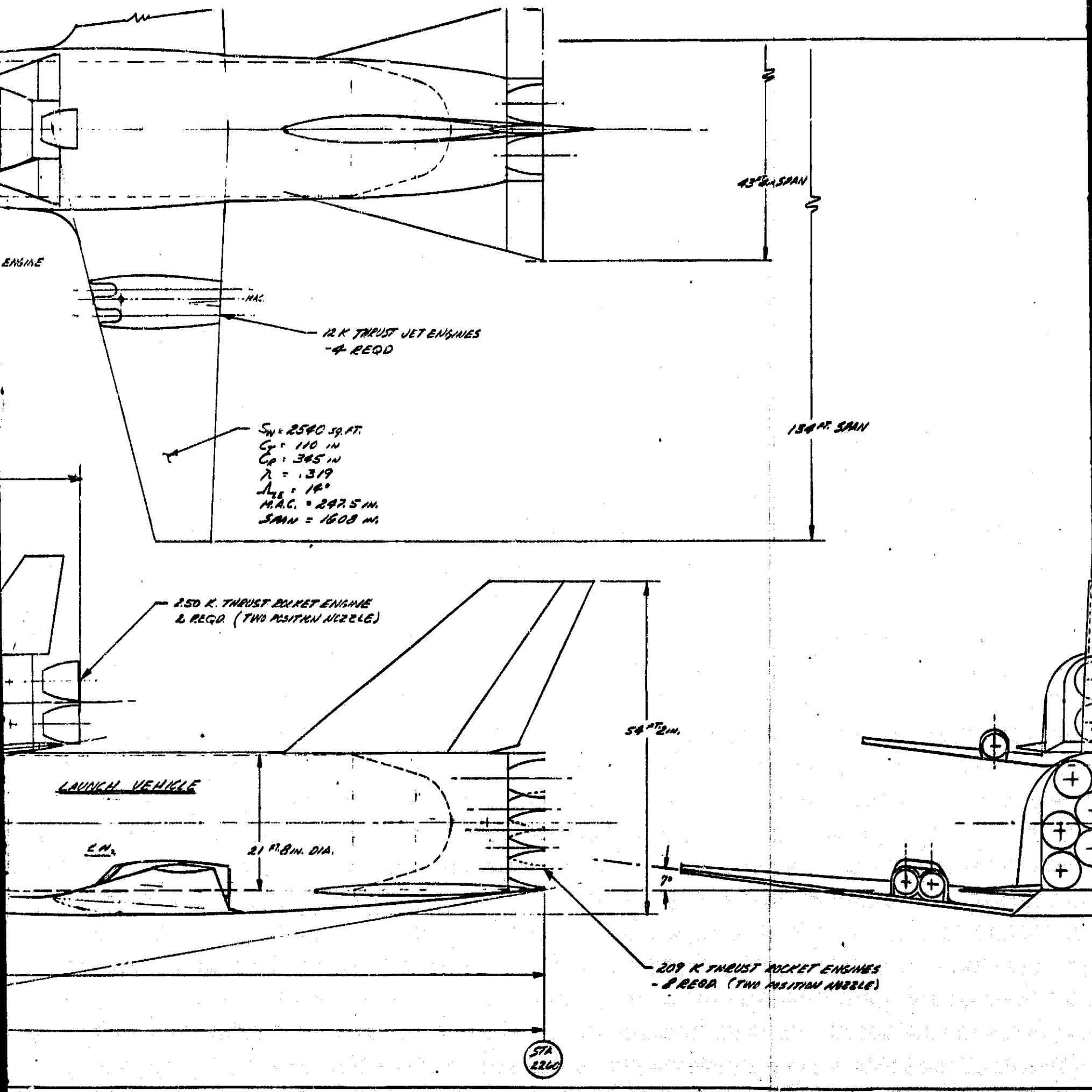

Figure 7.2-3. Baseline Config

FOLDOUT FRAME 2

Space Division
North American Rockwell

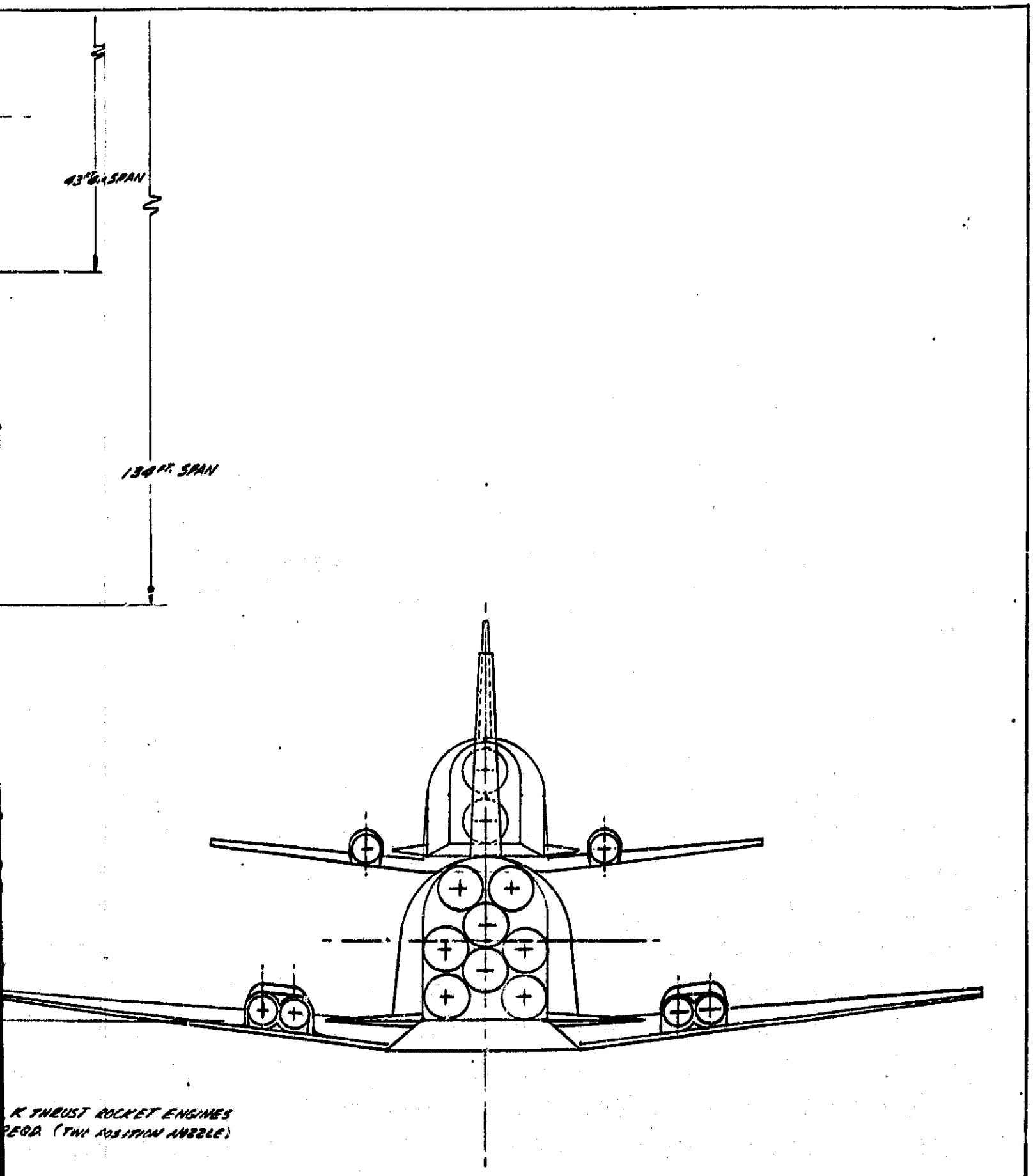

Figure 7.2-3. Baseline Configuration of 12,500-Pound-Payload Class

FOLDOUT FRAME 3

7-15, 7-16

SD 69-573-3

The drag of the composite configuration is shown in Figure 7.2-6. The expression used to evaluate drag due to lift at subsonic speeds was

$$\Delta C_{DL} = C_L^2/(.8\pi\, AR_W)$$

and at supersonic speeds

$$\Delta C_{DL} = (C_L)_W \tan \alpha_W$$

The results from the NR Newtonian flow program were used at the hypersonic Mach numbers. These drag data were used for the boost trajectory analysis.

Pitching moment data, C_{m_α} and $(C_m)_{\alpha FRL} = O$, are presented in Figure 7.2-7 for the composite configuration. The same methods were used for these data as were used for the lift curves. The data show the composite configuration to be stable throughout the Mach number regime, with neutral stability at the hypersonic Mach numbers.

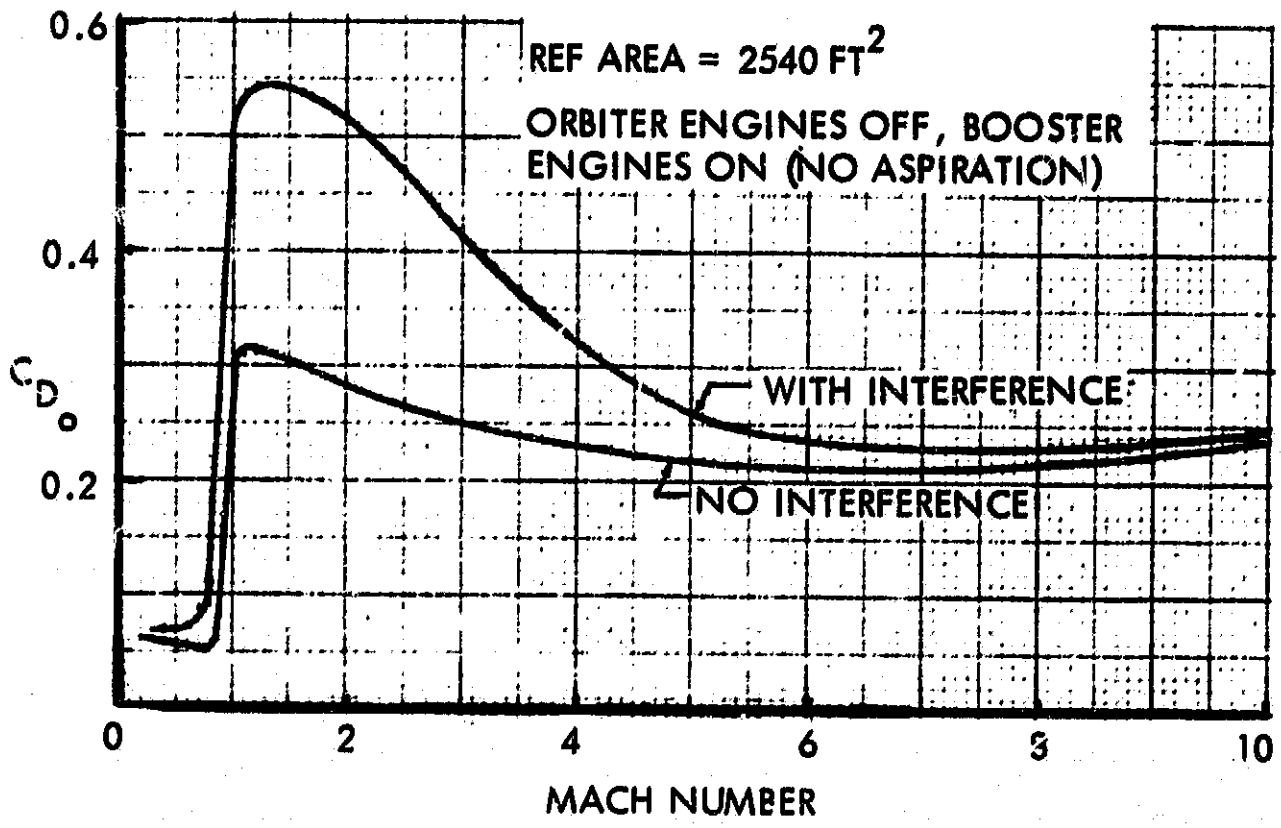

Figure 7.2-4. Zero Lift Drag During Boost

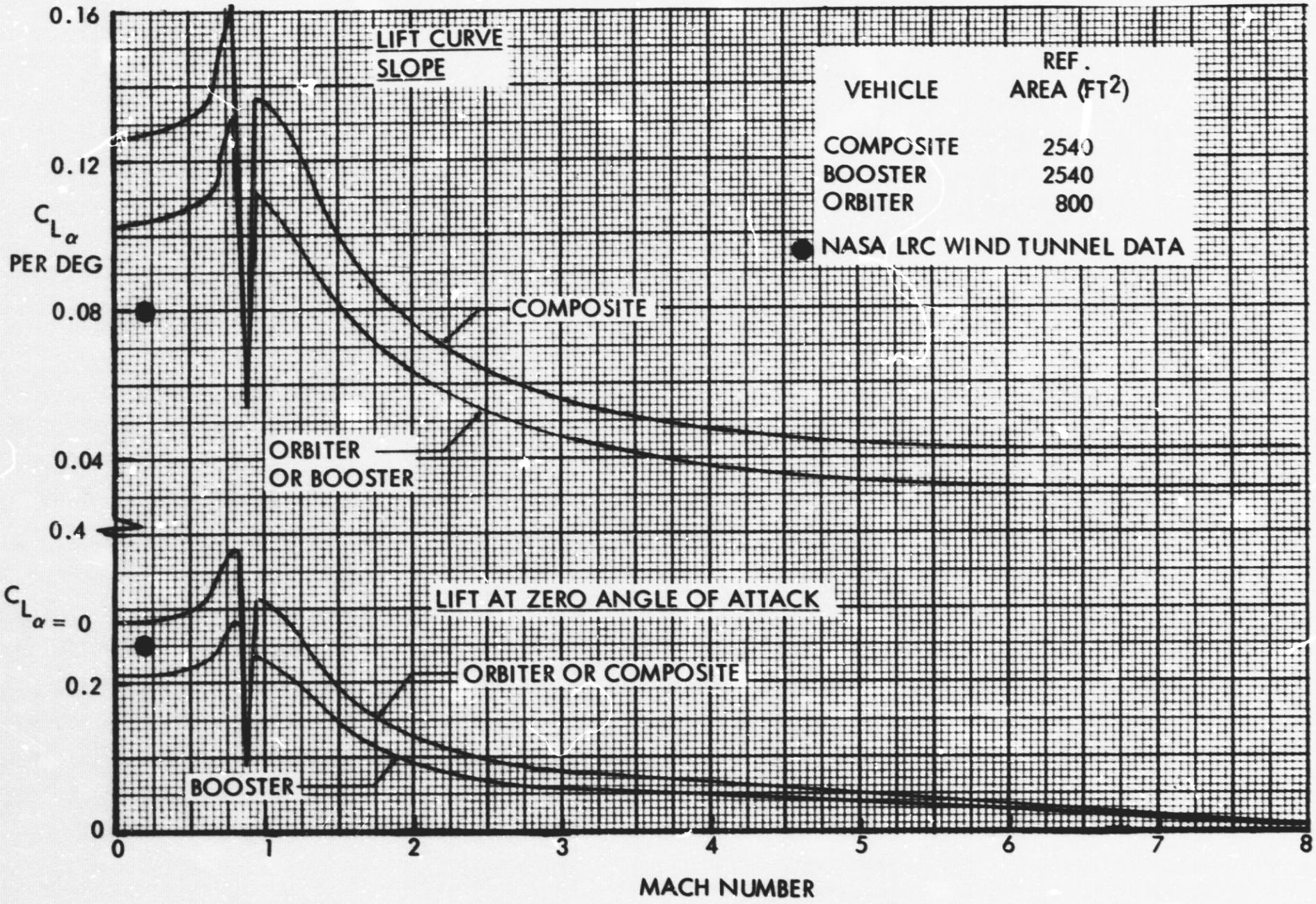

Figure 7.2-5. Lift Characteristics, 12,500-Pound Payload Class

Space Division
North American Rockwell

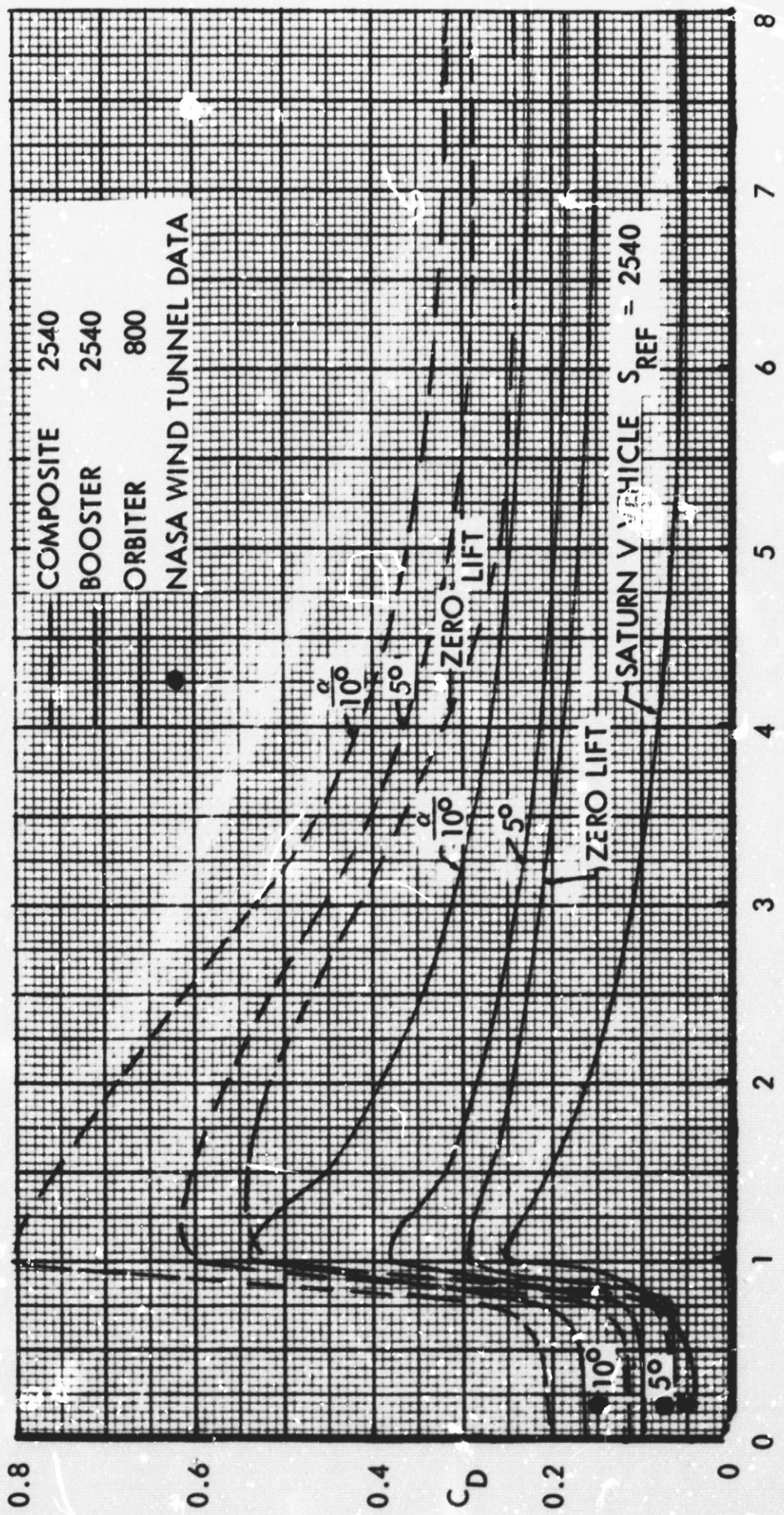

Figure 7.2-6. Drag Characteristics, 12,500-Pound Payload Class

Figure 7.2-7. Pitching Moment Characteristics for Composite Configuration, 12,500-Pound Payload Class

Booster Configuration

The baseline booster longitudinal data evaluated with the Newtonian flow hypersonic program are presented in Figures 7.2-8 and 7.2-9. Preliminary weight and balance estimates indicated that the booster center of gravity at burnout would be located at body station 1290, 59 percent of the body length. Exposed area of the horizontal surface on the baseline configuration (Figure 7.2-3) was 581 square feet. Estimates of the trim characteristics indicated that for the center-of-gravity location at station 1290, a horizontal surface of 581 square feet was not adequate to provide trim at 60-degree angle of attack. The exposed area required was estimated to be 1010 square feet for hypersonic trim.

Investigation of the horizontal surface requirement for subsonic trim indicated that a further increase in surface size would be required. The tail size required to trim subsonically at the high trim angle of attack was reevaluated based on the available NASA-Langley wind tunnel test data (Reference 7.2-5) on the baseline orbiter. The data were evaluated in parametric form (see Section 7.2-3) and the resultant booster tail sized for sufficient moment to compensate the wing body pitching moment with zero deflection on the elevator, was found to be 1400 ft^2. The 1400-ft^2 tail can provide trim hypersonically by using negative deflections on the elevator. Because of the large tails required for the booster and the orbiter baseline configurations, further parametric analysis was performed to decrease the tail size.

Orbiter Configuration

The baseline orbiter aerodynamic characteristics were estimated for hypersonic and subsonic Mach numbers. The subsonic characteristics were evaluated from the NASA-Langley wind tunnel data (Reference 7.2-5), and hypersonic characteristics from the NR Newtonian program. A comparison of the subsonic and hypersonic orbiter trim characteristics are presented in Figure 7.2-10. Analysis of the data indicated that an increased tail size was required for subsonic trim at 60-degree angle of attack and to provide sufficient control authority to pitch down to cruise at 5.5-degree angle of attack where maximum lift-to-drag ratio is obtained. The tunnel data indicated that the critical parameter which determined the size of the horizontal surface was the large wing plus body pitching moment existing at 55-degree angle of attack. To provide sufficient control authority for pitch-down, the horizontal surface was sized to obtain static longitudinal stability at 55-degree angle of attack for two cases: zero elevator deflection, and 30-degree down deflection of 50 percent of the horizontal surface. The horizontal surface sized for zero deflection was estimated to be 471 square feet, and the pitching moment characteristics which result are shown in

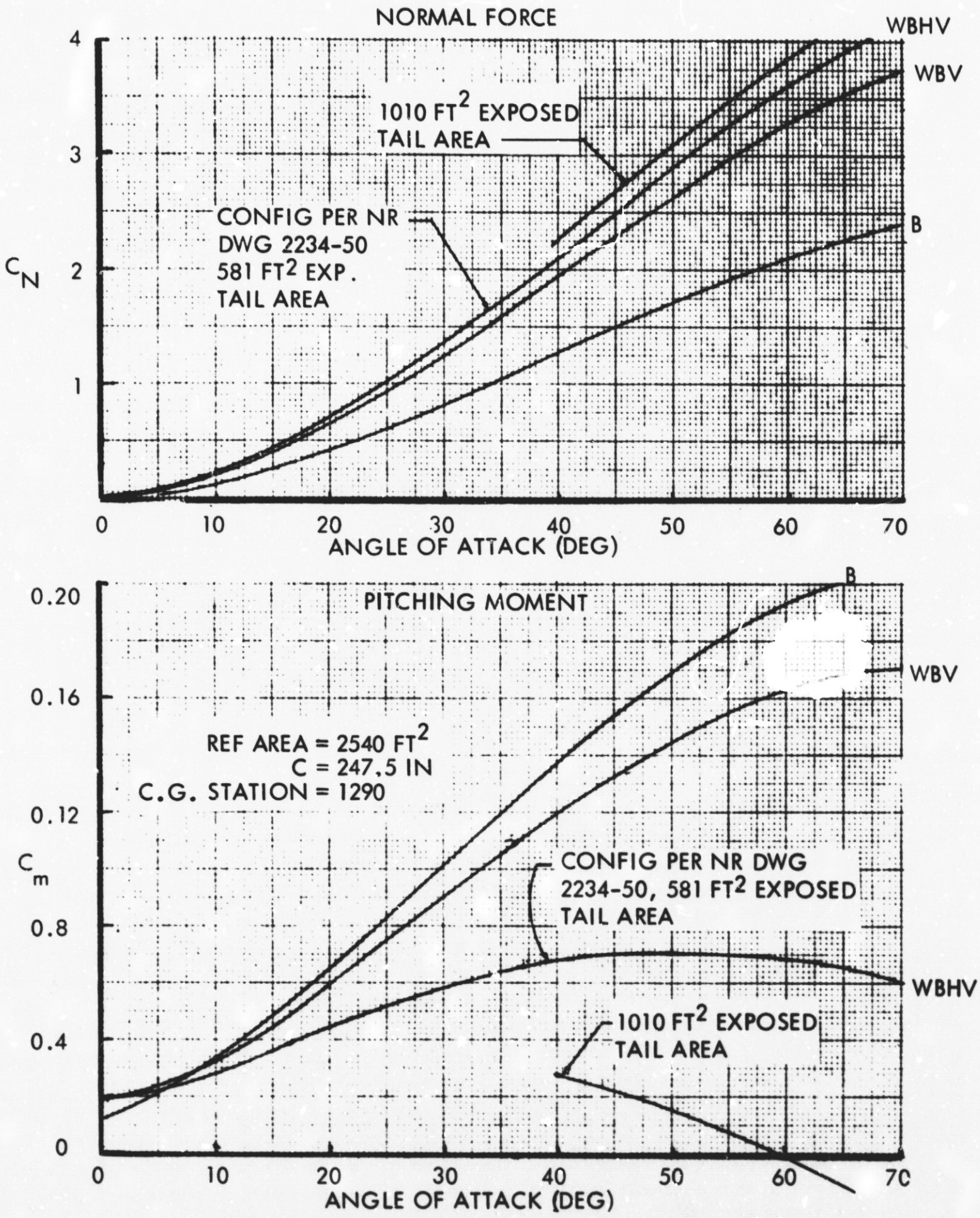

Figure 7.2-8. Normal Force and Pitching Moment Characteristics, Booster for 12,500-Pound Payload

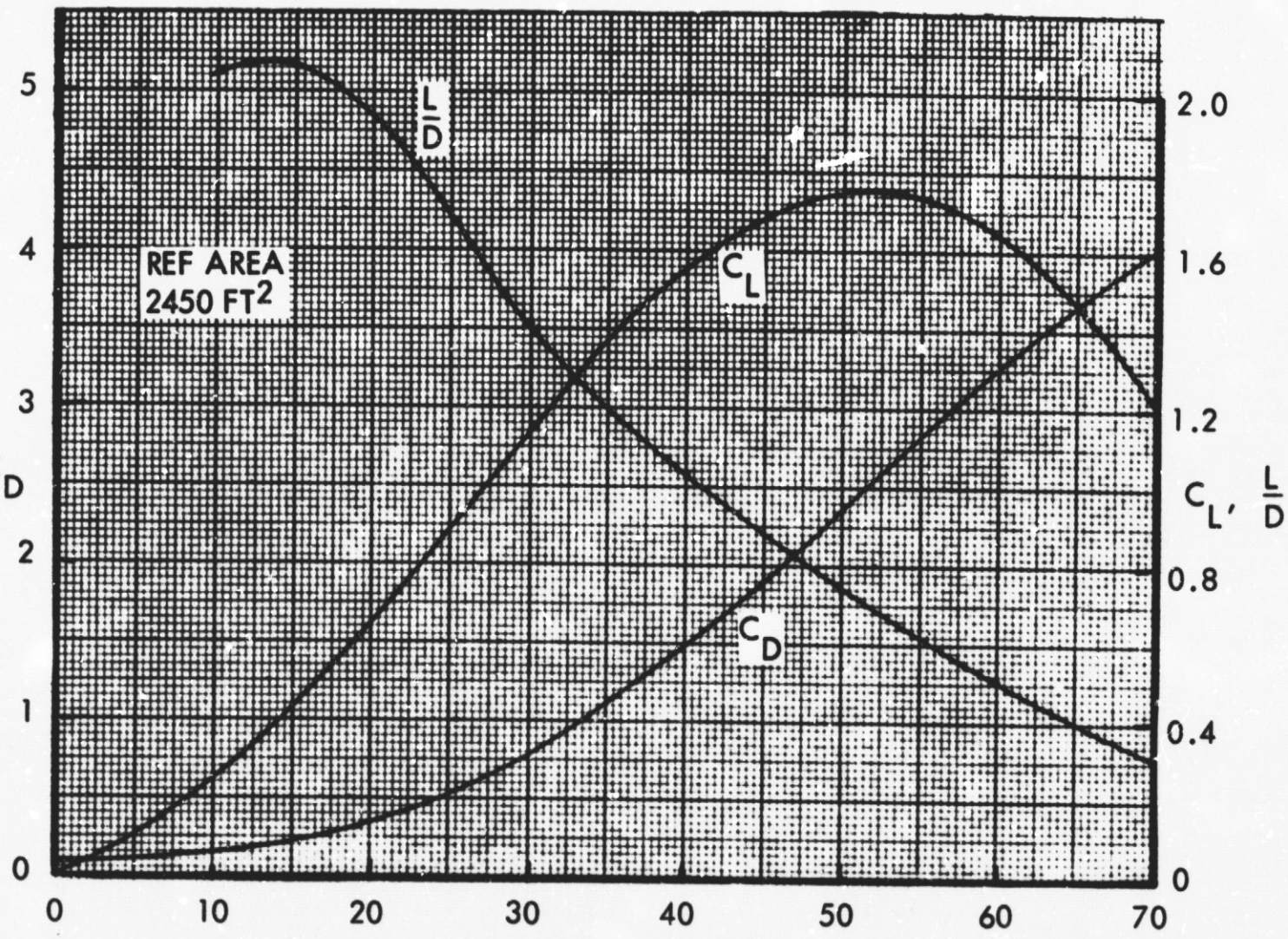

Figure 7.2-9. Lift and Drag Characteristics, Booster for 12,500-Pound Payload

Figure 7.2-10 for the center-of-gravity located at body station 650 (51.5 percent of the body length). Resizing for case 2 would allow the surface area to be reduced to 413 square feet. Subsequent studies of horizontal surface designs for the 50,000-pound payload class vehicles used the 30-degree deflection ground rule.

A higher fineness ratio nose shape was also tested in the Langley tunnel, and the results indicated a decrease in maximum wing body pitching moment. The resultant tail size was then estimated to be 398 square feet at zero elevator deflection or 349 square feet for a 50 percent elevator deflected 30 degrees. The elevator deflection ground rule implies that the aft-most center-of-gravity has been chosen, and if the center-of-gravity were further aft, difficulty would arise in pitching the orbiter down.

Hypersonic trim characteristics for the orbiter with 471 square feet exposed tail area are shown on the right-hand side of Figure 7.2-10. The data indicate that: (1) during ascent the orbiter is longitudinally stable, (2) the large horizontal tail, which was sized on the basis of subsonic stability, results in excess hypersonic stability and the vehicle will trim at 30-degree angle of attack. Two possible solutions to the excess stability are:

1. Fold the horizontal tail about a hinge line parallel to the X fuselage axis through a dihedral angle of 60 degrees. This could also aid directional stability because the vertical tail is completely shadowed at 60-degree angle of attack and does not contribute to directional stability. The orbiter now trims at 60-degree angle of attack.

2. Expose only 64.6 square feet of the horizontal tail and rotate the movable portion of 406.4 square feet 60 degrees, trailing edge up. The orbiter now trims at 60 degrees angle of attack.

The latter concept was selected because it represents the system of lightest weight.

Final aerodynamic characteristics for the 12,500-pound payload class orbiter are shown in Figure 7.2-11 for entry, transition to cruise, and landing flight conditions. Lateral directional stability derivatives are presented in Figure 7.2-12. The vehicle exhibits a stable dihedral effect, C_{ℓ_β}, for the complete angle of attack range. The directional derivative, C_{n_β}, is stable for the orbiter during ascent and is slightly unstable at the high angle of attack attitude during entry. This is not a problem, however. Six-degree-of-freedom entry simulations (see Section 7.5.4) demonstrated that the orbiter lateral/directional characteristics were stable during entry, and stability remained excellent for an unstable directional derivative an order of magnitude greater than the value shown on the figure for 60-degree

Figure 7.2-10. Orbiter Trim Characteristics

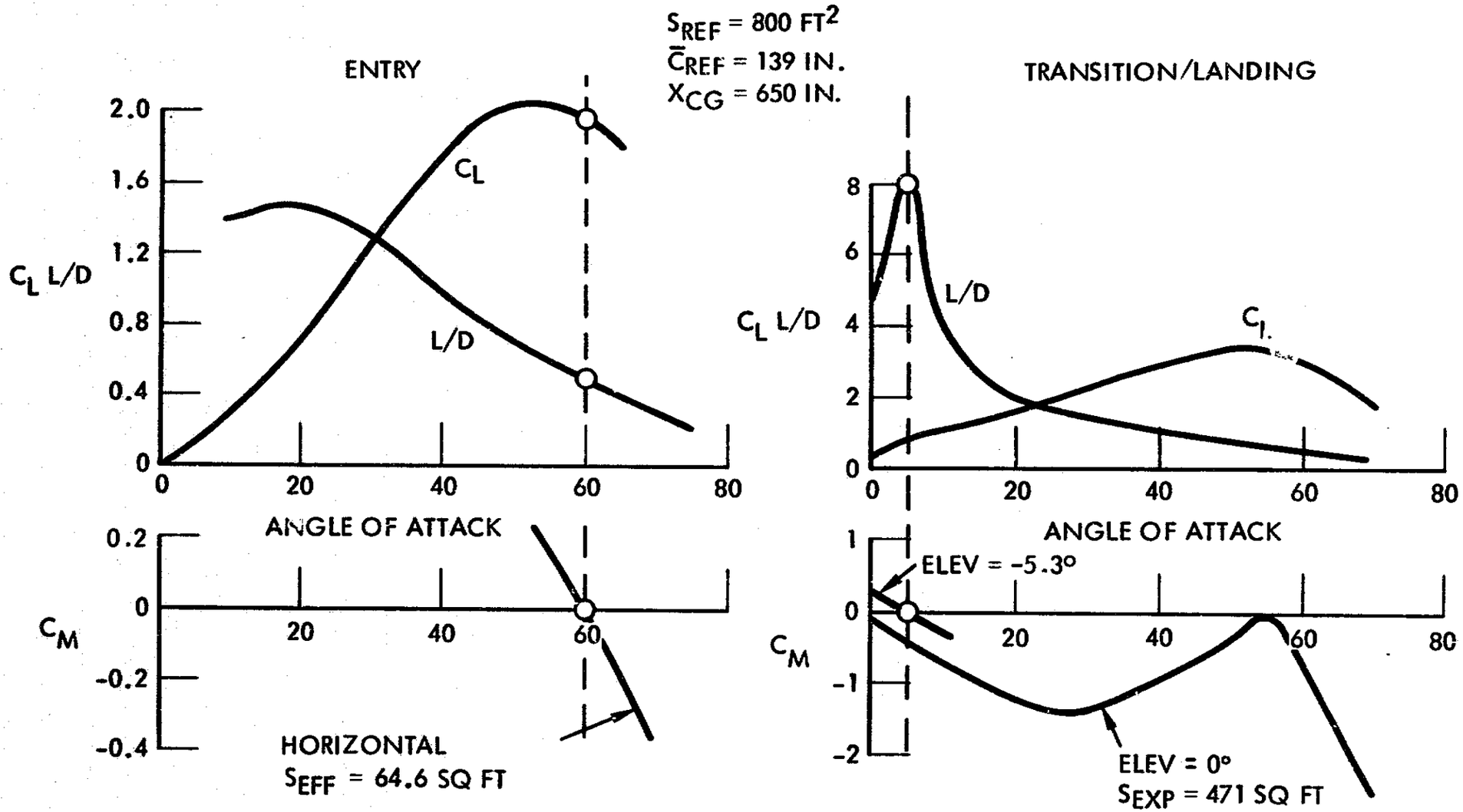

- STATICALLY STABLE AT HIGH & LOW α
- TRIMMABLE AT HIGH & LOW α
- SUBSONIC L/D = 8

Figure 7.2-11. Orbiter Aerodynamics

REF NR DWG 2234-50
$X_{C.G.}$ = 650 IN
$Z_{C.G.}$ = -19.9 IN
b REF = 900 IN
S REF = 800 FT^2

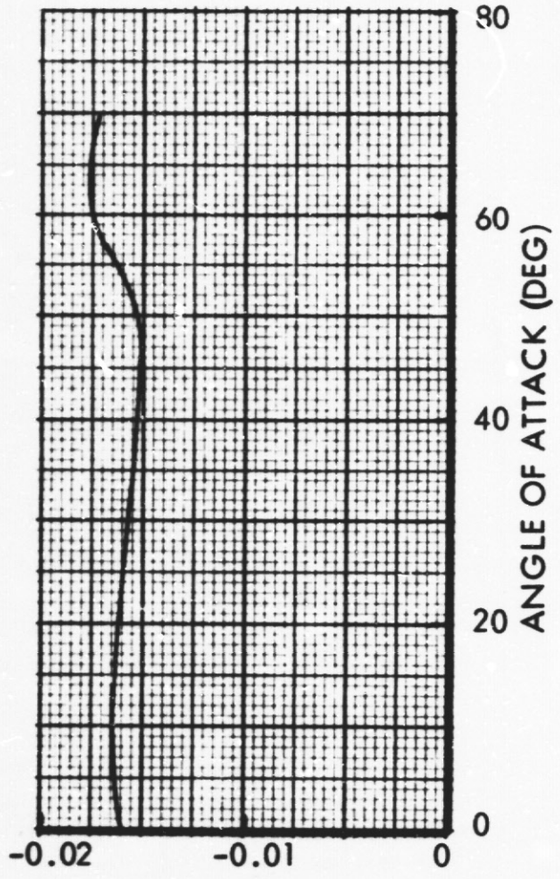

C_{Y_β}
(PER DEG)

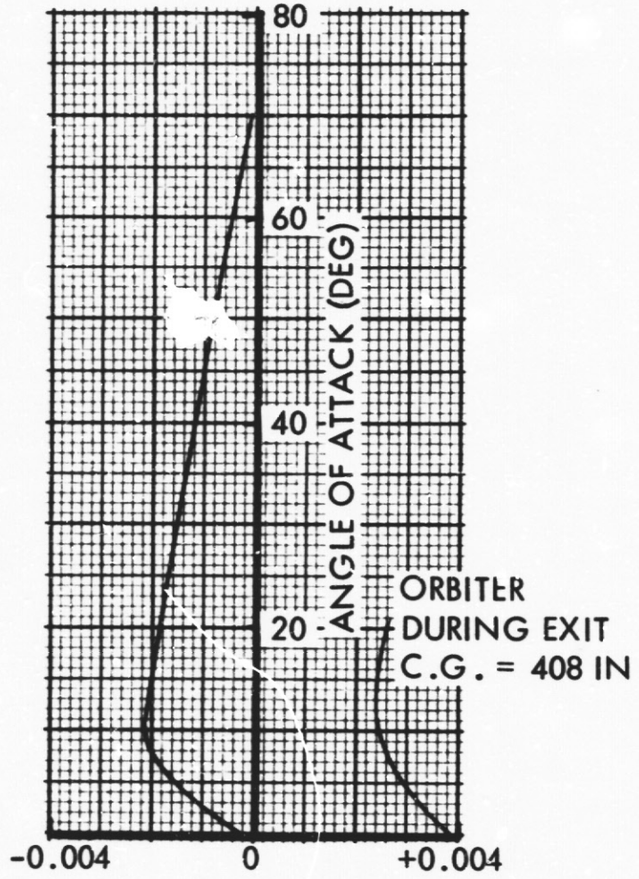

C_{n_β}
(PER DEG)

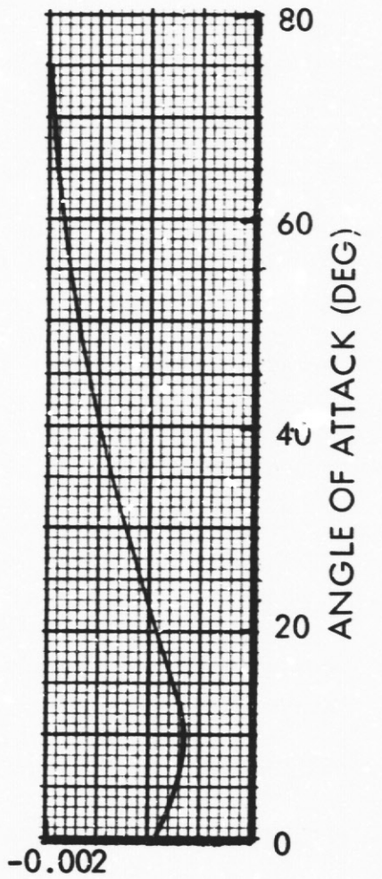

C_{ℓ_β}
(PER DEG)

Figure 7.2-12. Orbiter Hypersonic Lateral - Directional Characteristics, 12,500-Pound Payload Class

Space Division
North American Rockwell

angle of attack. Design changes which could provide static directional stability are (1) body shaping aft of the center of gravity, or (2) dihedral on the horizontal tail.

7.2.4 Design Improvements and Sensitivity Analysis

This section describes design improvements which were investigated to establish the design features which should be incorporated in the shuttle vehicle.

External Payload

Estimates of the variation in drag of a cargo pod mounted external to the orbiter are presented in Figure 7.2-13. The pod was configured with a hemispherical forward end since it was found that the weight increase associated with an aerodynamic fairing caused a greater performance degradation than the increased drag incurred by the hemispherical end. At the high angles of attack from entry to transition to cruise, the pod is shielded from the flow and will have small influence on aerodynamic characteristics.

Horizontal Tail Size Requirements and Body Shaping

The wind tunnel data obtained for the 12,500-pound-payload baseline orbiter showed that the horizontal tail should be sized to cancel the wing body instability existing at the high angle of attack during transition to subsonic cruise. These data showed that the body was the major contributor to the instability. Since body normal force is related to body planform area,

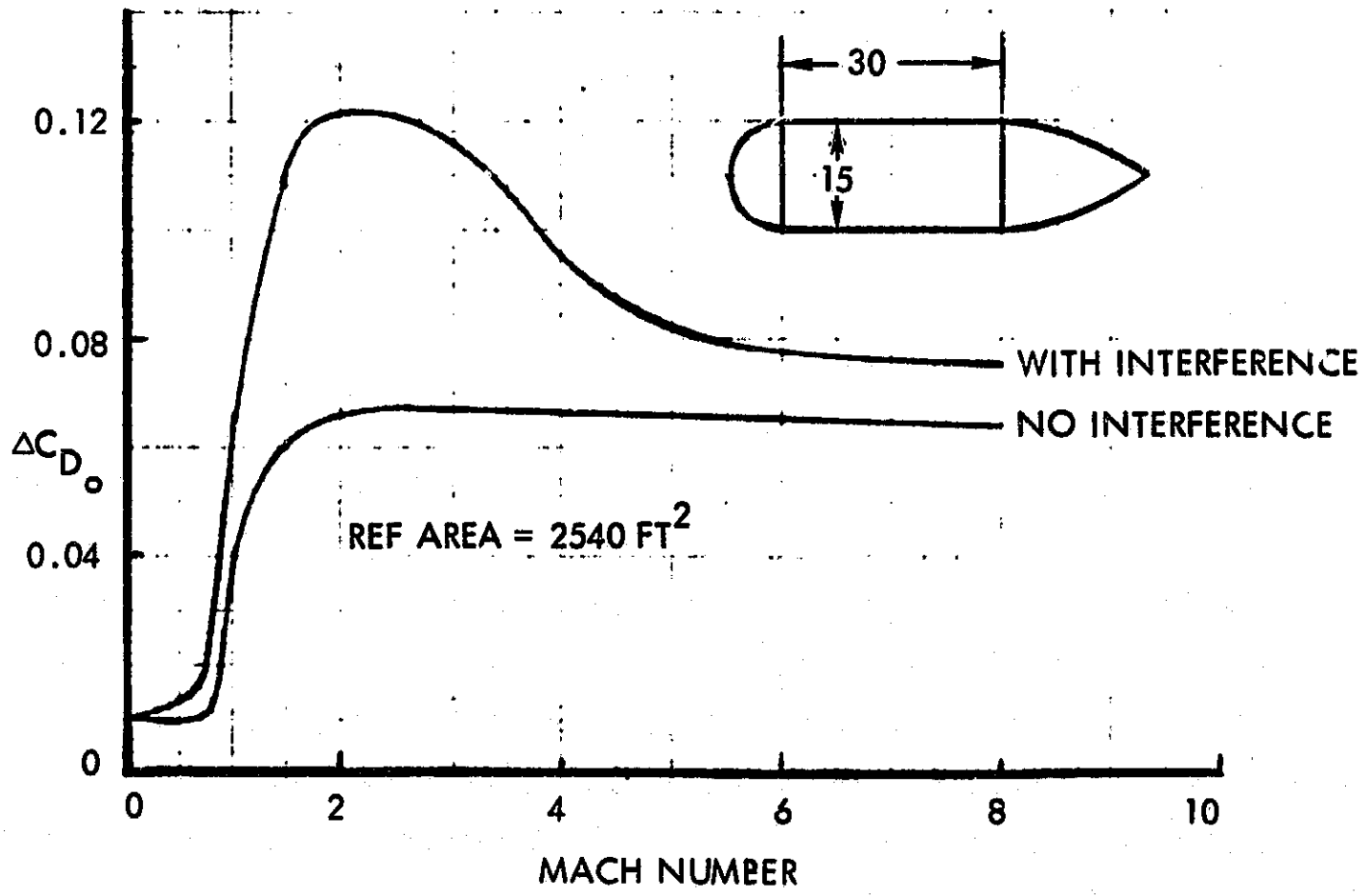

Figure 7.2-13. Drag of External Payload

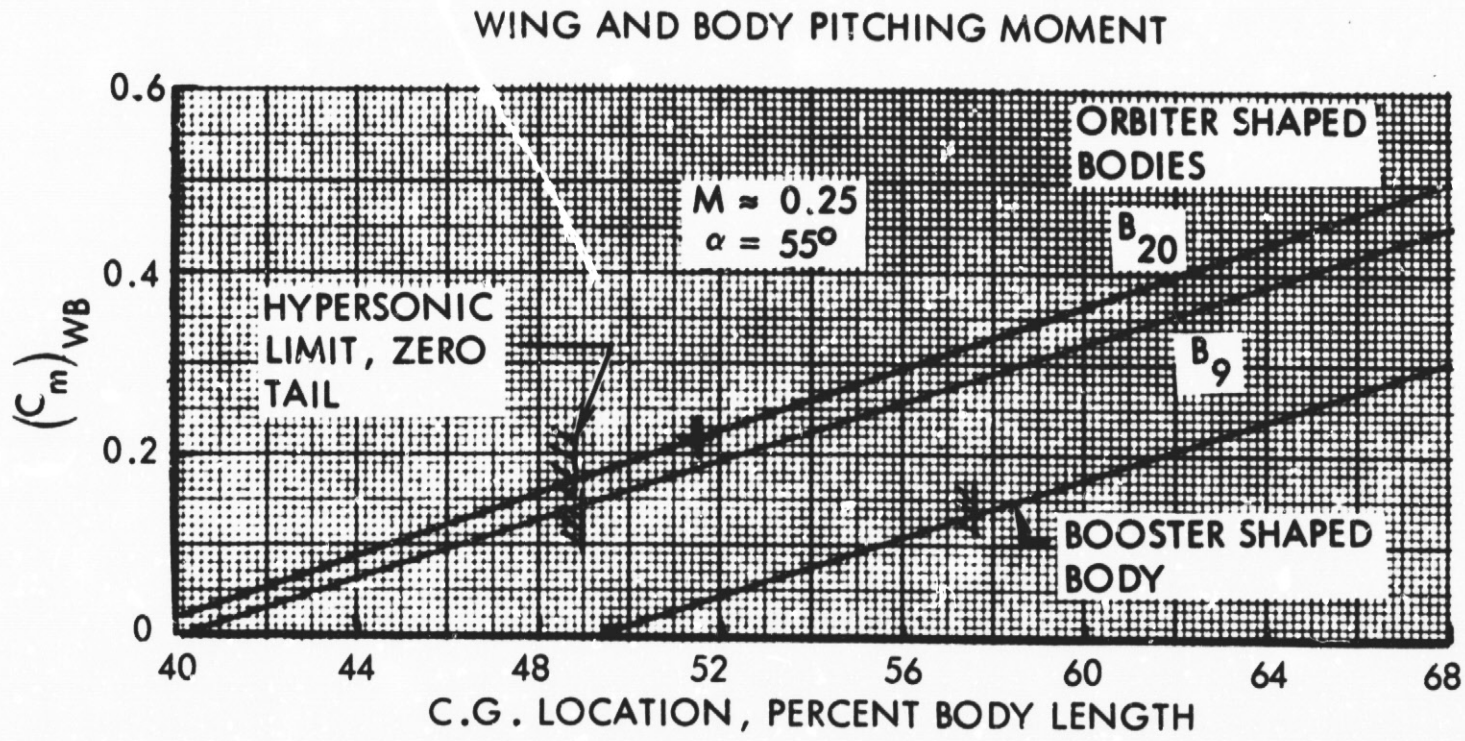

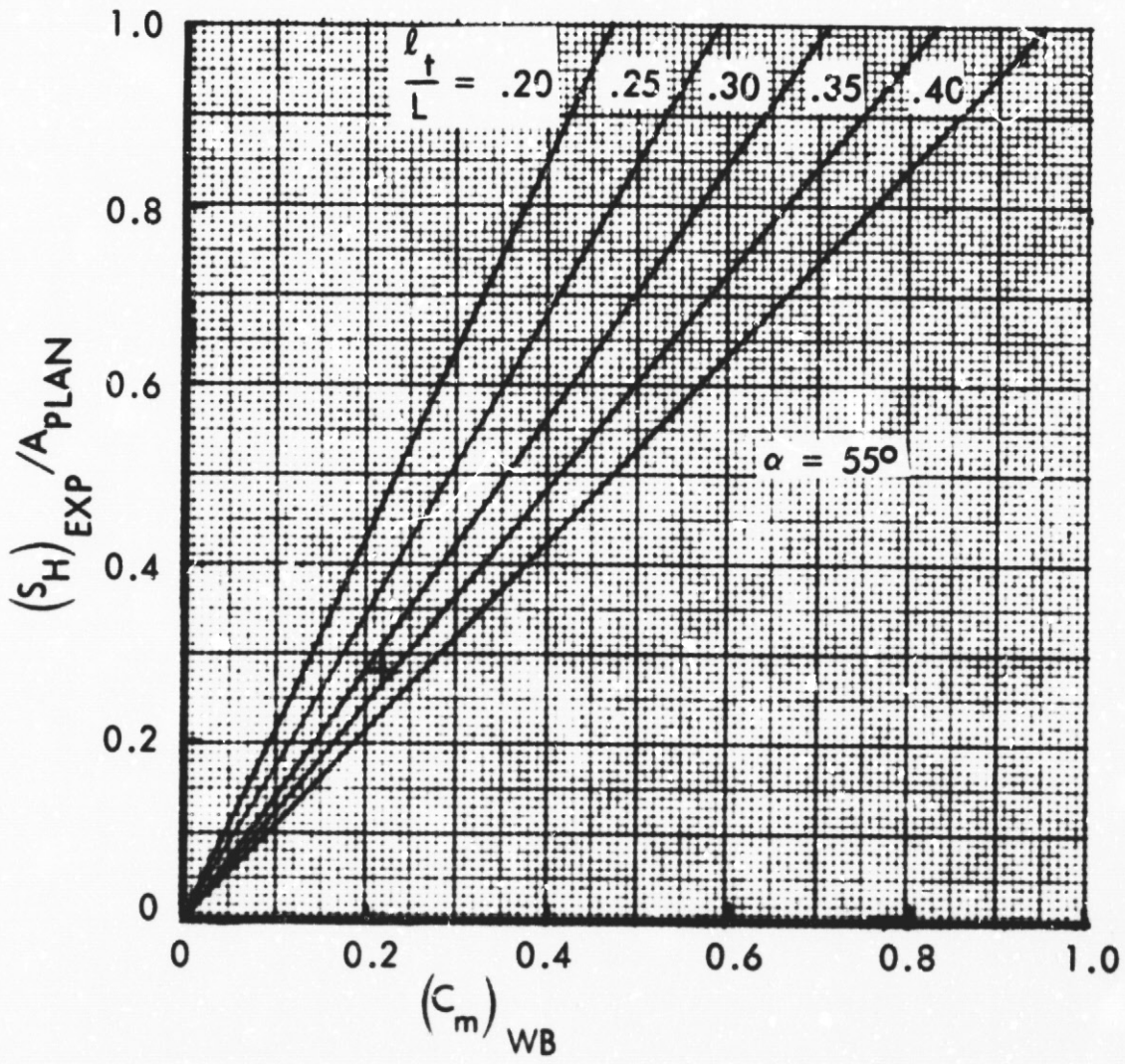

NOTES:

(1) L = BODY LENGTH
(2) A_{PLAN} = BODY PLANFORM AREA
(3) ℓ_t = 77% OF TAIL LENGTH TO EXPOSED PANEL
(4) + = 12.5 K CLASS ORBITER BASED ON LRC W.T. DATA
(5) $(C_m)_{WB} = M/qA_{PLAN}L$

Figure 7.2-14. Tail Size for Subsonic Trim

and center of pressure is related to planform centroid, a functional relation between wing body pitching moment, based on planform area, and center of pressure, may be developed. Once the wing body pitching moment has been determined, the tail size is estimated from the relation:

$$C_{m_{WB}} = \Delta C_p \frac{\ell_t \, (S_T)_{EXP}}{L \, (S)_{PLAN}}$$

where ΔC_p = 2.35 (from Langley data) at 55 degrees angle-of-attack

ℓ_t = tail length

L = body length

Tail size, as a function of plan area, was calculated for a wide range of center of gravity locations and tail lengths and presented in the form of design chart in Figure 7.2-14. The chart assumes the wing 1/4 mean aerodynamic chord station is located at the same station as the vehicle center of gravity. The tail size predicted by the design chart is 471 square feet (0.285 of the plan area) for the 12,500-pound-payload baseline orbiter.

When the tail size design chart was used to predict a tail size for a scaled orbiter with a 50,000-pound payload, the chart yielded a tail size of 1215 square feet for a center of gravity location of 50 percent of the body length. This tail was 46 percent of the total wing area. This unusually large tail size precipitated an investigation into the potential advantage of rounding the body to reduce the tail size.

Determination of the effects of corner radius on the body pitching moment was based on an estimation of crossflow drag coefficient. Previous work by Polhamus (Reference 7.2-1) indicated that the subcritical (i.e., laminar) crossflow drag coefficient and the Reynolds number at which the flow becomes supercritical are both strong functions of corner radius. The question arose as to whether one should use subcritical or supercritical crossflow characteristics. Use of subcritical crossflow drag coefficients would result in predicting a large horizontal surface size.

It was decided to base the estimates on subcritical crossflow drag. This was done because:

1. Wind tunnel data obtained during the Ames 6-by-6-foot tunnel tests of the NR 0.02 scale orbiter (Reference 7.2-6) indicated that the largest positive elevator deflection to trim at 60 degrees angle of attack occurs between Mach 0.5 and 0.6. This is illustrated in Figure 7.2-15.

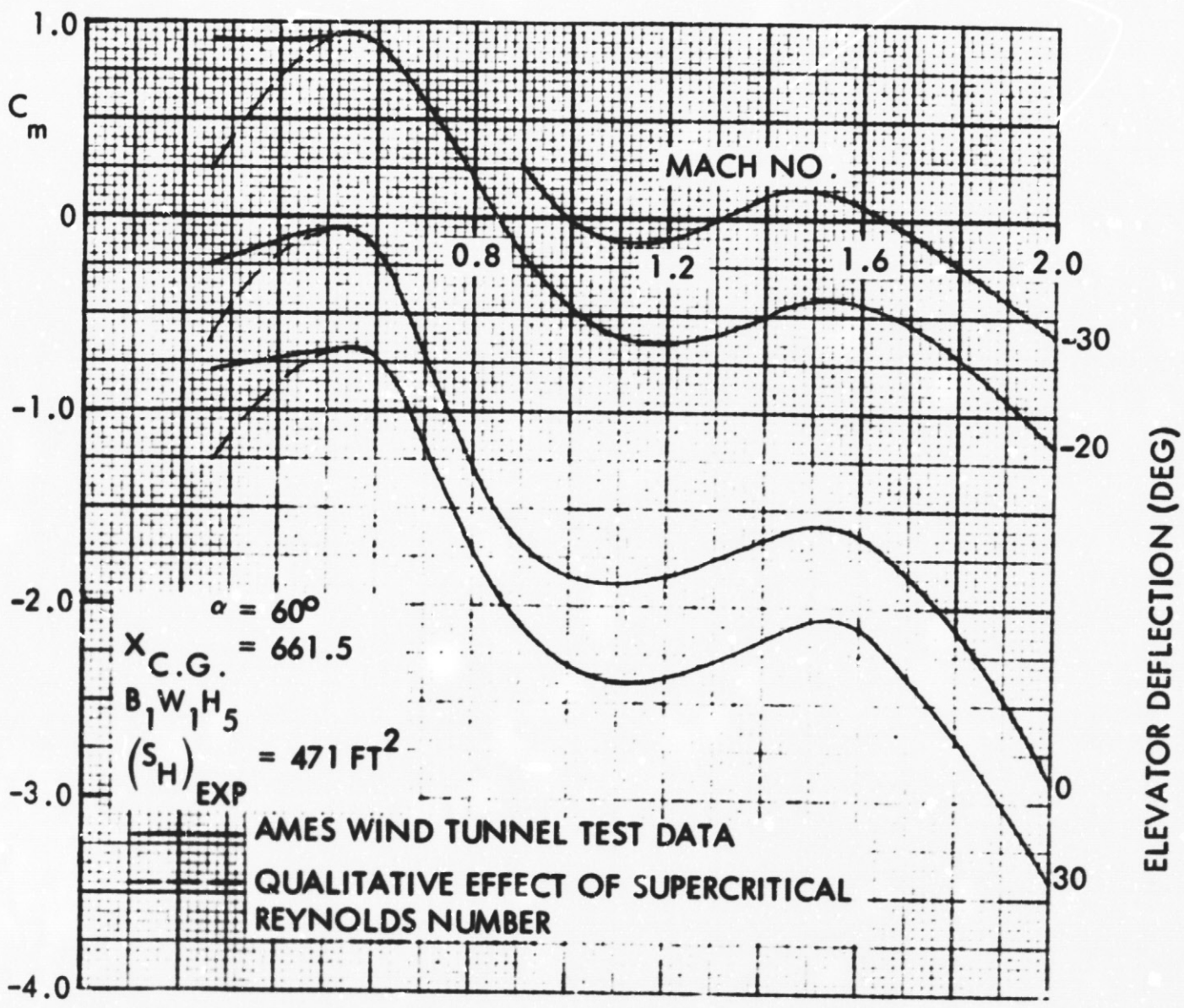

Figure 7.2-15. Effect of Mach Number on Pitching Moment Characteristics

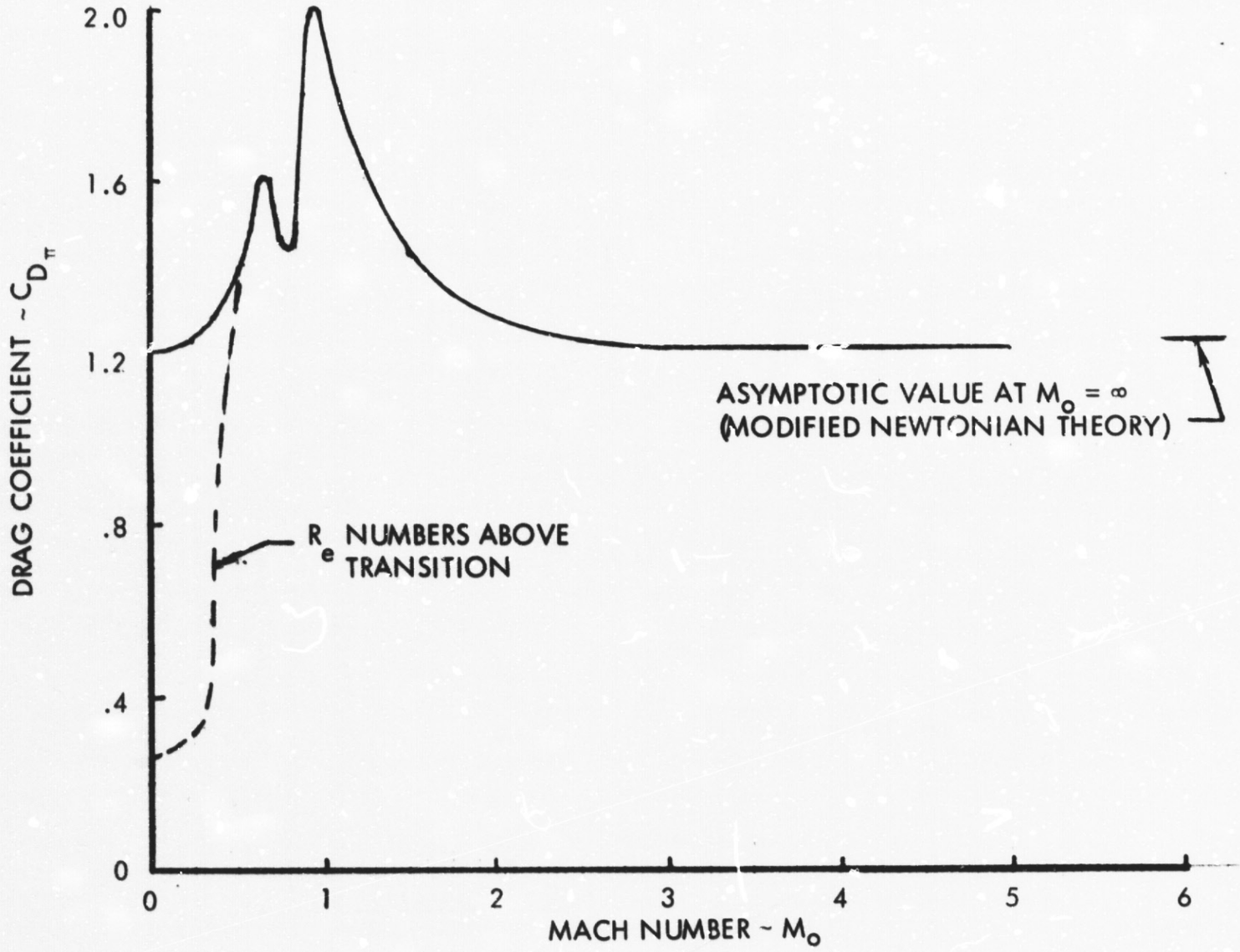

Figure 7.2-16. Drag of Infinite Circular Cylinder

Space Division
North American Rockwell

2. At speeds greater than the critical Mach number (approximately 0.5 for a cylinder, see Figure 7.2-16), the value of the crossflow drag coefficient for either subcritical or supercritical Reynolds numbers is the same and has a value slightly greater than the subcritical value at low Mach numbers.

Presented in Figure 7.2-17 is the correlation of crossflow drag coefficient for several cross-sectional shapes as a function of corner radius. The data reveals that crossflow drag for a rectangular shaped cross section becomes minimum for a corner radius of 33.3 percent of the width. Crossflow drag as a function of corner radius evaluated from the Langley tunnel test is also presented. The results from this correlation can then be applied to obtain more parametric data on wing body pitching moment as shown in Figure 7.2-18. The center of pressure is presented as a function of body centroid, and C_m wing-body as a function of center of gravity, center of pressure and corner radius. It is probable that a body can be found which will yield a tail size required for transition no larger than a tail size required for satisfactory static margin for cruise flyback and landing and still yield acceptable hypersonic performance. As a check on minimum tail size required, estimated $(S_T)_{EXP}/S_{ref}$ is presented in Figure 7.2-19 for a family of tail lengths as a function of (C_{m_α}) wing body which can be obtained experimentally or theoretically.

A 50,000 pound payload orbiter configuration was developed incorporating a body corner radius of 33.3 percent of the width, and compared to a configuration with sharp body corners, i.e., less than 2 percent of the body width. The sharp cornered orbiter is illustrated in Figure 7.2-20. Figure 7.2-21 shows the configuration with rounded corners. The effect of corner radius was twofold. First, the body subsonic crossflow normal load and thereby the horizontal tail size were substantially reduced as previously discussed. Second, the hypersonic W/C_LS and directional stability at high angle of attack were somewhat degraded. The directional stability was reduced. These effects on horizontal tail size with and without body corner radius are compared in Figure 7.2-22. For zero corner radius, the exposed horizontal tail size was 2520 square feet for the center of gravity located at 58 percent of the body length (Station 1368) using the parametric charts of Figure 7.2-14. The tail was sized for neutral stability at 55-degree angle of attack with zero elevator deflection. Incorporating a body corner radius of 33.3 percent of the body width allowed the tail size to be reduced to 1450 square feet. Sizing the surface for 30 degrees elevator deflection further reduced the tail size to 1170 square feet. Additional tail size reduction could be accomplished by utilizing a nose ogive with a higher fineness ratio shaped body, but this was not evaluated.

The orbiter hypersonic characteristics for the configurations shown in Figures 7.2-20 and 7.2-21 were evaluated by the Newtonian flow program.

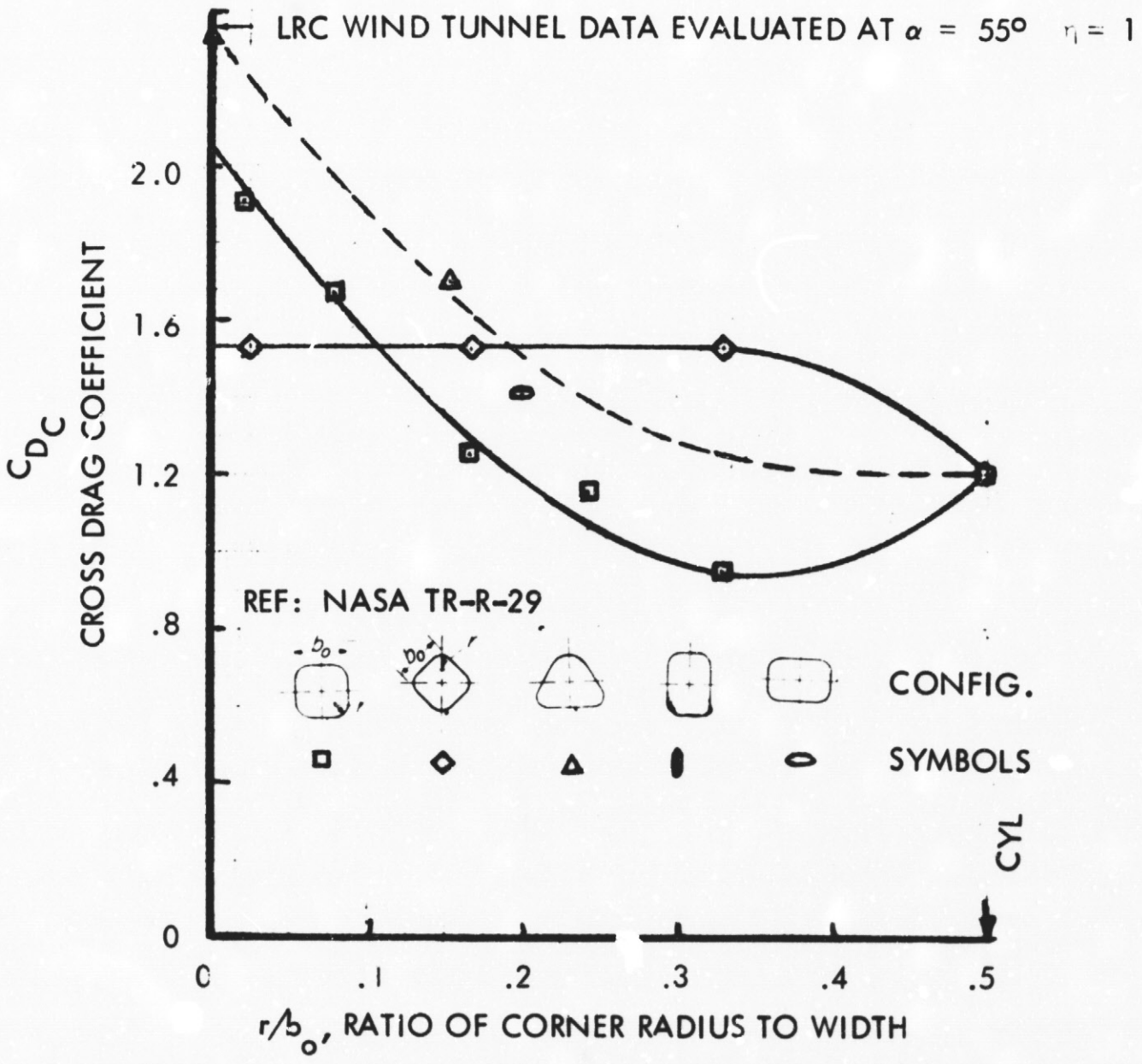

Figure 7.2-17. Effect of Corner Radius on Subsonic Cross Flow Drag Coefficient

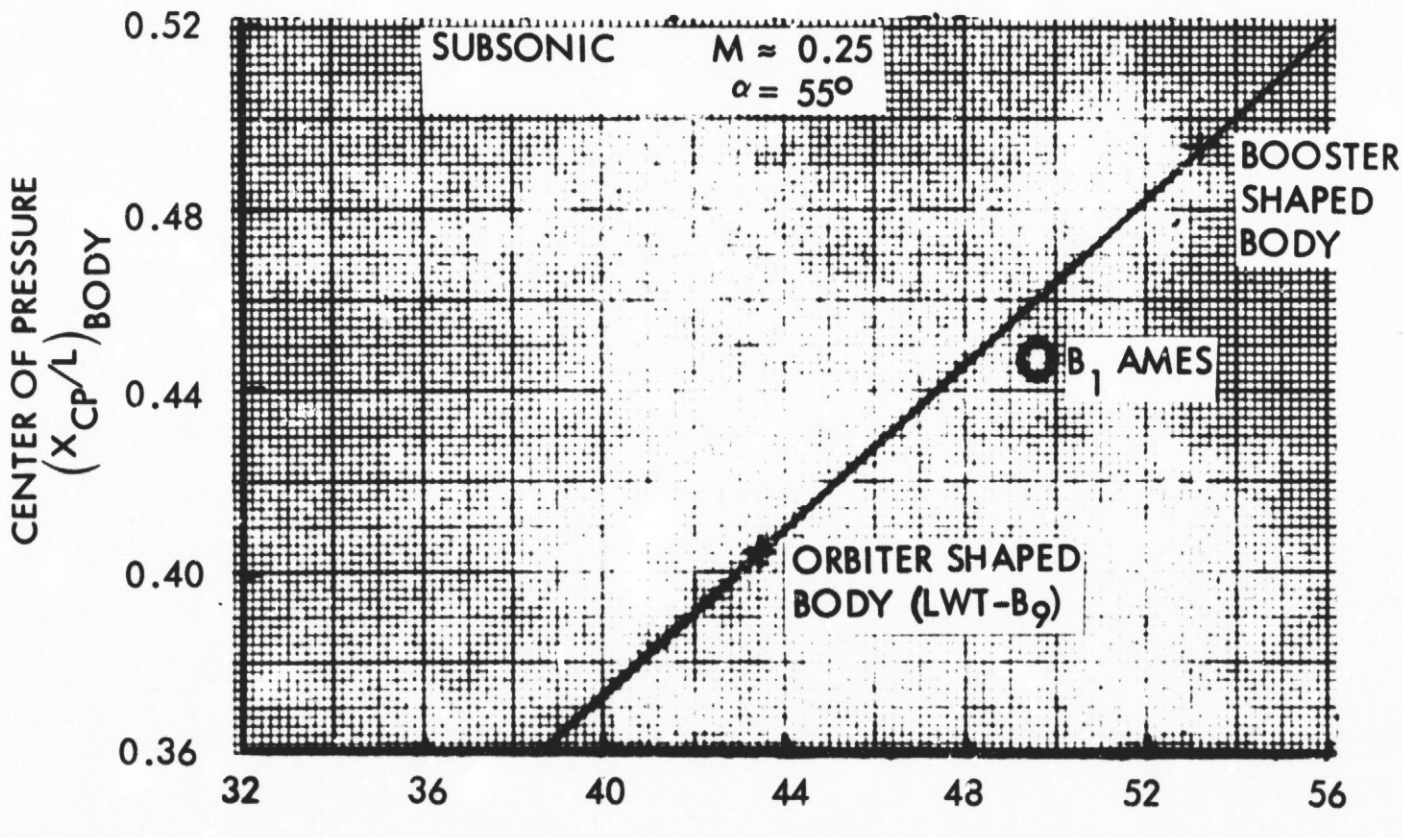

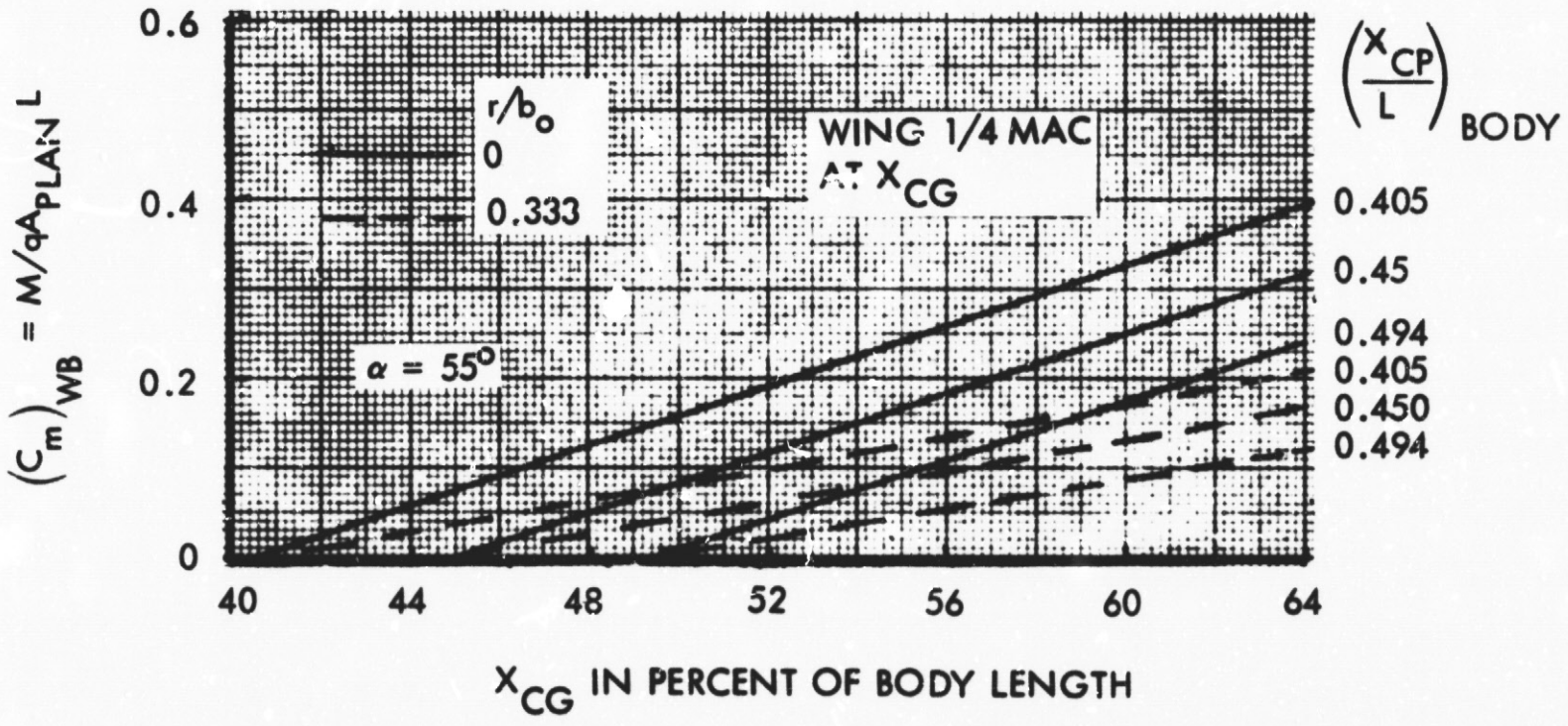

Figure 7.2-18. Effect of Corner Radius on Wing Body Pitching Moment

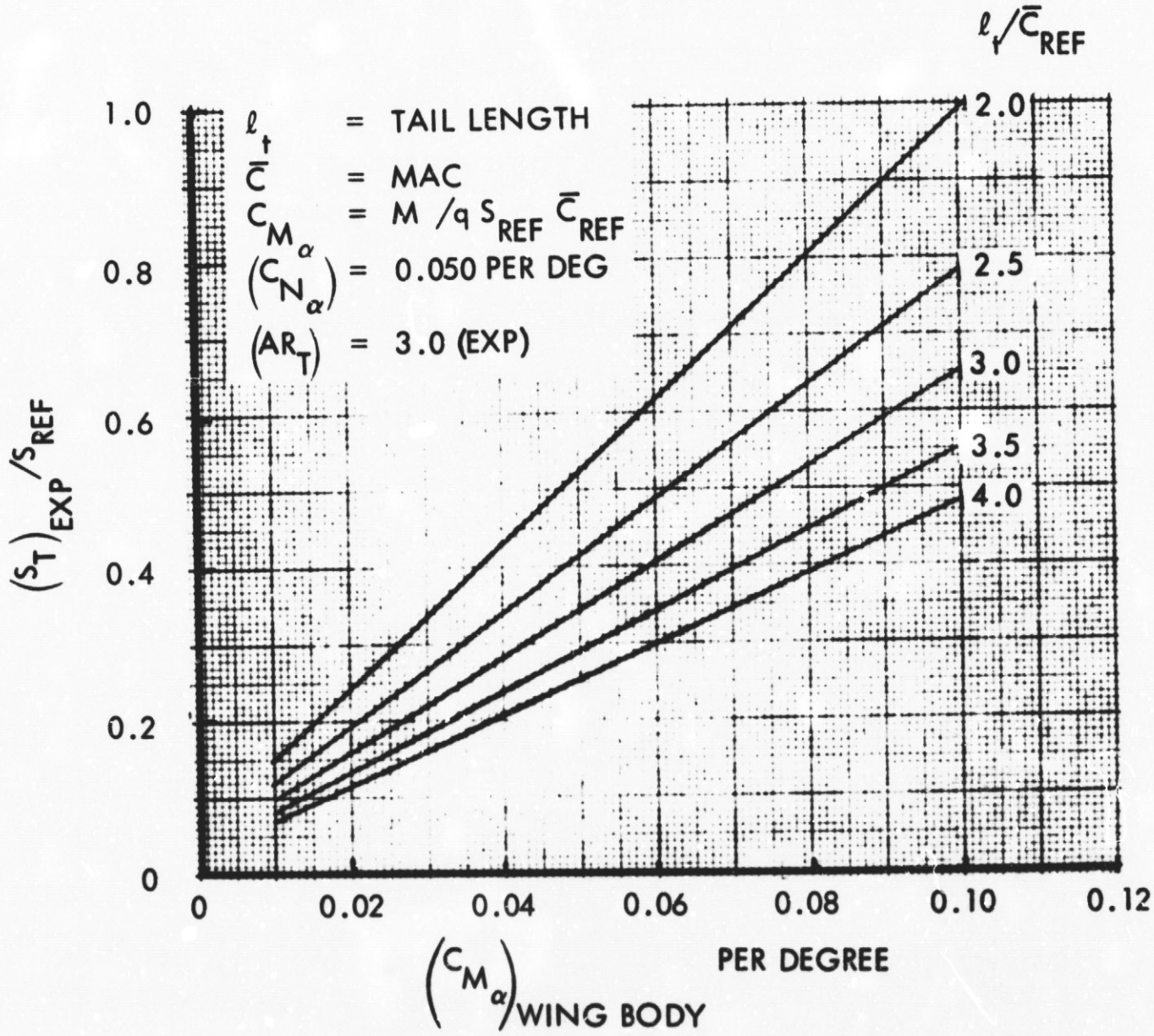

Figure 7.2-19. Estimated Subsonic Tail Size for 10 Percent Static Margin at Cruise

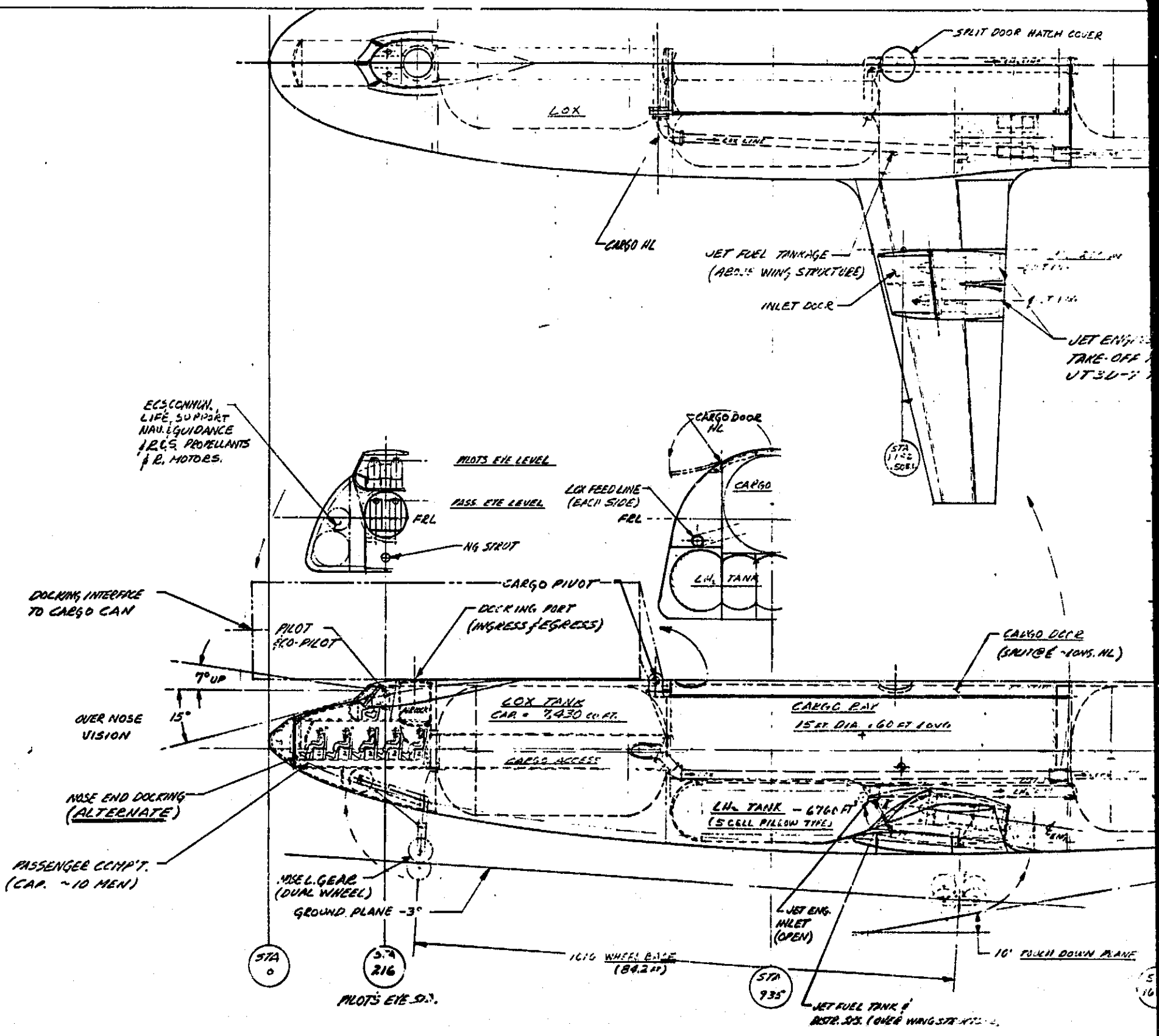

FOLDOUT FRAME 1

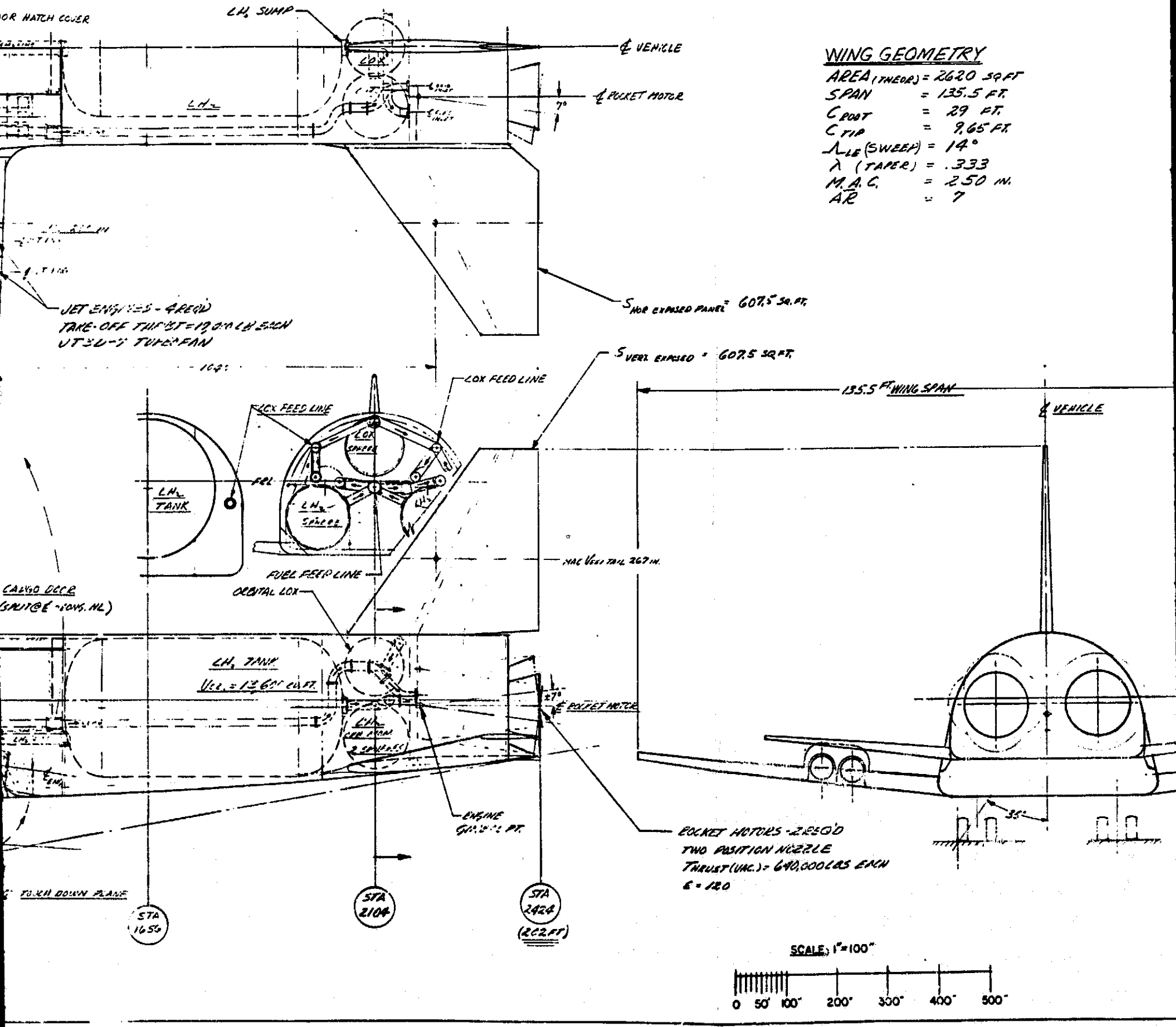

WING GEOMETRY

AREA (THEOR)	=	2620 SQ FT
SPAN	=	135.5 FT.
C_{ROOT}	=	29 FT.
C_{TIP}	=	9.65 FT.
Λ_{LE} (SWEEP)	=	14°
λ (TAPER)	=	.333
M.A.C.	=	250 IN.
AR	=	7

Figure 7.2-20. Orbiter Co
Payload

FOLDOUT FRAME 2

VEHICLE

ET MOTOR

HOR EXPOSED PANEL = 607.5 SQ. FT.

IER EXPOSED = 607.5 SQ FT.

WING GEOMETRY

AREA (THEOR.) = 2620 SQ FT
SPAN = 135.5 FT.
C_{ROOT} = 29 FT.
C_{TIP} = 9.65 FT.
Λ_{LE} (SWEEP) = 14°
λ (TAPER) = .333
M.A.C. = 250 IN.
AR = 7

STAGE WEIGHTS

PROPELLANT (LOX/LH$_2$) = 555,000 LBS.
TOTAL LAUNCH = 835,000 LBS.
RE ENTRY = 295,000 LBS.
LANDING = 243,000 LBS.
PROPELLANT (ON ORBIT) = 35,000 LBS.

TOTAL PLANFORM AREAS

S_{WING} = 2620 SQ FT (W/S_W = 90 PSF)
$S_{FUS.}$ = 5380 SQ FT.
S_{TOTAL} = 8000 SQ FT. ($W/S_{TOT.}$ = 30)

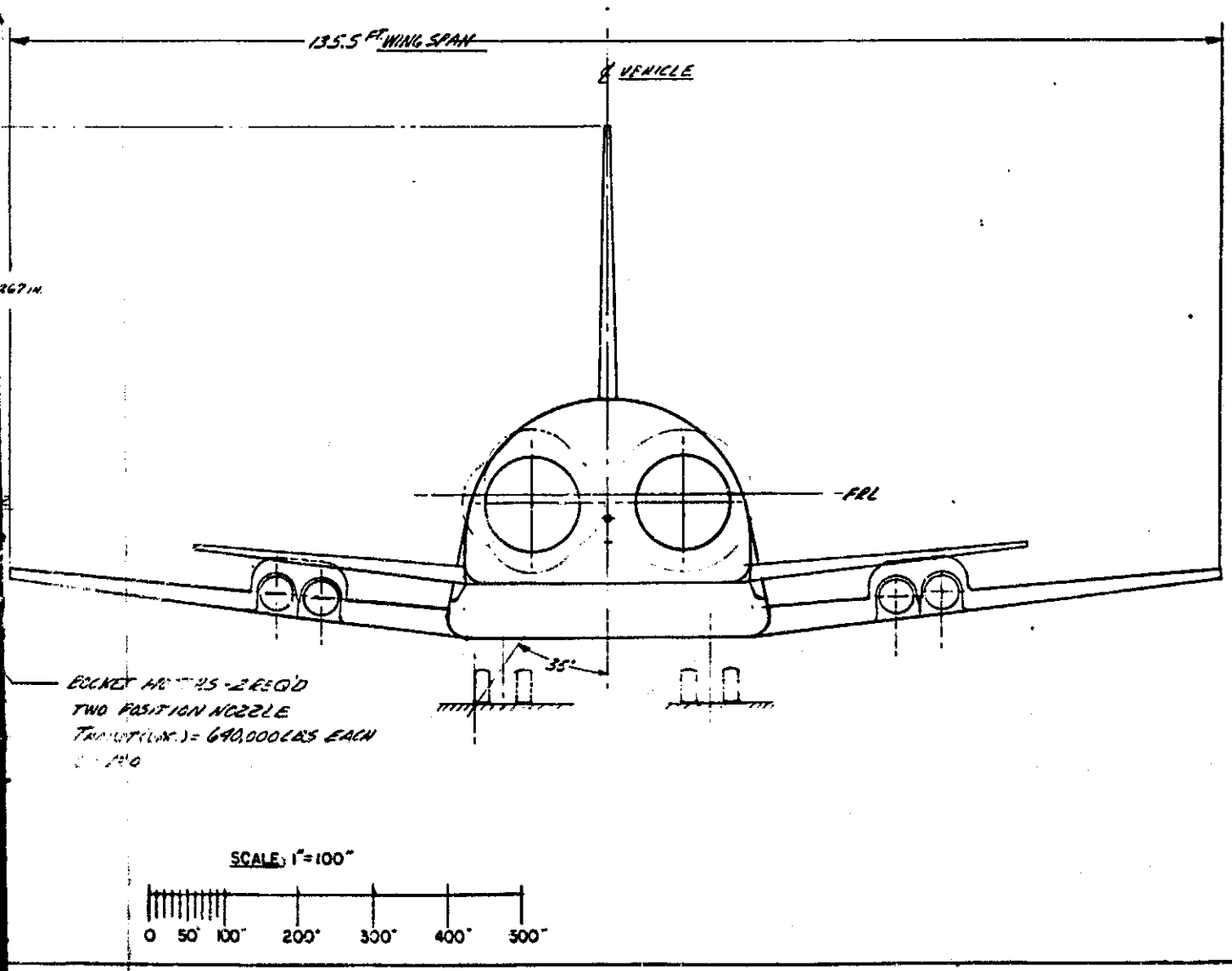

Figure 7.2-20. Orbiter Configuration, 50,000-Pound Payload Class

FOLDOUT FRAME 3

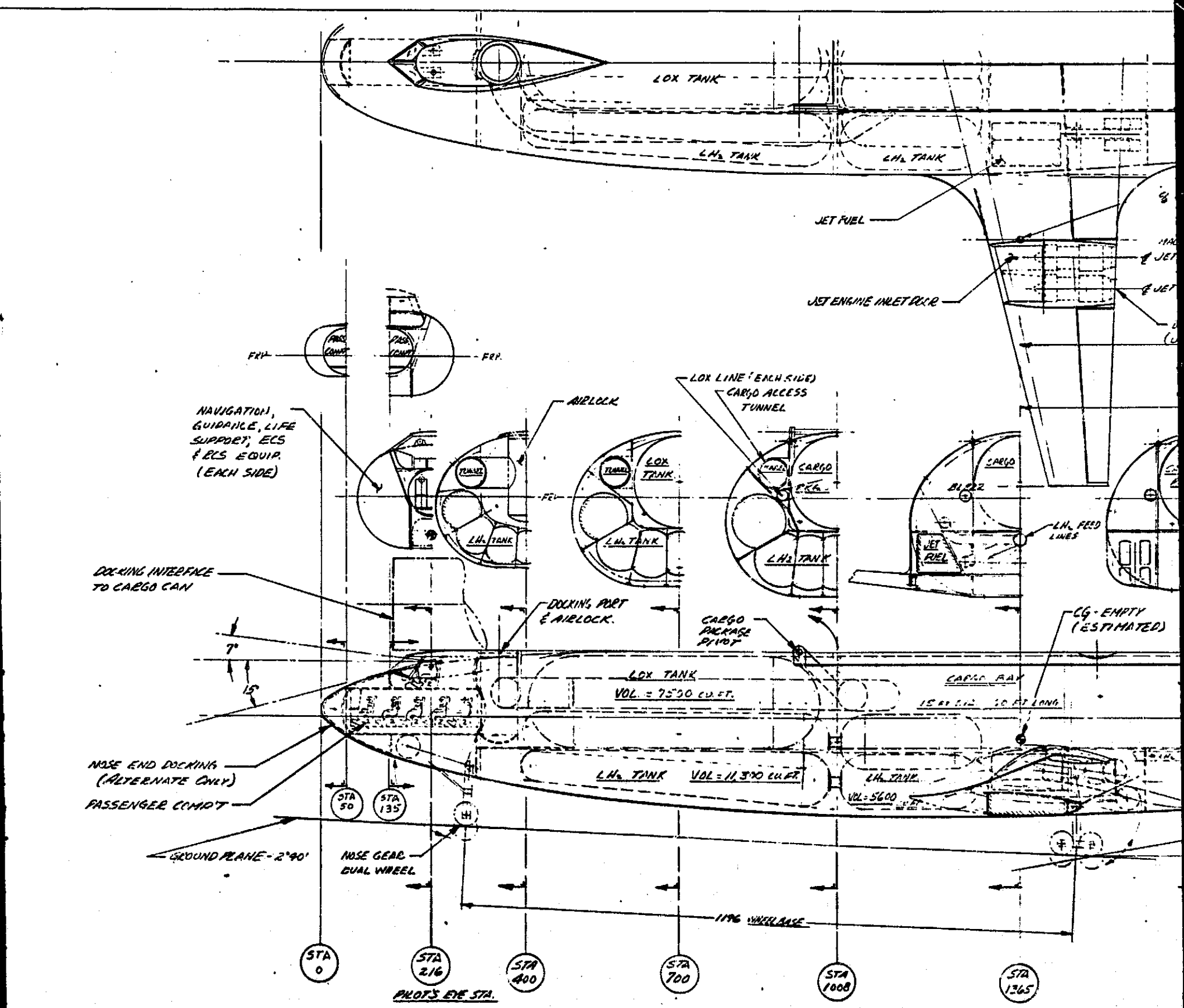

FOLDOUT FRAME 1

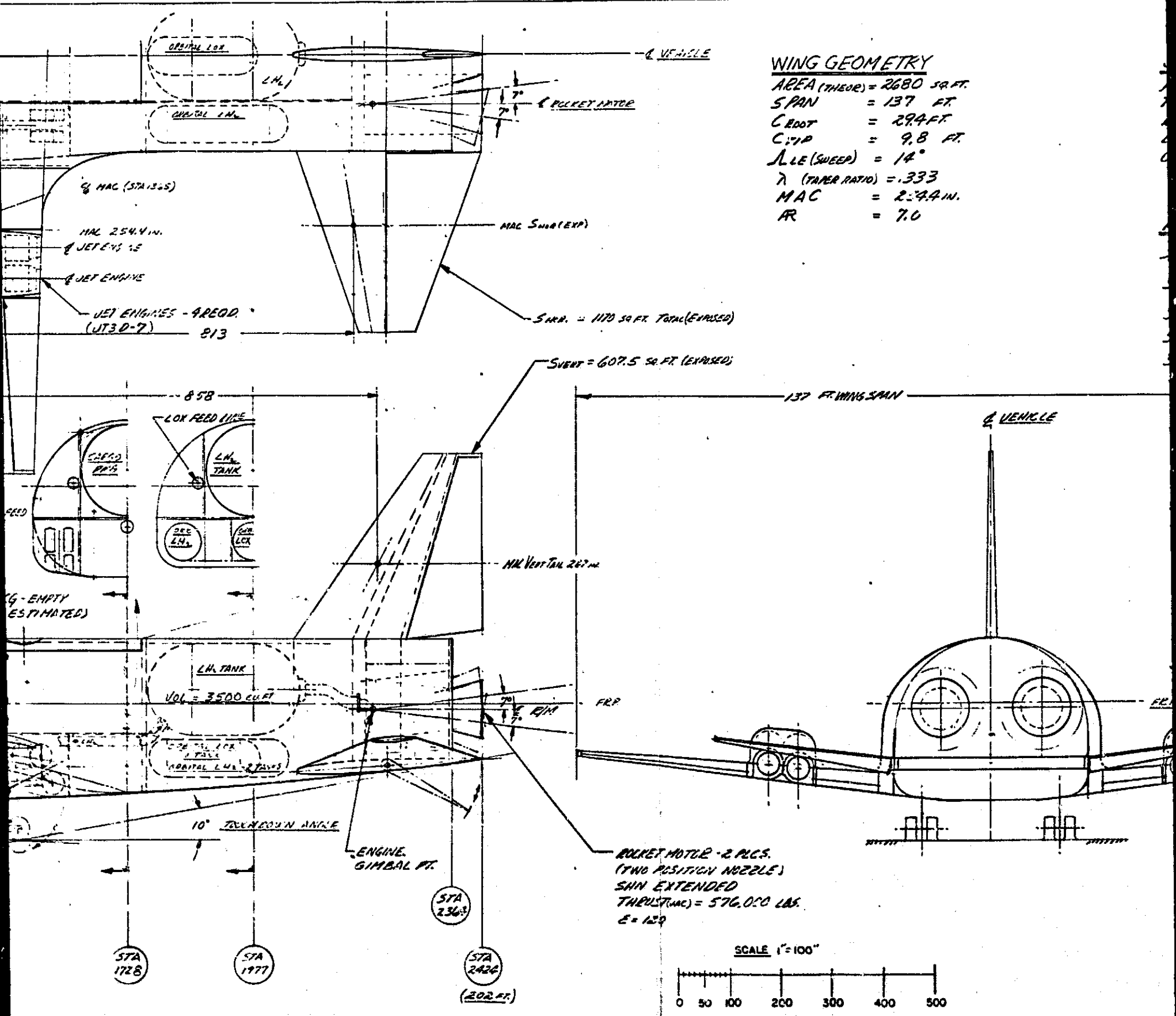

WING GEOMETRY

AREA (THEOR) = 2680 SQ. FT.
SPAN = 137 FT.
C_{EDOT} = 29.4 FT.
C_{TIP} = 9.8 FT.
Λ_{LE} (SWEEP) = 14°
λ (TAPER RATIO) = .333
MAC = 254.4 IN.
AR = 7.0

Figure 7.2-21. Orbiter Configuration Inco

FOLDOUT FRAME 2

Space Division
North American Rockwell

WING GEOMETRY

AREA (THEOR) = 2680 SQ. FT.
SPAN = 137 FT.
C_{ROOT} = 29.4 FT.
C_{TIP} = 9.8 FT.
Λ_{LE} (SWEEP) = 14°
λ (TAPER RATIO) = .333
MAC = 254.4 IN.
AR = 7.0

STAGE WEIGHTS

PROPELLANT (LO_2/LH_2) = 555,000 LBS.
TOTAL LAUNCH = 835,000 LBS.
RE-ENTRY = 295,000 LBS.
LANDING = 241,000 LBS.
ON-ORBIT PROPELLANT = 35,000 LBS.

AREAS

S_{WING} = 2620 SQ FT. ($\frac{W}{S_W} \approx 90$ PSF)
S_{FUS} = 5380 SQ FT.
S_{TOTAL} = 8000 SQ FT. ($\frac{W}{S_{TOT}} \approx 30$)
$S_{HOR. TAIL}$ = 1170 SQ FT. (EXPOSED)
$S_{VERT. TAIL}$ = 607.5 SQ. FT.

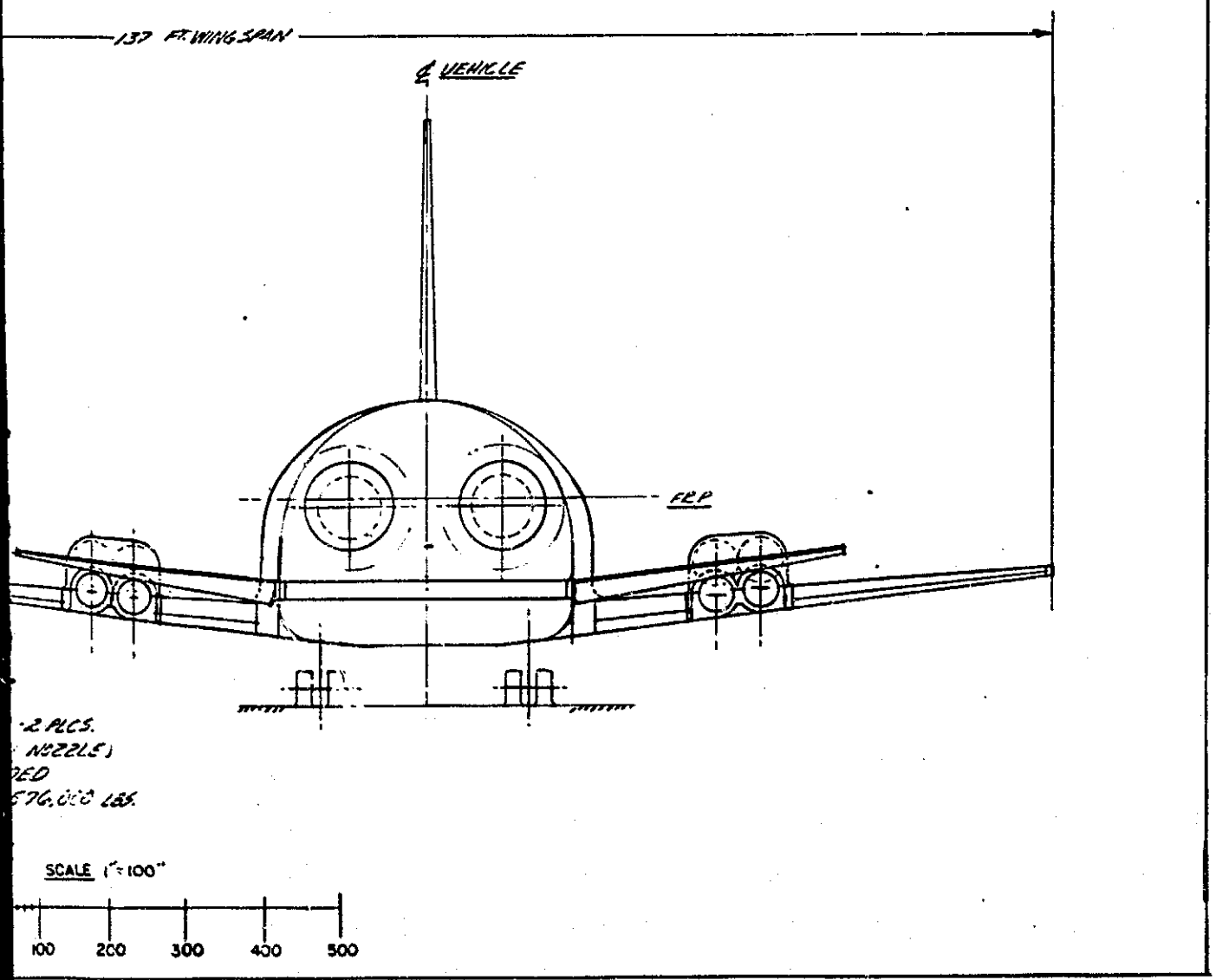

Figure 7.2-21. Orbiter Configuration Incorporating Body Corner Radius

FOLDOUT FRAME 3

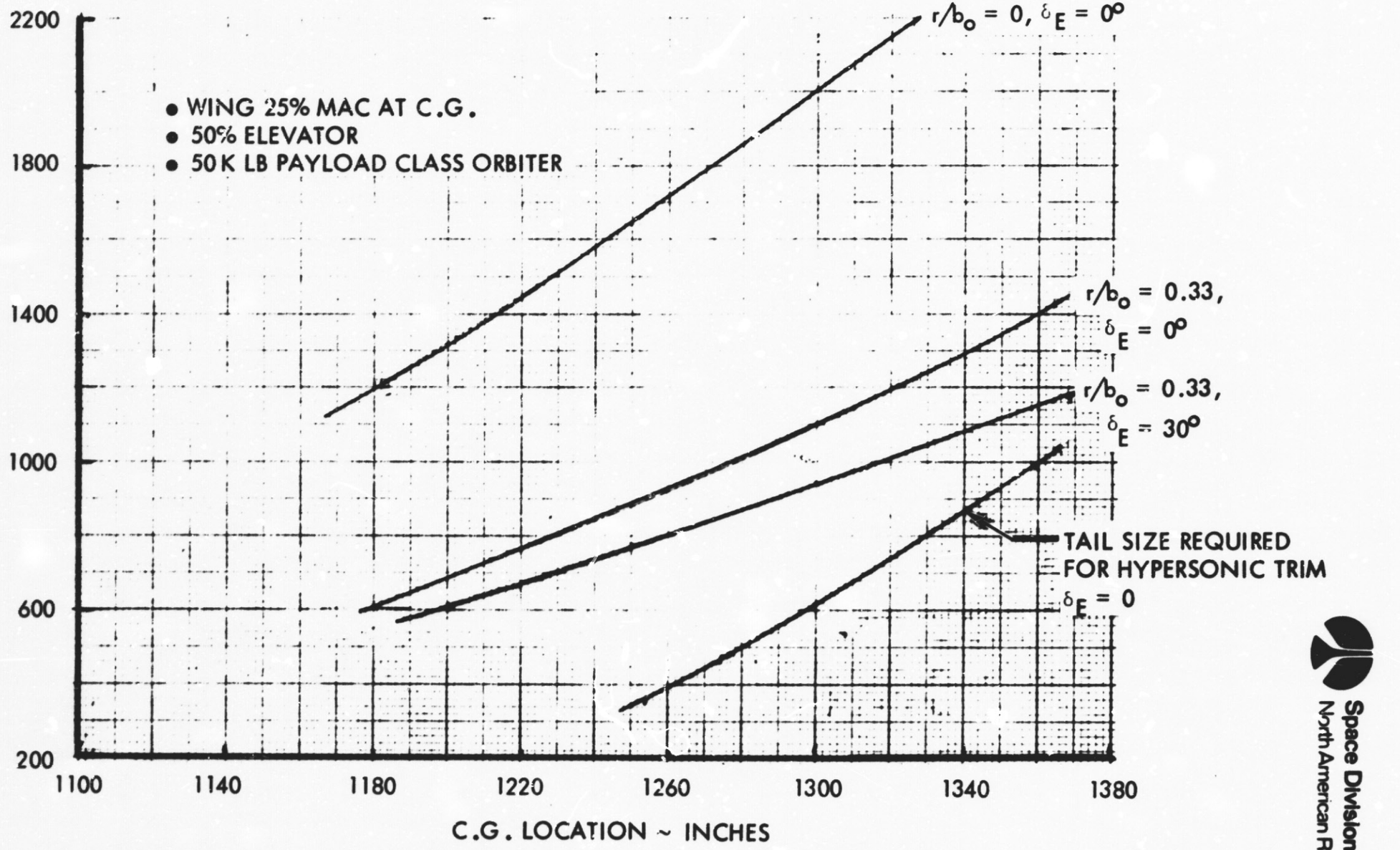

Figure 7.2-22. Effect of Body Corner Radius on Horizontal Tail Size

Space Division
North American Rockwell

The effects of body corner radius on lift, drag and L/D are compared in Figure 7.2-23. The effect on L/D at 60 degrees angle of attack was negligible; however, C_L was degraded by approximately 12 percent. Estimates of the resulting effects on weight and thermal environment are summarized in Table 7.2-1. Entry weight for the configuration with sharp corners was estimated to be 245,000 pounds, giving an entry lift loading (W/C_LS) of 39.1 pounds per square foot. Design thermal environment was based on W/C_LS = 50 pounds per square foot. Peak entry temperature is proportional to the (W/C_LS) to the 1/8 power over the range of interest, and the design environment for the square and round corner configurations was reduced accordingly. In addition, entry weight for the rounded corner configuration was reduced 9000 pounds to account for the weight saving due to the smaller horizontal tail. Temperatures at the body corner were scaled according to the heating rate distribution shown in Figure 7.4-2 . The ratio of maximum heating rate at the corner to maximum heating rate at the lower body centerline was estimated to be 1.7 and 1.3 for the sharp and rounded corner configuration respectively. As shown in Table 7.2-1, peak lower temperatures are not significantly different for the round and sharp corner designs. The round corner configuration exhibits a 100 F temperature advantage, and a 9000-pound weight saving.

The lateral directional estimates are presented in Figure 7.2-24. A stable dihedral effect is noted. The sides of the body forward of the center of gravity had roll in so that at high angle of attack the sides would be shaded in sideslip, resulting in improved directional stability due to the body at high α. The orbiter static directional derivative does exhibit some directional instability, negative C_{n_β}, in the body axis which, for the same center of gravity, increases as the corners of the body are rounded. However, for entry at high angle of attack, the directional derivative, C_{n_β}, is not the important parameter in defining vehicle stability. A six-degree-of-freedom parametric analysis of the vehicle directional stability characteristics indicated that for a negative C_{n_β} five times that estimated for the configuration with corner radius on the body, the vehicle was stable and controllable and used 1021 pounds of fuel in yaw and roll during reentry. With neutral and with stable C_{n_β}, only 8 to 9 percent as much fuel was used (Section 7.5.4). Though static directional instability can be acceptable during reentry, to minimize reaction control system fuel it is considered more favorable to design for a minimum of neutral stability. This can be accomplished by design improvements such as twin vertical tails rolled out, body shaping and/or dihedral on the horizontal tail. The effects on C_{n_β} of dihedral on the horizontal tail are indicated on the figure. With 30 degrees dihedral, neutral C_{n_β} is obtained.

These preliminary results indicated that the rounded corner configuration may have a weight advantage over the baseline configuration, and lateral/directional characteristics appear to be acceptable. However, additional investigations are required to evaluate the effects of corner radius

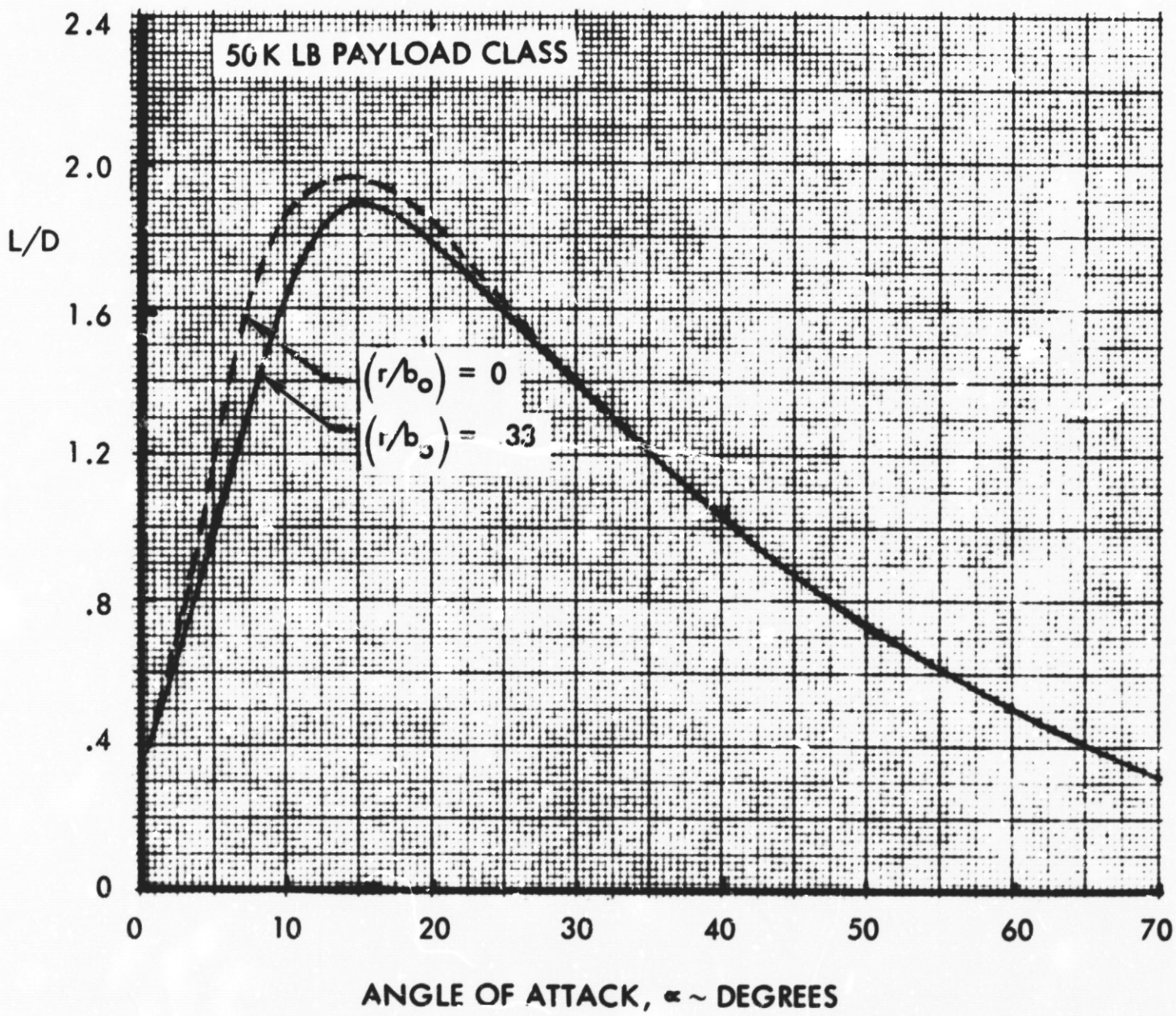

(a) Lift-to-Drag Ratio

Figure 7.2-23. Effect of Body Corner Radius on Orbiter Hypersonic Aerodynamics (Sheet 1 of 2)

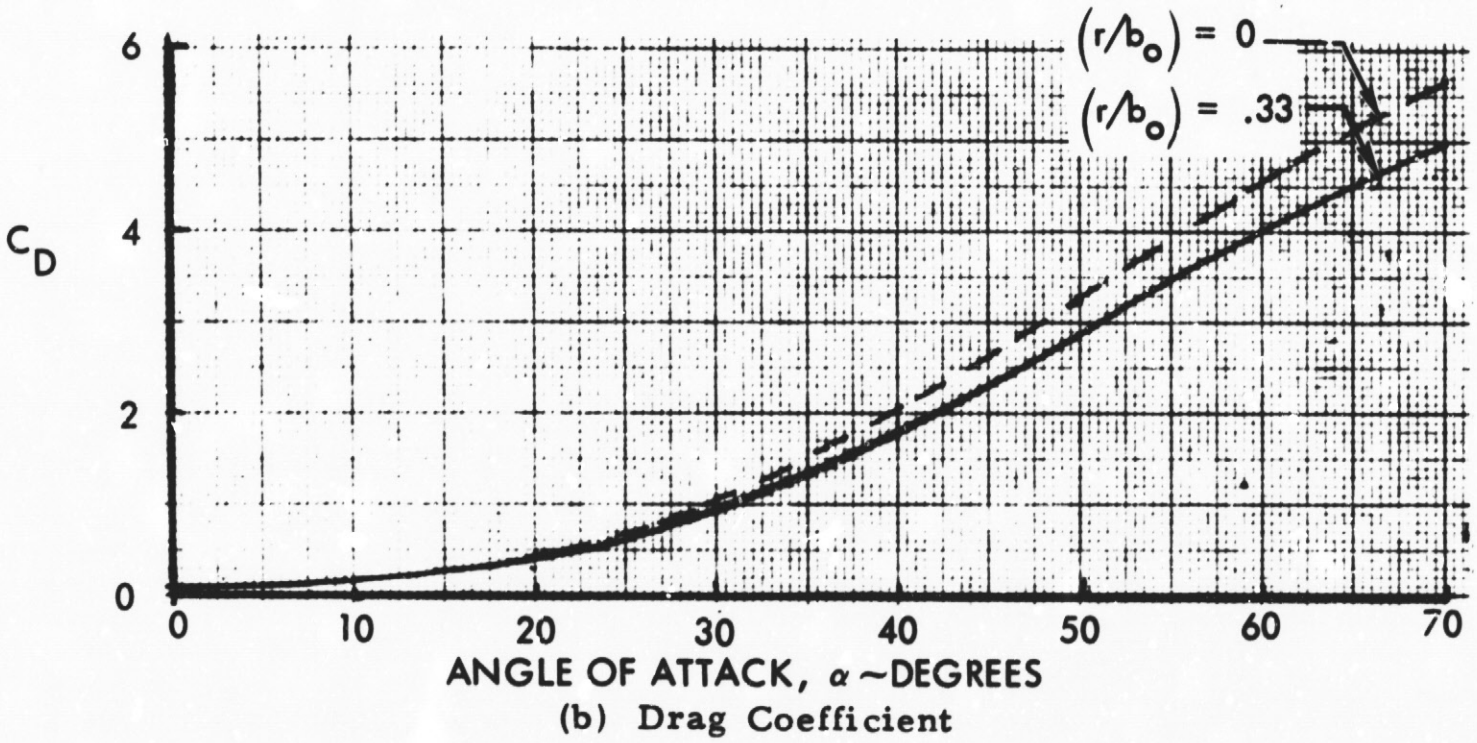

(b) Drag Coefficient

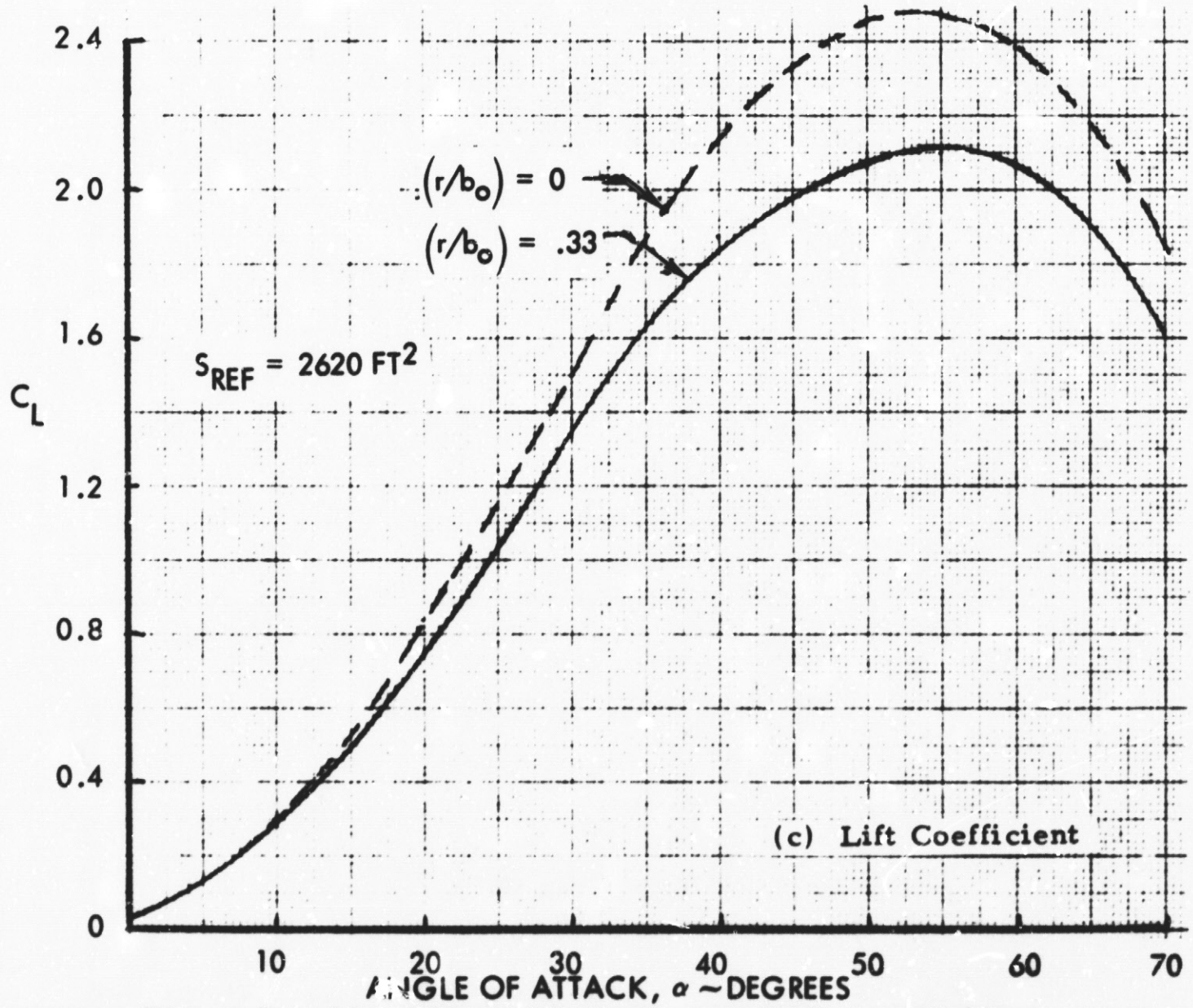

(c) Lift Coefficient

Figure 7.2-23. Effect of Body Corner Radius on Orbiter Hypersonic Aerodynamics (Sheet 2 of 2)

NOTES: 50K LB PAYLOAD CLASS ORBITER

X_{CG} = 1182 Z_{CG} = -35

b_{REF} = 1626 IN S_{REF} = 2630 FT^2

Mach = 8.0

O EFFECT OF ROUNDING BODY CORNER, r_{HORIZ} = 7°

X EFFECT OF ROUNDING BODY CORNER, r_{HORIZ} = 30°

Figure 7.2-24. Hypersonic Lateral/Directional Characteristics

Table 7.2-1. Body-Corner Radius Weight and Temperature Trade

50 K Orbiter
α = 60-Degree Entry

Body Configuration	C_L	$\frac{W}{C_L S}$ (lb/ft^2)	ΔW (lb)	Temp Ratio Due to $W/C_L S$	Temp on Body ℄ (F)	Temp at Body Corner (F)
Design thermal environment		50		1.0	1300	1550
Square corner	2.386	39.1		0.970	1250	1490
Round corner (r/b) = 0.33	2.080	43.2	-9000	0.982	1270	1390

on thermal environment, heat protection system design, and structural weight before the revised contour should be incorporated in the baseline configuration. Rounded corners certainly should be considered for the booster, where about 20,000 pounds of substructure are required in the present design for the standoff structure to support the flat bottom of the fuselage.

Directional Stability Improvements

The configurations exhibited unstable directional derivatives at hypersonic Mach numbers. This is not considered a very serious problem, as discussed in the previous section. However, reaction control system fuel consumption during entry will be reduced if stable or neutrally stable C_{n_β} is realized. Consequently, techniques to improve the directional characteristics were evaluated and are presented in this section. These are the effect of body shaping, vertical tail, twin versus single, and dihedral in the horizontal tail.

Vertical Tail, Twin Versus Single. A single vertical is completely shadowed and is ineffective at high angles of attack. One method to improve directional stability, if needed, at the hypersonic Mach numbers is to incorporate twin verticals which are rolled out. Rolling out basically increases the pressure coefficient due to angle of attack and its projection into the XZ plane, thereby increasing the side force aft of the center of gravity.

The most effective rollout position for zero toe-in angle can be found from the Newtonian model as follows:

$$Cy/K \frac{S_F}{S_{ref}} = -\cos\Gamma\left[\cos^2\eta_r - \cos^2\eta_L\right] \qquad (1)$$

Where η is the angle between the velocity vector and the normal to the left or right surface and where Γ is the roll-out angle:

$$\cos^2\eta_r - \cos^2\eta_L = 4 \sin\alpha \sin\Gamma \sin\beta \cos\Gamma$$

The side force in expression (1) can be maximized with respect to Γ to yield the maximum side force.

$$\frac{dCy}{d\Gamma} = 0 = \frac{d}{d\Gamma}\left[\cos\Gamma\left(\cos^2\eta_r - \cos^2\eta_L\right)\right] =$$

$$\frac{d}{d\Gamma}\left[4 \sin\alpha \sin\Gamma \sin\beta \cos^2\Gamma\right]$$

Differentiating the enclosed expression with respect to Γ yields:

$$4 \sin\alpha \sin\beta \left[\sin\Gamma(2\cos\Gamma)(-\sin\Gamma) + \cos^3\Gamma\right] = 0$$

Reducing the above equation further yields:

$$2 \sin^2\Gamma = \cos^2\Gamma \qquad (2)$$

The roll-out angle becomes approximately 35 degrees for maximum directional stability input.

Body Shaping. A second or alternate method in which to improve directional stability is to shape the body aft of the center of gravity by slightly rolling the sides out. The same Newtonian mechanism applies here as it did for rolled-out twin verticals. The left body side is shaded for positive sideslipping at any angle of attack. The expression for side force then becomes:

$$Cy/K \frac{S_F}{S_{ref}} = -\cos\delta \cos\Gamma(\cos^2\eta_r)$$

Where δ and Γ are the toe-in and roll-out angles, respectively, as shown in Figure 7.2-25, η is the angle between the velocity vector and normal to the right flat.

$$\cos n_r = -\cos\alpha\cos\beta\sin\delta\cos\Gamma + \sin\beta\cos\Gamma\cos\delta + \sin\alpha\cos\beta\sin\Gamma$$

The side force was evaluated at β = 5 degrees and a roll-out angle of 0, 5, and 10 degrees, and is presented in Figure 7.2-25. These data show that at 60-degree angle of attack: a roll-out angle of 5 degrees is about three times more effective than a vertical side, and a toe-in angle of 10 degrees diminishes the effectiveness by 2-1/2 times. This curve can be used to evaluate design improvement effects on sideslip.

Horizontal Tail Dihedral. A third method in which to improve directional stability hypersonically is to have a fixed amount of dihedral on the horizontal tail. The identical equations are used to describe sideslip as are used on the rollout vertical. Presented in Figure 7.2-26 is the effect of dihedral on sideslip for dihedral of 14 and 7 degrees. The sideslip at 60 degrees angle of attack is over three times as effective at 14 degrees dihedral as it is at 7 degrees, and the effect of negative incidence is degrading. It may be possible that an acceptable amount of fixed dihedral on the horizontal tail may be sufficient to design the configuration for neutral stability.

Wing Size, Sweep, Geometry to Reduce Flyback Propellant Requirements

The booster flyback range is a direct function of the cruise velocity. An increase in the cruise velocity could increase the flyback range proportionately. One way to increase the cruise velocity is to increase the wing drag divergence Mach number. It is possible to make a calculation of the onset of transonic flow over wings by using the local pressure coefficient on the wing upper surface and the local flow inclination computed from sweepback theory. The critical Mach number of the wing is thus found to be a function of the sweep angle, pressure loading, and airfoil section. These parameters may be manipulated to increase the wing drag divergence Mach number. The drag coefficient for a wing (based on reference area S_{ref} having an exposed area S_{exp}) is given by:

$$C_D = C'_D \cos^{\eta}\Lambda \frac{C_{D_{AR}}}{C_{D_{AR_\infty}}} \frac{S_{exp}}{S_{ref}}$$

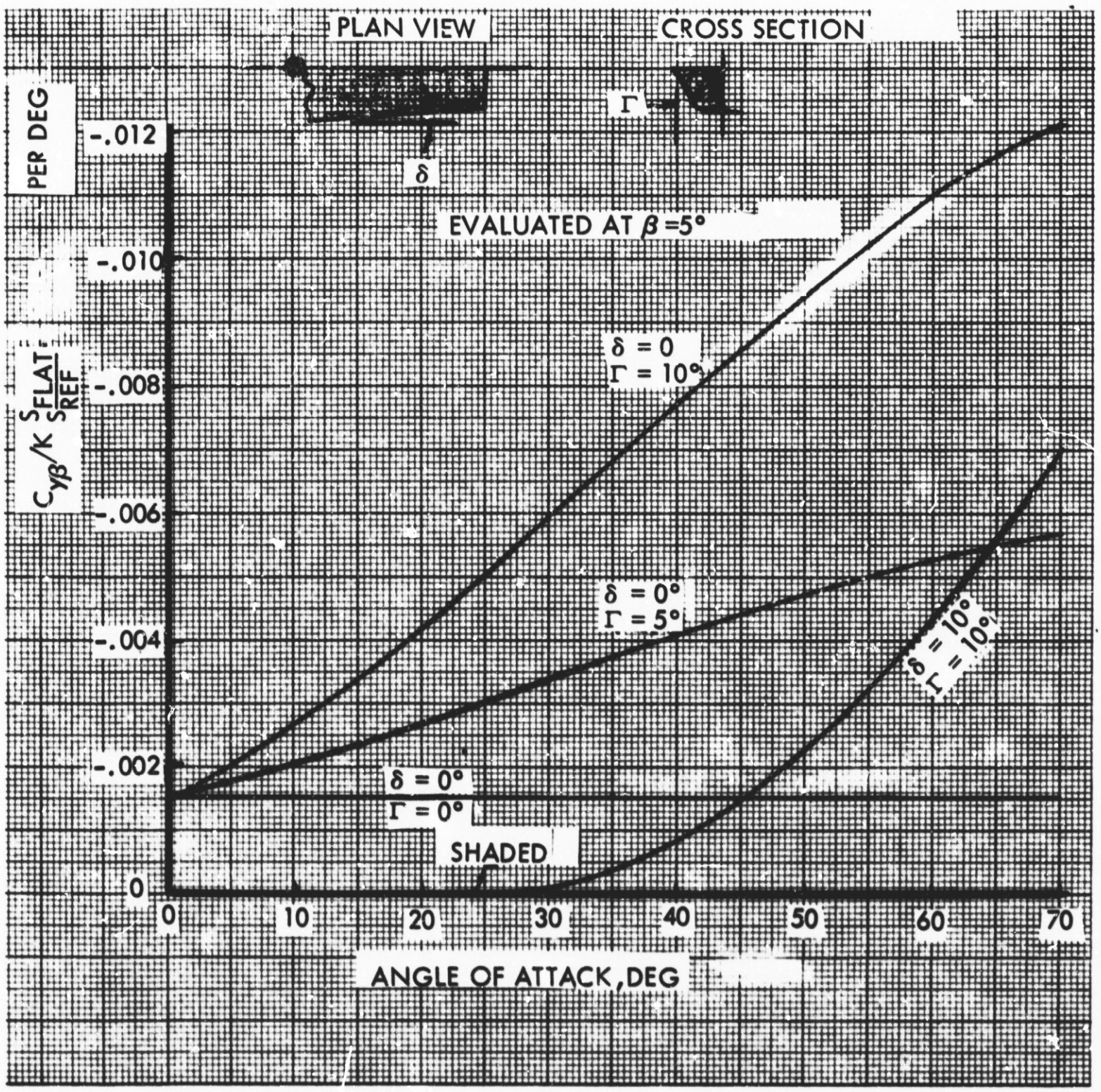

Figure 7.2-25. Effect of Body Shaping or Hypersonic Lateral/ Directional Characteristics

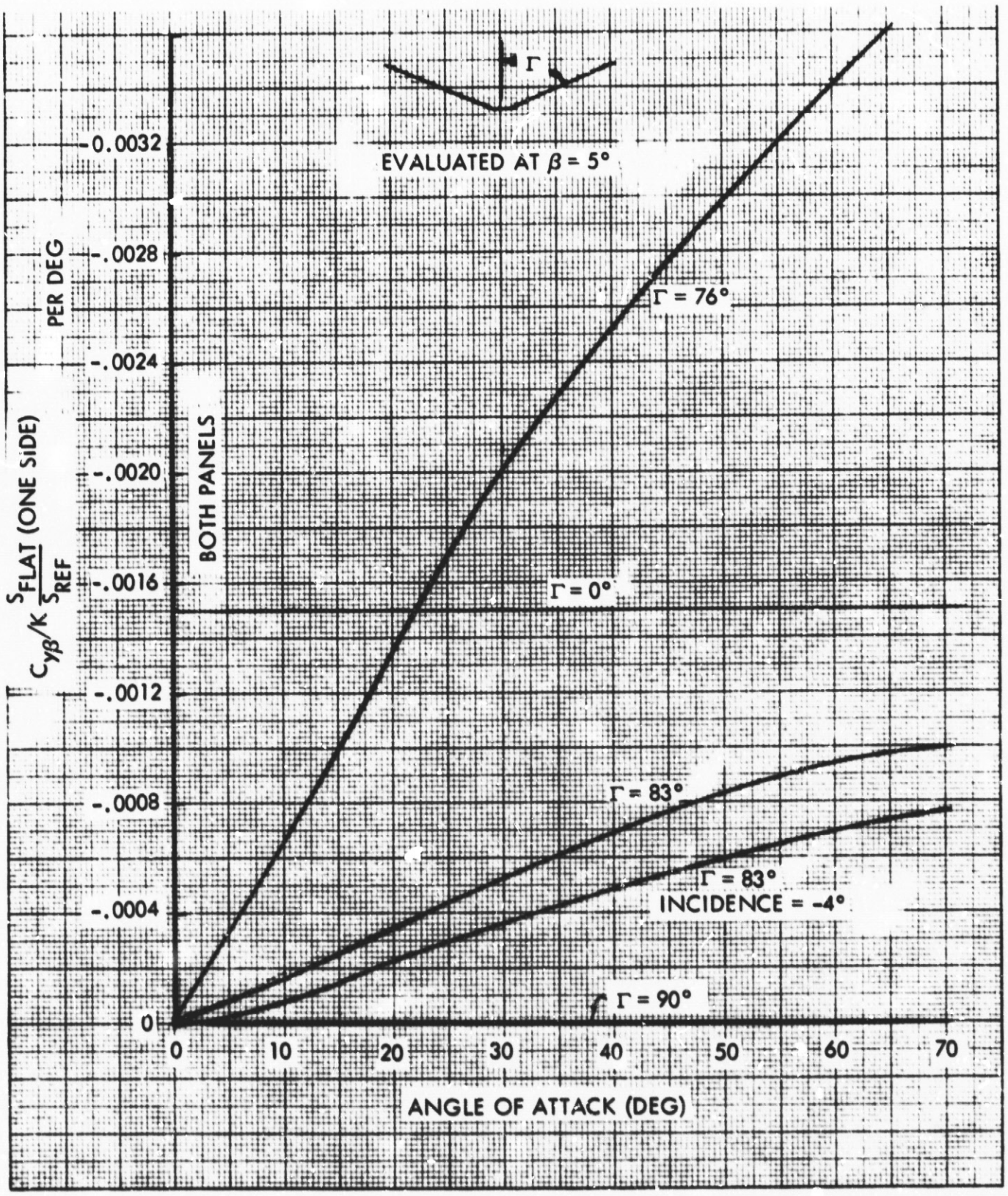

Figure 7.2-26. Effect of Horizontal Tail Dihedral on Hypersonic Lateral/Directional Characteristics

where

$$C'_D = C_D\,(\tau',\ M',\ AR = \infty)$$

is the two-dimensional airfoil section wave drag coefficient. The primed quantities denote effective thickness ratio and Mach number, namely

$$\tau' = \tau/\cos\Lambda$$

$$M' = M_\infty \cos^m \Lambda$$

where the value of the exponents n and m depend upon the leading edge sweep angle and Mach number.

For $\Lambda \leq 60$ degrees

(a) if $M_\infty \cos\Lambda \leq 2.8$
$n = 2.5$
$m = 0.5$

(b) if $M_\infty \cos\Lambda > 2.8$
$n = 3.0$
$m = 1.0$

The effect of wing sweep on leading edge drag is shown in Figure 7.2-27. The aspect ratio correction is presented in Figure 7.2-28. These data show that reducing the aspect ratio from 6 to 3 reduces the transonic wave drag approximately 38 percent. Thus reducing the aspect ratio will have a significant effect on increasing the cruise speed.

The effect on the wing drag divergence Mach number for the aspect ratio 7 ILRV wing is presented in Figure 7.2-29. These data show that the drag divergence Mach number may be increased 19 percent by increasing the wing sweep to 45 degrees. The increase in drag divergence Mach number will result in a 6 percent increase in range for a vehicle with no weight change. It is apparent that both wing sweep and aspect ratio exert a powerful influence on vehicle cruise Mach number. A tradeoff study of increased wing sweep and reduced aspect ratio may show a significant increase in flyback performance. The trade-off study must consider the impact of wing shape and size on vehicle weight.

Wings with highly swept leading edges and low aspect ratio fulfill the requirements for high performance and acceptable flying qualities in the transonic regions of flight. However, increasing the leading edge sweep and diminishing the aspect ratio, each taken as a measure by itself, reduces the lift curve of the configuration. The usable angle of attack at landing is limited by several factors (pilot's range of vision, tail ground clearance, landing gear length, etc.). The high-lift capability of the configuration at

Figure 7.2-27. Effect of Wing Sweep on Leading Edge Drag

Space Division
North American Rockwell

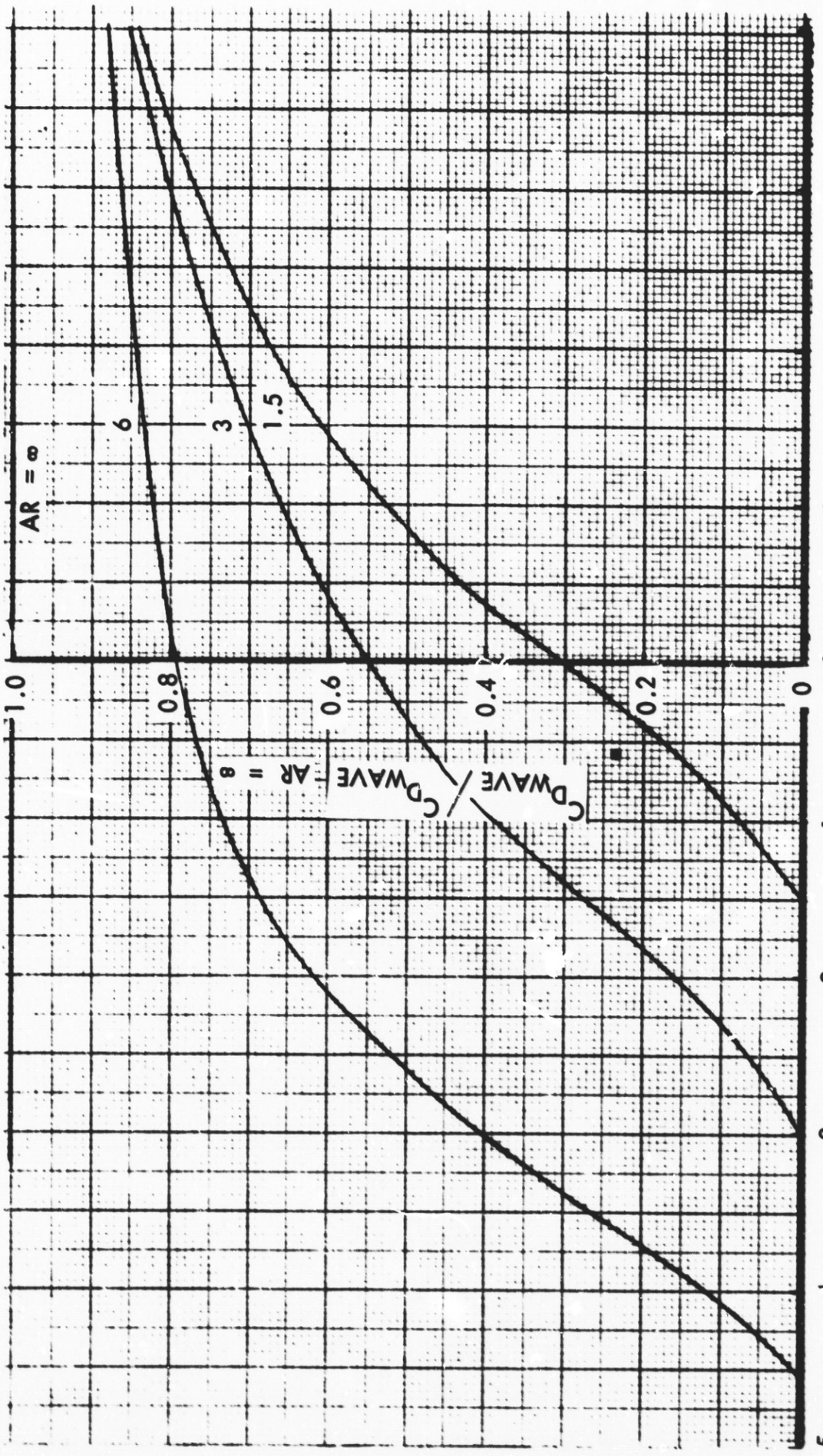

Figure 7.2-28. Aspect Ratio Wave Drag Correction

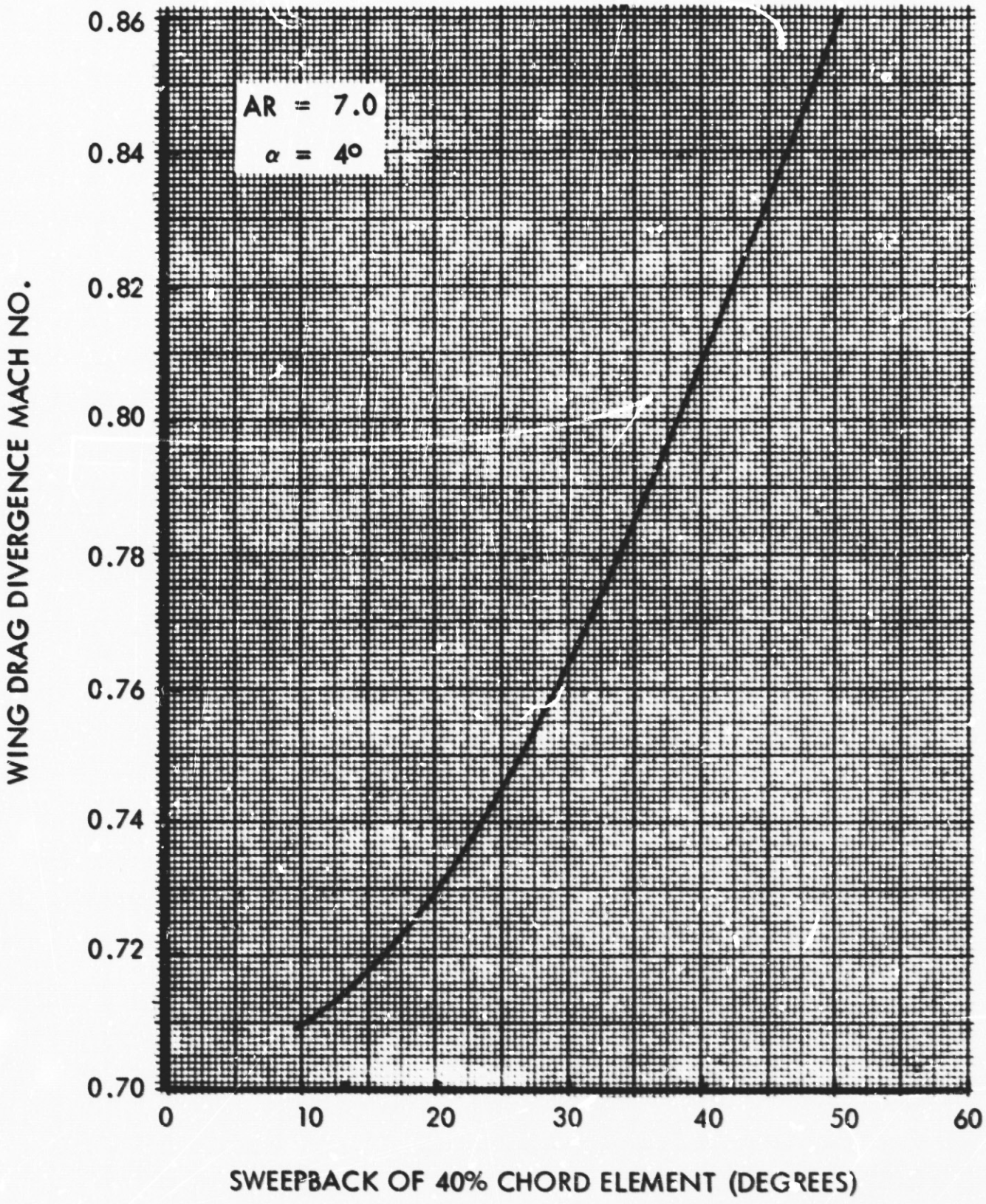

Figure 7.2-29. Effect of Sweep on Drag Divergence Mach No.

fixed angle of attack must be increased in some way if the landing speed is not to be increased. This is usually done by cambering the lifting surface with the aid of leading and trailing edge flaps. An alternate method is to use high-lift aerodynamics of canard configurations. The high-lift attainment of canards is achieved by taking advantage of the detached leading edge flows of two suitably arranged wings of appropriate relative size.

The canard also has the advantage of having a smaller stability-increasing aerodynamic center travel over the range from subsonic to supersonic flight. This is due to the absence of two important contributions which, for the conventional wing-tail configuration, favor the rearward travelling of the aerodynamic center, namely the reduction of the wing downwash from subsonic to supersonic flow, which causes a loss of tail efficiency and interference load induced by the wing on the fuselage.

In addition, the heavy propulsion system of the booster causes the center of gravity to be further aft relative to the orbiter body length. As the center of gravity moves aft, the moment arm of the horizontal stabilizer or conventional aft elevator decreases resulting in a larger aerodynamic surface. Preliminary analysis indicates that consideration of canard elevators with their longer moment arm becomes attractive for center of gravity locations greater than about 0.6L. The thermal environment of canards is estimated to be of the same order of magnitude but slightly more severe as compared to aft elevators due to the higher energy air in the region of the canards. Future studies should include evaluation of the canard concept, particularly for center of gravity locations of 0.6L or greater.

Turbojet Engine Location

The turbojets for cruise and landing for the baseline vehicle are located on the top surface of the wing with the nacelle leading edge raked back to avoid high heating. Alternate locations for these turbojets have been considered. Based on center of gravity considerations, it is desirable to locate them forward. Thus, a logical alternate location that was considered was to stow these engines in the fuselage near the nose during entry and deploy them outboard on pylons for subsonic cruise and landing. The major advantage to this scheme is the forward shift in center of gravity and resulting decreased empennage, and an aerodynamically cleaner wing. Disadvantages include the region of local heating on the fuselage sides due to engine exhaust and the increased complexity and weight associated with incorporating the variable engine location feature. Preliminary analysis indicated that the wing location was superior. Additional studies of alternate turbojet locations are recommended to substantiate these findings.

7.2.5 Results of NASA ARC Wind Tunnel Tests

The NR 0.02 scale orbiter model illustrated in Figure 7.2-30 was tested in the ARC 6-by-6-foot supersonic tunnel at Mach numbers from 0.25 to 2.0, angles-of-attack from -10 to 75 degrees, and sideslip angles from -4 to 8 degrees. Two fuselage nose sections, four horizontal stabilizers, and two vertical stabilizers were evaluated. Preliminary results of the tests indicate the following:

1. For a center-of-gravity location at approximately 0.53L, either of the horizontals having an exposed area of 471 square feet (H_4 or H_5) were adequate for the pitchdown maneuver and yielded an acceptable cruise static-stability margin. The smaller horizontal (approximately 350 square feet exposed area, H_6) was not acceptable. A plot of the longitudinal pitching moment characteristics of the model with the H_5 horizontal is shown in Figure 7.2-31.

2. At a high angle-of-attack (57 degrees), the model was laterally and directionally stable at Mach 2 but exhibited unstable directional derivatives at Mach numbers from 1.5 to 0.25. Additionally, the plots of rolling moment, yawing moment, and side force coefficients versus sideslip angle were erratic at Mach numbers lower than 2.0.

   Figure 7.2-22 shows that for the manner in which the shuttle vehicles are configured (inward sloping sides forward of the center of gravity)at a high angle-of-attack in supercritical flow, the entire fuselage contributes to static directional stability, while in subcritical flow the entire fuselage effects directional instability. This phenomenon may be a factor in the directional instabilities observed in the wind tunnel tests at high angles-of-attack.

3. For the H_5 horizontal, the elevator deflection required to trim the vehicle at an angle-of-attack of 60 degrees varied from about 28 degrees up at Mach 2 to approximately 18 degrees down at Mach 0.5. The variation in elevator deflection with Mach number is shown in Figure 7.2-32. From Figure 7.2-33 it may be seen that the predominant factor in elevator effectiveness was the shift in the center of pressure of the body.

It was not possible to simulate operational Reynolds numbers in the 6- by-6-foot supersonic tunnel. The Reynolds number based on model mean aerodynamic chord is approximately 0.9×10^6 at M = 0.6 in tunnel and is about 1.3×10^7 at the same Mach number operationally. Because of the low

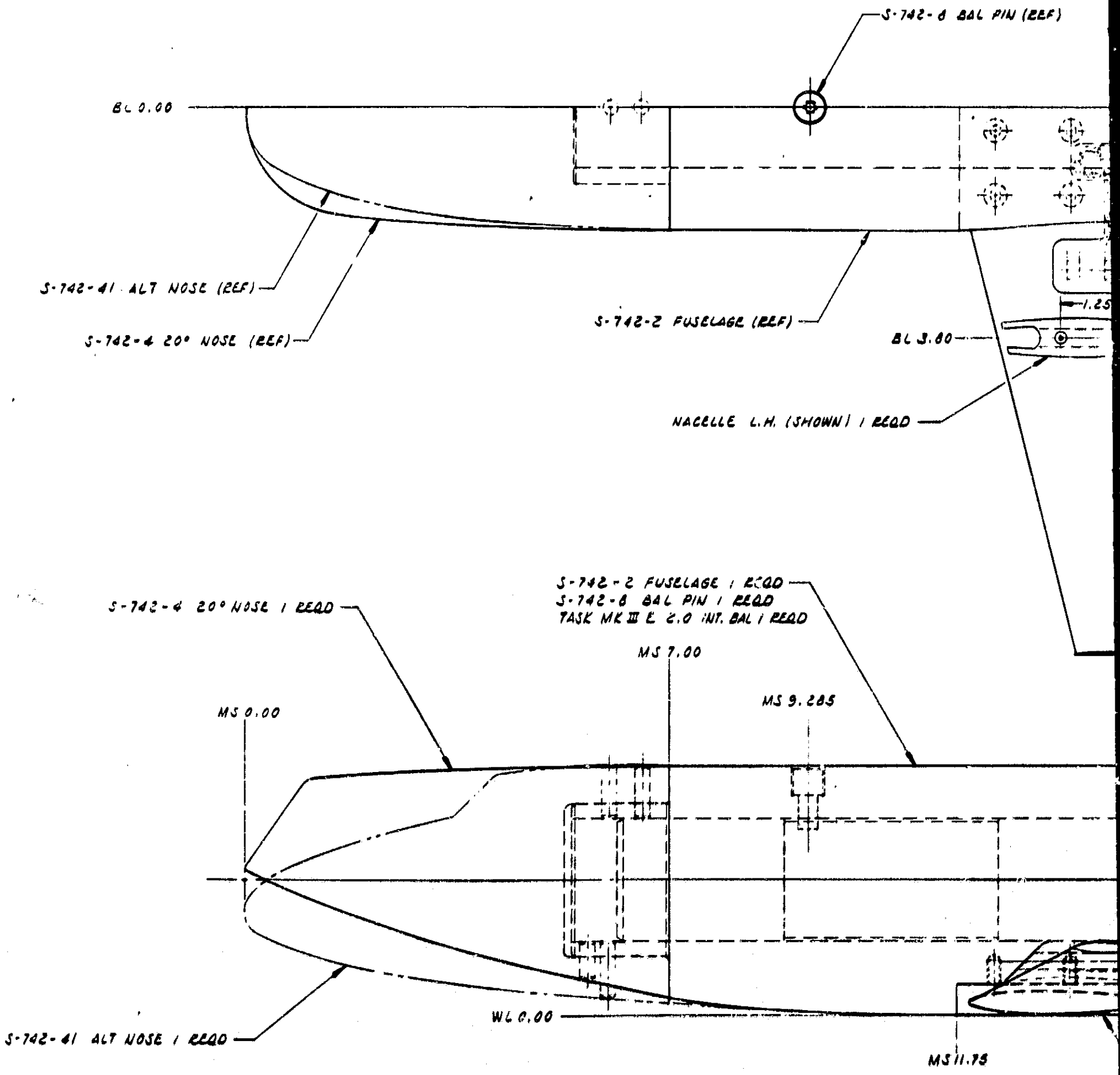

FOLDOUT FRAME 1

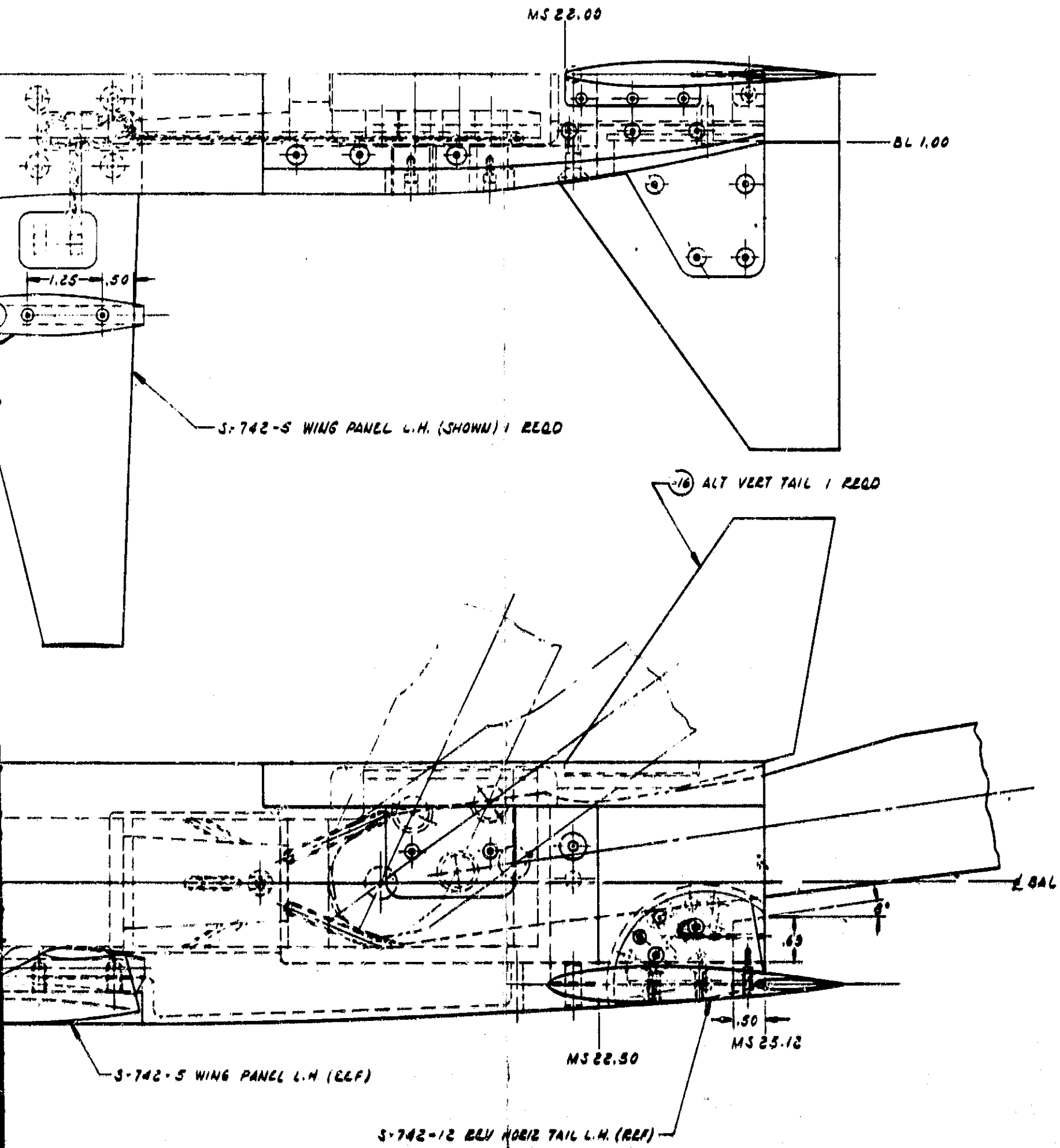

Figure 7.2-30. Wind Tunnel Model, 0.02 Scale Orbiter, 12,500-Pound-Payload Class (Sheet 1 of 3)

FOLDOUT FRAME 2

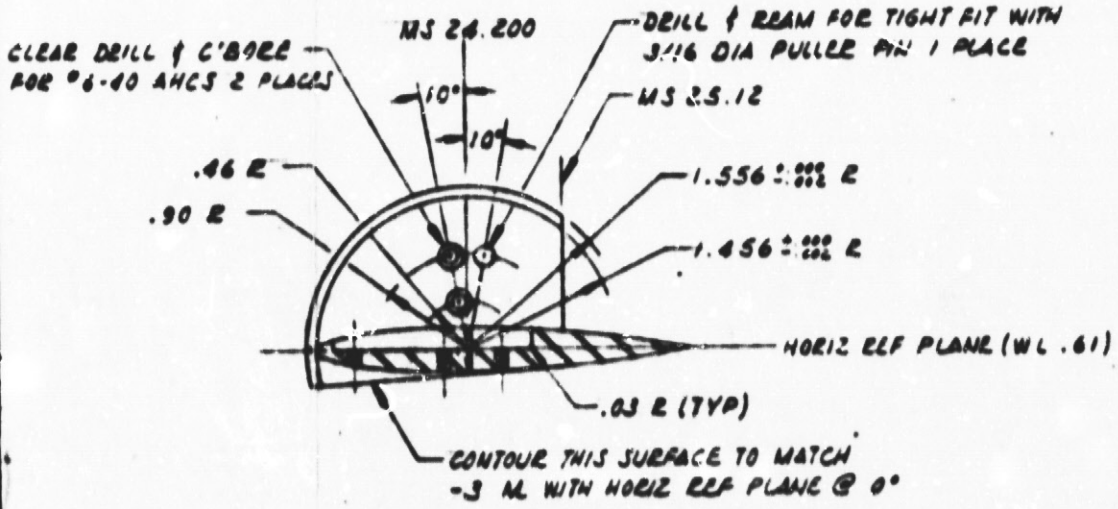

SECT. 13 - 13

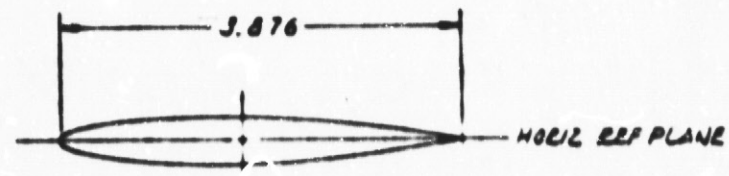

ROOT TEMP

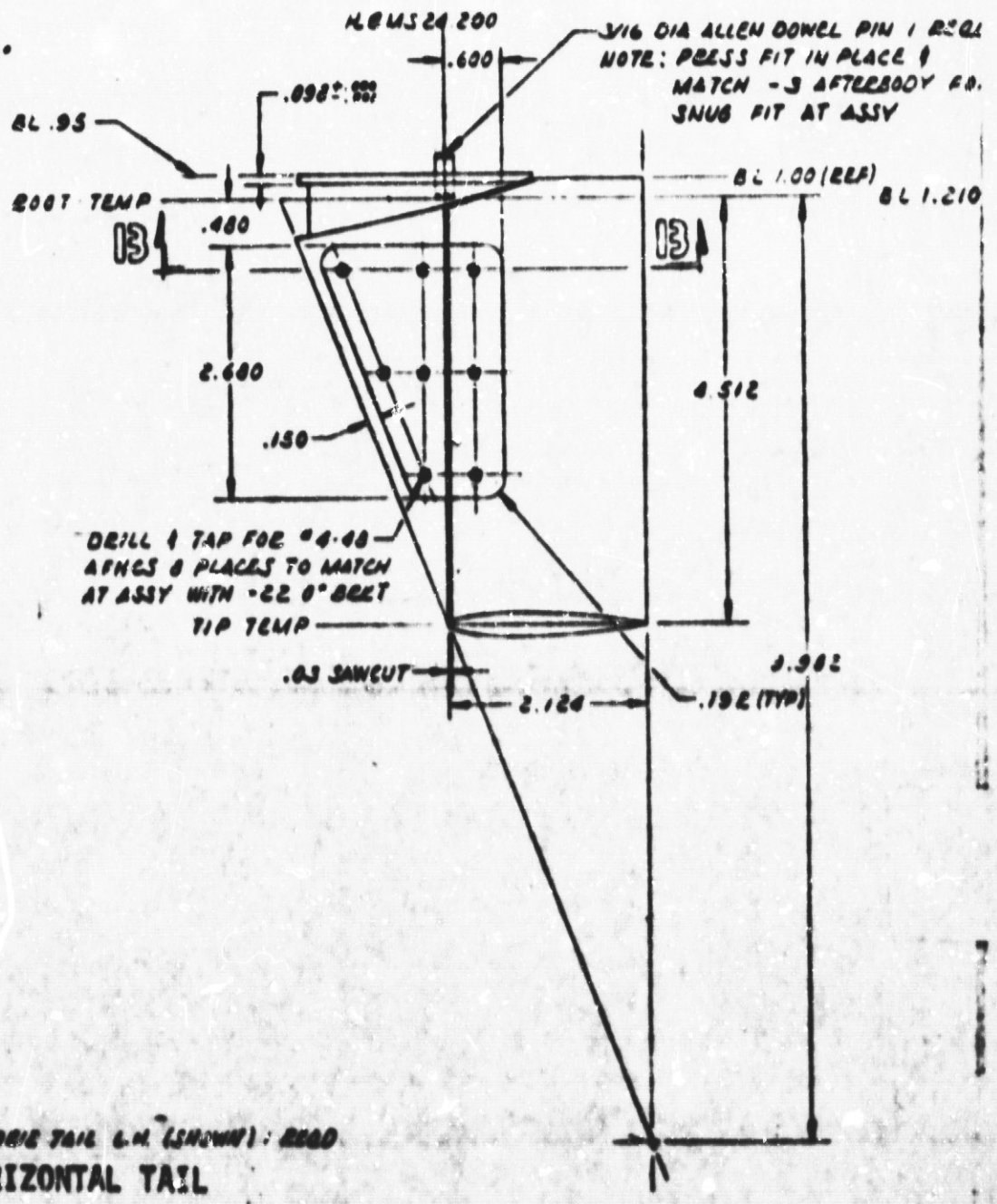

% C	ROOT TEMP X	ROOT TEMP 2Y	TIP TEMP X	TIP TEMP 2Y
0	0	0	0	0
1.25	.040	.070	.027	.039
2.5	.097	.095	.053	.052
5	.194	.127	.106	.069
7.5	.291	.140	.159	.081
10	.388	.164	.212	.090
15	.581	.189	.319	.103
20	.775	.205	.425	.112
30	1.163	.226	.637	.124
40	1.550	.233	.850	.127
50	1.938	.226	1.062	.124
60	2.326	.206	1.274	.113
70	2.713	.174	1.487	.095
80	3.101	.129	1.699	.071
90	3.409	.072	1.912	.040
95	3.682	.040	2.018	.022
100	3.876	.005	2.124	.003
LEG		.061		.034

DETAIL -14 ALTERNATE HORIZ TAIL L.H. (SHOWN): REQD

H5 HORIZONTAL TAIL

FOLDOUT FRAME 1

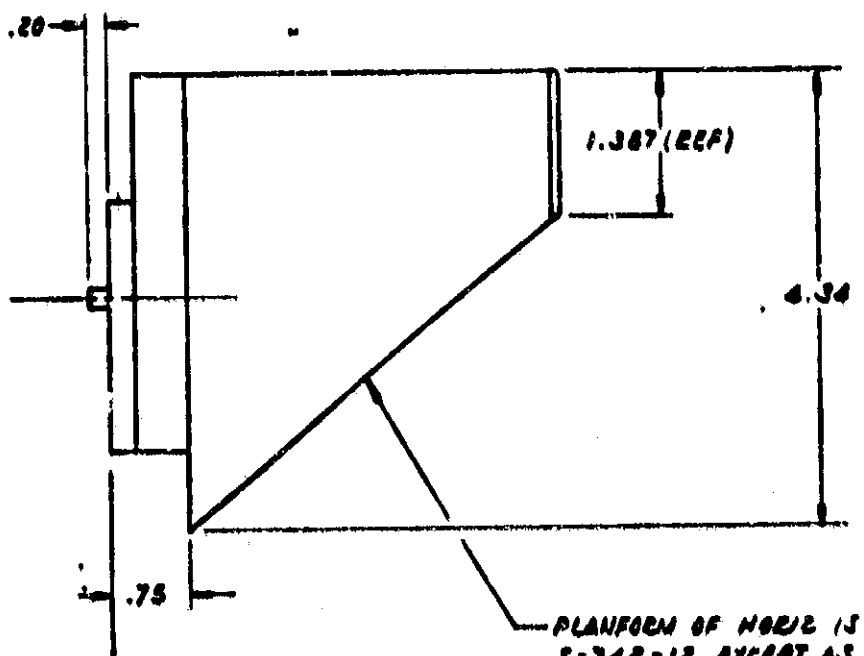

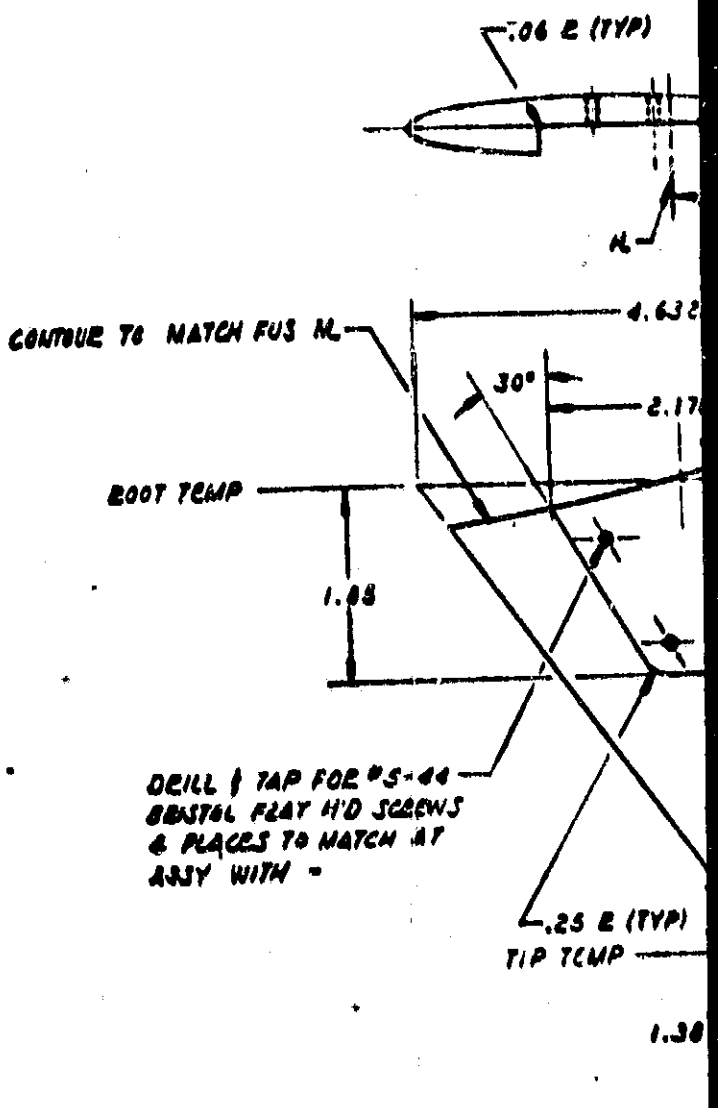

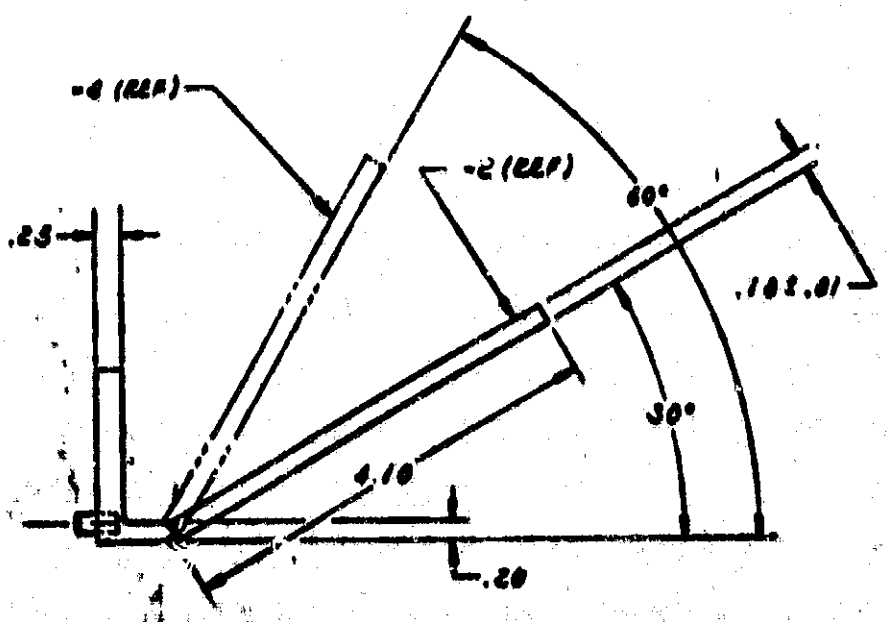

DETAIL

DETAIL "B" 30° DIHEDRAL HORIZ L.H. (SHOWN)

No. HORIZONTAL TAIL

Figure

FOLDOUT FRAME 2

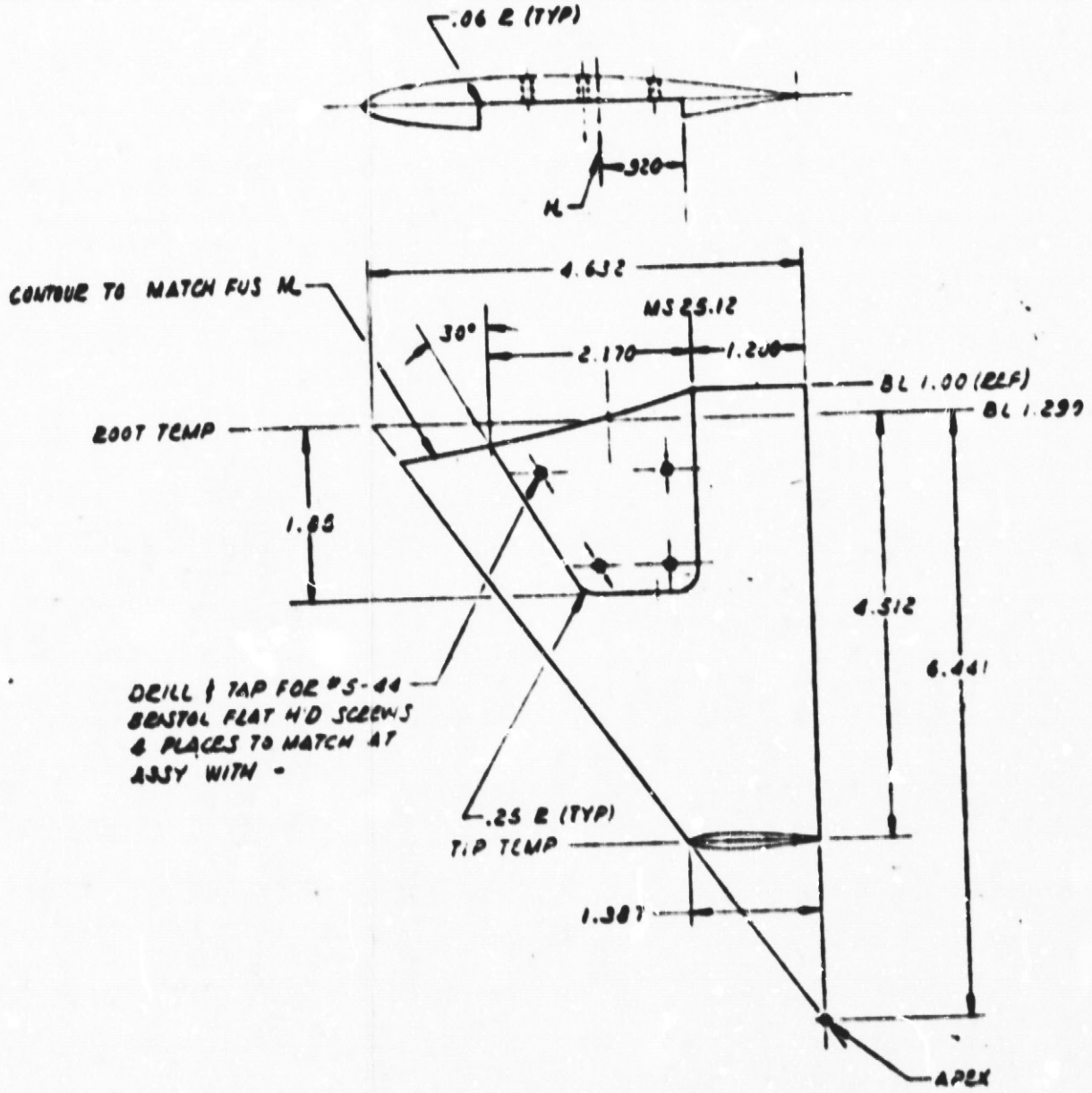

DETAIL -12 REVISED HORIZ TAIL L.H. (SHOWN)

-12 REVISED HORIZ TAIL TABLE OF ORD

%C	ROOT TEMP X	ROOT TEMP ±Y	TIP TEMP X	TIP TEMP ±Y
0	0	0	0	0
1.25	.058	.084	.017	.025
2.5	.116	.114	.035	.034
5	.232	.151	.069	.045
7.5	.347	.177	.104	.053
10	.463	.196	.139	.059
15	.695	.225	.208	.069
20	.926	.245	.277	.073
30	1.389	.270	.416	.081
40	1.853	.278	.555	.093
50	[illegible]	.270	[illegible]	.081
60	2.779	.246	.832	.074
70	3.242	.208	.971	.062
80	3.706	.154	1.110	.046
90	4.169	.086	1.249	.026
95	4.400	.048	1.318	.014
100	4.632	.006	1.387	.002
LER		.073		.022

H_4 HORIZONTAL TAIL

Figure 7.2-30. Wind Tunnel Model, 0.02 Scale Orbiter, 12,500-Pound-Payload Class (Sheet 2 of 3)

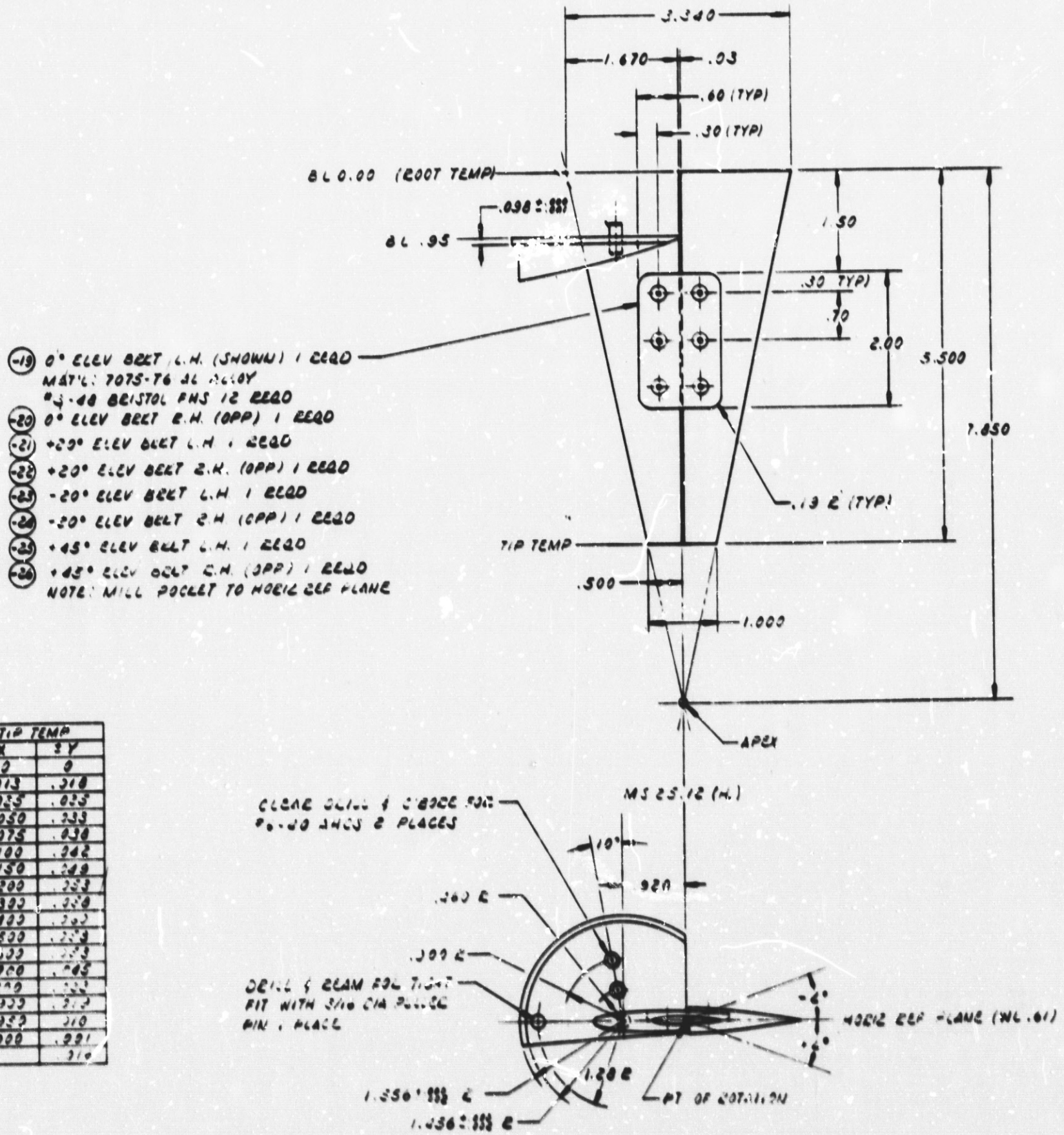

(-19) 0° ELEV BELT L.H. (SHOWN) 1 REQD
MAT'L: 7075-T6 AL ALLOY
#3-48 BRISTOL PHS 12 REQD
(-20) 0° ELEV BELT R.H. (OPP) 1 REQD
(-21) +20° ELEV BELT L.H. 1 REQD
(-22) +20° ELEV BELT R.H. (OPP) 1 REQD
(-23) -20° ELEV BELT L.H. 1 REQD
(-24) -20° ELEV BELT R.H. (OPP) 1 REQD
(-25) +45° ELEV BELT L.H. 1 REQD
(-26) +45° ELEV BELT R.H. (OPP) 1 REQD
NOTE: MILL POCKET TO HORIZ REF PLANE

% CHORD	ROOT TEMP X	ROOT TEMP ± Y	TIP TEMP X	TIP TEMP ± Y
0	0	0	0	0
.25	.342	.061	.013	.218
2.5	.084	.082	.025	.033
5	.167	.109	.050	.233
7.5	.251	.127	.075	.038
10	.334	.142	.100	.242
15	.501	.163	.150	.249
20	.668	.177	.200	.253
30	1.002	.195	.303	.258
40	1.336	.200	.403	.252
50	1.670	.195	.500	.253
60	2.004	.170	.603	.253
70	2.338	.132	.700	.245
80	2.672	.111	.800	.233
90	3.006	.062	.903	.213
95	3.173	.034	.953	.210
100	3.340	.034	1.000	.221
LE		.053		.210

DETAIL -17 TAPERED HORIZ STAB ASSY L.H. (SHOWN) 1 REQD (REF)

H_6 HORIZONTAL TAIL

FOLDOUT FRAME 1

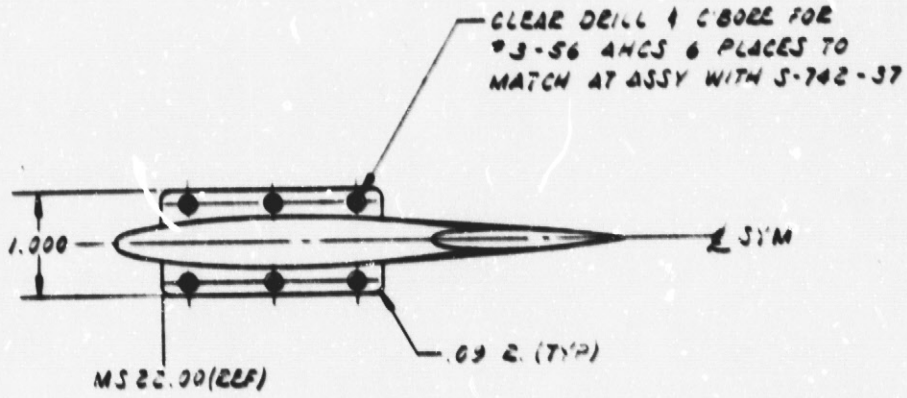

% CHORD	ROOT TEMP X	ROOT TEMP ±Y	TIP TEMP X	TIP TEMP ±Y
0	0	0	0	0
5	.205	.133	.091	.059
10	.415	.174	.182	.078
20	.821	.217	.365	.097
40	1.642	.246	.730	.109
60	2.463	.218	1.095	.097
80	3.284	.137	1.459	.060
95	3.899	.042	1.733	.018
100	4.105	.025	1.824	.002
LER		.065		.029

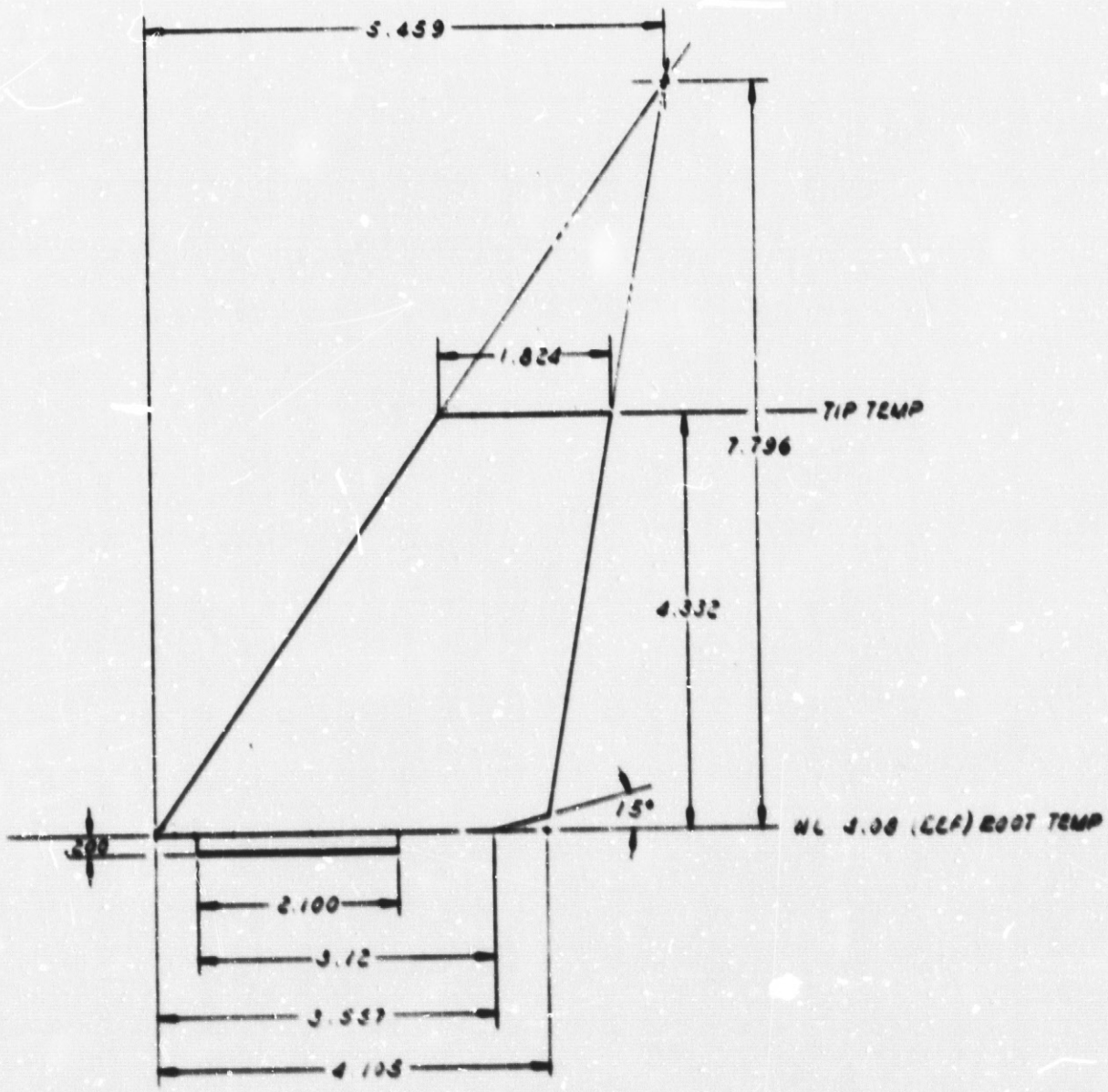

DETAIL -16 ALT VERT TAIL / CLAD (LER)

V_3 VERTICAL TAIL

Figure 7.2-30. Wind Tunnel Model, 0.02 Scale Orbiter, 12,500-Pound-Payload Class (Sheet 3 of 3)

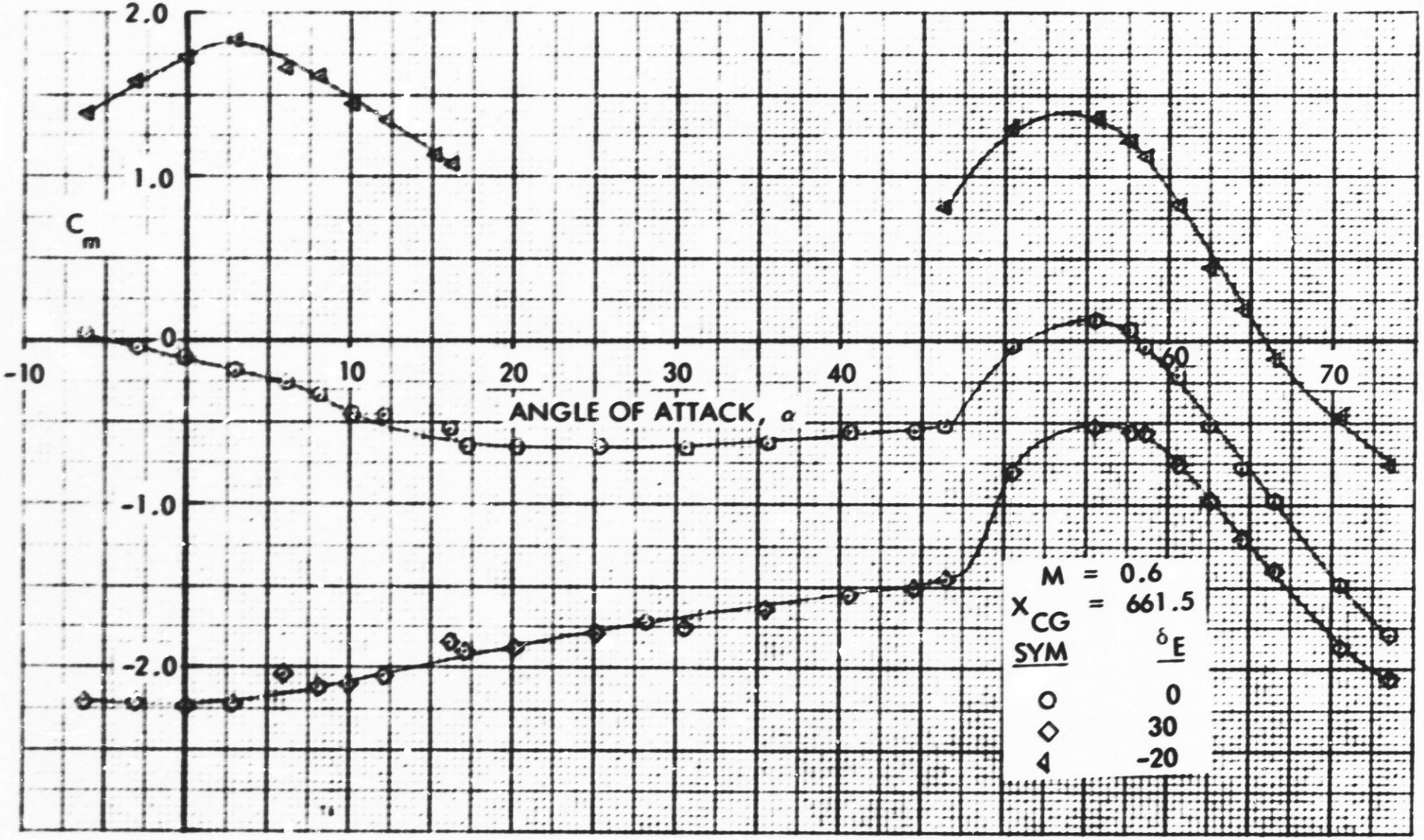

Figure 7.2-31. Longitudinal Pitching Moment Characteristics, $B_1W_1H_5$

Space Division
North American Rockwell

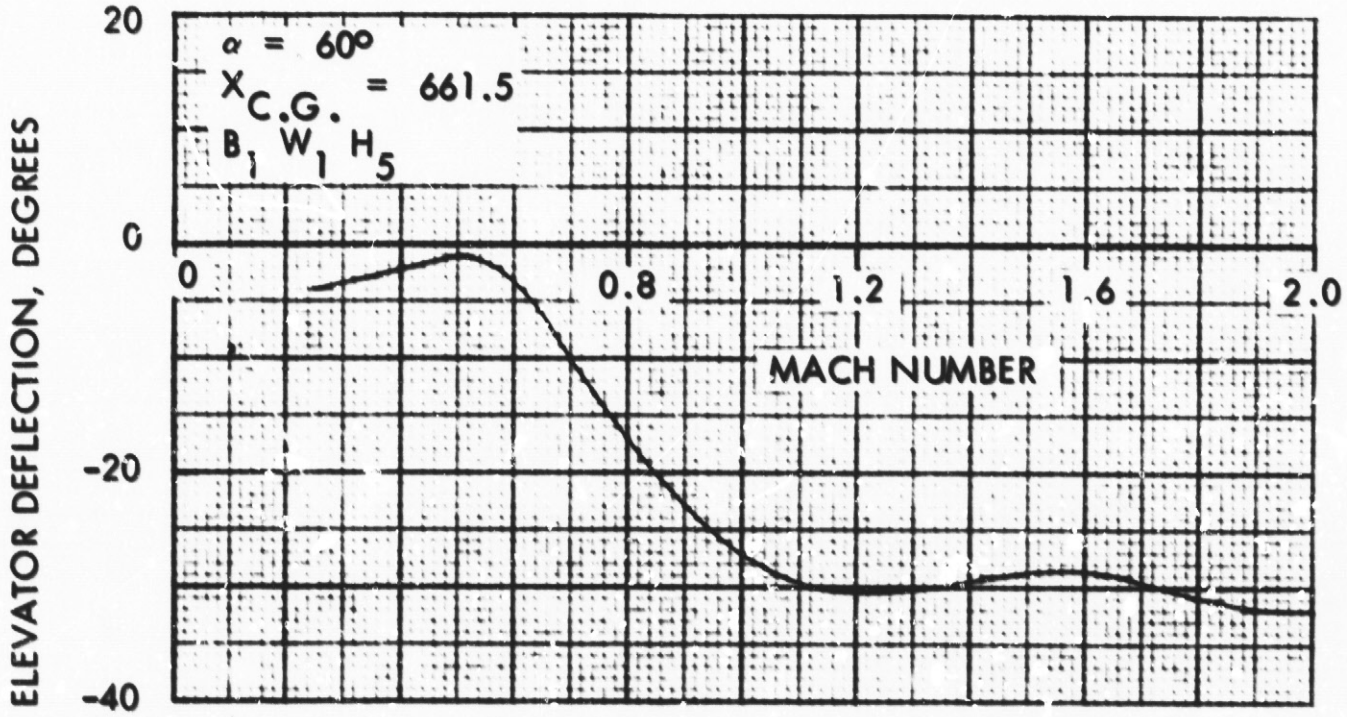

Figure 7.2-32. Elevator to Trim at 60-Degree Angle of Attack

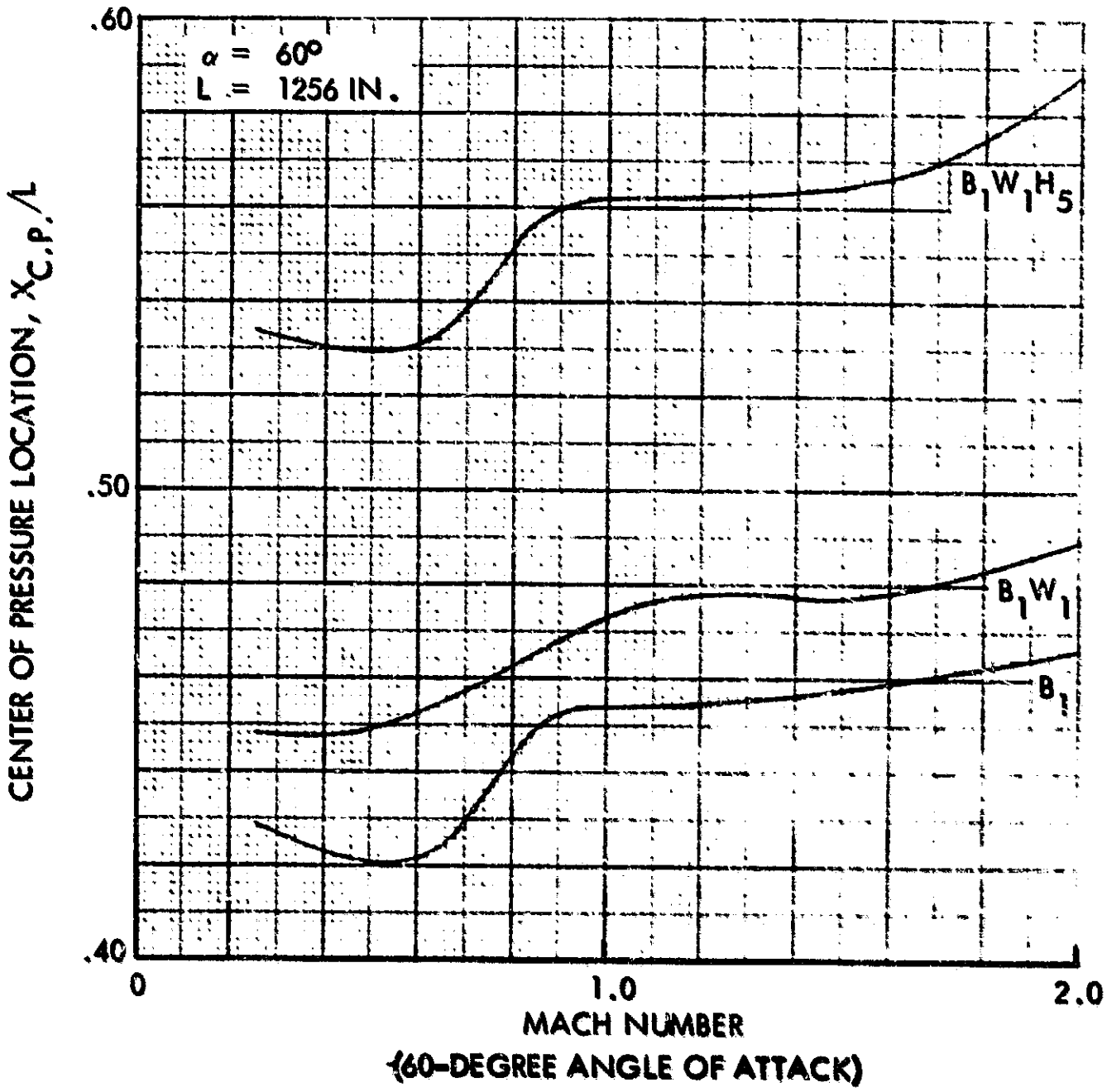

Figure 7.2-33. Center of Pressure Component Buildup (Sheet 1 of 2)

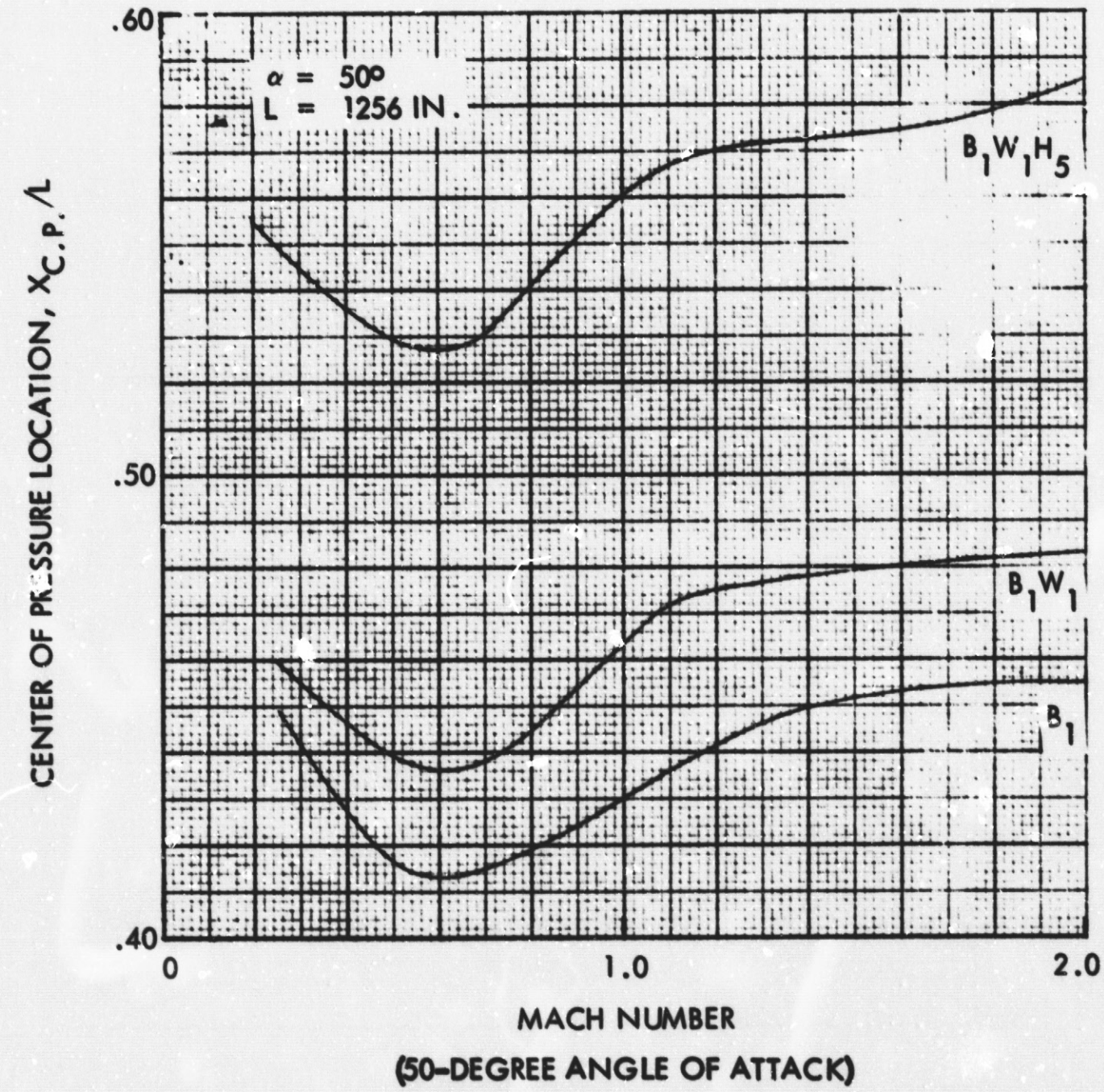

Figure 7.2-33. Center of Pressure Component Buildup (Sheet 2 of 2)

Reynolds numbers of the tests, direct application of the wind tunnel data to shuttle vehicle design can lead to erroneous conclusions in defining horizontal tail size requirements and in the lateral directional stability characteristics.

At high angles-of-attack, the fuselage experienced subcritical flow conditions in the wind tunnel, while actual flight conditions at a Mach number of 0.4 will be supercritical. The crossflow drag coefficient of the fuselage will be considerably less for supercritical flow as compared to subcritical (see Reference 7.2-1) if the horizontal were sized only for transition from a high angle-of-attack to cruise angle-of-attack at a Mach number of 0.4 and to provide cruise static stability, it would be significantly smaller than if based on subcritical fuselage crossflow. However, previous data indicates that at speeds greater than the critical Mach number (approximately 0.5 for a cylinder, Section 15 of Hoerner's "Fluid Dynamic Drag") the value of the crossflow drag coefficient based on either subcritical or supercritical Reynolds number is the same and has a value slightly greater than the subcritical value at lower Mach numbers. Since the vehicle must be trimmed at an angle-of-attack of 60 degrees at Mach numbers greater than the critical value, it appears that reducing the horizontal to that required in supercriticel flow is not warranted, and surface sizings should be based on the maximum body force anticipated.

The wind tunnel data indicated an increase (or "bump") in the body normal force coefficient at angles-of-attack of from 45 to 65 degrees due to adverse flow separation on the body. This phenomena was observed in both NASA tests at LRC (Reference 7.2-5) and the Ames tests in the 6 by 6-foot tunnel. The effect is illustrated in Figure 7.2-34. With control of the separation region on the body, it is believed that the positive "bump" in the C_N versus angle-of-attack curve would disappear.

The significance of the "bump" is in the estimation of elevator size required to perform the pitchdown maneuver (Figure 7.2-35) which shows the horizontal tail size required for a preliminary version of the 50,000 pound payload class orbiter.

Results of the wind tunnel test suggest that an alternate pitch-down flight mode could be developed which would permit reduction of the horizontal stabilizer size and possibly avoid the erratic lateral-directional behavior observed at Mach numbers below 1.5. One approach could be to perform the transition from high to cruise angle-of-attack in two steps: hold the initial 60-degree angle-of-attack until after the entry heating pulse is essentially over, then pitch down to a lower angle-of-attack, perhaps 40 degrees; maintain 40 degrees through transonic conditions, and pitch down to subsonic cruise. Another alternate mode would be to pitch down supersonically. Pitch dynamics, control, flight loads, transonic stability, and wing flutter characteristics must be analyzed to determine the best flight mode for pitch-down to cruise angle-of-attack.

Figure 7.2-34. Fuselage Normal Force Variation with Angle of Attack

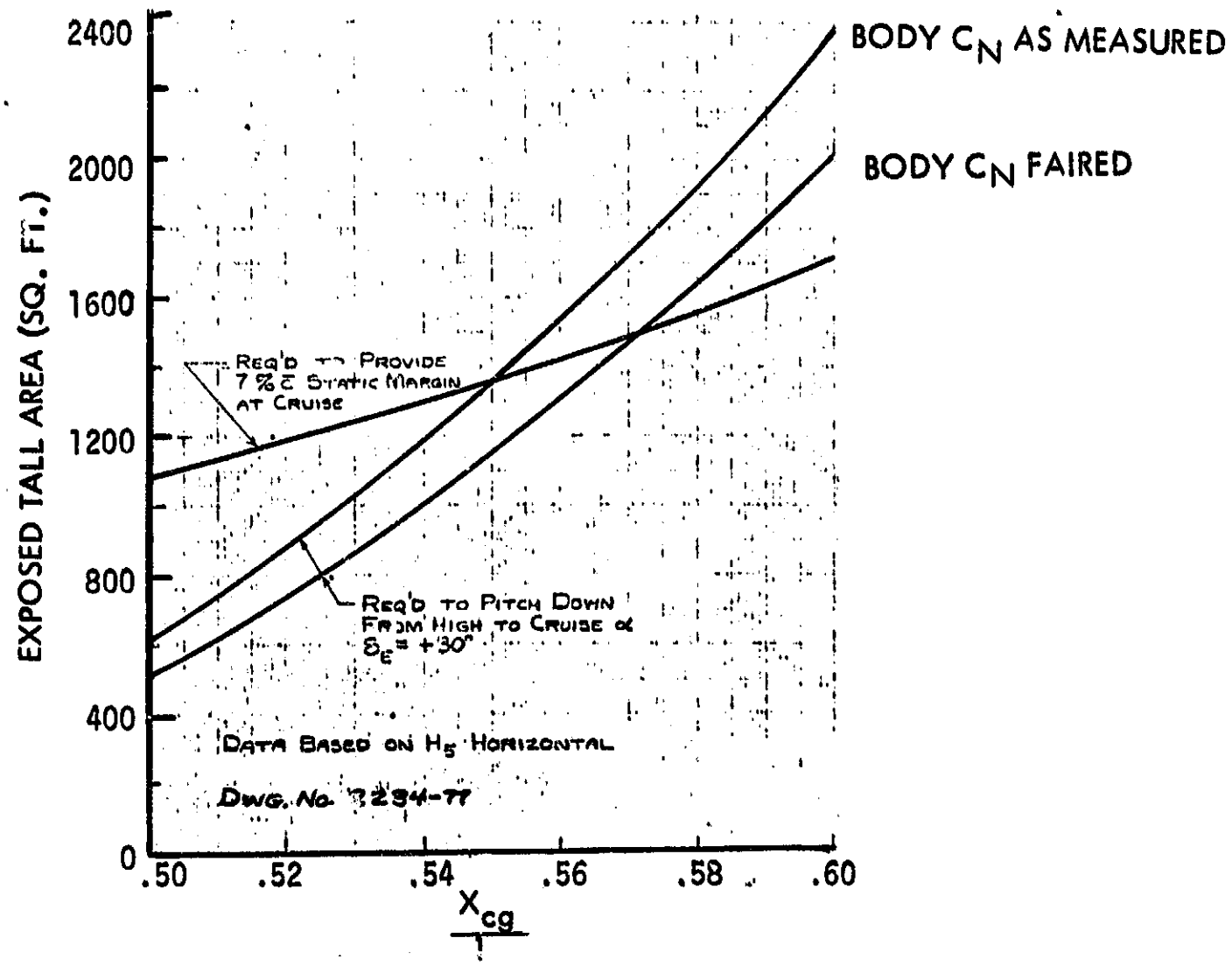

Figure 7.2-35. Effect of Fuselage Normal Force on Horizontal Tail Size Required for 50,000-Pound-Payload Orbiter

Figure 7.2-36 illustrates the effects of body nose shape on the body pitching moment and normal force characteristics. Because of the lower pitching moment occurring at high angles-of-attack, the rounded nose shape would require a smaller horizontal tail for pitchover to the low angle-of-attack for subsonic cruise. The two nose shapes tested were shown in Figure 7.2-30.

7.2.6 Conceptual Design Definition

The aerodynamic analyses supporting conceptual design of the 50,000-pound payload class system are reported herein. Aerodynamic characteristics of the 50,000-pound payload orbiter and booster are presented in this section; airloads are presented in Section 8.3. The subsonic, transonic, and supersonic aerodynamic derivatives were based on the results of wind tunnel tests conducted at the NASA-Langley and NASA-Ames Research Centers and were corrected for differing component planform areas and area centroids. Hypersonic characteristics were determined from Newtonian theory.

Composite Configuration

The 50,000-pound-payload class orbiter and booster mated configuration is illustrated in Figure 7.2-37. Estimates of zero-lift drag for the composite configuration during boost are presented in Figure 7.2-38. The data shown represent launch vehicle rocket engines burning (no aspiration) and orbiter stage engines not burning. Major subsonic drag items were the base and friction drags. At supersonic speeds the wave drag of the blunt nose, thick low sweep wings, and empennage were high. There is considerable uncertainty in the interference drag, and that shown was based on Titan III C experimental data. The drag due to lift is also shown in Figure 7.2-38. Estimation methods were the same as the 12,500-pound payload class configuration described in Section 7.2.3. These drag data were used for launch trajectory analyses (see Section 7.3.1).

Estimates of lift curve slope for the composite configuration during boost are presented in Figure 7.2-39. At transonic Mach condition, the data show an abrupt drop in C_{L_α} which is caused by the wing thickness ratio. This effect is desirable in terms of decreasing air loads in the transonic range. Lift characteristics at zero angle of attack are presented in Figure 7.2-39. The interference due to the influence of the orbiter wing vortex on the local flow field on the booster wing was estimated to be less than 7 percent.

Pitching moment data are presented in Figure 7.2-40 for the composite configuration. The same methods were used for estimation as were used on the lift curves. The data show the composite configuration to be stable

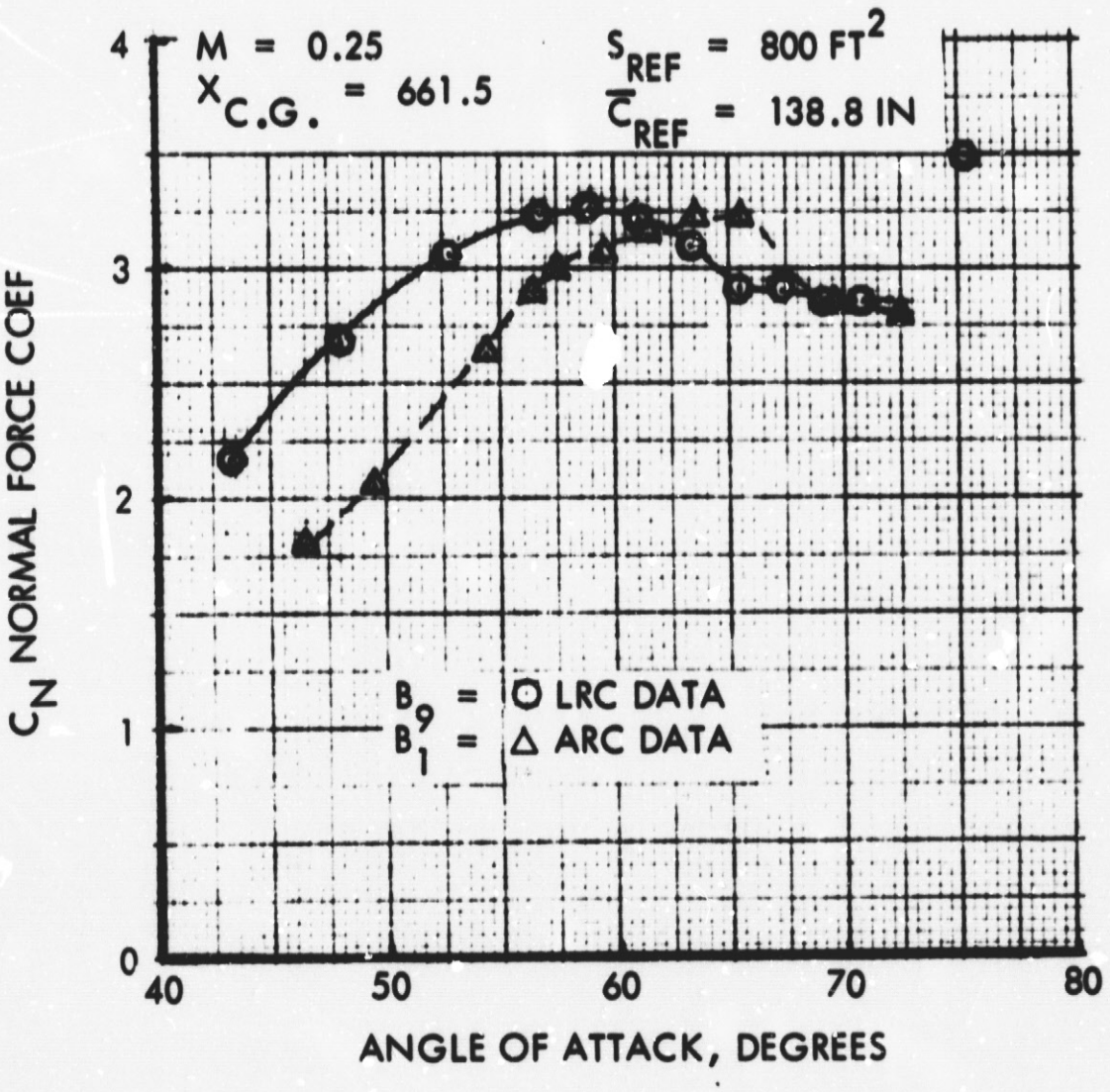

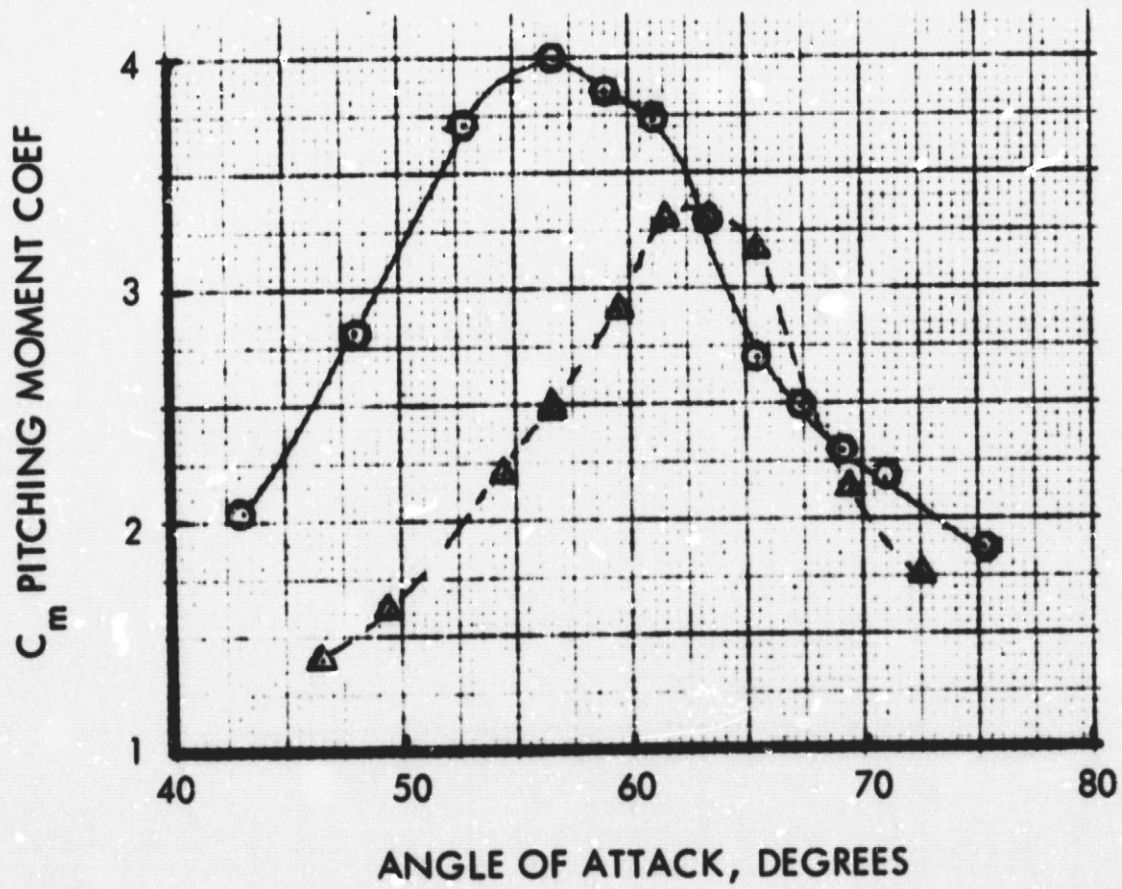

Figure 7.2-36. Effect of Body Nose Shape on Longitudinal Characteristics

PRECEDING PAGE BLANK NOT FILMED.

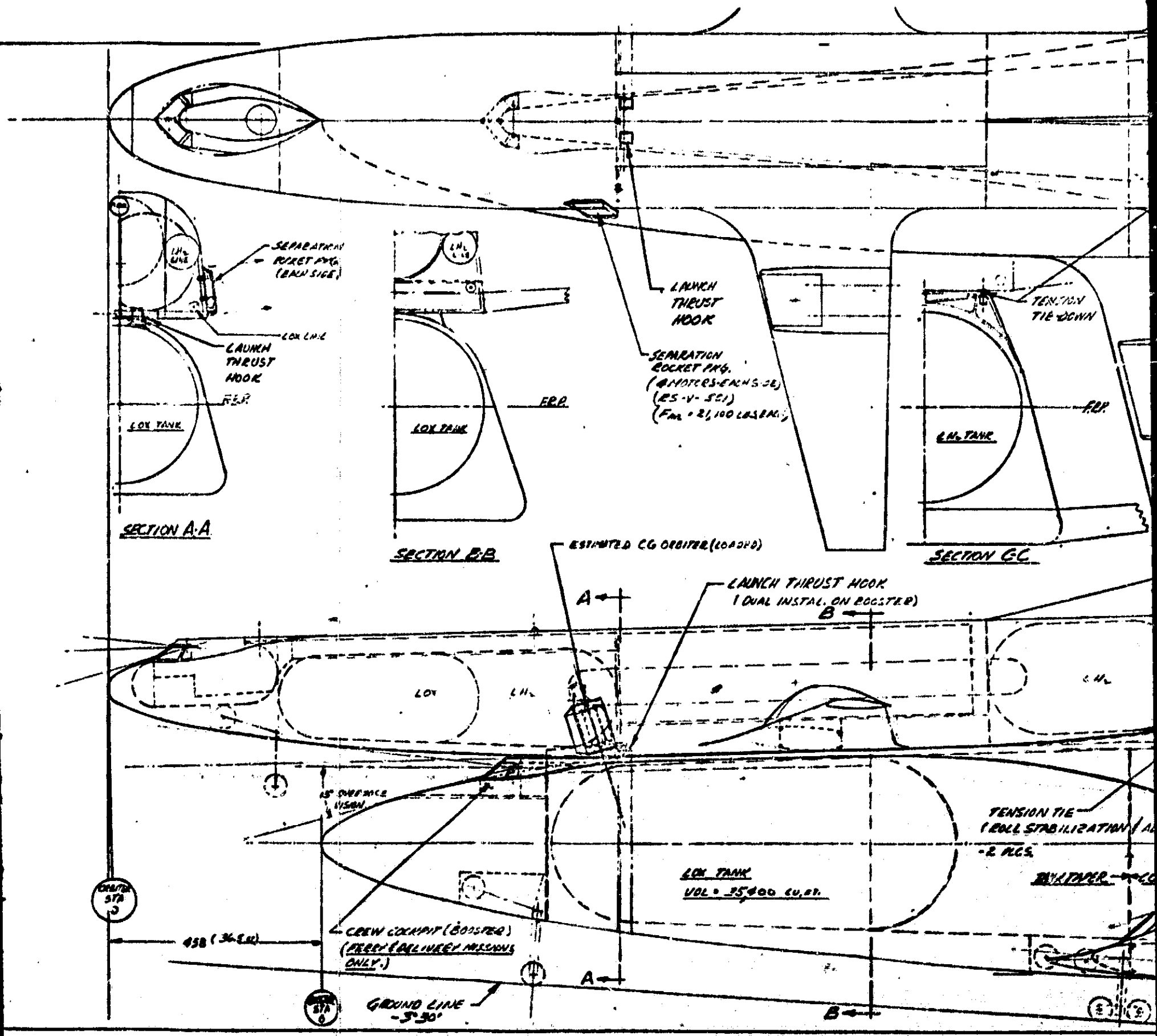

FOLDOUT FRAME 1

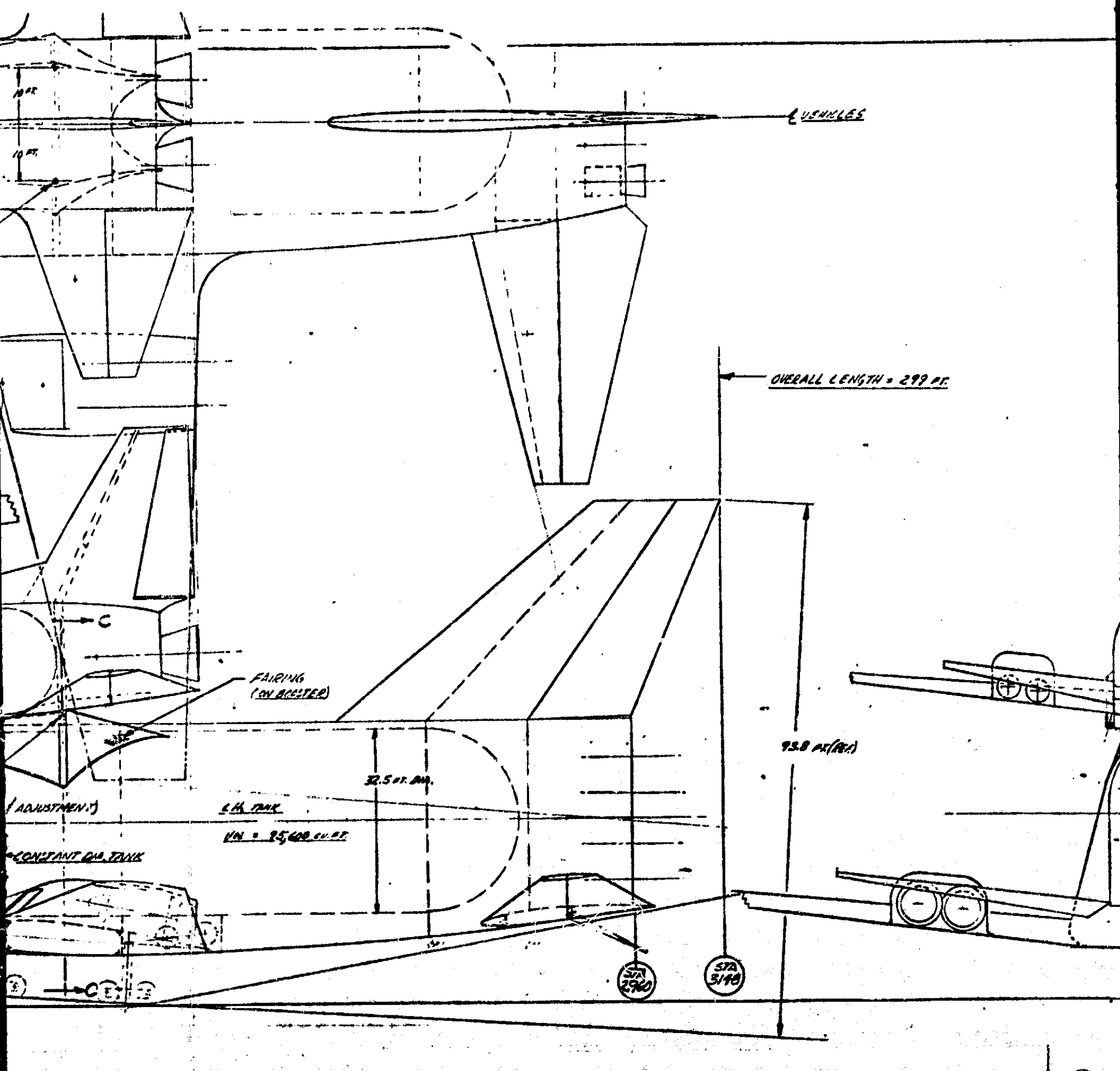

FOLDOUT FRAME 2

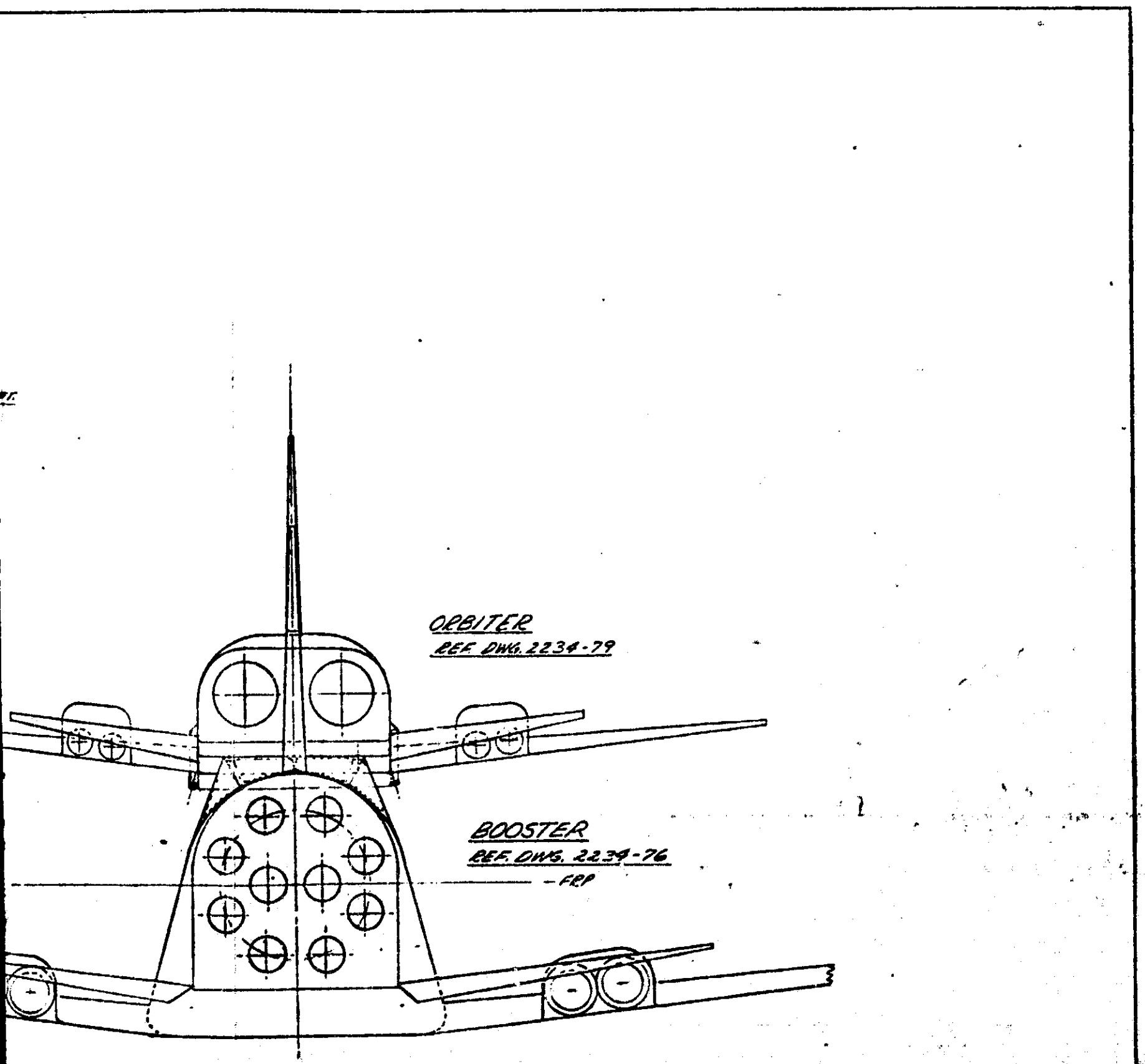

Figure 7.2-37. Orbiter-Booster Mated Configuration

FOLDOUT FRAME 3

UPSIZE PAGEMAT – 120% KEYLINE IMAGE AREA
BLOW UP CALLOUTS 120% – REDUCE TO 83% OF ORIGINAL

PLEASE MAKE CORRECTIONS ON TISSUE OVER LAYS
OR READING COPY IF AVAILABLE

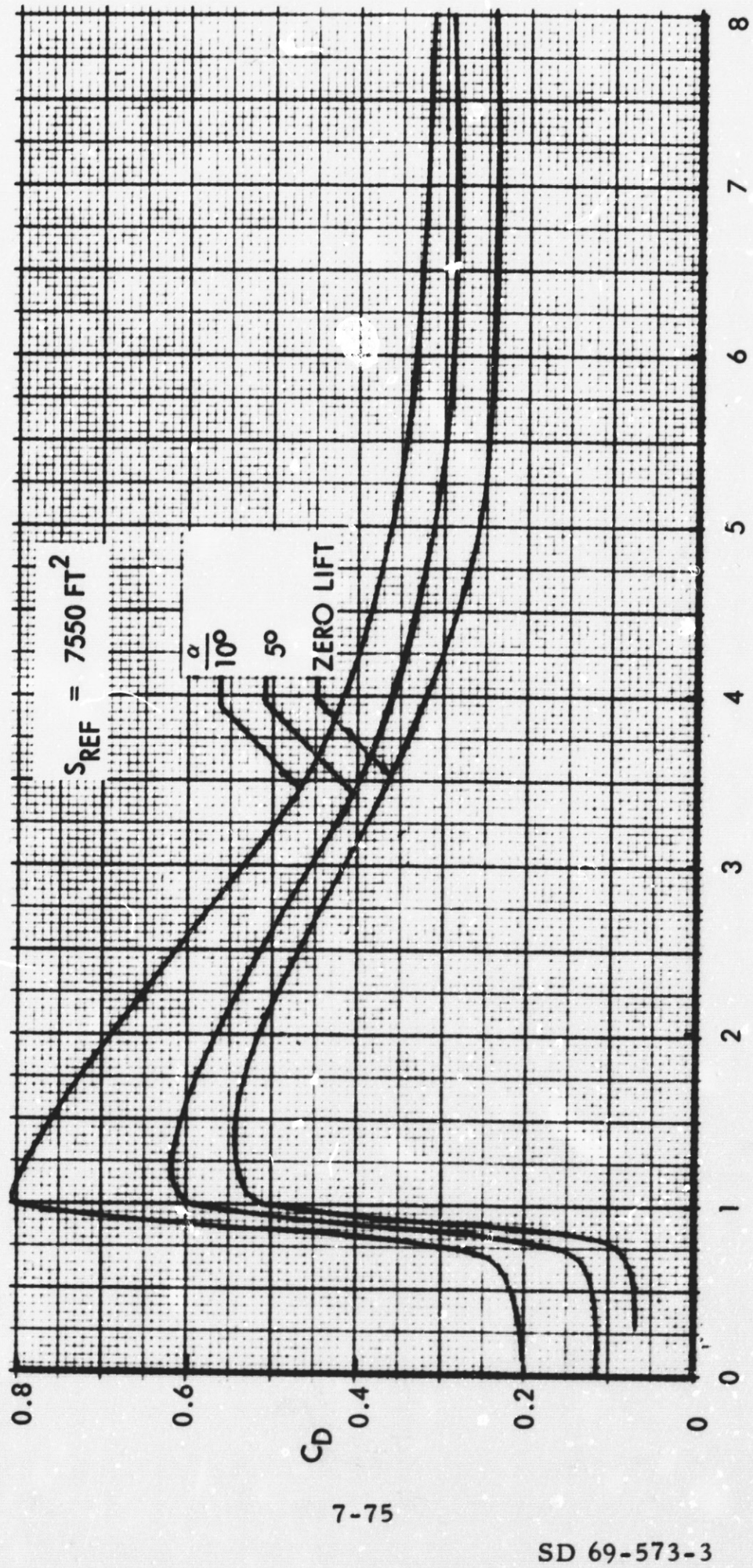

Figure 7.2-38. Drag Versus Mach Number, 50,000-Pound-Payload Class Composite Configuration

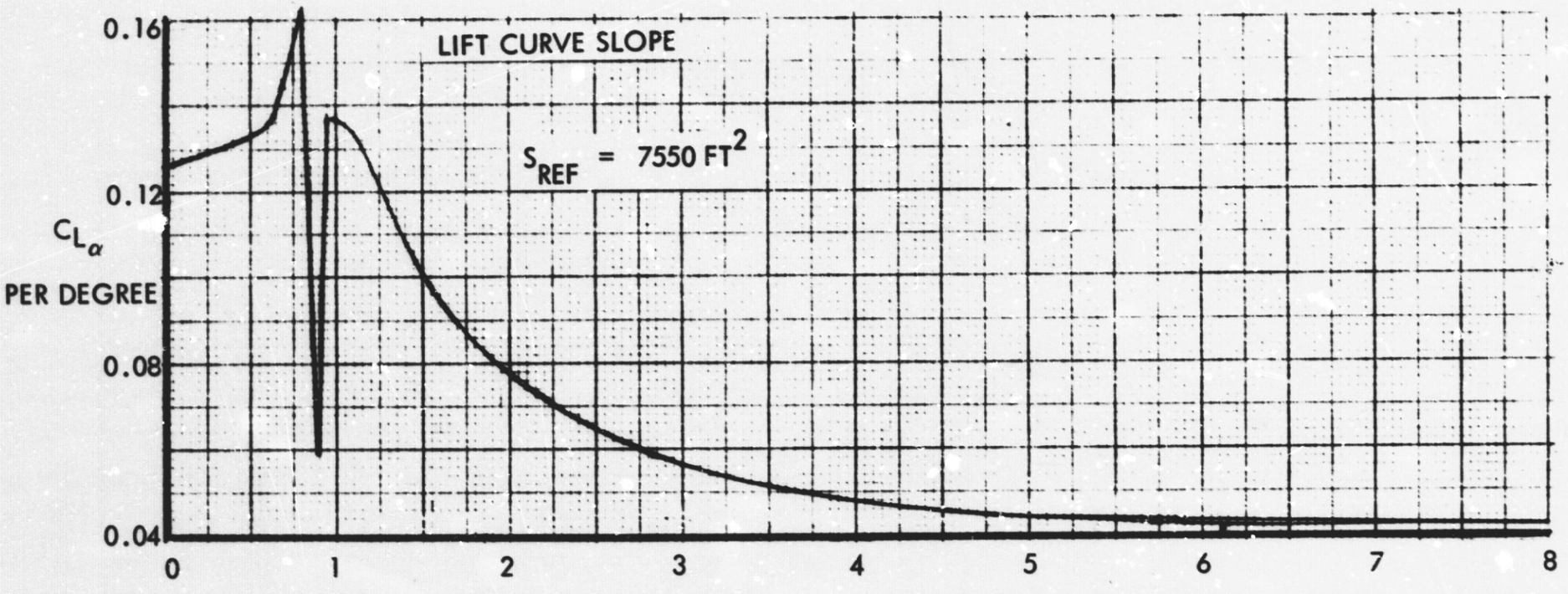

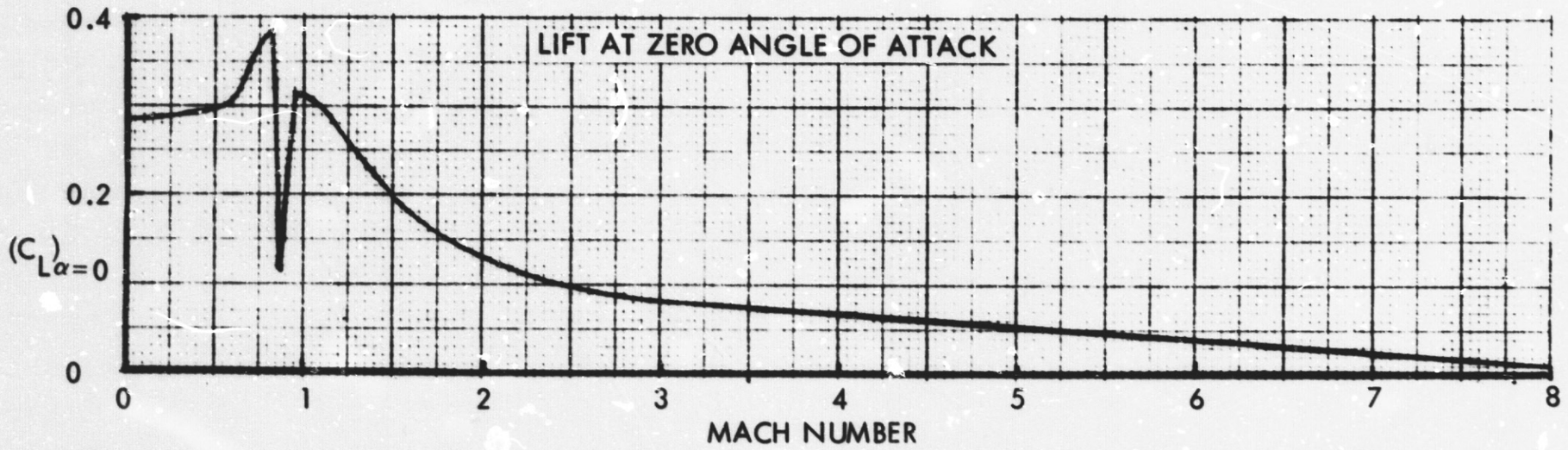

Figure 7.2-39. Lift Characteristics, 50,000-Pound-Payload Class Composite Configuration

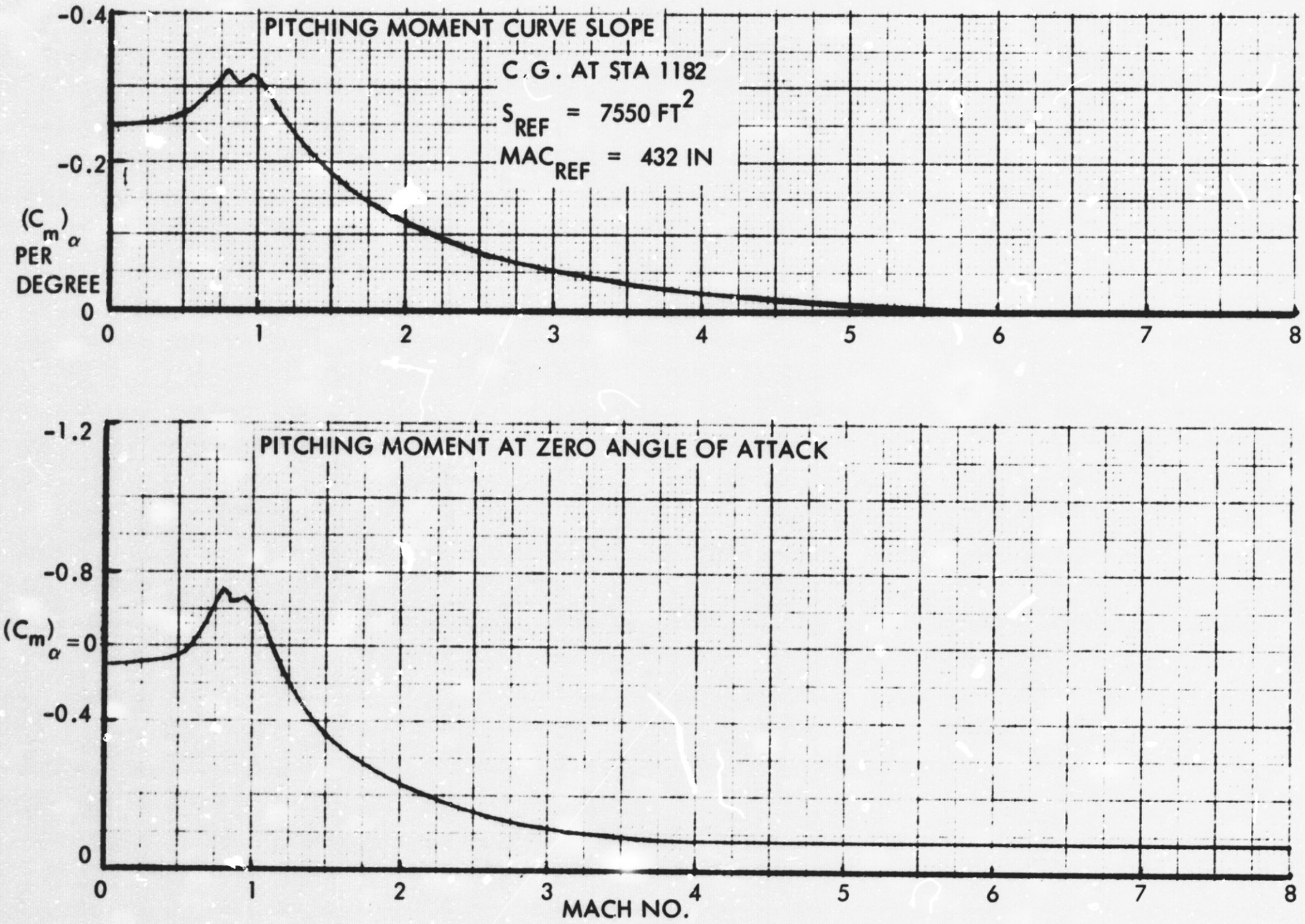

Figure 7.2-40. Pitching Moment Characteristics for 50,000-Pound-Payload Class Composite Configuration

Space Division
North American Rockwell

throughout the Mach number regime, with neutral stability at the hypersonic Mach numbers.

Orbiter Configuration

The 50,000-pound payload class orbiter configuration is illustrated in Figure 7.2-41. The orbiter hypersonic characteristics were evaluated by the Newtonian flow program and are shown in Figure 7.2-42. During reentry for the center of gravity at 58 percent of the body length, the configuration trims at a 44-degree angle-of-attack with zero elevator deflection, and at a 60-degree angle-of-attack with -24 degree deflection. The C_L at a 60-degree angle-of-attack is estimated to be 2.11, yielding a W/C_LS at entry of 42 pounds per square foot. Lift-to-drag ratio at a 60-degree angle-of-attack is 0.53. Subsonic characteristics are also illustrated. Maximum lift-to-drag ratio is 7.3 at about 5 degrees angle-of-attack.

The variation of the required exposed area of the horizontal tail for the 50,000-pound payload orbiter is shown in Figure 7.2-43. The criteria that establish horizontal tail size are the requirements to pitch down from high to cruise angle-of-attack and to provide a longitudinal static stability margin during cruise. The effect of these two requirements are illustrated. Three curves are shown for the horizontal tail size to perform the pitch down maneuver. One curve represents the area required to overcome the fuselage positive pitching moment as measured in the ARC tests including the positive "bump" in the C_N versus angle-of-attack curve at a high angle-of-attack as discussed previously (Figure 7.2-34). With control of the separation region on the body it is believed that the positive "bump" would disappear. Thus, the second curve represents a fairing of the body C_N versus angle-of-attack curve to remove this "bump". The model used in the ARC tests incorporated a small fixed flap aft of the body. The third curve shown represents an aft flap deflected 30 degrees and is the elevator effectiveness data used for design.

The horizontal tail area required to provide static stability margins at cruise of seven and zero percent are also shown in Figure 7.2-44. As indicated, for center-of-gravity locations forward of 58 percent of the length of the fuselage, the cruise stability margin requirement is critical in establishing the horizontal surface size.

Weight and balance estimates indicate the nominal orbiter center-of-gravity location at entry is 58 percent of the body length. The forward limit on center of gravity is established by hypersonic trim requirements. A forward travel of approximately 2 feet can be tolerated while still achieving trim at a 60-degree angle-of-attack. This would be accomplished

ITEM		
WING		
AREA (TOTAL)	FT^2	2890
ASPECT RATIO		7
TAPER RATIO		0.33
AIRFOIL		0014-64 ROOT 0012-64 TIP
M.A.C. (TOTAL)	FT	21.4
HORIZONTAL SURFACE		
AREA (EXPOSED)	FT^2	1150
ASPECT RATIO		3.0
TAPER RATIO		0.30
ELEVATOR AREA	FT^2	575
VERTICAL SURFACE		
AREA (EXPOSED)	FT^2	900
ASPECT RATIO		1.4
TAPER RATIO		0.36
RUDDER AREA	FT^2	300
AERODYNAMIC PERF		
PLANFORM AREA	FT^2	8190
PLANFORM LOADING	PSF	31
HYPERSONIC L/D		0.52
ENTRY LIFT LDG W/C_LS	PSF	42
SUBSONIC WING LDG	PSF	88
TOUCHDOWN SPEED	KNOTS	128

Figure 7.2-41. Orbiter Aerodynamic Configuration, 50,000-Pound-Payload Orbiter

Space Division
North American Rockwell

HYPERSONIC

TRIMMABLE AT HIGH & LOW α
L/D = 0.53 AT α = 60°

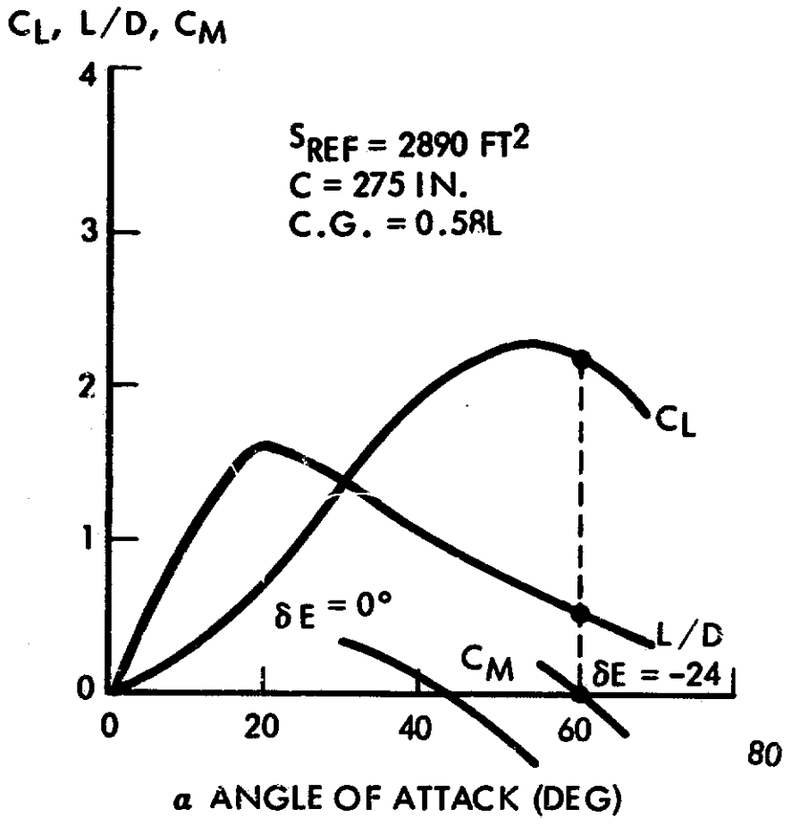

TRANSITION / GLIDE

TRIMMABLE AT HIGH & LOW α
$(L/D)_{MAX}$ = 7.3

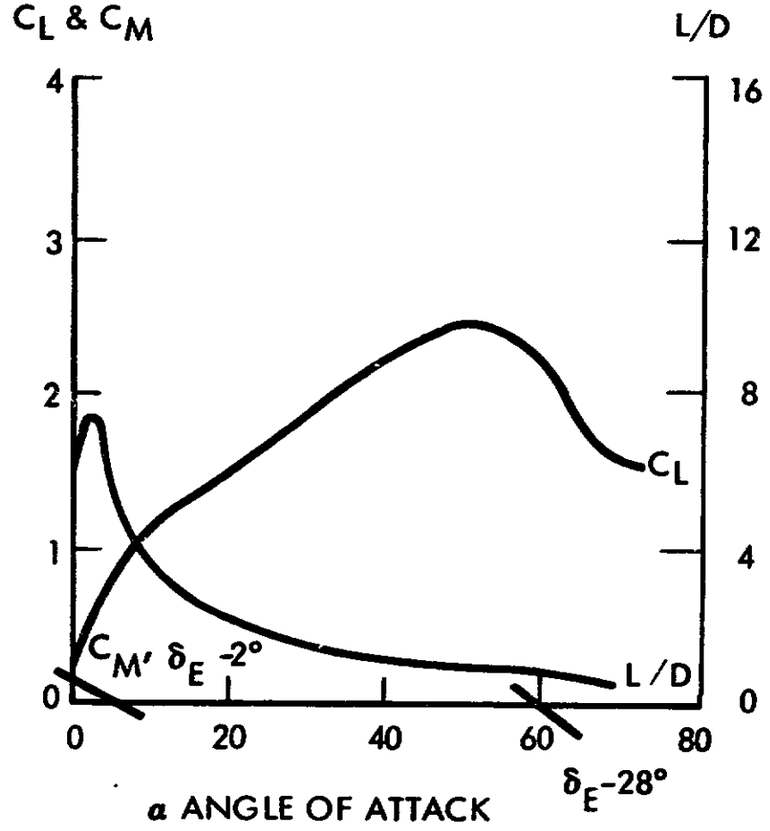

Figure 7.2-42. Orbiter Longitudinal Aerodynamic Characteristics, 50,000-Pound Payload Class

Space Division
North American Rockwell

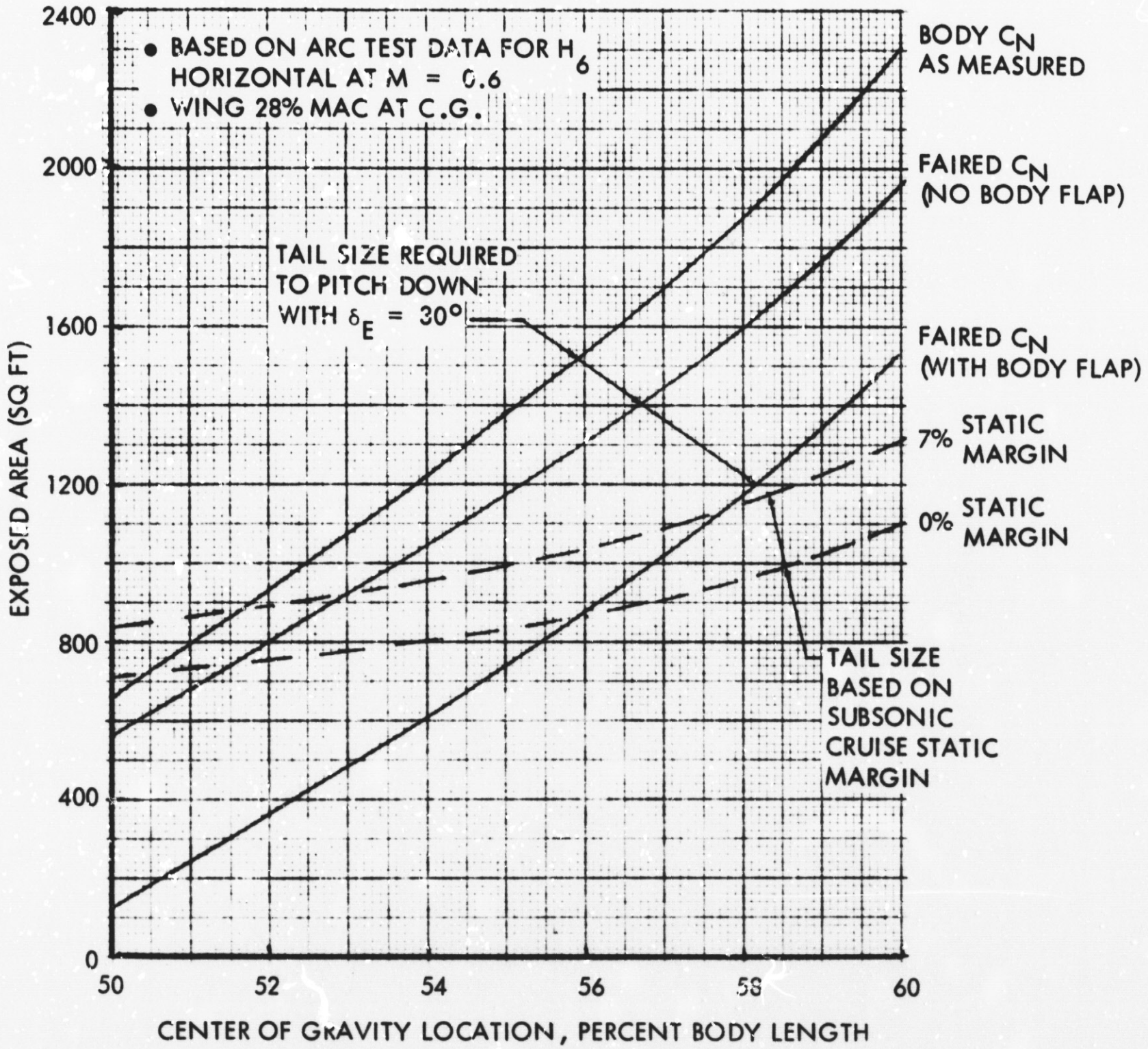

Figure 7.2-43. Horizontal Tail Size for 50,000-Pound Payload Orbiter

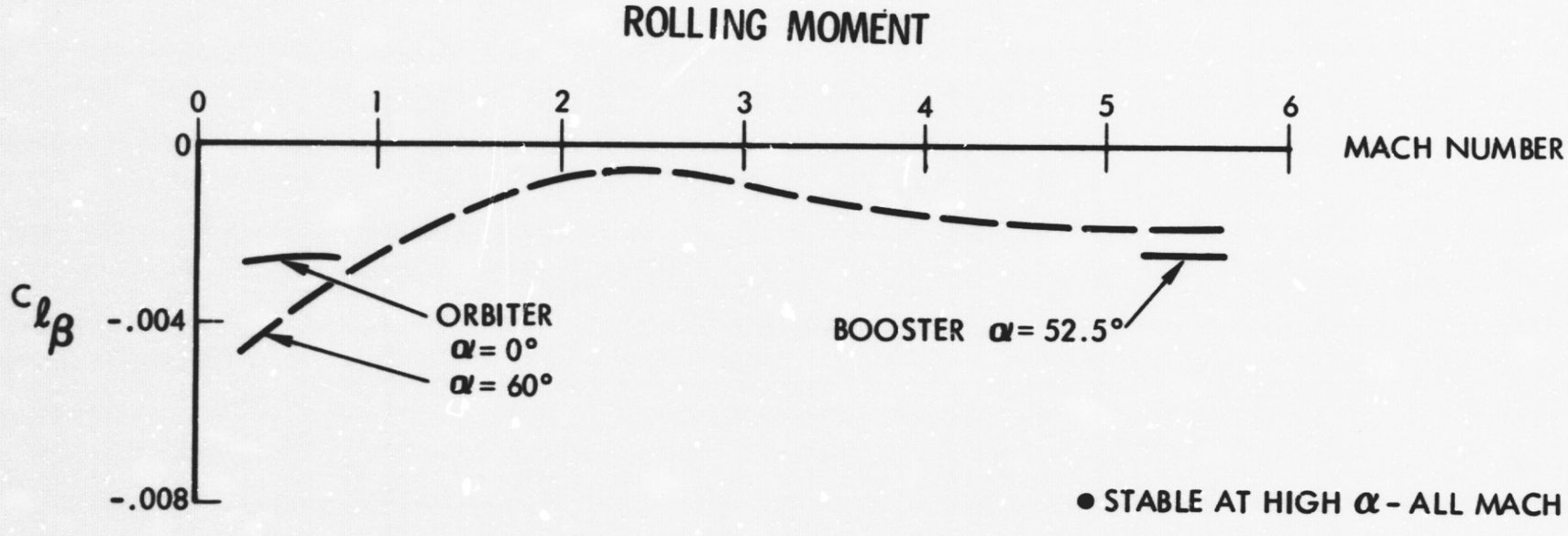

- STABLE AT HIGH α - ALL MACH NUMBERS
- 6 DOF SIMULATION CONFIRMS STABILITY & CONTROLLABILITY

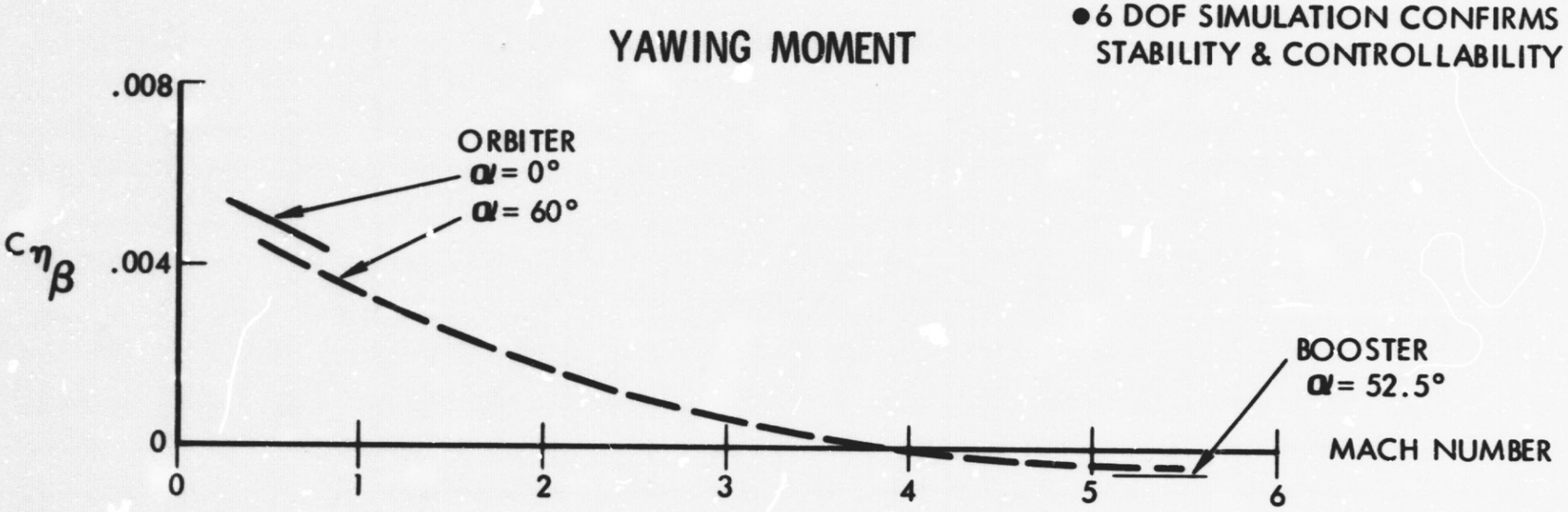

Figure 7.2-44. Lateral-Directional Characteristics

Space Division
North American Rockwell

with all of the elevator (50 percent of the planform) deflected out of the flow. To increase the margin on forward travel of the center of gravity would require redesign of the horizontal, such as relocating the hinge line. The aft limit on center of gravity travel is about 18 inches, where the static margin for subsonic cruise would be zero percent as compared to 7 percent for the nominal center of gravity location. These limits on vehicle center of gravity at entry were related to excursions in center of gravity of the 50,000-pound payload. The forward center of gravity limit corresponds to an 8-foot movement of the cargo center of gravity, while a 6.2-foot aft movement of the cargo center of gravity is allowable.

Lateral directional characteristics versus Mach number for high and low angles of attack are shown in Figure 7.2-44. Hypersonic data were estimated with the Newtonian flow program. ARC wind tunnel results from the 0.02 scale orbiter model were used for Mach numbers of 2.0 and below. The configuration exhibits static stability at all conditions with an essentially neutral directional derivative at hypersonic conditions.

Additional analyses should be made to optimize the cruise static margin for the shuttle system. Conventional fighter aircraft and operational passenger transports have static margins of approximately 0.05 times the mean aerodynamic chord. The Boeing SST incorporates a flight regime at negative static margin. However, flight at negative static margins requires considerable sophisticated attitude control equipment, including the capability to sense and correct for atmospheric perturbations such as gusts, winds, etc.

Booster Configuration

The booster aerodynamic characteristics were based on analysis of a preliminary configuration shown in drawing NR-2234-69, Figure 7.2-45. The aerodynamic data presented for this configuration is considered to be representative of the final booster aerodynamic configuration illustrated in Figure 7.2-46.

The subsonic and hypersonic longitudinal characteristics are presented in Figure 7.2-47. Subsonic performance was evaluated by use of parametric and Langley Research Center test data. The maximum lift-to-drag ratio was estimated to be 8.4 from the corrected Langley wind tunnel test data.

The booster hypersonic characteristics were obtained by using the NR Newtonian flow program. The booster trims at C_L maximum at a 52.5 degree angle of attack with the elevator trailing edge deflected up 7 degrees. The hypersonic (C_L) maximum and the corresponding lift-to-drag ratio were 1.86 and 0.69, respectively. The lateral directional stability characteristics were presented earlier in Figure 7.2-44. These data reflect a 7-degree

PRECEDING PAGE BLANK NOT FILMED.

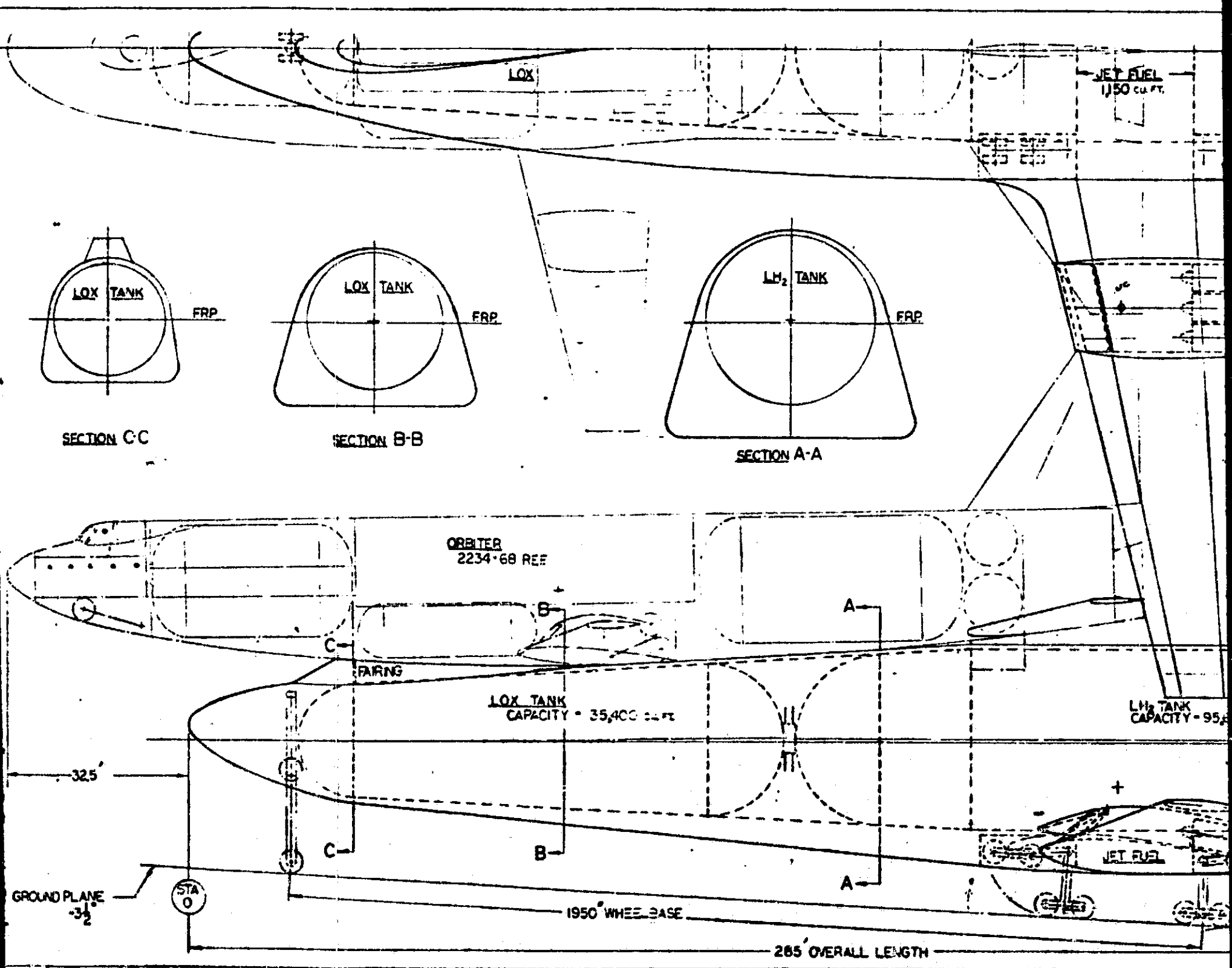

FOLDOUT FRAME 1

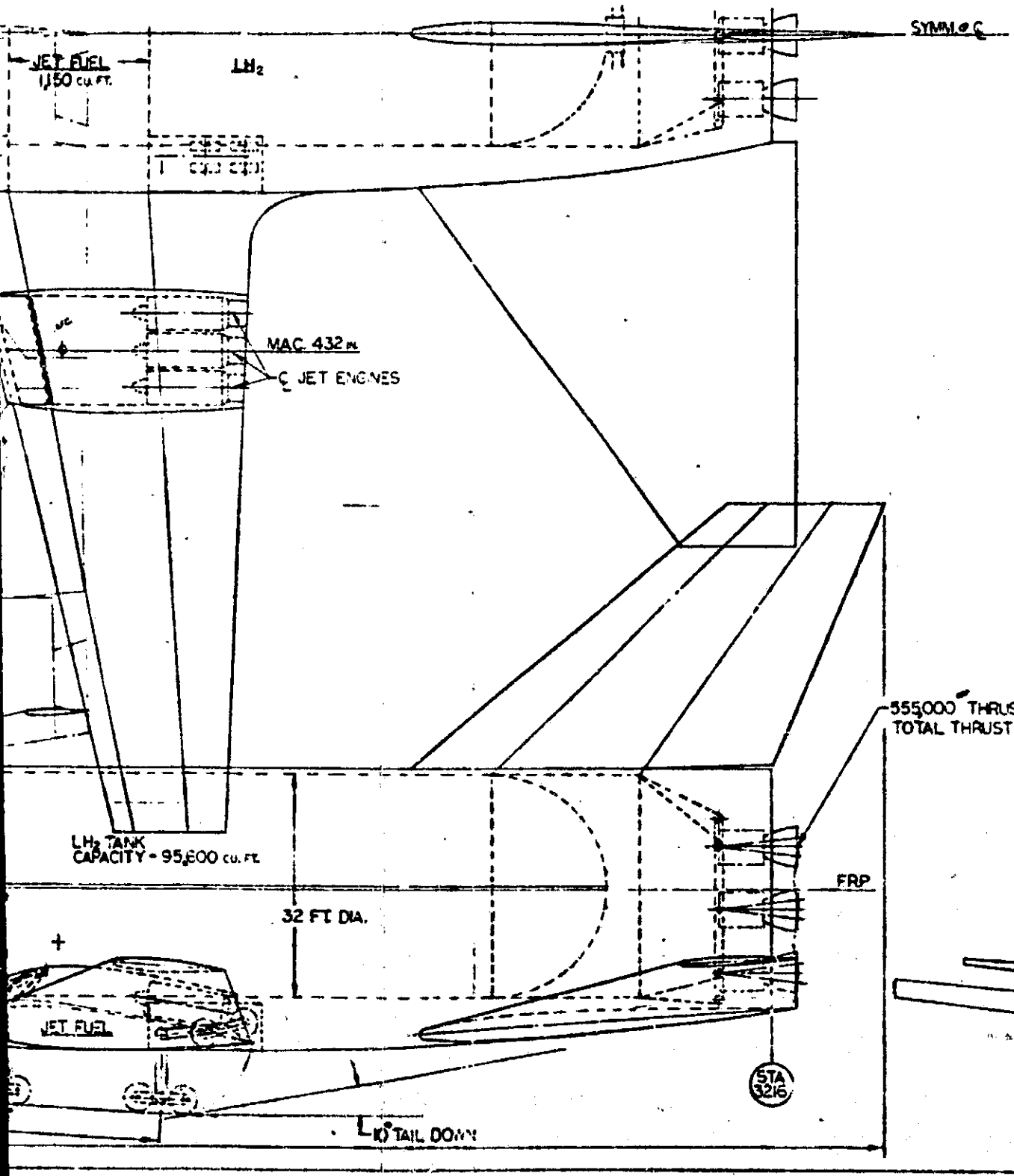

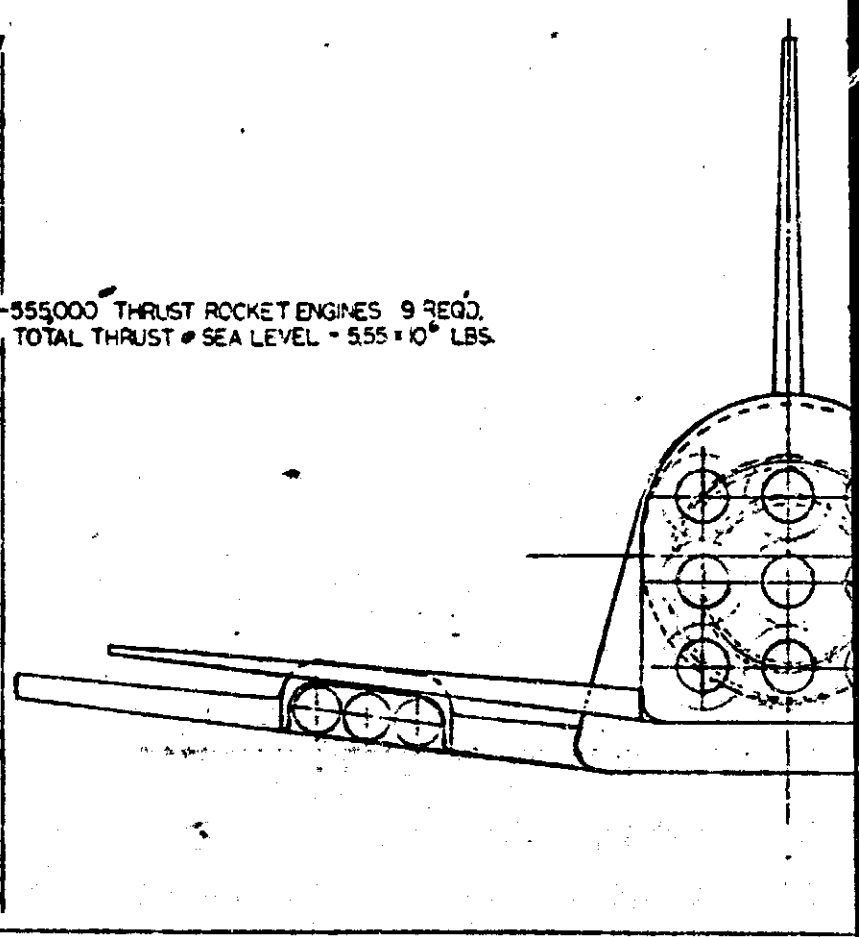

FOLDOUT FRAME 2

WING GEOMETRY

S_W = 7,550 sq. ft.
SPAN = 230 ft.
C_R = 49.8 ft.
C_T = 15.9 ft.
Λ_{LE} = 14°
λ = .319

STAGE WEIGHTS

PROPELLANT (LOX & LH_2)	=	2,600,000 LBS.
TOTAL LAUNCH	=	3,150,000 LBS.
REENTRY	=	550,000 LBS.
LANDING	=	494,000 LBS

TOTAL PLANFORM AREAS

S_{WING} = 7,550 sq. ft. $\left(\frac{W}{S_W} = 70 \text{ LDG.}\right)$

$S_{FUS.}$ = 11,310 sq. ft.

TOTAL = 18,860 sq. ft. $\left(\frac{W}{S}_{TOTAL} = 30 \text{ REENTRY}\right)$

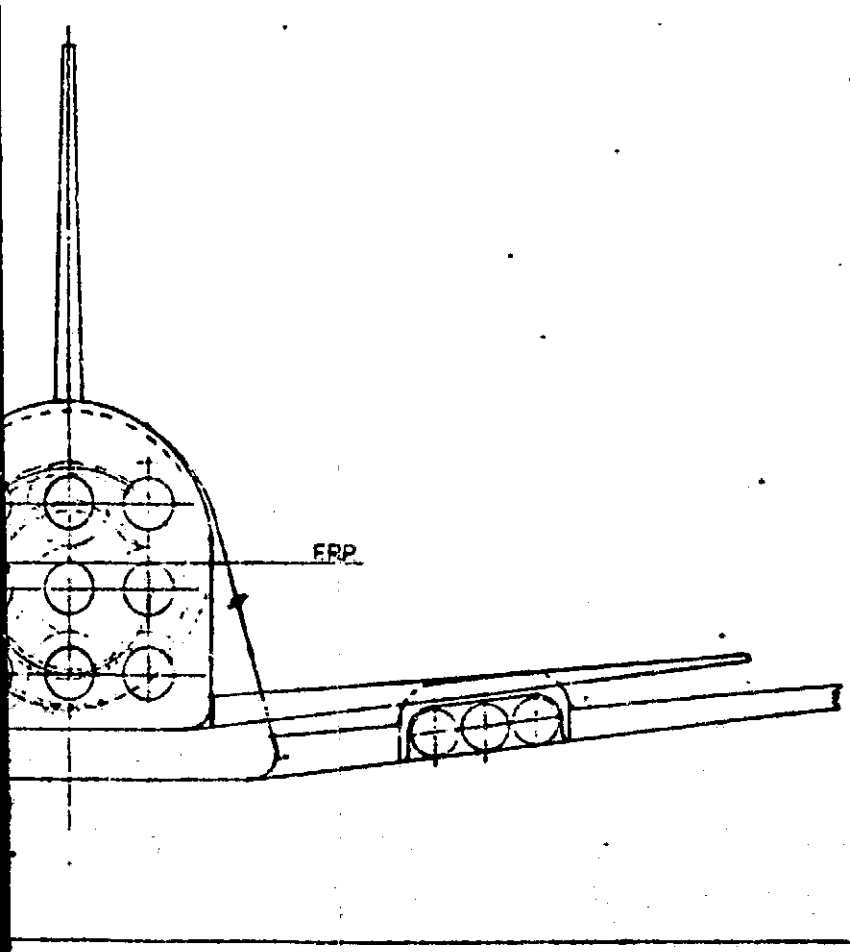

Figure 7.2-45. Launch Vehicle Configuration Concept

FOLDOUT FRAME 3

UPSIZE PAGEMAT – 120% KEYLINE IMAGE AREA
BLOW UP CALLOUTS 120% - REDUCE TO 83% OF ORIGINAL

PLEASE MAKE CORRECTIONS ON TISSUE OVERLAYS,
OR READING COPY IF AVAILABLE

ITEM		
WING		
AREA (TOTAL)	FT^2	7550
ASPECT RATIO		7.0
TAPER RATIO		0.32
AIRFOIL		0014-64 ROOT 0012-64 TIP
M.A.C.	FT	36
HORIZONTAL SURFACE		
AREA (EXPOSED)	FT^2	1800
ASPECT RATIO		4.5
TAPER RATIO		0.3
ELEVATOR AREA	FT^2	120
VERTICAL SURFACE		
AREA (EXPOSED)	FT^2	1408
ASPECT RATIO		1.05
TAPER RATIO		0.43
RUDDER AREA	FT^2	470
AERODYNAMIC PERF		
PLANFORM AREA	FT^2	18350
PLANFORM LOADING	PSF	29
HYPERSONIC L/D		0.69
ENTRY LIFT LDG W/C_LS	PSF	27
SUBSONIC WING LDG	PSF	63
TOUCHDOWN SPEED	KNOTS	112

Figure 7.2-46. Booster Aerodynamic Configuration, 50,000-Pound Payload Class

Space Division
North American Rockwell

HYPERSONIC

TRIMMABLE AT HIGH & LOW α
ENTER AT C_L MAX = 1.87
PITCH MODULATION CONTROLS G'S
L/D = 0.69 AT α = 52.5°

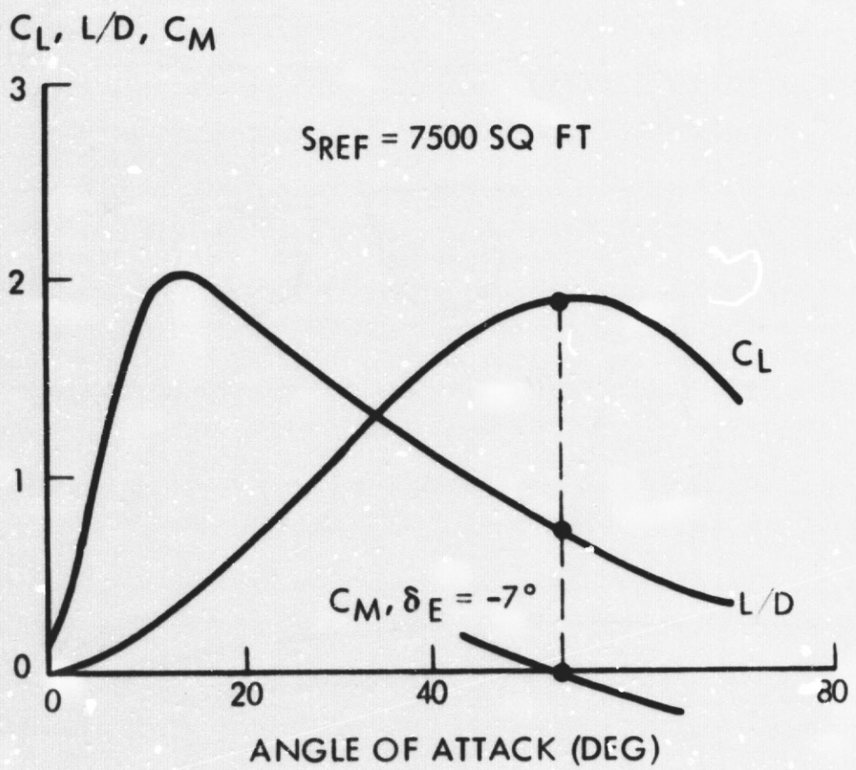

TRANSITION / CRUISE

TRIMMABLE AT HIGH & LOW α
$(L/D)_{MAX}$ = 8.4

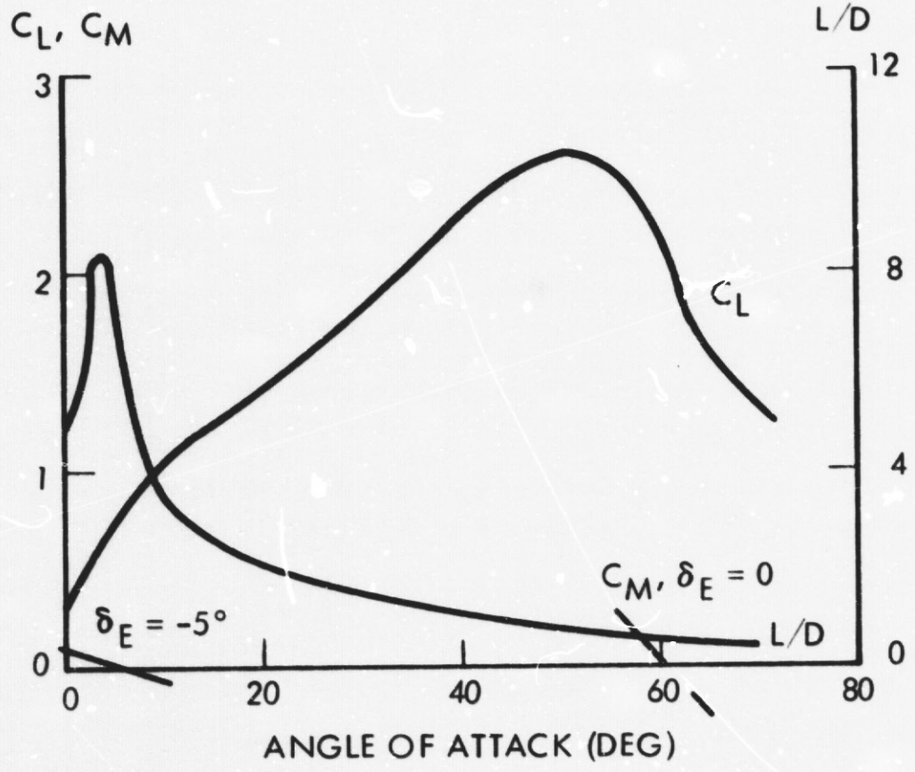

Figure 7.2-47. Booster Aerodynamics, 50,000-Pound Payload Orbiter

SD 69-573-3

Space Division
North American Rockwell

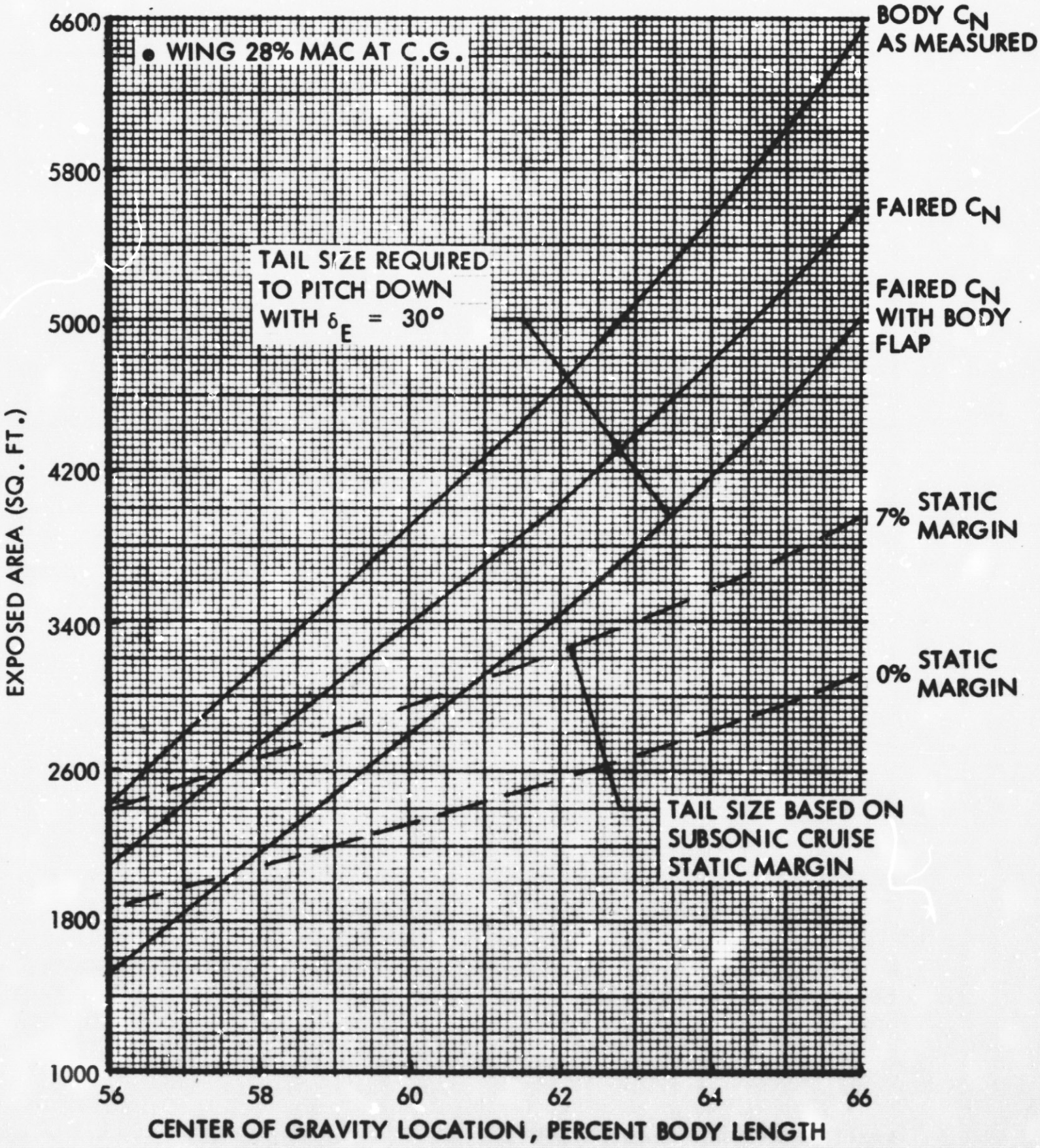

Figure 7.2-48. Effect of Body Center of Gravity Location on Booster Tail Size

dihedral on the horizontal tail and exhibit a slightly unstable derivative at a 52.5-degree angle of attack.

The variation of the required exposed area of the horizontal tail with the center of gravity for the baseline booster is presented in Figure 7.2-48. for the wing located with the 28-percent mean aerodynamic chord at the body's center of gravity. The criteria that establish horizontal tail size for the booster are the same as those applied to the orbiter and provide a longitudinal stability margin during cruise and during pitch down from high to cruise angle of attack. Three curves are shown for the horizontal tail size required to perform the pitch down maneuver. One curve represents the area required to overcome the wing body pitching moment. The second and third curves represent the elimination of the positive "bump" in C_N versus the angle-of-attack curve as measured in the ARC test. The effect of a 1200-square foot flap located under the body and deflected 30 degrees is also shown. The flap is hinged with the elevator. As in the case of the orbiter, it is believed that with control of the separation region on the body, the positive "bump" in C_N and in C_m would disappear, thus the tail size for pitch down was based on the "faired" C_N curve. The horizontal tail area required to provide static stability margins at cruise of seven and zero percent also are shown. As indicated on the figure, for a center-of-gravity location forward of 61 percent of the body length, the cruise stability margin requirement is critical in establishing horizontal surface size. However, weight and balance estimates indicated that the center of gravity would be considerably aft of 61 percent of the body length. A location aft of 65 percent was predicted for the configuration illustrated in Figure 7.2-45. From the data shown in Figure 7.2-48, a horizontal surface greater than 3760 square feet would be required.

Two approaches were considered to reduce the size of the horizontal surface:

1. Center of gravity control

2. Relocating the wing aft of the body center of gravity.

It is desirable to move the entry center of gravity forward and move the wing aft to reduce the tail size. The center-of-gravity location during reentry and transition can be moved forward by locating the fuel used for subsonic cruise forward of the landing center-of-gravity position.

The tail area required for pitch down from high to cruise angle-of-attack and for hypersonic trim at C_L maximum was evaluated for three center-of-gravity locations. The results are presented in Figure 7.2-49 as a function of wing location. Also shown is the tail area

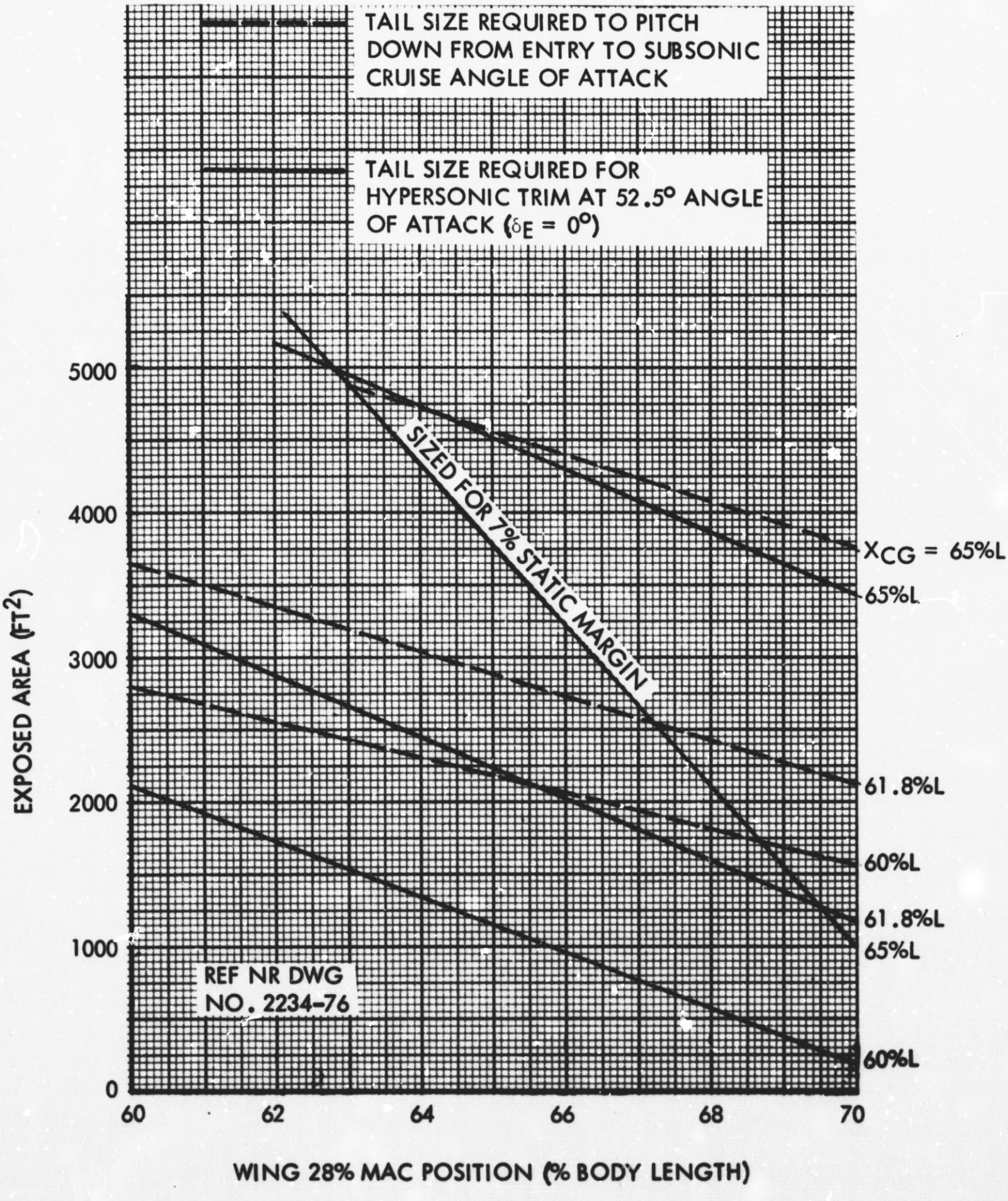

Figure 7.2-49. Effect of Wing Location on Booster Tail Size

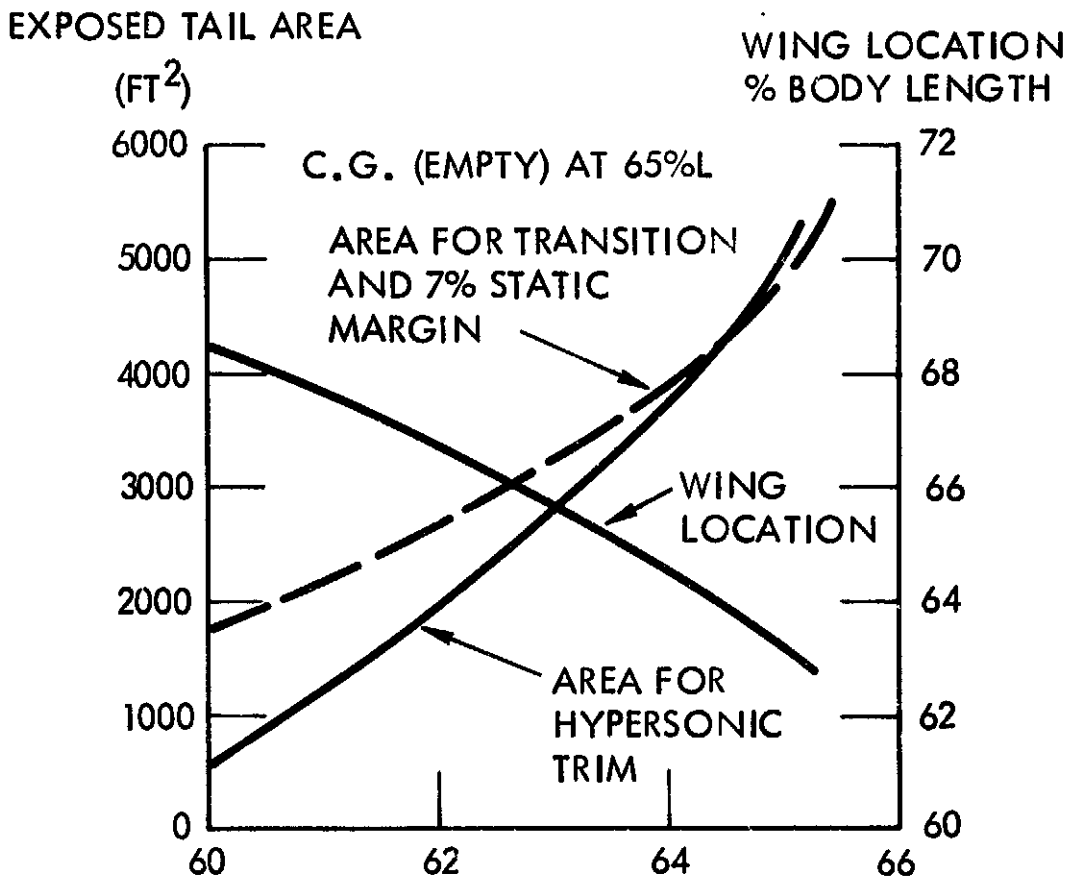

EXP WING AREA = 5430 FT²

BODY PLAN AREA = 12,920 FT²

Figure 7.2-50. Horizontal Tail Size for 50,000-Pound-Payload Booster

required for a 7 percent static margin at a center of gravity located at 65 percent of the body length. Notice that for the wing at 65 percent of the body length, the horizontal area required is 3760 square feet. The hypersonic and transition tail area requirements intersect the static margin requirement at specific wing and entry center-of-gravity locations. These intersections of the area required for transition and static margin are cross-plotted in Figure 7.2-50, as a function of the entry center-of-gravity location.

These curves reveal that as the wing is moved aft, the required area decreases for transition and a 7 percent static margin, and the corresponding center-of-gravity location required for reentry and transition moves forward. Also shown is the required hypersonic area to trim at C_L maximum.

For the final configuration, the entry center of gravity with the turbojet flyback fuel forward was located at 60 percent of the body length. For this case, the wing is located such that 28 percent of the mean aerodynamic chord is located at 68 percent of the body length.

Additional studies should be conducted to improve the booster aerodynamic configuration. Reshaping the forward body would reduce the tail size required for pitch over. However, it may be desirable to make a more fundamental change in the booster configuration. Because the center of gravity and wing are so far aft, it may be advantageous to develop a canard configuration, as discussed in Section 7.2.4.

7.3 FLIGHT MECHANICS

7.3.1 Summary

Flight mechanics analyses during the second phase of the subject study were directed toward establishment of the optimum reusable vehicle to maximize performance, and the generation of mission trajectories and performance data. Significant results were:

1. Optimum oxidizer/fuel mixture ratio is 6 to 1 for both the orbiter and booster stages.

2. Based on the use of two main engines on the orbiter and the same basic engine design on the two vehicle stages, 11 engines on the booster provide an optimum vehicle design.

3. To provide a 50,000-pound-payload delivery capability, the vehicle gross weight is 4.5 million pounds at launch.

4. Use of simultaneous booster and orbiter firing at lift off would result in a significant payload reduction (about 30 percent).

5. Use of high T/W turbojets in orbiter, hydrogen fuel in booster turbojets, and booster turbojets during ascent could reduce gross weight by approximately 0.75 million pounds.

6. Minimum on-orbit ΔV is 1215 feet per second compared to a design requirement of 1990 feet per second. Reducing the on-orbit ΔV to the minimum would allow a 10,000-pound payload increase.

7. Once-daily return of the orbiter to the recovery site is obtained by orbital phasing with no increase in deorbit ΔV required over direct descent.

8. Nominal orbiter lateral range is 190 nautical miles. This can be increased to 400 miles with no significant increase in entry thermal environment by entry at a 47.5-degree angle of attack.

9. Maximum lateral range capability is 1240 nautical miles achieved by entry at 20 degrees angle of attack. The thermal protection system weight increase is 22,000 pounds.

10. 1500 nautical miles ranging can be obtained with banking during entry, followed by subsonic cruise obtained by off-loading payload and adding turbojet fuel.

11. Booster flyback mode incorporates banked entry to reduce range by 24 percent over a straight-ahead entry. Flyback range is 310 nautical miles.

12. Further optimization of turbojet propulsion systems on orbiter and booster is required to reduce vehicle weight.

13. Nominal landing speeds are 113 knots for the booster and 128 for the orbiter.

14. In event of loss of a single booster or orbiter engine, the vehicle can still complete the primary mission.

15. In event of abort early in the launch trajectory, the orbiter can return to the launch site. Following late aborts, the capability exists to perform a successful entry, but insufficient performance exists to return to the launch site.

16. In event of failure of both orbiter engines following staging, excessive entry loads will result unless a fuel-dump capability is provided. Water landings are probable.

7.3.2 Launch Phase Analysis

Definition of logistics vehicle characteristics during the vehicle's ascent phase of the mission encompassed three major areas of investigation:

1. Establishment of optimum stage propellant distributions for vehicles to deliver payloads ranging from 7,700 to 50,000 pounds and definition of nominal ascent trajectories for use in environmental analyses.

2. Sensitivity analyses to establish performance impact of variation in vehicle design, weights, and operating modes

3. Definition of ascent and abort trajectories for selected vehicles

Concept Sizing

Identification of the optimum velocity distribution between the two stages of the logistics vehicle configured for various payloads was facilitated by definition of aerodynamic characteristics. The vehicle used as a basis for parametric sizing and performance studies was a configuration developed by NASA MSC. The configuration uses eight 260,000-pound sea level thrust engines on the booster and two engines of the same design, each delivering 300,000 pounds of vacuum thrust, on the orbiter. Aerodynamic characteristics described in Section 7.2.3, were established for this vehicle and scaled for use in parametric sizing of vehicles to deliver greater payloads. Stage propellant mass fractions based on weight scaling data were used in initial vehicle-sizing operations discussed in Volume IV.

The basic concepts investigated in the sizing analysis included:

1. 12,500-pound payload class - Payload established for vehicle with 2,080,000-pound lift-off thrust

2. 25,000-pound payload (15-foot-diameter by 30-foot cargo bay)

3. 25,000-pound payload (15-foot-diameter by 60-foot cargo bay)

4. 50,000-pound payload (15-foot-diameter by 60-foot cargo bay)

5. 50,000-pound payload (22-foot-diameter by 60-foot cargo bay)

For concept 1, the optimum stage propellant distribution was established to maximize payload with a vehicle lift-off weight of 1,664,000 pounds. For concepts 2 through 5, the optimum stage sizes were established to minimize vehicle gross weight and satisfy specified payload delivery requirements.

Ground Rules. Ground rules for sizing the above concepts were:

1. Minimum thrust-to-weight ratio T/W at liftoff of 1.25

2. Minimum booster sea level T/W of 1.125 with one engine out

3. Minimum orbiter sea level T/W of 1.125 (two engines)

4. Atmosphere used - 1963 Patrick up to 90 kilometers, extended to 700 kilometers by 1962 standard atmosphere.

5. Direct ascent to a 45- by 100-nautical-mile orbit inclined at 55 degrees.

6. Axial acceleration unconstrained

7. Excess ΔV requirement of 2,000 fps for on-orbit maneuvers and 225 fps for flight performance reserves assigned to the orbiter.

Approach. The vehicles for delivery of the previously specified payloads were sized parametrically through a multistage vehicle sizing program. The approach to determining the optimum stage sizes for each configuration considered stage mixture ratio and thrust-to-weight ratio. The vehicle delivering a 25,000-pound (15-foot by 30-foot cargo bay) payload was selected as a base point from which the optimum mixture ratio and thrust-to-weight ratio for each stage was determined. These values of mixture ratio and thrust to weight were then used to establish the optimum stage sizes for the remaining payload concepts.

Vehicle Characteristics. The ascent trajectory mode uses vertical ascent for 20 seconds followed by a gravity turn for the remainder of the first-stage operating period. For the second-stage operating period, the

trajectory is simulated by a linear tangent method for optimum pitch-plane steering. Vehicle gross weight versus mixture ratio and thrust-to-weight ratio are shown in Figures 7.3-1 and 7.3-2 for the 25,000-pound (15-foot by 30-foot cargo) payload configuration.

From Figure 7.3-1, the optimum mixture ratio is 6:1 in both stages for a thrust-to-weight ratio of 1.3. The optimum stage thrust-to-weight ratios were selected on the basis of using a propellant mixture ratio of 6:1 in both stages.

In Figure 7.3-2, the vehicle gross weight is a function of stage thrust-to-weight ratio and the number of engines on the booster. The analysis is based on use of two engines in the orbiter and the same basic engine design on both stages. A 10-engine system was selected for the booster. This resulted in a 1.25 T/W at liftoff and a corresponding orbiter T/W of 1.6 (vacuum). Selection of a 13-engine system is shown to result in the lowest gross weight system, but with the same engine design on each stage this would result in inadequate T/W on the orbiter for abort at sea level.

A 10-engine booster system was selected to minimize weight and booster engine system complexity. Comparable vehicle weights would be achieved with an 11-engine booster. Configurations, with the exception of the vehicle with 2,080,000-pound liftoff thrust, were sized on the basis of a propellant mixture ratio of 6:1 on both stages and T/W's of 1.25 and 1.6 in the booster and orbiter, respectively. Because of engine thrust constraints for the 2,080,000-pound lift-off thrust vehicle, a T/W of 1.56 was used for the orbiter. Stage characteristics for the five vehicles analyzed are presented in Tables 7.3-1 through 7.3.5. Payload for the 12,500-pound class vehicle was estimated to be 7700-pounds, as shown in Table 7.3-1.

Since no acceleration constraint was imposed in the sizing, the impact of limiting the acceleration during ascent was investigated. The vehicle delivering a 25,000-pound payload (15-foot by 30-foot cargo bay) was analyzed with a 3-g constraint in both stages. This would be accomplished by throttling or shutting down engines. A result of this constraint was an additional 640 pounds of propellant required in the orbiter to achieve the desired orbital conditions.

Nominal Trajectory Data. Nominal trajectories are displayed in Figures 7.3-3 and 7.3-4 for vehicles delivering 7700-pounds and 25,000 pounds of payload (15-foot by 30-foot cargo bay), respectively. Axial load has been limited to 3 g's in both stages during the ascent to a 45- by 100-nautical-mile orbit. The trajectory in Figure 7.3-3 was used as the design launch trajectory for the 12,500-pound-payload baseline vehicle.

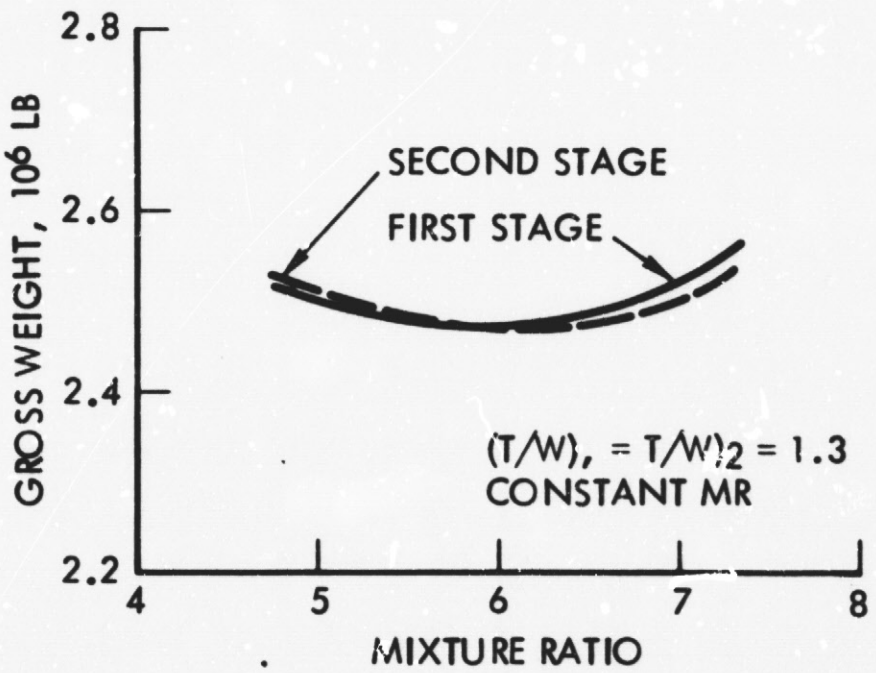

Figure 7.3-1. Vehicle Gross Weight versus Stage Mixture Ratio

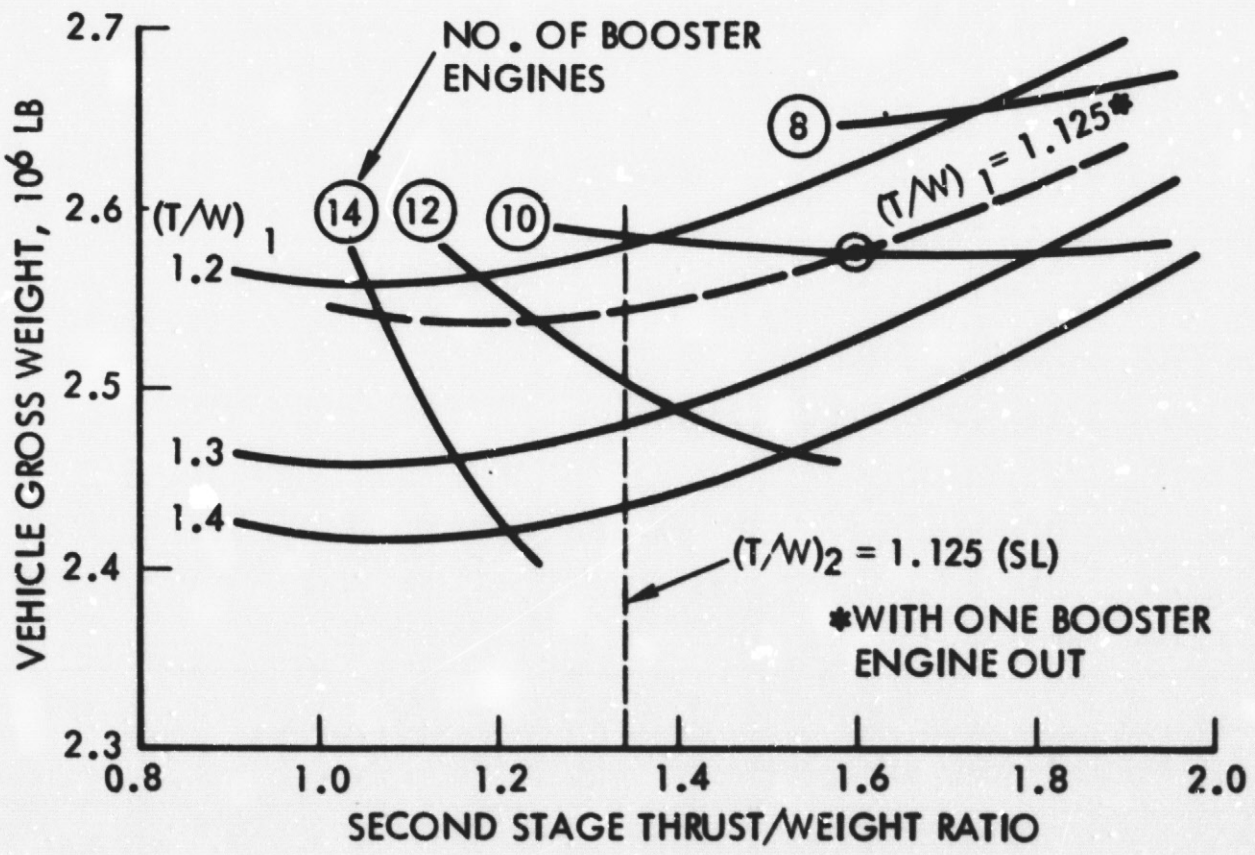

Figure 7.3-2. Vehicle Gross Weight versus Stage Thrust-to-Weight Ratio

Table 7.3-1. Characteristics of 7,700-Pound Payload Vehicle (12,500-Pound Class)

Vehicle Parameters	Stage 1	Stage 2
Gross weight, lb	1,664,000	385,100
Propellant, lb	1,018,200	294,800*
Burnout weight, lb	260,700	92,500**
Thrust (sea level), lb	2,080,000	
Thrust (vac), lb	2,286,336	600,000
Mixture ratio	6:1	6:1
Expansion ratio, ϵ	35:1	120:1
Number of engines	8	2
Thrust/weight, T/W_o	1.25	1.56
Characteristic velocity, ft/sec	12,950	17,648
Type of engine (pump, pressure, solid)	Pump	Pump
Propellant mass ratio, ν_B	.796	.755
Burnout velocity, ft/sec	7,616	25,883
Burnout altitude, ft	207,000	273,400
Reference area, square ft	2,540	
Orbital maneuvers, ft/sec		2,000
Flight performance reserves, ft/sec		225
Maximum dynamic pressure, psf	420	
Orbital and flight performance reserves propellant, lb		16,293

*Including orbital and flight performance reserves
**Excluding payload.

Table 7.3-2. Characteristics of 25,000-Pound Payload Vehicle (15- by 30-Foot Cargo Bay)

Vehicle Parameters	Stage 1	Stage 2
Gross weight, lb	2,576,000	469,000
Propellant, lb	1,729,000	325,000*
Burnout weight, lb	378,000	119,000**
Thrust (sea level), lb	3,220,000	
Thrust (vac), lb	3,539,464	750,000
Mixture ratio	6:1	6:1
Expansion ratio, ϵ	35:1	120:1
Number of engines	10	2
Thrust/weight, T/W_o	1.25	1.6
Characteristic velocity, ft/sec	15,200	15,235
Type of engine (pump, pressure, solid)	Pump	Pump
Propellant mass ratio, ν_B	.820	.732
Burnout velocity, ft/sec	9,873	25,883
Burnout altitude, ft	237,000	273,400
Reference area, square ft	5,080	
Orbital maneuvers, ft/sec		2,000
Flight performance reserves, ft/sec		225
Maximum dynamic pressure, psf	425	
Orbital and flight performance reserves propellant, lb		23,414

*Including orbital and flight performance reserves
**Excluding payload.

Table 7.3-3. Characteristics of 25,000-Pound Payload Vehicle (15- by 60-Foot Cargo Bay)

Vehicle Parameters	Stage 1	Stage 2
Gross weight, lb	2,730,000	526,400
Propellant, lb	1,813,000	386,000*
Burnout weight, lb	391,000	131,000**
Thrust (sea level), lb	3,412,500	
Thrust (vac), lb	3,751,000	842,240
Mixture ratio	6:1	6:1
Expansion ratio, ϵ	35:1	120:1
Number of engines	10	2
Thrust/weight, T/W_o	1.25	1.6
Characteristic velocity, ft/sec	14,920	15,530
Type of engine (pump, pressure, solid)	Pump	Pump
Propellant mass ratio, ν_B	.823	.734
Burnout velocity, ft/sec	9,583	25,883
Burnout altitude, ft	243,000	273,400
Reference area, square ft	5,080	
Orbital maneuvers, ft/sec		2,000
Flight performance reserves, ft/sec		225
Maximum dynamic pressure, psf	440	
Orbital and flight performance reserves propellant, lb		25,690

*Including orbital and flight performance reserves
**Excluding payload.

Table 7.3-4. Characteristics of 50,000-Pound Payload Vehicle (15- by 60-Foot Cargo Bay)

Vehicle Parameters	Stage 1	Stage 2
Gross weight, lb	3,479,000	740,700
Propellant, lb	2,269,000	523,700*
Burnout weight, lb	470,000	167,000**
Thrust (sea level), lb	4,348,750	
Thrust (vac), lb	4,780,200	1,185,100
Mixture ratio	6:1	6:1
Expansion ratio, ϵ	35:1	120:1
Number of engines	9	2
Thrust/weight, T/W_o	1.25	1.6
Characteristic velocity, ft/sec	14,400	15,900
Type of engine (pump, pressure, solid)	Pump	Pump
Propellant mass ratio, ν_B	.829	.758
Burnout velocity, ft/sec	9,243	25,883
Burnout altitude, ft	226,000	273,400
Reference area, square ft	6,200	
Orbital maneuvers, ft/sec		2,000
Flight performance reserves, ft/sec		225
Maximum dynamic pressure, psf	440	
Orbital and flight performance reserves propellant, lb		35,280

*Including orbital and flight performance reserves
**Excluding payload.

Table 7.3-5. Characteristics of 50,000-Pound Payload Vehicle (22- by 60-Foot Cargo Bay)

Vehicle Parameters	Stage 1	Stage 2
Gross weight, lb	4,007,200	739,500
Propellant, lb	2,731,000	506,800*
Burnout weight, lb	537,000	183,000**
Thrust (sea level), lb	5,009,000	
Thrust (vac), lb	5,505,000	1,183,200
Mixture ratio	6:1	6:1
Expansion ratio, ϵ	35:1	120:1
Number of engines	10	2
Thrust/weight, T/W_o	1.25	1.6
Characteristic velocity, ft/sec	15,600	14,850
Type of engine (pump, pressure, solid)	Pump	Pump
Propellant mass ratio, ν_B	.836	.735
Burnout velocity, ft/sec	10,670	25,883
Burnout altitude, ft	189,000	273,400
Reference area, square ft	6,200	
Orbital maneuvers, ft/sec		2,000
Flight performance reserves, ft/sec		225
Maximum dynamic pressure, psf	450	
Orbital and flight performance reserves propellant, lb		37,886

*Including orbital and flight performance reserves
**Excluding payload

Figure 7.3-3. Ascent Trajectory Profile, 12,500-Pound Payload Class, 45 by 100 N. Mi Orbit

SD 69-573-3

Space Division
North American Rockwell

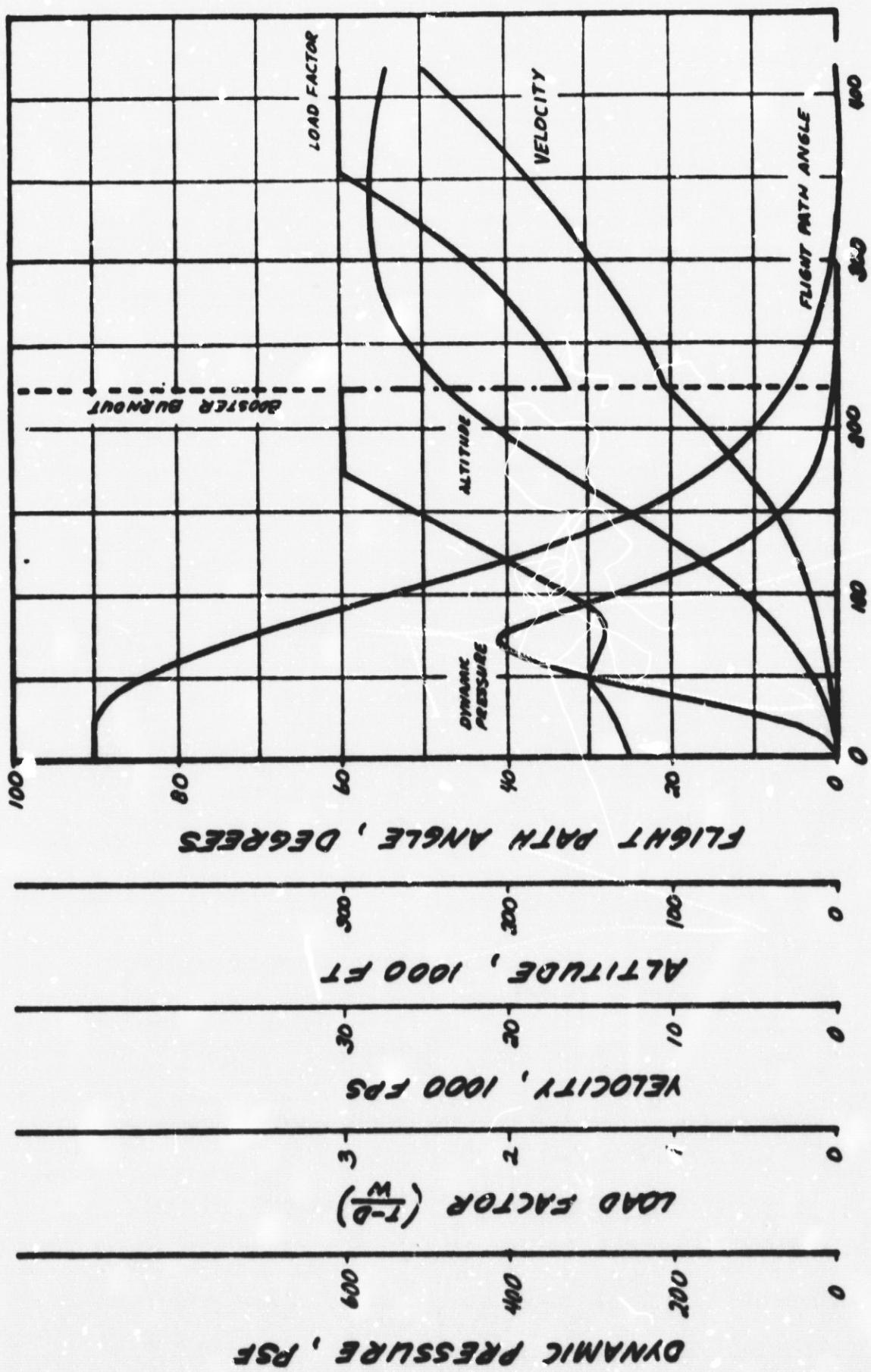

Figure 7.3-4. Ascent Trajectory Profile, 25,000-Pound Payload Class, 45 by 100 N. Mi Orbit

Alternative Mission Capability. The performance capability of the various payload class vehicles for alternative inclined orbits is shown in Figure 7.3-5. In determining payload, fixed stage propellant loads were assumed and the gross weight was allowed to vary to meet the desired orbit conditions. Ascent to orbit was assumed to be planar direct, with no constraints on launch azimuth.

Design Improvements and Sensitivity Analysis

The objective of the design improvements and sensitivity analysis was to evaluate candidate design and flight mode improvement concepts from a performance standpoint to aid in the final conceptual design selection.

External Payload Analysis. The impact on performance of locating the cargo bay outside the orbiter was evaluated with respect to the vehicle delivering 25,000 pounds of payload. This concept is defined in Table 7.3-2. The performance impact of increased drag from the external payload was assessed. Ground rules for the flight analysis were identical to those used for the vehicle with internal payload.

Trajectories were computed, and performance was established for design configurations with internal and external cargo resulting in the vehicle zero lift drag coefficients defined in Figure 7.3-6. Structural modifications required to locate the cargo bay externally were not reflected in this analysis.

The impact of the increased drag coefficient from the external cargo bay resulted in a loss of 3500 pounds of payload.

Performance Reserve Sensitivity Analysis. Vehicle gross weights are extremely sensitive to total mission velocity requirements. For the nominal mission, propellant is provided to allow 2000 fps in excess of that required to achieve a 45- by 100-nautical-mile orbit. This velocity allowance for on-orbit maneuvers includes contingencies. In view of the vehicle weight sensitivity to mission velocity, it is desirable to determine the impact of the maneuvering ΔV allowance. The influence of the on-orbit ΔV on the payload delivery capability of two vehicles was therefore established. Representative vehicles with nominal payload delivery capabilities of 25,000 pounds and 50,000 pounds were analyzed. Gross vehicle weight was held constant as the on-orbit reserves were varied from 0 to 2000 fps. Ascent propellant of each orbiter was considered fixed, whereas the total orbiter propellant varied as the orbital reserves changed. For the on-orbit ΔV range of 0-2000 fps, the orbiter mass fraction varied from 0.72 to 0.74 for the vehicle delivering 50,000 pounds, and 0.72 to 0.73 for the vehicle delivering 25,000 pounds of payload. The variation in payload with on-orbit ΔV allowance is presented in Figure 7.3-7 for the two specified vehicles.

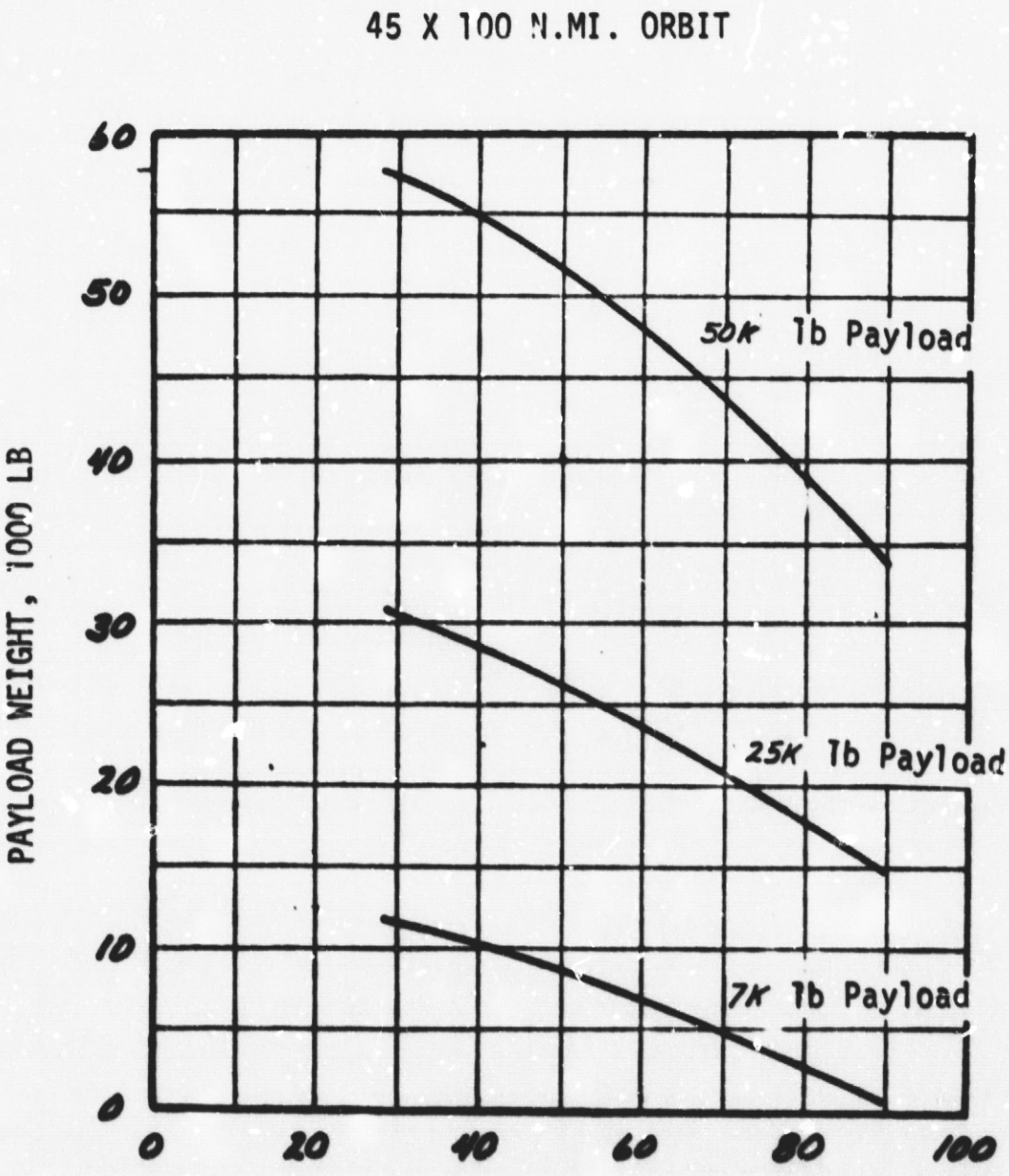

Figure 7.3-5. Effect of Inclination Angle on Payload

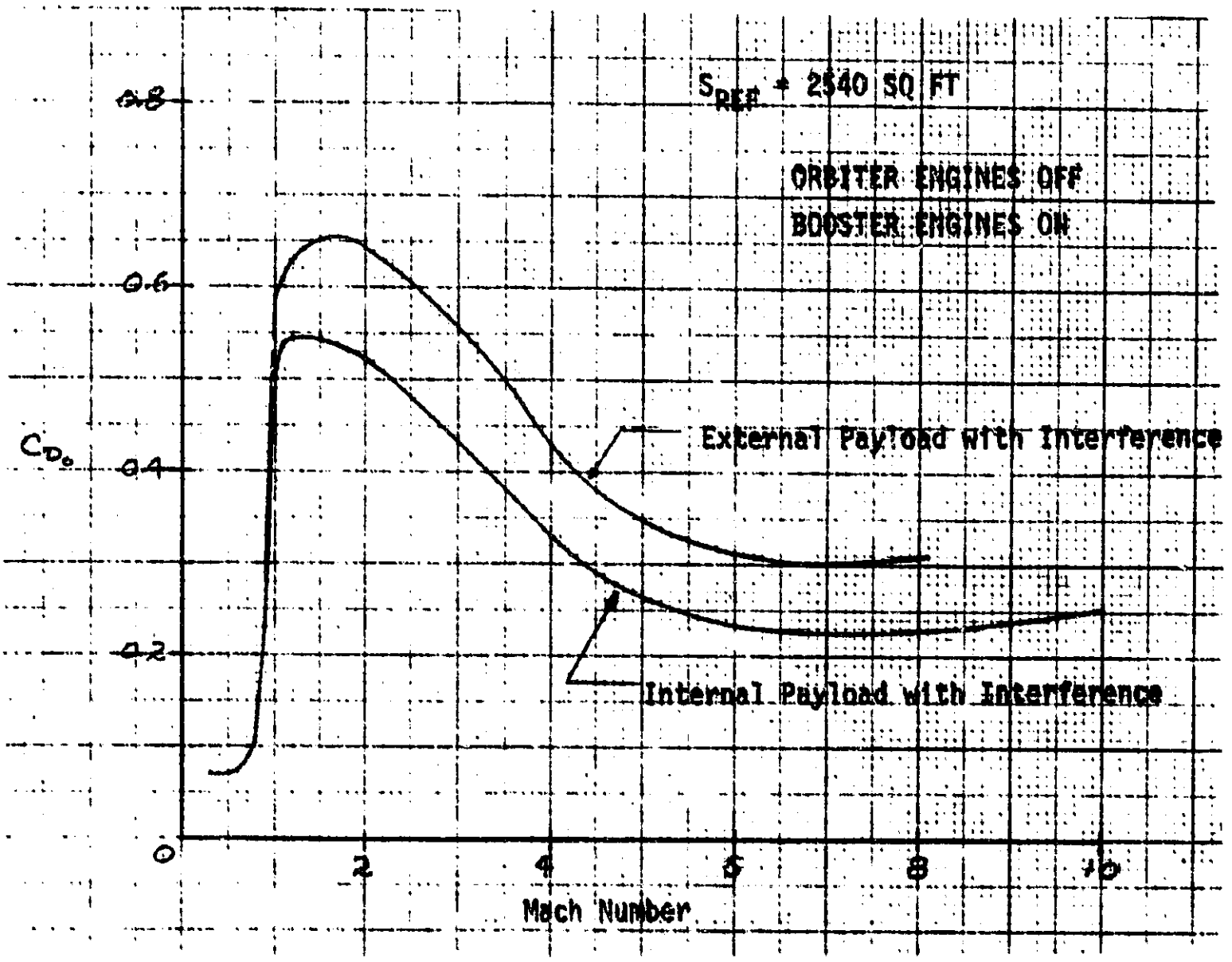

Figure 7.3-6. Zero Lift Drag Coefficient Vehicle with 25,000-Pound Payload (15-Foot Diameter by 30 Feet)

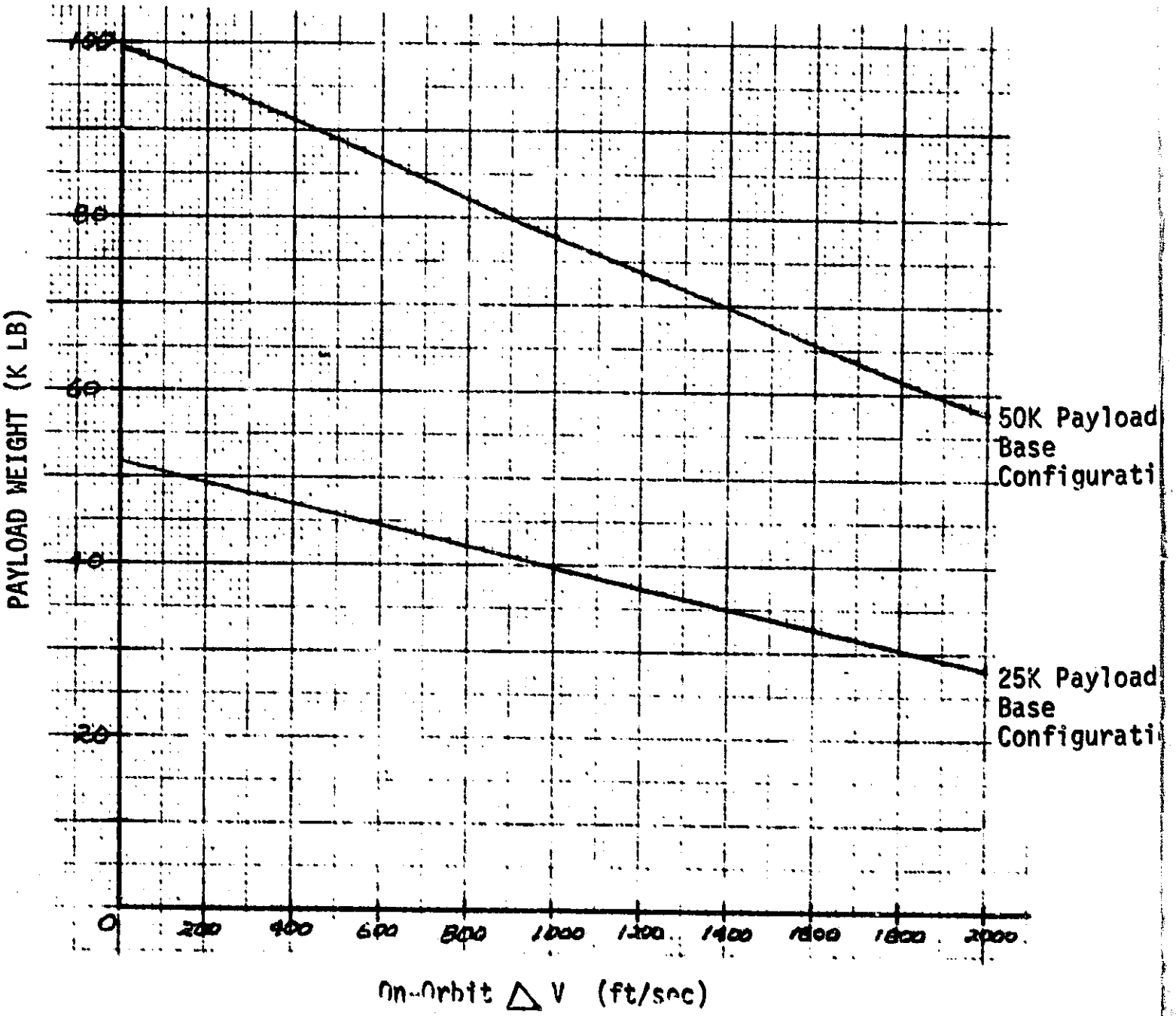

Figure 7.3-7. Payload Variation for Change in On-Orbit ΔV

It is projected that the nominal mission could be performed with an on-orbit ΔV allowance of 1215 fps. For this on-orbit ΔV, the payload of the vehicle delivering 25,000 pounds could be increased by 9000 pounds, and the vehicle delivering 50,000 pounds could deliver an additional 15,000 pounds of payload.

Gross Weight and Payload Sensitivity Analysis. The success of the shuttle vehicle is contingent upon achieving desired performance and limiting gross weight. During design evolution, however, it is likely that vehicle characteristics and system weights will change. It is therefore necessary to establish the impact of these changes in vehicle characteristics on the vehicle performance. Trade studies were therefore performed to define the payload change associated with variations in mission requirements, system weight, and engine performance. These studies were performed for a representative vehicle, defined in Table 7.3-6, capable of delivering a 50,000-pound payload to a 60- by 100-nautical-mile orbit.

For establishment of performance sensitivities, each stage parameter was analyzed separately to determine the effect on payload or vehicle gross weight. Table 7.3-7 summarizes performance and weight sensitivities of the vehicle delivering a 50,000-pound payload. The sensitivities are illustrated in Figures 7.3-8 and 7.3-9.

The performance partial of payload-to-stage-propellant weight was determined for constant stage burnout weight. The partial of payload-to-booster-vacuum thrust was determined on the basis that booster sea level thrust was held constant.

The sensitivity of payload to coast time between stages considered instantaneous thrust decay and buildup in the booster and orbiter, respectively.

The performance partial of payload to inclination assumed planar ascent with no range safety constraints.

Injection Altitude Sensitivity Analysis. The effects of orbit injection conditions on vehicle stage weights and flight characteristics were determined in order to evaluate the impact on ascent heating, booster flyback range and propellant requirements, and overall stage characteristics. The investigation was based on the following ground rules and assumptions:

1. Initial T/W of 1.25 on the booster and 1.6 on the orbiter

2. On-orbit velocity requirements reduced to reflect an increase in injection orbit altitude

Table 7.3-6. Characteristics of 50,000-Pound Payload Vehicle (60- by 100-Nautical-Mile Orbit, 15- by 60-Foot Cargo Bay)

Vehicle Parameters	Stage 1	Stage 2
Gross weight, lb	4,125,000	776,300
Propellant, lb	2,787,700	536,700*
Burnout weight, lb	561,100	189,600**
Thrust (sea level), lb	5,156,250	1,078,108 (ϵ = 35:1)
Thrust (vac), lb	5,667,956	1,242,064
Mixture ratio	6	6
Expansion ratio, ϵ	35	120
Number of engines	10	2
Thrust/weight, T/W_o	1.25	1.6
Characteristic velocity, ft/sec	15,400	15,221
Type of engine (pump, pressure, solid)	Pump	Pump
Propellant mass ratio, v_B	.832	.739
Reference area, square ft	6,310	
Orbital maneuvers, ft/sec		1,973
Flight performance reserves, ft/sec		228
Maximum dynamic pressure, psf	418	
Burnout velocity, ft/sec	10,114	25,800
Burnout altitude, ft	246,000	364,566
Burnout flight path angle, deg	8.6	0.
Maximum acceleration, g's	3.0	3.0

*Including orbital and flight performance reserves
**Excluding payload

Table 7.3-7. Performance Sensitivities
(Vehicle Delivering 50,000-Pound Payload)

Partial	Measurement	Booster	Orbiter	Range
$\frac{\partial W_{PL}}{\partial Isp}$	(lb/sec)	+770	+727	±5 sec
$\frac{\partial W_{PL}}{\partial W_{B.O.}}$	(lb/lb)	-.13	-1.0	±2%
$\frac{\partial W_{PL}}{\partial W_{p}}$	(lb/lb)	+.17	+.25	±2%
$\frac{\partial W_{PL}}{\partial T_{vac}}$	(lb/lb)	+.004	+.005	±5%
$\frac{\partial W_{PL}}{\partial t_{coast}}$	(lb/sec)	-----	-100	
$\frac{\partial W_{PL}}{\partial \Delta V_{\text{on orbit}}}$	(lb/fps)	-----	-22.	±1000 sec
$\frac{\partial W_{PL}}{\partial Inc}$	(lb/deg)	-----	-385	±10 deg
$\frac{\partial W_{o}}{\partial W_{PL}}$	(lb/lb)	-----	22	±5%
$\frac{\partial W_{o}}{\partial W_{B.O.}}$	(lb/lb)	3	22	±5%

$W_{B.O.}$, Stage burnout weight
W_p, Stage propellant weight
W_o, Gross vehicle weight
t_{coast}, Coast time between stages
Inc, Inclination
W_{PL}, Payload weight
W_{gross}, Stage gross weight, propellant plus burnout weight

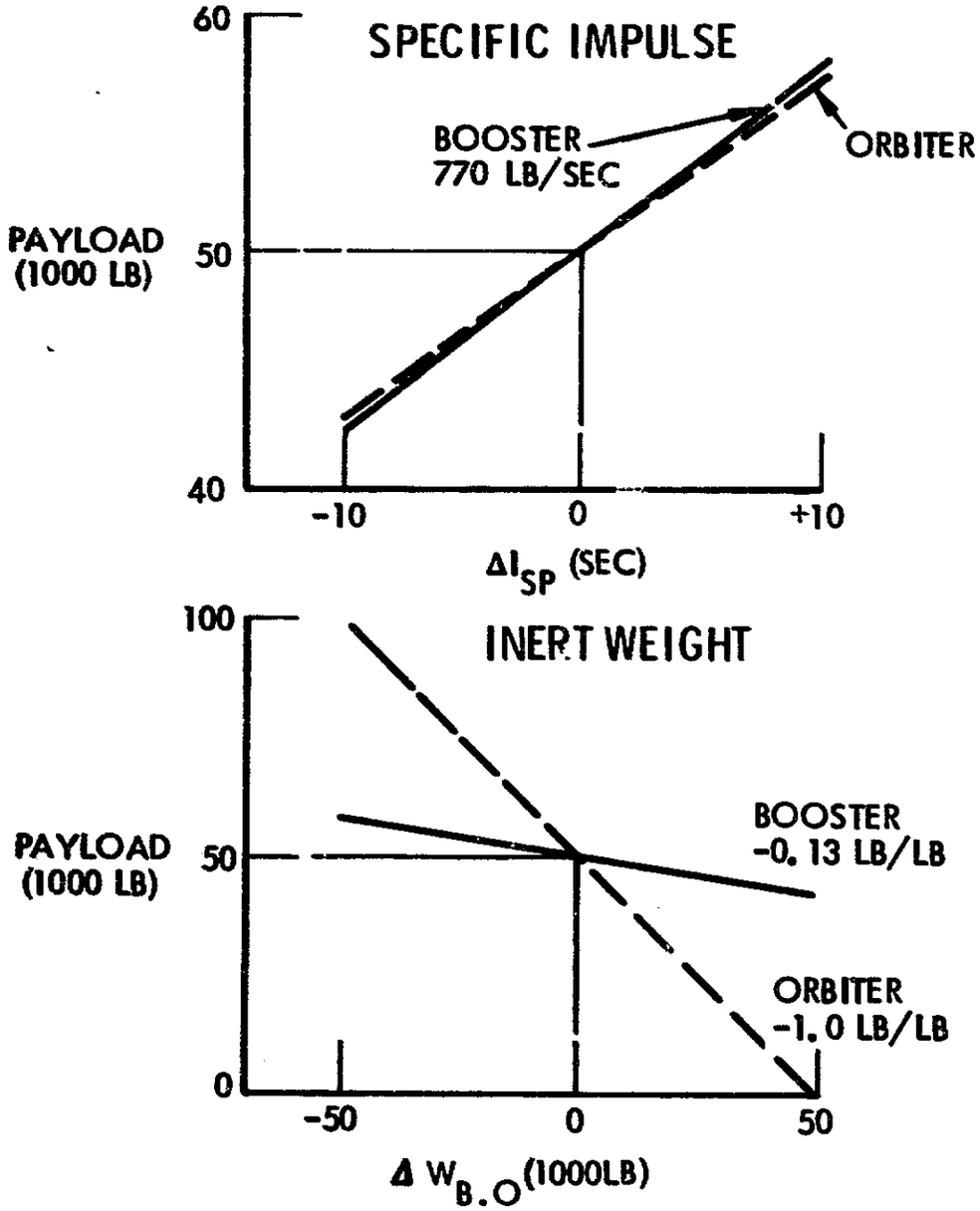

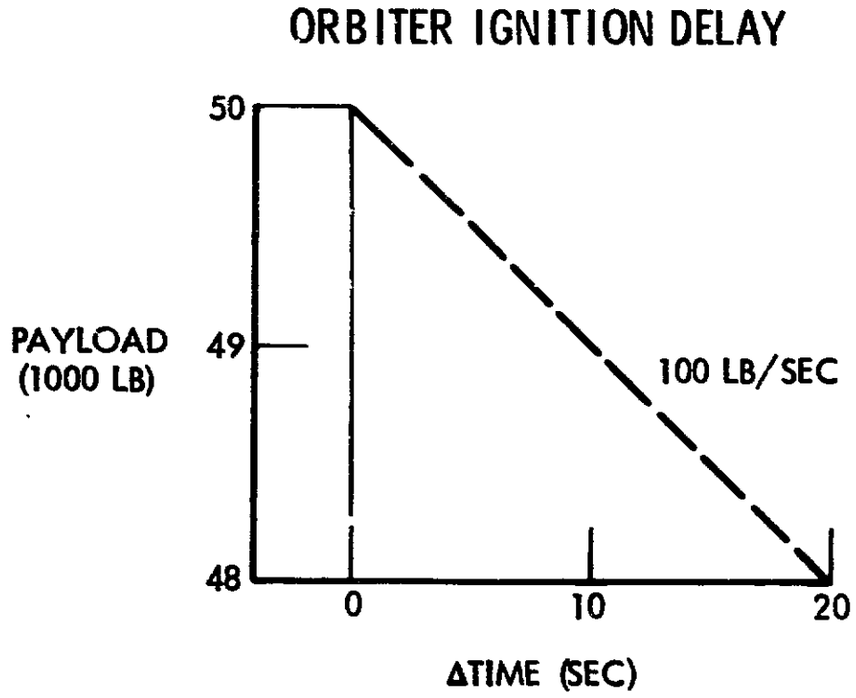

Figure 7.3-8. Payload Sensitivities for 50,000-Pound Payload Class

Space Division
North American Rockwell

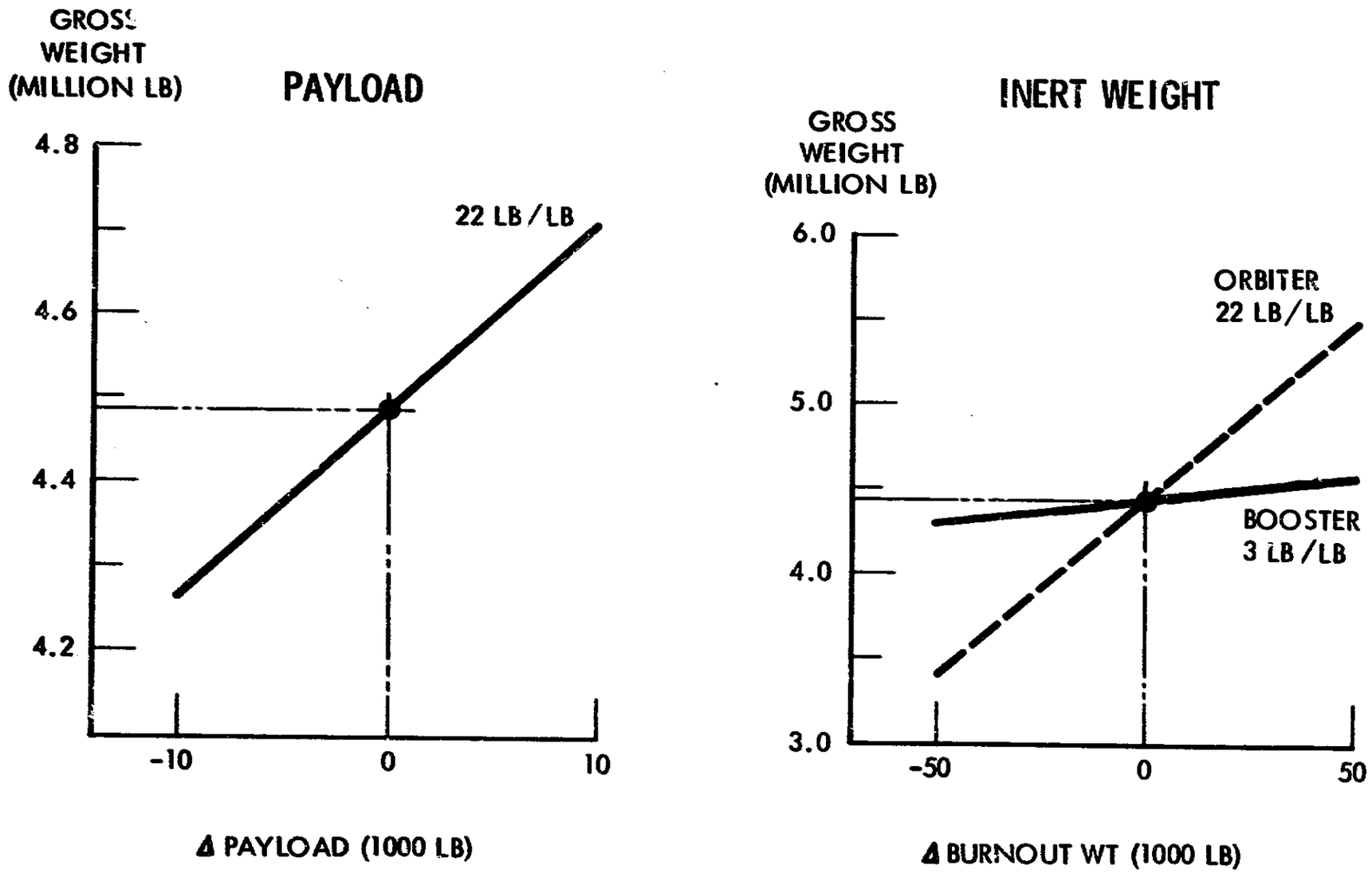

Figure 7.3-9. Gross Weight Sensitivities for 50,000-Pound Payload Class

Space Division
North American Rockwell

3. Zero lift, 3-g axial load constraint

4. Optimum stage sizes for specified orbit injection conditions

Selection of the nominal ascent trajectory was based on an evaluation of ascent heating and loads, booster flyback range and propellant requirements, and the subsequent impact on stage weight and size. Results presented in Table 7.3-8 indicate that the effect of injection conditions on stage weight is not large over the range of interest. An increase in launch weight of only 0.15 percent will result if the design injection orbit is changed from 45-by-100 to 60-by-100 nautical miles. It is noted that while booster size is increased, the orbiter size is decreased so that the net change is not large (6000 pounds). In addition, the maximum dynamic pressure during boost is essentially unchanged for the injection conditions investigated.

Orbiter drag losses during Hohmann transfer are estimated to be 40 fps for a 45-nautical-mile perigee altitude case (based on a W/C_DA of 1100 psf) and are negligible for injection into a 60- by 100-nautical-mile orbit or higher. The previously described sensitivity analysis indicated that within the range of injection orbits specified in Table 7.3-8, the injection altitude may be selected on a basis other than performance.

The ascent heating discussion in Section 7.4 indicates that the injection altitude should be 50 by 100 nautical miles or greater in order to prevent the thermal environment during boost from exceeding entry environment on critical areas of the orbiter. Investigations of booster flyback range as influenced by injection altitude are reported in Section 7.3.3 These results show that flyback range increases almost linearly with injection altitude. Consequently, a low injection altitude should be selected in order to minimize requirements for flyback propellant. Because thermal protection system development is an area of major technology advancement for the shuttle it was felt that the ascent conditions should not impose a more severe environment than already exists for entry. Therefore, a 50- by 100-nautical mile injection was selected for the design launch conditions.

Ascent Flight Mode Analysis - Lifting Versus Nonlifting. Studies were performed to determine if vehicle performance could be improved by providing a vehicle angle of attack that would produce lift during ascent. The configuration described in Table 7.3-6 was used for the flight mode analysis. For comparison, a baseline nonlifting trajectory and an optimum atmospheric ascent trajectory were obtained under the following conditions:

1. Direct ascent to a 60- by 100-nautical-mile, 55-degree inclined orbit
2. 3-g maximum axial acceleration in both stages
3. Optimum exoatmospheric steering initiated at orbiter ignition

Table 7.3-8. Injection Orbit Performance Effects
(50,000-Pound Payload)

Item	Units	Injection Orbit		
		45 by 100 nm	60 by 100 nm	80 by 100 nm
Launch Weight	K lb	4,119	4,125	4,194
Booster Characteristics				
Gross weight	K lb	3,336	3,349	3,426
Propellant weight	K lb	2,777	2,788	2,854
Entry weight	K lb	559	561	572
Thrust, sea level	K lb	5,148	5,156	5.242
vac	K lb	5,659	5,668	5,762
Ideal velocity	fps	15,300	15,400	15,600
Burnout velocity	fps	10,155	10,114	10,173
Burnout altitude	ft	222,000	246,000	282,000
Flight path angle	deg	6.3	8.6	11.9
Orbiter				
Gross weight	K lb	783	776	768
Propellant weight	K lb	543	536	529
Entry weight (with PL)	K lb	241	240	238
Thrust, vac	K lb	1,254	1,242	1,228
Ideal velocity	fps	15,100	15,200	15,100
Burnout velocity	fps	25,883	25,800	25,690
On orbit ΔV	fps	2,000	1,973	1,936

Figure 7.3-10 illustrates the flight characteristics of the resulting trajectories. The lifting trajectory is superimposed on the nonlifting trajectory (solid lines) by a series of symbols.

The basic difference between the two trajectories is that the nonlifting case was constrained to zero angle of attack, whereas the lifting case was simulated with a program that uses a closed-loop, steepest descent, optimization procedure to derive the optimum angle-of-attack history. (Lift and drag are a function of angle of attack and Mach number.) The resulting angle-of-attack history for the lifting trajectory is shown in Figure 7.3-11.

A performance comparison of the two flight modes revealed no significant difference in payload for the lifting and nonlifting ascent trajectories. Further investigation of the control necessary to maintain the specified angle-of-attack history would probably degrade the lifting flight mode, thereby making it less attractive than the nonlifting flight mode.

Effect of Winds on Ascent Performance. A cursory investigation was made of the effects of head winds on the baseline nonlifting flight mode. The method of analysis was based on the assumption that the launch vehicle pitch-attitude history in the presence of head winds was described by the nonlifting, no-winds, baseline flight mode. The control required to fly the programmed pitch attitude history was not assessed.

Figure 7.3-12 presents the wind profile used in this analysis in addition to the resulting angle-of-attack history up to booster burnout. The conditions at booster burnout are summarized in Table 7.3-9 for the trajectories with and without head winds.

Table 7.3-9. Vehicle Conditions at Booster Burnout

Conditions	No Winds	Head Winds
Inertial velocity (fps)	11,022	10,824
Altitude (ft)	248,711	250,808
Inertial flight path angle (deg)	7.78	7.99
Pitch attitude (deg)	16.395	16.395

The resulting loss in payload from head winds, compared to the no-winds nominal trajectory, was approximately 900 pounds.

Figure 7.3-10. Ascent Trajectory Profile, Lifting and Nonlifting Flight Modes 50,000-Pound Payload - (60 by 100 N. Mi. Orbit)

Space Division
North American Rockwell

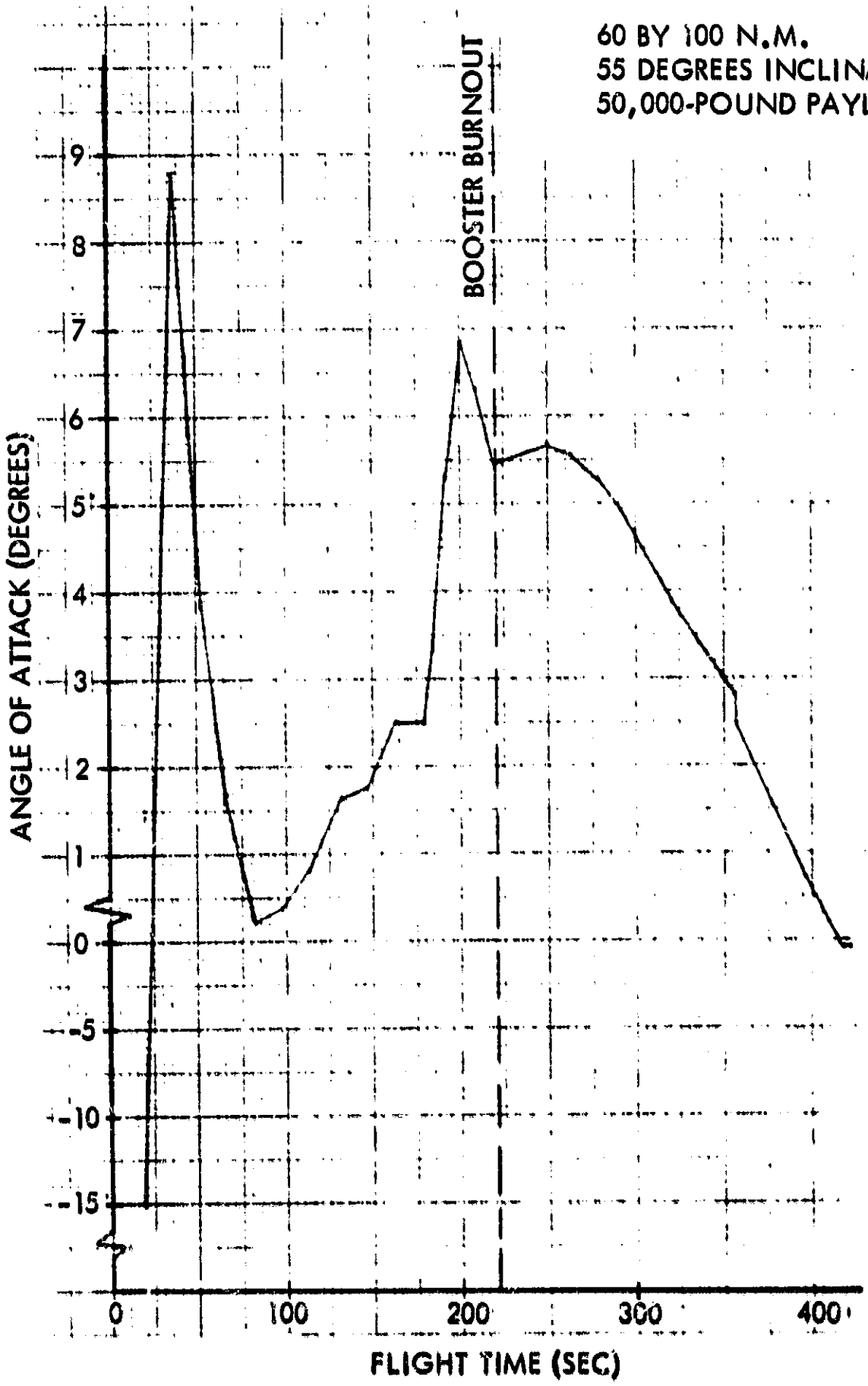

Figure 7.3-11. Angle of Attack History for Lifting Ascent

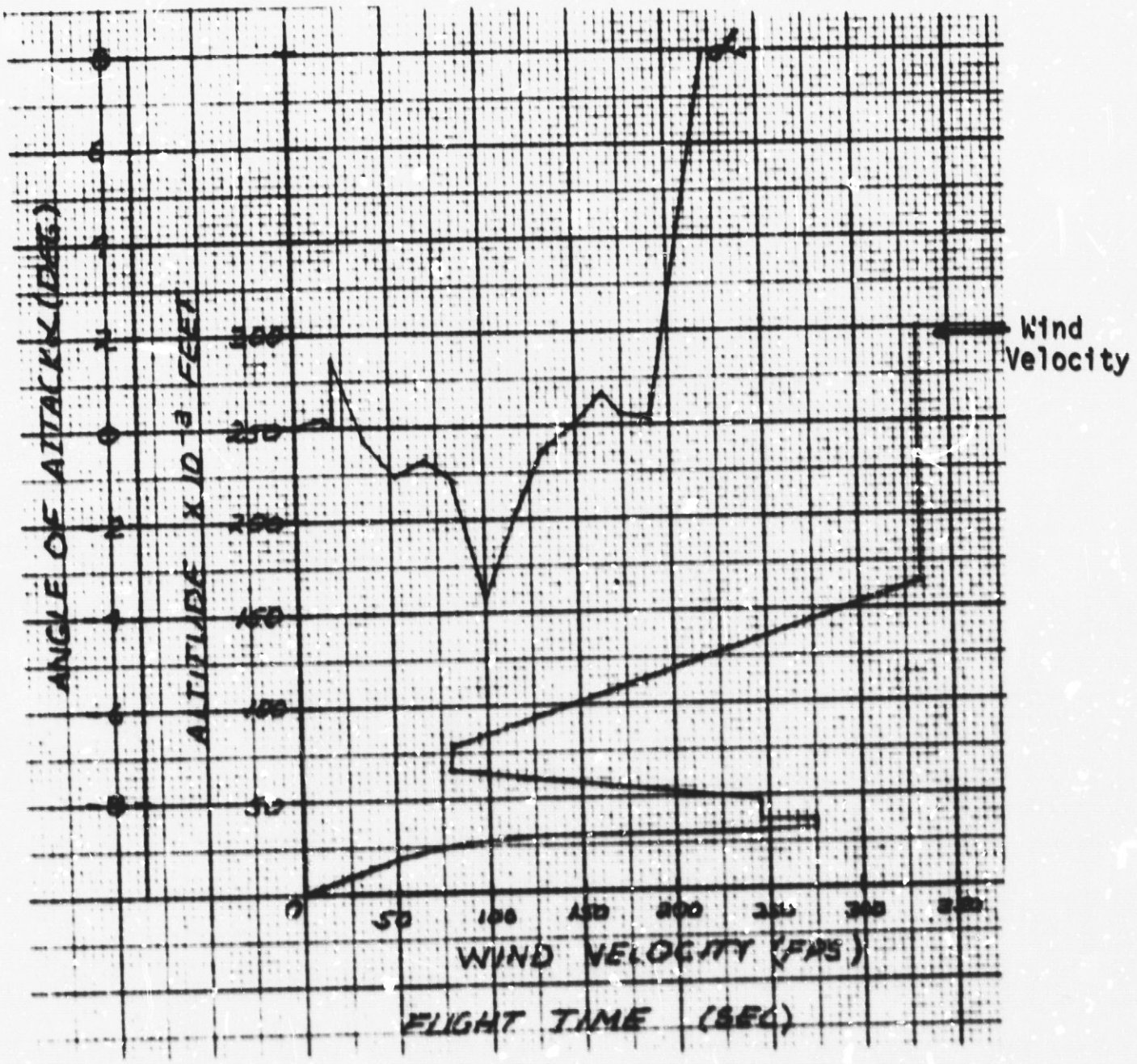

Figure 7.3-12. Wind Profile and Angle of Attack History

Flyback Analysis. The impact of booster flyback propellant on vehicle gross weight was investigated. The booster flyback propellant is treated as an incremental inert weight of the booster. Thus, for the booster that has a performance partial of -0.13 pounds of payload per pound of booster inert weight, a 1000-pound increase in flyback propellant would decrease payload by 130 pounds or, conversely, increase vehicle gross weight by 2860 pounds.

Turbojet Analysis. The effect on performance of using the booster turbojets during ascent was evaluated for the vehicle described in Table 7.3-6. The following assumptions and conditions were used in the analysis.

1. Four turbojets operating at maximum power setting (41,700 pounds sea level per engine decaying to 11,000 pounds at 40,000 feet)

2. Turbojets shut down 70 seconds after launch (Mach number of 0.95 and altitude of 30,000 feet)

3. Vehicle gross weight increased by 840 pounds to account for the turbojet fuel consumed during boost

The resulting decrease in orbiter propellant required for ascent and on-orbit maneuvers was 2600 pounds. Assuming the orbiter structure-to-propellant partial is 0.16, the net increase in payload delivery capability using turbojets during boost is approximately 3000 pounds.

Conceptual Design Definition

Baseline Nominal Trajectory - 50,000-Pound Payload. As a basis for environment and subsystem analysis, a trajectory was computed for the vehicle configured to deliver a 50,000-pound payload, which is described in Table 7.3-10. The vehicle was launched into a 50- by 100-nautical mile orbit, inclined 55 degrees, under the following ground rules:

1. Planar ascent direct to orbit injection

2. 3-g axial load limit in both stages

3. Zero lift ascent

4. Optimum pitch plane steering initially

The nominal ascent trajectory is illustrated in Figure 7.3-13. This trajectory was used for definition of an ascent design environment.

Abort Capability. The effect of an engine out in either the booster or orbiter was analyzed, using the baseline configuration (Table 7.3-10). The

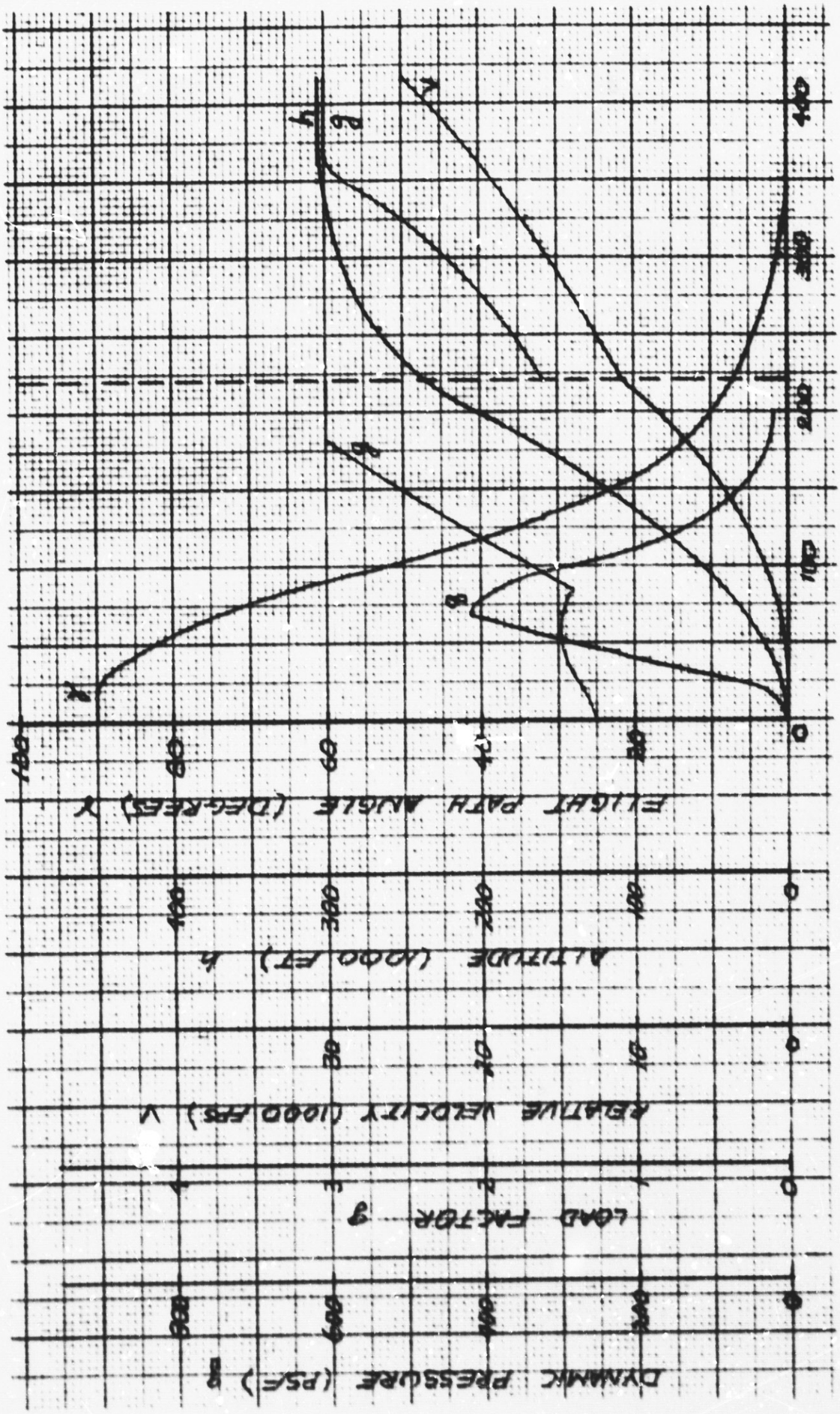

Figure 7.3-13. Nominal Ascent Trajectory Profile, 50,000-Pound Payload, 50 by 100 N.M. Orbit

Table 7.3-10. Characteristics of 50,000-Pound Payload Baseline Vehicle (50- by 100-Nautical-Mile Orbit)

Vehicle Parameters	Booster	Orbiter
Gross weight, lb	4,125,000	776,300
Propellant, lb (ascent)	2,787,700	496,600
Burnout weight, lb	561,100	189,600
Thrust (sea level), lb	5,156,250	1,078,108 (ϵ = 35)
Thrust (vac), lb	5,667,956	1,242,064
Mixture ratio	6	6
Expansion ratio, ϵ	35	120
Number of engines	10	2
Thrust/weight, T/W_o	1.25	1.6
Characteristic velocity, ft/sec	15,400	15,100
Type of engine (pump, pressure, solid)	Pump	Pump
Propellant mass ratio, v_B	.83	.74
Burnout velocity, ft/sec	10,189	25,855
Flight path angle, deg	7.0	0.
Burnout altitude, ft	230,000	303,740
Reference area, square ft	6,310	
Orbital maneuvers, ft/sec		1,990
Flight performance reserves, ft/sec		225
Maximum dynamic pressure psf	419	
Orbital and flight performance reserves propellant, lb		40,100

objective of this analysis was to determine whether the nominal mission can be accomplished after an engine failure during boost. The approach used in the analysis was to determine the velocity increment required to offset increased gravity losses with an engine failure in the booster or orbiter. This mission velocity increment was compared to the velocity allowance for performance reserves and on orbit ΔV contingency. On-orbit ΔV was determined by subtracting flight performance reserves from the remaining orbiter propellant after injection into a 50- by 100-nautical mile orbit. Results of this analysis are presented in Figure 7.3-14. Note that if one booster engine is lost at liftoff (a 10-percent reduction in thrust), the orbiter can still achieve orbit and perform the mission based on a minimum on-orbit ΔV requirement of 1215 fps. Likewise, if one orbiter engine fails at orbiter ignition (222 seconds after liftoff), the mission can still be completed with the resulting on-orbit ΔV of 1225 fps.

Alternative Launch Vehicle Configurations (3.0 and 3.5 Million Pound Gross Weight). Studies were conducted to determine the performance of several two-stage, reusable, shuttle vehicles. Optimum stage propellant distributions were determined for vehicles with gross weights of 3.5 million and 3.0 million pounds for two basic operating modes:

1. Sequential booster and orbiter firing

2. Simultaneous booster and orbiter firing at liftoff, with 100-percent thrust for booster and orbiter engines. The orbiter engines are throttled to 10-percent thrust 10 seconds after liftoff and return to full thrust after staging.

For a comparison of the vehicle performance with bell and aerospike engines, vehicles were defined with the following engines (both bell and aerospike engines are configured to provide the maximum diameter that can be achieved with the same vehicle base envelope, with allowance for gimbaling engines 7 degrees):

1. Bell engine (400,000-pounds sea level thrust) using different nozzles on booster and orbiter

2. Aerospike engines (400,000-pounds sea level thrust) identical design on booster and orbiter; each engine has a single combustor

3. Aerospike engines (800,000-pounds/400,000-pounds sea level thrust) of similar diameter on booster and orbiter; booster uses 800,000 pounds of thrust with dual combustors; orbiter uses 400,000 pounds of thrust with single combustor

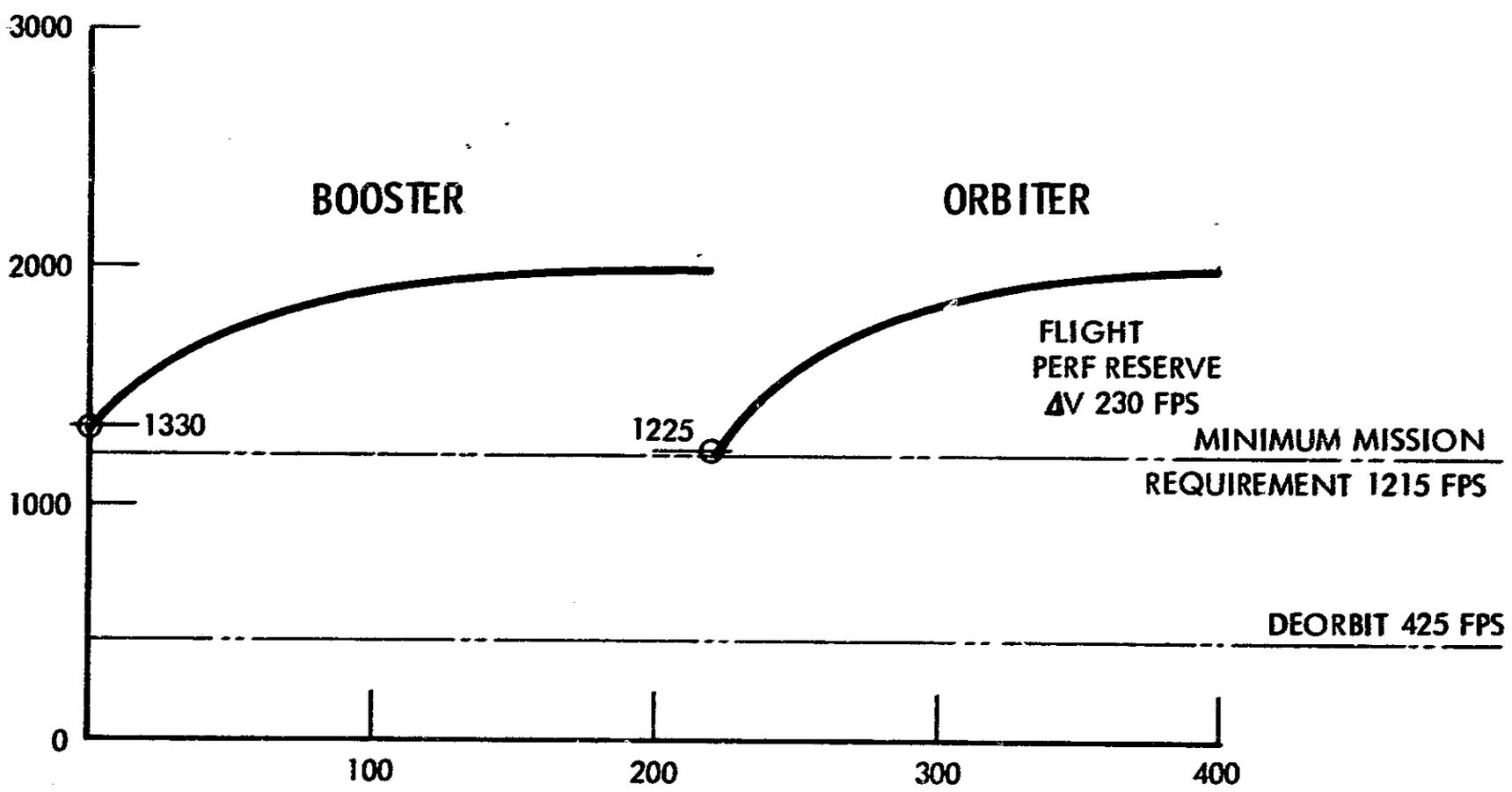

Figure 7.3-14. Ascent Performance - One Engine Out (50 by 100 N. Mi. Injection of 50,000-Pound Payload Class)

Engine characteristics used in this analysis are discussed in Volume IV. The stage propellant mass data used in the sizing evaluation are shown in Figure 7.3-15.

Vehicle weights, propulsion systems, and payloads for seven vehicles, encompassing the previously described propulsion systems, operating modes, and gross weights are summarized in Table 7.3-11.

It is noted that for vehicle performance to be maximized with the bell engine, different nozzles are used on the booster and orbiter. Orbiter engine nozzles are extended to increase expansion ratio after staging.

When aerospike engines are used, a significant vehicle performance improvement is achieved through the use of dual combustors on the booster engines. These booster engines deliver 800,000 pounds of sea level thrust. This facilitates use of a larger diameter engine (with 6 engines) than would be possible with a greater number of lower thrust engines.

It is observed that the payload for the vehicle with sequential firing mode is 7400 pounds to 9600 pounds greater than for a vehicle using simultaneous booster and orbiter firing at liftoff. This performance difference does not reflect the increase in base area or reduction in bell engine size, which would be necessary for the vehicle using simultaneous firing mode. This revision would be necessary to account for increased thrust vector angle required for the vehicle with simultaneous firing. Simultaneous booster and orbiter firing causes a significant shift in combined vehicle center of gravity during ascent. This requires additional thrust vector deflection above the normal engine gimbal (7 degrees minimum) required for control.

Three additional 3.5 million-pound configurations were sized in which different engines were used on the booster and orbiter. These configurations are defined in Table 7.3-12. The first configuration is identical to the aerospike dual combustor configuration of Table 7.3-11 except the diameters of the orbiter engines have been increased from 120 inches to the limit of 156 inches. The second and third configurations represent optimum thrust levels in the orbiter for a liftoff T/W of 1.25 and illustrate the comparative performance between the bell and aerospike engines. Table 7.3-12 summarizes the vehicle weights, propulsion systems, and payloads thus obtained. The performance of the aerospike engines is slightly better than the bell engine.

Payload Sensitivity to On-Orbit ΔV. The baseline system delivers 50,000 pounds of payload to a 270-nautical-mile, circular orbit at a 55-degree inclination and has an on-orbit ΔV of 2000 fps. The payload capability of alternative vehicles previously described is listed below:

Engine characteristics used in this analysis are discussed in Volume IV. The stage propellant mass data used in the sizing evaluation are shown in Figure 7.3-15.

Vehicle weights, propulsion systems, and payloads for seven vehicles, encompassing the previously described propulsion systems, operating modes, and gross weights are summarized in Table 7.3-11.

It is noted that for vehicle performance to be maximized with the bell engine, different nozzles are used on the booster and orbiter. Orbiter engine nozzles are extended to increase expansion ratio after staging.

When aerospike engines are used, a significant vehicle performance improvement is achieved through the use of dual combustors on the booster engines. These booster engines deliver 800,000 pounds of sea level thrust. This facilitates use of a larger diameter engine (with 6 engines) than would be possible with a greater number of lower thrust engines.

It is observed that the payload for the vehicle with sequential firing mode is 7400 pounds to 9600 pounds greater than for a vehicle using simultaneous booster and orbiter firing at liftoff. This performance difference does not reflect the increase in base area or reduction in bell engine size, which would be necessary for the vehicle using simultaneous firing mode. This revision would be necessary to account for increased thrust vector angle required for the vehicle with simultaneous firing. Simultaneous booster and orbiter firing causes a significant shift in combined vehicle center of gravity during ascent. This requires additional thrust vector deflection above the normal engine gimbal (7 degrees minimum) required for control.

Three additional 3.5 million-pound configurations were sized in which different engines were used on the booster and orbiter. These configurations are defined in Table 7.3-12. The first configuration is identical to the aerospike dual combustor configuration of Table 7.3-11 except the diameters of the orbiter engines have been increased from 120 inches to the limit of 156 inches. The second and third configurations represent optimum thrust levels in the orbiter for a liftoff T/W of 1.25 and illustrate the comparative performance between the bell and aerospike engines. Table 7.3-12 summarizes the vehicle weights, propulsion systems, and payloads thus obtained. The performance of the aerospike engines is slightly better than the bell engine.

Payload Sensitivity to On-Orbit ΔV. The baseline system delivers 50,000 pounds of payload to a 270-nautical-mile, circular orbit at a 55-degree inclination and has an on-orbit ΔV of 2000 fps. The payload capability of alternative vehicles previously described is listed below:

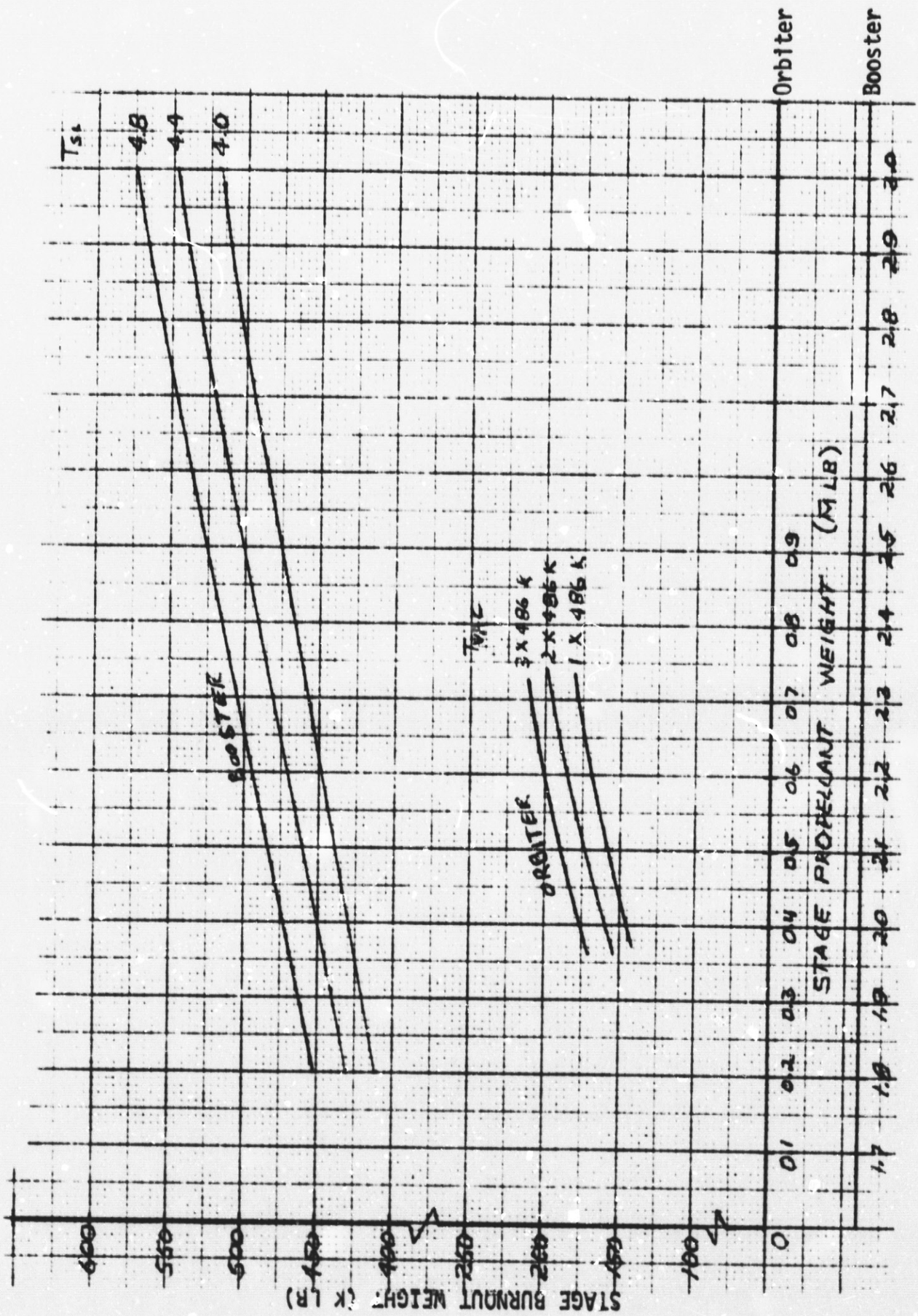

Figure 7.3-15. Stage Mass Data (3.0 and 3.5M Pound Gross Weight Vehicles)

Table 7.3-11. Vehicle Characteristics Summary*

Characteristic	Operating Mode						
	Sequential Firing				Simultaneous Firing		
Gross lift-off weight (1000 lb)	3000	3500	3500	3500	3000	3500	3500
Engine type	Bell	Bell	Aerospike dual combustor	Aerospike single combustor	Bell	Bell	Aerospike
Booster weight (1000 lb)	2329	2829	2816	2789	2329	2829	2816
Number of engines on booster	10	11	6	11	10	11	6
Booster engine thrust, F_{SL} (1000 lb)	400	400	800	400	400	400	800
Lift-off T/W	1.33	1.26	1.37	1.26	1.50	1.48	1.54
Orbiter weight (1000 lb)	671	671	684	711	671	711	684.4
Number of engines on orbiter	2	2	2	2	2	2	2
Orbiter engine thrust, F_{VAC} (1000 lb)	464	464	453	453	464	464	453
Payload (1000 lb)	12.2	31.8	30.6	23.3	4.8	22.2	24.3

Orbiter operates at full thrust for 10 seconds, then throttles to operate at 10 percent thrust

*Mission: 270-n mi orbit, 55-degree inclination - 2000 ft/sec above 45- by 100-n mi orbit

Table 7.3-12. Vehicle Characteristics With Optimized Engine Sizes*

Characteristics	Sequential Operating Mode		
Gross lift-off (1000 lb)	3500	3500	3500
Engine type	Aerospike	Aerospike	Bell
Booster weight (1000 lb)	2789	2847	2828
Number of engines on booster	6	7	7
Booster engine thrust, F_{SL} (1000 lb)	800	625	625
Lift-off T/W	1.37	1.25	1.25
Orbiter weight (1000 lb)	711	653	672
Number of engines on orbiter	2	2	2
Orbiter engine thrust, F_{VAC} (1000 lb)	486	450	450
Payload (1000 lb)	37.3	38.4	35.8

*Mission: 270 nm, 55 degree inclination, 220 ft/sec on orbit ΔV flight performance reserve, 45-by-100 nm insertion orbit

Vehicle Description	Payload (lb)
3.5 million pounds gross weight, sequential burn	31,800
3.0 million pounds gross weight, sequential burn	12,200
3.5 million pounds gross weight, simultaneous burn	22,200
3.0 million pounds gross weight, simultaneous burn	4,800

An investigation was completed to determine the payload sensitivity of alternative space shuttle configurations to on-orbit ΔV. Results are summarized in Figure 7.3-16. A payload trade was determined to establish the payload variation with on-orbit ΔV allowance. This assumes a one-to-one exchange of payload and on-orbit propellant. A payload increase of approximately 10,000 pounds may be obtained by reducing on-orbit ΔV allowance to the minimum acceptable value of approximately 1300 fps above the velocity in an orbit of 45 by 100 nautical miles.

Final Performance of the Study Concepts. Based on a detailed system analysis reported in Volume IV, the subsystem weights of a number of vehicles were revised. These revised weight data were used to derive final weights and trajectory characteristics of the vehicle delivering a 50,000-pound payload (15-foot by 60-foot cargo bay). Staging velocity was optimized for a liftoff T/W of 1.25 direct ascent to an orbit of 50 by 100 nautical miles at 55 degrees inclination. The stage propellant and structure data used in the sizing operation are illustrated in Figure 7.3-17. Table 7.3-13 summarizes the final stage weight and performance characteristics of the vehicle delivering a 50,000-pound payload. Note that, as a result of increased burnout weights in both stages, the vehicle gross weight has increased from 4.125 million pounds in the baseline vehicle to approximately 4.5 million pounds. The number of booster engines has increased from 10 to 11. Performance capability to alternate orbit inclinations is shown in Figure 7.3-18.

Two configurations were sized by using the data presented in Figure 7.3-17. Analyzed were configurations delivering a 25,000-pound payload within cargo bays 15 feet in diameter by 60 feet and 12 feet in diameter by 48 feet. Both vehicles were flown to the design orbital conditions described previously. Tables 7.3-14 and 7.3-15 summarize the stage weights and flight characteristics of these concepts.

7.3.3 Orbital Phase Analysis

Definition of logistic vehicle characteristics during the orbital phase of the mission encompassed two areas of investigation:

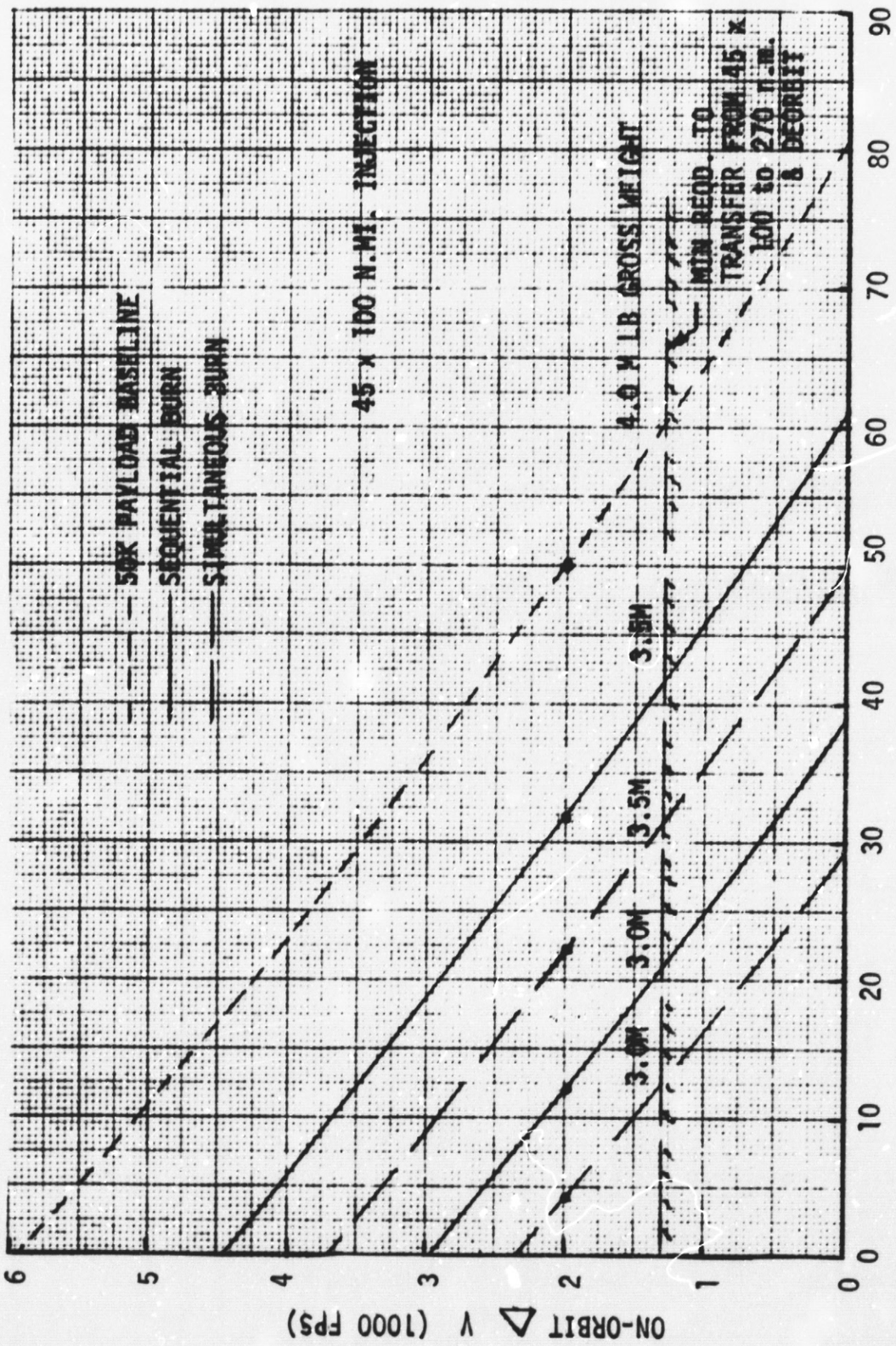

Figure 7.3-16. Payload Vs On-Orbit Maneuver Capability

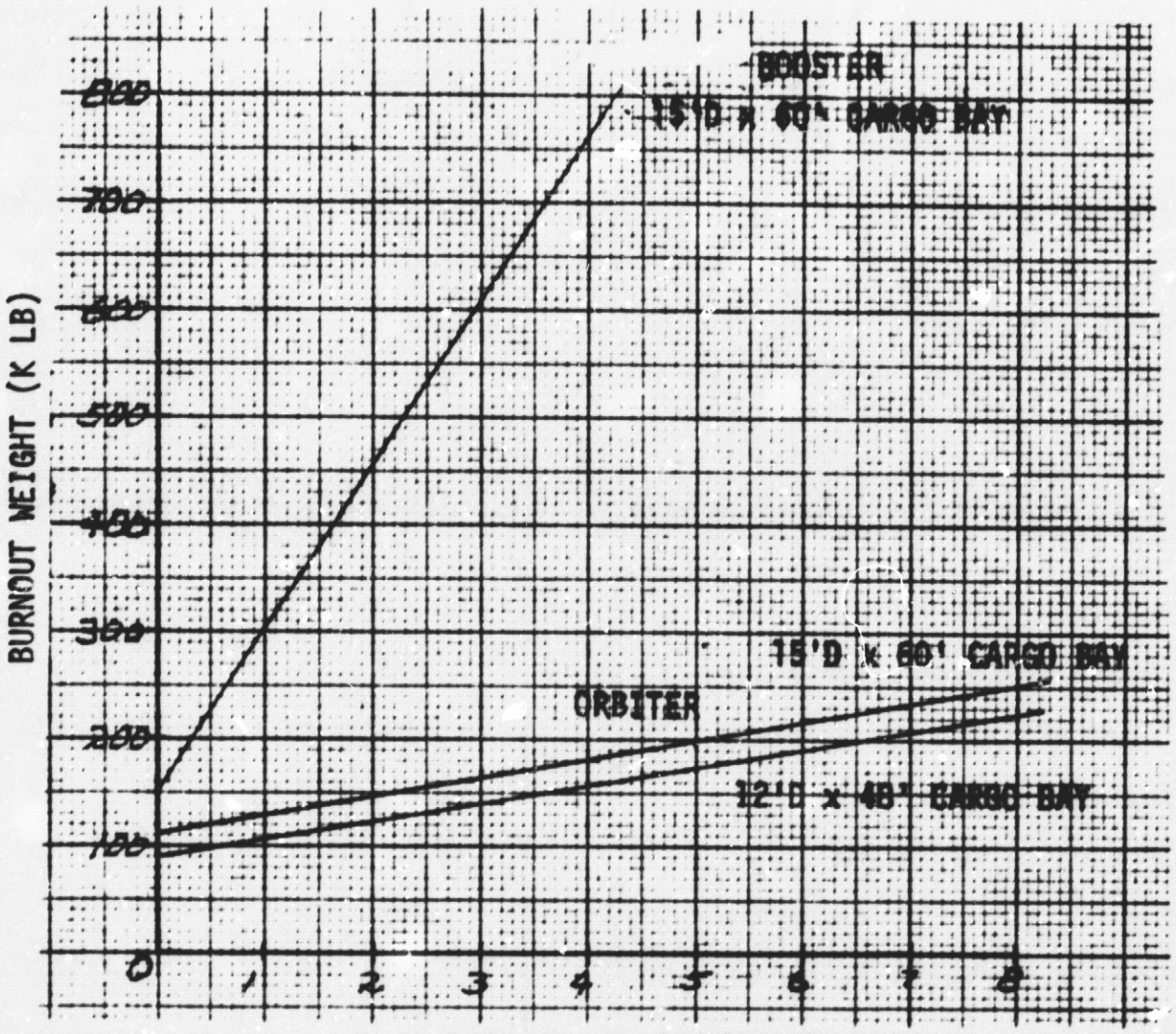

Figure 7.3-17. Stage Propellant Versus Burnout Weight

Table 7.3-13 Final Vehicle Characteristics 50,000-Pound Payload Configuration (15- by 60-Foot Cargo Bay, 50- by 100-Nautical-Mile Orbit)

Vehicle Parameters	Booster	Orbiter
Gross weight, lb	4,494,000	867,600
Propellant, lb (ascent)	3,017,000	560,300
Burnout weight, lb	609,200	214,300
Thrust (sea level), lb	5,617,200	
Thrust (vac), lb	6,205,900	1,180,000
Mixture ratio	6	6
Expansion ratio, ϵ	35	58/120
Number of engines	11	2
Thrust/weight, T/W_o	1.25	1.36
Characteristic velocity, ft/sec	15,380	15,310
Type of engine (pump, pressure, solid)	Pump	Pump
Propellant mass ratio, ν_B	.832	.738
Burnout velocity, ft/sec	10,866	25,855
Burnout angle, deg	6.9	0.
Burnout altitude, ft	245,000	303,806
Reference area, square ft	6,310	
Orbital maneuvers, ft/sec		1,990
Flight performance reserves, ft/sec		229
Maximum dynamic pressure, psf	430	
Orbital and flight performance reserves propellant, lb		43,000

- KSC LAUNCH
- 50 X 100 N MI INJECTION
- MAX G 3

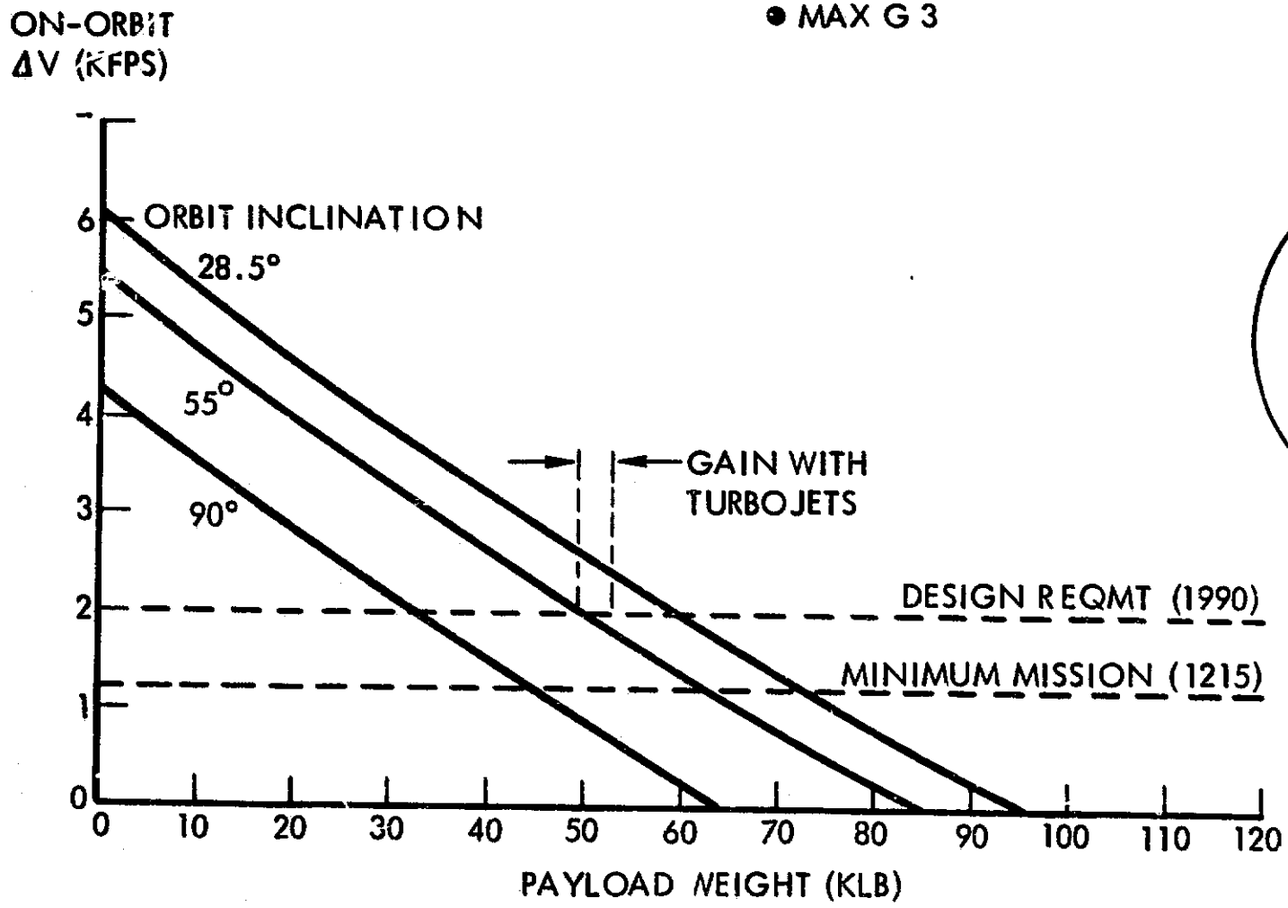

MAXIMUM PAYLOAD (LB)	
28.5° INCL	60,000
55° INCL	50,000
90° INCL	32,700

Figure 7.3-18. Payload Capability (50,000-Pound Payload System Alternate Orbits)

Table 7.3-14. Characteristics of 25,000-Pound Payload Configuration (15- by 60-Foot Cargo Bay, 50- by 100-Nautical-Mile Orbit)

Vehicle Parameters	Booster	Orbiter
Gross weight, lb	3,857,000	798,600
Propellant, lb (ascent)	2,524,000	527,700
Burnout weight, lb	534,300	207,900
Thrust (sea level), lb	4,821,300	
Thrust (vac), lb	5,326,500	1,118,000
Mixture ratio	6	6
Expansion ratio, ϵ	35	58/120
Number of engines	10	2
Thrust/weight, T/W_o	1.25	1.40
Characteristic velocity, ft/sec	14,674	15,969
Type of engine (pump, pressure, solid)	Pump	Pump
Propellant mass ratio, ν_B	.825	.731
Burnout velocity, ft/sec	10,254	25,855
Burnout angle, deg	7.7	0.
Burnout altitude, ft	234,000	303,806
Reference area, square ft	5080	
Orbital maneuvers, ft/sec		1,990
Flight performance reserves, ft/sec		229
Maximum dynamic pressure psf	465	
Orbital and flight performance reserves propellant, lb		38,000

Table 7.3-15. Characteristics of 25,000-Pound Payload Configuration (12- by 48-Foot Cargo Bay 50- by 100-Nautical-Mile Orbit)

Vehicle Parameters	Booster	Orbiter
Gross weight, lb	3,310,000	649,000
Propellant, lb (ascent)	2,179,400	434,100
Burnout weight, lb	481,600	165,000
Thrust (sea level), lb	4,137,500	
Thrust (vac), lb	4,571,100	960,000
Mixture ratio	6	6
Expansion ratio, ϵ	35	58/120
Number of engines	10	2
Thrust/weight, T/W_o	1.25	1.48
Characteristic velocity, ft/sec	14,838	15,948
Type of engine (pump, pressure, solid)	Pump	Pump
Propellant mass ratio, ν_B	.819	.736
Burnout velocity, ft/sec	10,269	25,855
Burnout angle, deg	7.7	0.
Burnout altitude, ft	236,000	303,806
Reference area, square ft	5,080	
Orbital maneuvers, ft/sec		1,990
Flight performance reserves, ft/sec		229
Maximum dynamic pressure psf	455	
Orbital and flight performance reserves propellant, lb		24,900

1. Establishment of event timelines and on-orbit ΔV requirements for rendezvous and deorbit phasing

2. Definition of time-phasing and ΔV requirements for return to ETR from a 270-nautical mile orbit

Rendezvous Profile

To determine minimum on-orbit maneuver requirements, a rendezvous profile was established, and event timelines and ΔV requirements were determined. The data were derived on the basis of the coelliptic sequencing rendezvous technique, a method employed for AAP earth-orbital operations. This technique affords a high degree of crew safety as well as providing opportunities for correcting maneuver dispersions more or less continuously. The resulting rendezvous profile is flexible enough to function for the entire phase window, including worst-case phase and lighting conditions.

Approach. The ILRV mission is concerned with ferrying men to and from a space station located in a 270-nautical mile circular earth orbit inclined 55 degrees to the equator. Launches are assumed to be coplanar with the target orbit, the target being at an arbitrary position in the orbit at that time. The approach to determining the rendezvous profile was to establish a sequence of maneuvers which, when accomplished, provide a specified relative geometry between vehicles for the terminal phase rendezvous maneuvers. These latter maneuvers, designated terminal phase insertion (TPI) and terminal phase finalization (TPF), are standardized and occur relative to solar lighting conditions. A minimum duration timeline was established to serve as a basepoint from which additional phase and waiting requirements (resulting from adverse target position at launch) could be based. The minimum duration sequence resulted from a favorable target position at launch and lighting conditions at TPF, requiring no additional coasting in orbit other than the minimum set for basic maneuvers. The maximum duration sequence was limited by the design requirement for a maximum of 24 hours ascent time.

Ground Rules for ILRV Rendezvous. The ground rules and assumptions used in this analysis were as follows:

1. Launch coplanar to target orbit plane from ETR

2. Target orbit 270-nautical-mile circular, 55-degree inclination

3. Orbiter is inserted into elliptic parking orbit

4. Total on-orbit ΔV = 2000 fps in excess of that required for ascent from a 45- by 100-nautical mile orbit

5. ILRV is rendezvous-active

6. AAP-type coelliptic sequencing rendezvous with terminal phase braking occurring in daylight

7. Coelliptic orbit 10 nautical miles below target orbit

8. Minimum coast between maneuvers - 1/2 revolution (except terminal phase).

9. Terminal phase coast through 130-degree transfer angle

10. Maximum ascent time of 24 hours

Rendezvous Technique. The basic rendezvous technique can be explained with the aid of Figure 7.3-19, depicting a rendezvous profile from a 80- by 100-nautical mile orbit. The ILRV is assumed to be in the insertion orbit at its perigee. Following a 1/2-revolution coast, the orbit is circularized to 100 nautical miles. The amount of coast time in the circular orbit (additional to the 1/2 revolution minimum) depends upon target phasing requirements. The subsequent phase adjust and NCC horizontal-burn maneuvers provide opportunities for correcting off-nominal maneuver dispersions. The CDH (constant Delta height) burn circularizes the ILRV orbit 10 nautical miles below the target orbit. The target lead angle at this point is a specified value such that following at least a 1/2-revolution coast to TPI (inertially fixed due to solar lighting), the TPI-burn thrust vector lies along the line-of-sight (LOS) to the target vehicle. The minimum coast time between CDH and TPI is 1/2 revolution; longer coast times to the TPI point will occur for arbitrary phasing situations (up to 1-1/2 revolutions).

Minimum Duration Rendezvous. The basic minimum duration rendezvous profile is pictured in Figure 7.3-19 with the accompanying timeline and ΔV requirements. The time to rendezvous (from insertion) takes 4.325 hours; maneuver requirements necessitate a total ΔV of 698.3 fps. No additional waiting is necessary over the minimum coast times required between maneuvers.

Rendezvous Profile for Arbitrary Phase Angle. The rendezvous profile for an arbitrary phase angle is presented in Figure 7.3-20. For this example, the target phasing requirement is 200 degrees greater than the minimum duration case; the total time to rendezvous is therefore increased to 17.64 hours, but ΔV requirements remain unchanged. Both target lead and lighting requirements are satisfied by waiting in the 100-nautical mile and 260-nautical mile non-circular orbits for lengths of time in excess of the 1/2 revolution minimum - the duration depending upon how much catch-up is required relative to the phase angle required at the CDH burn. The

BOOST TO 50-BY-100 NM ORBIT
MIN. TIME BETWEEN MANEUVERS = 1/2 REV
TPF BRAKING PERFORMED IN DAYLIGHT

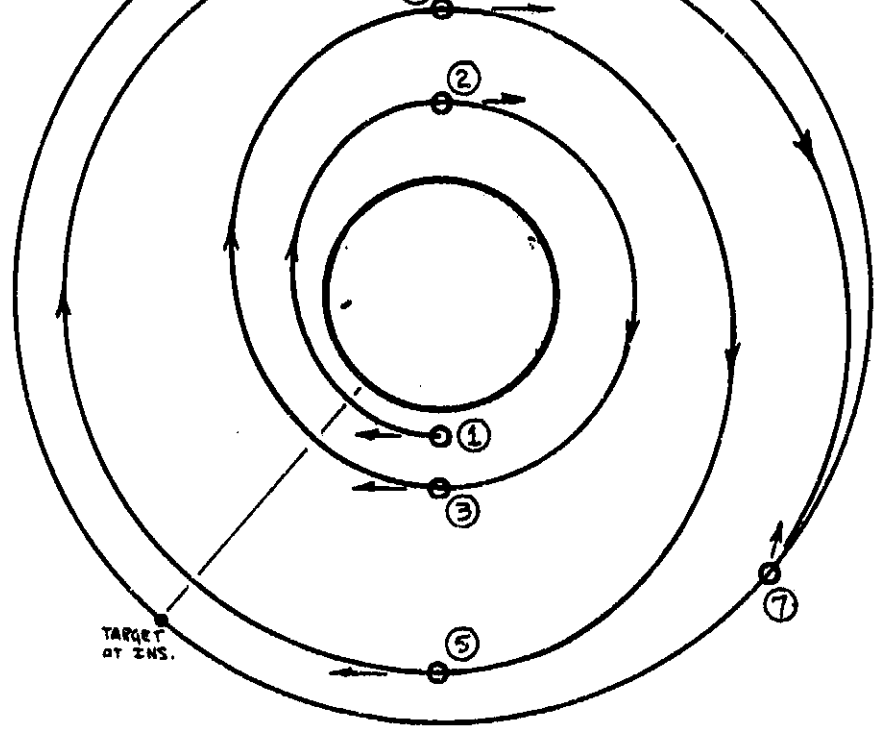

EVENT	ΔV (FPS)	RESULTING ORBIT, HA/HP (NM)	TIME BETWEEN EVENTS (HR)	TARGET LEAD (DEG)
1 INSERTION		50/100		240.20
2 CIRCULARIZE	91.0 HORIZ.	100/100	.732	26.23
3 PHASE ADJUST	142.3 HORIZ.	100/180	.735	14.02
4 NCC MANEUVER	279.1 HORIZ.	180/260	.748	4.65
5 CDH MANEUVER	136.9 HORIZ.	260/260	.773	1.03
6 TPI	22 27° ELEV.	260/271	.785	0.3
7 TPF	27 (THEORETICAL)	270/270	.550	0.0
TOTALS	698.3 FPS		4.325 HR.	

Figure 7.3-19. ILRV Mission Minimum Direction Rendezvous Profile

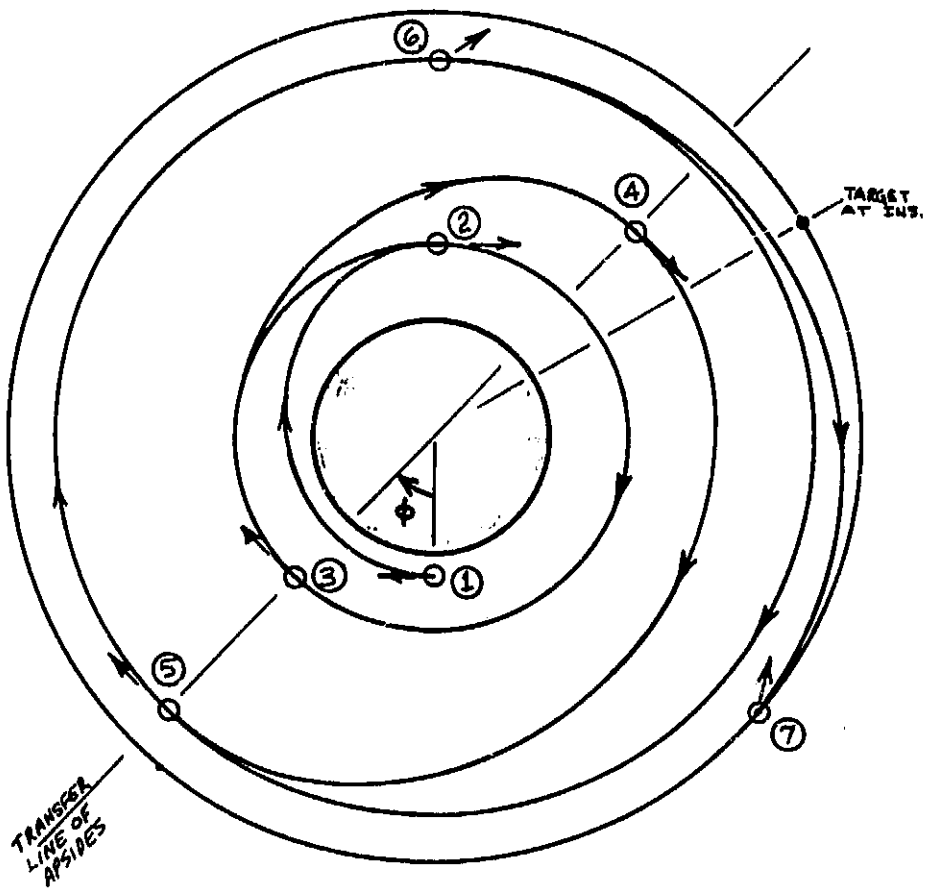

EVENT	ΔV (FPS)	RESULTING ORBIT, HA/HP (NM)	TIME BETWEEN EVENTS (HR)	TARGET LEAD (DEG)
1 INSERTION		50/100		240.20
2 CIRCULARIZE	91.0 HORIZ.	100/100	.732	226.23
3 PHASE ADJUST	142.3 HORIZ.	100/180	12.69	15.275
4 NCC MANEUVER	279.1 HORIZ.	180/260	.748	5.908
5 CDH MANEUVER	136.9 HORIZ.	260/260	.773	2.285
6 TPI	22 27° ELEV.	260/271	2.145	0.3
7 TPF	27 (THEORETICAL)	270/270	.550	0.0
TOTALS	698.3 FPS		17.64 HR	

Figure 7.3-20. ILRV Mission Rendezvous Profile, Arbitrary Phase Angle

required target lead at CDH is determined from the coast time to TPI, relative catch-up rate of the ILRF in the 260-nautical mile orbit, and the correct target phase angle at TPI. The phase adjust maneuver out of the 100-nautical mile circular orbit thus commences when, advancing the vehicle to the CDH point, the phase angle is equal to the required value for that CDH position.

Phase Window Summary. The entire phase window for ILRV rendezvous is shown in Figure 7.3-21 referenced from the point of orbit insertion conditions. Minimum duration (corresponding to 0-degree phasing) requires 4.325 hours, while 360-degree phasing requires 26.4 hours. The requirement for 24-hour maximum ascent time is exceeded slightly for 360-degree phasing. The sawtooth nature of the curve results from the requirement for 1/2 revolution durations between maneuvers and the fact that TPI/TPF positions in orbit are fixed. The inset curve of Figure 7.3-21 shows required target lead at CDH as a function of the phase adjust maneuver position (phase) in the 100-nautical mile orbit. As phase increases, the required phase angle decreases to a minimum value required for exactly 1/2 revolution coast from CDH to TPI. If phase is increased further, the required phase angle would theoretically correspond to less than 1/2 revolution coast; because of ground rules, however, the phase angle jumps up to the value corresponding to an additional 1 revolution coast from CDH to TPI. Hence, the time to rend zvous jumps at the end of each extra revolution in the 100-nautical m waiting orbit, decreases slightly from that value while in the new 100-nautical-mile orbit, and then jumps again at the end of the new orbit.

The maximum duration rendezvous timeline is summarized in Table 7.3-16, for the mission constrained so that total ascent time does not exceed 24 hours.

Descent Maneuver Requirements

Mission and design requirements for the orbiter specify that the return opportunity to the primary landing site shall be at least once every 24 hours (Section 4.0). The primary landing site is the Eastern Test Range (ETR). An investigation was made of descent from a 270-nautical mile orbit to ETR to define the descent flight mode and return performance capability of the orbiter.

Approach. Return from orbit to a selected landing site within a prescribed time interval requires that the orbiter perform a maneuver such that the recovery site is contained within the orbiter entry and landing footprint at the time of deorbit. In deorbit from a near-earth orbit to a specific touchdown site there are two times a day at which the orbit and landing site are coplanar. At one opportunity the spacecraft will approach the site from the descending direction. At these times, however, the spacecraft might be

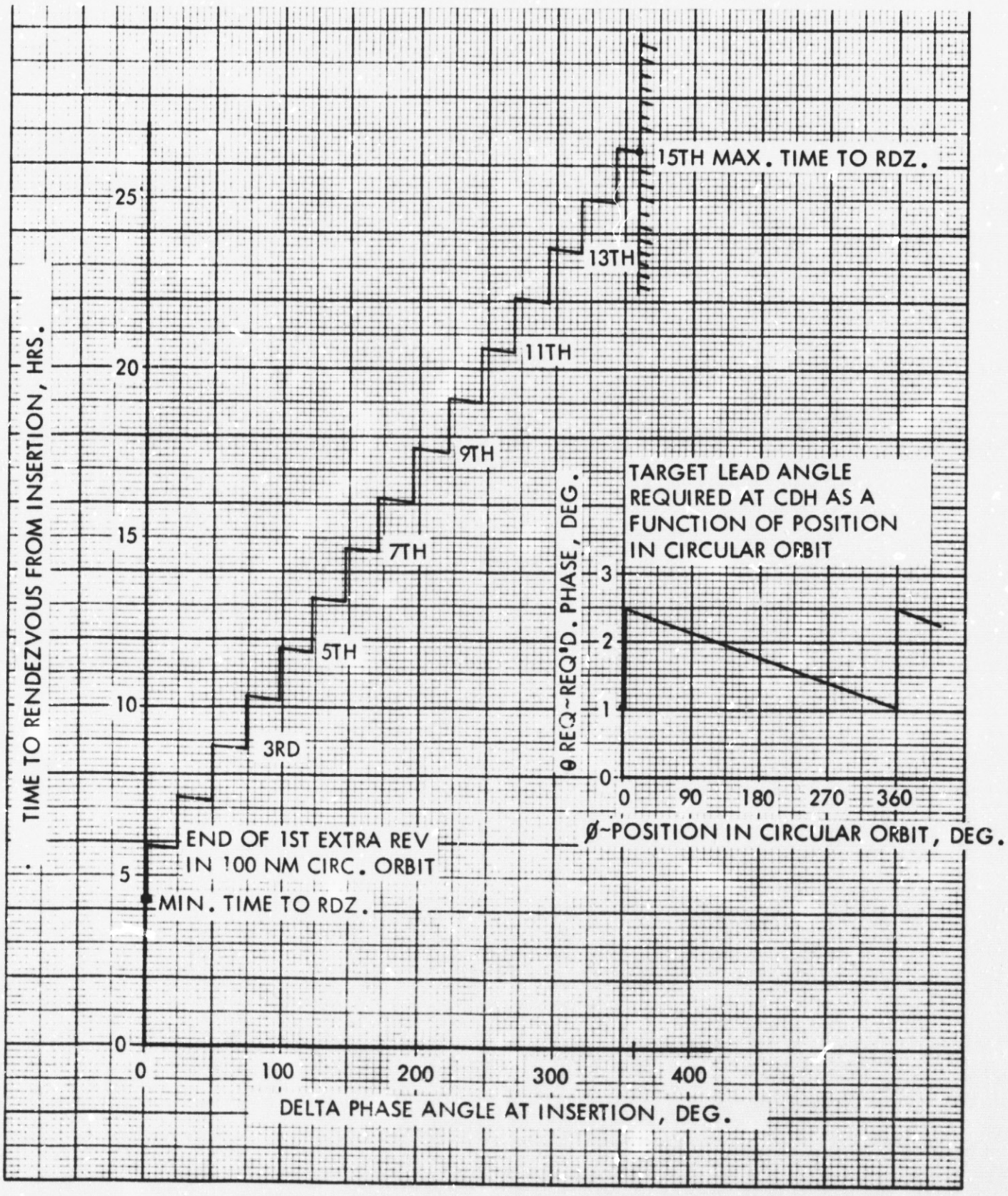

Figure 7.3-21. Time to Rendezvous Versus Phase Angle Difference at Insertion

Table 7.3-16. ILRV Rendezvous Maximum-Duration Timeline

Maximum Duration Constrained to 24-Hour Design Requirement

Event	ΔV (fps)	Resulting Orbit (n mi)	Time Between Events (hr.)	Target Lead (deg.)
1 Insertion	--	50/100	--	357.84
2 Circularization	91.0	100/100	.727	343.85
3 Phase Adjustment	142.3	100/180	19.845	14.02
4 NCC Maneuver	279.1	180/260	.748	4.65
5 CDH Maneuver	136.9	260/260	.773	1.03
6 TPI	22.0	260/271	.785	0.3
7 TPF	27.0 (Theor.)	270/270	.550	0.0
Totals	698.3		23.428	

at an arbitrary position within the 360-degree inplane arc of the orbit. Only a portion of the arc can be used as a deorbit point (window) due to various limits of propellant, systems accuracy, tracking, lighting, etc. The following problem usually exists. If the spacecraft is located within the deorbit window, the touchdown site may be out of the plane of the orbit and out of the landing footprint, or if the spacecraft is located in time when the orbit and site are coplanar, the spacecraft is outside of the deorbit window. This problem can be solved by out-of-plane capability in the form of lateral aerodynamic range or lateral thrusting, or by coplanar transfer to another orbit (phasing) whose period (after a sustained number of orbits) will result in the spacecraft arrival in the inplane window at the appropriate time for a coplanar deorbit.

The approach to defining descent maneuver requirements was to establish the out-of-plane ranging requirements for daily return capability as affected by orbital inclination, and the delay times associated with orbital phasing. Out-of-plane ranging by aerodynamic maneuvering during entry was combined with orbital phasing to establish the deorbit ΔV requirement and the maximum phasing time which would guarantee at least once daily return to ETR.

Computational Model. The attainment of a 100-percent probability of daily return capability requires that the spacecraft arbitrarily be located at any inplane position (i.e., 360-degree window) within the orbit plane. Figure 7.3-22 shows the significance of the 360-degree phase window criteria on the out-of-plane recovery requirements. The figure is a sketch of the rotating earth relative to a fixed inclined orbit plane. For convenience of illustration, assume the spacecraft phase is defined as zero at the ascending crossing of the equator (N). At some appropriate time, deorbit is performed with a subsequent left lateral maneuver to touch down when ETR is located at point A. Now consider later deorbit points spaced in the orbit plane through 360 degrees of phase position. As the vehicle advances to each deorbit point and accomplishes entry and touchdown, the recovery site advances from A to B. The time span between the touchdown from the first point to the last is one orbital period plus the extra interval of time resulting from the recovery site velocity component in the direction of the orbital track. The worst case out-of-plane is obviously when the left lateral out-of-plane range angle ($-\rho$) is numerically equal to the right lateral angle ($+\rho$).

The incident angle of the meridian planes A and B is

$$\Delta\Gamma_L = \omega\,(P + t_{L_2} - t_{L_1}) \qquad (1)$$

which equals the sum of the earth rotation and nodal regression rates (ω) multiplied by the time of travel of the site from A to B ($P + t_{L_2} - t_{L_1}$).

The associated precession of the line of nodes (i.e., change in longitude of the ascending node) is

$$\Delta\Gamma = -\omega P \qquad (2)$$

The out-of-plane angle ρ relative to the longitude of the ascending node was evaluated for a range of orbital inclinations.

Out-of-Plane Requirements. The results of out-of-plane requirements are presented in Figure 7.3-23 for all inclination values. The figure shows that the out-of-plane requirements for once daily return to ETR are a near-linear boundary zigzagging between the 180 and 360 degree phase windows as inclination is increased.

The physical significance of Figure 7.3-23 can be more readily understood by the following sketches representing orbital ground tracks crossing the latitude of ETR. In each case, the point representing ETR is located to define the largest tangential circle, the radius of which represents the out-of-plane requirement. Sketch A is the 360-degree phase window for twice-daily return.

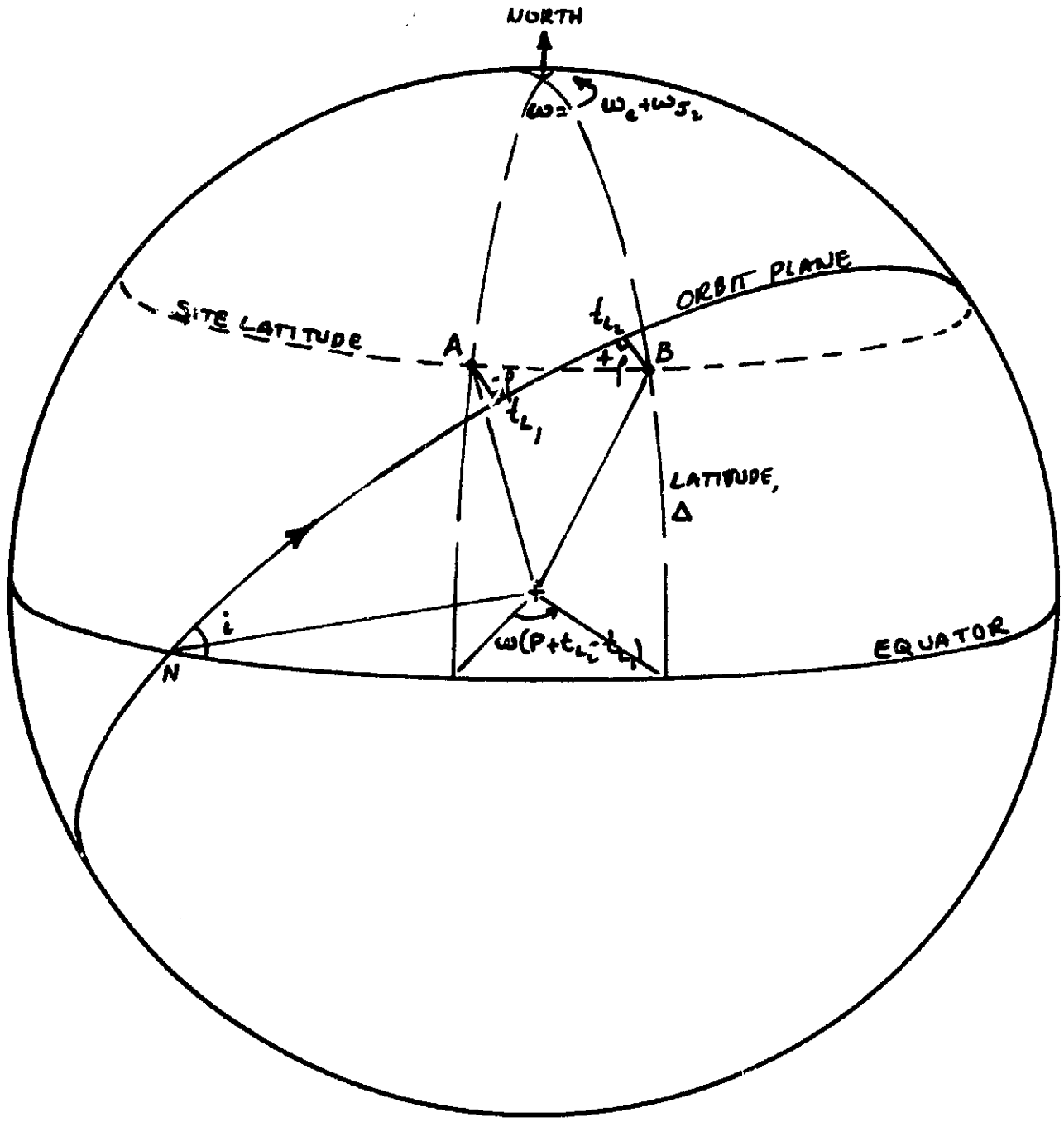

Figure 7.3-22. 360-Degree Descent Phase Window Definition

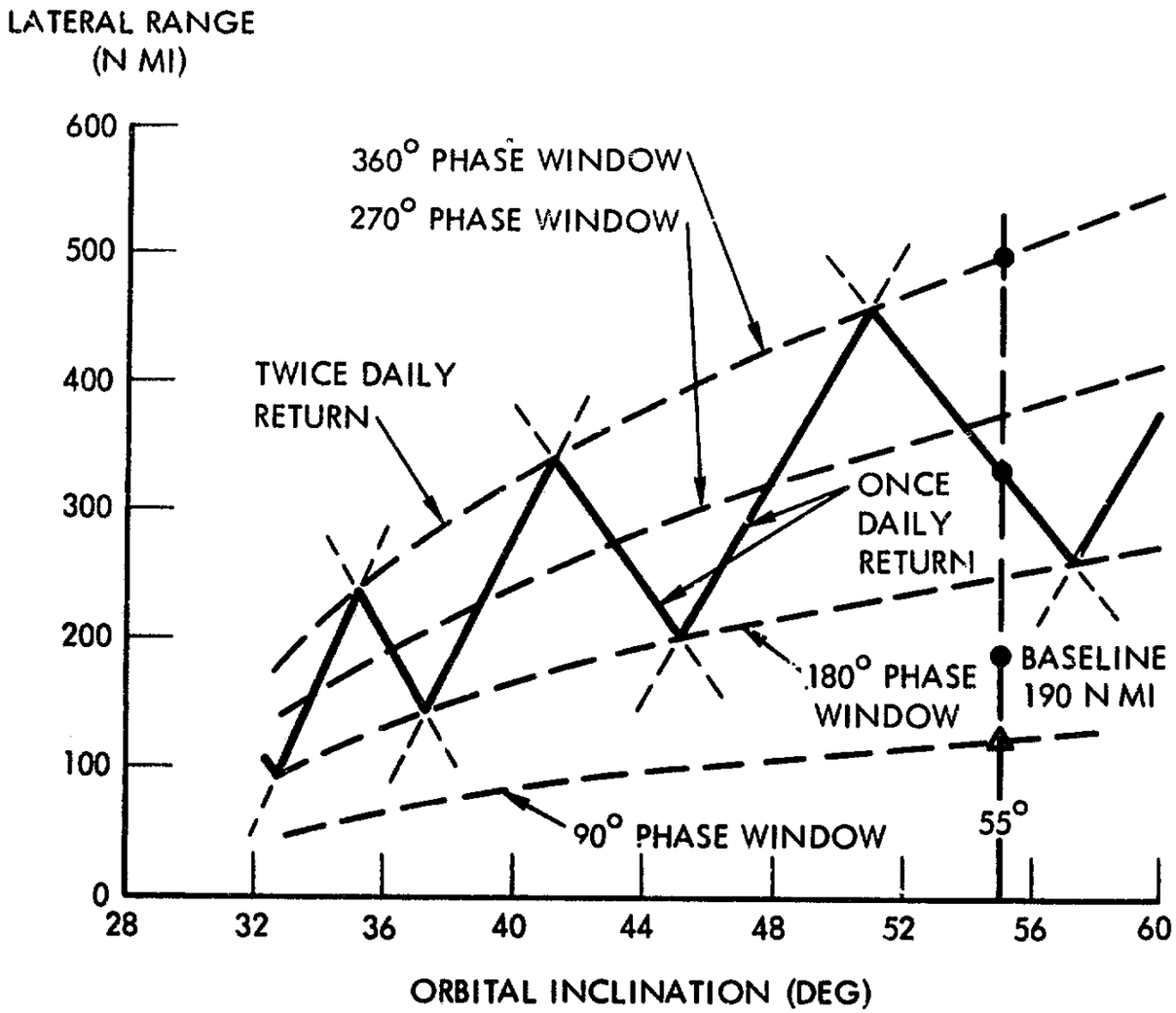

- TWICE DAILY RETURN 495 N MI LATERAL RANGE (α = 43°)
- ONCE DAILY RETURN 335 N MI LATERAL RANGE (α = 51°)
- BASELINE ORBITER REQUIRES DEORBIT PHASING (13.69 HRS)

Figure 7.3-23. Lateral Range Requirements - Direct Return to ETR, 270-Nautical Mile Orbit

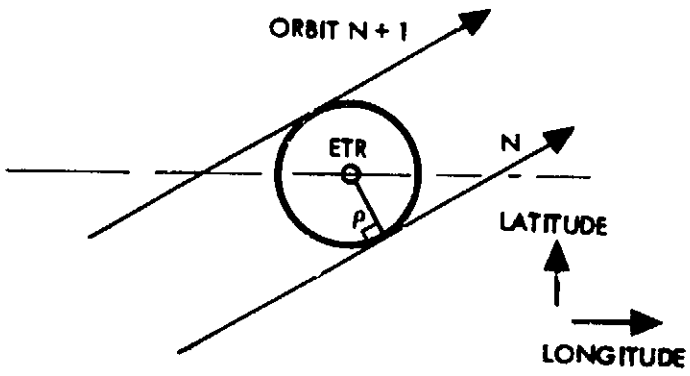

SKETCH (a) 360° WINDOW, TWICE DAILY RETURN

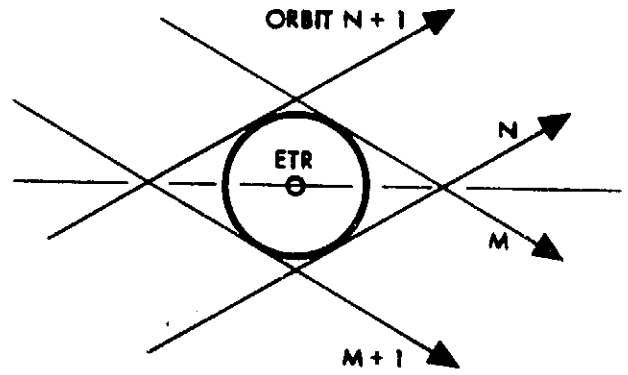

SKETCH (b) 360° WINDOW, TWICE DAILY RETURN - MATCHED PHASE WINDOWS OF ASCENDING AND DESCENDING SOLUTIONS

The peaks of the zigzag curve are indicative of the ascending and descending tracks crossing at the latitude of ETR as shown in Sketch B. The troughs of the zigzag curve are indicated by the case where the two circles in Sketch C are of equal radius.

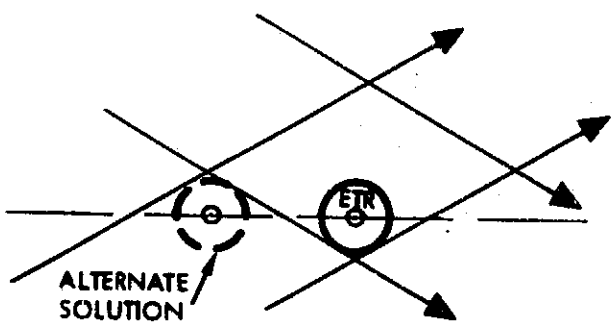

SKETCH (c) PERFECTLY AUGMENTED 180° WINDOWS

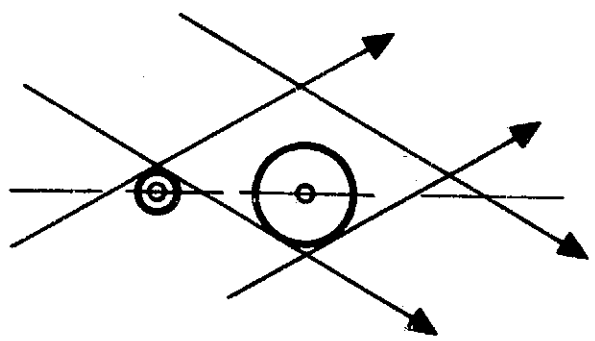

SKETCH (d) PARTIALLY AUGMENTED WINDOWS

Sketch D is an example of partially augmented windows as shown in Figure 7.3-23 by the near straight line limits of once-daily returns. The larger circle is the out-of-plane requirement shown by the solid line. The smaller circle represents out-of-plane values below the 180-degree phase window, hence, are not guaranteed daily solutions, but are valid operational solutions for some vehicle phase positions.

For the nominal ILRV mission at 55-degree inclination, Figure 7.3-23 indicates that for twice daily return to ETR, a lateral range of 500 nautical miles is required. Once-daily return requires 335 nautical miles of lateral range. These ranges are for direct descent from the 270-nautical mile circular orbit.

In-Plane Phasing Orbits. The out-of-plane requirements presented in Figure 7.3-23 can be reduced to essentially zero by the technique of inplane phasing without expenditure of additional deorbit ΔV in excess of the coplanar deorbit value. The technique is simply to divide the deorbit maneuver into two in-plane changes of state with a waiting period between the first burn and the final deorbit burn. The corrections to out-of-plane angle at touchdown by phasing involve a catchup phasing angle rate since a partial deorbit maneuver decreases the energy of the ellipse and decreases its period. To reduce the waiting time for phasing further, the expenditure of extra ΔV to increase the energy of the phasing ellipse will cause a retarding phasing angle rate. After an appropriate wait in a retarded phasing orbit, the deorbit maneuver can be efficiently performed at apogee.

The phase retard per orbit and the phase advance per orbit are supplementing to form a total phasing adjustment capability per orbital period, dependent on the mission orbital altitude, atmospheric drag limitations on perigee of the catchup orbit, and ΔV or other restraints on the apogee of the ellipse. This total phasing adjustment capability expressed in nodal adjustment per orbital period is,

$$\delta\Gamma = \omega \left[(P_{MAX} \cdot P_o) + (P_o - P_{MIN}) \right] = \omega (P_{MAX} - P_{MIN}) \qquad (3)$$

The maximum number of phasing orbits would be for a 100 percent adjustment of the longitude of the ascending node regression per orbit

$$N = \omega P_o/\delta\Gamma = P_o/(P_{MAX} - P_{MIN}) \qquad (4)$$

The maximum time for phasing

$$t = N P_{MAX} = P_o P_{MAX}/(P_{MAX} - P_{MIN}) \qquad (5)$$

Combined Lateral Ranging and Descent Phasing. Computations using Equation 5 for horizontal retro and posigrade in-plane maneuvers at the appropriate apogee and perigee positions were combined to provide the trade-off in Figure 7.3-24. The perigee altitude of the transfer conic was limited to 100 nautical miles to avoid drag losses. The highest apogee selected was 600 nautical miles. In order to limit the entry environment to the design value (corresponding to entry from a 270 nautical mile orbit at -1.5-degree flight path angle), an additional burn was performed to transfer back from any phase-retard orbit to the 270 nautical mile circular orbital altitude before performing the deorbit maneuver.

An example will illustrate use of Figures 7.3-23 and 7.3-24. At a hypersonic lift to drag ratio of 0.50, the orbiter has a lateral range of 190 nautical miles this corresponds to a phase window capability of about 135 degrees. From Figure 7.3-23, it is noted that a 240 degree window is required for once daily return. The deficit of 105 degrees of phase window could be compensated with orbital phasing. From Figure 7.3-24, at the minimum deorbit ΔV line, interpolation between 90 and 180 degrees yields 13.7 hours maximum time required for phasing. The important feature to note is that the mission requirement of one return to ETR at least once in 24 hours is readily met by use of combined phasing and lateral ranging during descent with no additional deorbit propellant requirements. These results are shown in Figure 7.3-25 which illustrates the two deorbit burns required.

If additional deorbit propellant is available, the worst case descent time can be reduced by use of a higher energy phasing orbit. Assuming a total mission on-orbit ΔV of 2000 feet per second, 1200 feet per second ΔV is the maximum which would be available for descent maneuvers. This would allow reducing the worst case delay time to 6.6 hours by phasing in a 270-by-510 nautical mile orbit. Final deorbit is performed at 270 nautical miles in order to not exceed design thermal environment.

The use of descent phasing in conjunction with lateral ranging is discussed further in Section 7.3.4.

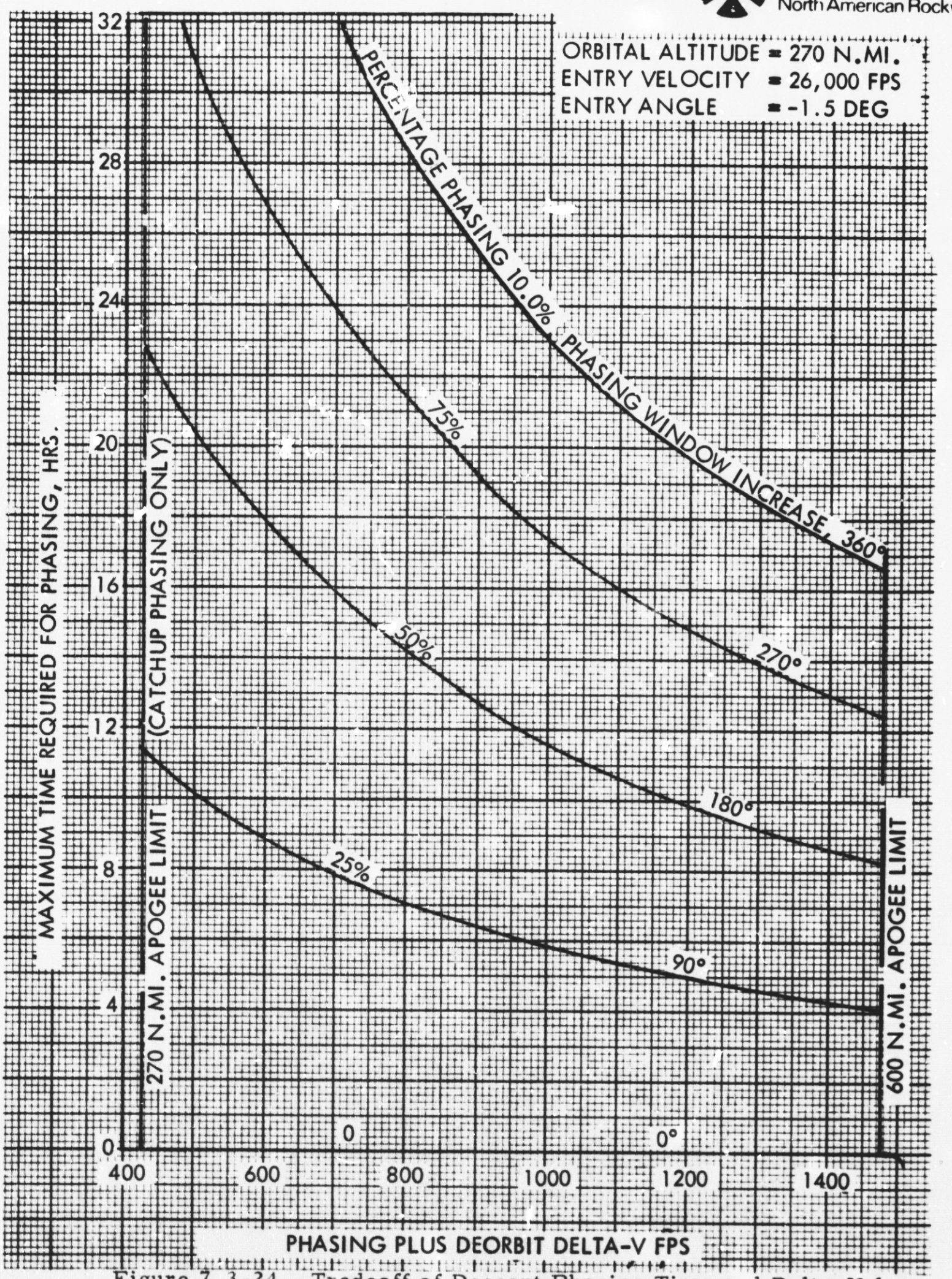

Figure 7.3-24. Tradeoff of Descent Phasing Time and Delta-V for Various Phase Window Increases

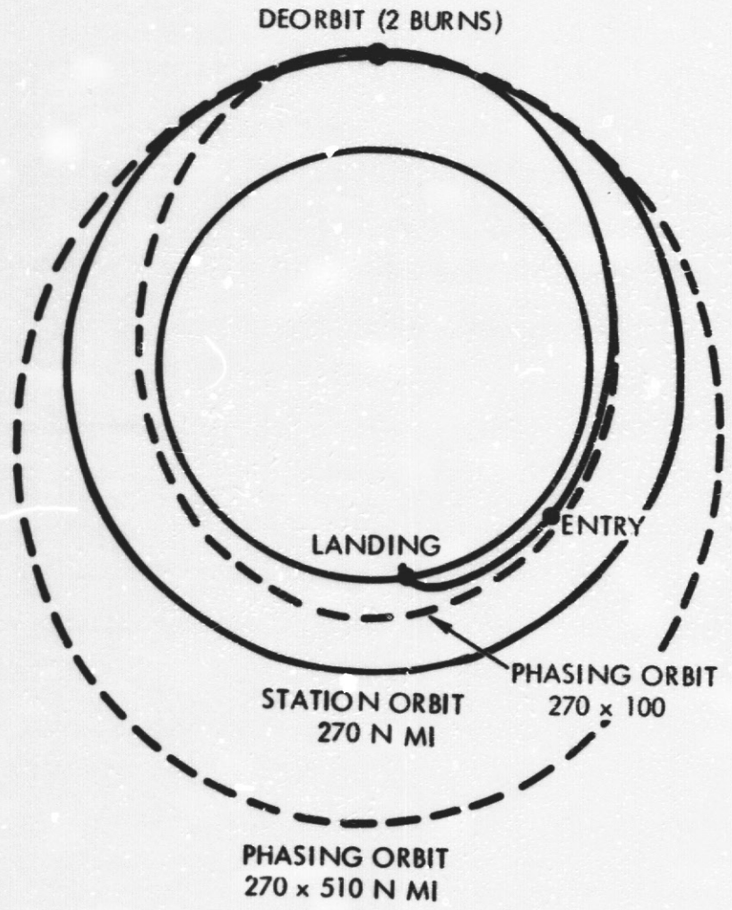

RETURN OPPORTUNITY	ΔV (FPS)	DELAY ORBITS	DELAY TIME (HRS)	REMARKS
ONCE DAILY	① 295 ② 130 425 TOTAL	9	13.69	• WORST CASE PHASING • MIN ΔV
ONCE DAILY	① 388 ② 812 1200 TOTAL	4	6.61	• MAX ΔV AVAILABLE • MIN DELAY TIME FOR WORST CASE PHASING

Figure 7.3-25. Return Site Phasing - 50,000-Pound Payload Orbiter, Cross Range = 190 Nautical Miles

Space Division
North American Rockwell

7.3.4 Entry Phase Analysis

Definition of logistic vehicle characteristics during the entry phase of the mission encompassed four major areas of investigation:

1. Development of orbiter entry trajectories for use in environmental analyses

2. Sensitivity analyses to establish the effect of entry lift loading on orbiter entry performance and design environments

3. Evaluation of alternative approaches to improve the lateral ranging capability of the baseline orbiter

4. Establishment of optimum booster descent mode to minimize flyback range

Concept Sizing

To facilitate establishment of sizes and weights of the logistic vehicle concept defined by NASA MSC, it was necessary to define parametric entry performance and design environment. The approach was to develop banked and unbanked entry trajectories for selected values of lift loading parameter W/C_LS. These data established the cross range capability of the MSC concept and were used to define entry thermal environment. In addition, the sensitivity of lateral range, peak heating, and heat load to lift loading was established.

Design entry trajectories were computed for the orbiter for two values of the lift parameter (W/C_LS of 32.3 and 50.0 psf) and for both unbanked and banked entry, using aerodynamic performance estimated for the 12,500-pound baseline (Section 7.2.3). The flight mode used maintained the pitch attitude of the orbiter at an angle of attack of 60 degrees (L/D of 0.5) throughout entry. The roll attitude varied in the following manner: either zero or 50 degrees until pullout; modulated roll after pullout to keep altitude constant until the equilibrium glide condition with roll attitude at either zero or 40 degrees is reached; and zero or 40 degrees roll maintained until the velocity is decreased to 3000 fps. Both right and left roll entries were computed. The initial and final conditions used for computing the trajectories are given in Table 7.3-17 and a summary of the results is presented in Table 7.3-18. All trajectories were computed with rotating-earth effects included.

The lateral range realized from a right-roll entry is seen to be appreciably greater than that realized from a left-roll entry; however, the average

of the right and left lateral ranges (i.e., 190 nautical miles) represents the true measure of the orbiter's performance. Although the change in W/C_LS from 32.3 to 50.0 psf does change the magnitude of the right and left lateral ranges, it has negligible effect on the average lateral range.

The primary effect of increasing W/C_LS from 32.3 to 50.0 psf is to increase the maximum stagnation heat transfer rate by 15 percent during an unbanked entry and by 27 percent during a banked entry.

A lateral range of 190 nautical miles is realized by flying a banked entry of 50 degrees prior to pullout and 40 degrees during equilibrium glide. (The value of 190 nautical miles was computed by averaging the lateral ranges realized from an entry flown with roll always to the right with that of an entry flown with roll always to the left). The banked entry results in a stagnation heat transfer rate 10 percent greater than the unbanked entry when W/C_LS is 32.3 psf and 17 percent greater when W/C_LS is 50.0 psf. However, the corresponding stagnation heat load is decreased by 15 percent when W/C_LS is 32.3 psf and by 12 percent when W/C_LS is 50.0 psf.

Weight estimates for the 12,500-pound payload class vehicle indicated that the lift parameter would be approximately 50 pounds per square foot. Consequently, the nominal entry design trajectory for W/C_LS of 50.0 psf was selected.

Table 7.3-17. Initial and Final Conditions for Orbiter Entry Trajectories

	Inertial	Relative
Initial conditions:		
Flight time, sec	0.0	0.0
Velocity, fps	25,992.5	25,134.1
Altitude, ft	400,000.0	400,000.0
Flight-path angle, deg	-1.500	-1.551
Inclination, deg	55.000	57.903
Longitude, deg	0.0	0.0
Latitude, deg	0.0	0.0
Azimuth, deg	35.000	32.097
Longitudinal range, nm	0.0	0.0
Lateral range, nm	0.0	0.0
Heading angle, deg	0.0	0.0
Final condition:		
Velocity, fps		3,000.0

Table 7.3-18. Summary of Design Entry Trajectories

Quantity	W/C_LS = 32.3 PSF				W/C_LS = 50 PSF			
	UnLanked Entry (Ø=0/0)	Unbanked Entry (-Ø=0/0)	Banked Entry (Ø=50/40)	Banked Entry (-Ø=50/40)	Unbanked Entry (Ø=0/0)	Unbanked Entry (-Ø=0/0)	Banked Entry (Ø=50/40)	Banked Entry (-Ø=50/40)
At Pullout								
Time, sec	268.1	268.1	295.1	296.7	283.0	283.0	314.9	317.0
Altitude, ft	268,190	268,190	258,760	258,450	261,220	261,220	251,310	250,960
Velocity, fps	24,119	24,119	23,190	23,137	24,153	24,153	23,200	23,138
Dynamic pres., psf	8.2	8.2	12.5	12.6	12.0	12.0	17.8	18.0
Total load factor	0.57	0.57	0.87	0.88	0.54	0.54	0.80	0.81
At Terminus								
Time, sec	994.4	989.7	812.4	799.5	1019.2	1014.6	839.5	826.3
Altitude, ft	141,610	141,590	138,040	137,760	131,370	131,350	127,940	127,690
Velocity, fps	3,000	3,000	3,000	3,000	3,000	3,000	3,000	3,000
Long range, nm	2,990	2,979	2,432	2,408	3,096	3,085	2,545	2,521
Lateral range, nm	99	-10	216	-154	102	-5	220	-161
Heading angle, deg.	5.0	1.6	43.6	-38.9	5.1	1.9	43.6	-38.6
Maximum Values								
Dynamic pres., psf	24.9	24.9	29.8	30.3	38.6	38.7	46.6	47.3
at Time, sec	888	880	736	720	896	888	776	760
Total load factor	1.72	1.73	2.06	2.10	1.73	1.73	2.08	2.12
at Time, sec	888	880	736	720	896	888	776	760
[1]Stag. heat rate, Btu/ ft^2/sec at Time, sec	40	40	44	44	46	46	54	54
	256	256	264	272	272	272	288	288
[1]Stag. heat load, Btu/ ft^2	20,750	20,680	17,710	17,530	25,470	25,400	22,460	22,240

[1]Reference radius = 1 ft.

Design Improvement and Sensitivity Analysis

Wing Loading and Angle of Attack Trades. An investigation was conducted to determine the effects on orbiter entry performance and environment of varying the wing loading from 58 to 162 psf and the angle of attack from 40 to 70 degrees. The aerodynamic characterisitics used for the 16 combinations of wing loading (W/S) and angle of attack (α) are given in Figure 7.3-26. (The baseline orbiter configuration with a wing loading of 90 psf and an angle of attack of 60 degrees has an L/D of 0.5 and a W/C_LS of 50.0 psf.) The initial and final conditions used in computing the entry trajectories are given in Table 7.3-26. The results shown in Figures 7.3-27 and 7.3-28 were computed by averaging the values realized from an entry flown with roll always to the right with that of an entry flown with roll always to the left.

Figure 7.3-27 shows the effect on the orbiter's ranging performance of varying wing loading and angle of attack. Both lateral and longitudinal range increase greatly as angle of attack is decreased; however, lateral range is almost unaffected and longitudinal range increases only 10 percent as wing loading is increased.

Figure 7.3-28 shows the effect on the orbiter's entry environment of varying wing loading and angle of attack. The primary effect of decreasing the angle of attack is to increase the stagnation heat load and the primary effect of increasing the wing loading is to increase the maximum value of the stagnation heat transfer rate. Because of the dip in the curve of stagnation heat transfer rate as the angle of attack is varied, an appreciable increase in lateral range can be realized without a corresponding increase in stagnation heat transfer rate. For example, the lateral range of the baseline configuration can be increased from 190 to 400 nautical miles by decreasing the angle of attack from 60 to 47.5 degrees while maintaining the same value of maximum stagnation heat transfer rate. However, the corresponding stagnation heat load is increased by 45 percent.

The effect on entry performance and environment of decreasing the angle of attack to 20 degrees was investigated for the baseline orbiter configuration (wing loading of 90 psf). The aerodynamic characteristics used are given in Figure 7.3-29 and the results are presented in Figure 7.3-30. At an angle of attack of 20 degrees, a lateral range of 1400 nautical miles can be realized (if viscous interaction effects are ignored). However, the maximum stagnation heat transfer rate is increased by 49 percent and the stagnation heat load is increased by 374 percent.

Lateral Ranging. The baseline orbiter designed for entry at 60 degrees angle of attack has a lateral range capability of approximately 190 nautical miles. This capability, combined with orbital phasing during descent has been shown to be adequate to meet the ILRV mission requirement of a return

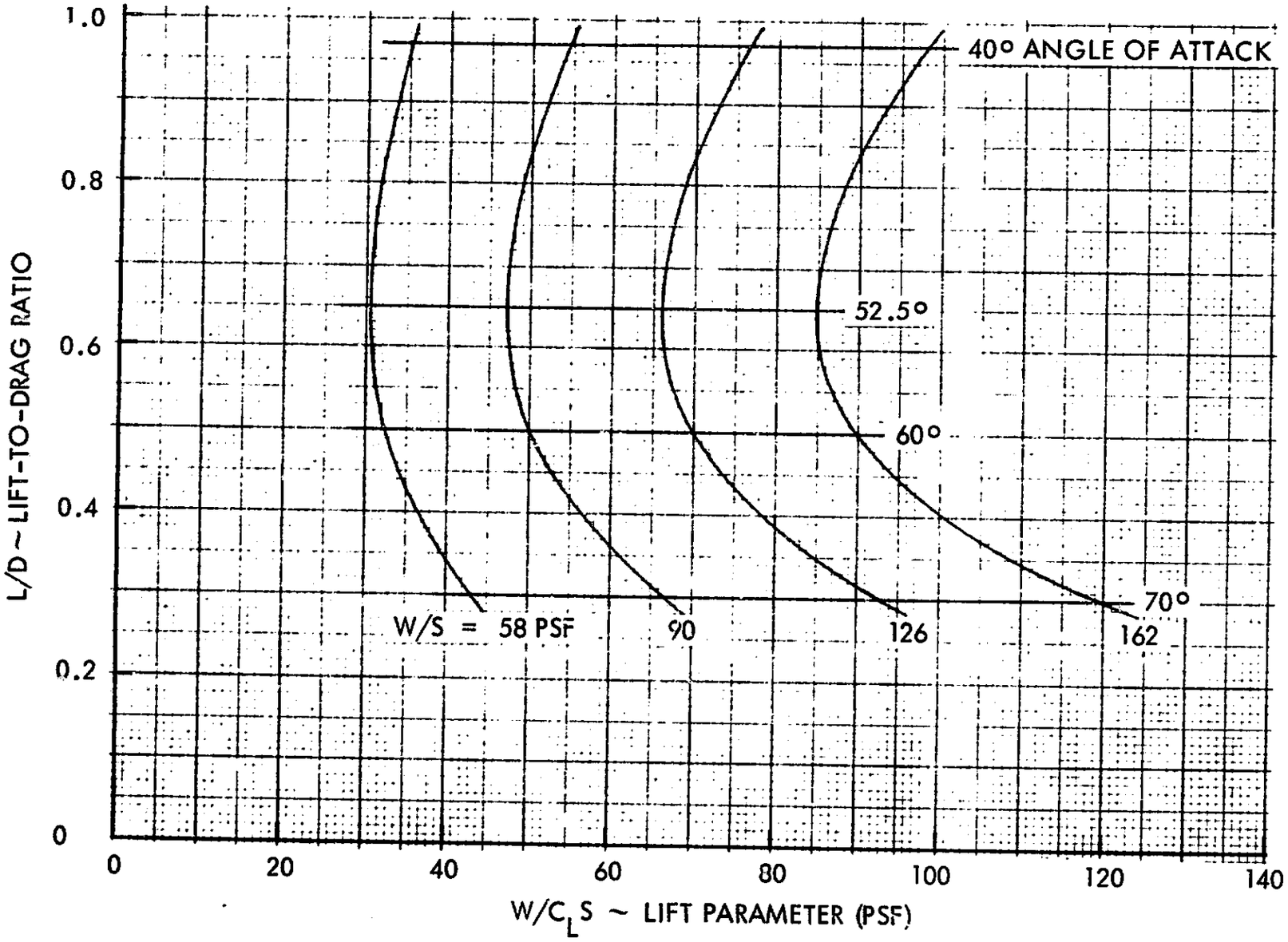

Figure 7.3-26. Effect of Wing Loading and Angle of Attack on Aerodynamic Characteristics of Orbiter

Figure 7.3-27. Effect of Wing Loading and Angle of Attack on Entry Performance of Orbiter

Space Division
North American Rockwell

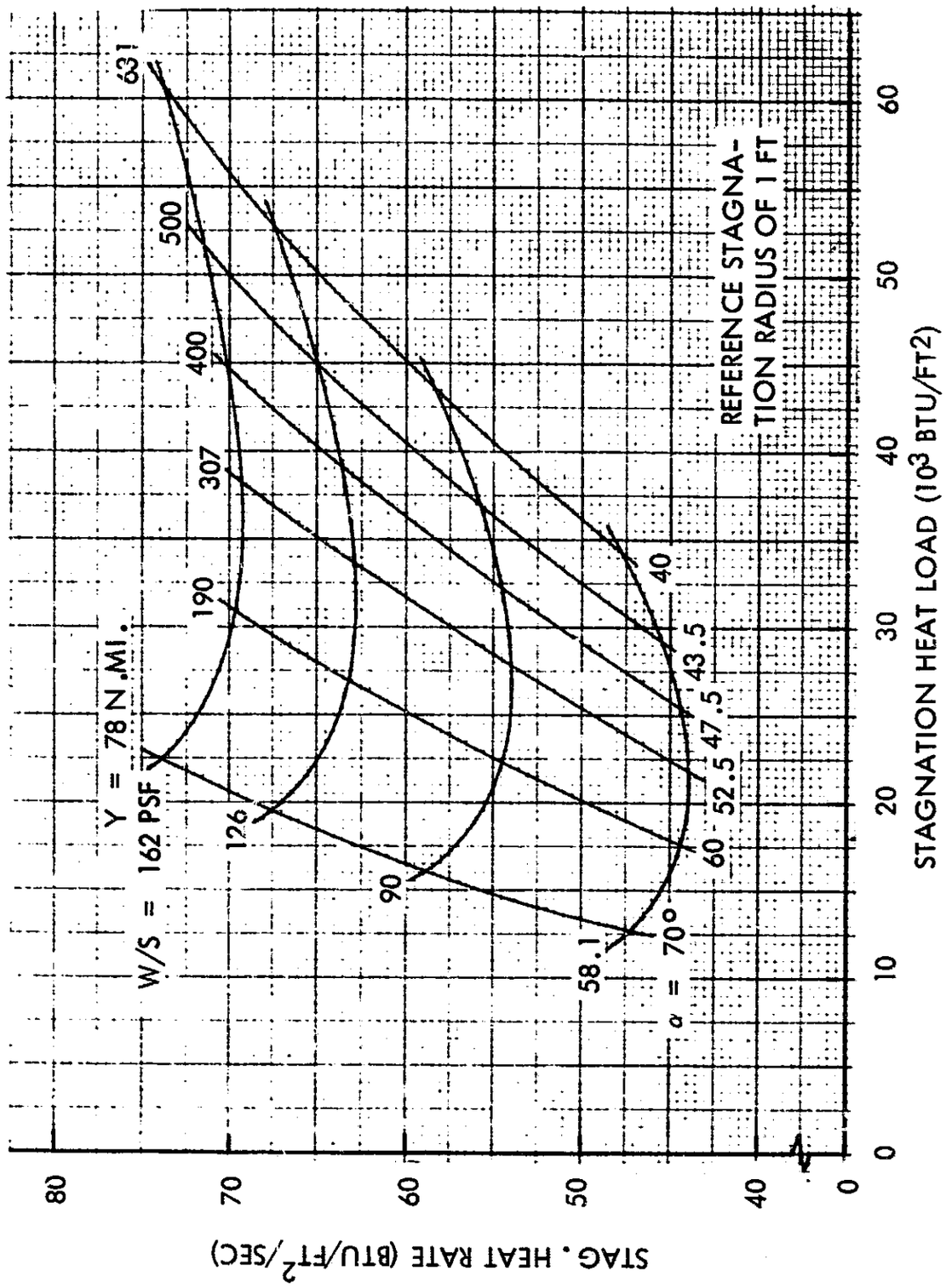

Figure 7.3-28. Effect of Wing Loading and Angle of Attack on Entry Environment of Orbiter

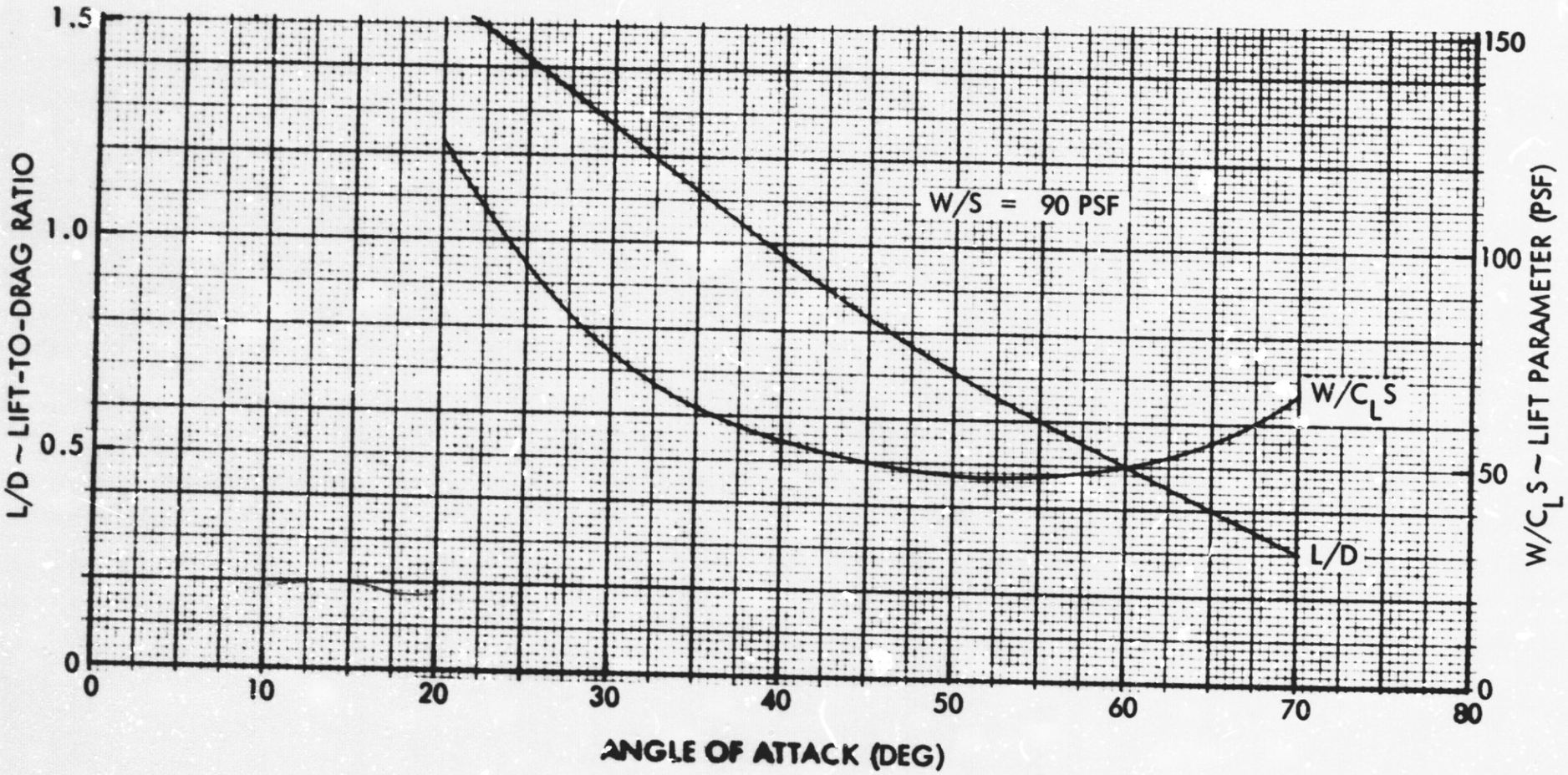

Figure 7.3-29. Effect of Angle of Attack on Aerodynamic Characteristics of Baseline Orbiter

Figure 7.3-30. Effect of Angle of Attack on Entry Performance and Environment of Baseline Orbiter

opportunity to the primary landing site (ETR) at least once every 24 hours. Some missions have been identified which require lateral ranging capability as great as 1500 nautical miles, and NASA requested an investigation of alternative approaches to improve the lateral range performance of the baseline orbiter. Five approaches were considered:

1. Orbital phasing before entry
2. Subsonic cruise, using fuel obtained by reducing the payload weight
3. Orbital plane change, using rocket propellant obtained from the on-orbit ΔV budget and from reducing payload weight
4. Improved hypersonic performance capability obtained by reducing the angle of attack during entry
5. Combinations of the above

In case (4) above, the entry thermal environment will be more severe at the leading edges of wing and tail surfaces, at the body nose region, and along the lower surfaces where turbulent flow will be experienced due to flight at lower altitudes. For this case, two approaches were considered: (a) the angle of attack is decreased as velocity decreases in a manner designed to prevent the wing leading edge temperature from exceeding the design value, and (b) the angle of attack is decreased with no constraint on wing leading edge temperature. Velocity limits for case (a) are shown later in Table 7.4-4.

Orbital Phasing. At the nominal entry angle of attack of 60 degrees, the baseline orbiter has a lateral range of 190 nautical miles. The ILRV mission requirement for the orbiter to have the capability to return to the launch site within 24 hours can be met by lateral ranging, deorbit phasing, or a combination of both. For direct return from a 270-nautical mile 55-degree orbit, a lateral range of about 500 nautical miles is required for twice daily return and 335 nautical miles for at least one daily return (Section 7.3.2). With the ILRV lateral range of 190 nautical miles, the maximum descent phasing time will not exceed 24 hours if descent phasing is employed. For a guaranteed once daily return, an equivalent lateral range of 335 miles is obtained by combined phasing and aerodynamic maneuvering. The phasing time required is 13.7 hours. The total velocity increment required for the phasing plus deorbit maneuver is 425 feet per second and is equal to the nominal deorbit requirement. This is 75 feet per second less than the design retro velocity.

Increased equivalent lateral ranging can be obtained by additional phasing or by expending additional propellant. For 24 hours phasing, an additional equivalent lateral range of about 260 nautical miles is possible

without expending more than the nominal deorbit ΔV of 425 feet per second. This would increase the ranging capability of the baseline from 190 to 450 nautical miles. This is apparent from Figures 7.3-23 and 7.3-24. Figure 7.3-24 indicates that for a maximum phasing time of 24 hours, a phasing window increase of 189.5 degrees is obtained. As seen from Figure 7.3-23, this corresponds to about 260 nautical miles of lateral range.

Further increases in equivalent lateral ranging can be realized with expenditure of additional phasing plus deorbit propellant. The relationship is illustrated in Figure 7.3-24. For a nominal mission, the maximum on-orbit propellant available will provide 1200 feet per second ΔV. As shown on the figure, a 360-degree phase window increase would be realized with 1200 feet per second phasing plus deorbit ΔV at a maximum phasing time of 19.7 hours. For a 270-nautical mile circular orbit at 55 degrees inclination, the corresponding lateral range increase is about 495 nautical miles. If the maximum phasing time is 24 hours, the equivalent lateral range increase would be about 630 nautical miles, or a total ranging of 820 nautical miles when combined with aerodynamic maneuvering during entry.

Subsonic Cruise. Using subsonic cruise after entry, a maximum additional range of 855 nautical miles can be obtained by exchanging payload for turbojet fuel. The range versus payload trade for the 50,000-pound payload orbiter is illustrated in Figure 7.3-31. A maximum of 845 nautical miles could be obtained at zero payload when the 2,000 fps on-orbit ΔV is maintained.

Orbital Plane Change. If the total on-orbit propellant is used for a plane change maneuver, an increase in lateral range of 260 miles could be obtained. However, approximately 1000 fps is required for ascent, rendezvous, and docking at the space station. If the remaining 1000 fps is used for a plane change maneuver, an additional lateral range of approximately 130 nautical miles could be obtained. This gives a total range of 320 nautical miles resulting from a combined plane change plus aerodynamic maneuver. Additional ranging can be obtained by off-loading payload and adding propellant to make the plane change. If all the payload were converted to plane change propellants, a maximum of 720 nautical miles would be obtained when the 2000 fps on-orbit ΔV is maintained. Subsonic cruise is less costly than the plane change maneuver in terms of payload loss.

Hypersonic Maneuver. The previous discussions of ranging have been restricted to the baseline case where the angle of attack at entry is 60 degrees. As discussed in the previous section, a significant increase in lateral ranging can be obtained if the angle of attack is reduced so that the hypersonic performance capability of the orbiter is increased. Evaluation of the hypersonic aerodynamic characterisitics of the 50,000-pound payload class orbiter

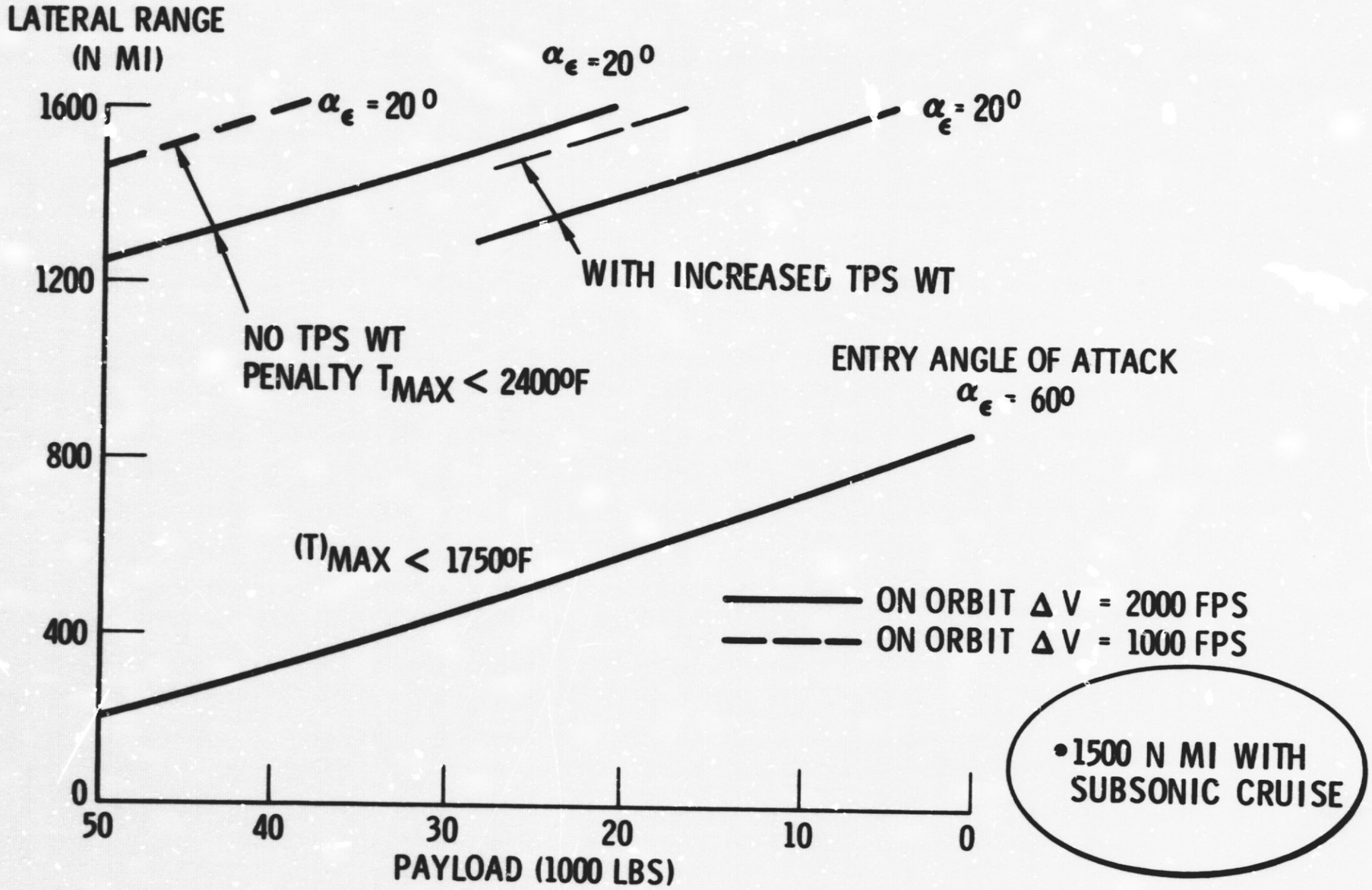

Figure 7.3-31. Lateral Range Capability With Subsonic Cruise

Space Division
North American Rockwell

indicates that the maximum lift-to-drag ratio is approximately 1.56 obtained at an angle of attack of about 20 degrees. For this case, the maximum lateral range with 50,000-pound payload is approximately 1240 nautical miles when accounting for the effects of viscous interactions on the hypersonic performance characteristics. The effects on entry thermal environment are indicated in Figure 7.3-32 for points on the body surface. Maximum temperatures are not expected to exceed 2300 F over 90 percent of the surface area. However, the stagnation heat load is about 5.2 times as great as for entry at 60 degrees angle of attack. Correlation of thermal protection system (TPS) weight with heat load indicated that TPS weight varied with the 1/3 power of the stagnation heat load. This results in a 72 percent increase (22,000 pounds) in TPS weight. These results represent only a gross approximation to the impact on the vehicle design due to entry at 20 degree angle of attack. The effect on entry control and design loads was not considered. In addition, a more extensive study of thermal environment is required to confirm the feasibility of this approach.

Combined Ranging. The improved lateral ranging which could be achieved with subsonic cruise following entries at 60-degree and 20-degree angle of attack is illustrated in Figure 7.3-31. The previous discussion indicated that to enter at 20 degrees angle of attack, a 22,000-pound increase in TPS weight would be required. For a fixed size orbiter, this amounts to 22,000 pounds reduction in payload. Combining reduced angle of attack entry with subsonic cruise, a 1500-nautical mile range capability would be obtained with 15,000-pound payload capability. If the on-orbit ΔV requirement were reduced by 1000 ft/sec, 1500 nautical miles cross range could be obtained with 28,000 pounds payload for entry at 20 degrees angle of attack.

Booster Turnaround Trades. To support selection of the end boost injection altitude discussed in Section 7.3.2, an investigation was conducted to determine the effect on booster entry performance and environment of varying the injection altitude of the boost trajectory from 45 to 80 nautical miles. The results are presented in Figure 7.3-33 for a straight-ahead entry without any pitch modulation. The flight mode used maintained the pitch attitude of the booster at an angle of attack of 60 degrees throughout entry and varied the roll attitude in the following manner: 180 degrees until apogee and zero degrees thereafter. The initial and final conditions used in computing the trajectories are given in Table 7.3-19. Figure 7.3-33 shows that as the injection altitude is increased, the maximum normal load factor experienced by the booster during entry increases from 3.23 to 6.35 and the associated flyback range increases from 392 to 515 nautical miles.

In an effort to decrease the flyback range, an investigation was conducted of the turnaround performance and environment realized from flying banked entries. Normal load factor was restrained from exceeding a specified value by modulating the pitch attitude of the booster. The flight mode

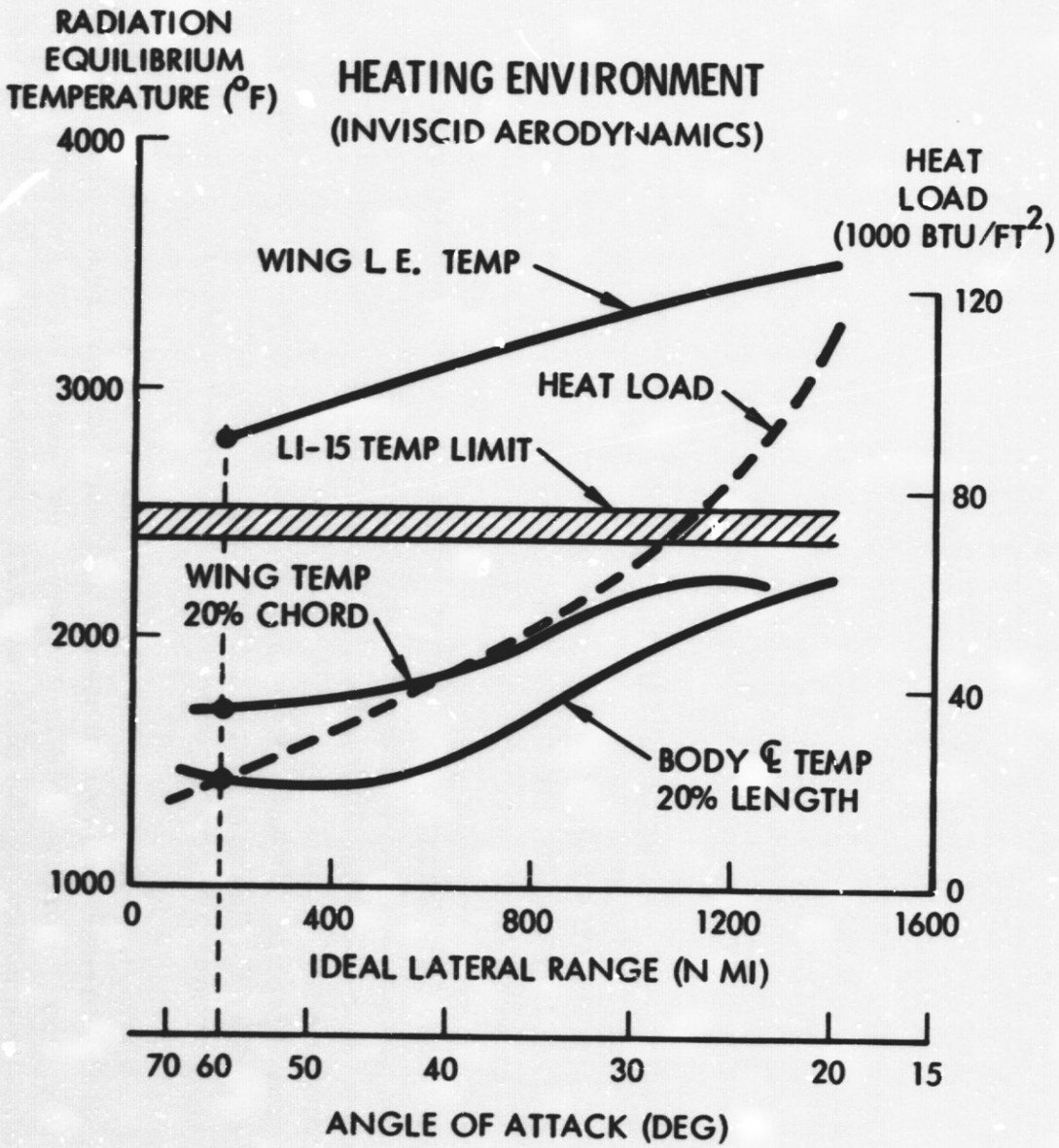

- MAX RANGE N MI
  - 1400 IDEAL
  - 1240 ACTUAL
- AT MAX RANGE TEMP < 2300 °F OVER 90 PERCENT SURFACE AREA
- HEAT LOAD 5.2 TIMES BASELINE AT MAX RANGE, 72 PERCENT INCREASE IN TPS WEIGHT (22,000 LB)
- 1500 N MI WITH CRUISE PROPELLANT, PAYLOAD REDUCED TO 15,000 LB

Figure 7.3-32. Orbiter Lateral Range Capability at Reduced Angle of Attack, 50,000-Pound Payload Orbiter

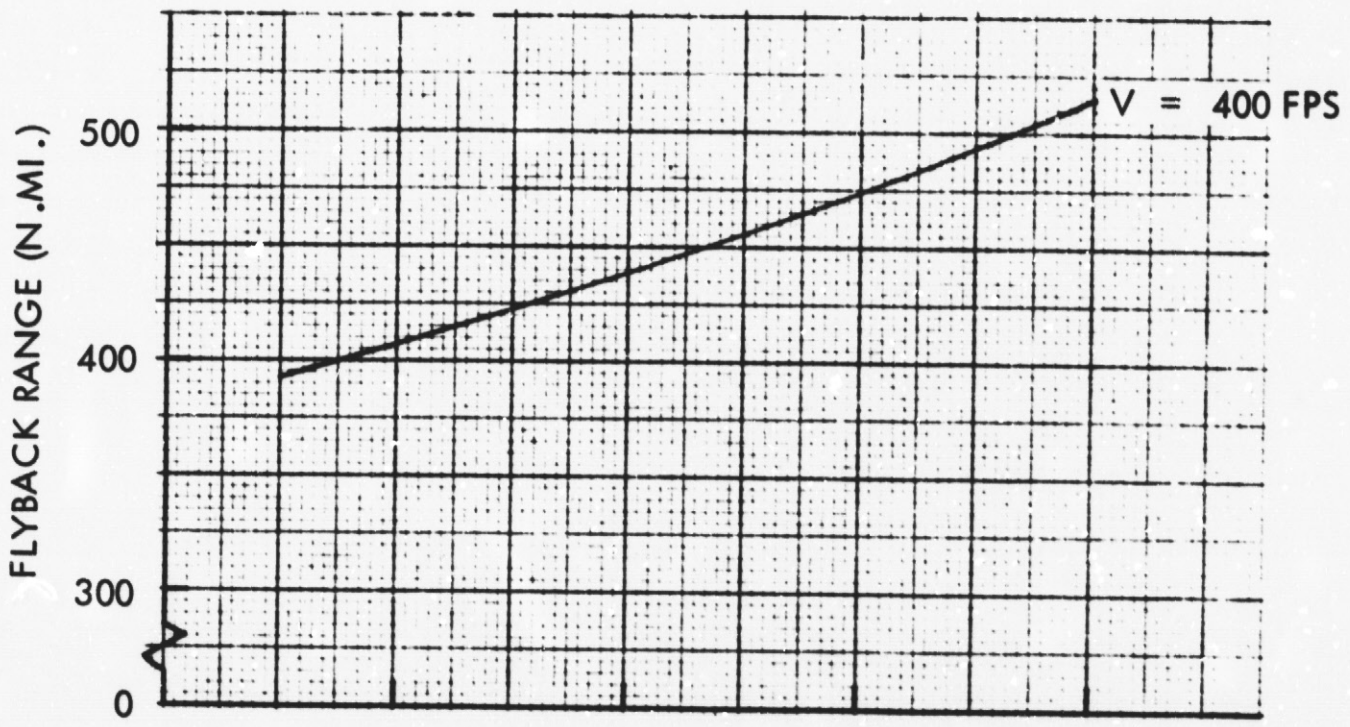

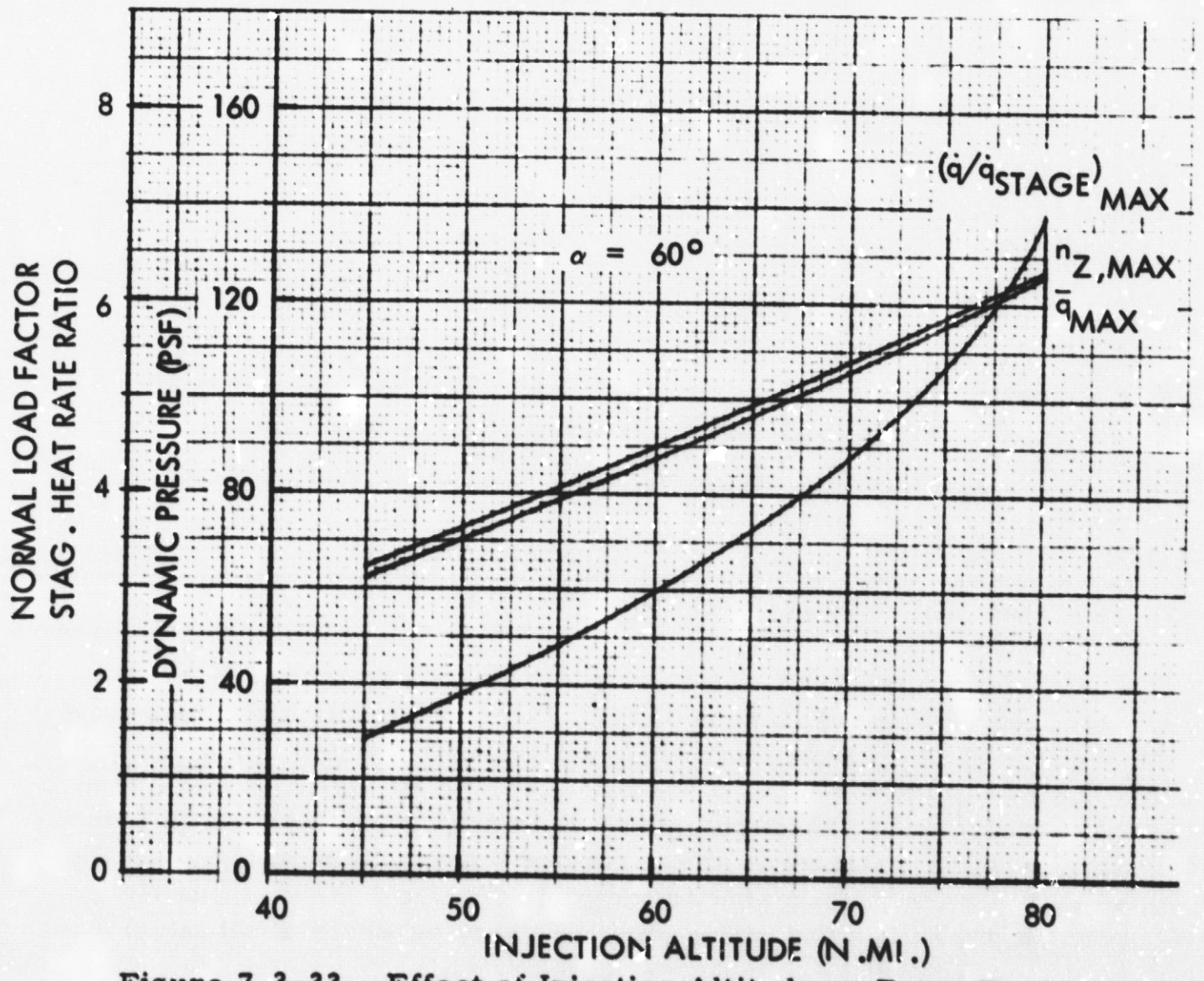

Figure 7.3-33. Effect of Injection Altitude on Entry Performance and Environment of Booster

used varied the pitch attitude to provide the following schedule of angle of attack: 52.5 degrees (maximum lift coefficient) until the specified normal load factor was reached; modulated angle of attack to hold a constant normal load factor until either the angle of attack was 52.5 degrees or the 180-degree turnaround was completed; and either 15 or 4.5 degrees during the glide following the completion of the turnaround. The roll attitude varied in the following manner: 90 degrees until the resultant load factor reached 0.5; 60 degrees until completion of the 180-degree turnaround; and zero degrees until the velocity is decreased to 400 fps. The aerodynamic characteristics used for the booster are given in Table 7.3-20. The results of the investigation are presented in Figures 7.3-34, -35, and -36.

Table 7.3-19. Initial and Final Conditions for Booster Turnaround Trajectories

	Injection Altitude (Nautical Miles)			
	45	50	60	80
Initial conditions:				
Flight time, sec	0.0	0.0	0.0	0.0
Relative velocity, fps	10,139.0	10,082.0	10,040.0	10,173.0
Altitude, ft	233,700.0	242,000.0	256,700.0	281,800.0
Flight-path angle, deg	5.94	6.68	8.30	11.93
Inclination, deg	57.16	57.17	57.18	57.18
Longitude, deg	280.57	280.56	280.55	280.58
Latitude, deg	29.90	29.88	29.87	29.90
Azimuth, deg	38.72	38.70	38.69	38.70
Longitudinal range, nm	98.90	97.80	96.90	99.50
Lateral range, nm	0.0	0.0	0.0	0.0
Heading angle, deg	0.0	0.0	0.0	0.0
Weight, lb	559,200.0	558,800.0	561,100.0	572,500.0
Final condition:				
Relative velocity, fps	400.0	400.0	400.0	400.0
*measured from launch site				

Presented in Figures 7.3-34 and -35 are the results of the effect of varying the injection altitude from 45 to 60 nautical miles and the normal load factor limit from 2.5 to 4.0. Minimum angle of attack and the associated maximum dynamic pressure experienced during the turn while normal load factor is held constant are shown plotted versus flyback range in Figure 7.3-34, and versus normal load factor in Figure 7.3-35. The flyback range shown in these figures was computed using an angle of attack of

Table 7.3-20. Aerodynamic Characteristics of Booster

Mach No.	α = 0°	α = 15°	α = 30°	α = 45°	α = 52.5°	α = 60°
C_L - LIFT COEFFICIENT						
0.0	0.560	1.280	1.750	2.400	2.600	2.150
0.5	0.560	1.280	1.750	2.400	2.600	2.150
0.9	0.500	1.351	1.740	2.350	2.600	2.150
1.1	0.160	1.330	1.700	2.300	2.500	2.050
2.0	0.035	0.600	1.250	1.850	1.980	1.900
3.0	-0.070	0.400	1.130	1.760	1.860	1.780
30.0	-0.070	0.400	1.130	1.760	1.860	1.780
C_D - DRAG COEFFICIENT						
0.0	0.0530	0.4740	1.2238	2.5263	3.3548	3.5833
0.5	0.0530	0.4740	1.2238	2.5263	3.3548	3.5833
0.9	0.0530	0.4740	1.2168	2.5000	3.3548	3.5833
1.1	0.0530	0.4586	1.1888	2.4731	3.3333	3.5345
2.0	0.0700	0.2727	0.8741	2.0556	2.7500	3.4545
3.0	0.0700	0.2000	0.7902	1.9556	2.6957	3.3905
30.0	0.0700	0.2000	0.7902	1.9556	2.6957	3.3905
L/D - LIFT-TO-DRAG RATIO						
0.0	10.57	2.70	1.43	0.95	0.775	0.60
0.5	10.57	2.70	1.43	0.95	0.775	0.60
0.9	9.43	2.85	1.43	0.94	0.775	0.60
1.1	3.02	2.90	1.43	0.93	0.75	0.58
2.0	0.50	2.20	1.43	0.90	0.72	0.55
3.0	-1.00	2.00	1.43	0.90	0.69	0.525
30.0	-1.00	2.00	1.43	0.90	0.69	0.525
Reference area = 7550 square feet						

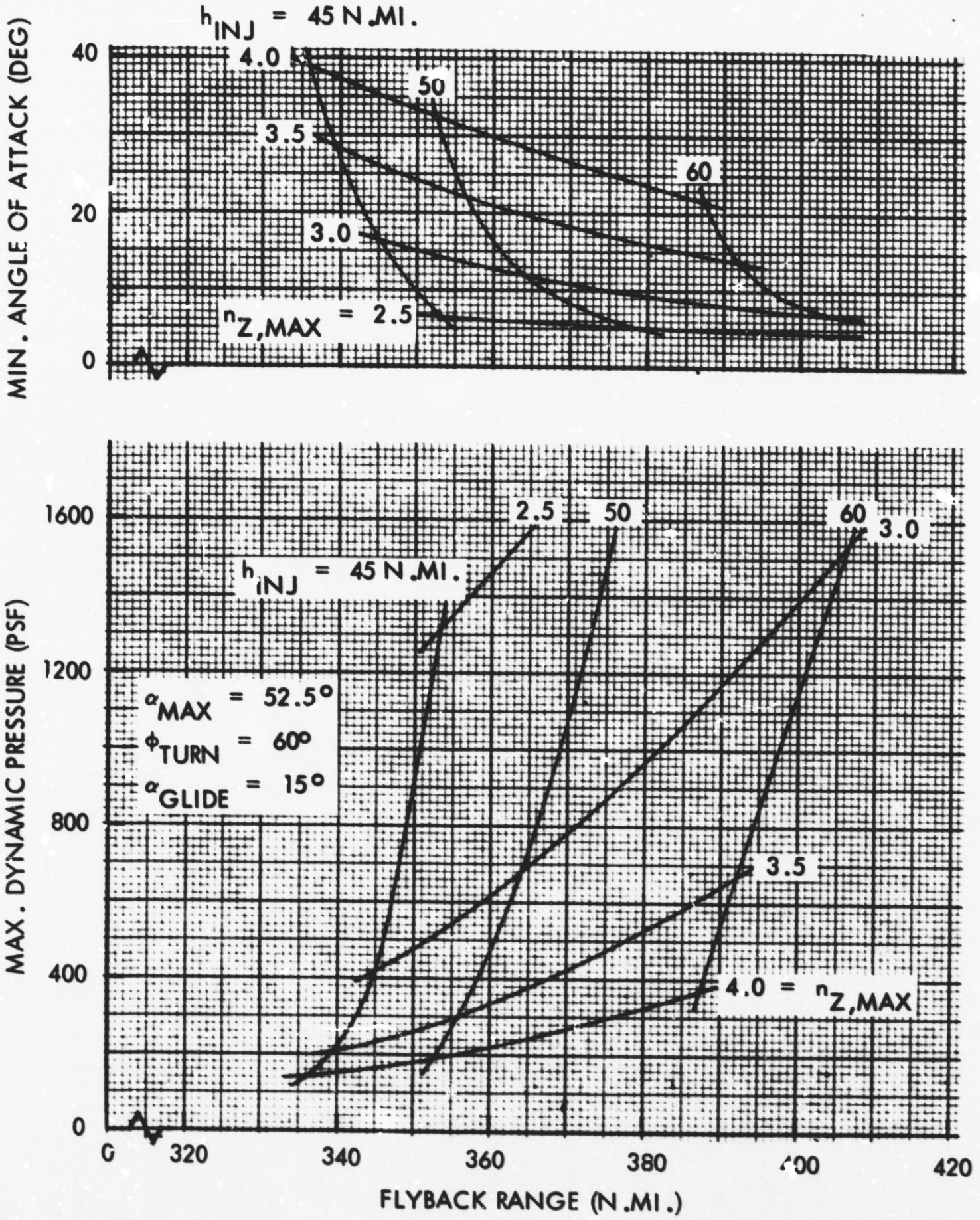

Figure 7.3-34. Effect of Injection Altitude and Normal Load Factor Limit on Turnaround Performance and Environment of Booster

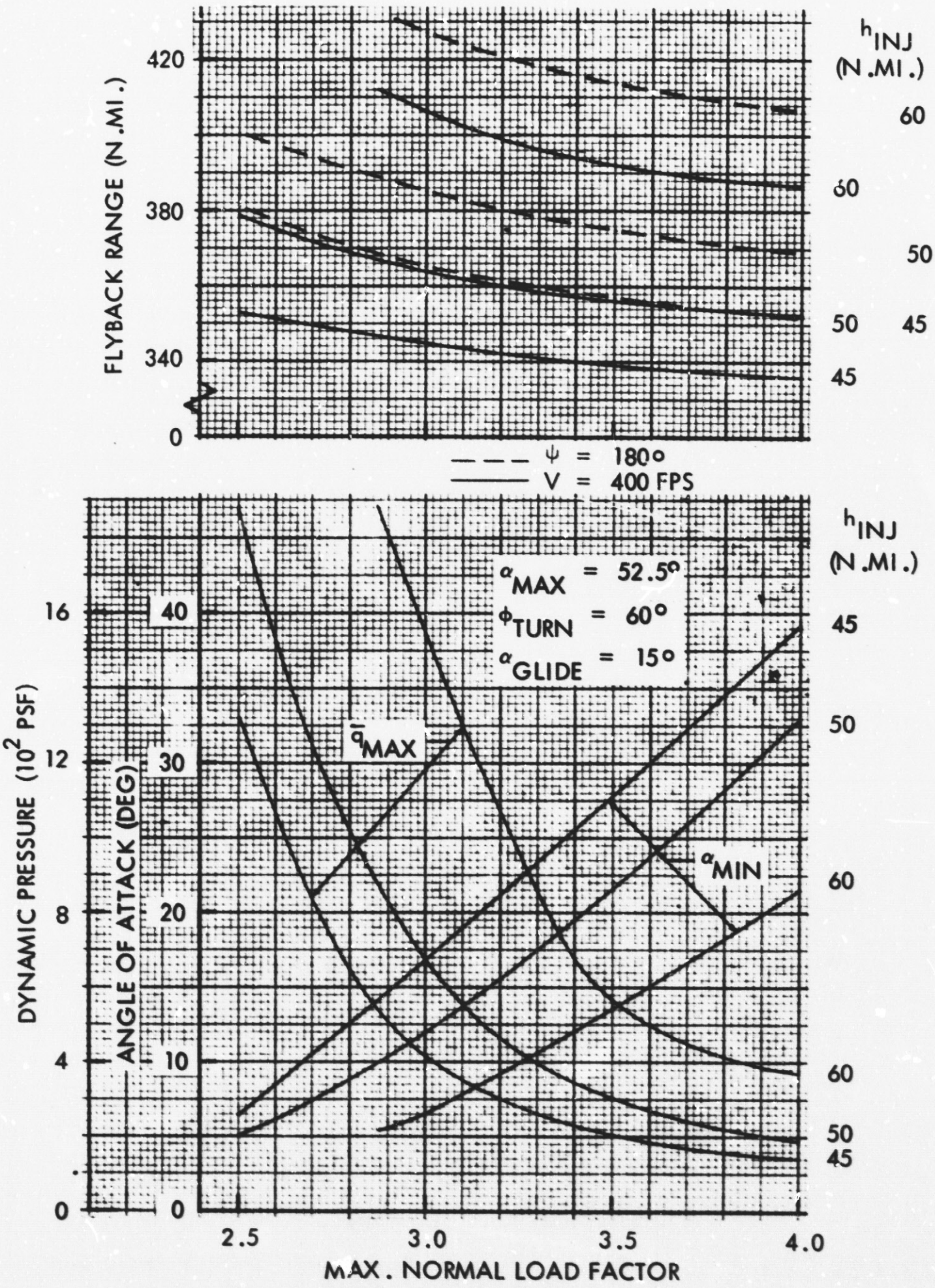

Figure 7.3-35. Effect of Injection Altitude and Normal Load Factor Limit on Turnaround Performance and Environment of Booster

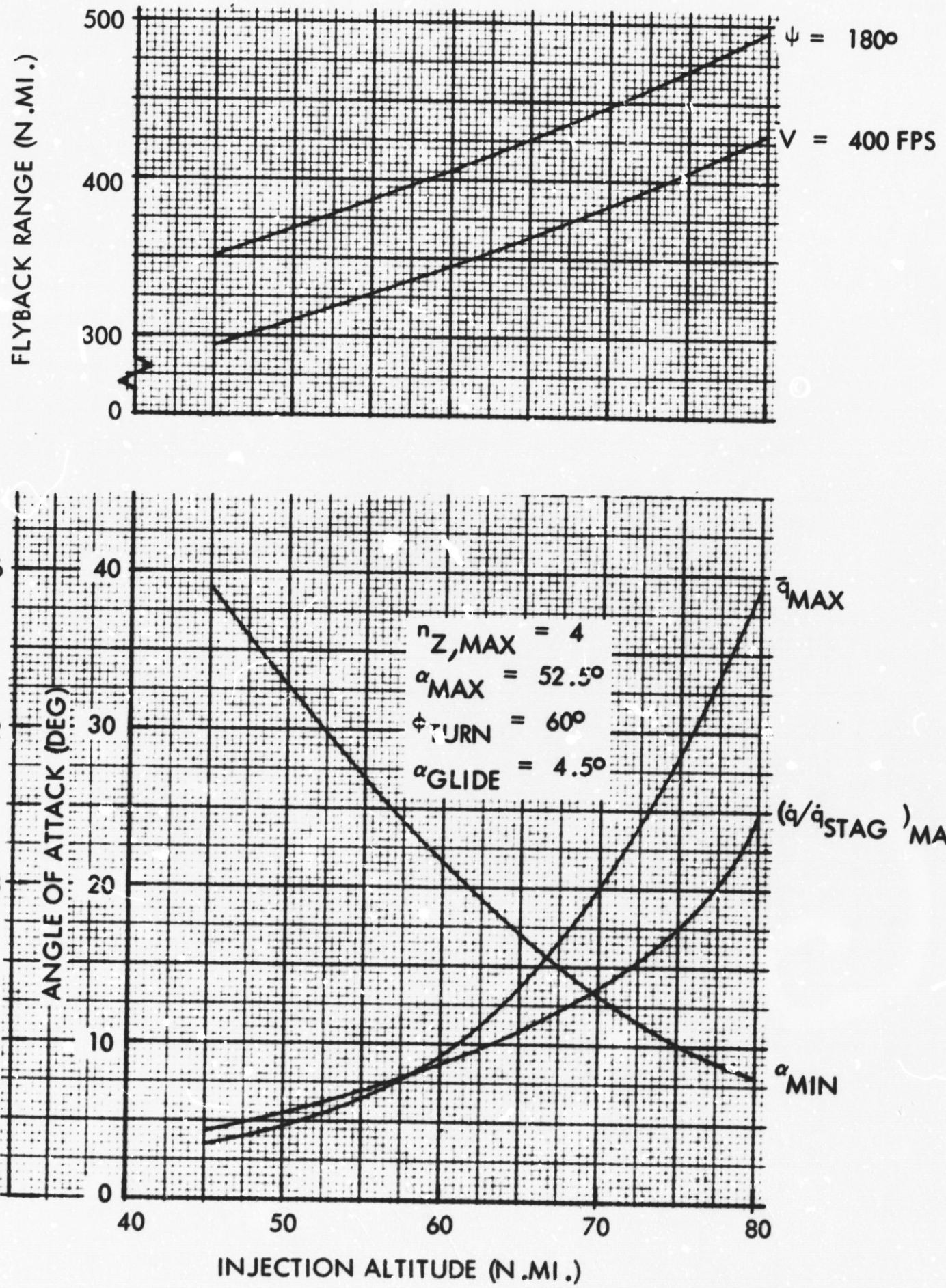

Figure 7.3-36. Effect of Injection Altitude on Turnaround Performance and Environment of Booster with Normal Load Factor Limited to 4.0

15 degrees during the glide following the completion of the turnaround. At even the lowest injection altitude of 45 nautical miles, dynamic pressure is observed to increase rapidly for normal load factors lower than 3.0. At injection altitudes greater than 60 nautical miles even a normal load factor limit of 4.0 will not prevent the dynamic pressure from becoming excessive.

Presented in Figure 7.3-36 are the results of the effect of varying the injection altitude from 45 to 80 nautical miles while limiting the normal load factor to 4.0. The flyback range shown in this figure was computed using an angle of attack of 4.5 degrees during the glide following the completion of the turnaround. Both the dynamic pressure and the stagnation heat transfer ratio increase rapidly for injection altitudes above 60 nautical miles. The effectiveness of reducing the flyback range while at the same time performing a 180-degree turnaround maneuver can be evaluated by comparing this figure with Figure 7.3-33. At the injection altitude of 50 nautical miles, the flyback range is reduced from 408 to 310 nautical miles with an accompanying increase of normal load factor from 3.65 to 4.00 and dynamic pressure from 70 to 189 psf.

Conceptual Design Definition

Orbiter Entry Flight Mode Definition. To provide a basis for environment and subsystem analysis, an entry flight mode and design trajectory was developed for the 50,000-pound payload orbiter. The orbiter entry phase begins at 400,000 feet altitude after deorbit from a 270-nautical mile circular orbit.

A banked maximum lateral-range entry trajectory was selected as the design entry trajectory for the 50,000-pound payload orbiter. Th. flight mode used maintained the pitch attitude of the orbiter at an angle of attack of 60 degrees (L/D of 0.5 and W/C_LS of 50.0 psf) throughout entry. The roll attitude varied in the following manner: 50 degrees until pullout; modulated roll after pullout to keep altitude constant until the equilibrium glide condition with roll attitude at 40 degrees is reached; and 40 degrees roll maintained until the velocity is decreased to 3000 fps. Although both right and left roll entries were computed, the right roll entry trajectory was the one used as the design entry trajectory. The initial and final conditions used for computing the design trajectory were given in Table 7.3-17. Rotating-earth effects were included in the trajectory computations.

The nominal entry profile is illustrated in Figure 7.3-37. After deorbit, the orbiter is banked 50 degrees and pitched up so that the angle of attack will be 60 degrees during entry. Initial conditions at 400,000 feet altitude are a relative velocity of 25,134 feet per second at a flight path angle of -1.55 degrees. The 50-degree bank angle is maintained during the initial plunge until pullout at a velocity of 23,200 feet per second at approximately 250,000 feet. Then

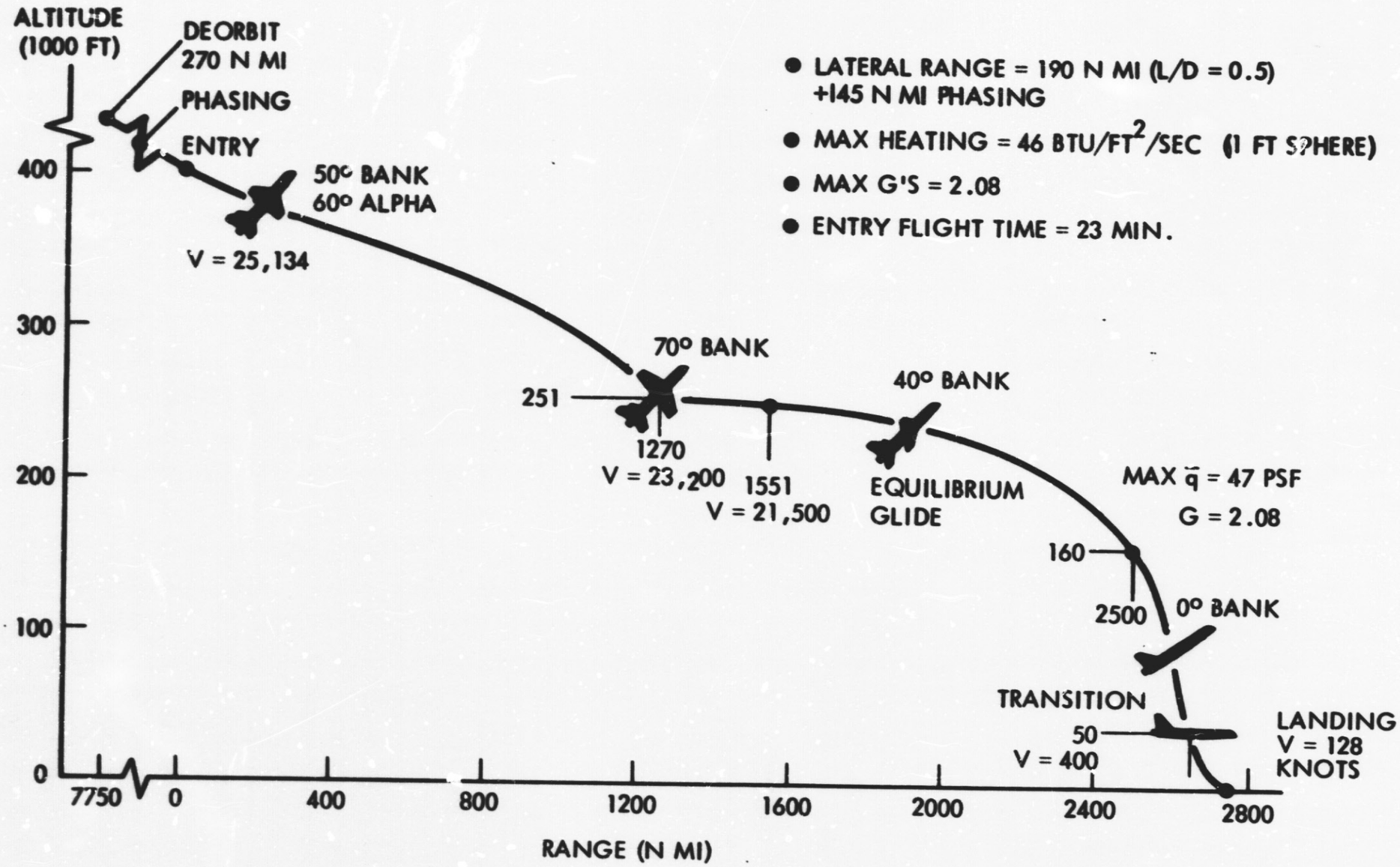

Figure 7.3-37. Orbiter Entry Profile, 50,000-Pound Payload Orbiter

SD 69-573-3

Space Division
North American Rockwell

the bank angle is modulated to hold constant altitude and the vehicle continues to decelerate until equilibrium glide conditions are reached at a velocity of about 21,500 feet per second. During equilibrium glide, the bank angle is varied according to guidance commands to reach the recovery site. The case illustrated is the maximum lateral ranging case for which the bank angle was maintained at 40 degrees during equilibrium glide. The maximum dynamic pressure is 47 psf reached at 160,000 feet altitude at about Mach 6. Maximum load factor is a slightly greater than 2 g. The maximum aerodynamic heating rate is 46 Btu/square foot/second based on stagnation point heating of a one-foot diameter sphere. When the heading angle reaches 90 degrees, the bank angle is reduced to zero. Transition to subsonic glide occurs at 50,000 feet altitude at 0.4 Mach number. The turbojets are ignited at 20,000 feet and operated at reduced throttle setting, ready for use in event of a wave-off during landing. Orbiter landing speed is 128 knots, power off. Total flight time from 400,000 feet altitude is approximately 23 minutes.

The flight conditions at significant points during the design entry are given in Table 7.3-21. Time-history plots of several trajectory quantities are given in Figure 7.3-38. The lateral range of 220 nautical miles shown in the table and the figure is that experienced during an entry flown with roll always to the right. Averaging this value of lateral range with the value realized from an entry flown with roll always to the left gives a lateral range of 190 nautical miles.

Booster Turnaround Flight Mode Definition. A banked entry/turnaround trajectory was used as the design entry trajectory for the 50,000-pound payload booster. It was selected on the basis of minimized flyback range. The nominal booster descent profile is shown in Figure 7.3-39. Initial conditions used were those for a boost trajectory having an injection altitude of 50 nautical miles (Table 7.3-19). The flight mode used varied the pitch attitude of the booster to provide the following angle-of-attack schedule: 52.5 degrees (maximum lift coefficient) until the normal load factor of 4.0 was reached; modulated angle of attack to hold the normal load factor at 4.0 until the angle of attack was again 52.5 degrees; 52.5 degrees until the 180-degree turn was completed; and 4.5 degrees during the glide after completion of the turnaround. The roll attitude varied in the following manner: 90 degrees until the resultant load factor reached 0.5; 60 degrees until completion of the 180-degree turnaround; and zero degrees until the velocity decreased to 400 fps. Aerodynamic characteristics used for the booster are presented in Table 7.3-20.

The flight conditions at significant points during the turnaround are given in Table 7.3-22. Time-history plots of several trajectory quantities are given in Figure 7.3-40. All quantities shown, except time, are referenced to the launch point. Time is referenced to the staging point.

Table 7.3-21. Flight Conditions at Significant Points During Entry of Orbiter

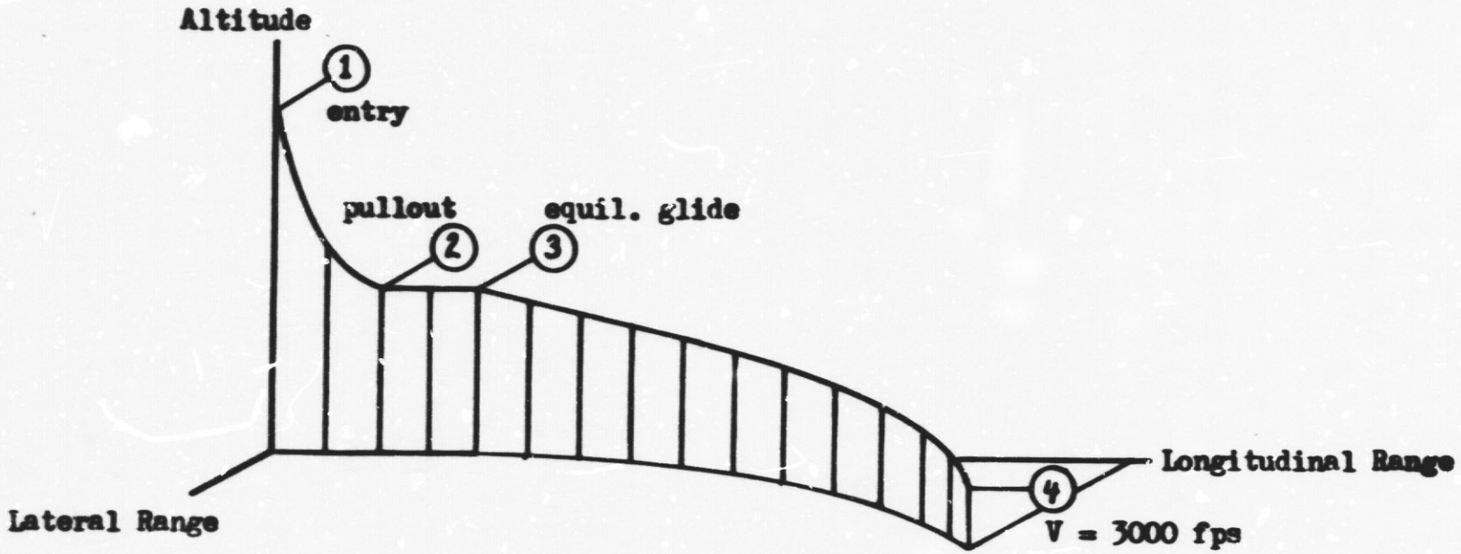

	1	2	3	4	MAX. LOAD
Bank angle, deg	50.0	50.0/69.6	40.0	40.0	40.0
Angle of attack, deg	60.0	60.0	60.0	60.0	60.0
Flight time, sec	0.0	314.89	392.72	839.55	776.0
Relative velocity, fps	25,134.1	23,200.2	21,541.1	3,000.0	6,425.8
Altitude, ft	400,000.	251,315.	251,315.	127,937.	160,775.
Flight-path angle, deg	-1.55	0.00	0.00	-10.80	-4.19
Mach number	19.13	25.33	23.52	2.90	5.94
Dynamic pressure, psf	0.01	17.82	15.36	40.43	46.56
Resultant load factor	~0	0.80	0.69	1.81	2.08
Longitudinal range, nau. mi.	0.0	1,269.4	1,551.7	2,545.4	2,505.7
Lateral range, nau. mi.	0.0	10.0	26.5	219.6	192.8
Heading angle, deg	0.0	2.35	4.29	43.56	23.12

Space Division
North American Rockwell

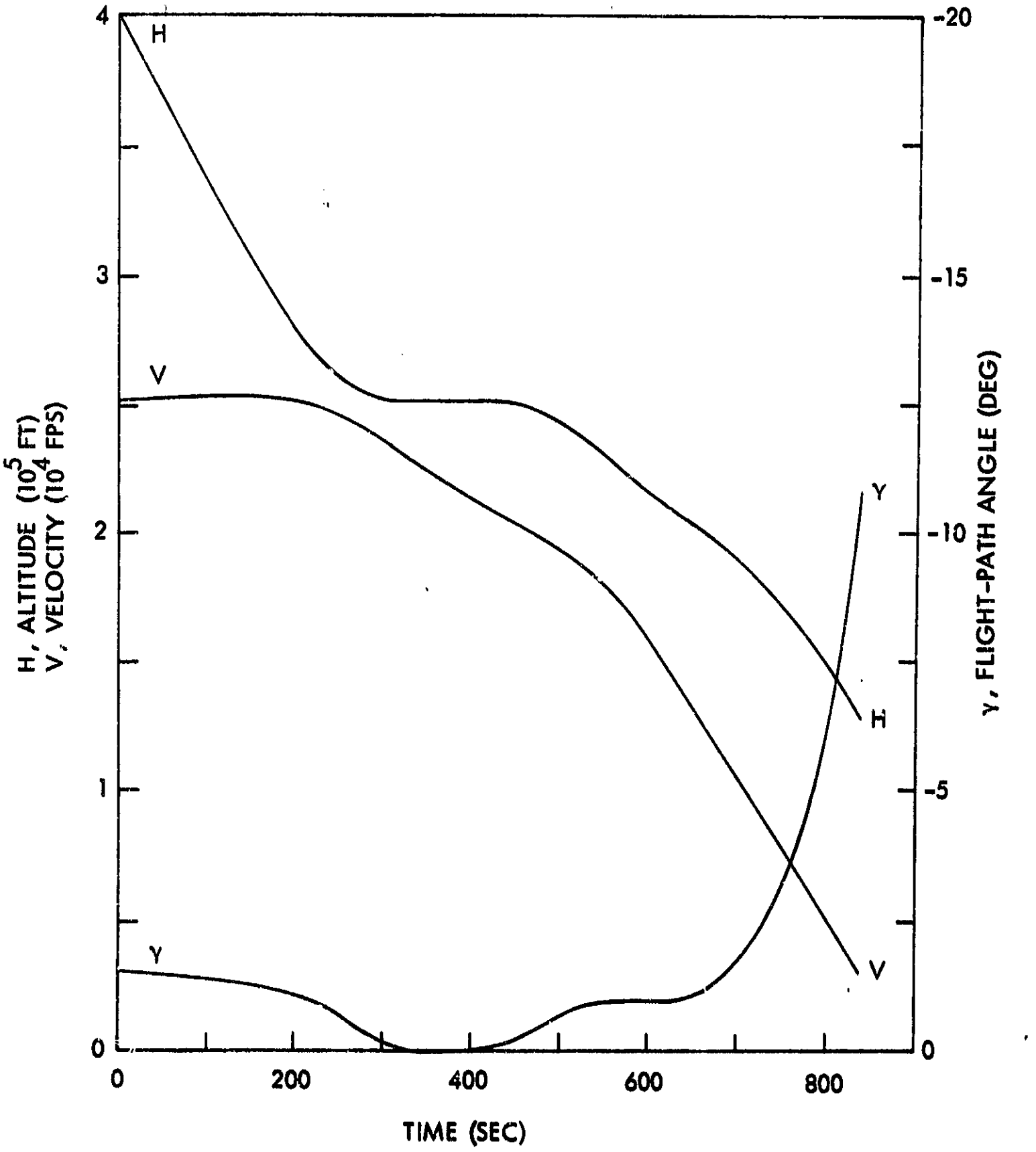

Figure 7.3-38. Time History of Design Entry Trajectory of 50,000-Pound Payload Orbiter (Sheet 1 of 3)

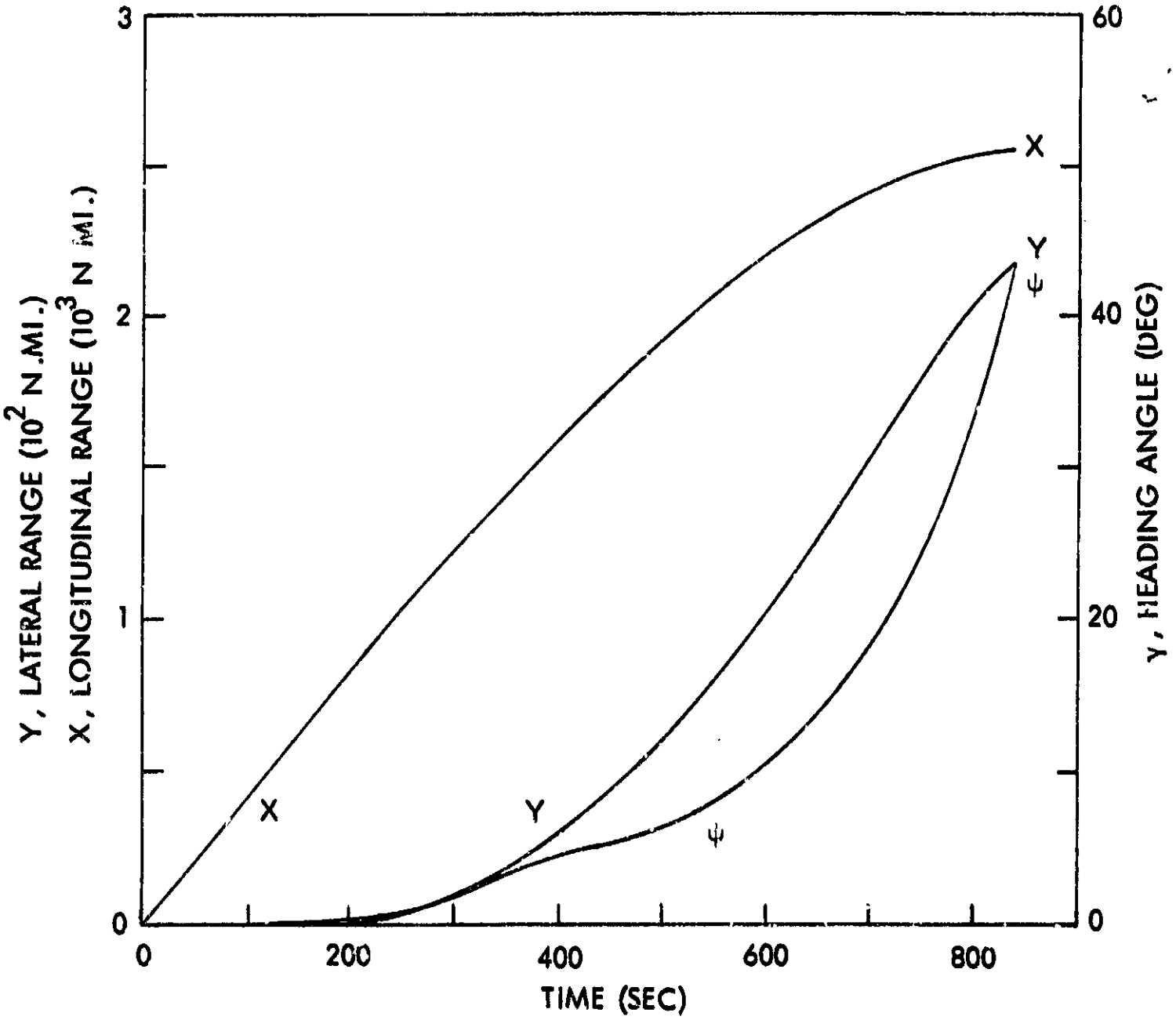

Figure 7.3-38. Time History of Design Entry Trajectory of 50,000-Pound Payload Orbiter (Sheet 2 of 3)

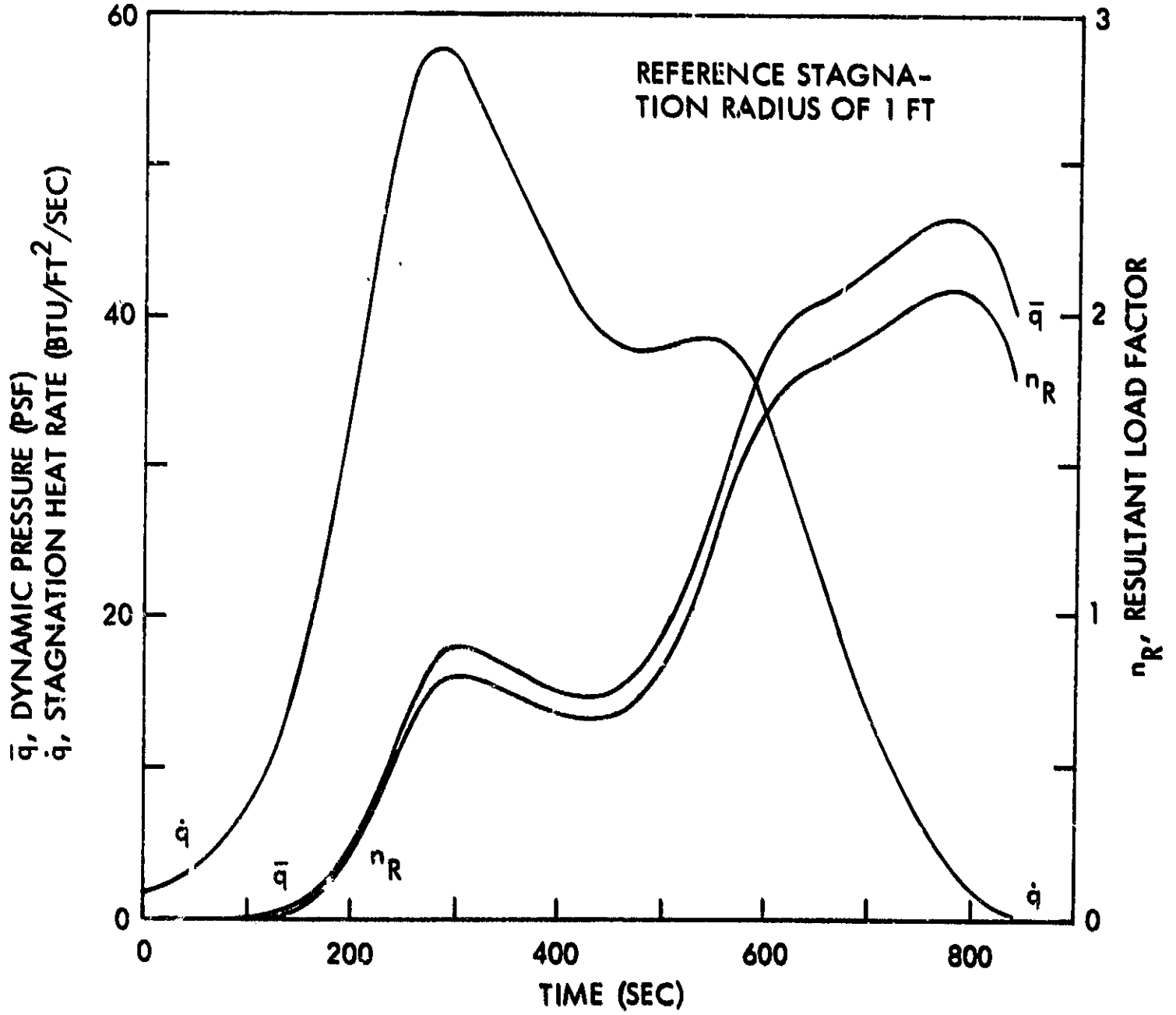

Figure 7.3-38. Time History of Design Entry Trajectory of 50,000-Pound Payload Orbiter (Sheet 3 of 3)

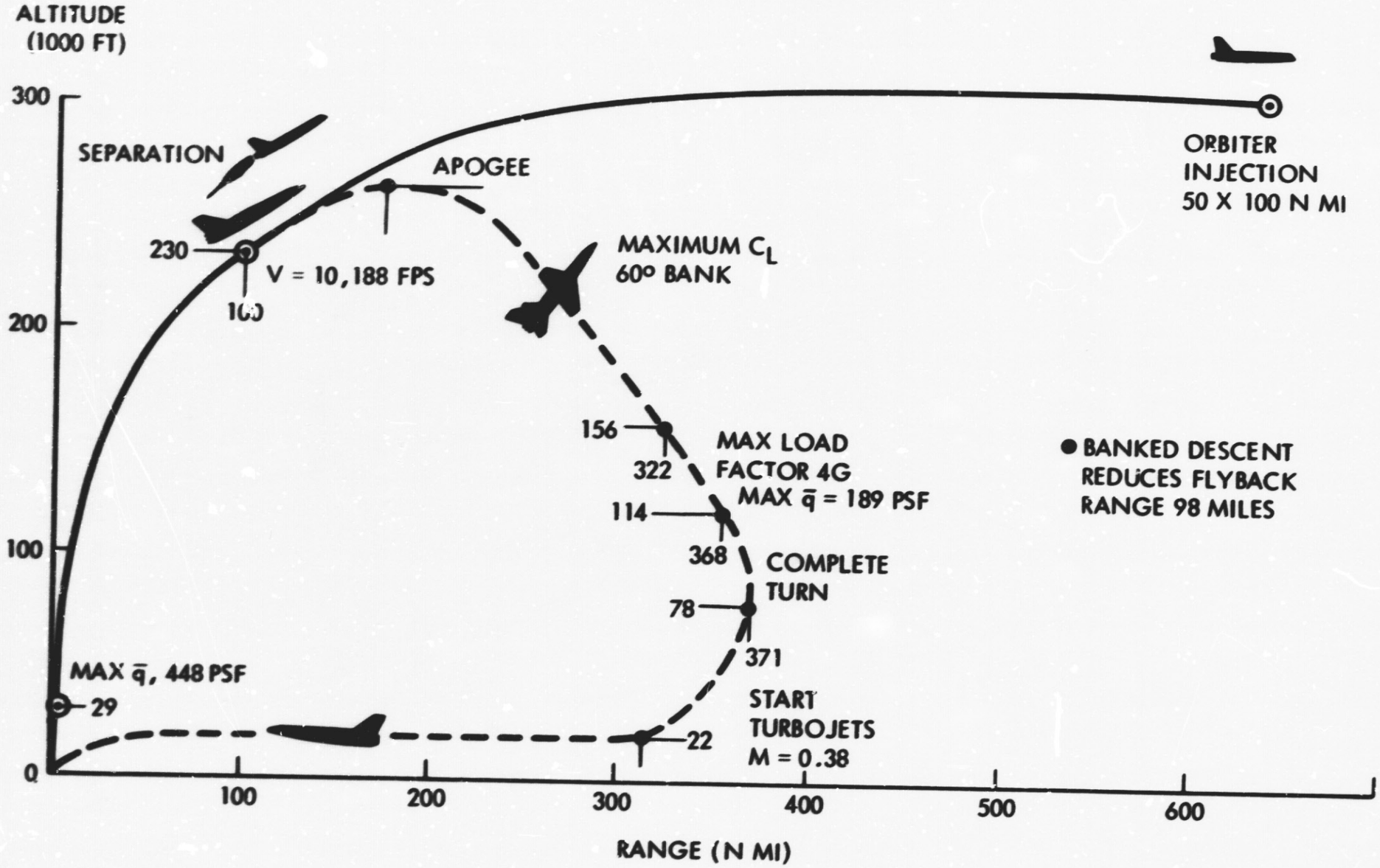

Figure 7.3-39. Booster Descent Profile

SD 69-573-3

Space Division
North American Rockwell

Table 7.3-22. Flight Conditions at Significant Points During Turnaround of Booster

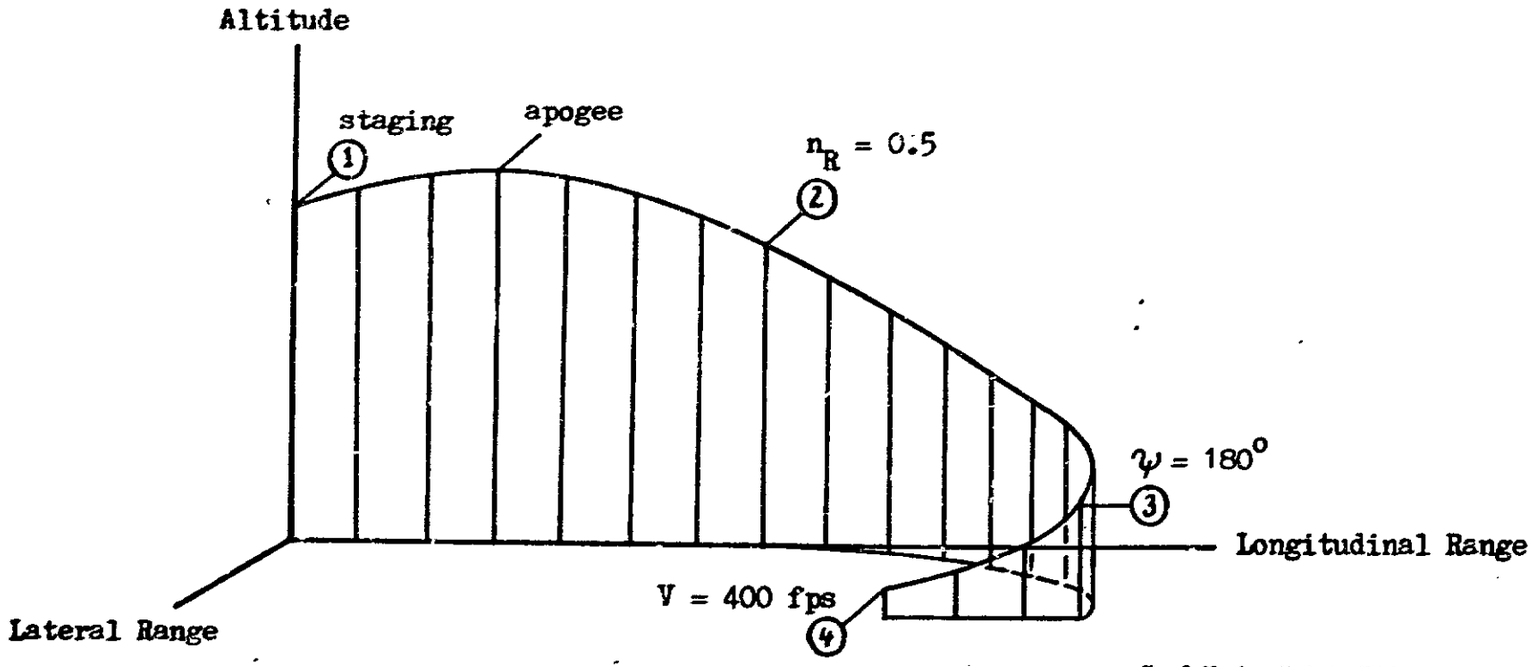

	①	②	③	④	MAX. LOAD
Bank angle, deg	90.0	90.0/60.0	60.0/0.0	0.0	60.0
Angle of attack, deg	52.5	52.5	52.5/4.5	4.5	32.7
Flight time, sec	0.0	105.36	292.12	947.42	176.0
Relative velocity, fps	10,082.0	9,763.2	720.4	400.0	5,457.1
Altitude, ft	242,000.	221,172.	78,425.	22,077.	120,362.
Flight-path angle, deg	6.68	-9.11	-53.20	-6.20	-5.96
Mach number	10.71	9.79	0.74	0.39	5.34
Dynamic pressure, psf	5.12	11.37	23.99	94.44	188.91
Resultant load factor	0.23	0.50	1.38	1.00	4.02
Longitudinal range, nau. mi.	97.8	266.5	369.0	310.4	355.9
Lateral range, nau. mi.	0.0	2.3	49.2	48.2	18.0
Heading angle, deg	0.0	2.00	180.00	182.39	32.85

Space Division
North American Rockwell

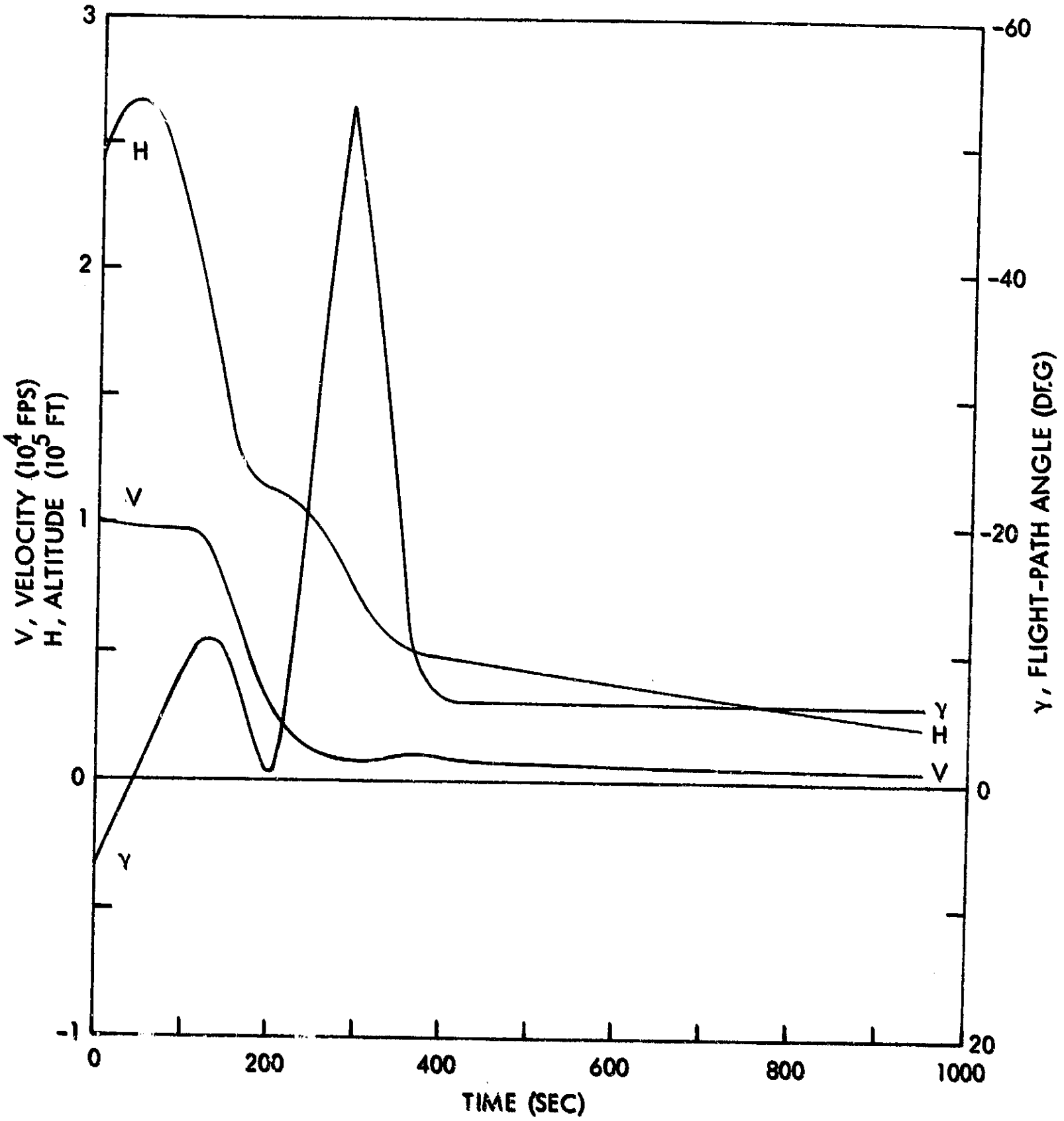

Figure 7.3-40. Time History of Design Turnaround Trajectory of 50,000-Pound Payload Booster (Sheet 1 of 3)

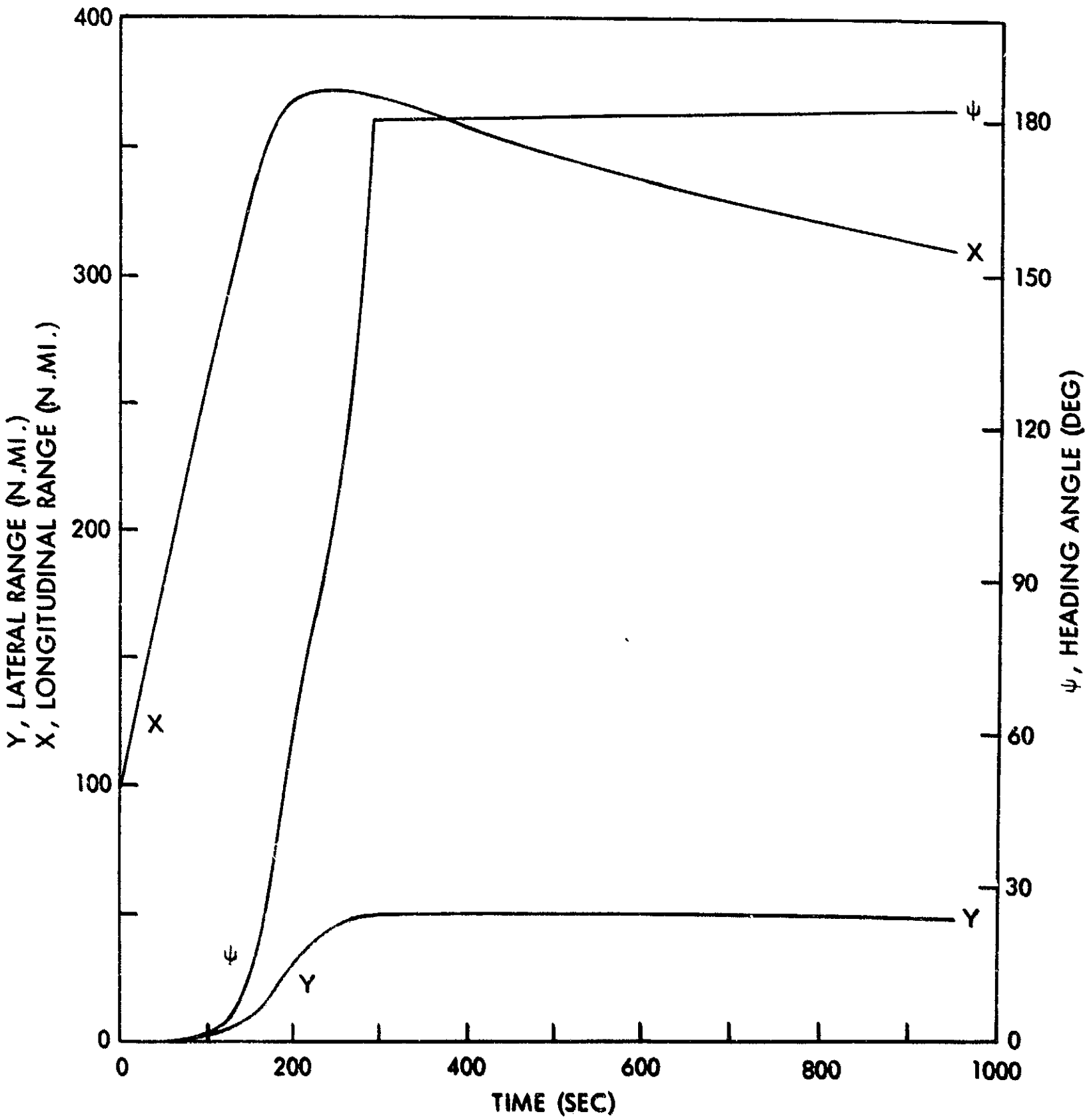

Figure 7.3-40. Time History of Design Turnaround Trajectory of 50,000-Pound Payload Booster (Sheet 2 of 3)

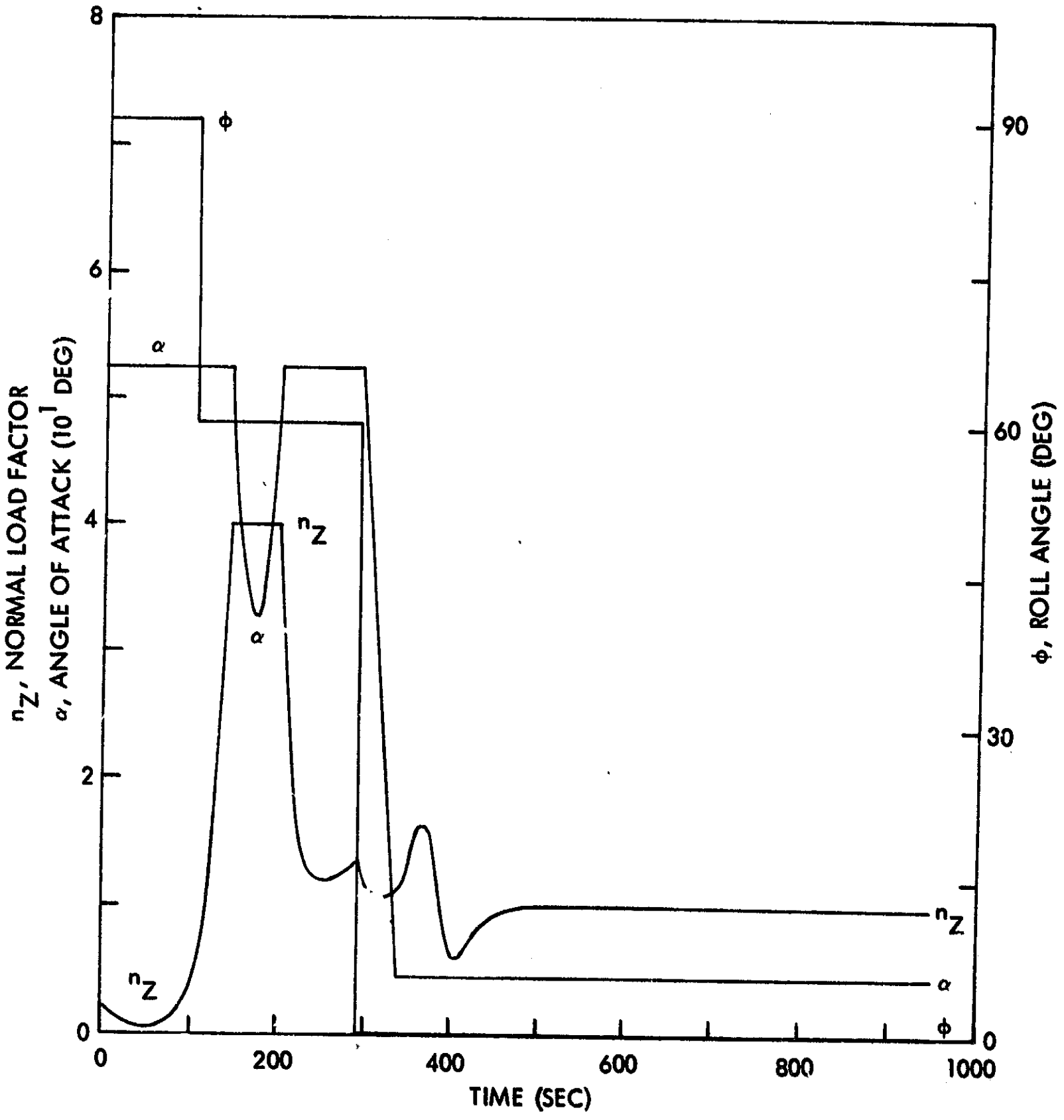

Figure 7.3-40. Time History of Design Turnaround Trajectory of 50,000-Pound Payload Booster (Sheet 3 of 3)

7.3.5 Approach and Landing

Definition of logistics vehicle characteristics during the approach and landing phase of the mission encompassed three major areas of investigation:

1. Optimization of booster flyback cruise performance and definition of cruise-back propulsion system requirements

2. Sensitivity studies to establish performance impact of variations in booster and orbiter go-around systems

3. Definition of orbiter and booster landing characteristics

Ground rules for initial sizing of systems and definition of approach and landing characterisitics were:

1. Wing loading of 70 psf for the booster and 90 psf for the orbiter

2. Booster flyback range of 230 nautical miles

3. Sufficient fuel for two go-around maneuvers

4. Aerodynamic performance of booster and orbiter based on evaluation of LRC wind tunnel results (Reference 7-5)

5. Propulsion system performance based on Pratt & Whitney JT3D-7 turbojet

The approach was to determine optimum cruise conditions, to minimize booster flyback fuel requirements, and to define the performance characteristics for a range of landing weights corresponding to vehicles with payloads over the range of 10,000 to 50,000 pounds.

Concept Sizing

To support studies to size the MSC shuttle vehicle concept over the specified payload range, it was necessary to determine thrust and fuel requirements for booster and orbiter subsonic flight conditions as a function of landing weight. Maximizing flyback range depends upon maximizing the Brequet range factor, V x (L/D)/SFC. It requires satisfying the aerodynamic and propulsion requirements simultaneously. The aerodynamic requirements are specified in terms of the lift-drag ratio. The propulsion requirements are specified in terms of the thrust available and fuel consumption. A convenient display of aerodynamic and propulsion requirements is in the form of a cruise map (Figure 7.3-41). The cruise map presents level-flight drag or

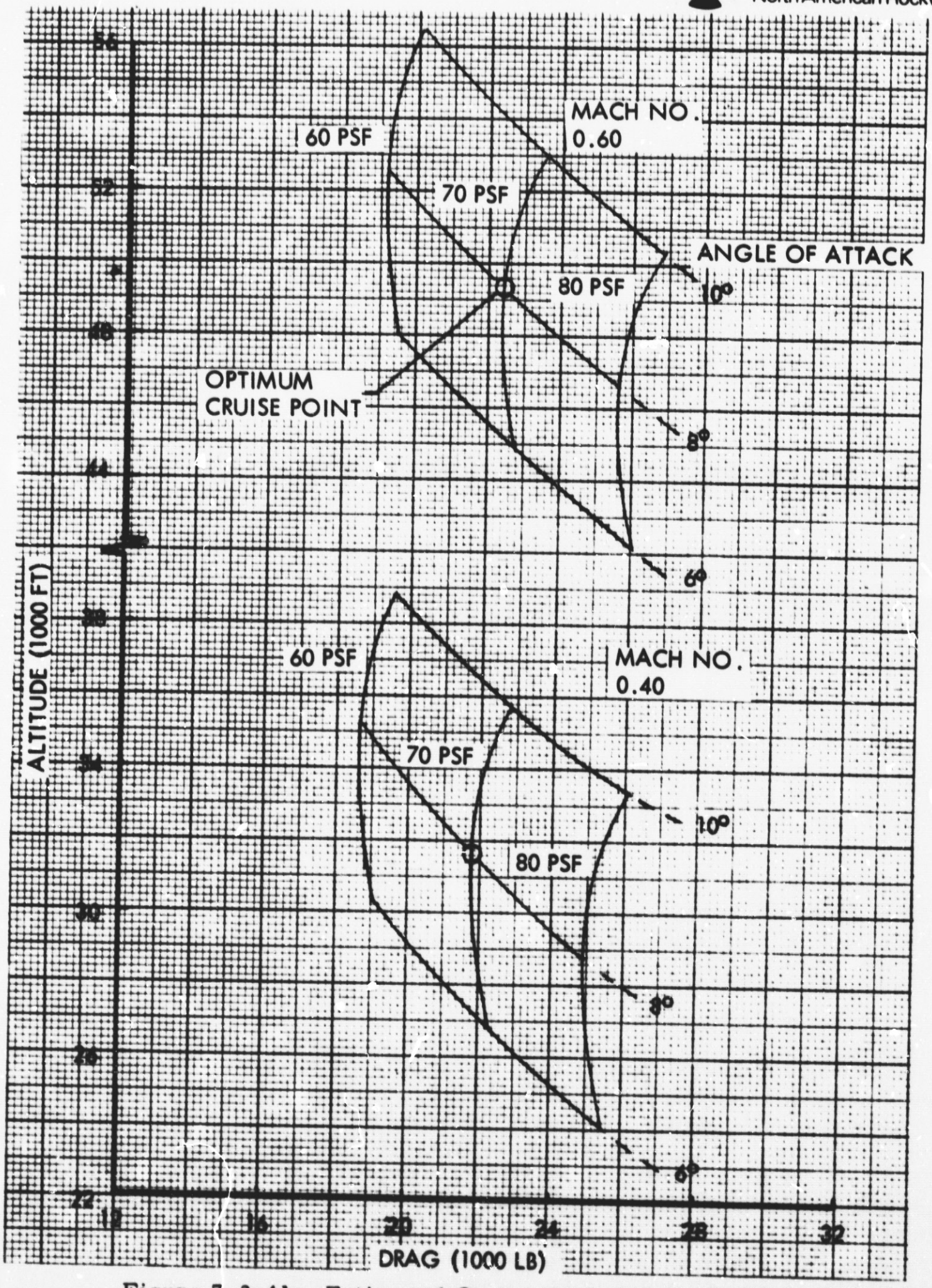

Figure 7.3-41. Estimated Optimum Cruise for Booster, 12,500 Lb Payload Class System

thrust as a function of altitude at a constant Mach number, with wing loading and angle of attack as parameters.

The P&W JT3D-7 engine performance for M = 0.4 and M = 0.6 is displayed in Figure 7.3-42. The maximum continuous cruise thrust available and the thrust required for a fixed-wing loading are presented in Figure 7.3-43. Referring to Figure 7.3-43, it may be seen that the aerodynamic requirement for flight at (L/D) max is satisfied by the engine cruise thrust at M = 0.4 at 30,000 feet altitude. Engine thrust is inadequate to fly at the altitude required for (L/D) max at M = 0.6. Booster cruise optimization results for initial concept sizing are summarized in Figure 7.3-44. Maximization of cruise range for a fixed velocity depends upon maximization of the term (L/D)/SFC from the Brequet range factor. The curve in the upper left-hand corner of Figure 7.3-44 is for cruise at maximum L/D at 0.4 Mach number. It illustrates that the optimum cruise condition occurs at about 32,000 feet for wing loadings of from 70 to 80 psf. Drag and maximum continuous cruise thrust at the optimum cruise altitude are shown on the curve in the upper right corner of the figure. Thrust characteristics are for 4 P&W JT3D-7 engines and represent the 12,500-pound-payload-class baseline. The fuel required for 230 nautical miles of cruise is displayed in Figure 7.3-44 for the various payload class vehicles. These data include fuel for two go-around maneuvers, presented in Figure 7.3-45.

Landing Performance. The landing performance is based on the lift characteristics presented in Figure 7.3-46. The clean wing data are based on the LRC wind tunnel tests. Flap effectiveness is based on the characteristics of a 70-percent-span slotted flap deflected 20 degrees.

The maximum usable lift coefficient is limited by the 10-degree tail-down ground angle. The maximum trimmed lift coefficient is 1.6 (angle of attack = 8 degrees) with flaps and gear down. It results in touchdown speeds of 129 knots and 114 knots for the 12,500-pound-class orbiter and booster. These touchdown speeds compare favorably with touchdown speeds of contemporary transport aircraft—130 to 140 knots. The speed over a 50-foot obstacle is based on an approach made at an angle of attack for (L/D) max flaps and with gear down. The approach speeds are 144 knots for the orbiter and 127 knots for the booster.

Sensitivity Analysis

Investigations of booster and orbiter subsonic cruise performance were conducted during the concept sizing phase. They showed that significant weight penalties can result from provisions for flyback and go-around capability. Fuel required for the 12,500-pound-class booster flyback was shown

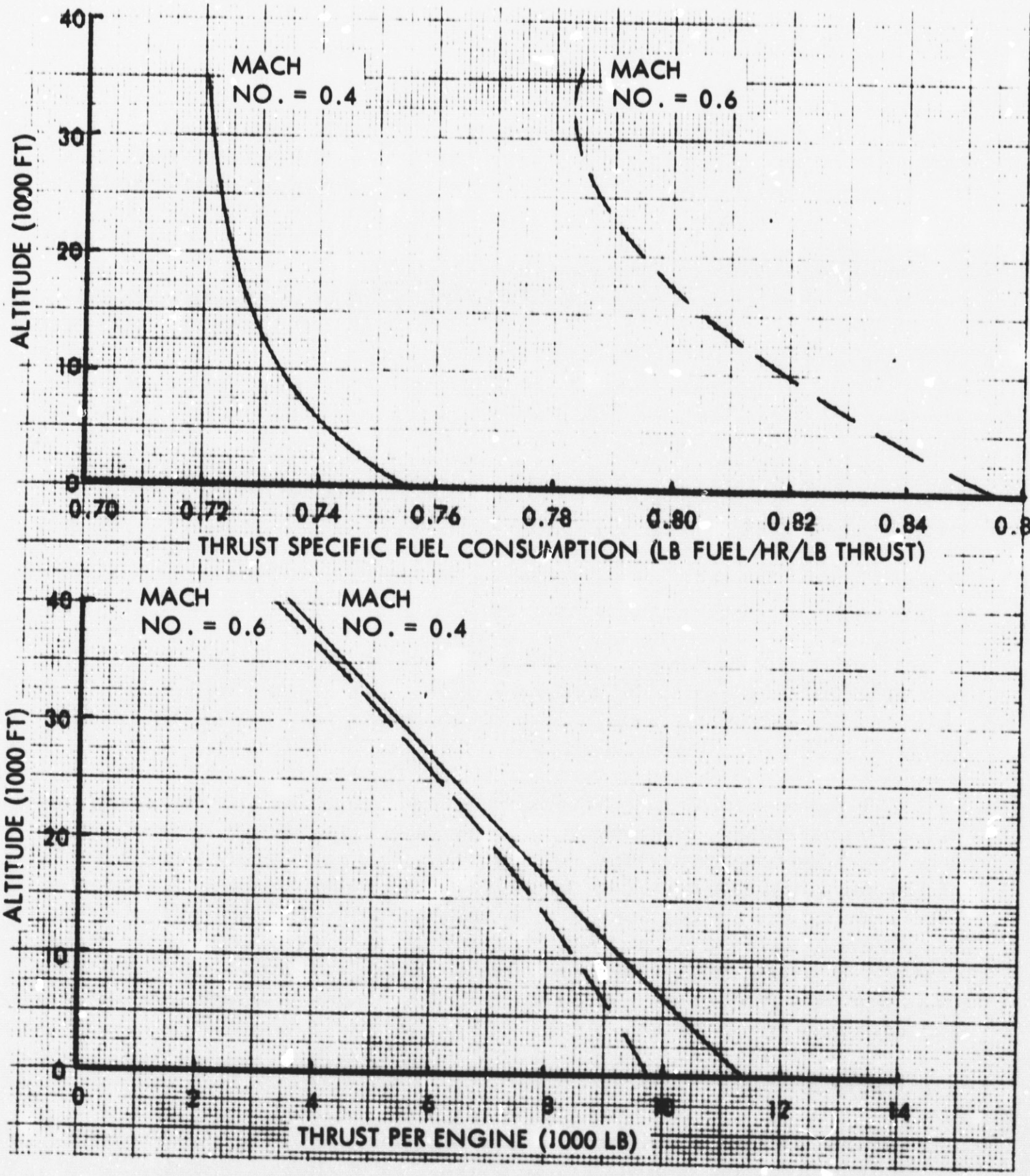

Figure 7.3-42. Thrust and Drag Characteristics for Booster Cruise, 12,500-pound Payload Class System

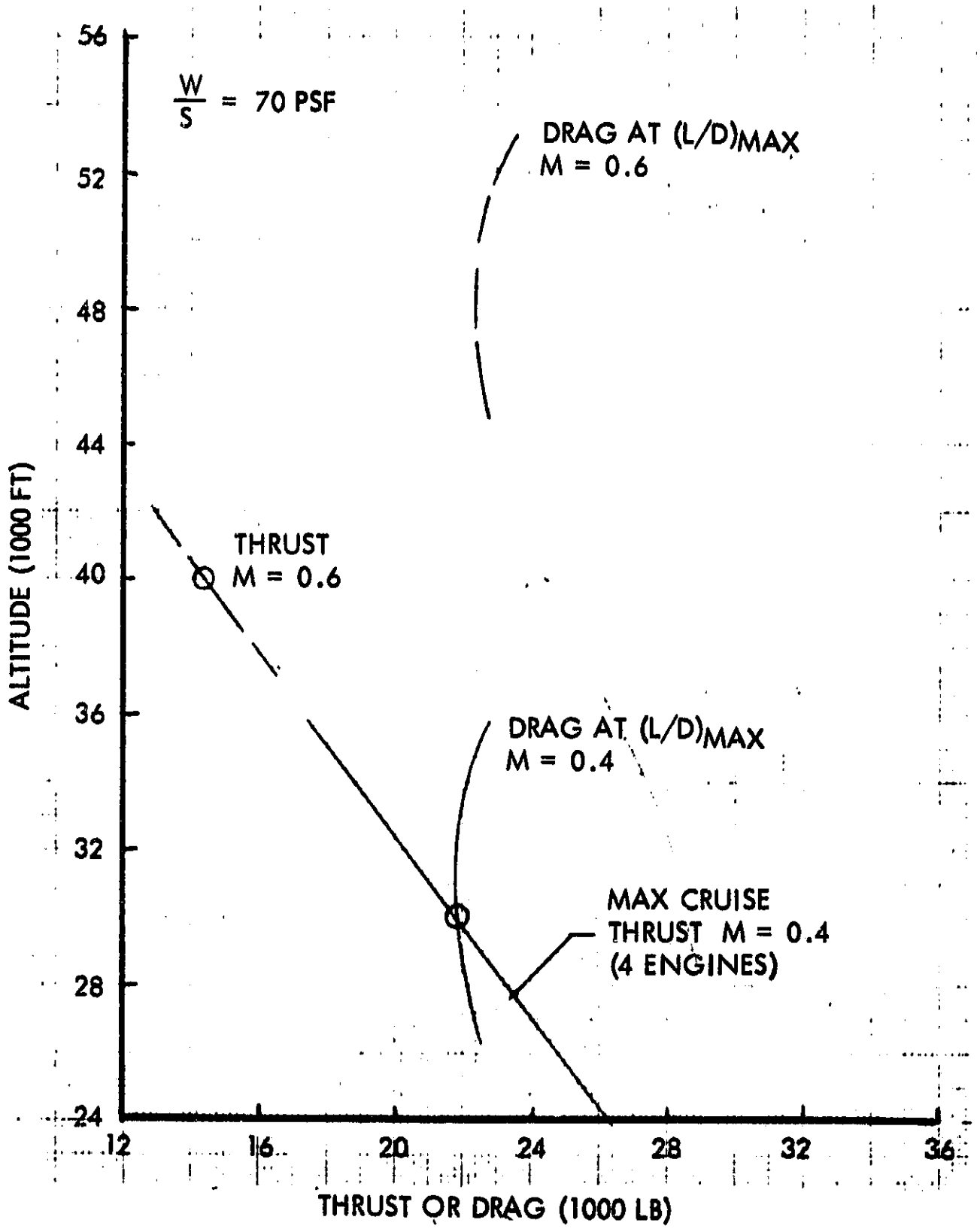

Figure 7.3-43. P&W JT3D-7 Turbojet Engine Performance

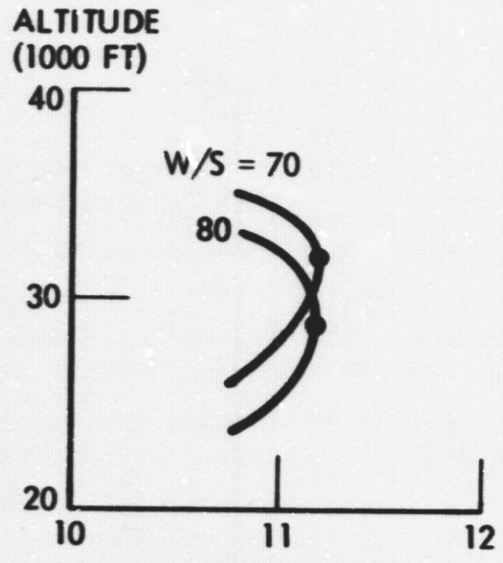

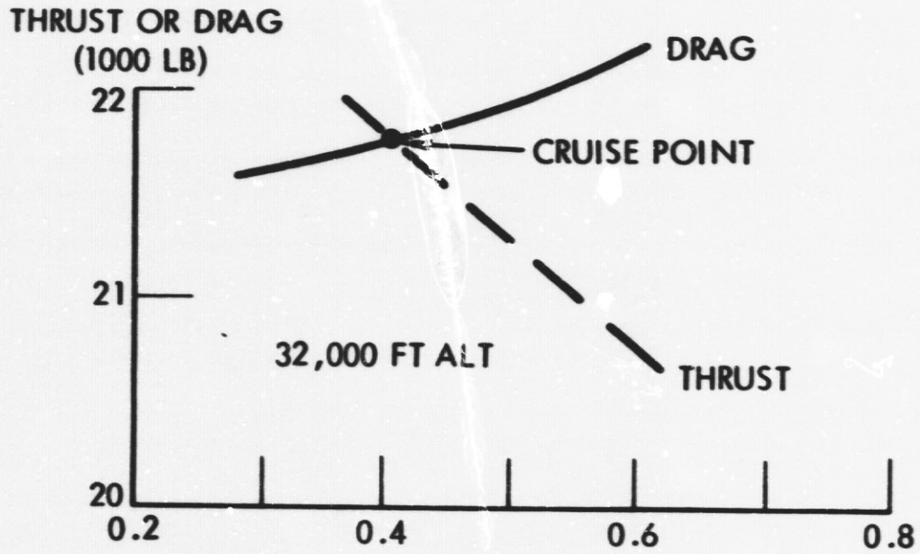

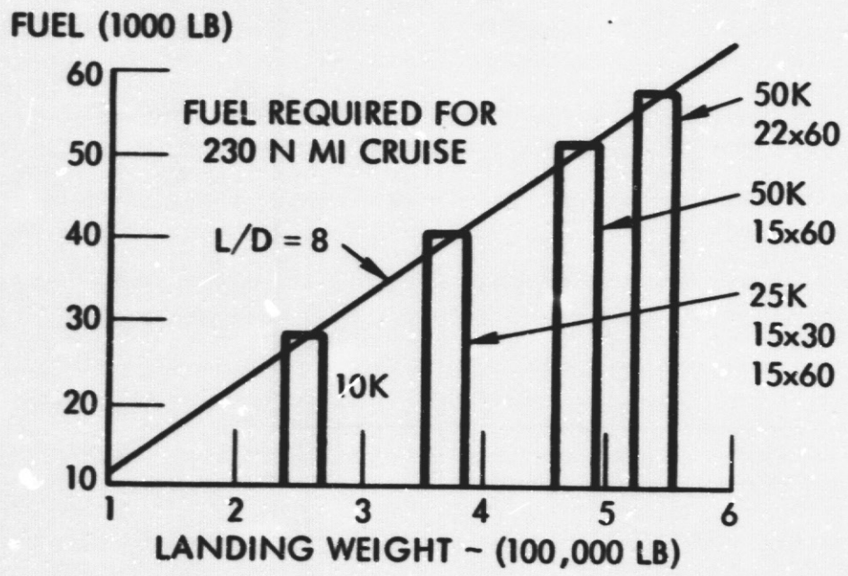

- OPTIMUM CRUISE ALTITUDE IS 32,000 FT, MACH 0.4
- FUEL REQUIRED IS APPROXIMATELY 10% OF LANDING WEIGHT

Figure 7.3-44. Booster Cruise Optimization, 12,500-pound Payload Class System

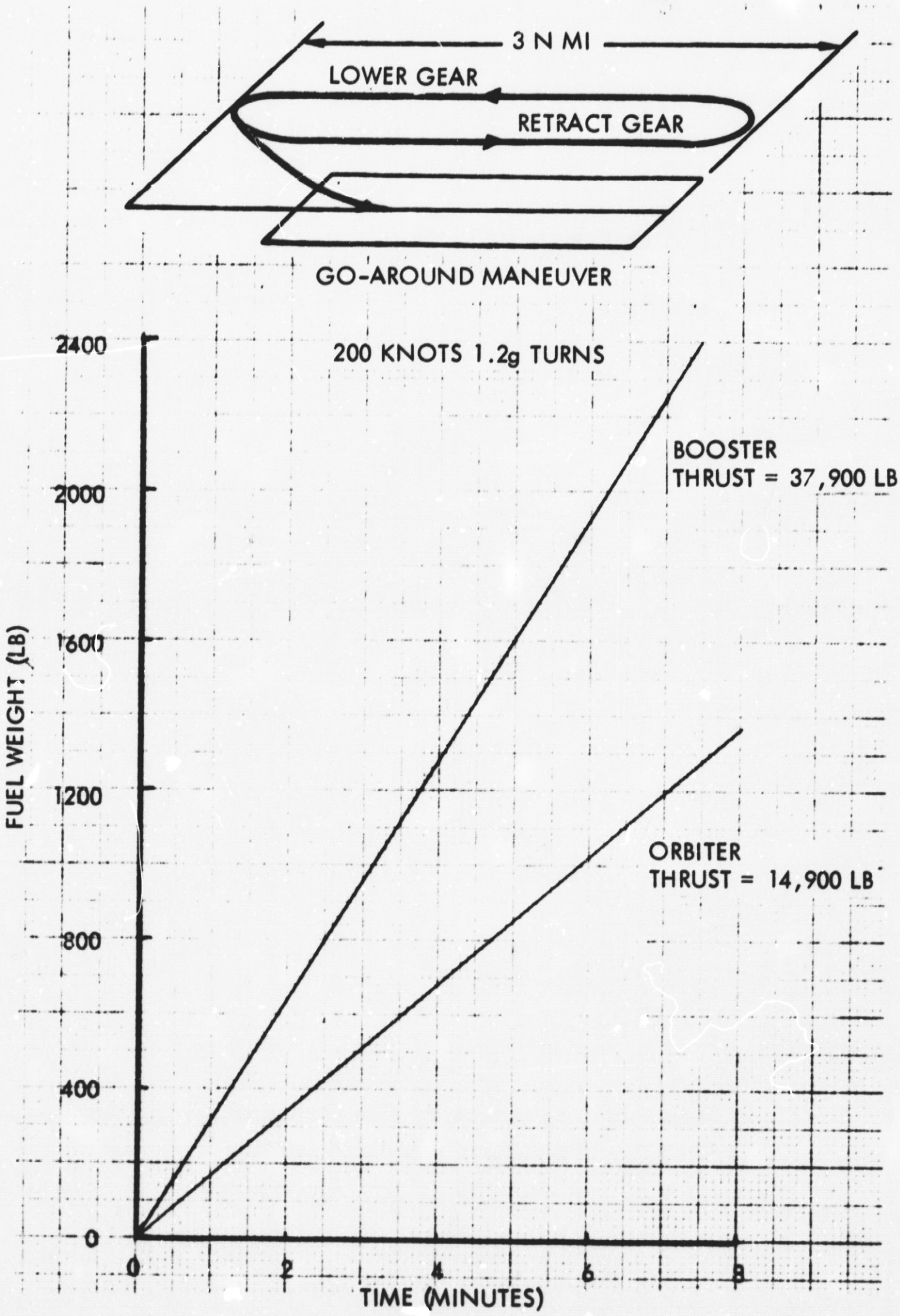

Figure 7.3-45. Go-Around Fuel Requirements, 12,500-pound Payload Class System

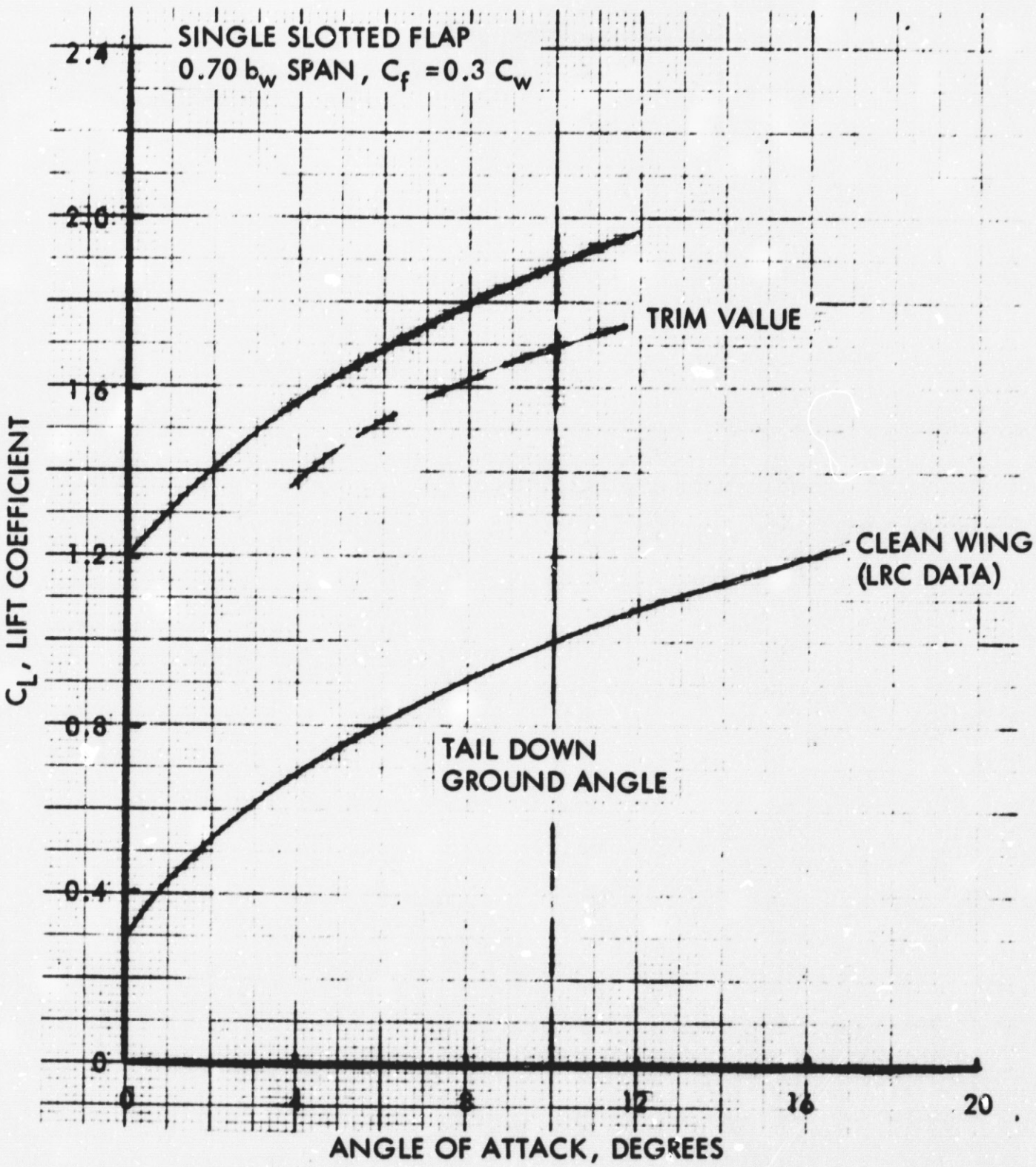

Figure 7.3-46. Landing Flap Effectiveness

to be approximately 10 percent of the landing weight, with turbojet engines amounting to an additional 5 percent of the landing weight. For the orbiter, engines and fuel for go-around capability accounted for about 10 percent of the landing weight. Because of the extreme sensitivity of shuttle system size and gross weight to orbiter and booster inert weight, it is important to minimize the weight of these air-breathing propulsion systems. For example, stage gross weight and payload sensitivity studies discussed in Section 7.3.2 indicate that, for a 1000-pound saving in orbiter go-around propulsion system weight, the vehicle gross weight will be reduced by 22, 000 pounds.

Orbiter Payload Sensitivity to Go-Around System. Studies were conducted to determine the vehicle performance improvement that could result from other approaches to providing go-around capability for the 50, 000-pound-payload-class orbiter.

The baseline design incorporates four JT3D-7 turbojets and sufficient fuel for two go-around maneuvers during landing. System weights required to provide this capability are presented in Figure 7.3-47. The orbiter payload gain associated with other go-around systems and landing situations was investigated. Four cases were considered:

1. Delete one go-around. Retain the baseline turbojet system, but reduce the fuel quantity to that required for one go-around. Engine operating time was reduced from 12 to 6 minutes using four JT3D-7 engines.

2. Straight-in approach at reduced thrust margin. Case 1 employs the baseline turbojet system, which has adequate thrust for climb-out after a landing wave-off. Eliminating the climb-out capability would permit deletion of two of the JT3D-7 engines.

3. Delete the go-around propulsion system.

4. Replace the JT3D-7 engines. Substitute advanced high thrust-to-weight ratio turbojets.

The payload gains that could result are illustrated in Figure 7.3-47.

In the baseline vehicle, 82 percent of the go-around propulsion system is from the engines themselves. Only 18 percent is fuel weight. Consequently, the payload gain from reduced engine operation (Case 1) is small.

Reducing the available thrust margin by deletion of two engines can provide a payload gain of 8520 pounds (Case 2). This is approximately the gain that could be realized by reducing the nominal on-orbit maneuver budget

BASELINE SYSTEM

ITEM	WEIGHT (LB)
4 JT3D-7	17,040
FUEL FOR 2 GO-AROUND	3,200
TOTAL	20,240

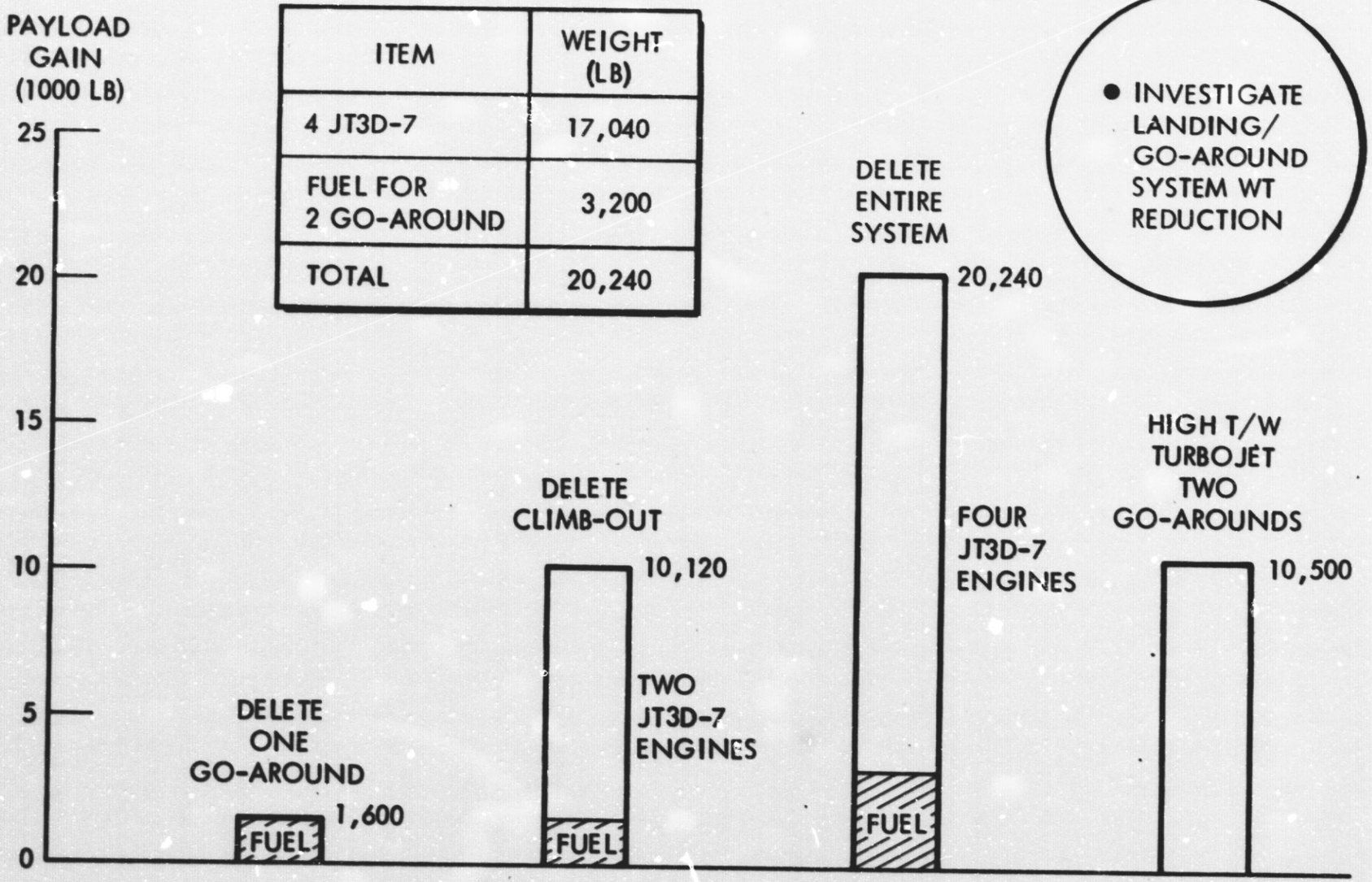

- INVESTIGATE LANDING/ GO-AROUND SYSTEM WT REDUCTION

Figure 7.3-47. Payload Sensitivity to Go-Around Capability, 50,000-Payload Orbiter

Space Division
North American Rockwell

by 600 fps. The maneuver budget has about 700 fps excess ΔV above that required to transfer from the 45-by 100-n mi injection condition, rendezvous with the space station at 270 nautical miles, and deorbit. An operational trade should be conducted to evaluate the reduced mission flexibility resulting from reduced ΔV versus that resulting from reduced go-around capability.

Deletion of the entire go-around propulsion system (Case 3) results in a 20,240-pound increase in payload capability. This is based on a one-to-one trade of propulsion system weight for payload. It does not account for the small gains that could be realized by reoptimization of the booster and orbiter vehicles.

Replacing the JT3D-7 engines with an advanced high thrust-to-weight (T/W) turbojet can provide a payload gain of 10,500 pounds over the baseline system. The high T/W system evaluated has the same performance capability as the baseline system using four JT3D-7 engines. Four high T/W engines are required. System weights were estimated to be:

1.	4 engines	4800 lb
2.	Fuel for 2 go-around maneuvers	4940 lb
	Total:	9740 lb

Design of the high T/W propulsion system was based upon data obtained from the Allison Division of General Motors. The data are a result of USAF contracts to develop a high T/W engine. Allison has built a high T/W flight-weight engine that is under test in England as part of the US/UKSJ99 Direct Lift Jet Engine Program. This engine was designed for vertical take off and landing applications with relatively short duty cycles and relatively short total life compared to conventional cruise propulsion systems. As such it would be particularly well suited for the ILRV application. The basic engine under test in England has a thrust of 8916 pounds, specific fuel consumption of 1.0, and a dry weight of 465 pounds, resulting in a T/W = 19:1.

Scaled for application to the 50,000-pound payload class orbiter, the engine had the following characteristics:

Thrust = 18,000 pounds/engine
SFC = 1.1 pounds/pounds-hour
Weight = 1,200 pounds
T/W = 15:1

The reduced thrust-to-weight ratio reflects addition of a power takeoff pad to the flight-weight test engine. The pad provides power for the orbiter vehicle during its landing operations.

The foregoing results demonstrate the large payload gains that could be realized by incorporating an alternative go-around system in the orbiter. Deletion of the go-around capability is not recommended, but the high thrust-to-weight turbojet system should be investigated further.

Performance Sensitivity to Booster Go-Around System. A brief investigation was performed of the sensitivity of shuttle vehicle performance to booster go-around capability. The performance partial for the booster is -0.13 pounds of payload per pound of booster inert weight (see Section 7.3.2). Changes in go-around system weights were treated as changes in inert weight. For the 50,000-pound-payload class, approximately 10,800 pounds of turbojet fuel are reserved for go-around. Deletion of this capability would result in a 1400-pound increase in orbiter payload for a given vehicle.

Use of hydrogen fuel for the turbojets is discussed in Section 8.7 of Volume 4. A potential payload increase of 5500 pounds was estimated if hydrogen were used for fly-back and go-around.

Conceptual Design Definition

To minimize weight of the booster air-breathing propulsion system, an optimization study of flyback cruise performance was made. The optimization was based on matching thrust required to cruise at maximum L/D with thrust available from the turbojet propulsion system. A flyback range requirement of 300 miles was used.

Aerodynamic and propulsion requirements are presented in the form of a cruise map (Figure 7.3-48). The cruise map presents level-flight drag or thrust as a function of altitude at a constant Mach number. Wing loading and angle of attack are parameters. The cruise map lift-and-drag characteristics are based on low-speed wind tunnel data from the LRC and ARC tests. The conditions for level-flight cruise at (L/D) max, with wing loading and Mach number as parameters, are shown in Figure 7.3-49. This plot was obtained by plotting the loci of the (L/D) max points from the cruise maps. Each point on this cruise carpet represents level flight cruise at an angle of attack for maximum lift-drag ratio. Engine thrust is superimposed upon the cruise carpet. The intersection of the thrust required (drag) curves with the thrust available curves represents an equilibrium cruise condition. When the wing loading is known, the cruise carpet curves define the Mach number and altitude for cruise. Optimum cruise is seen to correspond to flight at 0.52 Mach number at 32,000 feet (75 psf wing loading). Six JT9D-15 engines are required.

Fuel required for cruise is presented in Figure 7.3-50. It may be seen that a flyback range of 300 nautical miles requires 36,200 pounds of fuel plus 10,500 pounds for two go-around maneuvers.

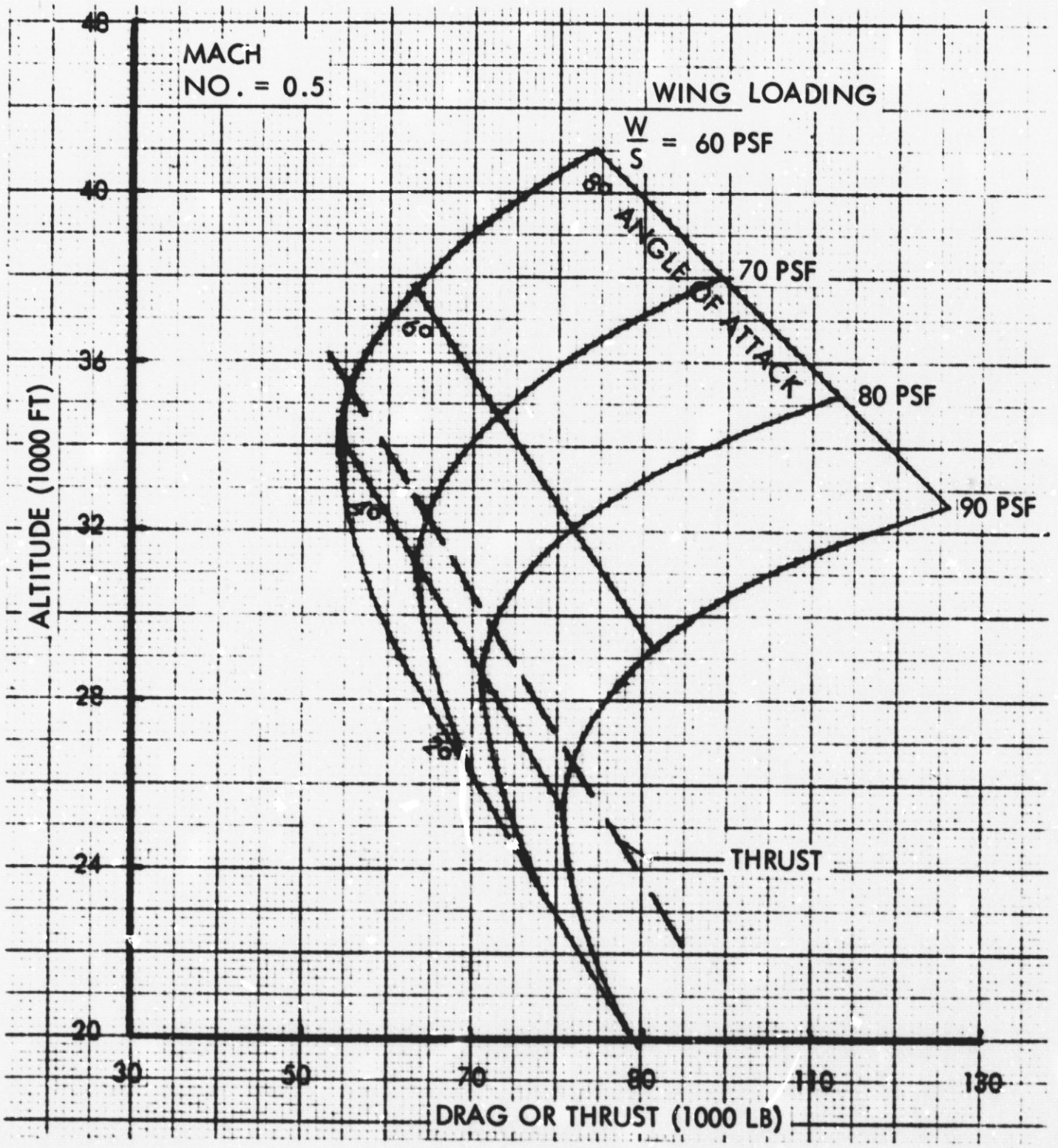

Figure 7. 3-48. Conditions for Booster Level Flight Cruise, 50,000-pound Payload Class System

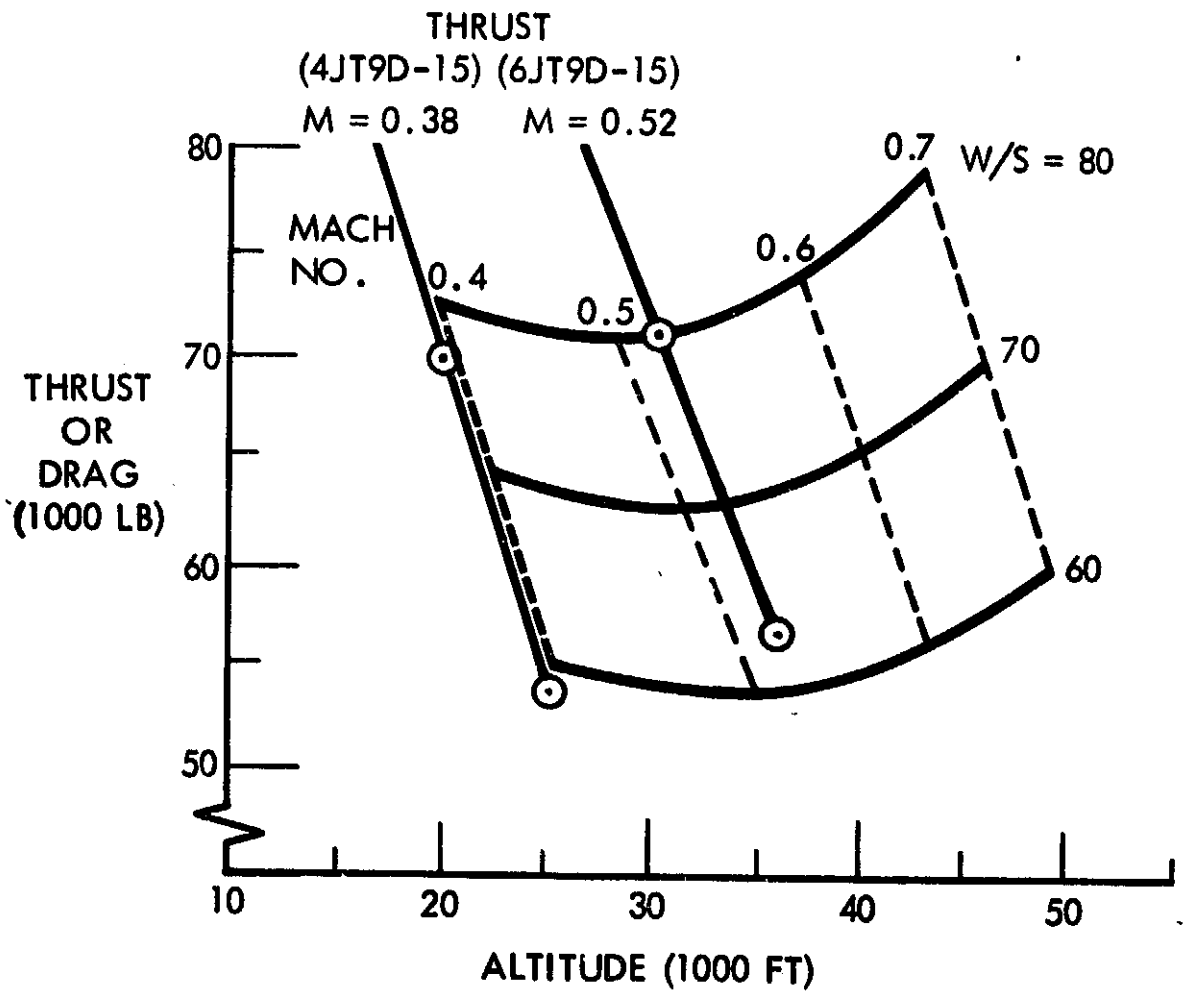

Figure 7.3-49. Conditions for Level Flight Cruise at Maximum Lift-to-Drag Ratio

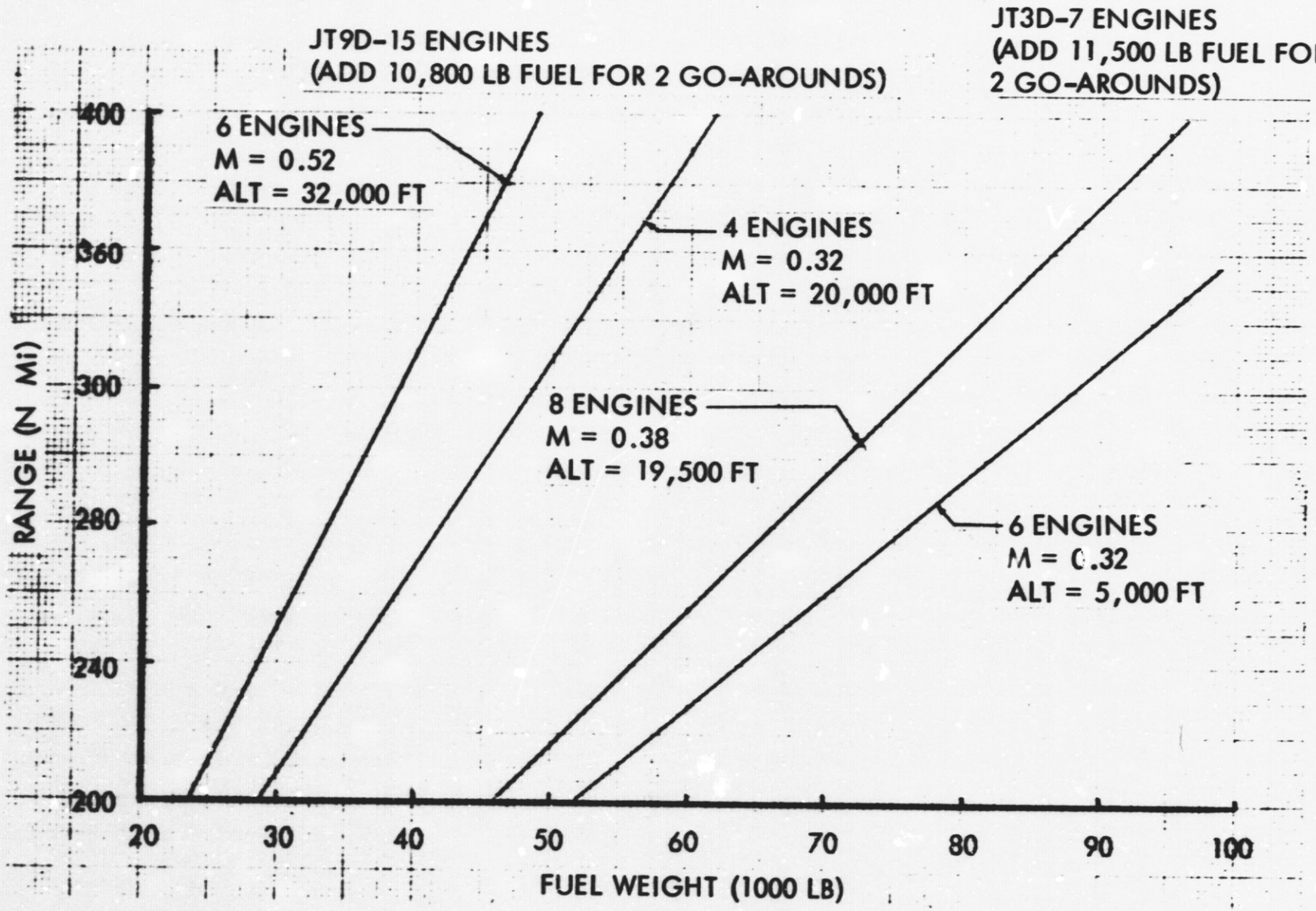

Figure 7.3-50. Fuel Requirements for Booster Cruise Back

A similar investigation was performed using the smaller JT3D-7 engines. All cruise calculations were based on the requirement of flight at conditions for maximum lift-drag ratio. The effect of fuel load and the number of engines on range are shown in Figure 7.3-50.

Optimization of the Brequet range factor yields the maximum range for a given mass ratio. It does not necessarily follow that, for a fixed range, the system weight is minimized. The effect of flying off optimum (lower cruise velocity), using four JT9D-15 engines instead of six, is also presented in Figure 7.3-50. A flyback range of 300 nautical miles requires 45,200 pounds of fuel for this condition, a 25-percent increase in fuel weight. However, total system weight must include the weight of the engines and fuel. Summarized in Table 7.3-23 are the total propulsion system weights (engine plus fuel) for selected types and number of engines. The data are based on a cruise range of 300 nautical miles. It is noted that the lowest-weight system is not the one designed for optimum cruise Mach number. Instead it is the one using the least possible number of engines. The saving in engine weight is greater than the increased fuel weight required for cruise at off-optimum conditions. The selected system for the 50,000-pound-payload-class booster uses 4 JT9D-15 engines.

Landing Performance. The landing-flap effectiveness was presented in Figure 7.3-46. The flap is a single slotted flap with a span of 70 percent of the wing span and a 30-percent chord. Flap effectiveness and trim levels were estimated from NR Report NA-68-414 (Reference 7-7). The lift-drag budget for landing is presented in Table 7.3-24.

Landing performance is summarized in Figure 7.3-51. Thrust and drag characteristics during approach and landing for the booster and orbiter are displayed on the left side of the figure. The approach is made at 200 knots true air speed at a trimmed lift coefficient of 1.38 with flaps and gear down. The orbiter, with flaps and gear down, has an excess thrust margin that results in a rate of climb of 1570 feet per minute. This rate of climb is adequate for climb-out after a missed approach. The flaps and gear-down rate of climb of the booster is 1750 feet per minute. These data show that the orbiter and booster both possess an adequate excess thrust margin for a missed approach.

An approach may be successfully made with one engine out. However, little thrust exists for climb-out. An approach with one engine out would be considered an emergency. Thus the requirement for go-around would be redundant.

Landing-ground-roll and touchdown-speed characteristics are also summarized in Figure 7.3-51. It is interesting to note that, if the flaps were not deflected, the touchdown speed of the orbiter would increase to

Table 7.3-23. Comparison of Booster Cruise-Back Engine and Fuel Weights

Cruise Condition		Turbojet Engines				Fuel Required for 300-nmi Range (lb)	Total Propulsion System Weight	Remarks
Mach Number	Altitude (ft)	Type	Number Required	Weight Per Engine (lb)	Total Engine Weight			
0.52	32,000	JT9D-15	6	8470	50,820	36,200	97,820	• Optimum cruise Mach number = 0.52 • 10,800 pounds of go-around fuel
0.38	20,000	JT9D-15	4	8470	33,880	45,000	89,680	
0.38	20,000	JT3D-7	8	4260	34,080	71,000	116,580	• Optimum cruise Mach number = 0.38 • 11,500 pounds of go-around fuel
0.32	7,000	JT3D-7	6	4260	25,560	82,000	119,060	

Space Division
North American Rockwell

THRUST MARGIN

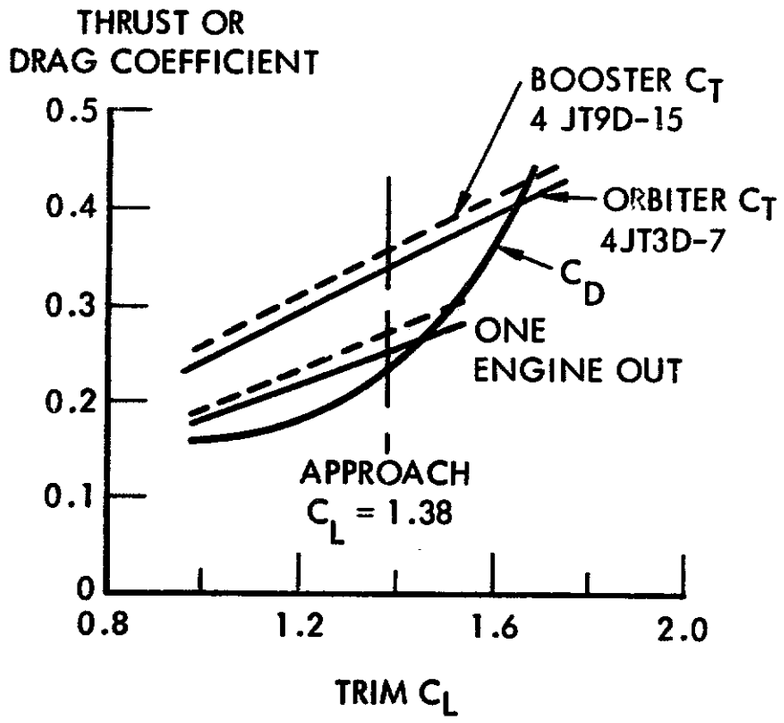

	NOMINAL	ONE ENGINE OUT
• BOOSTER	1.52	1.29
• ORBITER	1.43	1.20

LANDING SPEED

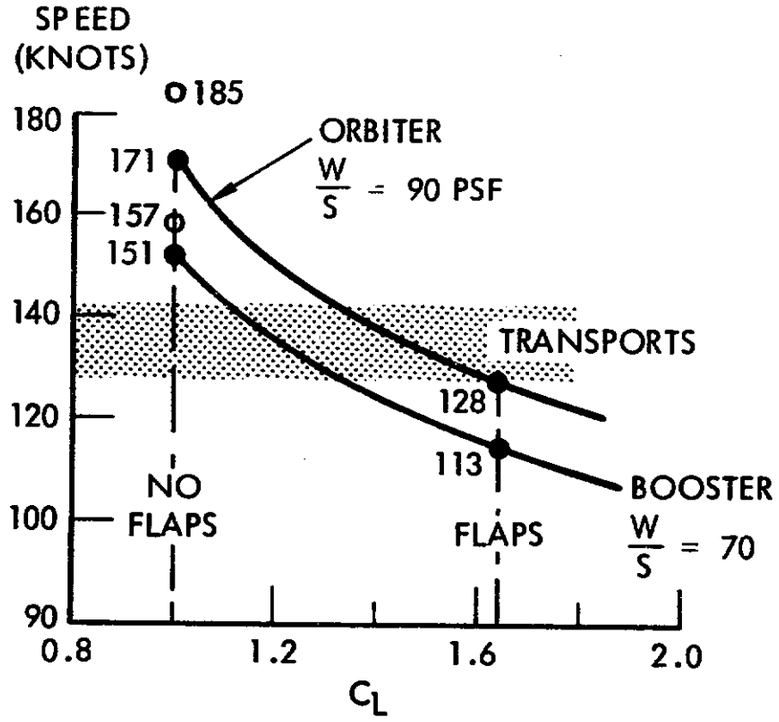

- LANDING SPEED COMPARABLE TO PRESENT DAY TRANSPORTS
- LANDING DISTANCE (FT)

	BOOSTER	ORBITER
50 FT OBSTACLE	2350	3000
GROUND RUN	2010	2800
TOTAL	4360	5800

Figure 7.3-51. Landing Characteristics, 50,000-Pound Payload System

Space Division
North American Rockwell

171 knots. The maximum touchdown speed is associated with a landing performed at an elevated runway on a hot day. The touchdown speed for the orbiter landing at Denver (5000 feet altitude) on a hot day is 185 knots. The touchdown velocity for the booster for the same conditions is 157 knots. A possible trade off exists between the additional weight and complexity of the landing flap system and the additional touchdown speed.

The fuel for one go-around maneuver is shown in Figure 7.3-52. The go-around course is a three-mile racetrack course with a 1.2-g turn at both ends. The time for one go-around is six minutes.

Table 7.3-24. Landing Lift-Drag Budget

Item	C_L	C_D
Clean wing ($\alpha = 8°$)	0.90	0.120
Flaps	0.91	0.164
Elevator	-0.18	0.012
Gear	0	0.024
Total	1.63	0.320

7.3.6 Launch Abort Analysis

The ILRV design requirement regarding system failures states that the system will fail operationally after the first failure and fail safe after the second failure. These are noncatastrophic failures. The system is not designed for abort capability in the event of major structural failure in the booster or orbiter, for example. An investigation of launch abort was conducted where the failures considered were related to engine-out contingencies in the primary rocket propulsion system.

The booster has 11 rocket engines, all ignited at lift-off. If one engine fails any time during first-stage operation, the vehicle has the capability of completing the primary mission. This was demonstrated in Section 7.3.2. If two engines fail at lift-off, the total mission cannot be accomplished. However, the thrust-to-weight margin is sufficient to permit the vehicle to continue the boost trajectory until a safe separation can be accomplished and the orbiter can return to a landing site.

If one engine fails on the orbiter any time after staging, the vehicle has the performance capability to complete the primary mission. This was also demonstrated in Section 7.3.2. If both orbiter engines fail, a launch abort

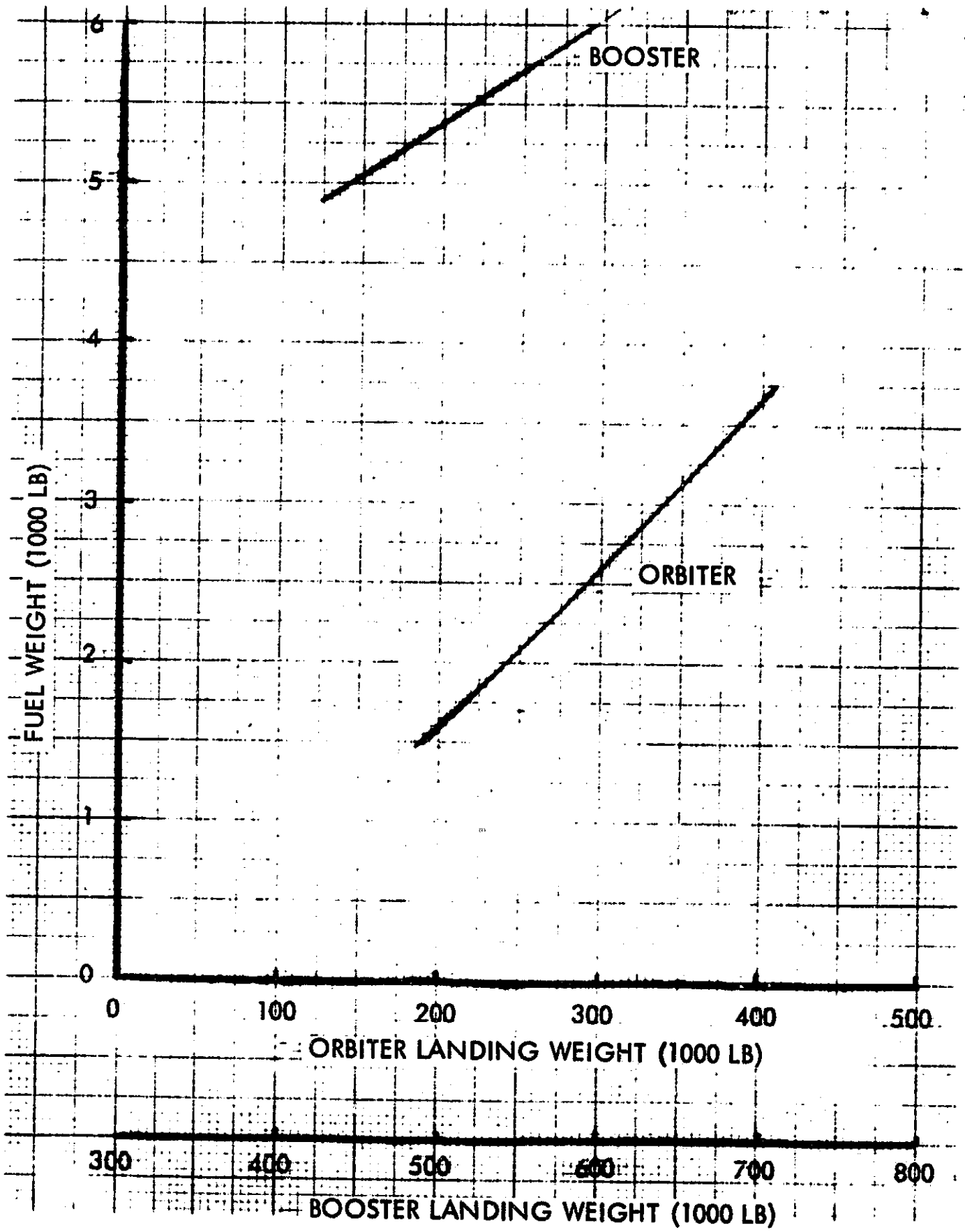

Figure 7.3-52. Effect of Landing Weight on Go-Around Fuel Requirements (One Go-Around)

condition results. The impact of abort conditions on vehicle design and performance characteristics was evaluated through an investigation of launch aborts. The objectives of this evaluation were to:

1. Identify feasible flight modes for orbit or launch aborts.

2. Evaluate the capability of the 50,000-pound-payload-class orbiter to recover from a launch abort situation.

3. Determine the capacity, if any, of the orbiter to return to the launch site in event of an abort.

The approach was to investigate aborts from three areas of the launch profile: early pre-staging, late pre-staging, and post-staging. Orbiter angle of attack, bank angle, and thrust were varied to identify feasible flight modes that would allow maneuver to a touchdown point without incurring excessive load factors and heating. The abort conditions were taken from a launch trajectory to a 60 by 100 nautical miles orbit inclined at 55 degrees. Aborts from a staging point corresponding to launch to a 50-by 100-nmi orbit were also considered. Maximum load factors were defined, and flight modes were investigated to limit the design load factors to 4 g's normal and 3 g's axial. The stagnation heating rate was calculated for a one-foot radius sphere to compare relative severity in heating during abort.

Pre-Staging Aborts

Pre-staging aborts fall naturally into two general classes: early and late aborts. For the early aborts the nominal launch profile passes through the flight regime where, if it were not for the large positive flight path angle, the orbiter would be able to maintain a level altitude or would be able to glide in an equilibrium condition. For the early aborts then, the problem is mainly one of removing the large positive flight path angle without losing excessive altitude or speed.

For the late aborts, the problem is one of too much potential energy and not enough kinetic energy. For this kind of an abort, the orbiter is far above its equilibrium glide ceiling. If an abort occurs, the orbiter falls at a steep flight path angle with attendant large load factors. The concern in this case is not one of minimum altitude, as for the early aborts, but one of maximum load factor and heating rates.

Early Aborts. A brief examination of early aborts indicated that the orbiter has the performance capability to accomplish the abort and return to the launch site. There is, however, a constraint on time from lift-off at which the mission can be terminated. The altitude and velocity at abort must be sufficient to preclude unacceptable attitudes or altitudes from being

achieved during the period necessary for (1) booster thrust decay, (2) separation, and (3) orbiter thrust buildup. A detailed analysis has not been performed to establish the earliest acceptable abort time; however, it is estimated that this time may be on the order of 10 to 20 seconds, depending on vehicle thrust-to-weight ratios. Two early abort cases were considered: near-pad abort and an abort near maximum dynamic pressure. For the near-pad abort, it was assumed that the orbiter would fly the nominal launch trajectory until sufficient altitude and velocity had been reached to allow pitch-over the equilibrium cruise. Boost at maximum orbiter thrust was performed for 68 seconds, when an altitude of 26,000 feet was reached. The dynamic pressure was 411 psf. At this point, the orbiter engines were throttled to about 30 percent full thrust, and the vehicle was pitched down, using gimbal control. The vehicle descended to 20,000 feet, where a loiter pattern was maintained. From 6 to 9 minutes of powered cruise flight were available to fly back to the recovery site. Upon depletion of the rocket propellants, the vehicle descends and lands in the normal manner. The flight profile is shown in Figure 7.3-53.

The second case investigated was an abort at 68 seconds into the nominal launch trajectory. It was assumed that the booster engines were shut down and separation had been accomplished in the normal manner. The orbiter engines were ignited at full thrust, and a pitch-down maneuver was accomplished. Again, the orbiter engines were throttled to about 30 percent thrust, and a loiter pattern was flown at 20,000 feet to burn the orbiter fuel. A maximum of 11 minutes (81 miles) of powered flight time was available. Descent and landing is accomplished in the normal manner.

Late Aborts. Investigation of pre-staging aborts occurring late in the launch trajectory indicated the orbiter has the capability to accomplish an entry within vehicle design limits using angle of attack modulation and thrust. However, performance may be insufficient to return to the launch site. For launch into the 55-degree inclination orbit, land recovery of the orbiter is possible by banking toward the continental U.S.

Examination of pre-staging aborts with regard to the design criteria that the system will fail safe after the second failure reveals that the abort itself results from the first failure. The second failure could be loss of thrust on one orbiter engine. This would be the worst design case. Loss of both orbiter engines is a third system failure and is not a design condition. Excessive load factors would result during nonthrusting aborts, as shown in Figure 7.3-54. These data were obtained for a full orbiter flying straight ahead at full positive lift at the maximum trimable angle of attack, estimated to be 17 degrees. As expected, the most critical abort point in terms of load factor is at the staging point. For a launch trajectory of 60 by 100 nautical miles, a peak total load factor of 6.7 g's was computed. This is reduced to 6.0 for the nominal launch trajectory. If the angle of attack could be varied during entry, the peak load factor could be reduced. The benefit of this technique is indicated in the figure by the cross-hatched area. The total load

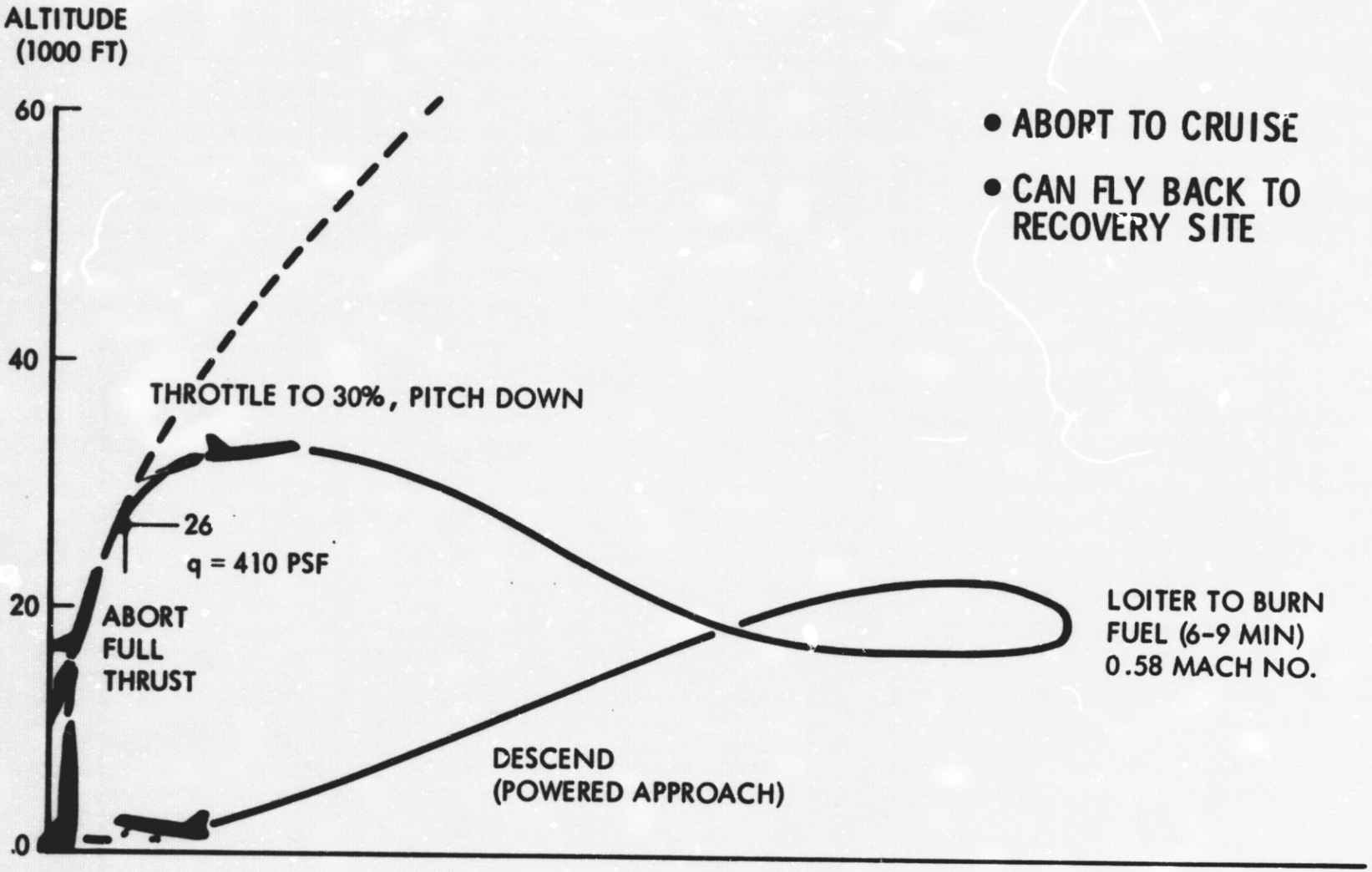

- ABORT TO CRUISE
- CAN FLY BACK TO RECOVERY SITE

Figure 7.3-33. Flight Profile Low-Altitude Abort, 50,000-Pound Payload Orbiter

MAXIMUM TOTAL LOAD FACTOR ON ORBITER

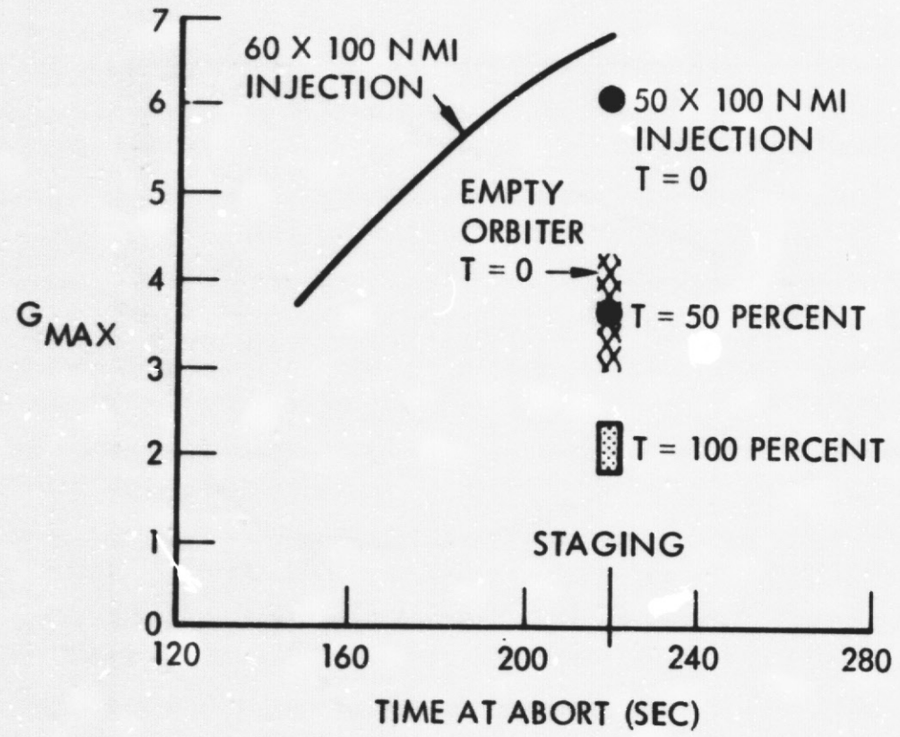

- EXCESSIVE LOADS WITH NON THRUSTING ORBITER (REQUIRES FUEL DUMP)
- SINGLE ENGINE ABORT $G_{MAX} = 3.6$

RECOVERY FOOTPRINT SINGLE ENGINE ABORT

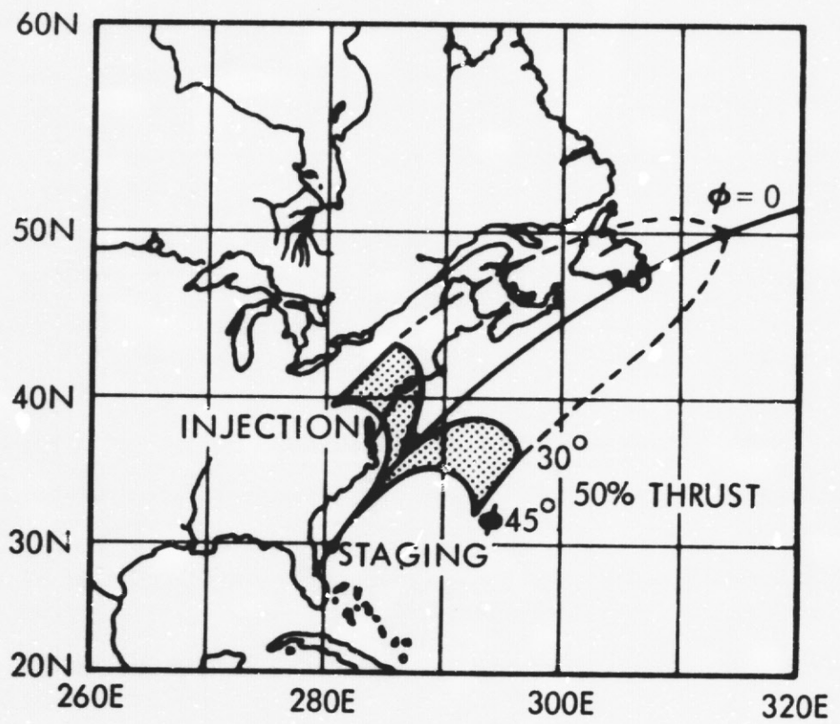

- LAND RECOVERY POSSIBLE

Figure 7.3-54. Prestaging Abort Performance 50,000-pound Payload Orbiter

Space Division
North American Rockwell

factor was reduced from 6.0 to 4.2 g's by limiting the normal load factor to 4.0 g's by angle-of-attack modulation. However, high heating rates and excessive dynamic pressure were experienced. The peak dynamic pressure reached was 4115 psf as compared to 47 psf during a nominal orbiter entry trajectory. The maximum reference stagnation heating rate was 65 Btu/ft^2/sec compared to 46 for a nominal entry. These results indicate that severe weight penalties would probably be incurred if it were a requirement to design for nonthrusting pre-staging aborts.

The design case for prestaging aborts will occur during thrusting aborts. Prestaging aborts with orbiter thrust were investigated to determine whether the orbiter could return to the launch site and to establish the resultant design environment. It was assumed that the orbiter was fully loaded and that all systems were operable. The abort objective was to return to the launch site within 4-g normal and 3-g axial load factor limits, using the three control variables of rocket thrust, angle of attack, and bank angle. The combinations examined in increasing order of effectiveness and complexity were (1) maximum angle of attack at full lift and zero thrust, (2) maximum angle of attack at full lift with thrust, and (3) maximum angle of attack constrained by both the weight loading and the load factor limit, bank angle other than zero to effect a turn, and thrust to aid in both load factor reduction and to maximize integrated range.

Straight ahead aborts from the launch trajectory of 60 by 100 nautical miles, including staging with the fully loaded orbiter at maximum trim angle of attack of 17 degrees and zero thrust, established that a maximum resultant load factor of about 7 g's occurs during abort from the staging point. The flight mode for these aborts was full negative lift to apogee and full positive lift thereafter. The addition of thrust at apogee and maintaining angle of attack at the maximum for the existing propellant loading was effective in reducing the load factor within limits (4 g's).

If full thrust were available, peak load factor could be limited to the nominal entry value, as indicated in Figure 7.3-54. For 50-percent thrust, corresponding to one orbiter-engine failure, a peak total load factor of 3.65 g's was experienced during a straight-in abort.

In an attempt to return to the launch site from the staging point of the launch trajectory of 50 by 100 nautical miles, the orbiter was banked to minimize the radius of turn, and the angle of attack was modulated to limit the peak load factors to 4.0. Rocket thrust was applied to maximize the integrated range. A combination of the three control variables was established. It resulted in near maximum return-to-pad performance of the orbiter. However, it was not possibe to return to the launch site with all available rocket propellant used, the maximum L/D glide terminated about 340 nautical miles short of the launch site. Refinements to the flight mode would not be expected to overcome this ranging deficit, and return to alter-

native sites was briefly considered. The recovery footprint for aborts at 50-percent thrust is shown in Figure 7.3-54. Land recovery is possible for banked turns to the left.

These data were obtained for thrusting aborts where thrust was applied at apogee and a maneuver performed in an attempt to return to the launch site. Results indicate that the orbiter should be designed for a total load factor of 4.0 to account for the abort case with one engine out. Additional investigations are required to determine the impact of the resulting loads and thermal environment on weight and vehicle structure, thermal protection, and control system design. Other flight modes should also be considered, such as thrusting to continue the ascent trajectory and then performing a power-off entry in the normal manner, in an effort to reduce the severity of abort design environments.

Post-Staging Aborts

If an orbiter engine fails, the vehicle has the capability to complete the primary mission, and the "fail operational" criteria are met. A second failure could be loss of thrust from the remaining orbiter engine. Consequently, nonthrusting post-staging aborts were investigated.

Initial conditions were taken from a preliminary boost trajectory to an orbit of 60 by 100 nautical miles at a 55 degree inclination. For entry at the design angle of attack (60 degrees) to be performed, it is necessary that the orbiter fuel be expended so that the vehicle can be trimmed at 60 degrees. With a full fuel load, the orbiter would enter at about a 15-degree angle of attack, and the orbiter is not designed for the heating environment that would result. Thus, it was assumed that the fuel had been dumped in some manner before entry.

The flight mode was to fly zero bank at a 60-degree angle of attack until pullout, hold altitude by modulating the bank angle, and full lift after the bank was reduced to zero. The maximum deceleration loads (g-loads) encountered during entry after an abort are shown in Figure 7.3-55 as a function of abort time and boost velocity. The figures show that an abort from the nominal trajectory could lead to a resultant load factor as high as 5.3 with the flight mode described.

A flight mode using angle-of-attack modulation was investigated as a means of reducing these loads. The resultant force coefficient of the orbiter increases with angle of attack; therefore, the loads can be decreased by angle-of-attack modulation. The abort at 287 seconds (peak g) was investigated to determine how much the load could be reduced and how much modulation would be required. The orbiter entered at zero bank and maximum C_L (52.5-degree angle of attack) until the resultant load factor built up to a specified level. At that point, the angle of attack was decreased to maintain the desired load factor (and increased to 52.5 degrees as the

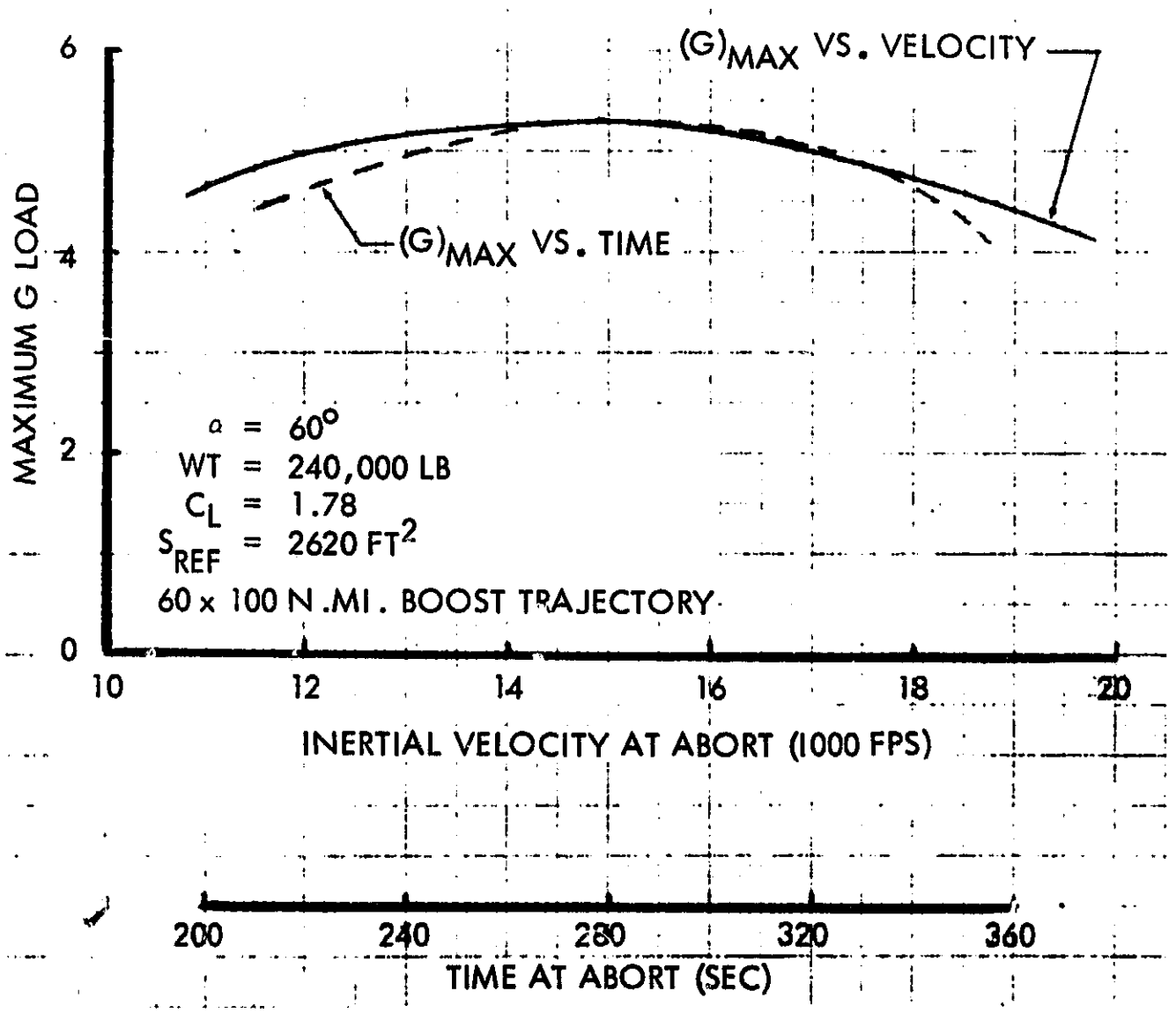

Figure 7.3-55. Maximum G Loads During Nonthrusting Poststaging Abort, 50,000-pound Payload Class Orbiter

vehicle decelerated). Figure 7.3-56 gives the load factor history for no angle-of-attack modulation and with modulation neces ary to hold several load factors. As the maximum load factor is reduced, the minimum angle of attack is reduced, and the time of load application is increased. The amount of angle-of-attack modulation required for various load factors is given in Figure 7.3-57. This curve shows that the load factor can be reduced to near 2.0 g's if there is no restriction on minimum trim angle of attack. For an estimated minimum trim angle of attack of about 40 degrees for the empty orbiter, a maximum load factor of 3.7 g's results.

The energy level for these aborts is too low for return to the launch pad. The distance to the pad after an entry is illustrated in Figure 7.3-58. The change in range increases almost linearly as the maximum load factor is reduced. For the lift modulation case discussed, the flyback range to the launch site is 880 miles. Water landing will result from straight ahead entry after abort from a nominal ILRV launch trajectory. Splashdown points are illustrated in Figure 7.3-59. Additional investigations are required to determine the orbiter cross-range capability during abort. Figure 7.3-60 compares the heating-rate time histories that would occur during an abort with an empty orbiter employing angle-of-attack modulation. The maximum heating rates are only about half the level reached during an abort from the staging point with a full orbiter, as discussed earlier. They are well within the 46 btu/ft^2/sec value achieved for the entry design case.

Abort Flight Modes Summary

Launch abort investigations have identified feasible flight modes for orbiter aborts. Results indicate that the successful entry can be performed with the orbiter from pre- and post-staging aborts, providing one engine is available for trajectory shaping during aborts prior to staging. In the event of a nonthrusting post-staging abort, fuel dump will be required, and it will be necessary to modulate angle of attack during entry to avoid excessive load factors. Additional analysis is required to identify recovery capability and abort regions from which land landings can be accomplished and to define entry load and thermal environment, vehicle control, and separation characteristics.

The following flight modes were identified:

1. For early aborts, including pad abort, an effective abort technique is to remain on the nominal launch profile until an aerodynamically controllable state is reached, then transfer to level flight, choosing a combination of angle of attack and thrust level appropriate to the velocity and altitude condition. When the vehicle reaches an equilibrium condition, the bank angle can be adjusted for the desired turning performance as the fuel is depleted.

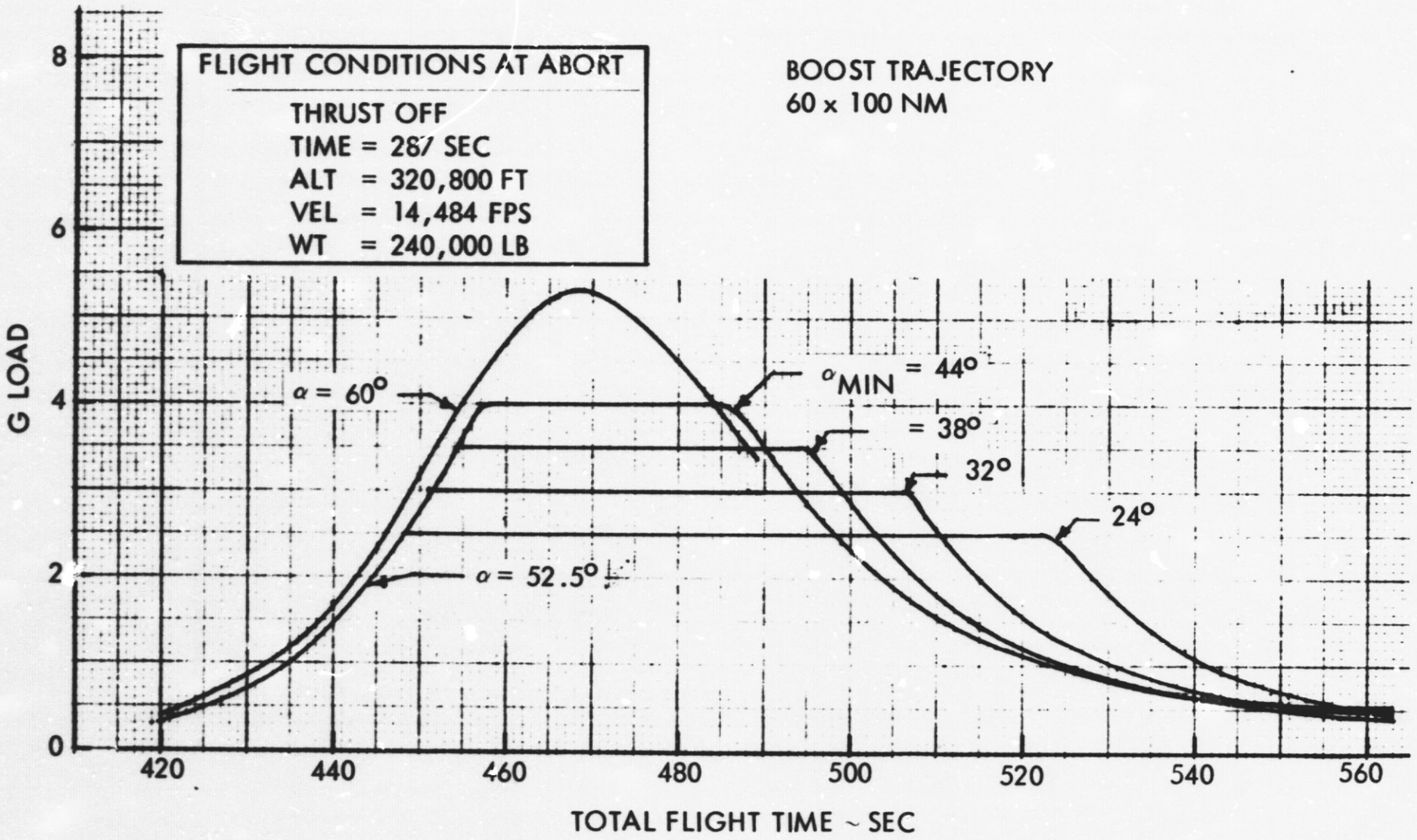

Figure 7.3-56. Abort G Loads with Angle of Attack Modulation, 50,000-pound Payload Class Orbiter

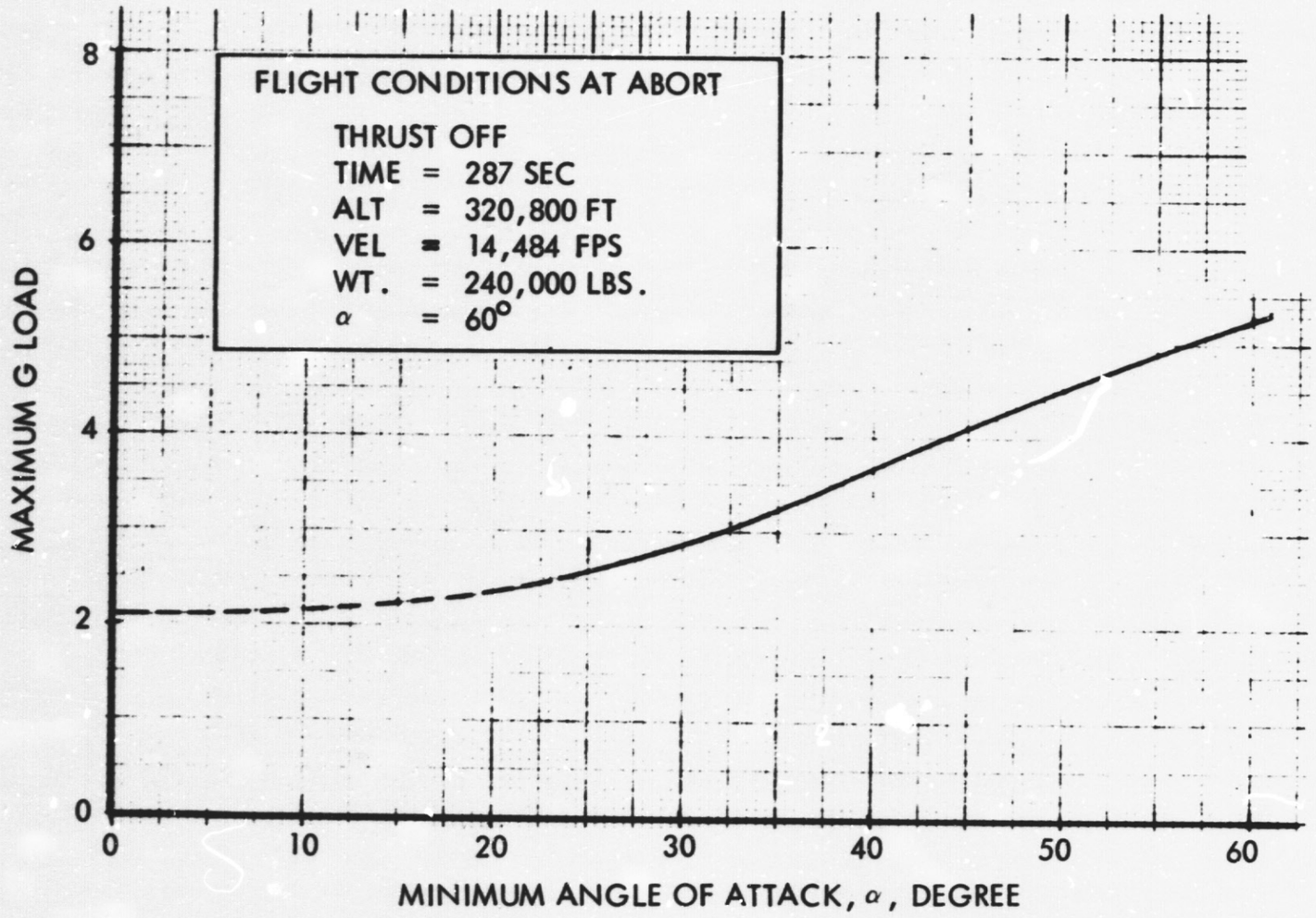

Figure 7.3-57. Angle of Attack Modulation Required for Restricting Maximum Load Factor, 50,000-pound Payload Class Orbiter

Space Division
North American Rockwell

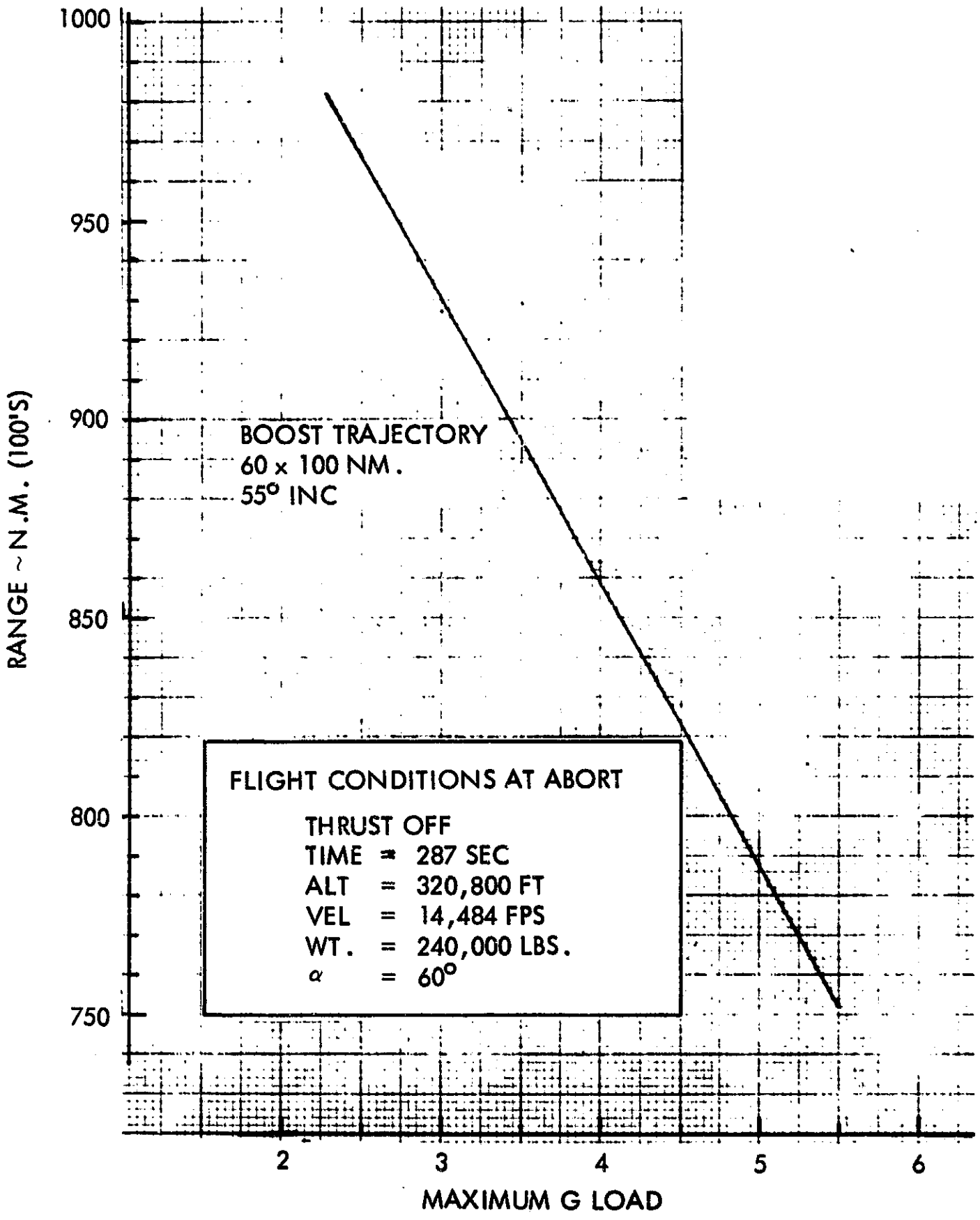

Figure 7.3-58. Variation of Abort Range with Maximum G Load, 50,000-pound Payload Class Orbiter

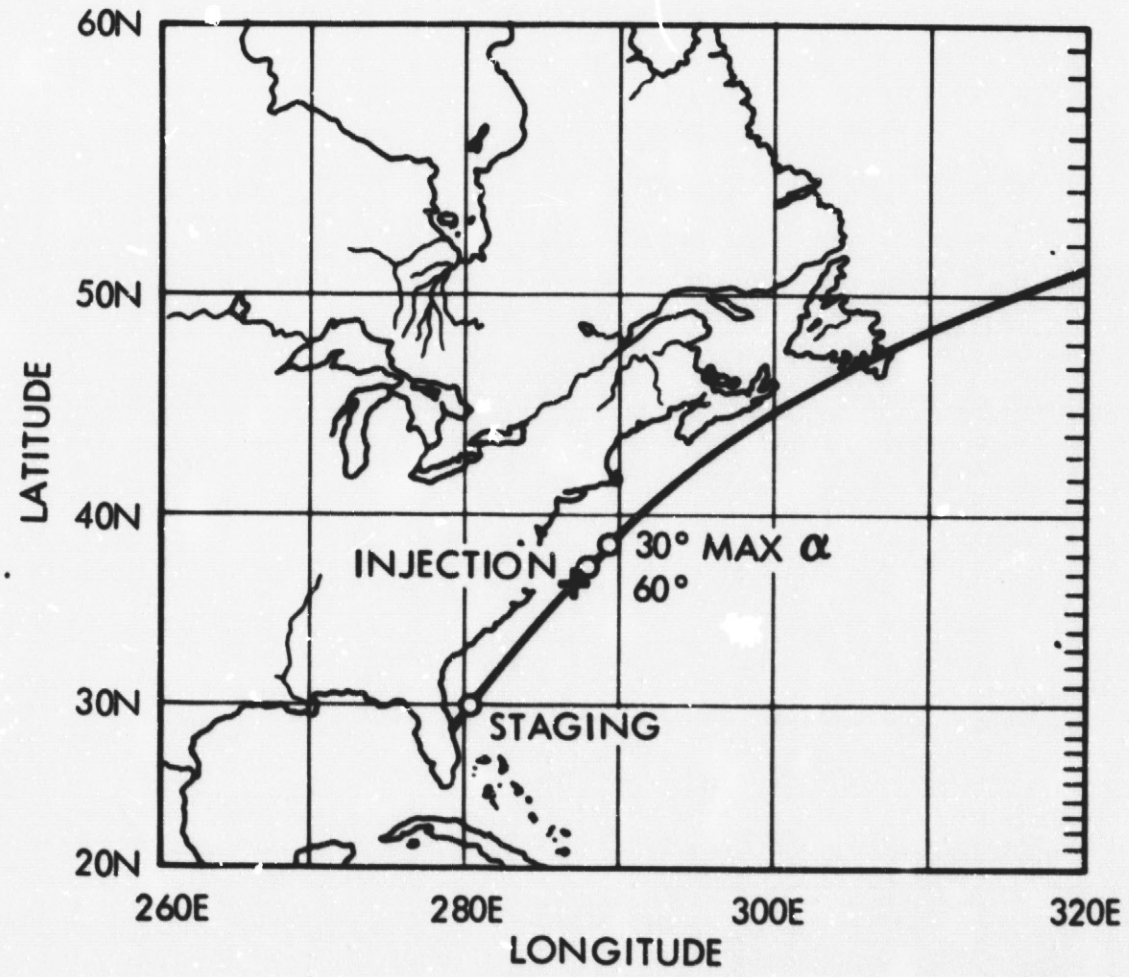

Figure 7.3-59. Splashdown Points Following Non-Thrusting Post-staging Aborts, 50,000-pound Payload Class Orbiter

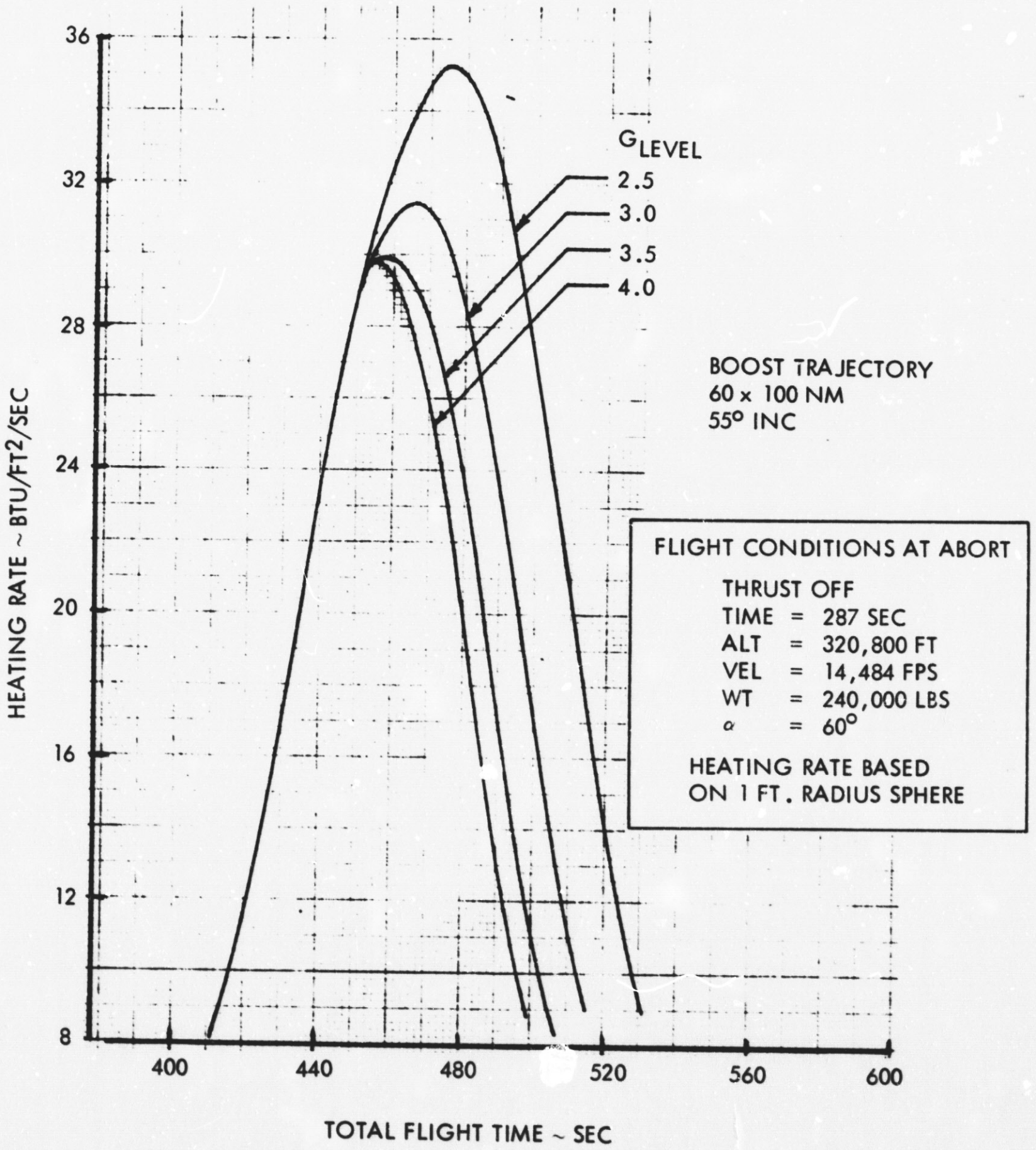

Figure 7.3-60. Stagnation Heating Rate During an Abort

2. For late aborts prior to staging, the capability exists to enter successfully within vehicle design limits using angle-of-attack modulation and thrust. However, performance capability is insufficient for the vehicle to return to the launch site.

3. For post-staging aborts with the dry orbiter, entry can be completed within vehicle design limits if angle-of-attack modulation is employed. Performance capability is insufficient for return to the launch site.

7.4 THERMAL ENVIRONMENT

Aerodynamic heating analyses during the record phase of the study were directed toward establishment of thermal environment during ascent and entry in order to determine design requirements for the thermal protection system.

7.4.1 Summary

Definition of thermal environment encompassed four major areas of investigation:

1. Establishment of aerodynamic heating environment for the MSC baseline orbiter and booster (12, 500 pound payload class)

2. Evaluation and correlation of NASA-provided thermal test data

3. Sensitivity analyses to establish the effect of wing loading and angle of attack on thermal environment during entry

4. Definition of ascent and entry heating design heating environments for the 50,000-pound payload class orbiter and booster

Significant results were:

1. The most severe thermal environment on the upper surface of the wings and fuselage occurs on the orbiter during boost. Maximum temperatures are 700 F at the wing 20 percent chord and 500 F on the body

2. Because of the low wing loading, laminar heating predominates during entry

3. The most severe thermal environment for the majority of the vehicle occurs during entry. Maximum temperatures over 90 percent of the surface area do not exceed 1500 F on the orbiter and 1400 F on the booster

4. Peak wing leading edge temperatures are 3000 F on the orbiter and 2200 F on the booster in non-interference areas

5. Considerable uncertainty exists as to the severity of interference heating. Orbiter wing temperatures could reach 3750 F in local hot spots

6. Over the range from 60 to 40 degrees angle of attack during entry, orbiter lower surface temperatures do not vary more than 100 F

7.4.2 Analysis Methods

The aerodynamic heating criteria used in analyzing the booster and orbiter were based on theories and data from the literature on similar configurations. The assumptions were verified by correlation of heating data provided by NASA MSC.

Flow Field Model

The flow field model was established for attached and separated flow regions over an angle-of-attack range of 0 to 70 degrees. For attached flow regions, pressure coefficients were computed by Newtonian theory:

$$\frac{C_p}{C_{p\ stag}} = \sin^2 (\theta + \alpha),$$

where θ is the local surface deflection of the vehicle. For negative-flow deflection angles ($\theta + \alpha < 0$), C_p of zero was assumed. Consistent with previous studies and test data on lifting bodies, local flow properties were computed by normal shock expansion for angles of attack greater than 40 degrees and by oblique shock theory for angles of attack smaller than 40 degrees. Two-dimensional strip streamlines were assumed for all angles of attack for the wing and horizontal tail and for the vertical tail at $\alpha = 0$ degrees. For $\alpha < 20$ degrees, two-dimensional strip theory was used on the fuselage. At higher angles of attack, an axisymmetric streamline pattern was used (References 7.4-1 and 7.4-2).

For $\alpha < 40$ degrees, where normal shock expansion yields low local Mach numbers, a gradual transition model was used. Onset of transition at $Re_{ONSET} = 500,000$ was assumed, and fully developed turbulent flow at $Re_{FT} = 1 \times 10^6$ was used based on local properties. For a $\alpha < 40$ degrees, transition onset at $Re_{ONSET} = 1 \times 10^6$ was used, and fully developed turbulent flow at $R_{eFT} = 2 \times 10^6$ was used, corresponding to the high local Mach numbers resulting from the oblique shock local properties.

Leading-edge heating was based on the stagnation heating theory of Hoshizaki (Reference 7.4-3) for entry and the theory of van Driest (Reference 7.4-4) for ascent. Heating dependency on sweep angle, Λ, was computed by

$$\frac{\dot{q}_\Lambda}{\dot{q}_{\Lambda = 0}} = \cos^{3/2} (\Lambda_{eff})$$

where $\Lambda_{eff} = \sin^{-1}(\cos\alpha \sin\Lambda)$. Laminar attached flow heating distributions for the 12,500-pound-payload configurations were computed by the local similarity theory of Cohen (Reference 7.4-5) for the fuselage centerline and wing over an angle-of-attack range of 40 to 70 degrees. Calculations with the laminar reference enthalpy method, as formulated in Reference 7.4-5, showed agreement within ten percent with the local similarity method. The simpler reference enthalpy method was therefore used for computing time histories of heating rates.

The transitional heating, when the local Reynolds number was between the onset value, $R_{e_{ONSET}}$, and the fully turbulent value, $R_{e_{FT}}$, was based on a combination of the laminar and turbulent (Reference 7.4-6) reference enthalpy methods. Zero pressure gradient heating data across a transition zone generally exhibit the behavior indicated by the reference enthalpy Stanton-Reynolds number plot shown below.

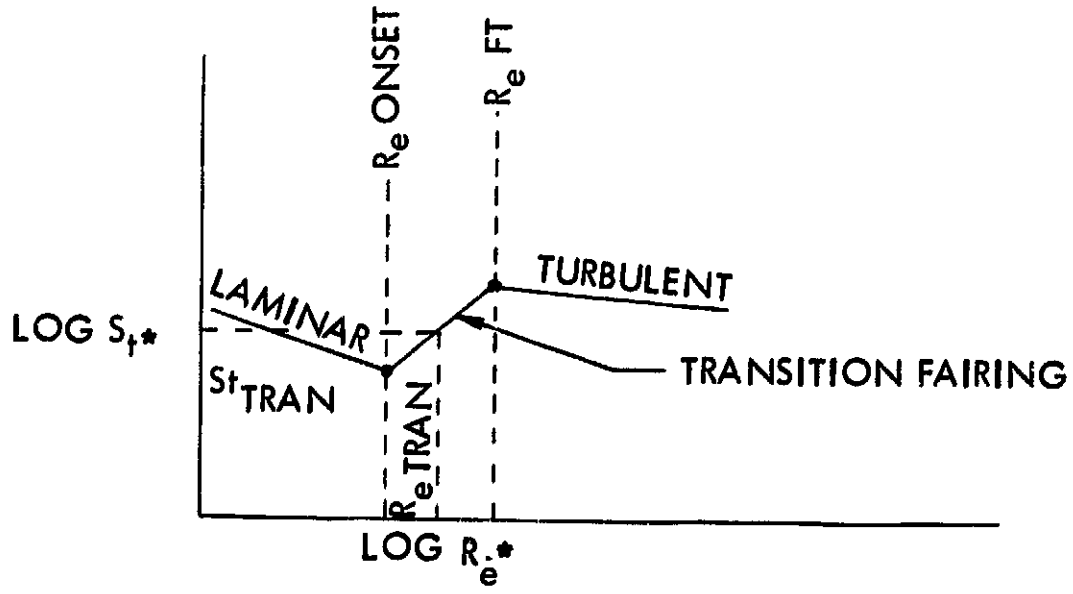

For heating computations in the transition zone, the reference Reynolds number in the transformed * plane corresponding to $R_{e_{ONSET}}$, $R_{e_{FT}}$, and $R_{e_{TRAN}}$ were computed, and the transitional reference Stanton number St^*_{TRAN} was derived from the transition fairing. This procedure was repeated for each time cut and body location. When the local Reynolds number exceeded the specified fully turbulent Reynolds number, heating was calculated by the turbulent reference enthalpy method of Eckert (Reference 7.4-6), assuming the virtual origin of the boundary layer at the vehicle nose. For flow on the fuselage, when axisymmetric streamlines were assumed, the laminar heating was determined by

$$\dot{q}_{\substack{\text{axisymmetric}\\ \text{laminar}}} = \dot{q}_{\substack{\text{flat}\\ \text{plate}\\ \text{laminar}}} \sqrt{3}$$

The turbulent heating was determined by

$$\dot{q}_{\substack{\text{axisymmetric}\\ \text{turbulent}}} = \dot{q}_{\substack{\text{flat}\\ \text{plate}\\ \text{turb}}} \quad 2^{1/5}$$

Heating in the transition zone was handled in a manner corresponding to the transition heating behavior on cones.

In the nose region of the fuselage and the leading-edge region of the wing, the assumption of Newtonian pressure is invalid because of the asymmetry of the shock. In these regions, the stagnation and leading edge heating was established from Apollo data and faired into the Newtonian/local similarity results downstream of the stagnation point. The stagnation point location was determined from Apollo data for the wing and MSC temperature sensitive paint test wind tunnel data for the fuselage. The stagnation heating was computed for the local radius of curvature at the assumed stagnation point and modified by Apollo data at the same angle of attack for non-Newtonian velocity gradients. The leading edge heating was determined by the heating rise on the Apollo torus relative to the actual stagnation point:

$$\frac{\dot{q}_{L.E.}}{q_{stag}} = \left(\frac{\dot{q}_{torus}}{q_{stag}}\right)_{Apollo}$$

At medium angles of attack, where Apollo data were not available, a fairing between the Newtonian results at low angles of attack and the Apollo data at high angles of attack was used. Results for the wing and fuselage for the 12,500-pound-payload configuration are shown in Figure 7.4-1 as heating normalized to stagnation heating to a one-foot-radius sphere. The heating ratios for the 50,000-pound payload are 0.715 times the 12,500-pound payload ratios because of the increase in size for the 50,000-pound payload configuration.

The heating to the chines of the fuselage was determined from the heating at the centerlines, useing the flat-faced cylinder data of References 7.4-7 and 7.4-8. A factor of 1.7 was applied to the centerline heating to obtain the chine heating. Figure 7.4-2 gives the estimated heating distribution normalized to the centerline heating for the sharp corners and for a rounded corner configuration, where

$$\frac{r_{corner}}{R_{body}} = 2/3$$

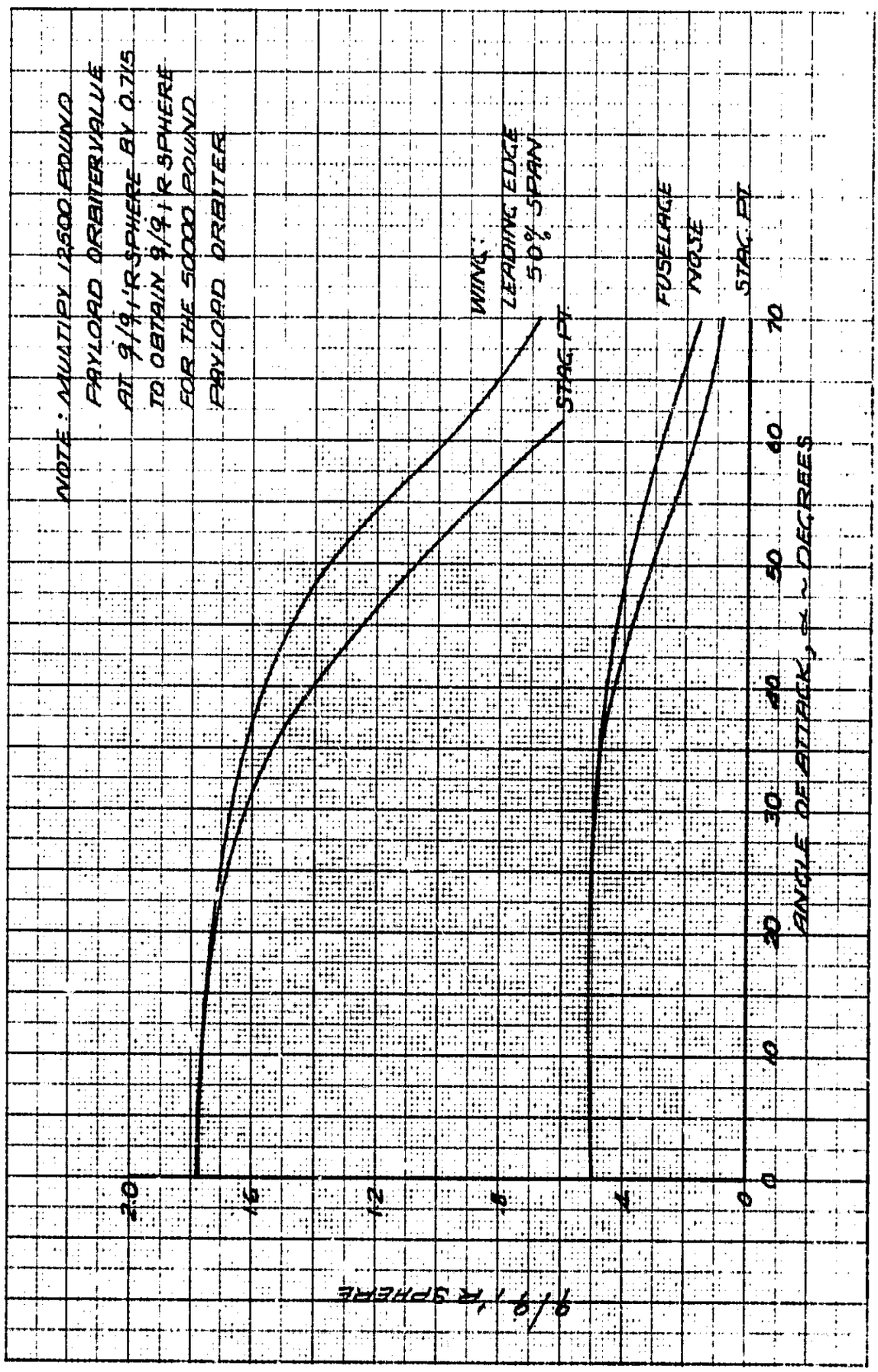

Figure 7.4-1. Stagnation Point and Leading Edge Heating Approximations, 12,500-Pound Payload Orbiter

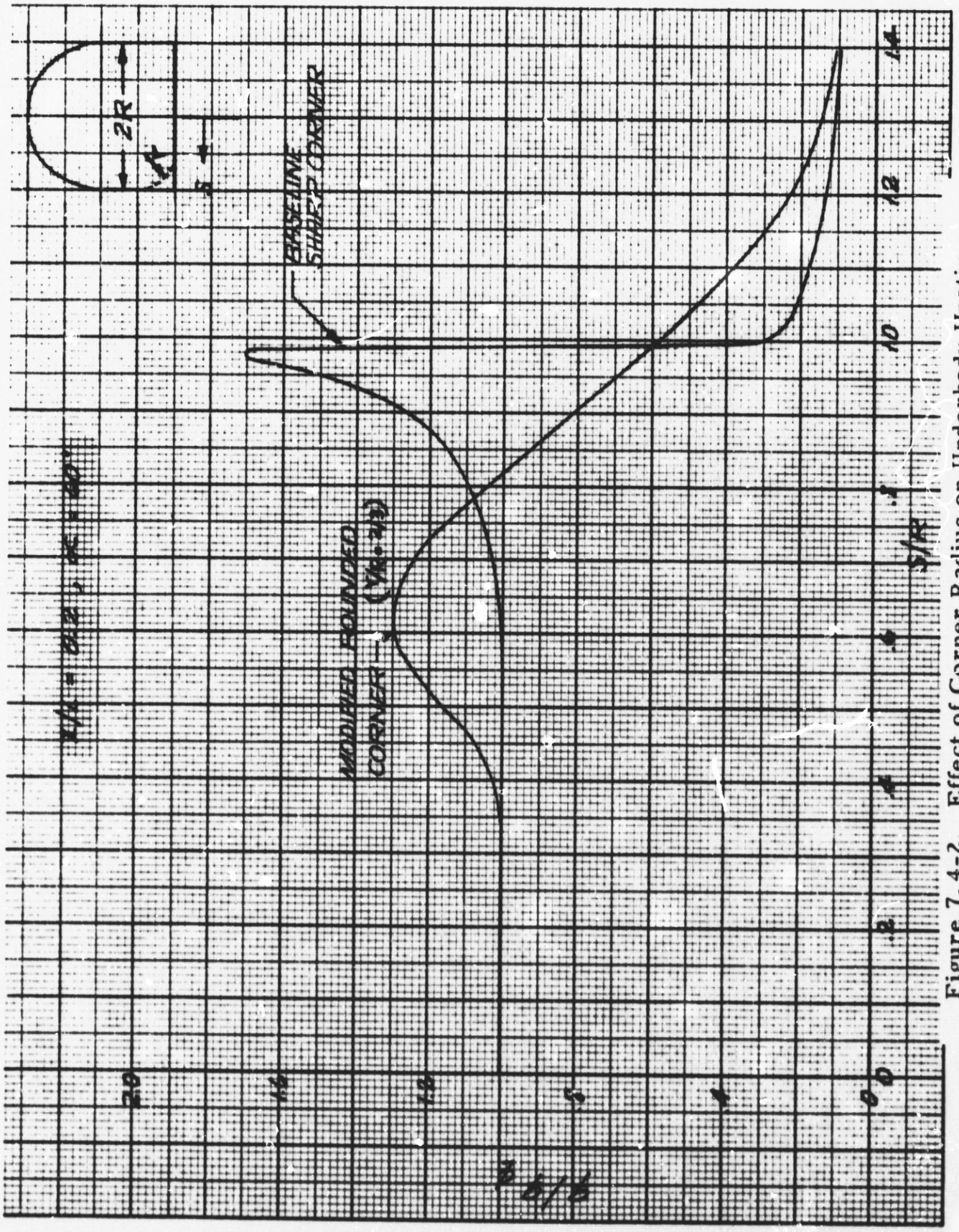

Figure 7.4-2. Effect of Corner Radius on Underbody Heating

The sides and top of the fuselage are wetted by the flow, which expands over the chines. For heating calculations, a two-dimensional boundary layer with $C_p = 0$ was assumed to originate at the chines and to remain attached to the tangent point of the flat sides and curved upper surface. Beyond this point of separation, the Chapman relation of Reference 7.4-9 was applied ($q_{separation} = 0.56\, q_{attached}$). The distribution of heating referenced to a point one foot from the chines is shown in Figure 7.4-3.

The heating to the upper surface of the wing at $\alpha = 60$ degrees was based on wake heating results of Apollo and other blunt bodies. This heating was taken as three percent of the stagnation point heating:

$$\dot{q}_{\substack{upper \\ surface}} = \frac{0.0628}{\sqrt{chord\ (ft)}}\, \dot{q}_{\substack{1'\,R \\ sphere}}$$

The interference heating to the control surface leading edges during ascent and entry was estimated from the data of Reference 7.4-10, -11, and -12. For direct shock impingement, a factor of four relative to undisturbed stagnation heating was applied. For the wing at $\alpha = 60$ degrees, the flow inclination to the leading edge should lessen the severity of the impingement, and a factor of three relative to the undisturbed $\alpha = 60$-degree environment obtained from the MSC paint test results was applied at 20-percent chord. Interference heating from shock interactions was estimated from the MSC paint test data and from References 7.4-13 and 7.4-14.

Test Data Correlation

Where applicable, the above method of analysis was applied to the NASA MSC 1/200 scale paint test data results obtained at NASA LRC at a freestream Mach number of eight and to data obtained from the MSC Arc Jet facility at a Mach number of six. Data for the wing and fuselage were available at 60-degree angle of attack and data or data interpolations were available for the fuselage at angles of attack of 15 and 45 degrees. At a 60-degree angle of attack, the paint test results and hypersonic tunnel results were in good agreement. Figure 7.4-4 gives the results of the correlation of the fuselage and wing data with the heating criteria specified above. Agreement is good on the aft section of the wing, but the leading edge region was too thin for reliable data to be obtained. The fuselage heating model underestimated the paint test data by approximately 20 percent in the afterbody region. This could be within the accuracy of the data and data reduction scheme or could indicate a stronger cross-flow on the

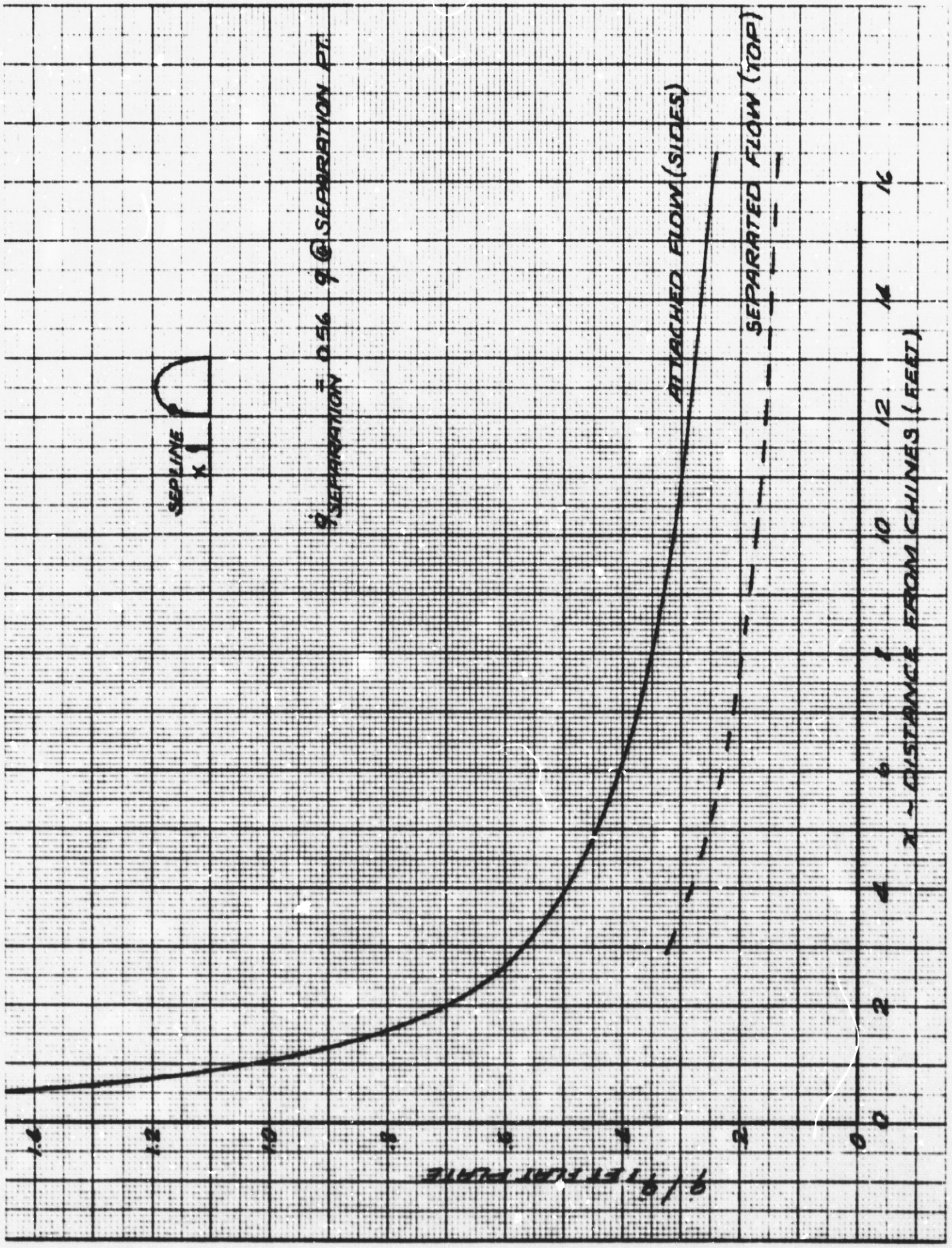

Figure 7.4-3. Heating Distribution to Sides and Top of Fuselage

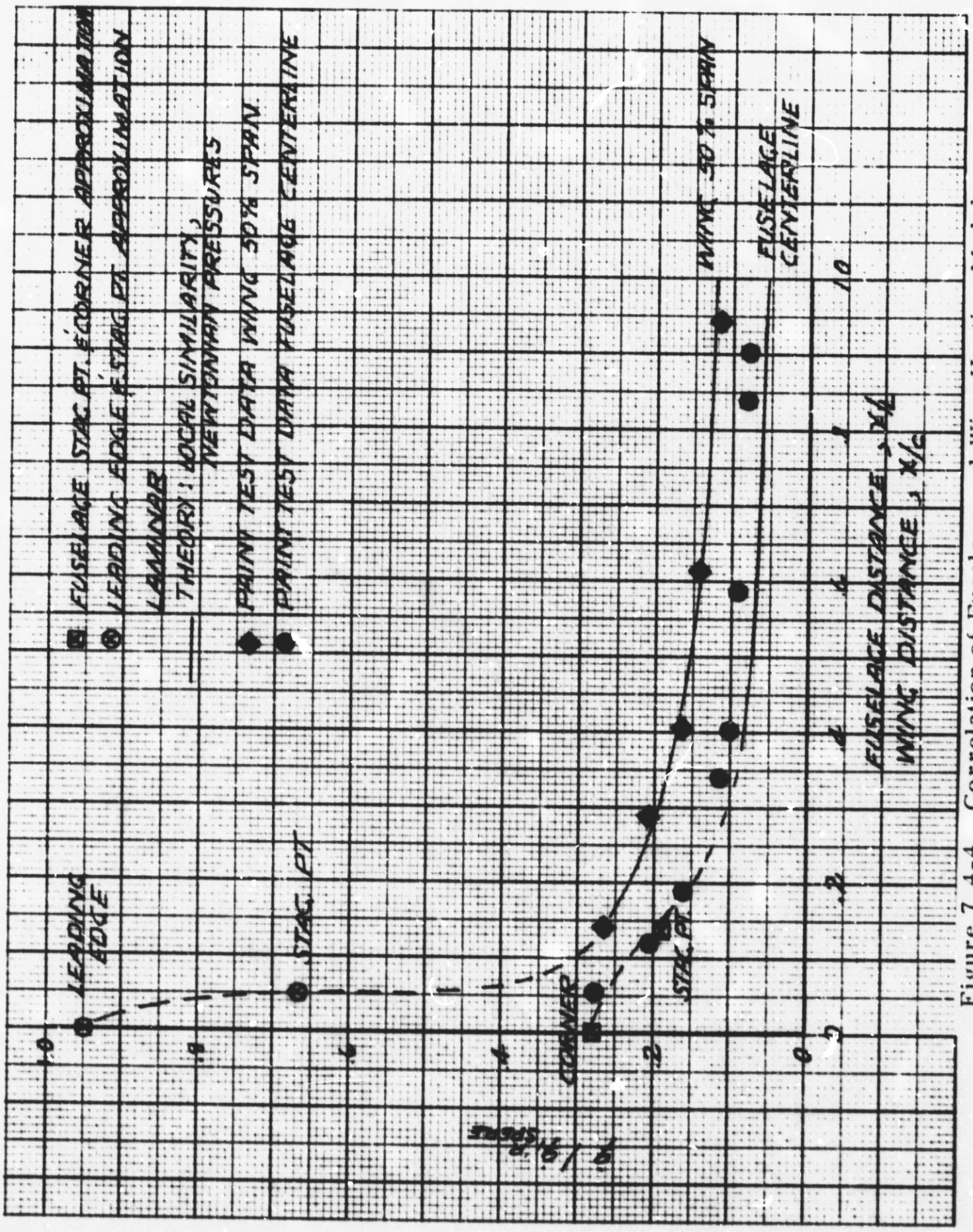

Figure 7.4-4. Correlation of Fuselage and Wing Heating Models (α = 60 Degrees)

afterbody or swallowing of the entropy layer by the boundary layer. The possibility of transition from normal shock expansion to oblique shock properties is also indicated by the correlation of the fuselage data at a 45-degree angle of attack (Figure 7.4-5). Although the difference between the paint test and the Arc Jet test data is large, qualitatively the data do not decay as rapidly on the afterbody as for isentropic expansion. Because of the length of the vehicle, it is possible that the body is not entirely isentropic at high angles of attack. The correlation of fuselage data at a 15-degree angle of attack is given in Figure 7.4-6. The isentropic expansion and oblique shock theories differ by about the same amount as the two sets of data. Because of the variation in the data, it is not possible to evaluate the validity of the flow model from these heating data alone.

Additional data were provided for the sides and top of the fuselage and the upper surface of the wing. The data for the upper surface of the wing indicated $0.01 \leq q/q_{1'R\,sphere} \leq 0.03$. At 50-percent span, the heating model developed here yields $q/q_{1'R\,sphere} = 0.0203$. The analytical model assumed for the fuselage is about 40 percent above the paint test data on the side of the vehicle and twice the experimental data on the top of the vehicle. Thermocouple data for the wing at $\alpha = 60$ degrees (run at LRC) were not received in time for correlation of results.

7.4.3 Baseline Vehicle (12,500-Pound Payload Class)

To support definition of sizes and weights of the logistics vehicle concept defined by NASA-MSC it was necessary to establish the thermal design environment for a range of entry conditions. Aerodynamic heating was computed for the 12,500-pound payload class orbiter and booster concept shown in Figure 7.2-3. Entry environments were defined for a parametric matrix of wing loadings from 58 psf to 162 psf over an angle-of-attack range from 20 to 60 degrees. Ascent environments were defined for a series of launch trajectories. This section presents the design heating data for the 12,500-pound payload class vehicle. The parametric data are discussed in Section 7.4.4.

For entry at a 60-degree angle of attack and a wing loading of W/S = 90 psf, the reference environments used with the heating factors in the previous section yield maximum radiation equilibrium temperatures (assuming surface emissivity of 0.8) as follows for the 12,500-pound-payload-class baseline orbiter:

Fuselage nose	2100 F
Fuselage stagnation point	1850 F
Wing leading edge 50-percent span	2900 F (non-interference region)

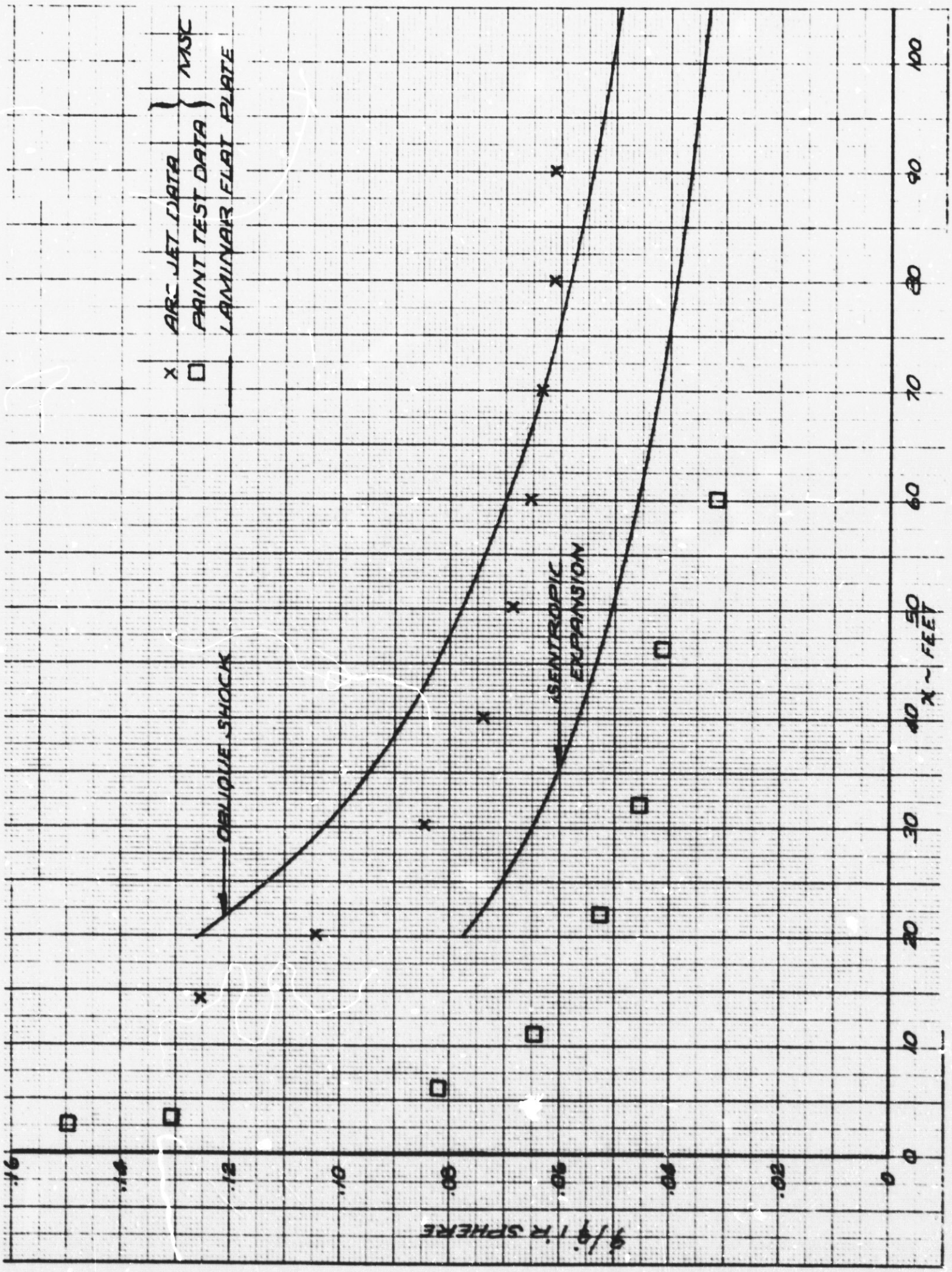

Figure 7.4-5. ILRV Fuselage Data Correlation (α = +45 Degrees)

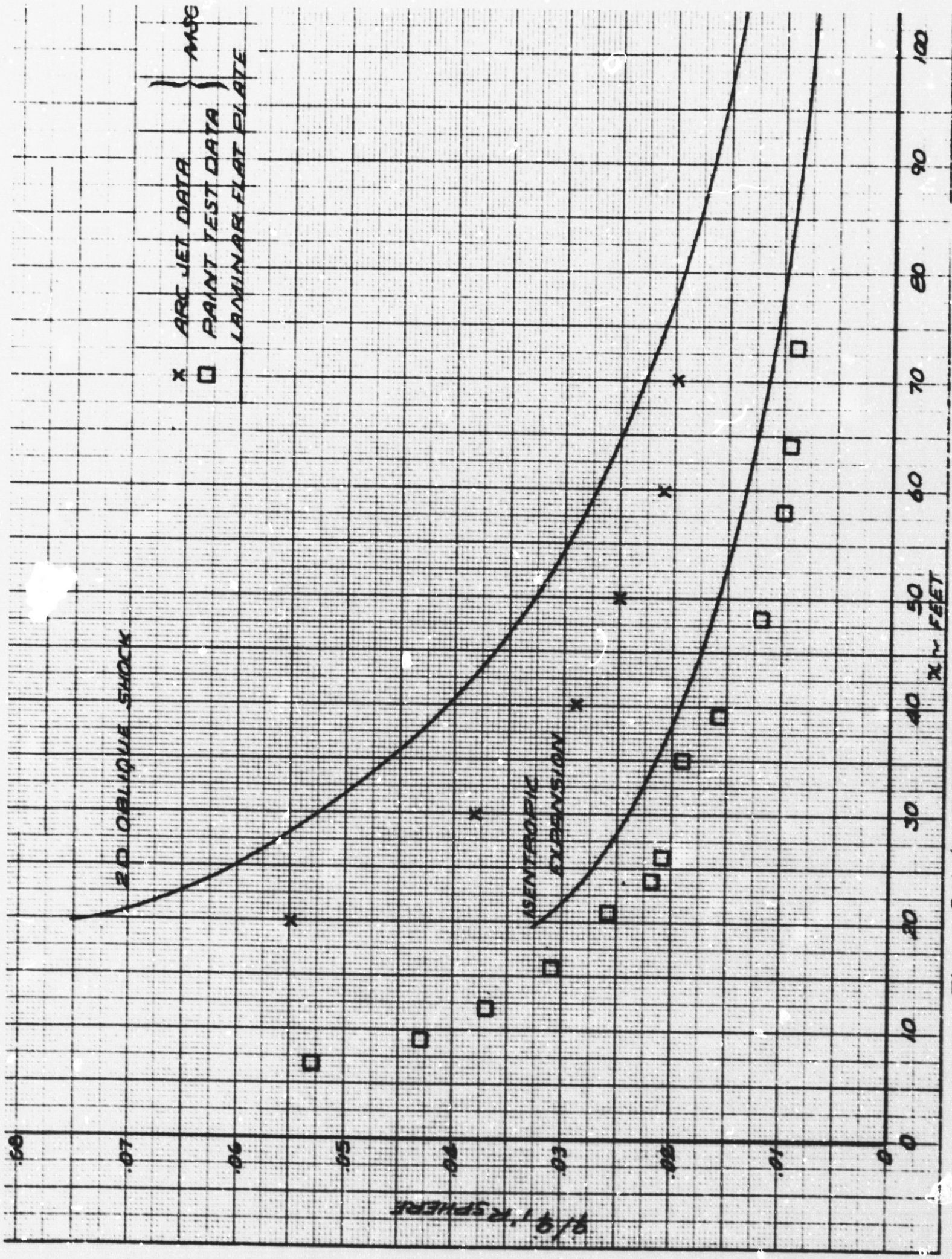

Figure 7.4-6. ILRV Fuselage Data Correlation (α = 15 Degrees)

Wing leading edge 20-percent span	3850 F (interference region)
Wing stagnation point 50-percent span	2620 F
Upper wing 50-percent span	800 F

The environments for the wing underside at 50-percent span (non-interference) and 20-percent span (interference region) are given in Figure 7.4-7. These leading edge and interference heating environments were based on low Reynolds number, low Mach number, wind tunnel tests. On a full-scale flight from earth orbit, the Mach number and Reynolds number range during entry will change the magnitude and extent of the interference heating. Additionally, vortex interaction is certain to cause premature transition of the boundary layer to turbulent flow in the interference regions. For certain configurations and flow conditions, References 7.4-10 and -11 show that shock impingement heating at a leading edge can exceed theoretical heating by a factor of 7 to 10 in localized areas. Reference 7.4-11 shows impingement heating on a flat surface can exceed undisturbed heating by a factor of 15 and cause transition of the boundary layer to turbulent flow. For these reasons, the above interference heating analysis is only qualitatively indicative of the severity of the interference problem.

The temperature distribution on the fuselage centerline and chines for the 12,500-pound-payload configuration with W/S = 90 is given in Figure 7.4-8. Estimated temperature concentrations and heat loads over the entire vehicle are summarized in Figure 7.4-9.

7.4.4 Design Improvements and Sensitivity Analysis

Effects of Injection Altitude on Ascent Heating

To support selection of the design launch trajectory, ascent heating was defined for the 12,500-pound and the 50,000-pound payload booster and orbiter for the 45, 80, and 100 by 100-nmi ascent trajectories. Figure 7.4-10 gives the reference sphere heating at orbiter burnout and before separation. For the range considered, burnout above 50 nautical miles is needed to prevent the ascent temperatures from exceeding entry temperatures on the leading edge of the wing. The booster and orbiter afterbody temperatures were about 600 F to 700 F. With the interference factors on the booster fuselage, temperatures reached 1300 F. Table 7.4-1 gives the maximum ascent heating rates for the booster and orbiter for surface inclination angles of 0, 5, and 10 degrees at the fuselage centerline. These inclination angles correspond to underbody centerline locations of X/L of approximately 0.5, 0.3, and 0.15 for the orbiter, and 0.7, 0.5 and 0.1 for the booster. They are approximately the same for both the 12,500-pound and 50-pound payload configuration. The 0 series also applies to the upper

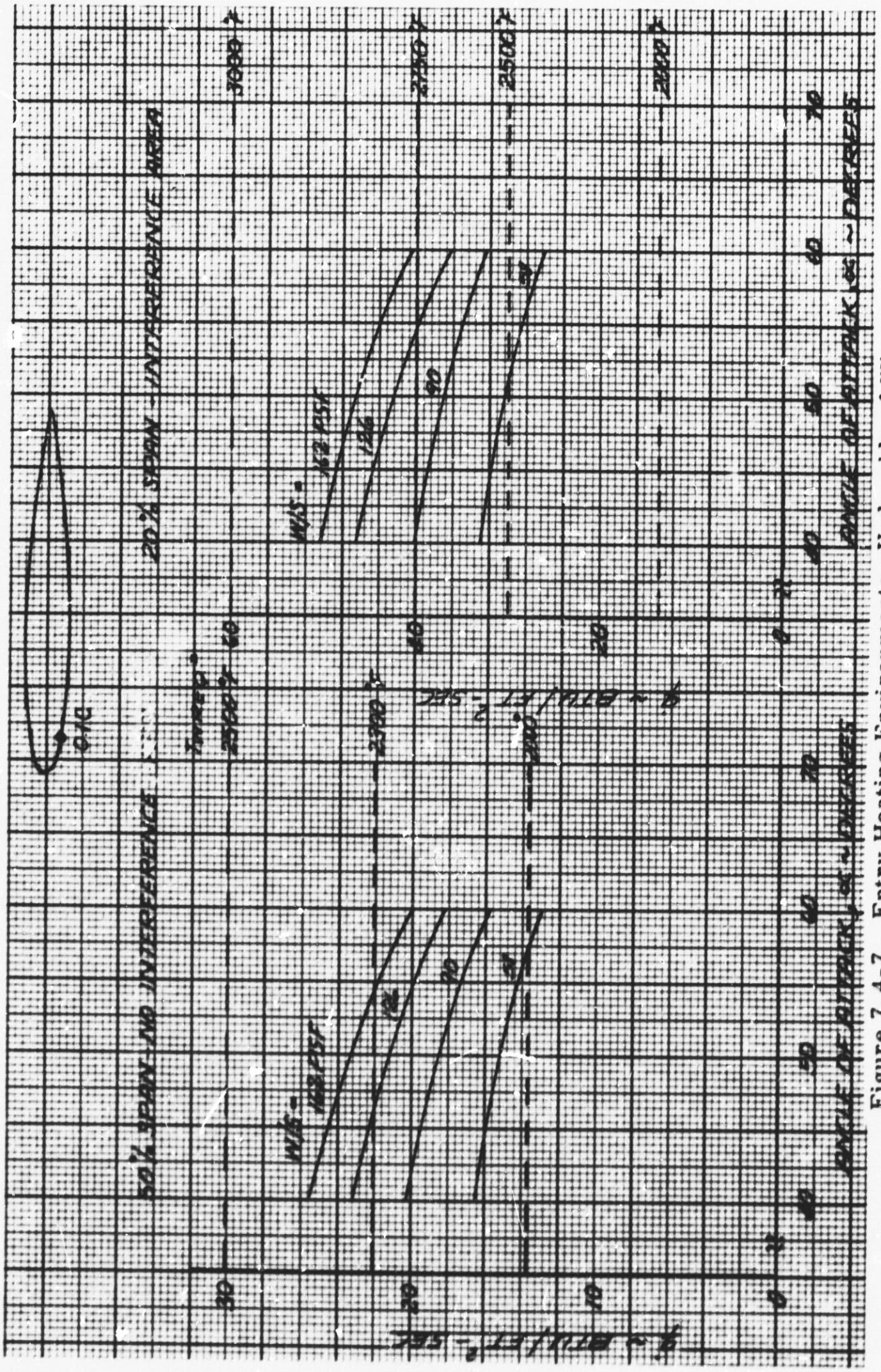

Figure 7.4-7. Entry Heating Environments, Underside of Wing — 12, 500-Pound Configuration

Figure 7.4-8. Orbiter Entry Environments, Underside of Body— 12,500-Pound Configuration

Space Division
North American Rockwell

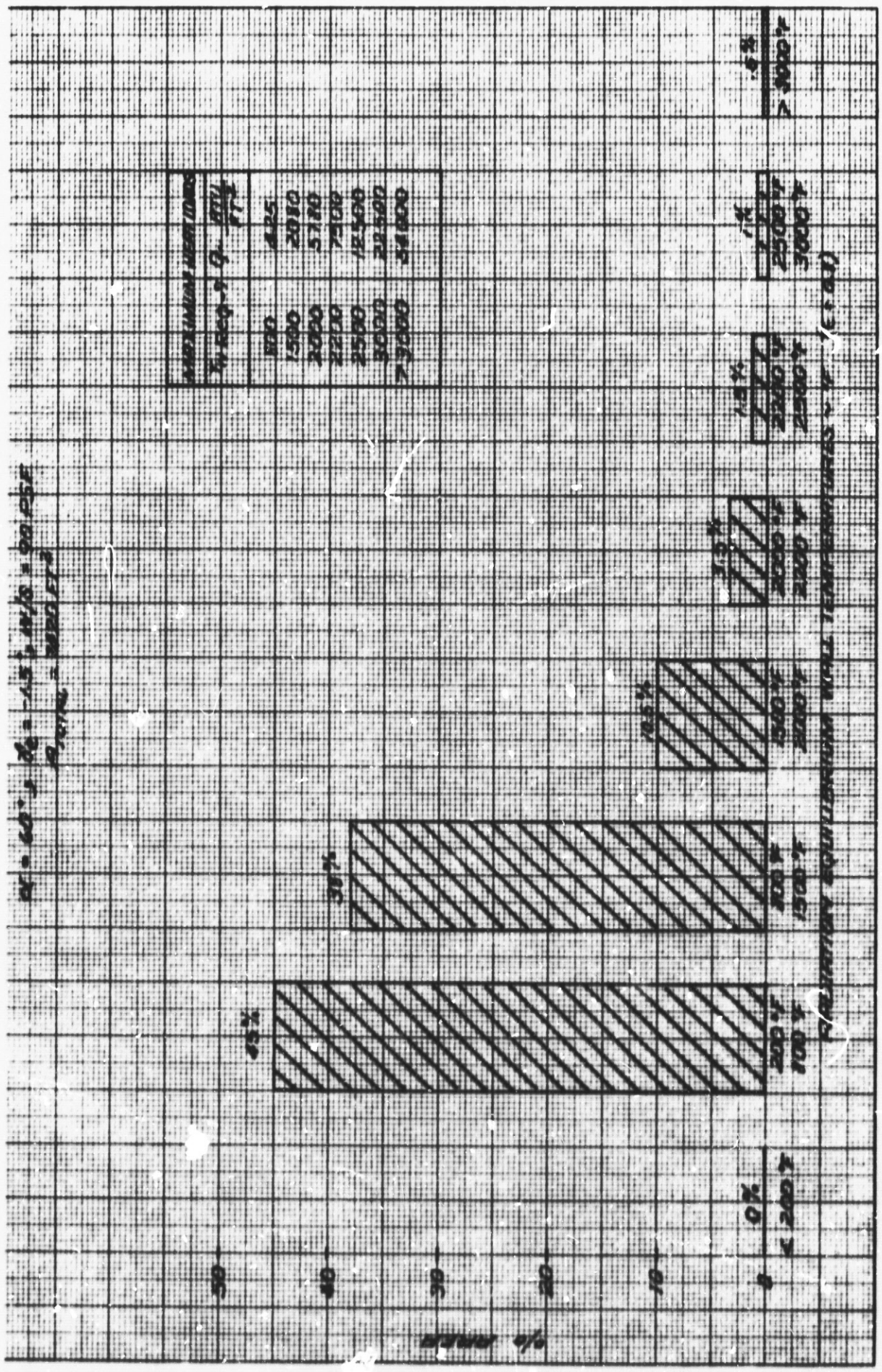

Figure 7.4-9. ILRV Temperature Concentrations, 12,500-Pound Configuration

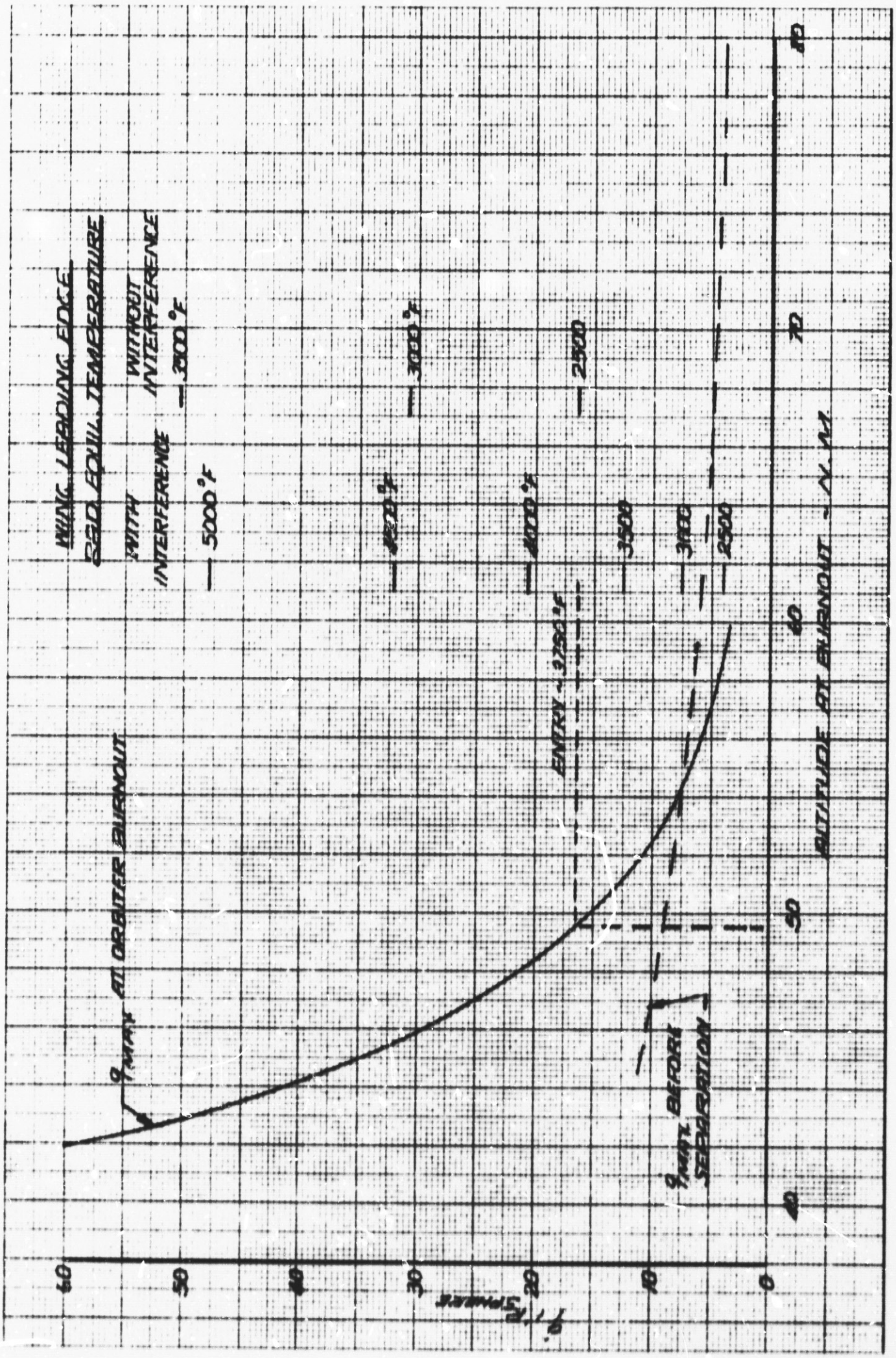

Figure 7.4-10. Ascent Heating at Orbiter Burnout

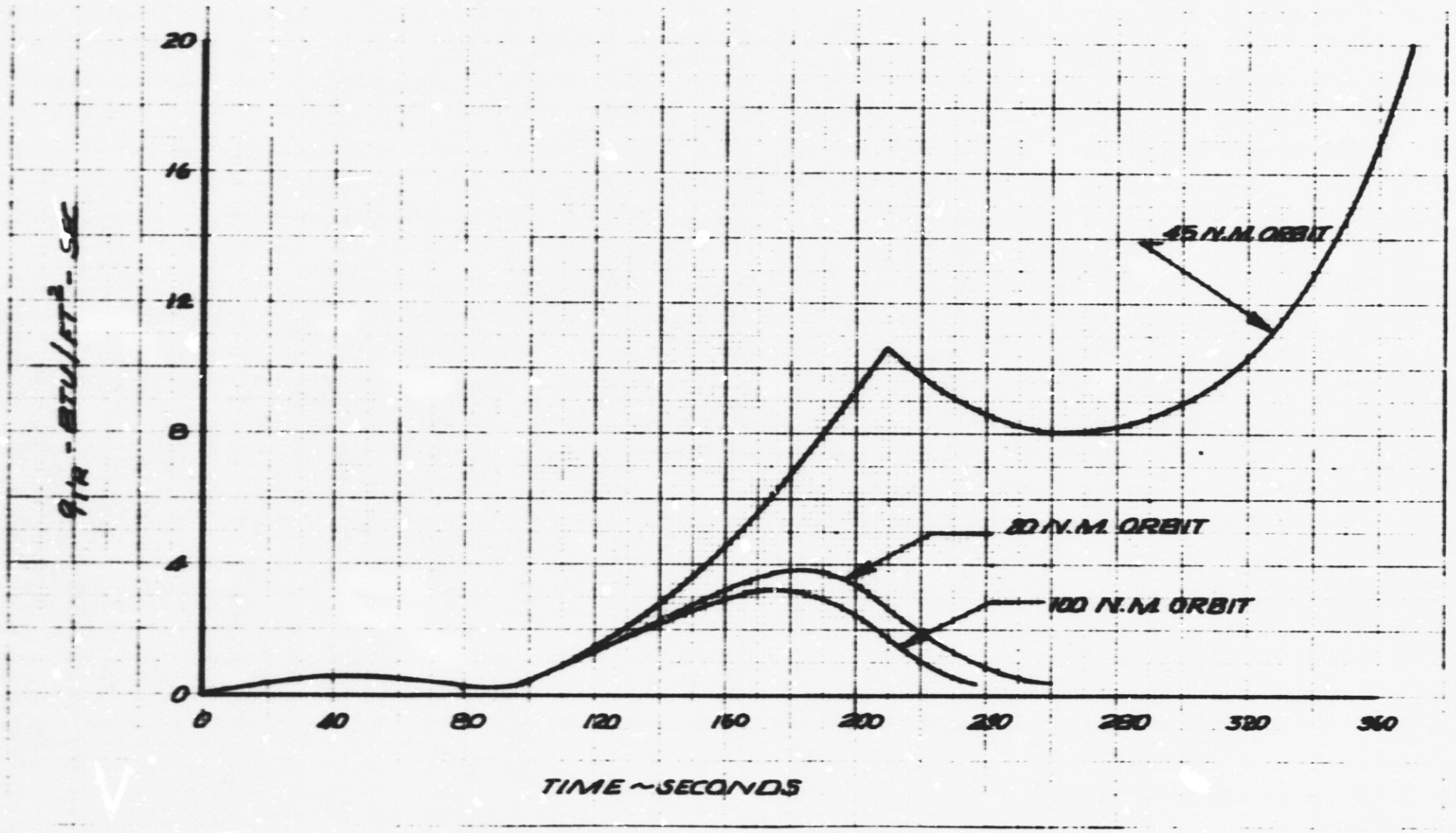

Figure 7.4-11. Ascent Heating, One-foot Radius Sphere

Space Division
North American Rockwell

Table 7.4-1. Maximum Ascent Heating Environments on Fuselage Centerline

Trajectory	Heating Rates (Btu/ft^2 - sec)				
	Configuration				
Orbit Insertion Altitude (nm)	Surface Inclination θ (deg)	12,500-lb Orbiter	12,500-lb Booster	50,000-lb Orbiter	50,000-lb Booster
45	0	0.38	0.32	0.32	0.30
45	5	0.45	0.49	0.40	0.40
45	10	0.68	0.65	0.62	0.60
80	0	0.38	0.33	0.32	0.30
80	5	0.40	0.36	0.35	0.33
80	10	0.50	0.48	0.48	0.42
100	0	0.36	0.32	0.32	0.30
100	5	0.40	0.36	0.36	0.36
100	10	0.50	0.45	0.43	0.40

surface of the orbiter. Table 7.4-2 summarizes the interference heating during ascent. Time histories of stagnation heating to a one-foot-radius reference sphere during the 45-, 80-, and 100- by 100-nmi trajectories are given in Figure 7.4-11 for a 0 F wall temperature.

Effects of Wing Loading and Angle of Attack on Entry Heating

To determine the sensitivity of the shuttle vehicle design to entry thermal environment, a parametric investigation of entry trajectories was conducted. For the 12,500-pound-payload-class orbiter, a matrix of 48 entry trajectories was computed, all for an entry angle of -1.5 degrees. For each of the angle-of-attack and wing loading (W/S) combinations listed (Table 7.4-3), three bank angle (Ø) schedules were run. These were 0°/0°, 50°/40°, and -50°/-40°. The first number is the bank angle before constant altitude deceleration. The second number is the bank angle after constant altitude deceleration.

For heating, there is negligible difference between the 50°/40° and -50°/-40° bank case. Both will exceed the Ø = 0°/0° case. All parametric heating was therefore based on the Ø = 50°/40° trajectories. The heating rates and loads referenced to a one-foot-radius sphere are given in Figure 7.4-12 for the trajectory matrix.

Table 7.4-2. Ascent Interference Heating Factors ($\dot{q}/\dot{q}_{1'R\ Sphere}$, $\alpha = 0$)

Area	50,000-lb Orbiter - No Interference	50,000-lb Orbiter Interference	50,000-lb Booster - No Interference	50,000-lb Booster Interference	12,500-lb Orbiter - No Interference	12,500-lb Orbiter Interference	12,500-lb Booster - No Interference	12,500-lb Booster Interference
Fuselage nose	0.775		0.61	2.44	0.74		0.69	2.76
Wing leading edge	1.20	4.8	0.995	3.82	1.74	6.96	1.30	5.20
Vertical fin	0.98	1.47	0.675	1.01	1.80	5.76	1.12	3.59
Horizontal fin	1.28	4.1	0.975	3.12	0.612		0.375	

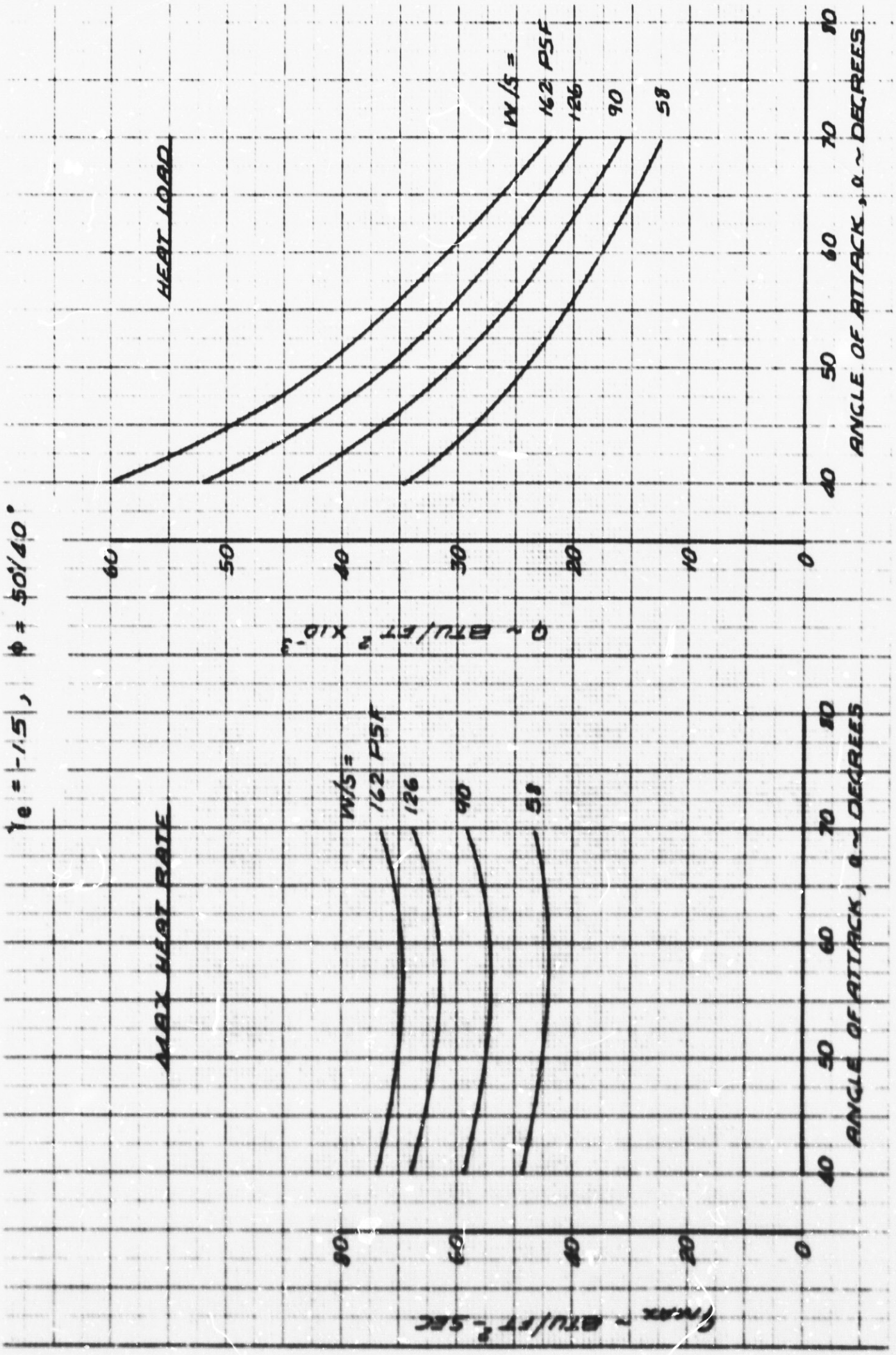

Figure 7.4-12. Reference Stagnation Point Heating, One-foot Radius Sphere

Table 7.4-3. Trajectory Matrix

α (deg)	W/S (psf) 58.1	90	126	162	L/D
70	W/C_LS (psf) = 43.05	54.58	93.33	120	0.30
60	32.81	50	70	90	0.50
52.5	30.41	47.10	65.93	84.77	0.65
40	35.24	54.58	76.41	98.24	0.97

Entry at a 40-degree angle of attack does not yield a significant increase in temperature over most of the body relative to the nominal 60-degree for the baseline. If the higher leading edge temperatures at the 40-degree angle of attack are tolerable, entry at 40 degrees is feasible. Entry at lower angles of attack results in a significant thermal penalty on the body, primarily because of the assumed change in the flow field from normal shock expansion to oblique shock dependency. The change in flow field assumption and transition criteria is a restrictive assumption of this analysis. The transition criteria will depend on the local Mach number, wall temperature, trajectory condition, and cross-flow effects. The flow field will gradually undergo transition from normal shock expansion to oblique shock. Location on the body at a given trajectory condition at which oblique shock is applicable is dependent on shock shape, Mach number, boundary-layer thickness, and cross-flow. A more refined flow field analysis would be desirable to isolate the angle-of-attack maneuver permitted for various heating constraints.

Reducing the orbiter angle of attack during entry will improve the hypersonic aerodynamic performance and result in increased laterial range. If this could be done without an increase in peak heating rate over the baseline design value, improved ranging performance could be obtained without a major impact on the design of the thermal protection system. Consequently, an investigation was conducted to determine the angle of attack and velocity limits constrained to a specified thermal design environment. Two cases were considered:

1. Limit the peak heating rate to the maximum value experienced during the nominal entry at a 60-degree angle of attack.

2. Limit the peak temperature to 2000 F.

Table 7.4-4 gives the maximum velocity at which pitch-down to a lower angle of attack is permissible so as not to exceed the baseline environments for entry at a 60-degree angle of attack or 2000 F for various constraints. The most severe constraint is the wing leading edge in the interference region. The reference leading edge heating and the interference factor both increase with decreasing angle of attack.

Table 7.4-4. Maximum Permissible Pitch-Down Velocity and Angle of Attack for Obtaining Baseline Temperatures on Wing Leading Edges

Angle of Attack - α	$(q/q_{1'R})_{CLEAN}$	$q_{1'R}$ (Btu/ft^2-sec)	Time (sec)	Max Velocity (fps)	Remarks
60°	0.95	54.0		25.0 K	
52.5°	1.30	39.5	658	17.5 K	Non-
40°	1.68	30.5	1045	13.89 K	interference
30°	1.72	29.8	1400	12.74 K	50-Percent Span
20°	1.75	29.3	1842	10.95 K	
60°	2.55	54.0		25.0 K	
52.5°	3.85	39.5	690	16.40 K	Interference
40°	5.23	30.5	1080	12.98 K	Region
30°	5.77	29.8	1463	11.25 K	20 Percent Span
20°	6.26	29.3	1910	9.51 K	

If the temperatures of the leading edges and the chines are allowed to exceed the baseline values for entry at a 60-degree angle of attack, entry can be performed at a reduced angle of attack. The estimated entry temperature concentrations of the 12,500-pound payload orbiter for entry at 40 degrees are shown in Figure 7.4-13 for W/S = 90 psf. Comparison of these data with those shown in Figure 7.4-9 indicates that pitch-down to 40 degrees is of little significance to the thermal concentrations. However, the loads are increased, indicating increased thermal-protection-system weight. Lateral range trades are discussed further in Section 7.3.4.

7.4.5 Conceptual Design Definition (50,000-Pound-Payload Class)

As a basis for definition of thermal protection system design requirements, aerodynamic heating environments were defined for the 50,000-pound-payload-class booster and orbiter. Maximum radiative equilibrium temperatures used for design are summarized in Figure 7.4-14.

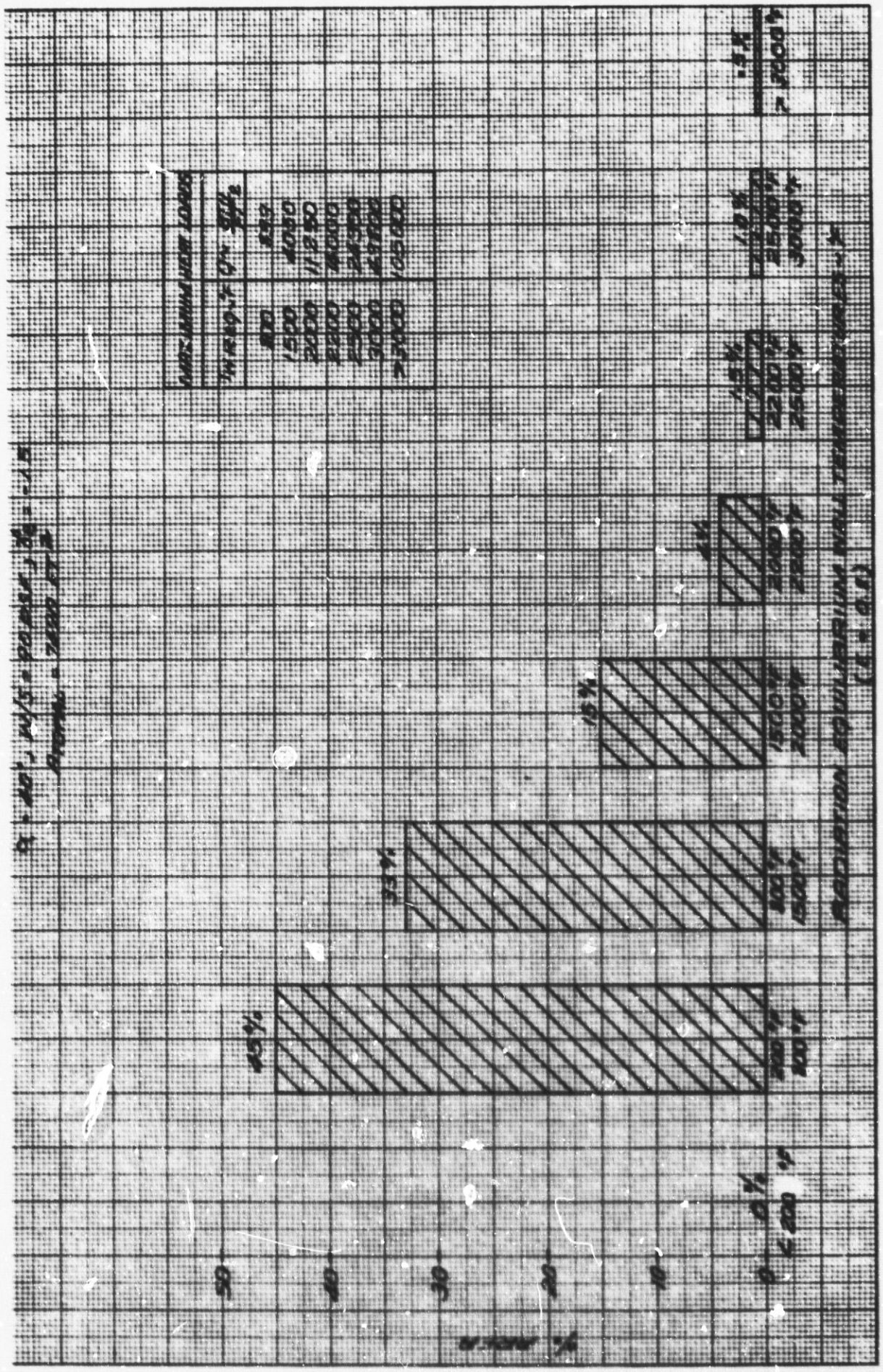

Figure 7.4-13. ILRV Temperature Concentrations, 12,500-Pound Configuration

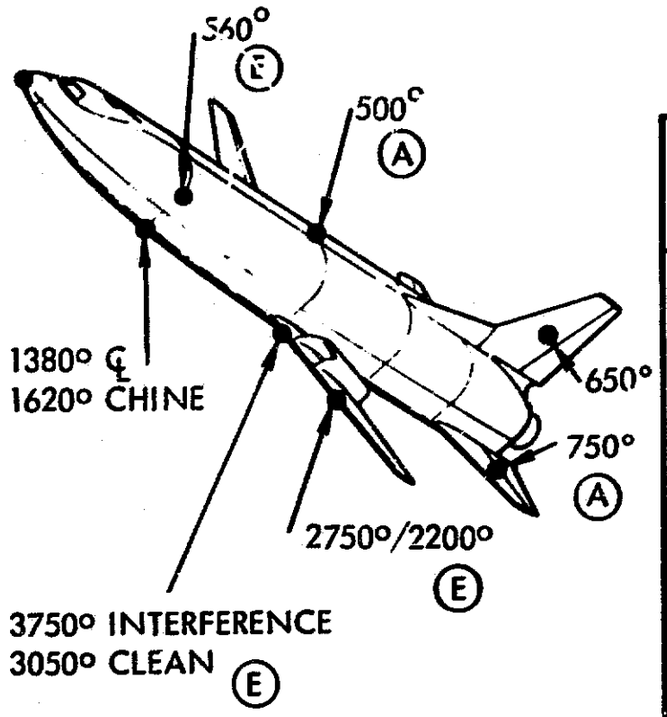

- ORBITER

  90% AREA < 1500°F

- BOOSTER

  90% AREA < 1400°F

LOCATION	CRITICAL FLIGHT CONDITIONS	RADIATION EQUILIBRIUM TEMPERATURE (°F)	
		BOOSTER	ORBITER
FUSELAGE			
NOSE	ENTRY	1275	1860
LOWER SURFACE 20%	ENTRY	1380	1420
LOWER SURFACE 80%	ENTRY	1220	1450
CHINE	ENTRY	1530	1620
SIDE	ENTRY	540	560
UPPER SURFACE	ASCENT	500	500
WING			
L.E. (NO INTERFERENCE)	ENTRY	2200	3000
LOWER SURFACE 20%	ENTRY	1400	1700
UPPER SURFACE 20%	ASCENT	650	700
HORIZONTAL SURFACE			
L.E.	ENTRY	2020	3450
LOWER SURFACE	ENTRY	1390	1500
UPPER SURFACE	ASCENT	600-650	700
VERTICAL SURFACE			
L.E.	ASCENT	1730	2320
SIDE	ASCENT	600-650	650

Figure 7.4-14. Thermal Environment Summary, 50,000-Pound Payload Class

Space Division
North American Rockwell

T_W = 800 F, α = 52.5° - 33°

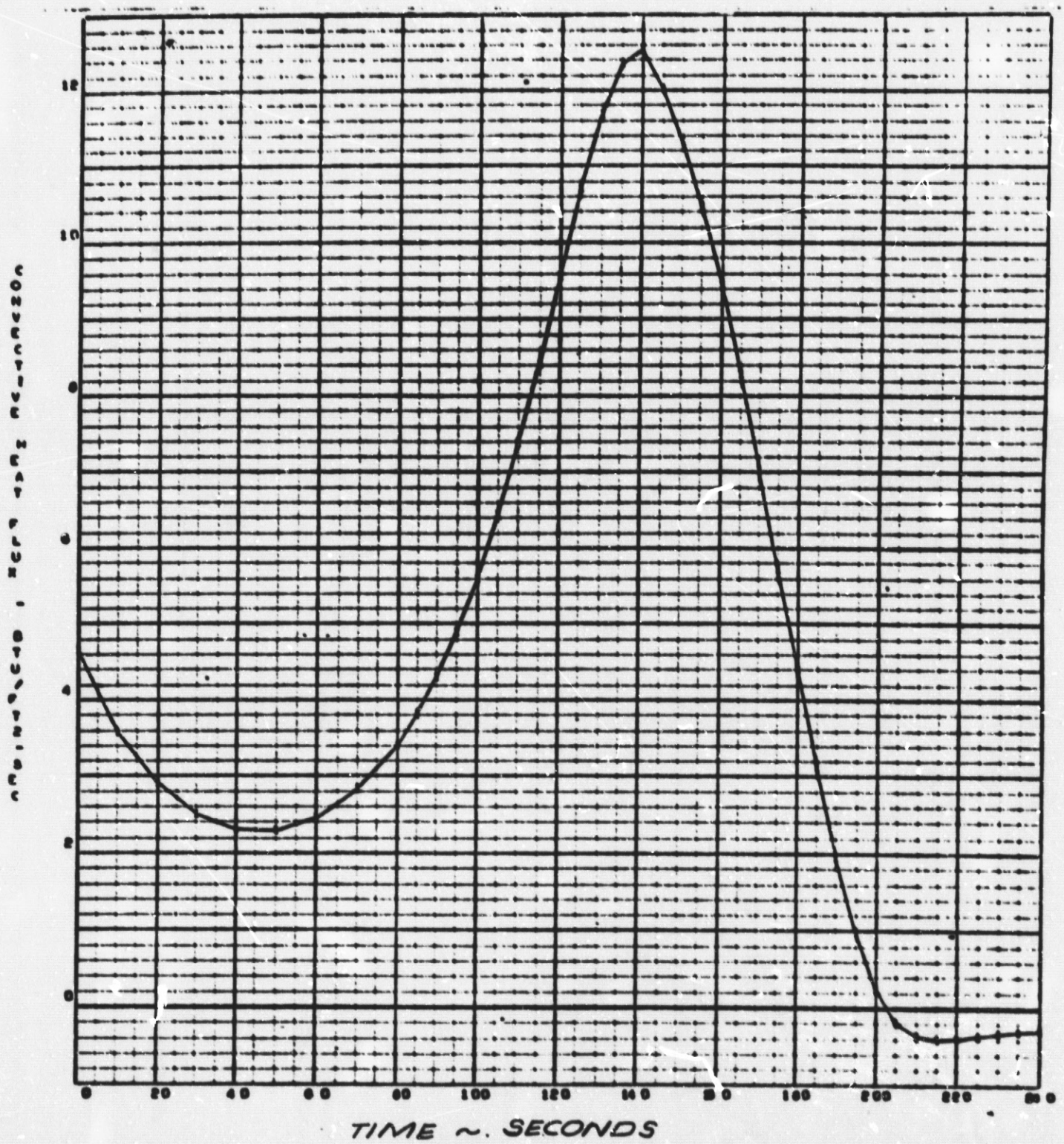

Figure 7.4-15. Stagnation Heating to a 1-Foot Radius Sphere During 50,000-Pound Class Booster Flyback

Booster Heating Environment

Ascent heating experienced by the booster was presented in Tables 7.4-1 and 7.4-2. These data were used to determine peak radiation equilibrium temperatures at selected body points. They were then compared with corresponding entry environment. It was found that maximum temperatures were experienced during boost on the upper surfaces of the body, wings, and horizontal tail, and on the vertical-tail leading edge and sides. These temperatures are listed in Figure 7.4-14.

Descent heating was defined for the 50,000-pound-payload booster executing a 4-g flyback trajectory after separation during launch to a 50- by 100-nmi orbit (see Section 7.3.4). Figure 7.4-15 gives a time history of stagnation heating to a one-foot-radius reference sphere for the booster descent trajectory. Time histories for fuselage and wing locations at 0.8 X/L and 0.8 X/C, respectively, are shown for the same trajectory in Figures 7.4-16 and 7.4-17. During the trajectory, the vehicle was pitched down from a 52.5-degree angle of attack to 33 degrees and subsequently pitched up to the original 52.5-degree angle of attack. Fig-7.4-18 gives the maximum temperature distributions on the underside of the fuselage and the wing at 50-percent span when the trajectory is executed at both a constant 52.5-degree angle of attack and the variable angle of attack described above. The radiation equilibrium temperatures over 90 percent of the fuselage and wing are less than 1400 F.

Orbiter Heating Environment

The 50,000-pound-payload entry environment is qualitatively similar to that of the 12,500-pound payload. The wing loading and aerodynamics were assumed to remain the same as for the 12,500-pound-payload vehicle, so the trajectory was the same. A time history of the stagnation point heat transfer to a one-foot-radius sphere executing the 50,000-pound-payload ILRV orbiter entry at a 60-degree angle of attack is given in Figure 7.4-19. Time histories for fuselage and wing locations of 0.8 X/L and 0.8 X/C, respectively, are shown for the same trajectory in Figure 7.4-20 and 7.4-21. The reduced W/C_LS of the 50,000-pound-payload vehicle yielded 40-percent lower heating rates in the laminar regions, but the increased size promoted earlier transition on the afterbody, which increased the turbulent heating.

The heating rates and loads for the leading edge reference heating (a one-foot-radius sphere) and the fuselage side and top reference heating (a one-foot-long flat plate at $C_p = 0$) are given in Figure 7.4-22. These environments were used with Figure 7.4-1 to specify environments for the leading edges and fuselage side and top surfaces. No provision was made for transition to turbulent flow for upper fuselage heating. Thus the present analysis is restricted to higher angles of attack.

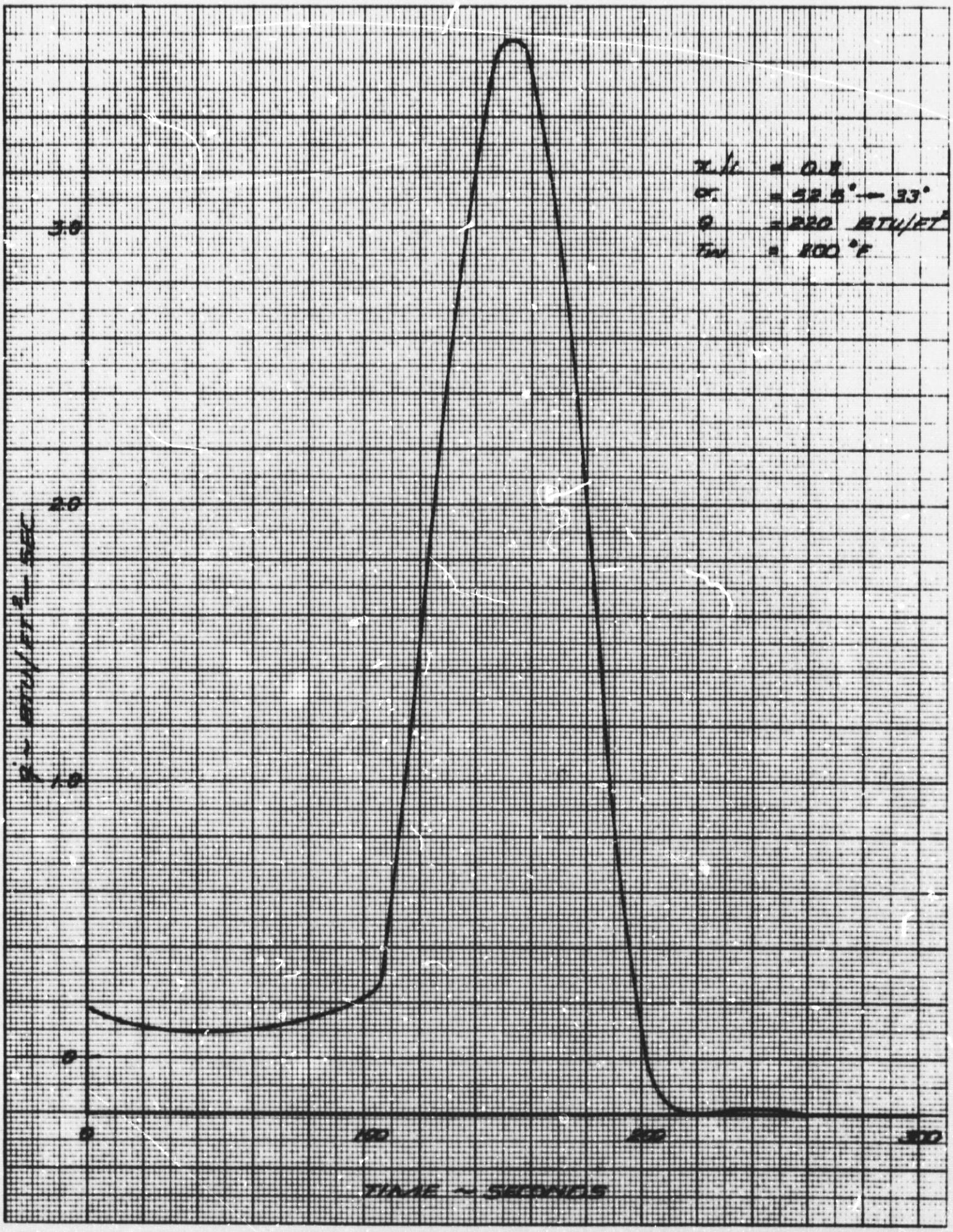

Figure 7.4-16. Booster Fuselage Heating History During Flyback

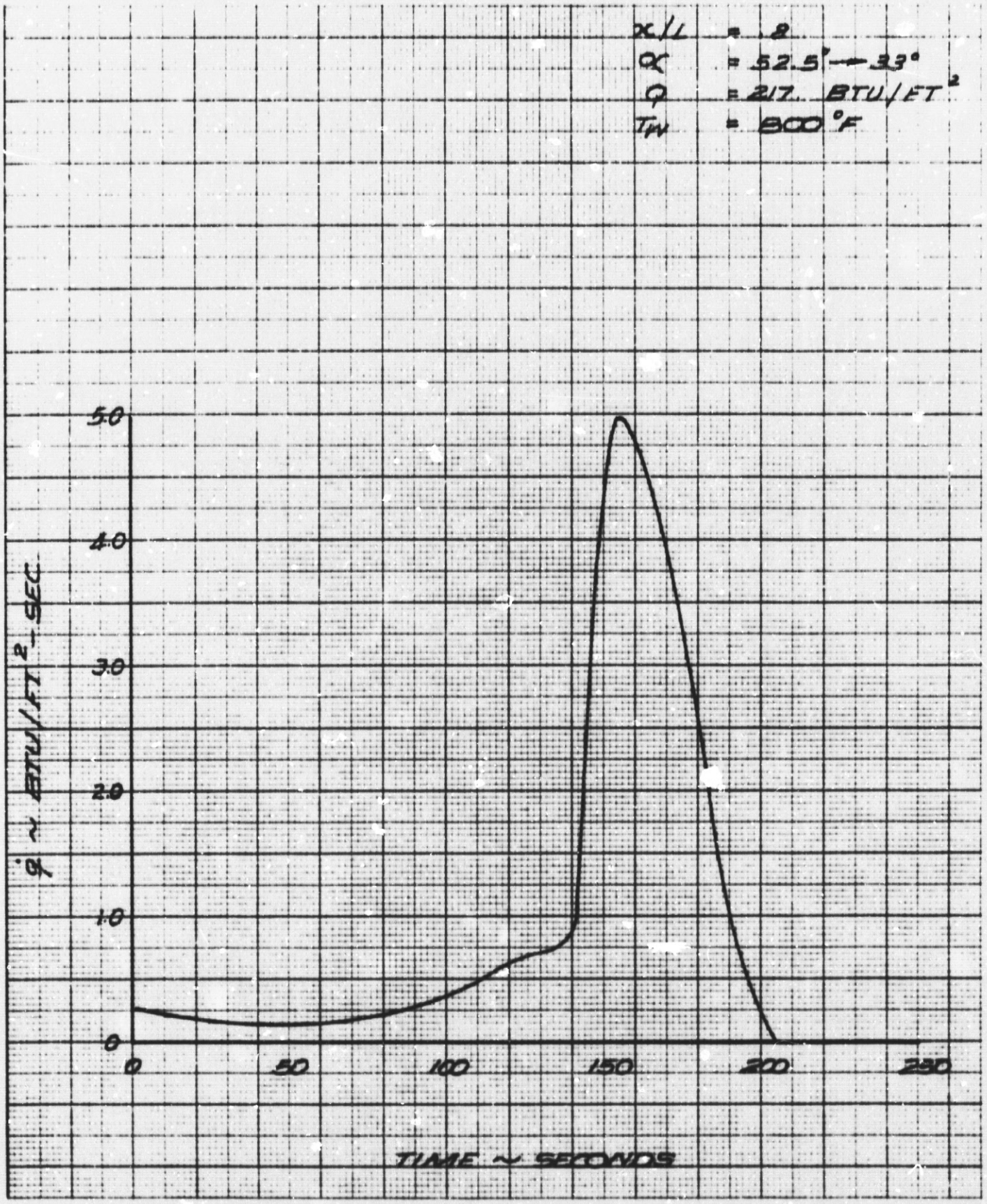

Figure 7.4-17. Booster Wing Heating History During Flyback

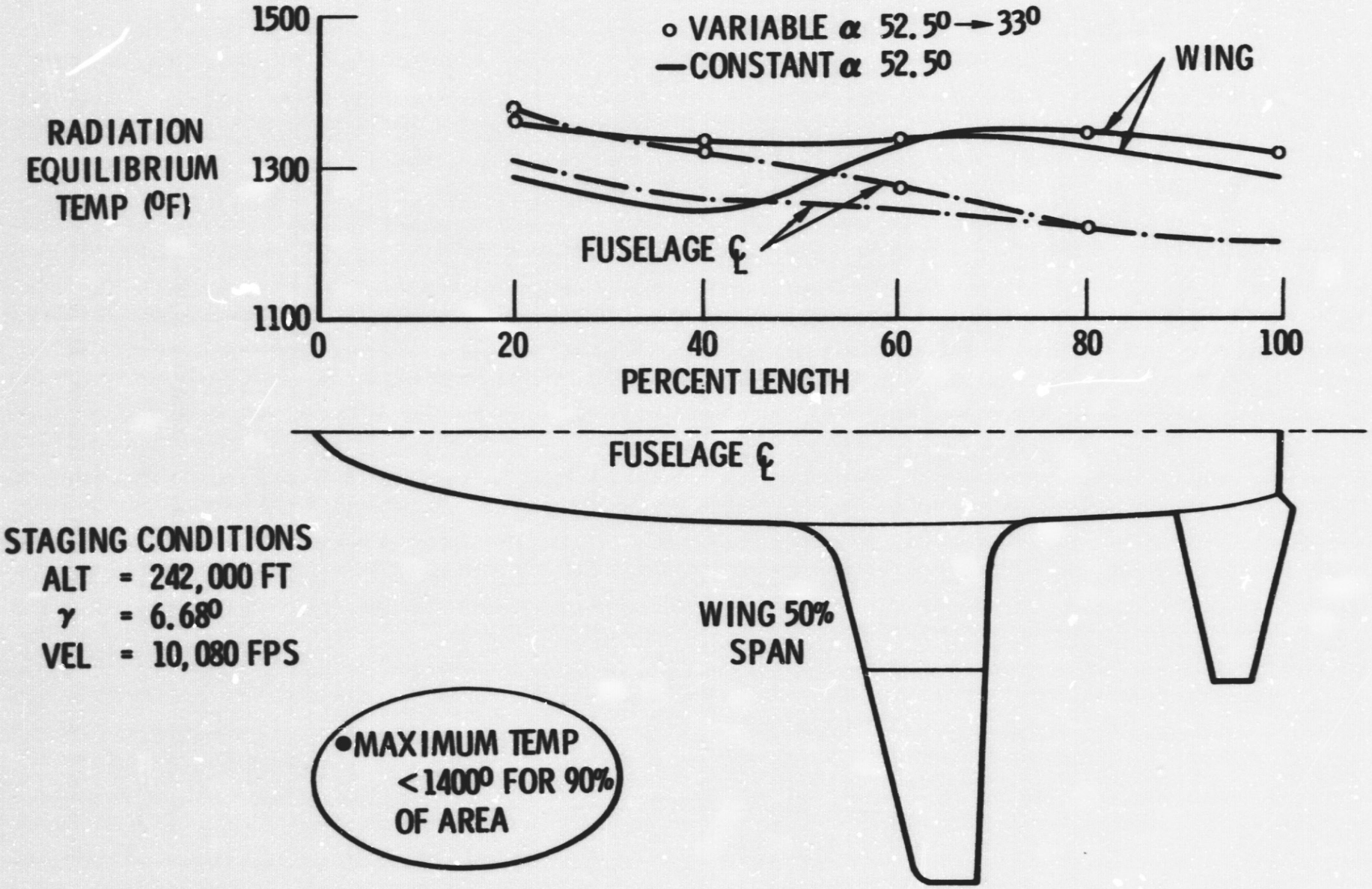

Figure 7.4-18. Booster Maximum Temperature Distribution During Flyback

Space Division
North American Rockwell

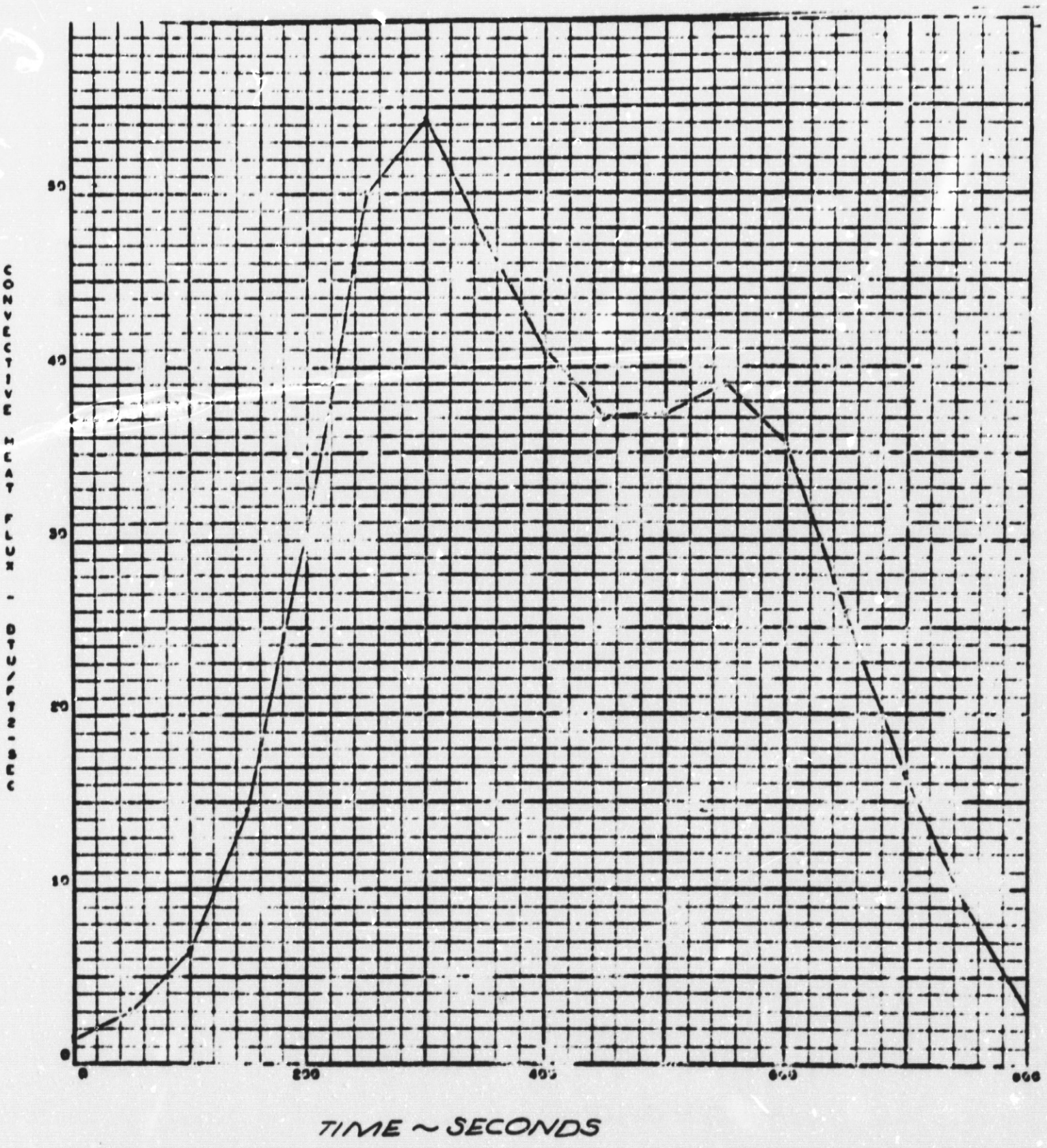

Figure 7.4-19. Stagnation Heating to a 1-Foot Radius Sphere During 50,000-Pound Class Orbiter Entry

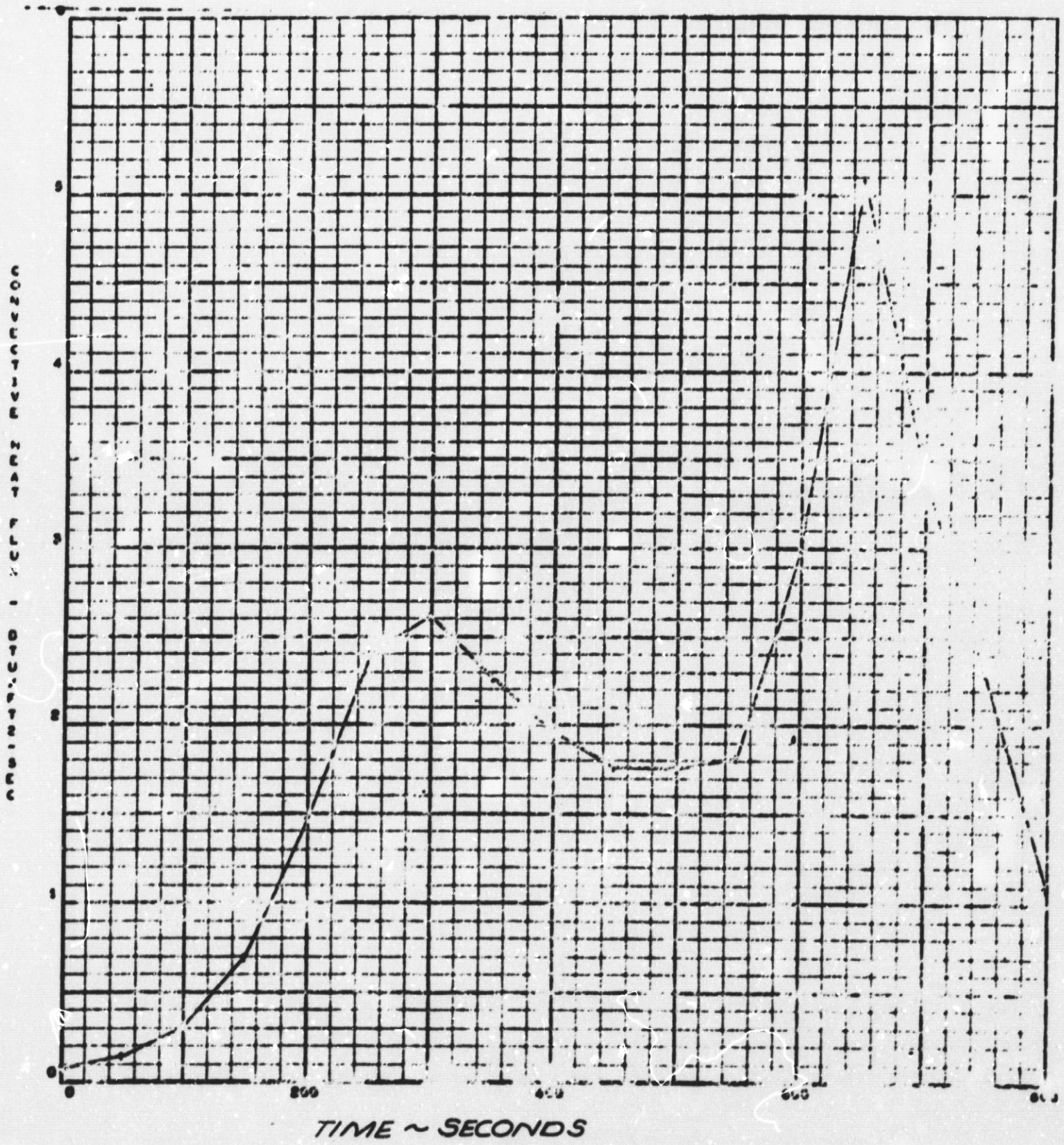

Figure 7.4-20. History of Entry Heating on Fuselage of 50,000-Pound Class Orbiter

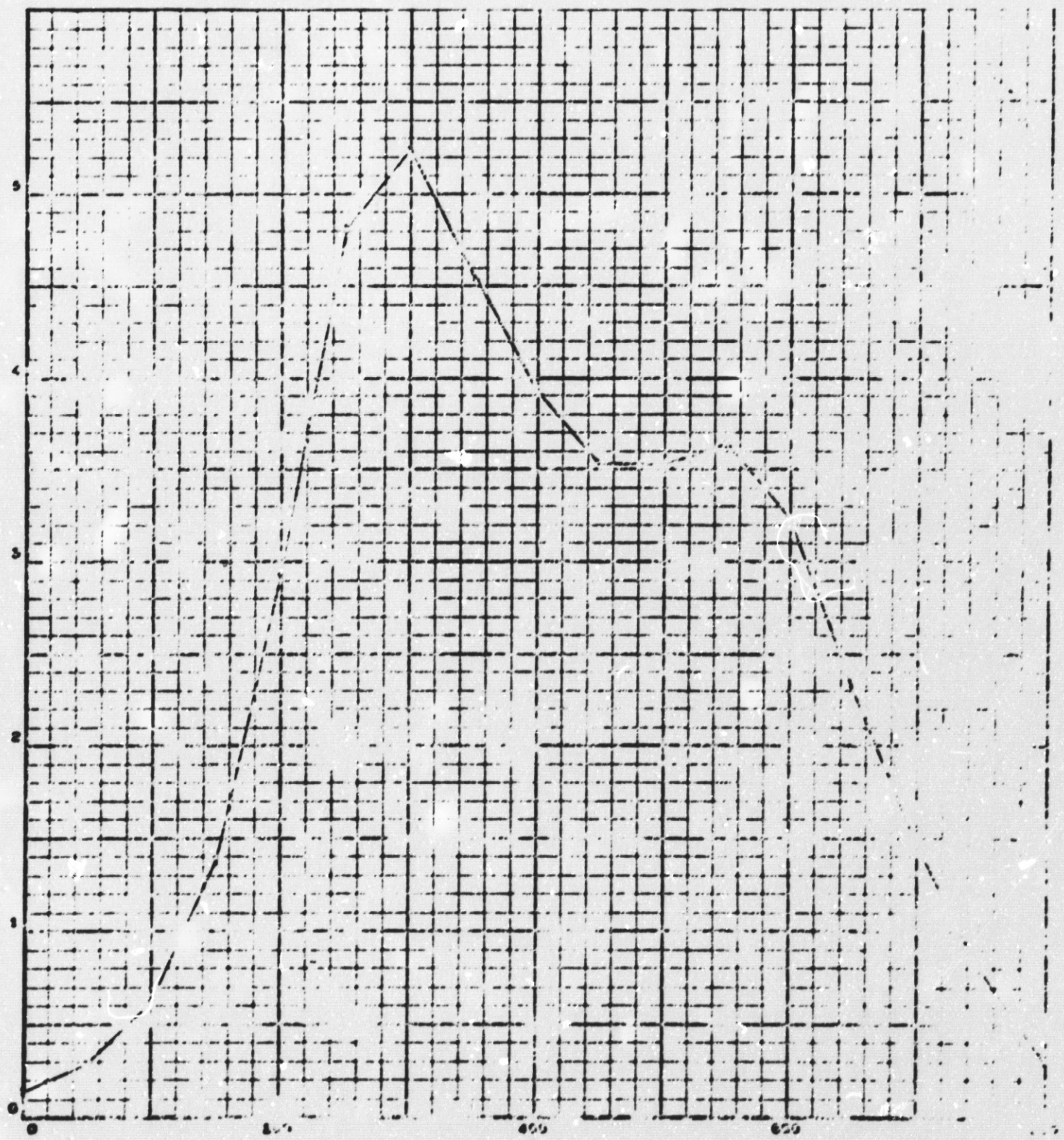

Figure 7.4-21. History of Entry Heating on Wing of 50,000-Pound Class Orbiter

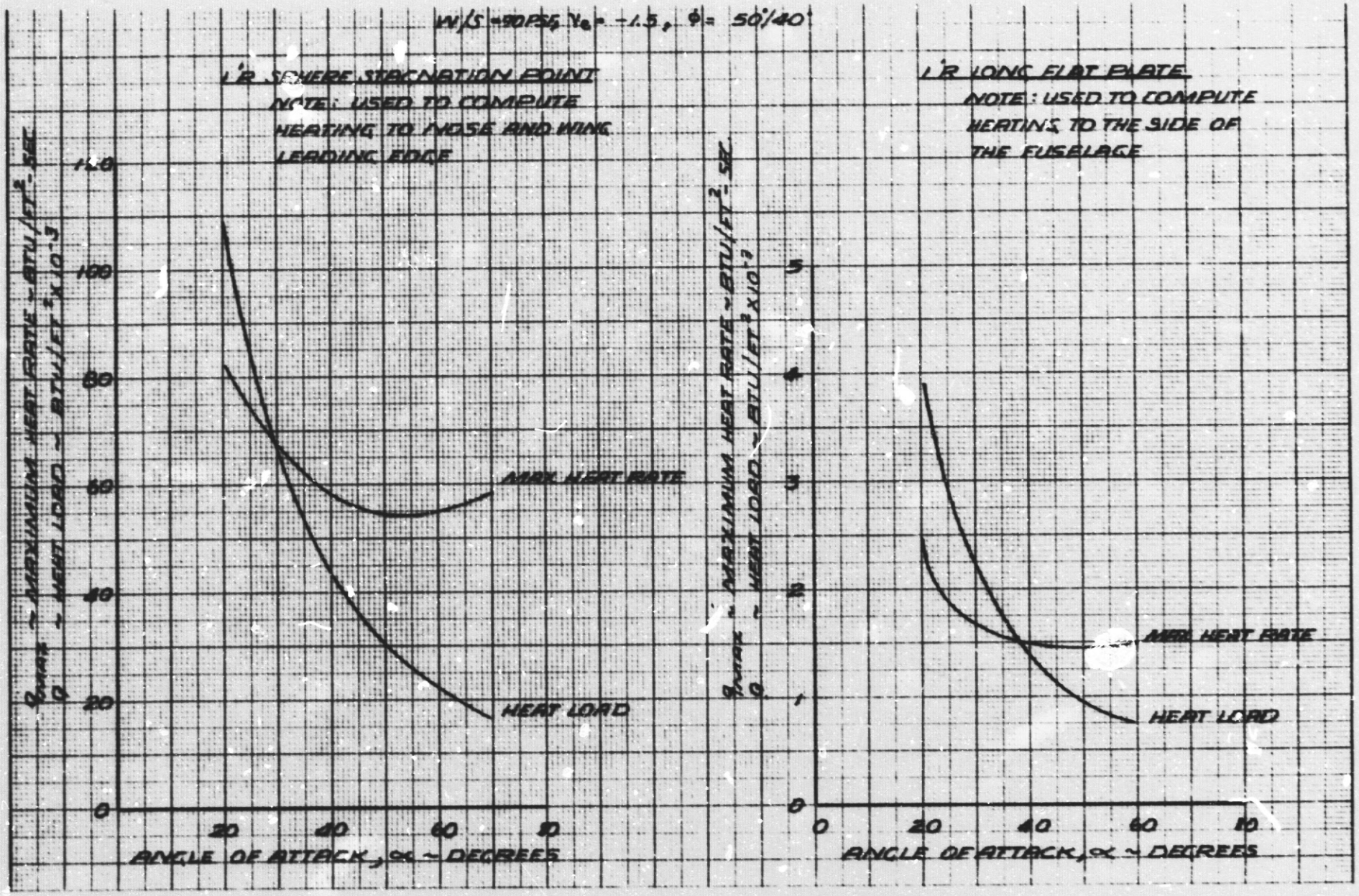

Figure 7.4-22. Reference Heating Rates and Loads

Space Division
North American Rockwell

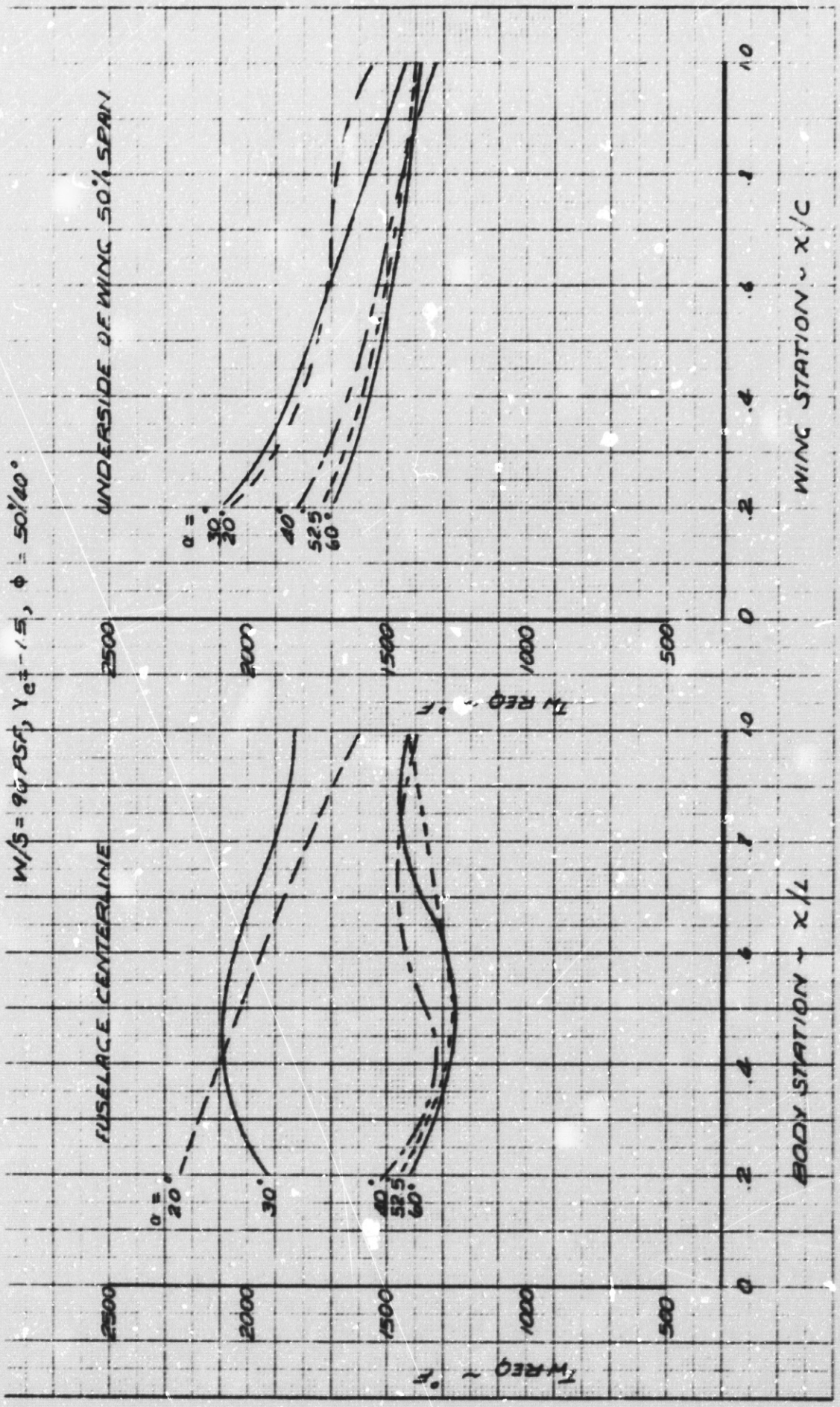

Figure 7.4-23. Orbiter Entry Heating Environments, 50,000-Pound Configuration Payload

The 50,000-pound payload orbiter entry radiation equilibrium wall temperatures and heat loads for the fuselage centerline and wing underside are given in Figures 7.4-23 and 7.4-24, respectively. The chine temperatures are 200 F to 400 F hotter than the centerline for the sharp corner vehicle. Rounding the corners, where the corner radius is 33 percent of the fuselage width, lowers the heating so that the chines are 100 F to 200 F cooler than the centerline.

The 50,000-pound payload orbiter entry radiation equilibrium wall temperatures and heat loads for the fuselage centerline and wing underside are given in Figures 7.4-23 and 7.4-24, respectively. The chine temperatures are 200 F to 400 F hotter than the centerline for the sharp corner vehicle. Rounding the corners, where the corner radius is 33 percent of the fuselage width, lowers the heating so that the chines are 100 F to 200 F cooler than the centerline.

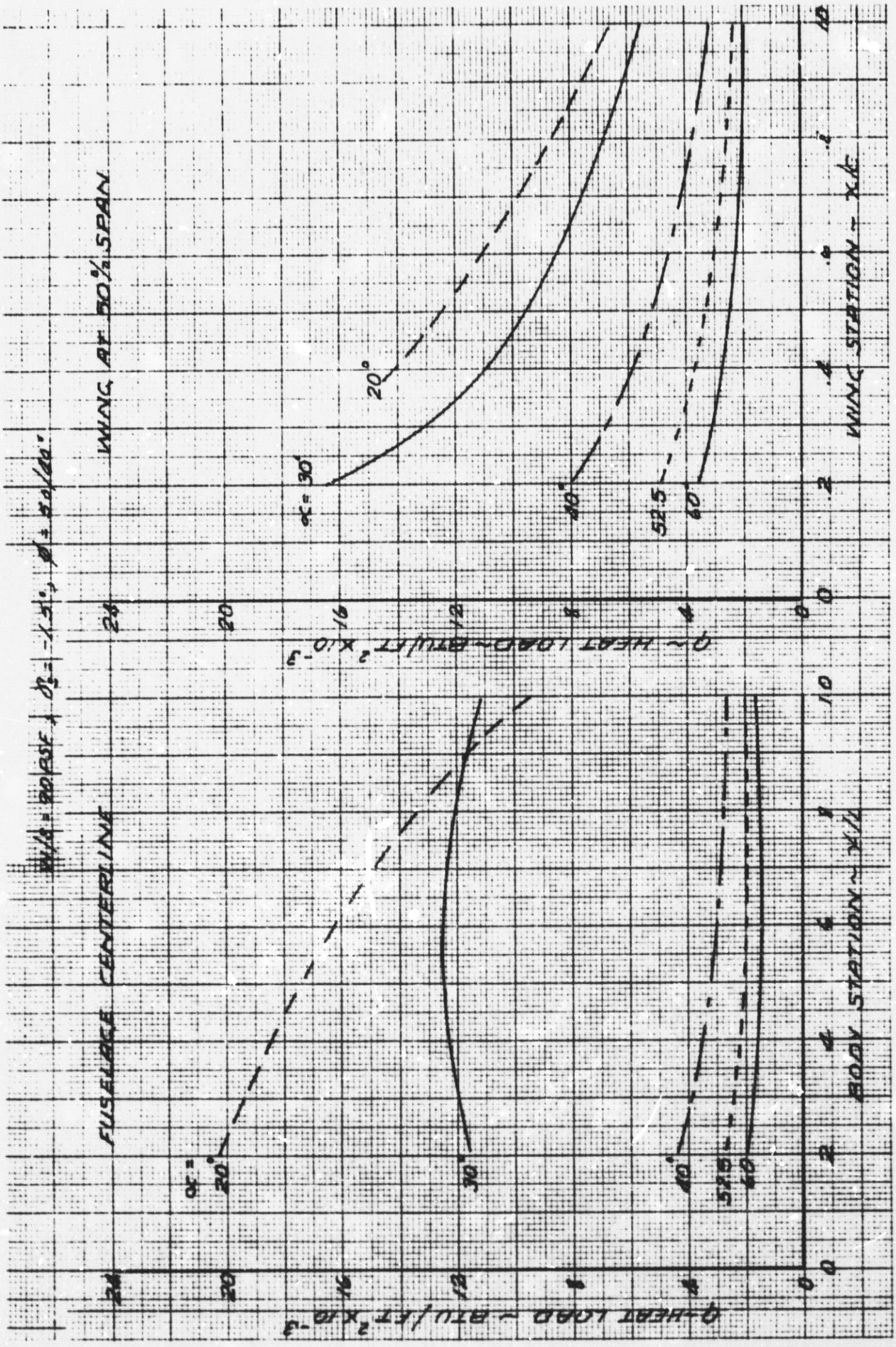

Figure 7.4-24. Orbiter Entry Heating Loads, 50,000-Pound Payload Class

7.5 CONTROL ANALYSES

7.5.1 Summary

Flight control analyses during the second phase of the study were directed toward identification of control requirements and feasibility for ascent, separation, entry, and transition to cruise portions of the flight. In addition, reaction control system thruster and fuel requirements were identified. Significant results were:

1. Ascent control is accomplished through thrust vector control of the main booster engines. A 7 degree gimbal angle limit was selected for design.

2. Control simulations have shown that the vehicle can be controlled along a programmed flight path angle during boost, and that maximum q alpha does not exceed 2970 psf-degrees when the vehicle flies through a 95 percent wind with a gust.

3. Adequate orbiter and booster separation can be provided by separation rockets located on the orbiter and fired to provide lateral translation. Total rocket weight is 3600 pounds. Delay of seven seconds in orbiter ignition is required to avoid orbiter rocket plume impingement on the booster.

4. Entry control simulations have shown that an RCS providing 0.5 degree per second^2 angular acceleration is adequate control authority. The vehicle is stable and well damped.

5. Unstable directional derivatives ($C_{n_\beta} < 0$) are not significant to vehicle controllability. Unstable roll (C_{ℓ_β}) could result in loss of vehicle control during entry.

6. Pitch down from high to low angle of attack is smooth and well damped using an elevator command incorporating gain scheduling.

7.5.2 Ascent Control Concepts

Control concepts for the ascent phase of the mission were defined for both the 12,500- and 50,000-pound payload class vehicles. The design objective of the ascent control system is to control the vehicle along an optimum trajectory dictated by the guidance and navigation system, and in a manner so that structural loading limits will not be exceeded. Effective limiting of structural loads is concerned with those loads caused by wind shear, gusts, engine gimbaling, and sudden engine failure.

The approach was to identify alternative control concepts to fly the desired trajectory, and perform a digital computer simulation accounting for winds, gusts, and engine gimbaling. A comparison of the pitch and yaw plane dynamics and trajectory attitude deviations established the preferred concept for the specified size vehicle.

Ascent Control, 12,500-pound Payload Class Vehicle

The reference trajectory for control analysis of the 12,500-pound payload class vehicle was determined for injection into a 45- by 100-nautical mile orbit, as discussed in Section 7.3.2. Using this trajectory as the desired flight path, a rigid body analysis was conducted to identify an ascent control concept capable of controlling the vehicle through wind shear and gusts without exceeding loading limits.

Three control concepts were investigated. In Concept A (attitude control), the vehicle is commanded to fly a desired attitude, θ_c. For this concept the attitude command is set equal to the flight path angle, γ_{Ref}, of the reference point mass trajectory. Concept B (load minimum) attempts to reduce the aerodynamic loading, q alpha, by commanding the vehicle to a trim angle of attack during the high dynamic pressure region from 13,000 to 67,000 feet altitude. Concept C attempts to do the same by allowing the vehicle to drift free with the wind during the same dynamic pressure region (i.e., the aerodynamics are stable, and the attitude control system is briefly disabled during the wind shear penetration).

The analysis was performed using a simplified digital computer program which calculates the pitch and yaw plane dynamics separately. All aerodynamic data, mass data, reference flight path angle, dynamic pressure, Mach number, vehicle velocity, and wind velocity profile with gust are put in the program as linear or nonlinear functions. The wind profile is a 95 percent design profile with a design gust occurring at the region of maximum dynamic pressure. Control loop gains were sized for a natural frequency of 1.2 radians per second and a damping ratio of 0.7. Preliminary gains were 0.32 for the attitude loop and 0.46 for the rate loop.

Each of the three control concepts was analyzed for two directions of wind velocity in the pitch and yaw planes. The results are summarized in Figure 7.5-1. The values shown are those obtained at the highest dynamic

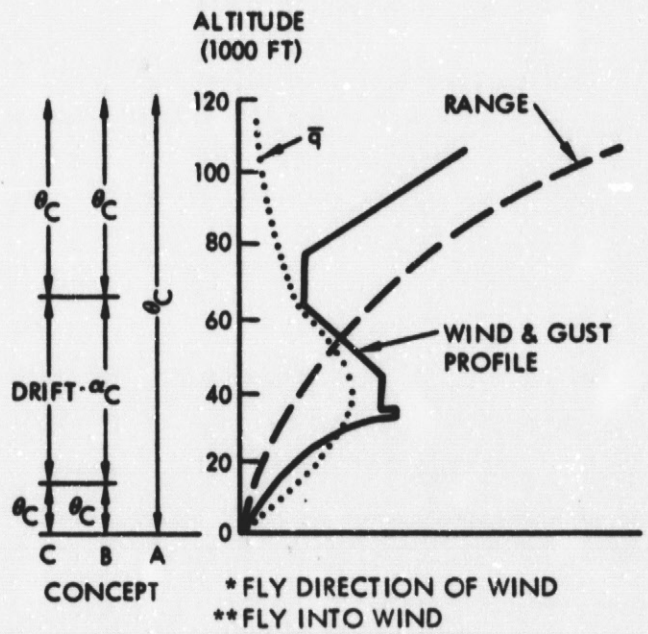

* FLY DIRECTION OF WIND
** FLY INTO WIND
\+ WIND FROM RIGHT
++ WIND FROM LEFT

FINDINGS

- FLYING INTO WIND GIVES WORST CONDITION
- OPTIMIZATION OF ALTITUDE FOR SWITCHING & CONCEPTS B & C CAN REDUCE $\bar{q}\alpha$
- CONCEPT B GIVES SMALLEST LOAD, GREATEST DEVIATION IN ATTITUDE

PARAMETER	CONTROL CONCEPT		
	A	B	C
$\bar{q}\alpha_{max}$	*-1780.0	-900.0	-1720.0
	**-2970.0	-1190.0	-2000.0
α	-4.4°	-2.1°	-4.4°
	-11.5°	-3.0°	-5.0°
θ_{ERROR}	-12.0°	-26.0°	-17.0°
	-26.0°	-30.0°	-25.0°
B_p	-4.4°	-1.0°	-1.9°
	-7.8°	-1.3°	-1.9°
$\bar{q}\beta_{max}$	+-1160.0	610.0	870.0
	++ 1181.0	-610.0	-850.0
β	-2.9°	1.5°	2.2°
	2.9°	-1.5°	-2.1°
ψ_{ERROR}	-5.0°	-11.0°	-10.0°
	5.0°	11.0°	10.0°
B_y	-2.1°	1.2°	0°
	2.1°	-1.2°	0°

Figure 7.5-1. Ascent Control Concepts, 12,500-Pound Payload Class System

load, q alpha and q beta. The wind directions used were from front and back for pitch and from right and left for yaw dynamics. The terms shown are defined as:

$\bar{q}\alpha$, $\bar{q}\beta$	maximum pitch/yaw dynamic loading, lb deg/ft^2
α, β	pitch/yaw angle of attack and maximum load
θ , ψ	pitch/yaw deviation from desired attitude at maximum load
β_p, β_y	pitch/yaw deflection of the engines at maximum load

The dynamic loading experienced with Concept A is 2970 psf-degrees and is least for Concept B. Concept B also requires the smallest engine deflection. However, it allows maximum deviation from the desired attitude. Dynamic loading in the yaw plane is sizable enough to warrant consideration. Flying into the wind results in greatest loading for all concepts. The maximum roll moment due to aerodynamic loading was calculated to be 575,000 foot-pounds. If the four outboard engines are used for control, they need to be deflected 3.5 degrees (equivalent to 2.5 degrees in yaw) to counteract this moment.

Use of the free drift method or the angle of attack load alleviation technique causes large temporary attitude deviations which perturb the ascent trajectory and possibly impact payload capability. These results indicate that the vehicle can be controlled to keep loads low during boost. Concept B can be used to minimize structural loading. This concept alleviates loading by commanding the vehicle to a trim attitude. Further analysis is needed to establish the altitude span during which load alleviation is to be used for best results. A method must be determined for the blending of commands from one control phase to the next, and the effect of engine failure should be investigated.

Ascent Control, 50,000-Pound Payload Class Vehicle

Three ascent control concepts were investigated for the 50,000-pound payload class vehicle. Control system performance was compared with regard to ability to steer the boost vehicle along an optimum trajectory through wind shear and gusts without exceeding structural loading limits. The approach was similar to that followed for the 12,500-pound payload class vehicle. The reference point mass trajectory was for injection into a 50- by 100-nautical mile orbit.

In concept A, the vehicle was commanded to follow the flight path angle of the point-mass trajectory using the control system of Figure 7.5-2; in Concept B an attempt was made to alleviate aerodynamic loading ($q\alpha$) by minimizing angle of attack during the high dynamic pressure region between 28,000 and 60,000 feet altitude; the same objective was attempted in Concept C by reducing actuator displacement whenever structural loading exceeded some preset limit. This is similar to the action of a g-limiter in a conventional manned aircraft.

Pitch control and trajectory dynamics were run in three degrees-of-freedom and yaw dynamics in one degree-of-freedom. Head and tail winds were generated using a 95 percent wind profile with a gust near max $q\alpha$. The same profile was used in the yaw axis.. Four runs were made: control Concepts A and B were each simulated for head and tail winds; wind also was inserted in the yaw axis simultaneously with the pitch axis. Concept C was analyzed by making estimates based on the time histories obtained for Concept A. In all cases, a 7-degree engine gimbal limit was used. Results are summarized in Table 7.5-1 for all three concepts. Pitch and yaw dynamics are shown in Figure 7.5-3 for Concept A.

A maximum q alpha of 2700 psf-degrees was experienced using flight path control (Concept A), even with a head wind, which was the worst case. Some deviation from the nominal flight path was experienced with a head wind, resulting in a loss in terminal altitude from about 202,000 feet to 181,000 feet, due largely to the ±7 degree actuator limits. Reference to Figure 7.5-3 shows two nearly equal peaks in structural loading as indicated by the $q\alpha$ time history: The first occurred about 78 seconds after launch, right after the wind gust and maximum $q\alpha$. This peak resulted from undamped oscillations in vehicle attitude because the actuator was hard over in an effort to force the vehicle back to the reference flight path angle against the wind. These oscillations would be damped without seriously altering the trajectory by allowing the actuator to leave its stops during the peaks. A g-limiter which overruled the actuator command whenever $q\alpha$ exceeded about 1900 or 2000 should provide adequate performance in this respect.

The second structural loading peak occurred about 127 seconds from launch. Angle of attack had increased to 20 degrees, and the flight path angle finally had been driven close enough to the reference value to permit the actuator to leave its stops, whereupon angle of attack began to decrease rather abruptly. Inasmuch as this peak was relatively broad, it could not be eliminated without increasing trajectory error, making it imperative that any load relief applied be as small as possible, both in duration and magnitude. Otherwise, the large amount of lift produced by the wings would cause large trajectory deviations, as contrasted with a conventional missile with very limited lifting capability.

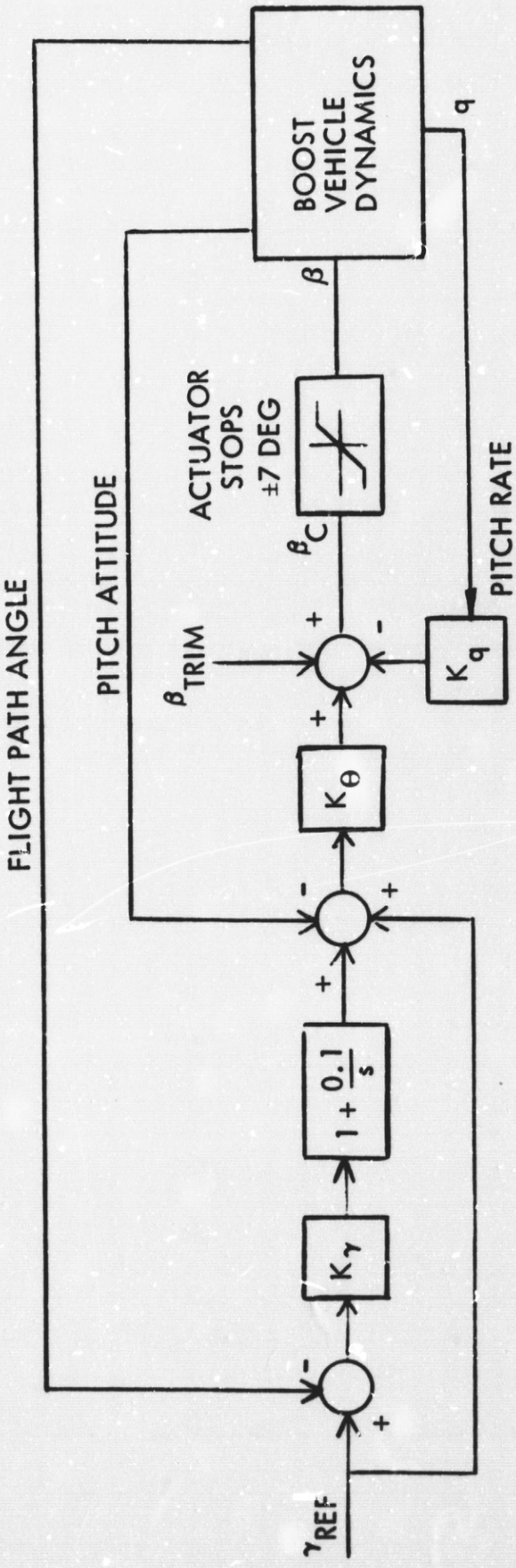

Figure 7.5-2. Boost Flight Path Control System, 50,000 Pound Payload Class Vehicle

Table 7.5-1. Summary of Results of Ascent Control Simulation, 50,000-Pound Payload Class Vehicle

Parameter	Control Concept		
	A	B	C (est.)
$\bar{q}\alpha_{max}$ (psf-deg)	* 1130	-900	800
	** -2700	-1847	2000
α	3.2°	-2.2°	2.3°
	-6.5°	-4.5°	-4.8°
$\gamma_{ERROR_{max}}$	-3°	14°	-3°
	-12°	-35°	-18°
B_p	7° (Limit)	7° (Limit)	7° (Limit)
	-7° (Limit)	-7° (Limit)	-7° (Limit)
$\bar{q}\beta_{max}$ (psf-deg)	2700	1750	---
	-2700	-1750	---
β	8.2°	4.2°	---
	-8.2°	-4.2°	---
$\psi_{ERROR_{max}}$	2.5°	31°	---
	-2.5°	-31°	---
B_y	5.2°	1°	---
	-5.2°	-1°	---

*Fly direction of wind
**Fly into wind

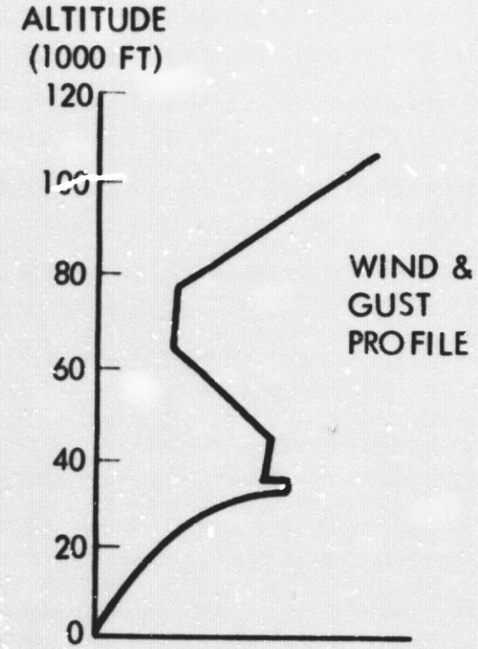

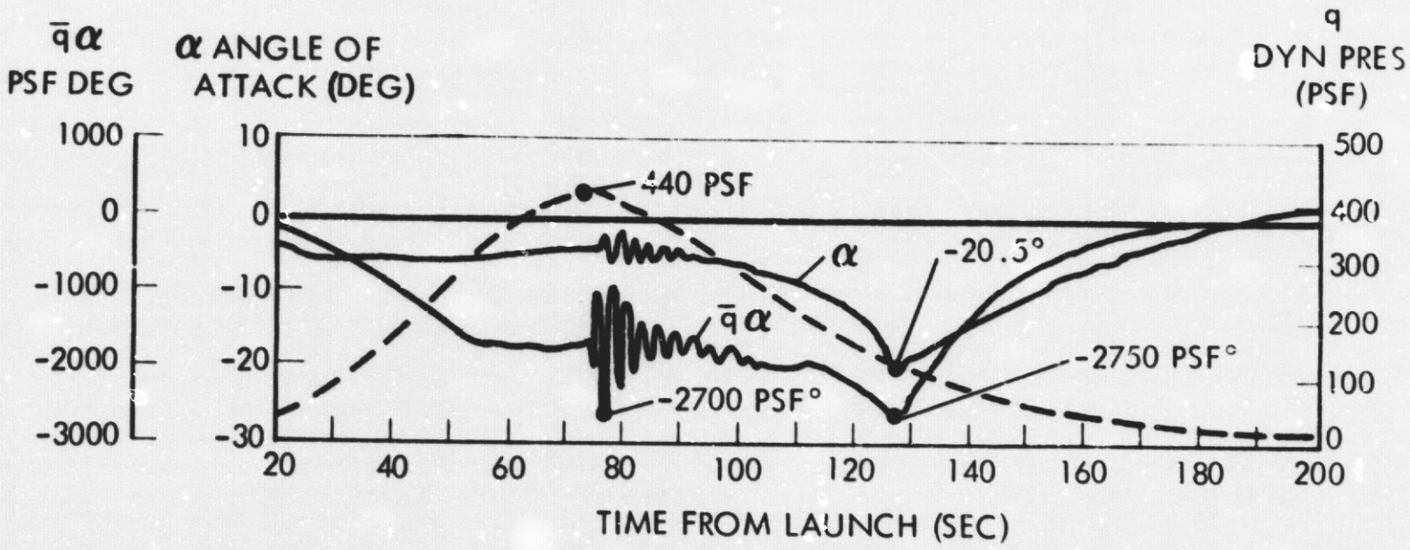

- FLYING INTO WIND GIVES WORST CONDITION
- MAX $\bar{q}\alpha$ = 2750 PSF -DEG
  $\bar{q}\beta$ = 2700 PSF -DEG
- MAX GIMBAL TRAVEL 7°

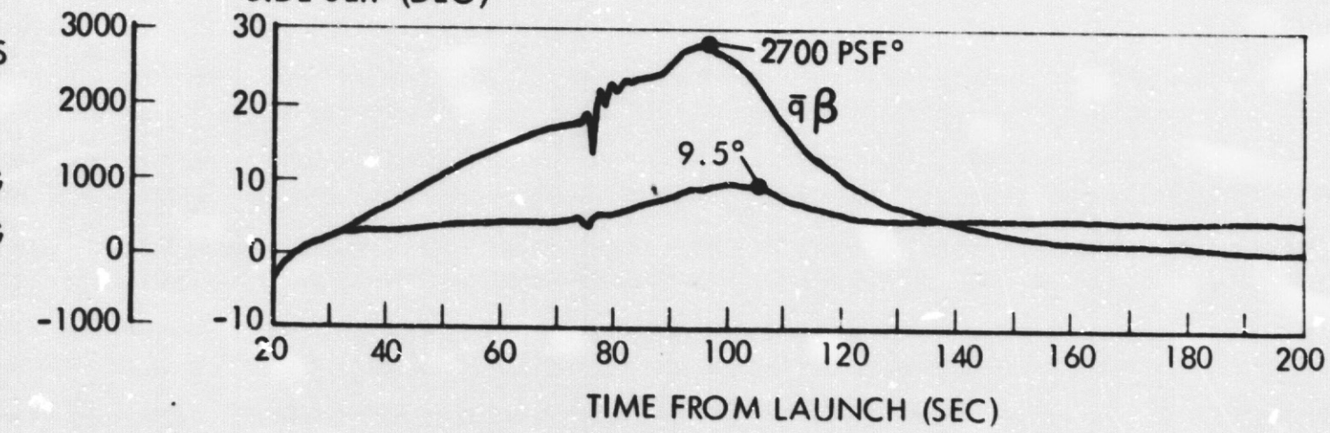

Figure 7.5-3. Ascent Control Simulation for 50,000-Pound Payload Class

These observations were confirmed by the runs using Concept B for control. Controlling angle of attack instead of flight path angle during the period of high loads reduced these loads temporarily, but caused extreme trajectory deviations, and high loads during recovery. Although these problems could be alleviated to some extent by redesign of the control system, Concept C appears to be superior in the sense that flight path deviations are minimized for a given structural load limit.

Yaw plane loading due to sideslip induced by lateral wind shear was sizable; maximum roll moment was calculated to be 575,000 foot-pounds. If the four outboard engines are used for roll control, deflections of 3.5 degrees (2.5 in pitch and 2.5 in yaw) are required to counteract this moment.

Of the three boost control concepts studied, Concept A (flight path angle control) minimized trajectory deviations. Concept B (minimum load control during the period of high dynamic pressure) reduced loads temporarily, but resulted in unacceptable trajectory deviations. Concept C (aircraft type q-limiting) minimizes flight path deviations for a given structural load limit, and appears most promising. Adaptation of a load-alleviation technique from manned aircraft, rather than from conventional boosters, is reasonable in view of the large lifting surfaces on the shuttle boost configuration. Also, it is likely that a g-limiter will be desirable during entry and subsonic flight, making possible a consolidation of hardware for various mission phases.

Perhaps the most significant problem area, as compared to currently operational boost configurations, is the tendency toward increased trajectory deviations due to wind, because of the large amount of lift generated by the vehicles, and the impact on control system design in terms of load relief.

7.5.3 Separation Analysis (50,000-Pound Payload Vehicle)

Booster/orbiter separation occurs at an altitude above 200,000 feet for vehicles investigated during the second phase of the study. Dynamic pressure ranges from 17 psf to about 5 psf, depending on stage optimization results. This section presents results of studies to establish the sequence of events and design requirements for the separation system.

Separation of the orbiter and booster vehicles is complicated by adverse aerodynamic proximity effects. In the attached configuration, a large negative normal force coefficient is developed which negates separation with only aerodynamic forces. To augment separation, the orbiter was equipped with separation rocket engines installed to provide added body Z axis translation forces. Consideration was given to installing the rocket engines on the booster, but this was found to be unacceptable due to the large X center of gravity shift during boost. The latter concept was judged unsatisfactory for abort cases.

Study Ground Rules

1. A minimum separation distance of 100 feet is required prior to full thrust of the orbiter main engine.

2. Maximum time delay from separation to orbiter main engine ignition is 10 seconds.

3. Attitude control of the booster and orbiter is required throughout the separation sequence.

Study Assumptions/Rationale

1. Constant dynamic pressure (no significant change in $\bar{q}$ for the small time increment considered in the analysis).

2. Both the booster and orbiter rigidly controlled to the separation attitude (attitude control via RCS is assumed and angular oscillations between attitude deadbands are not considered significant for separation analysis).

3. Constant booster/orbiter mass (change in mass is negligible over the 10-second time interval).

4. Interference aerodynamics used in the analysis are given in Figure 7.5-4. The normal force due to proximity effects was assumed to be acting on the orbiter vehicle only.

Solid propellant rocket engines were installed about the outer periphery of the orbiter in a YZ plane passing through the vehicle center of gravity. Two clusters of four engines each were mounted so that each thrust vector points through the center of gravity of the fully loaded configuration. To prevent possible damage to the booster, the clusters were installed on opposite sides of the vehicle and canted 29 degrees (rotated from -Z to +Z)

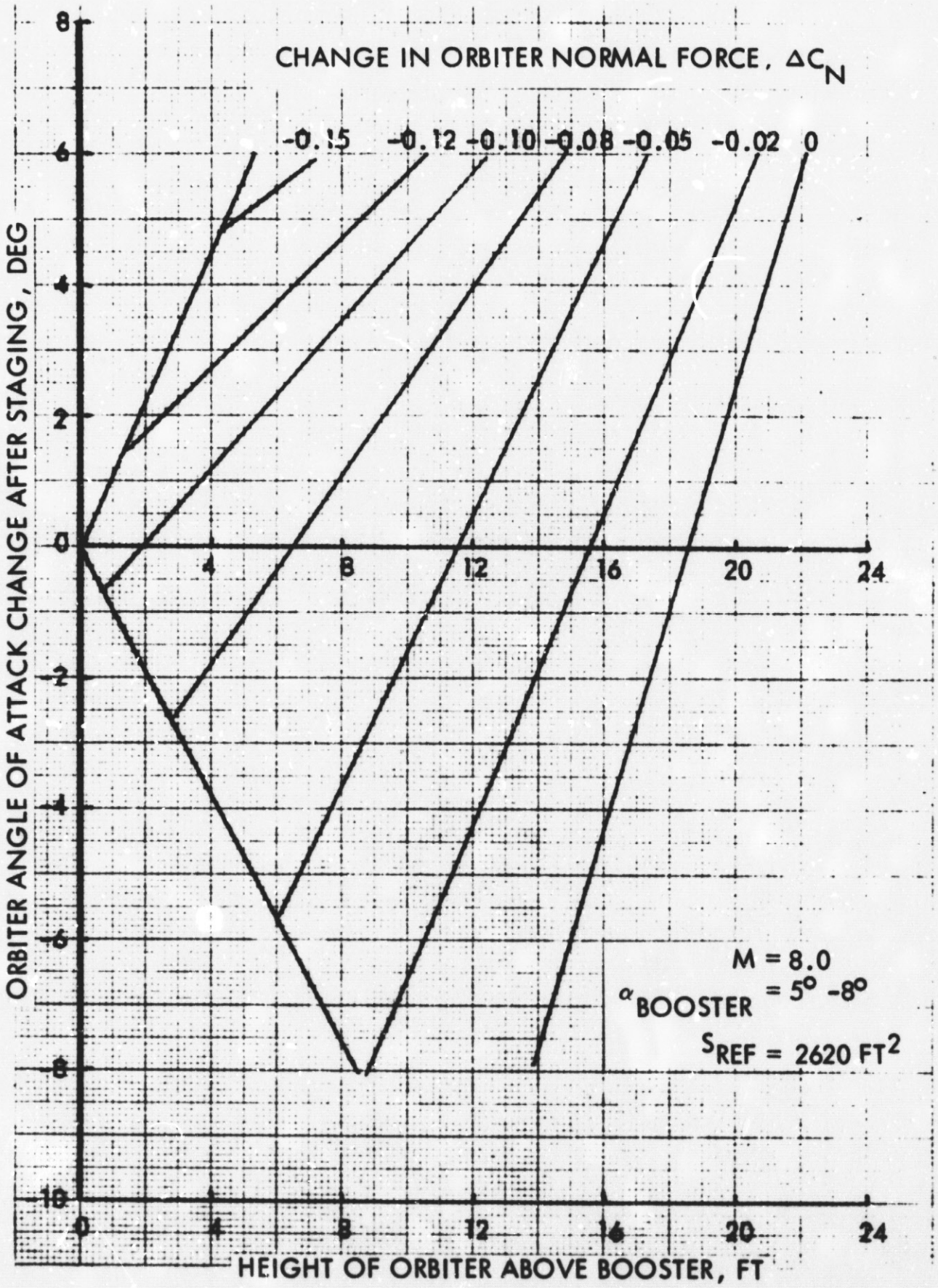

Figure 7.5-4. Booster Interference on Orbiter

with respect to the YZ plane. Each rocket engine develops 20,000 pounds of thrust (160,000 pounds total) with a two-second burn time. This configuration provides a resultant 140,000 pounds of thrust in a "Z" body axis direction and accelerates the orbiter above the booster. A separation engine-out failure would produce approximately 9700 pounds of side force but would not develop torque unbalance.

The thrust build-up characteristics of the orbiter rocket engines were obtained from estimated transient characteristics provided by Pratt & Whitney. Build-up to 20 percent thrust required approximately 1.4 seconds, and an additional 5 seconds were required to reach 100 percent thrust. Rocket plume heating data were provided informally by NASA MSC (Reference 7-8) for thrust levels from 17 to 100 percent.

Study results are summarized in Figure 7.5-5 which illustrates the relative position of the orbiter and booster during separation. The orbiter is shown in the condition which resulted in maximum plume heating. The staging sequence is as follows:

t = -2 : Booster/orbiter RCS attitude hold

Booster engine shutdown

t = 0 : Booster shutdown complete

Separate orbiter/booster

Ignite separation rockets

t = 7 : Ignite orbiter engines

Detailed relative displacements are shown in Figures 7.5-6 and 7.5-7. Figure 7.5-6 illustrates the relative portions of the orbiter and booster without orbiter thrust. Note that the difference in the relative trajectories was negligible for the angles of attack investigated. Figure 7.5-7 shows a comparison of the zero angle of attack case with two trajectories where separation was augmented with orbiter main engine ignition at separation and at 2 seconds following separation. Each of these trajectories assumed the main engine valves opened to 20 percent thrust. The plus X translation experienced by the orbiter as a function of time from main engine ignition is shown in Figure 7.5-8.

INITIAL CONDITIONS

- V = 11,000 FPS
- q = 10.5 PSF
- ALT = 230,000 FT

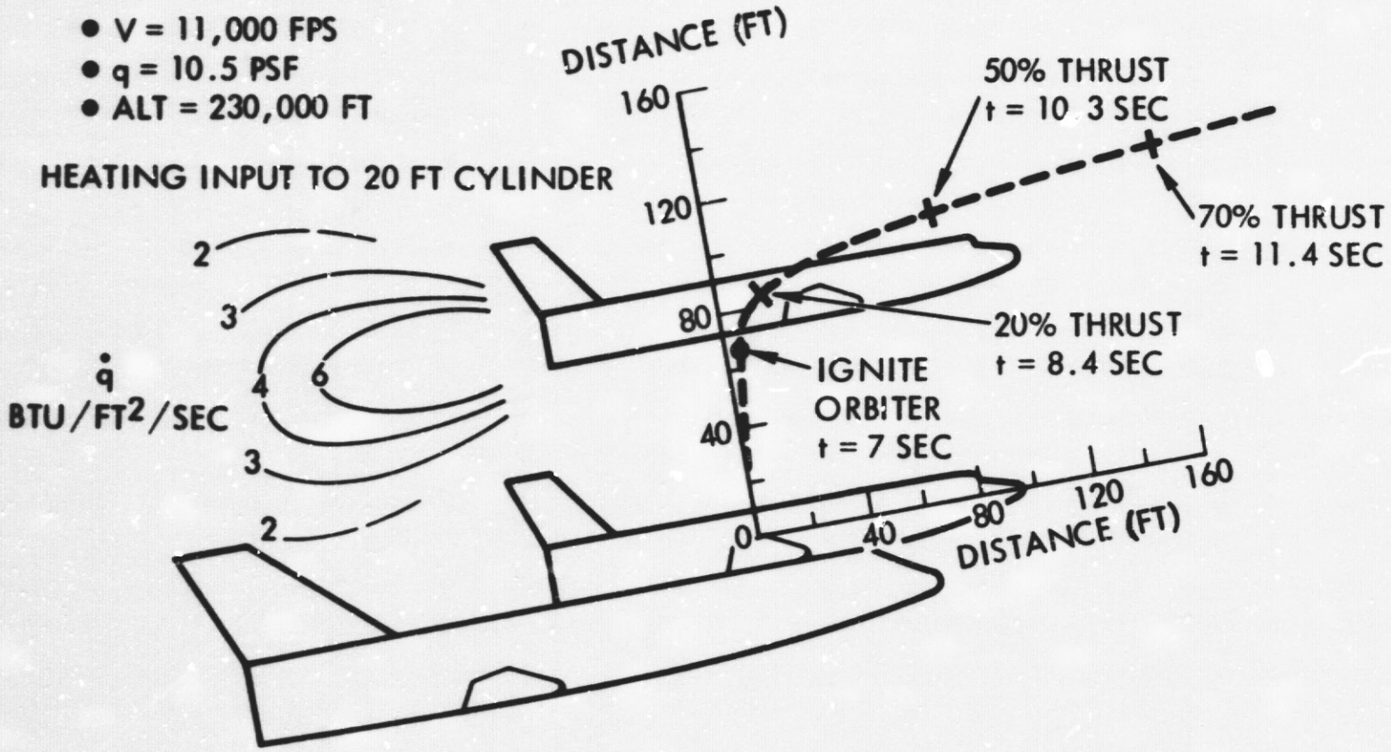

GROUND RULES

- ATTITUDE HOLD
- ORBITER IGNITION DELAY
- AVOID PLUME HEATING

SEPARATION ROCKETS - ADEQUATE SYSTEM

- T/W = 0.19
- ITOTAL = 320,000 LB-SEC
- WT = 3600 LBS LOADED / 1200 LB EMPTY

STAGING SEQUENCE

- t = -2 BOOSTER SHUTDOWN
- t = 0 SEPARATE, IGNITE SEP ROCKETS
- t = 7 IGNITE ORBITER ENGINES

Figure 7.5-5. Separation Concept for 50,000-Pound Payload Orbiter

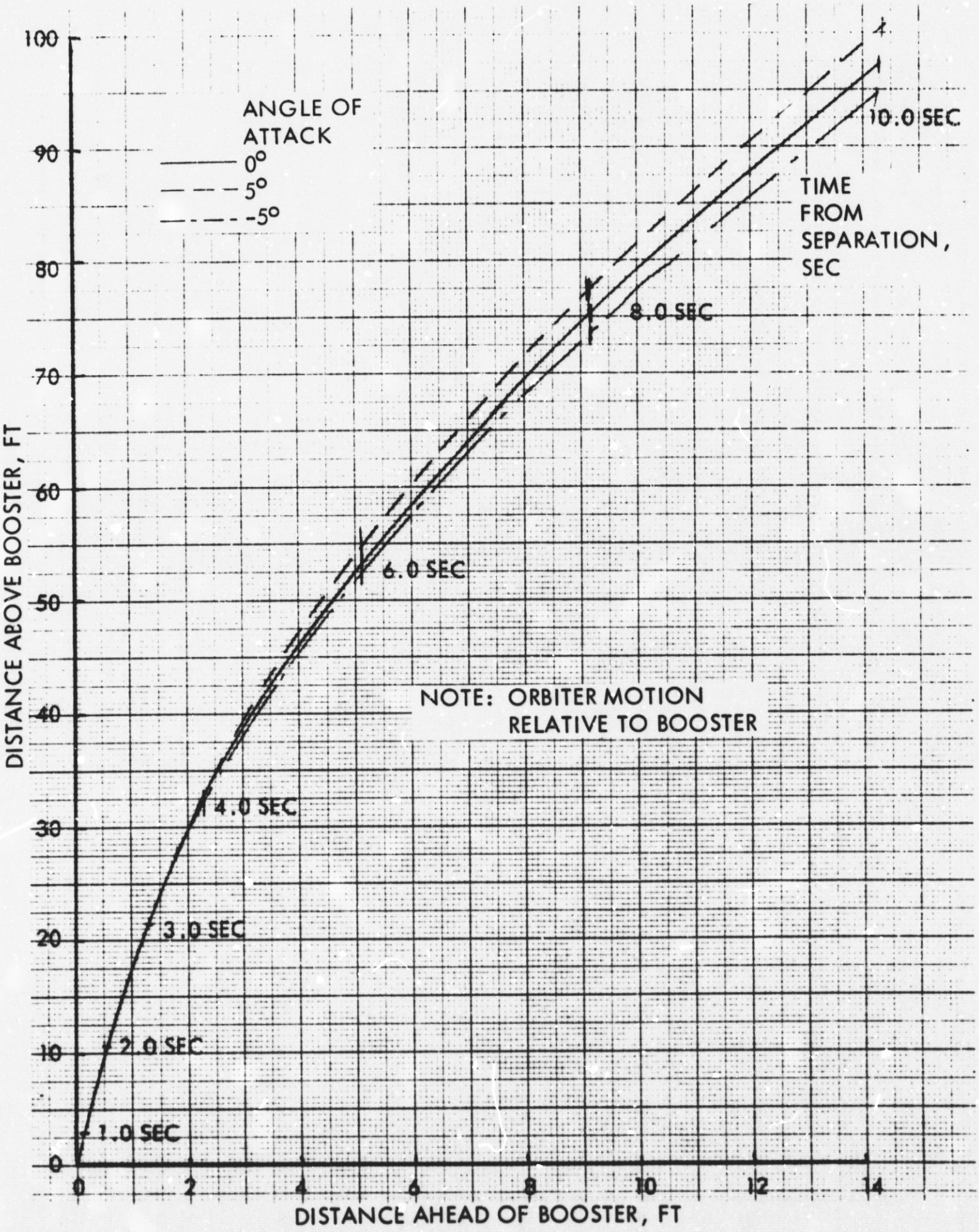

Figure 7.5-6. Booster - Centered Relative Motion, No Orbiter Thrust

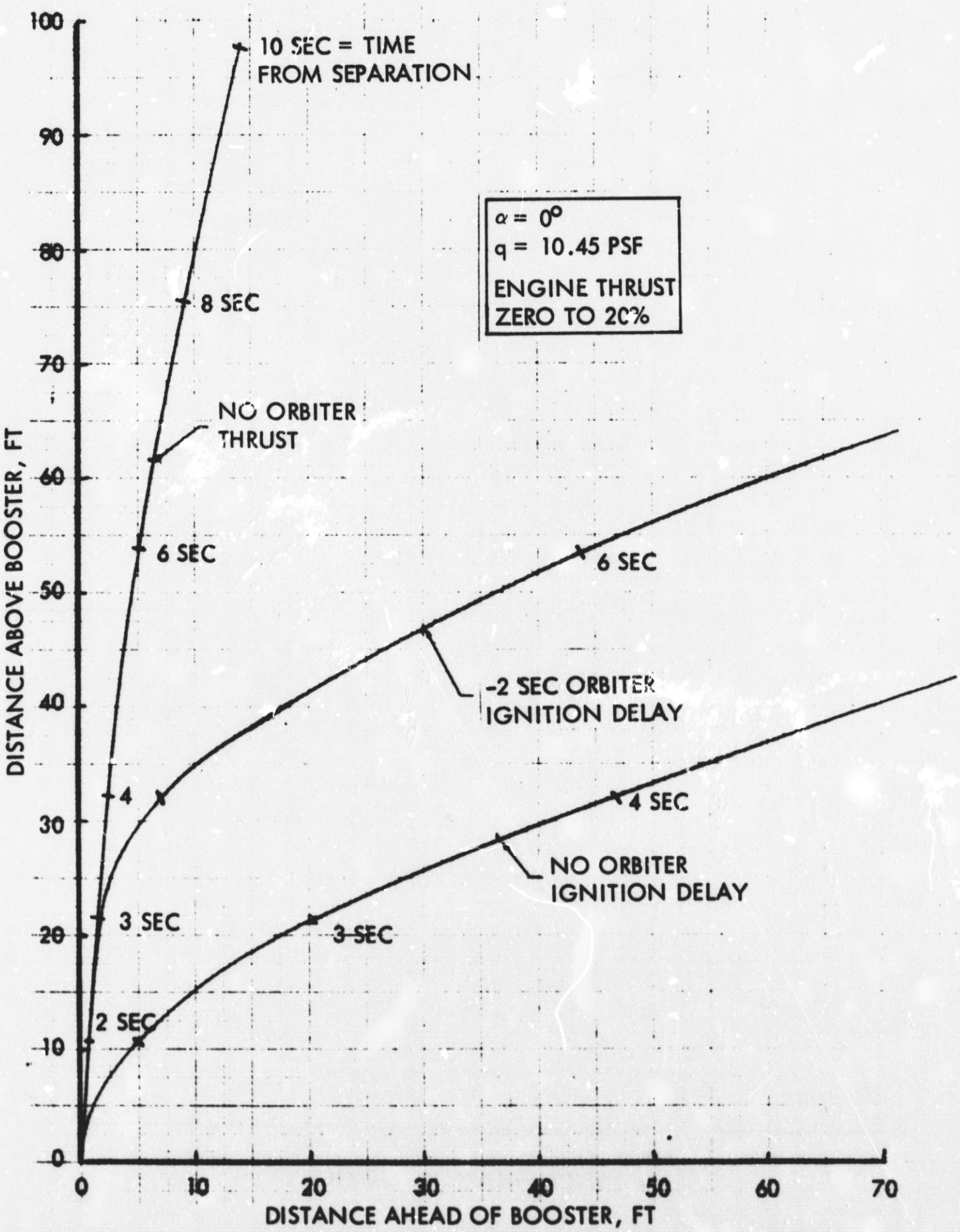

Figure 7.5-7. Booster-Centered Relative Motion, with Orbiter Thrust

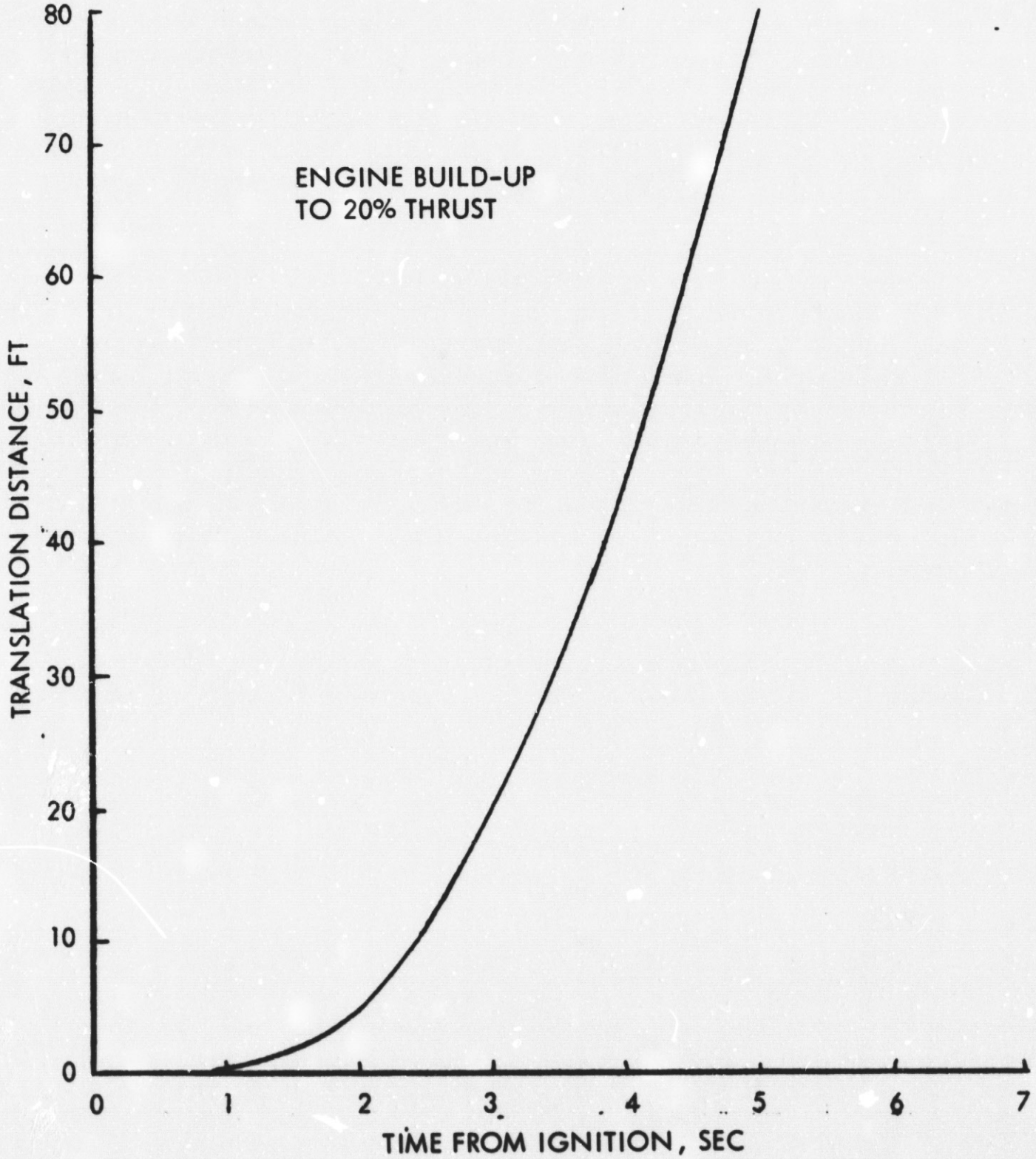

Figure 7.5-8. Orbiter Translation Due to Main Engine Thrust

RCS Requirements

The RCS is utilized in an attitude hold mode during separation. Two parameters that influence the sizing of the RCS pitch thrusters are aerodynamic torques and moments due to thrust misalignment of the separation rockets. Figure 7.5.9 provides a comparison of booster/orbiter pitching moments versus angle of attack when the vehicles are in the separation environment. If an angle of attack of minus 5 degrees at separation is assumed, then the curve can be extrapolated to indicate a 50,000-foot-pound requirement for RCS torque to oppose aerodynamic moments on both vehicles.

The orbiter center of gravity uncertainty was assumed to be 1.0 percent of the characteristic length; this equates to approximately 0.21 feet. With this thrust misalignment, the separation rockets could produce 33,600 foot-pound about any axis of the orbiter. Consequently, the total moment developed by aerodynamic and rocket forces in the pitch axis could be 83,600 foot-pound. It is recommended that the pitch control authority be 25 percent larger than the maximum external torques. Therefore, a total pitch control moment of 104,500 foot-pound would be required on the orbiter and 62,500 foot-pound on the booster for attitude hold authority during separation.

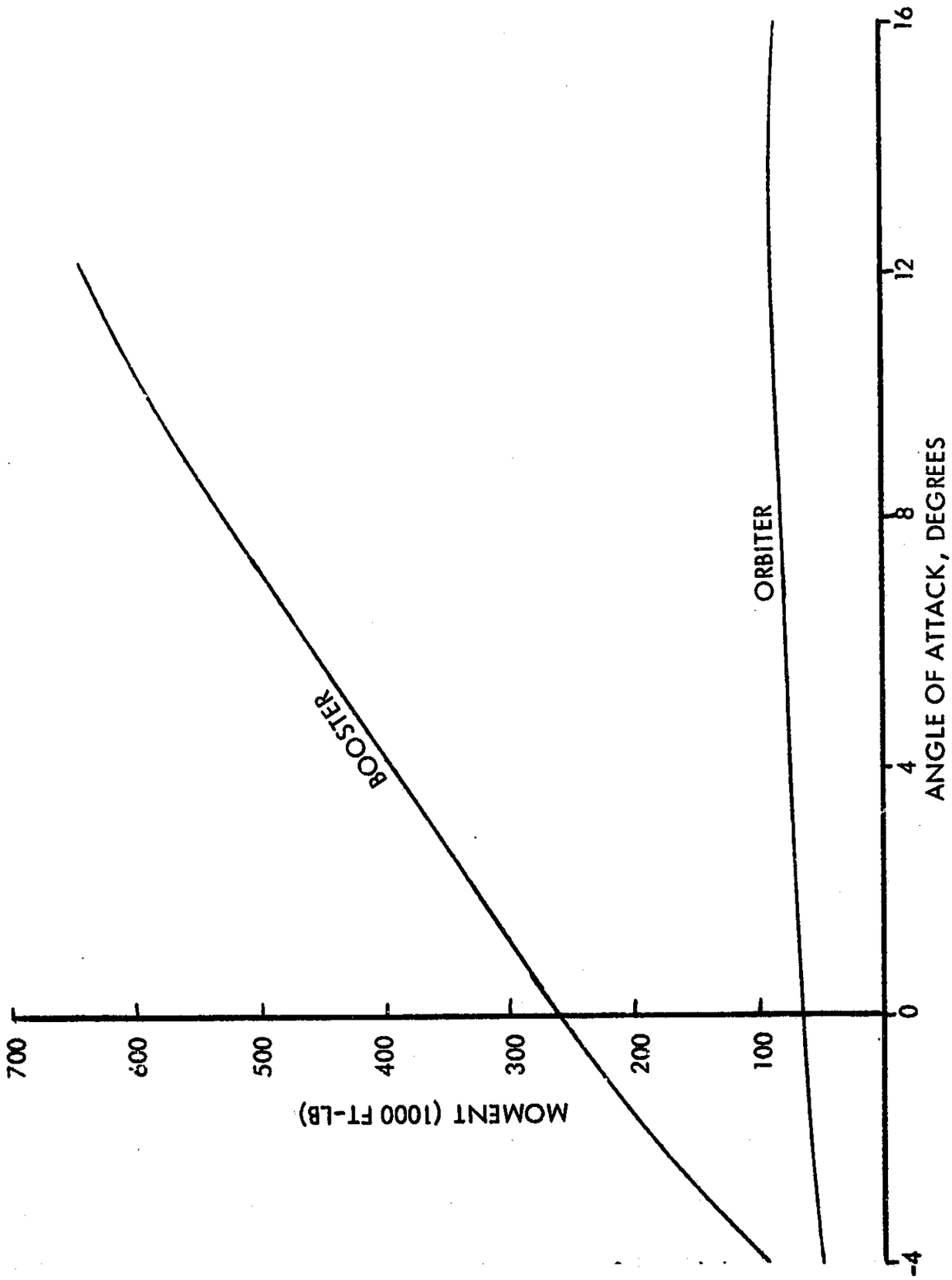

Figure 7.5-9. Pitching Moments at Booster-Orbiter Separation

7.5.4 Control System Simulation

Stability and control characteristics of the shuttle vehicle were assessed by performing a 6-degree of-freedom digital simulation to define the entry response of the 50,000-pound payload class orbiter configuration. The simulation is diagrammed in Figure 7.5-10. Included are a study of the effects of yaw and roll stability characteristics and a study of response for the pitch-down transition from entry to cruise attitude.

The simulation was performed in three parts:

1. The entry trajectory was flown with variable directional stability for three cases:

   a. Stable directional derivative ($C_{n_\beta} > 0$)

   b. Neutrally stable ($C_{n_\beta} = 0$)

   c. Unstable ($C_{n_\beta} < 0$)

   In each case, a 95-percent wind profile was used, oriented to hit the vehicle broadside. Results were then compared for control system effectiveness in performing stabilization and attitude hold functions and for RCS fuel consumption.

2. The entry trajectory was flown with variable dihedral effect for three cases:

   a. Stable dihedral effect ($C_{\ell_\beta} < 0$)

   b. Neutrally stable ($C_{\ell_\beta} = 0$)

   c. Unstable ($C_{\ell_\beta} > 0$)

3. A pitch-down maneuver to low angle of attack was performed by the elevator in response to an angle-of-attack command. Stabilization was provided by a pitch rate damper loop. Inasmuch as there were two stable pitch attitudes, control action was required to force the vehicle from one stable state at 60 degrees to the other at a 15-degree angle of attack, while damping the motion to prevent any significant overshoot. In view of the highly nonlinear

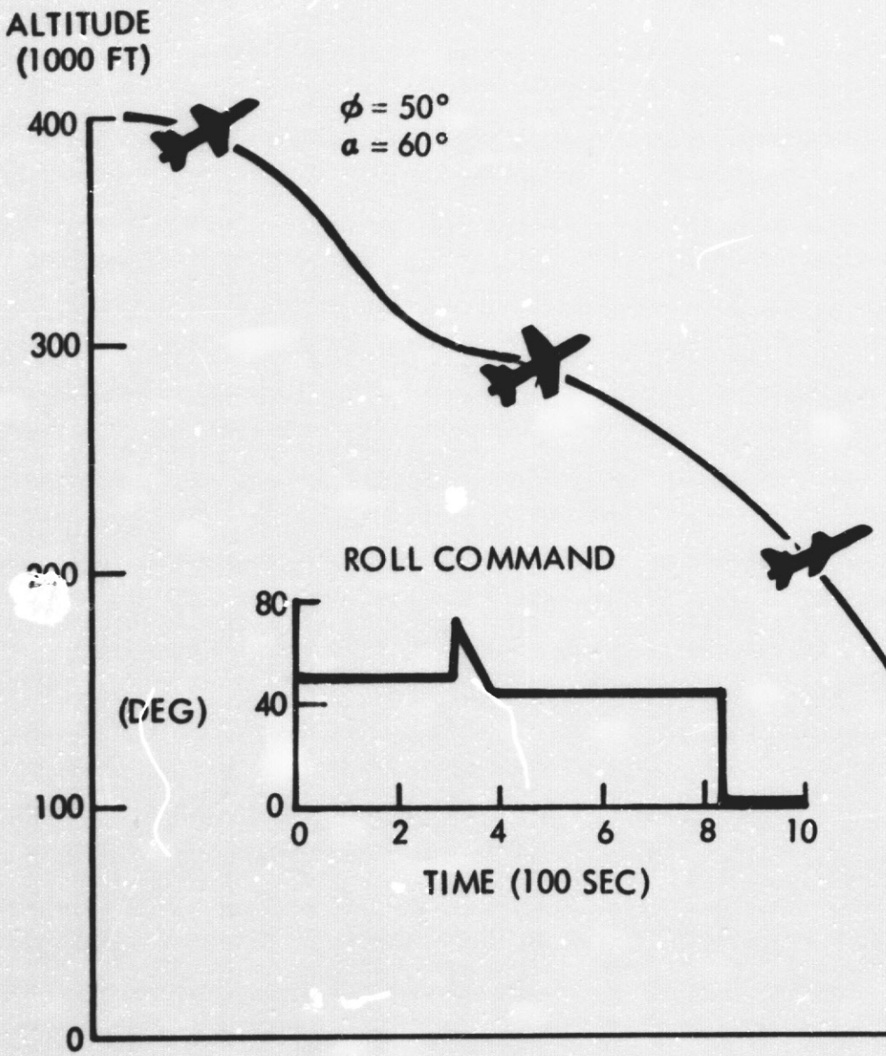

ENTRY CONTROL
- MODE-MAXIMIZE LAT RANGE
- LOW HEATING
- FIXED PITCH ATTITUDE, BANK ANGLE MODULATION FOR RANGING
- RCS DAMPING IN ALL 3 AXES
- ATTITUDE CONTROL IN ROLL & YAW
- 0.5 DEG/SEC^2 ACCEL

PITCH DOWN CONTROL
- ELEVATOR COMMAND
- GAIN SCHEDULING

VARIABLES
- C_{n_β} 0.01, 0, -0.01
- C_{ℓ_β} -0.002, 0, +0.002
- WINDS 95% YAW PLANE

Figure 7.5-10. Orbiter Entry Control Simulation

Space Division
North American Rockwell

and unconventional nature of the pitch moment coefficient, there was some question as to what restrictions on vehicle design would be required for this phase of the mission (e.g., tail size). Air-speed variations during the pitch-down maneuver also were studied.

Entry Simulation

The control system provided reaction jet damping in all three axes and attitude control in the roll and yaw axes (Figure 7.5-11 and 7.5-12). Conventional phase plane switching logic was used for attitude control in the pitch and yaw axes, while the pitch damper used a simple dead band. Since the orbiter is stable in pitch and trims at a 60-degree angle of attack, no pitch attitude control is needed. Commands to the roll and yaw jets are coordinated to provide roll about the relative wind vector in response to guidance commands, while minimizing sideslip. Turn coordination is essential because the roll stability axis differs from the roll body axis by the high (60-degree) angle of attack.

The control system studied accepts roll angle commands from the guidance input, which, for these simulations, was programmed as a function of time. The roll command was based on an entry trajectory to provide maximum cross range. The guidance scheme called for a constant (50 degree) bank angle until the flight path angle reached zero. Altitude was held constant by banking until an equilibrium glide condition was reached at a 40-degree bank angle. Bank angle was then held constant until aerodynamic velocity dropped to 3000 fps, then reduced immediately to zero (wings level) until pitch-down at 400 fps.

Effects of Directional Stability Variations on Orbiter Entry Simulation. Simulation time histories appear in Figures 7.5-13, -14, and -15. Figure 7.5-13 is for a vehicle that is statically stable in yaw (positive C_{n_β}); Figure 7.5-14 for neutral stability; and Figure 7.5-15 for unstable C_{n_β}. In each case, the trajectory began at 400,000 feet and was terminated at about 130,000 feet. Inertial velocity started at 25,992.5 fps, and the run continued until the total vehicle velocity with respect to the atmosphere was 3000 fps. Vehicle response was stable and well damped in all cases, indicating that the control system functioned well for either stable or unstable directional derivatives.

Results of the study are summarized in Table 7.5-2. The only serious problem was sharply increased fuel consumption for the unstable C_{n_β} case. Roll jet on-time increased by a factor of about 15, and yaw jet on-time by

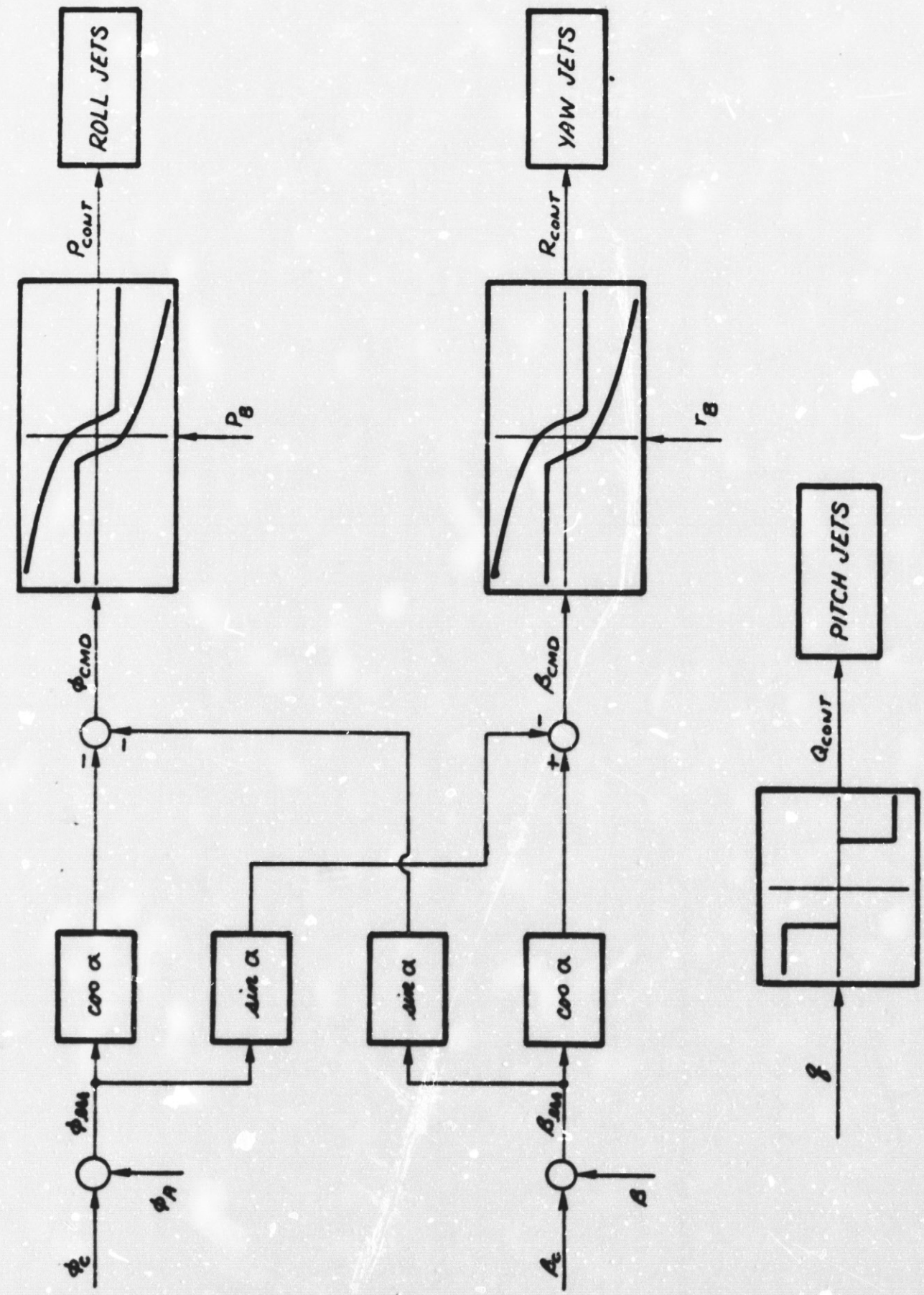

Figure 7.5-11. Entry Control System Block Diagram

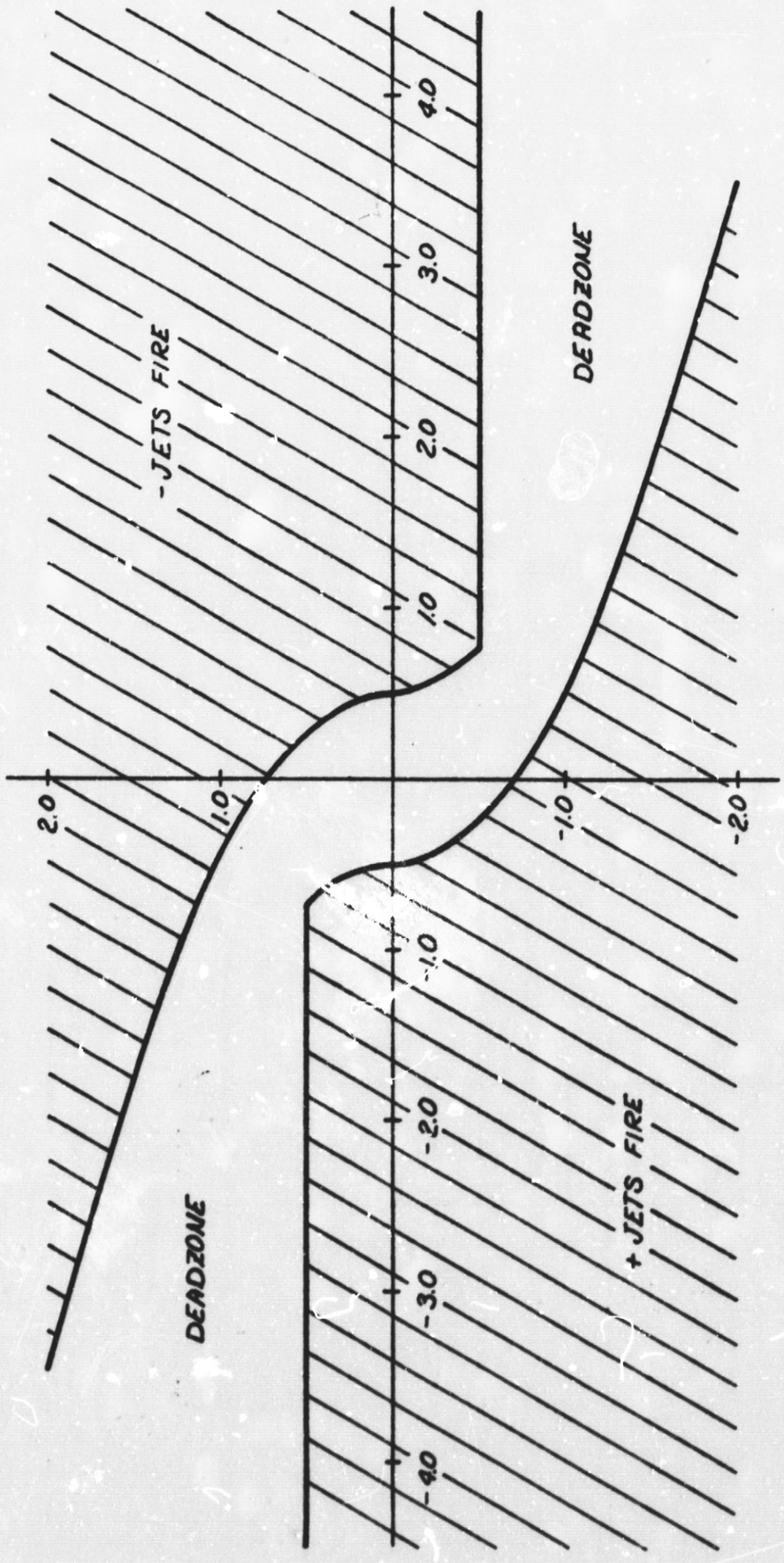

Figure 7.5-12. Roll and Yaw Phase Plane

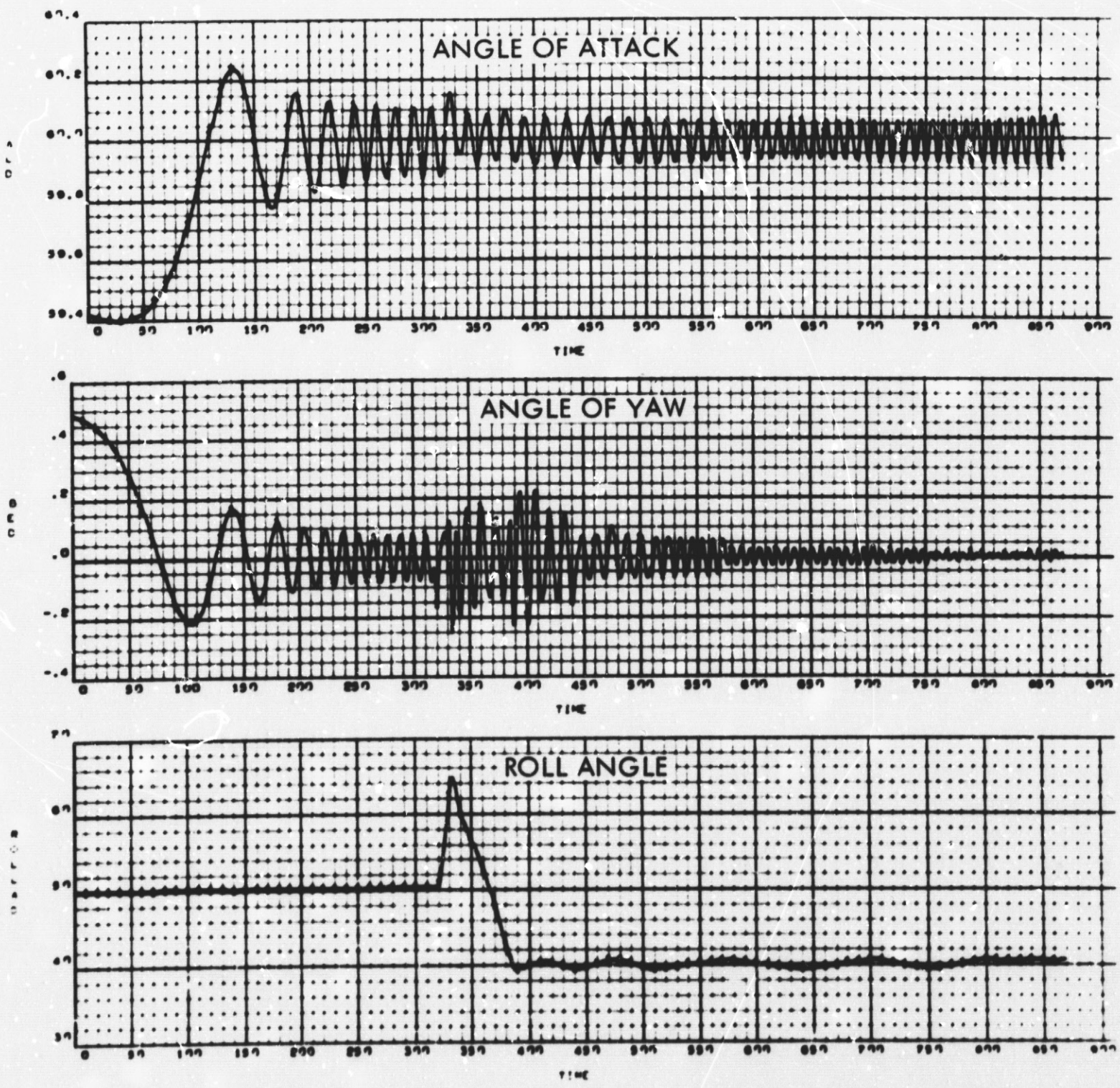

Figure 7.5-13. Orbiter Entry Simulation Time History, Stable C_{n_β}

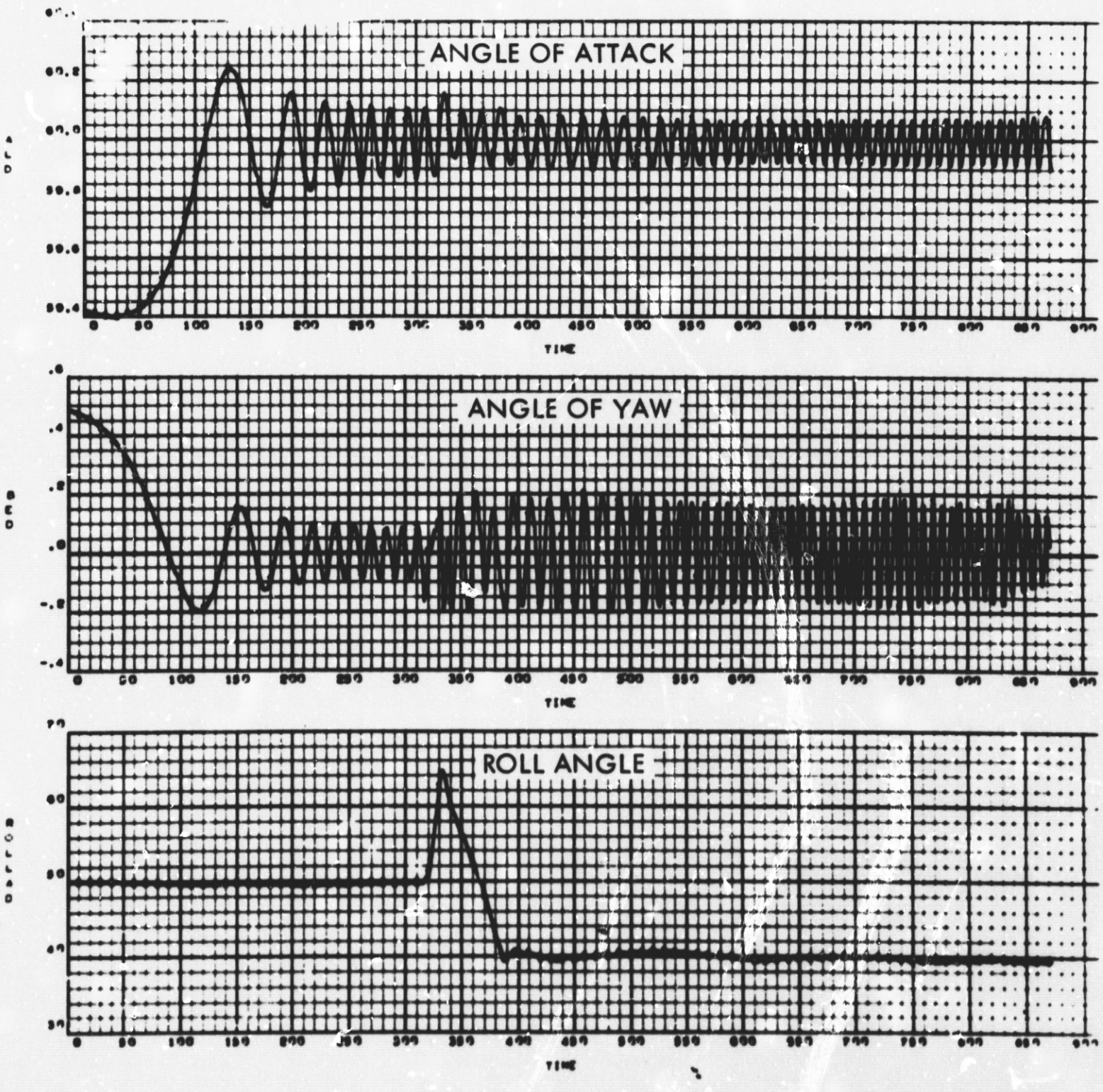

Figure 7.5-14. Orbiter Entry Simulation Time History, Neutrally Stable C_{n_β}

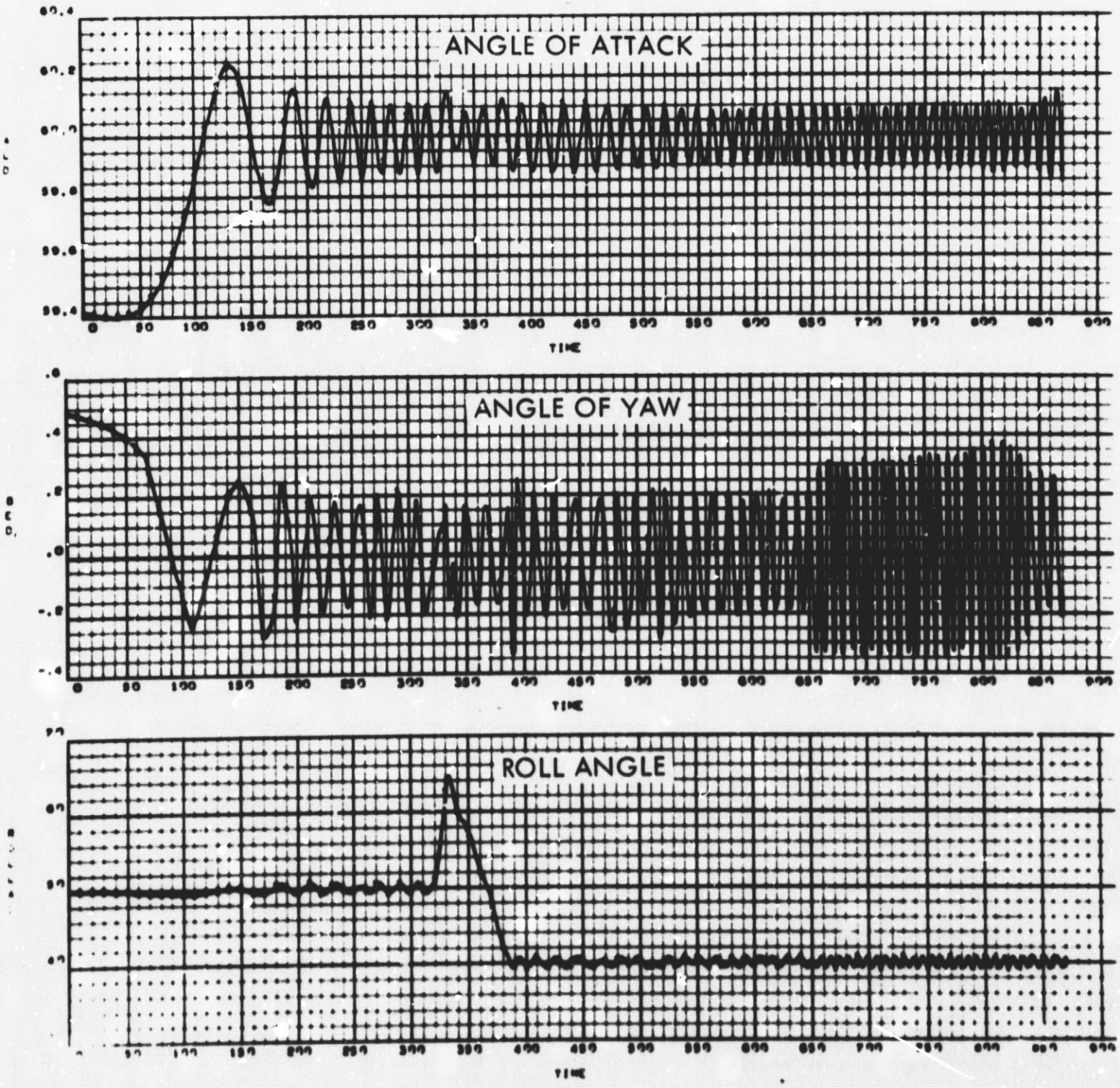

Figure 7.5-15. Orbiter Entry Simulation Time History, Unstable C_{n_β}

a factor of about 10. Propellant consumptions are presented in Table 7.5-3. The pitch damper jets never fired. Aerodynamic forces along the Y-axis remained small in all cases, indicating good turn coordination.

Table 7.5-2. Orbiter Entry Stability Simulation Results

Yaw Moment Coefficient C_{n_β} (per degree at 60° angle of attack)		0.01 (stable)	0.0 (neutral)	-0.01 (unstable)
Jet on time (sec) (870-sec run)	Roll	4.0	4.7	60.0
	Pitch	0.0	0.0	0.0
	Yaw	10.4	9.0	103
Peak sideslip β (Degrees)		0.25	0.22	0.38
Y-Axis Aerodynamic Force Y_B (lb)		110	240	470
Peak aerodynamic moments (ft-lb)	Roll	2800	6300	12,000
	Pitch	9300	10,000	17,000
	Yaw	1450	13	60,000
Peak body rate oscillations (deg/sec)	Roll	0.1	0.15	0.5
	Pitch	0.05	0.06	0.1
	Yaw	0.13	0.0	0.55

The jet on-time results in Table 7.5-2 do not include the roll maneuver to wings-level attitude. Neither do they involve rate limits in the phase plane logic. Figure 7.5-16 illustrates results, including the final roll maneuver, 0.5 deg/sec roll rate limiting (to conserve RCS fuel), but without wind. It is readily seen that most of the RCS fuel was consumed during this final maneuver in the presence of fairly large aerodynamic forces, with roll, pitch, and yaw jet on time increasing to 33, 34, and 46 seconds, respectively.

To summarize, a vehicle with stable or neutrally stable directional derivatives is readily controlled. However, fuel consumption increases sharply for unstable C_{n_β} the reaction jet engines must be large enough to overcome any of the unstable aerodynamic moments generated. Since these moments increase for larger vehicle oscillations, vehicle attitude must be closely controlled for unstable C_{n_β} if vehicle stability is to be maintained.

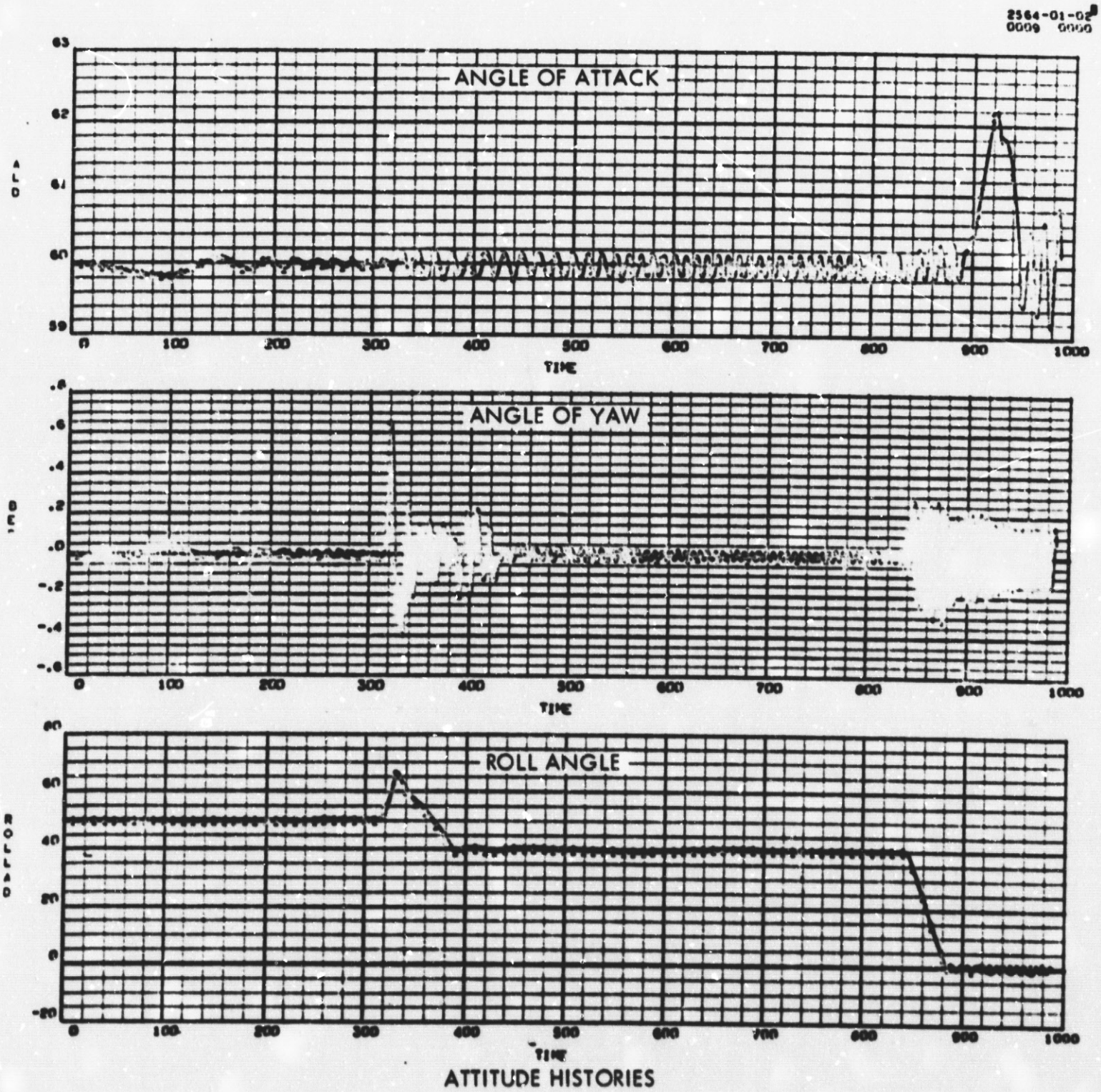

ATTITUDE HISTORIES

Figure 7.5-16. Orbiter Entry Simulation Including Final Roll Maneuver (Sheet 1 of 2)

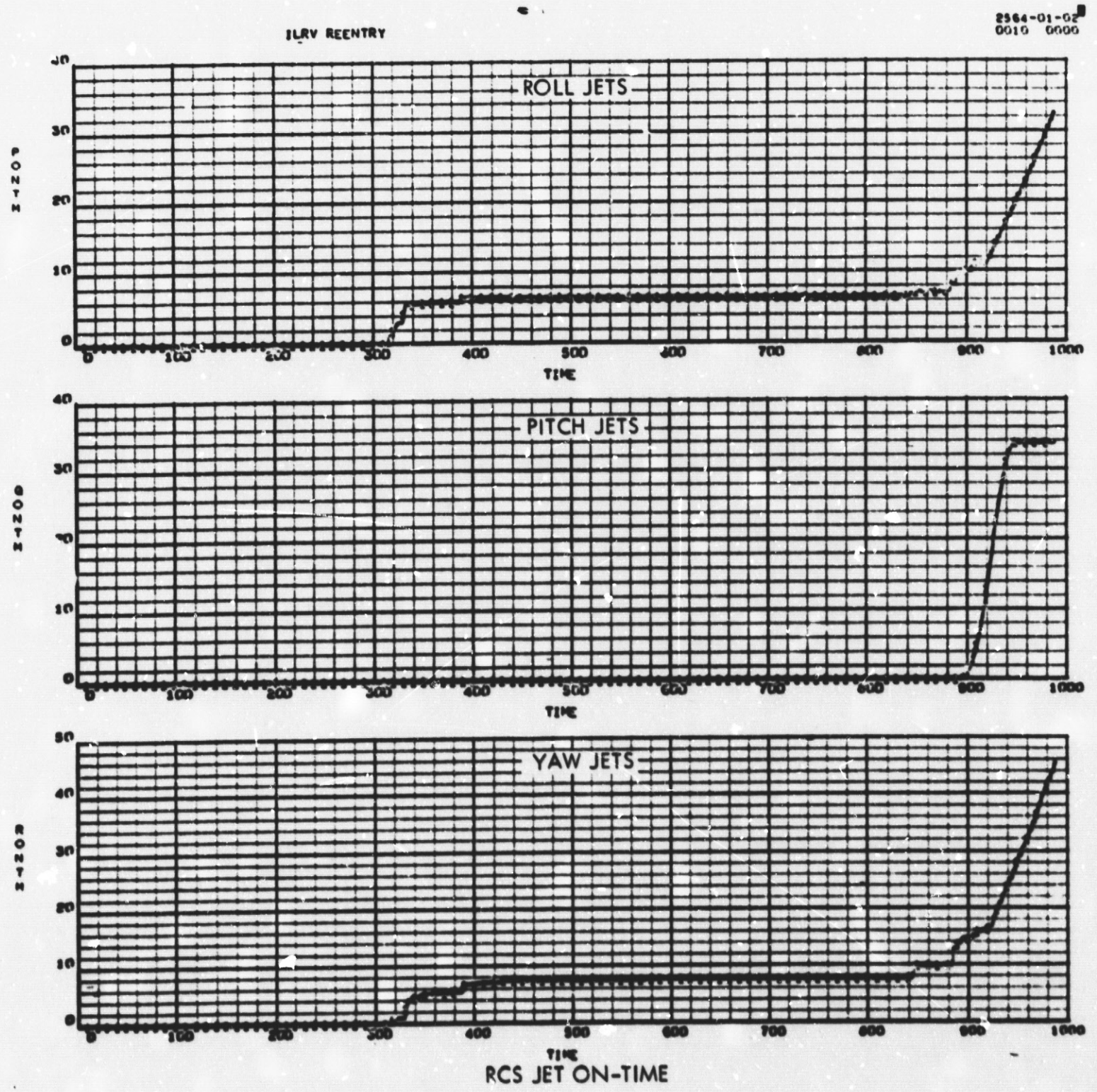

Figure 7.5-16. Orbiter Entry Simulation Including Final Roll Maneuver (Sheet 2 of 2)

If vehicle attitude exceeds a critical value, recovery with reaction jet control is impossible. In the case considered, the jets were sized to provide an angular acceleration of 0.5 deg/sec^2 in all axes, neglecting aerodynamics moments. This value provided good performance, but any reduction in RCS thrust would tend to increase the risk of losing control of a vehicle with unstable directional characteristics.

Effects of C_{ℓ_β} Variations on Orbiter Entry Simulation. In the previous simulation, a stable C_{ℓ_β} derivative was used. The value of C_{ℓ_β} was assumed fixed at -0.002, and C_{n_β} was varied from -0.01 to +0.01. It was desired to test the effects on vehicle performance and fuel consumption of variations in C_{ℓ_β}. Runs were made with values of 0.0 and +0.002. Results are shown in Table 7.5-3 together with those from previous runs.

It is significant that when positive (unstable) values of C_{ℓ_β} were used, the reaction jets were unable to stop the final roll maneuver at wings-level attitude prior to the pitch-down maneuver. This problem could be resolved. Either the aerodynamic control systems could be used for this maneuver, or the reaction jet control logic could be modified to reduce sideslip by shutting off jets in whichever axis is rolling faster than required for precise turn coordination.

Table 7.5-3 indicates that an unstable value (+0.002) of C_{ℓ_β} increases consumption of RCS propellant about 60 percent, although not nearly as much as an unstable value of C_{n_β}. It was assumed that three jets, each producing 800 pounds of thrust were used in each axis (one jet failed in each axis). The resulting accelerations were 4.6, 0.5, and 0.5 degrees/second^2 in the roll, pitch, and yaw axes, respectively. In view of the increased roll acceleration, results were not strictly comparable with earlier runs. Inasmuch as the simulation did not give propellant consumption directly, it was computed for each axis by multiplying jet on time in seconds by consumption rate given by

$$\dot{W} = \frac{\text{Number of Jets x Thrust/Jet}}{I_{sp}} = \frac{3 \times 800}{380} = 6.32 \text{ lb/sec}$$

To summarize, satisfactory entry trajectories were obtained with neutrally stable C_{ℓ_β}, although there is always some risk with an unstable vehicle that sideslip will increase to a point where unstable aerodynamic moments will exceed the total available RCS moments and make recovery impossible.

Table 7.5-3. Effects of C_{ℓ_β} Variations on Orbiter Entry

C_{ℓ_β}	C_{n_β}	Wind	Acceleration (deg/sec^2)			RCS On Time (seconds)			Propellant Used (lb)		
			Roll	Pitch	Yaw	Roll	Pitch	Yaw	Roll	Pitch	Yaw
-0.002	0.01	Yes	0.5	0.5	0.5	4.0	0.0	10.4	25.3	0.0	65.8
-0.002	0.0	Yes	0.5	0.5	0.5	4.7	0.0	9.0	29.7	0.0	56.8
-0.002	-0.01	Yes	0.5	0.5	0.5	60.0	0.0	103.0	369.0	0.0	652.0
+0.002	-0.009	No	4.6	0.5	0.5	19.0	0.0	26.0	*	*	*
0.0	-0.009	No	4.6	0.5	0.5	4.4	0.0	16.0	27.2	0.0	101.1

*Reaction jets did not stop final roll maneuver to wings level at a velocity of 3000 fps.

Transition to Cruise Simulation

The entry angle of attack (60 degrees) is maintained until the orbiter has reached subsonic flight. At approximately 400 fps velocity, a pitch-down maneuver is performed, and the orbiter glides at maximum L/D to the recovery site. A control simulation of the maneuver was conducted to verify the capability of the orbiter to perform the transition to horizontal flight.

The control system used is illustrated in Figure 7.5-17. Pitch-down is accomplished by an elevator command. Gain scheduling was incorporated to compensate for large variations in air speed and altitude during and after the maneuver. Control simulation results are presented in Figures 7.5-18 and 7.5-19. The maneuver was initiated at an altitude of 54,000 feet at a velocity of 400 fps. Dynamic response was smooth and well damped. There was little or no overshoot even though it was necessary to maneuver from one stable equilibrium point to another with nonlinear aerodynamic moments. Figure 7.5-18 illustrates the elevator deflection in degrees, the total pitching moment in foot-pounds, and the angle-of-attack history during the maneuver. Altitude, velocity, and dynamic pressure histories are illustrated in Figure 7.5-19.

Inspection of the pitching moment history shown in Figure 7.5-18 indicates that the pitch RCS system could be used to augment elevator authority, thereby allowing a reduction in size of the elevator surface. A moment of 162,000 foot-pounds is available from the pitch jets of the 50,000 pound-payload-class orbiter. The maximum moment developed by the elevator was about 750,000 foot-pounds, rapidly decaying to zero as the vehicle pitched down. As now sized, the RCS can provide about 20 percent of the peak aerodynamic moment, and will supply an equivalent integrated moment by maintaining the jet on for five seconds. Additional investigations of combined RCS plus aerodynamic control should be conducted to minimize orbiter vehicle weight. Similar studies are required for the booster.

7.5.5 Reaction Control System Requirements

To support logistic vehicle subsystem definition, studies were conducted to define reaction control system design requirements. Definition of these requirements encompassed two major areas of investigations:

1. Establishment of RCS angular acceleration rates for adequate vehicle control.

2. Definition of RCS propellant requirements to support sizing of the RCS fuel system.

K_α = 1.3

K_q = 5.0

$\bar{q}_{ACTUAL}$ = DYNAMIC PRESSURE

$\bar{q}_{DESIGN}$ = $\bar{q}$ USED IN 1 DOF PROGRAM (24.0)

Figure 7.5-17. Pitch-Down Control System

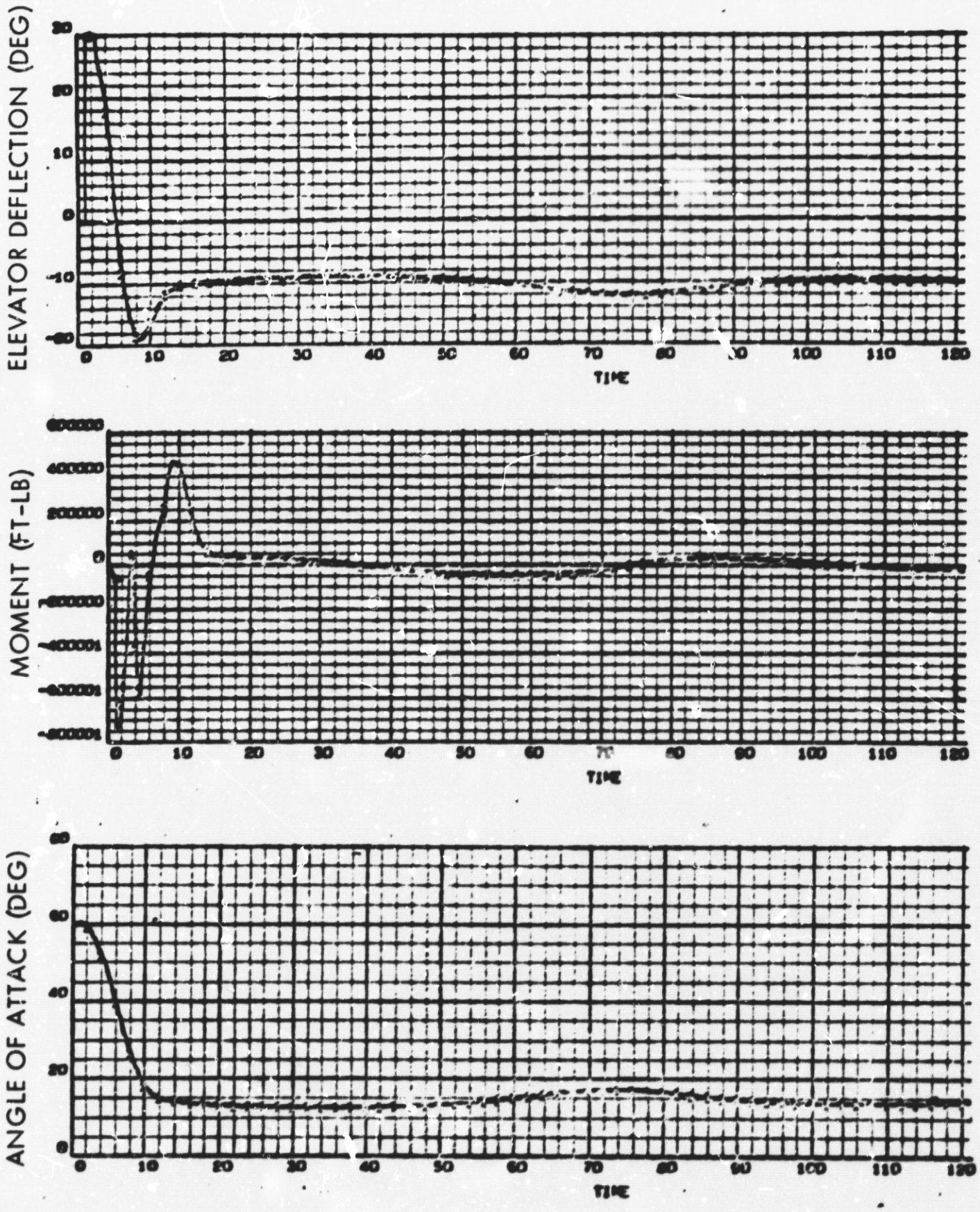

Figure 7.5-18. Pitch-Down Maneuver Time Histories: Elevator Deflection, Pitch Moment, Angle of Attack

Page intentionally left blank

Control Authority

System requirements were based on the following considerations:

1. Attitude hold in case of a main engine failure
2. Maneuver requirements during separation
3. Attitude hold during orbital coast periods
4. Vehicle maneuver rate and acceleration requirements during entry
5. Allowable mounting distance from center of gravity
6. Supression of disturbance torques during entry

The first six items were considered for preliminary system sizing. Suppression of disturbance torques during entry should be considered for final sizing.

Orbiter and booster RCS moment requirements are summarized in Table 7.5-4 for various mission phases. Orbiter entry control simulations reported in the previous section indicated that adequate control authority was obtained with roll and yaw jets sized to give an angular acceleration of 0.5 degrees per second squared. This value was used for the yaw jets. However, for the roll jets, the design requirement was determined from a one-engine-out condition on the orbiter. For this case, a pitch command will cause a rolling moment that must be cancelled by roll RCS jets. The requirement was based on counteracting an instantaneous 3- and - 1/2-degree gimbal command. Further analysis on limiting engine gimbal angle excursion and on transient recovery capability may allow the roll jet size to be reduced.

Pitch jets are used for stabilization and attitude control during separation of the orbiter and booster. The control moments required were 104,500 foot-pounds, as discussed in Section 7.5.3. Authority was increased to provide a pitch acceleration of 0.5 degrees per second squared, consistent with the yaw channel.

Translational acceleration requirement was based on Apollo CSM criteria. A translational acceleration of 0.1 ft/sec^2 is provided.

Booster RCS sizing was based on providing 0.5 deg/sec^2 angular acceleration in all axes. Additional studies should be conducted to confirm the adequacy of this requirement for entry control and maneuvers during flyback, and for augmentation of the pitch-down maneuver after entry.

Table 7.5-4. RCS Requirements Summary,
50,000-Pound Payload Class

	AXIS	REQUIREMENT		
		SOURCE	ANGULAR ACCEL (DEG/SEC^2)	MOMENT FT-LB
ORBITER	ROLL	ONE ASCENT ENGINE OUT	4.6	240,000
	PITCH	SEPARATION ATTITUDE HOLD	0.5	162,000
	YAW	ENTRY CONTROL	0.5	176,000
	TRANS-LATION	DOCKING (APOLLO CRITERIA)	0.1 FT/SEC^2	800 LBS TRANS-LATION
BOOSTER	ROLL	POST SEPARATION COAST	0.5	147,000
	PITCH	POST SEPARATION COAST	0.5	750,000
	YAW	POST SEPARATION COAST	0.5	830,000

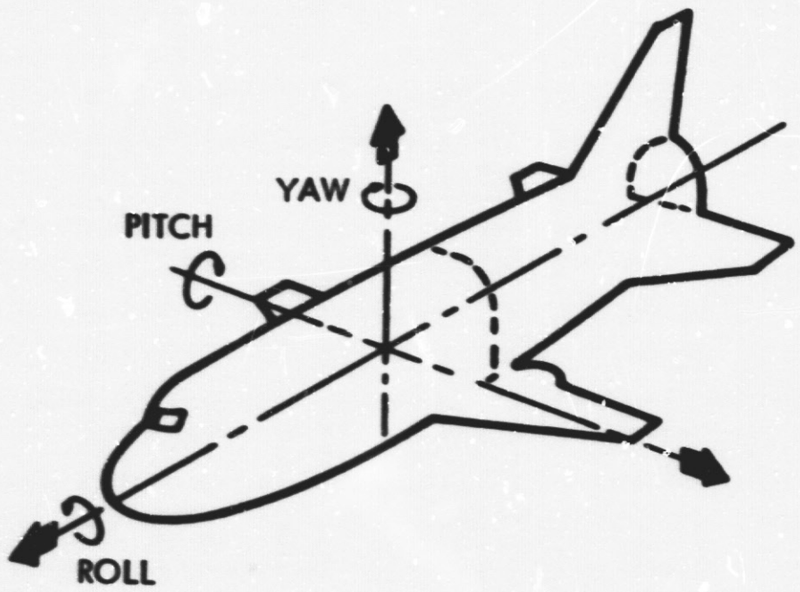

RCS Propellant Consumption

RCS propellant consumption was estimated to support RCS fuel system sizing. The estimate was based on preliminary mission considerations, approximate vehicle mass data, main engine thrust levels, and an assumed set of preliminary RCS performance requirements. From a preliminary mission time line, Table 7.5-5 was constructed to show the various RCS functions, along with the associated forcing functions that will define propellant consumption.

Consumption During RCS Translations. As indicated in Table 7.5-5, the translation jets are used to null ΔV residuals and for docking maneuvers. It was estimated that 50 fps are required of the RCS for these functions. With an average vehicle mass of 260,000/32 slugs, RCS I_{sp} of 380 seconds, and a 5-percent stabilization consumption added, the RCS fuel consumption for translation is

$$W_t = 1.05 \frac{260,000 \times 50}{32 \times 380} = 1070 \text{ pounds}$$

Propellant Consumption for Limit Cycling. It was assumed that ±5 degrees of dead band is acceptable during limit-cycle attitude hold. The average time between RCS pulse firing for the roll, pitch, or yaw channel is then

$$\text{delta t} = \frac{10 \overline{\text{deg}}}{0.0150 \text{ deg/sec}} = 675 \text{ sec}$$

A 30-ms pulse duration was assumed. The effective I_{sp} will be lower than nominal, a value of 200 lb-sec/lb_m being selected. For each cycle of minimum impulse firing, the fuel consumption is

$$W_{pitch} = W_{yaw} = \frac{(0.030)(1000)\,2}{200 \frac{\text{lb-sec}}{\text{lb}_m}} = 0.300 \text{ lb}_m$$

$$W_{roll} = \frac{0.030\,(1000)\,2}{200} = 0.300 \text{ lb}_m$$

On a per-hour basis, the fuel consumption for all three channels is

$$W = 3600 \frac{(3)\,(0.300)}{675}\,(2) = 9.6 \text{ lb/hr}$$

Table 7.5-5. Forcing Functions for RCS Propellant Consumption

Mission Phase	RCS Activities	Forcing Functions and Parameters				
		No. of Pitch & Yaw Maneuvers	No. of Roll Maneuvers	Translation Maneuvers & ΔV Residuals (fps)	No. of Hours in ±5 deg Limit Cycle	ΔV (fps)
Circularization	Limit cycle				0, 75	
	Orbit circularize burn - null residuals			ϕ, 5	0, 2*	100
Phasing	Attitude limit cycle				20	
	Attitude maneuver (align & trans)	3	2			
	Hohmann transfer				0, 6*	100
	Attitude limit cycle				0, 75	
	Tgt orbit circularize burn, att. maneuver	2	1		0, 6*	300
	Attitude control				0, 5	
Rendezvous	Attitude maneuver (1st rendezvous burn)	2	1		0, 1*	50
	Attitude control (rendezvous nav)	2	1			
	Attitude control (trim maneuver)	2	1			
	+X translation (plane change)			15		
	Attitude control (nav shift)	3	1			
	Midcourse correction (R, P, Y)			4.5		
	Attitude maneuver (rendezvous burn)	2				
	Attitude control (roll - rendezvous burn)		1		0, 1*	50
	Attitude maneuver	1	1			
Docking	Null Y-velocity residual			1		
	ΔV X			4		
	ΔV Z			5		
	Attitude maneuver (dock. att)	2	1			
	Attitude control				.25	
	Null closure rates -					
	Translation maneuver					
	ΔV Z			4		
	ΔV Y			3		
	Add closure rates (X, Y, Z)			1		
	Reduce closure rates (X, Y, Z)			5		
Deorbit	Space station separation (ΔV Z)			3		
	Attitude maneuver (alignment)	1	1			
	Attitude limit cycle				0, 5	
	Attitude maneuver (deorbit burn)	2	1			
	Attitude control (roll - deorbit burn)				1, 0*	500
	Attitude limit cycle				0, 75	
Entry	Attitude limit cycle				0, 1*	
	Totals	22	12	50	26	1300

*Equivalent to Wide Limit Cycle

From Table 7.5-5, the total time in limit cycle is estimated at 26 hours, hence:

$$W = (39.5)(9.6) = 389 \text{ pounds}$$

Propellant Consumption During Attitude Maneuvers. During attitude maneuvers, sustained thrusting of the RCS jets for one second was assumed, at an I_{sp} of 380 seconds. One pulse is required to start and one to stop each maneuver. Accordingly, the fuel consumption per maneuver is

$$W_{roll} = W_{pitch} = W_{yaw} = \frac{(2)(2)(1000)(3 \text{ sec})}{380} = 31.6 \text{ lb/maneuver}$$

From Table 7.5-5, there are 22 pitch and yaw maneuvers and 12 roll maneuvers in the orbital phases so that the total consumption is

$$W = (34)(31.6) = 1073 \text{ pounds}$$

Consumption Under One Main Engine ΔV. When only one main engine is used to provide ΔV, the lateral displacement from the vehicle centerline to the engine centerline is 72.5 inches. In the vertical plane, the displacement between vehicle center of gravity and thrust center is approximately 2 feet. Since the engines are mounted side by side, the ΔV maneuver will be performed with more yaw engine deflection than with pitch deflection for maintaining thrust pointing through the center of gravity.

With a distance of 1000 inches between the engine and center of gravity, a vehicle mass of (260,000/32) slugs, and an effective roll moment arm of 2 feet, the amount of unbalanced roll angular impulse per one fps of ΔV is

$$I_{roll} \cong \frac{260,000}{32} (2 \text{ ft}) \quad 2 \times 12 = 390 \text{ lb-ft-sec/fps}$$

With a roll lever arm of 70 feet and an I_{sp} of 380 seconds assumed, the RCS fuel needed to correct the unbalanced angular impulse is

$$W_{\Delta V} = \frac{390}{380 \times 70} = 0.0147 \frac{\text{lbm}}{\text{fps}} \Delta V$$

From Table 7.5-5, the total required ΔV is 1300 fps so that the propellant weight required is

$$W_{\Delta V} = 0.0147 (1300) = 19 \text{ lb}_m$$

On-Orbit RCS Propellant Estimates. With the various consumptions collected, the on-orbit portion of RCS propellant consumptions was estimated to be:

RCS translation	1070 lb
RCS limit cycling	389
Attitude maneuvers	1073
One-engine ΔV	19
Subtotal	2551
4-percent line traps assumed	102
6-percent gauging errors assumed	153
10-percent mission contingency assumed	255
Total	3061 lb

These values were established as minimum requirements for RCS fuel system sizing.

8.0 DESIGN ENVIRONMENTS

8.1 SUMMARY

This section of the report presents design trajectories, air loads, thermal environment, and structural loads for the 12,500-pound-payload class, MSC baseline and the 50,000-pound-payload concept. Significant results of the environment analyses were:

1. Maximum $q\alpha$ during boost is 2940 psf-deg, with 95 percentile ETR winds aloft.

2. Maximum acceleration is 3.0 g's for both stages.

3. Maximum g's during entry are 4.0 for the booster and 2.1 for the orbiter.

4. Maximum $q\alpha$ condition is the most critical load case for the majority of the vehicle.

5. Prelaunch is the design condition for the hold-down of the vehicle at the aft end of the booster.

8.2 12,500-POUND-BASELINE DESIGN ENVIRONMENT

Design structural and thermal environments were computed for the 12,500-pound-baseline booster and orbiter vehicles to support evaluation and vehicle sizing studies. The configuration is shown in NR Drawing No. 2234-50, (Figure 7.2-3).

8.2.1 Design Trajectories

Design trajectories were prepared for use in structural sizing and weight scaling of the 12,500-pound-payload baseline system. The vehicle was launched into an orbit of 45 by 100 nautical miles at 55 degrees inclination. Maximum dynamic pressure was 420 psf and it occurred 72 seconds after lift-off. Staging occurred at 203,800 feet at a velocity of 8,035 fps and flight path angle of 9.3 degrees.

The booster descent-trajectory mode was banked entry. It was selected to reduce booster flyback range. After separation, the orbiter engines were ignited, and the orbiter was boosted to the parking orbit of 45 by 100 nautical miles. End boost velocity was 25,883 fps. Launch and booster descent design trajectory data are summarized in Figure 8.2-1.

Orbiter entry was at a constant L/D of 0.50. It was obtained by flying at a constant angle of attack of 60 degrees throughout entry until pitch-over was initiated at 43,000 feet altitude. The roll attitude was varied during entry to maximize lateral range. Design entry trajectory parameters are presented in Figure 8.2-2. Maximum load factor during entry was 2.1 g's, which occurred at 161,000 feet altitude. During the transition maneuver, a peak load factor of 2.5 was obtained.

8.2.2 Design Thermal Environment

The design heating environment was computed for the 12,500-pound baseline orbiter. The ascent environment was based on launch into an orbit of 45 by 100 nautical miles, as described in Section 8.2.1. Entry environment was computed for a 60-degree angle of attack along a flight path angle of -1.5 degrees. Lift loading, W/C_LS, was 50 pounds per square foot. Results are summarized in Table 8.2-1. Temperatures are radiation equilibrium temperatures for an emissivity of 0.8. Environments for the wing do not include interference effects. Small-scale test data indicated that an interference region could exist on the underside of the wing near the 20-percent span location. It is estimated that local heating rates can be increased by a factor of 3 in flow interference regions. This will increase the leading edge temperature to 3850 degrees. The design should be based on this temperature.

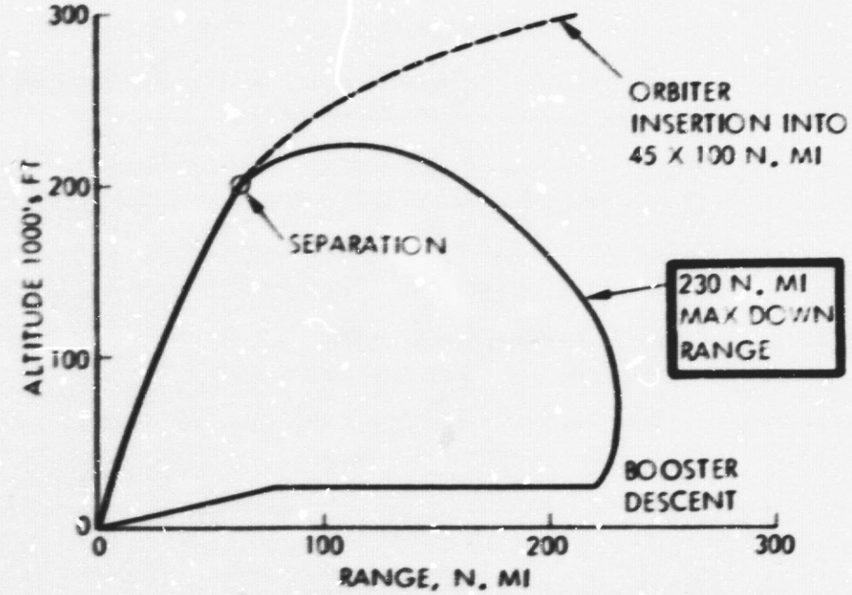

ASCENT

	FLIGHT CONDITION	TIME SEC	ALTITUDE FT	VELOCITY FT/SEC	LOAD FACTOR g's	DYNAMIC PRESSURE PSF
ASCENT	MAXIMUM DYNAMIC PRESSURE	72	28,600	940	1.46	420
	STAGING	201	203,800	8034	3.0	17
	END BOOST	425	273,400	25,883	3.0	
BOOSTER DESCENT	APOGEE	237	227,000	7520		5.
	MAX LOAD	337	126,000	4030	4.0	79
	TRANSITION	456	59,900	400	2.5	200
	LANDING		0	107 KNOTS		

Figure 8.2-1. Ascent Design Trajectory Parameters
(12,500-Pound Class Baseline)

Space Division
North American Rockwell

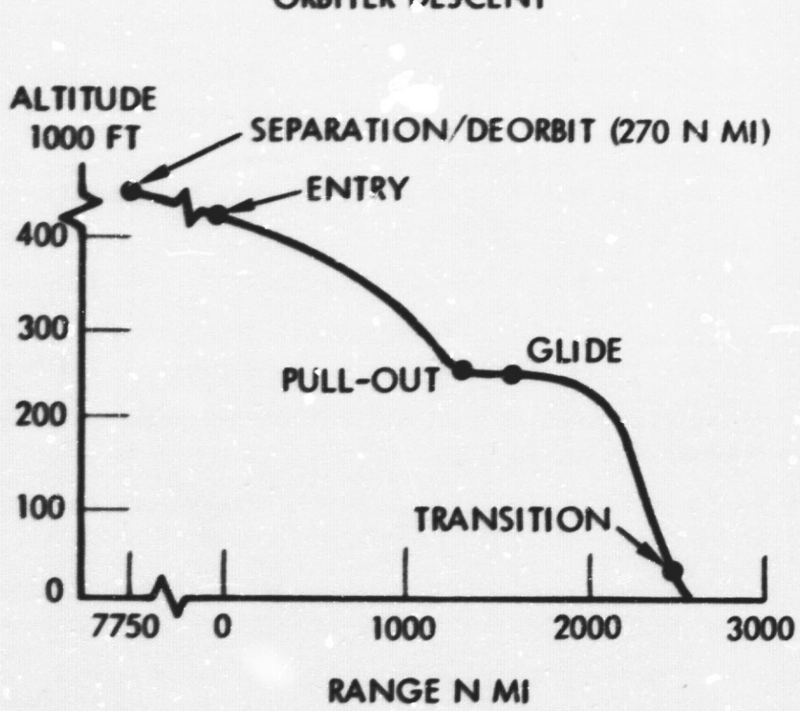

ORBITER DESCENT CONDITION	TIME (SEC)	ALTITUDE (1000 FT)	VEL (1000 FPS)	LOAD FACTOR G'S	DYNAMIC PRESSURE PSF
DE-ORBIT	33 MIN	270 N MI	24.55	0	0
ENTRY	0	400	26.00	0	0
PULLOUT	315	251	23.20	0.8	17.8
BEGIN GLIDE	393	251	21.54	0.7	15.4
MAX n_R/q	776	161	6.43	2.1	46.6
END ENTRY	840	128	3.00	1.8	40.4
TRANSITION	992	43	0.40	2.5	301.0
LANDING	1730	0	129 Kts		

Figure 8.2-2. Orbiter Design Trajectory
(12,500-Pound Class Baseline)

Table 8.2-1. Thermal Environment Summary
(12,500-Pound-Payload Class)

Location	Critical Flight Conditions	Radiation Equilibrium Temperature (°F) Orbiter
Fuselage		
Nose	Boost	2500
Lower surface (stag)	Entry	1850
Lower surface (80% of length)	Entry	1300
Chine (20% L)	Entry	1850
Side	Entry	560
Upper surface	Ascent	800
Wing (50% span)		
Leading edge (no interference)	Entry	2900
Lower surface (20% chord)	Entry	2200
Upper surface (20% chord)	Ascent	800
Horizontal surface		
Leading edge	Entry	3300
Lower surface	Entry	2000
Upper surface	Ascent	800
Vertical surface		
Leading edge	Ascent	2600
Side	Ascent	650

8.2.3 Air Loads

Aerodynamic load distributions were estimated at four flight conditions:

1. Maximum q α during boost.
2. Entry at α = 60 degrees
3. Subsonic transition
4. Landing with flaps down.

Figures 8.2-3 and 8.2-4 are the normal load distributions on the fuselage for the orbiter, booster, and composite configurations for the selected maximum q α case, which occurs at M = 1.1. The first curve is d (dN/dx)/dα. The latter curve is the composite configuration dN/dx evaluated at angles of attack of 4, 7, and 10 degrees. The method used to obtain the normal load distribution was based on NASA-CR-413, Linear Aerodynamic Loads on Cone-Cylinders at Mach Numbers From .7 to 2.0. The wing contribution was evaluated from the USAF Stability and Control DATCOM. Figure 8.2-5 presents the axial load distribution. It was obtained by fairing a component drag buildup.

Presented in Figures 8.2-6 through 8.2-9 are the estimated normal and axial load distribution for the orbiter and booster during entry at a 60-degree angle of attack. Hypersonic Newtonian flow was used to estimate these data, and the developed expressions are:

$$\frac{dC_N}{dx} = \frac{\Delta C_N}{\Delta x} = \frac{2 \sin^2 (\alpha + \epsilon) \cos \epsilon \, (\Delta A)}{\Delta x \, (S_{ref})}$$

$$\frac{dC_A}{dx} = \frac{\Delta C_A}{\Delta x} = \frac{2 \sin^2 (\alpha + \epsilon) \sin \epsilon \, (\Delta A)}{\Delta x \, (S_{ref})} = \frac{dC_N}{dx} \tan \epsilon$$

The load distribution at landing with flaps down is presented in Figure 8.2-10. It was assumed that the angle of attack at touchdown could be no more than 10 degrees.

8.2.4 Structural Loads (12,500-Pound-Payload Class)

Structural loads were computed for the 12,500-pound baseline booster and orbiter vehicles. The loads were generated by a modified rigid-body analysis. Load stations and the sign convention used for loads computation

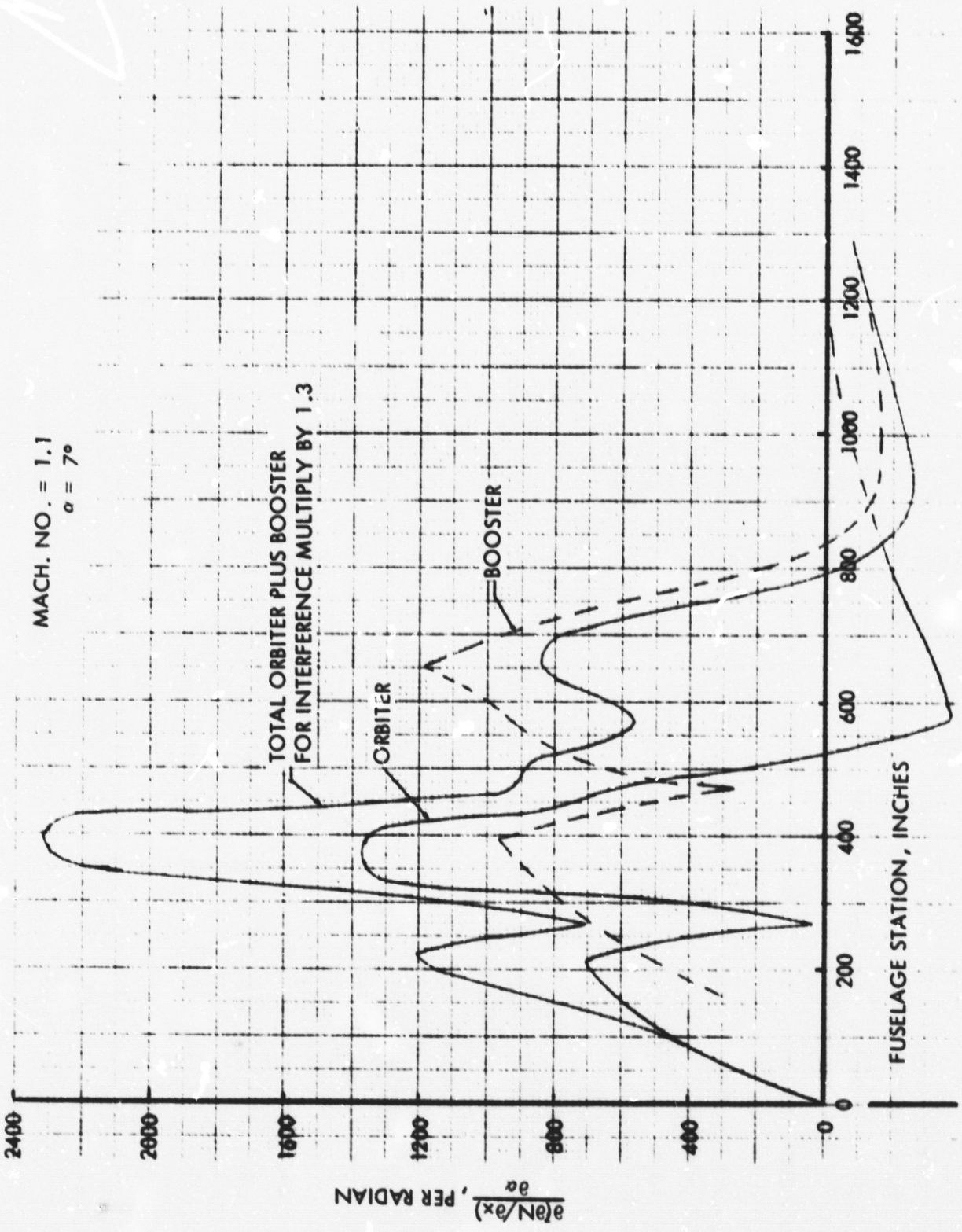

Figure 8.2-3. Normal Airload Distribution During Launch, Maximum q Alpha

TOTAL WING LOAD, LB

ANGLE OF ATTACK	BOOSTER	ORBITER
4°	725,000	228,000
7°	995,000	314,000
10°	1,265,000	362,000

SPANWISE C.P. AT MAC

CHORDWISE C.P. AT $\frac{X}{C}$ = 0.475

Figure 8.2-4. Effect of Angle of Attack on Airload Distribution During Launch, Maximum q Case

Figure 8.2-5. Axial Load Distribution During Launch, Maximum q Alpha

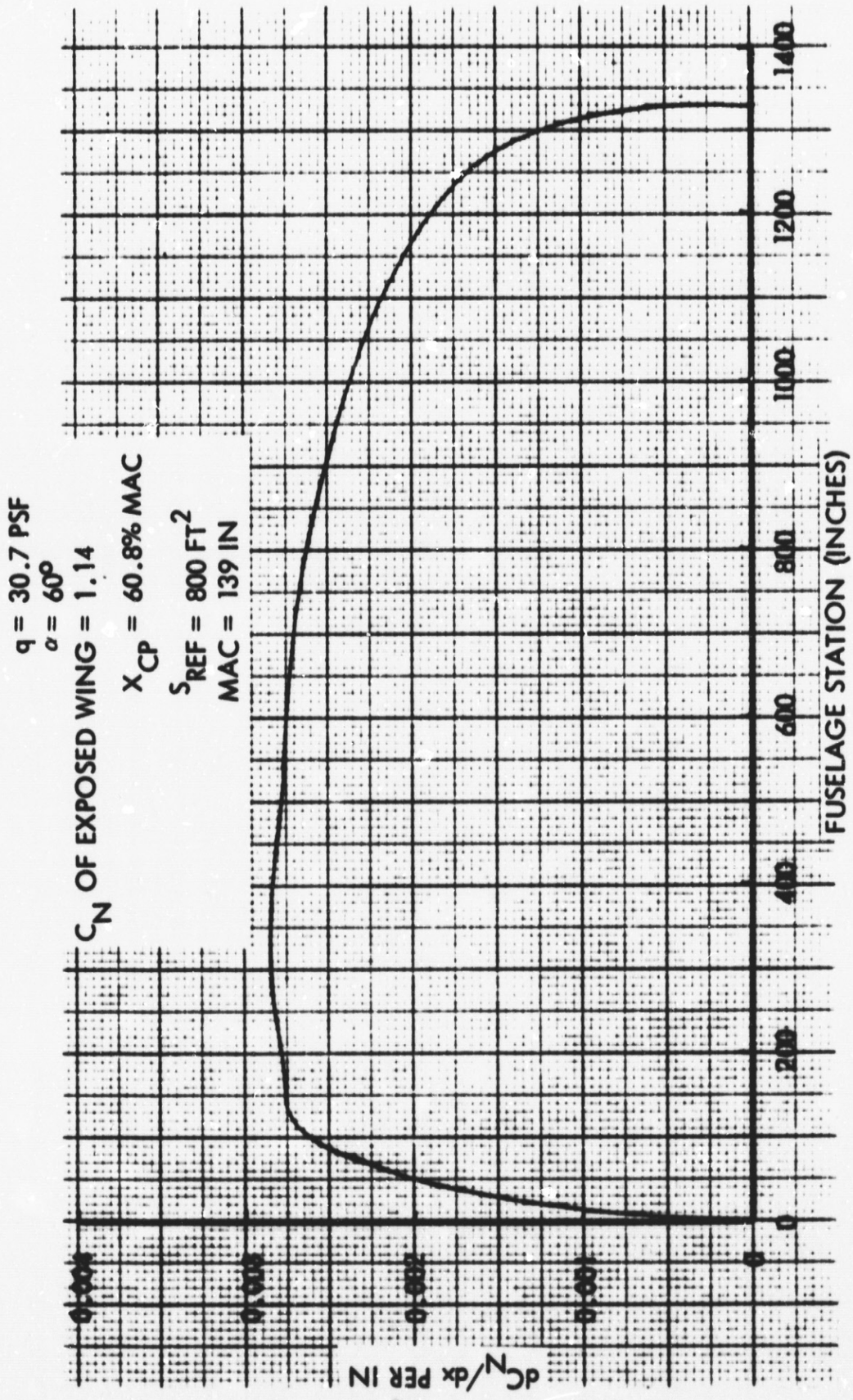

Figure 8.2-6. Normal Load Distribution During Orbiter Entry

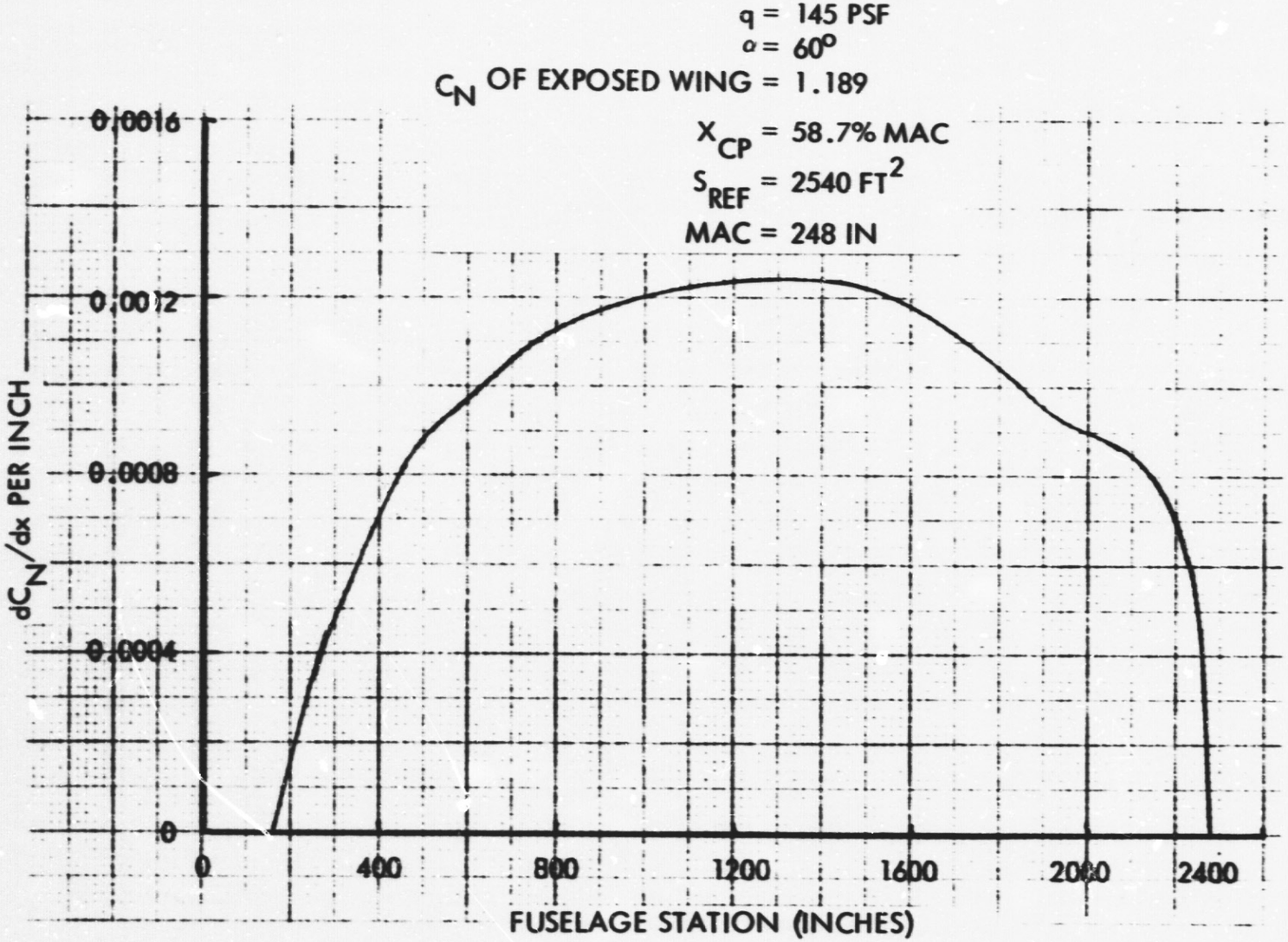

Figure 8.2-7. Normal Load Distribution During Booster Entry

Space Division
North American Rockwell

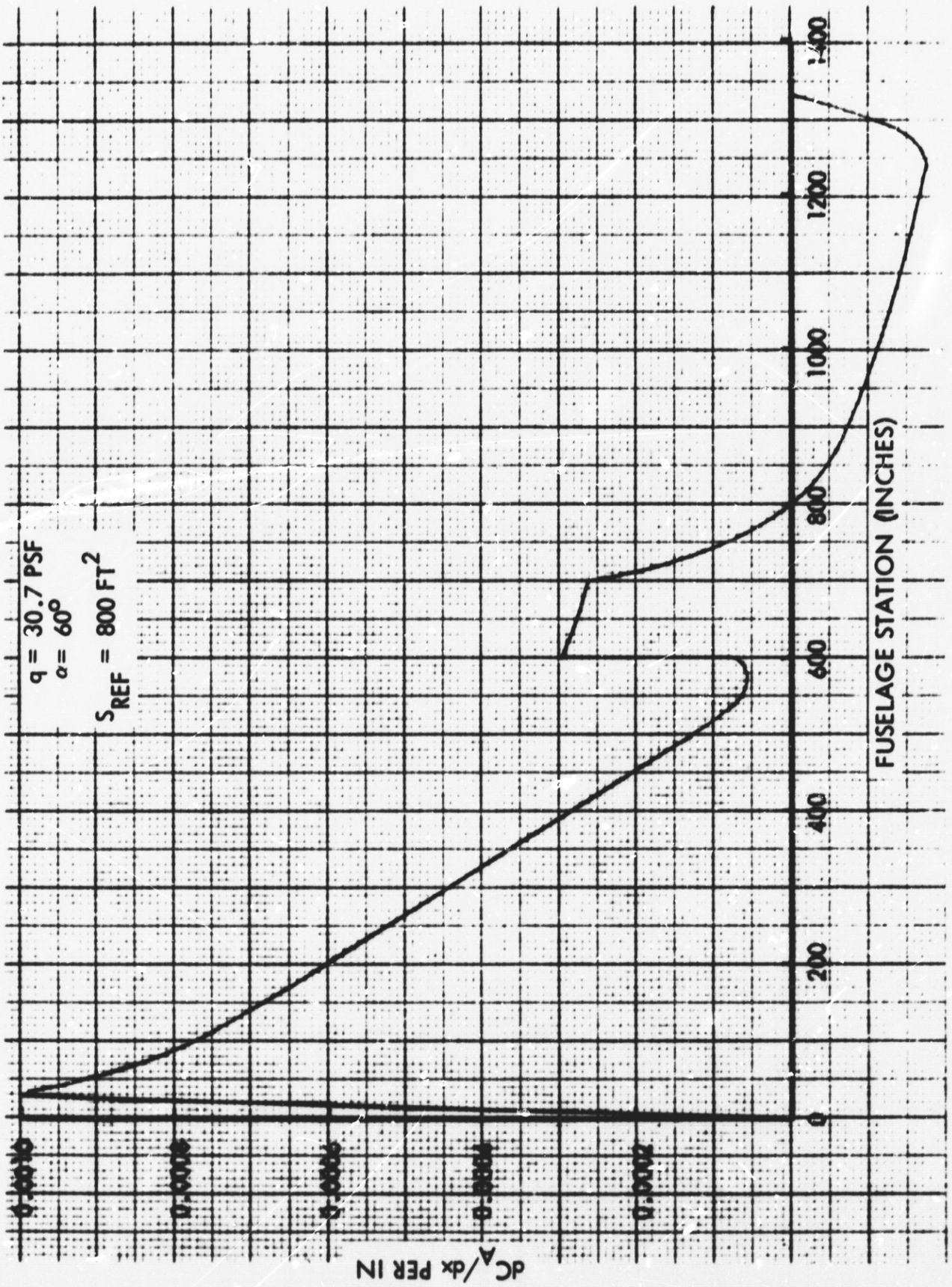

Figure 8.2-8. Axial Load Distribution During Orbiter Entry

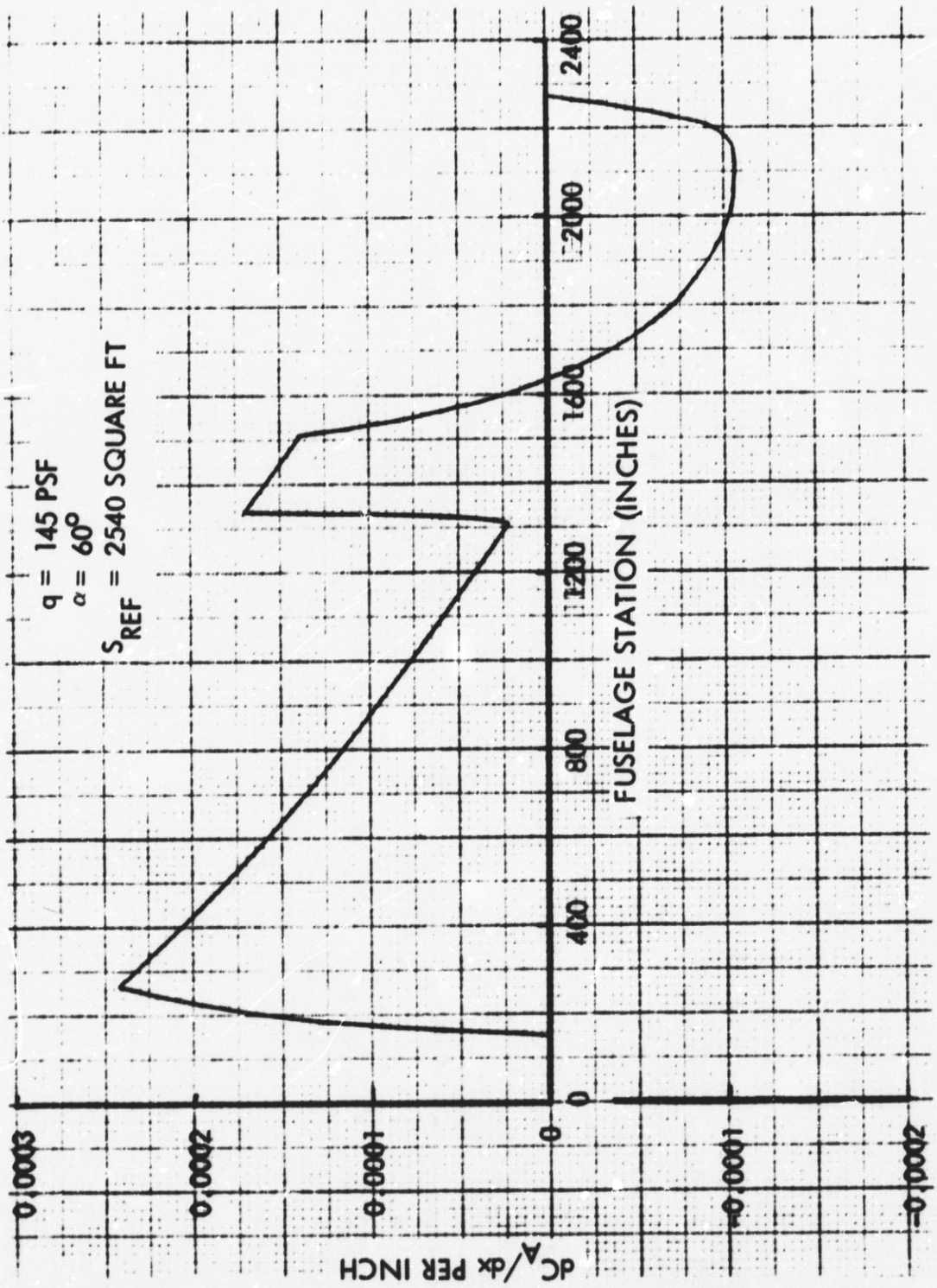

Figure 8.2-9. Axial Load Distribution During Booster Entry

Figure 8.2-10. Load Distribution During Orbiter Landing with Flaps Deflected

are shown in Figure 8.2-11. The orbiter and booster are joined by two attachments at the locations shown. The forward attachment was assumed to transmit transverse load (shear) only. The aft attachment was assumed to transmit both transverse and axial loads.

Estimated dynamic magnification factors were used to account for the following transient effects: prelaunch wind gusts and vortex shedding, horizontal gusts at maximum q α during boost, thrust-induced axial dynamics during boost, vertical gusts during subsonic cruise, and landing dynamics.

Critical body loads at certain stations of interest are summarized in Table 8.2-2. In comparing the loads, it becomes apparent that maximum q α is the most critical load condition. Subsonic maneuver during flyback and landing produce critical loads at certain locations of the orbiter and the booster. Prelaunch is the design condition for the hold-down of the vehicle at the aft end of the booster.

Detailed loads are presented in Figures 8.2-12 through 8.2-29. Loads on the booster fuselage are given in Figures 8.2-12 through 8.2-19. Orbiter body loads are presented in Figures 8.2-20 through 8.2-27 for the following conditions:

1. Prelaunch - 99.9 percentile ground winds
2. Maximum q α - angle of attack 7 degrees = 2940 psf-deg
3. Maximum acceleration first stage - 3 g's
4. Maximum acceleration second stage - orbiter only, 3 g's
5. Entry
6. Subsonic maneuver - 2.5 g's
7. Landing

The prelaunch loads in Figure 8.2-13 were computed for the booster centerline tilted 2 degrees so that the combined center of gravity of the fueled booster and orbiter lies over the center of the hold-down locations at the base of the booster. If there were no 2-degree tilt, the maximum base bending moment shown in Figure 8.2-13 would increase by a factor of 2 because of the offset orbiter.

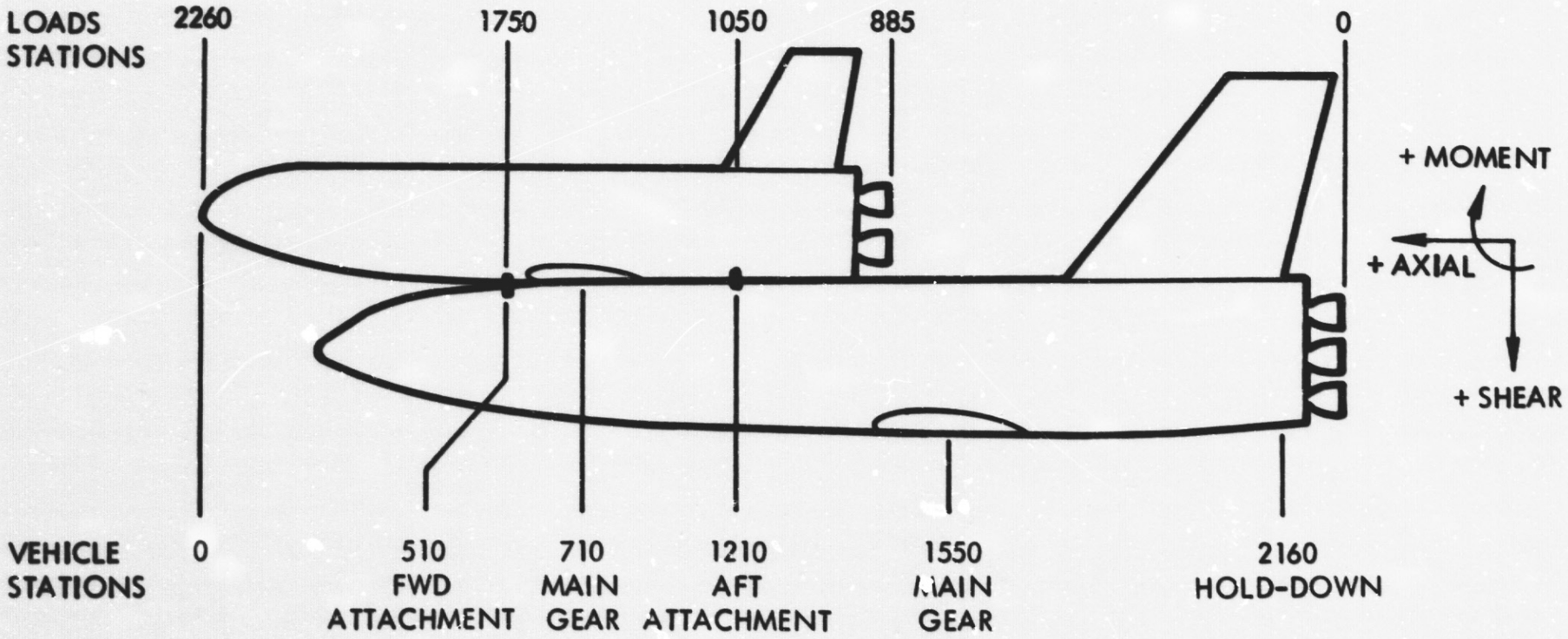

LOADING CONDITIONS

- PRE-LAUNCH
- MAXIMUM $q\alpha$ BOOST = 2340 PSF
- MAXIMUM ACCELERATION FIRST STAGE
- MAXIMUM ACCELERATION SECOND STAGE
- ENTRY
- SUBSONIC MANEUVER
- LANDING

Figure 8.2-11. Structural Loading Conditions

Table 8.2-2. Structural Design Loads Summary (12,500-Pound-Payload Class)

Loads Stations	Condition	Limit Loads		
		Shear x 10^{-3} (lb)	Axial x 10^{-3} (lb)	Moment x 10^{-6} (in.-lb)
Booster				
Hold-down station	Pre-launch	-68	-1351	132 (no tilt) 65 (tilt)
Main landing gear	Max qα	-470	-1750	-160
	Landing	-150	-85	-95
Aft attachment	Max qα	340	-1561	-66
	Landing	95	-30	-60
Forward attachment	Landing	46	-15	-9
	Max qα	-31	-113	5
Orbiter				
Aft attachment	Max accel	-3	-960	-
	Max qα	-24	-610	-16
Main landing gear	Max qα	-86	-477	-36
	Landing	-60	-35	-28
Forward attachment	Landing	62	-21	-18

Space Division
North American Rockwell

Wing and tail loads are listed in Figure 8.2-28. The wing loads are computed for the critical maximum $q\alpha$ and subsonic 2.5'g maneuver conditions. The vertical tail loads are computed for the maximum $q\alpha$ condition only.

The loads on the attachments joining the booster and orbiter are given in Figure 8.2-29. These loads are computed for the maximum $q\alpha$ and the first-stage maximum acceleration conditions.

Figure 8.2-12. Booster Fuselage Bending Moments, 12,500-Pound Payload Class

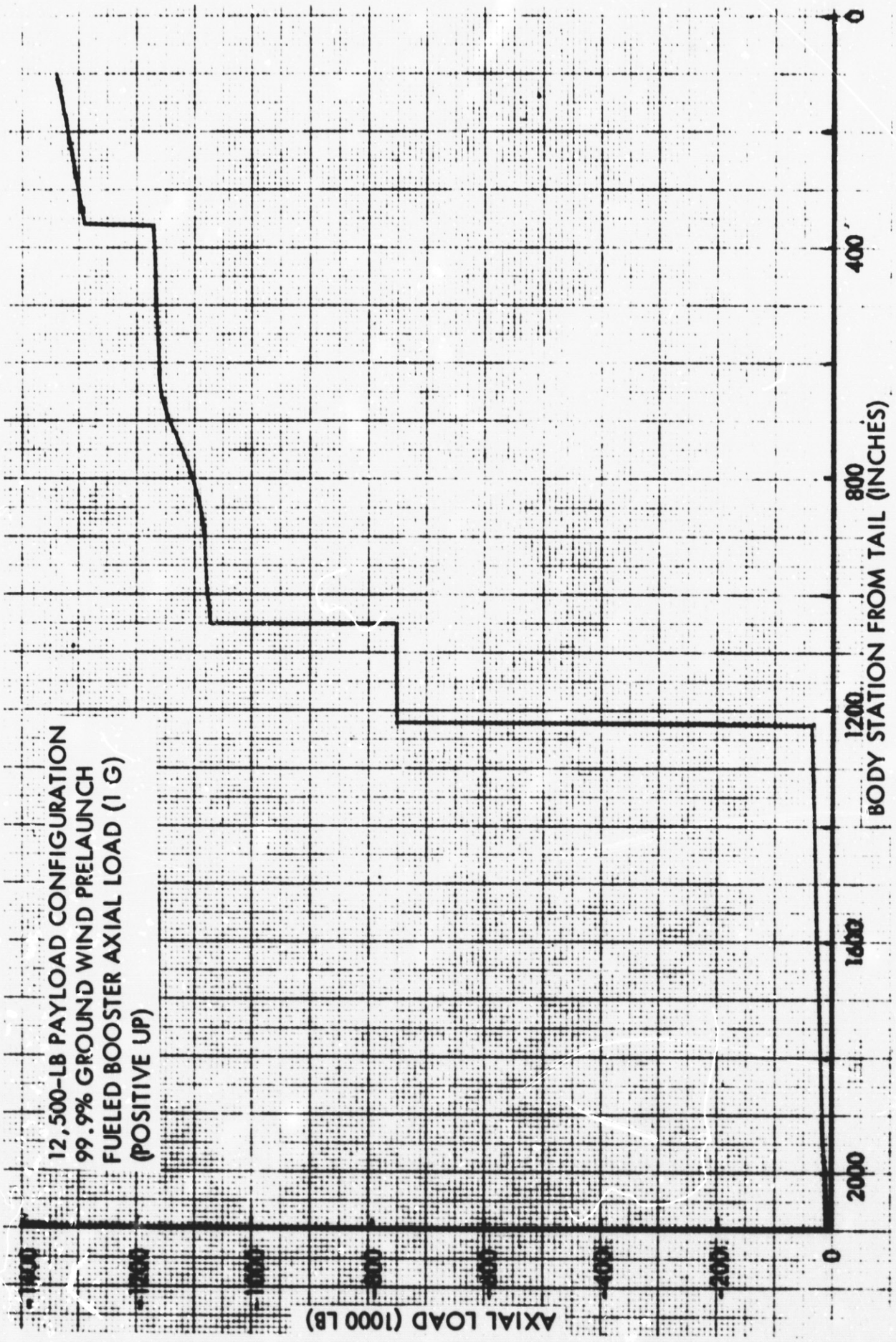

Figure 8.2-13. Booster Prelaunch Loads (Sheet 1 of 3)

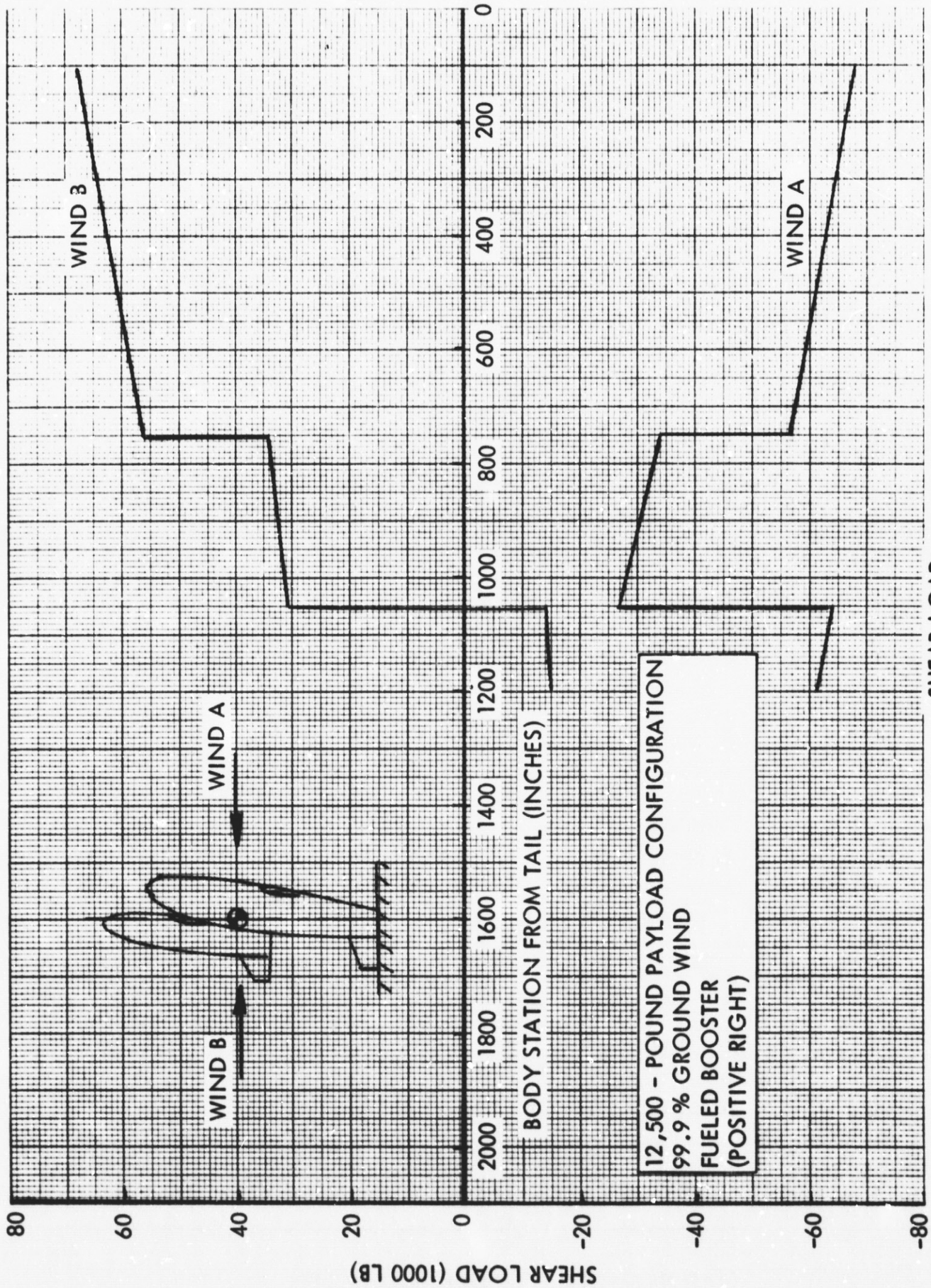

Figure 8.2-13. Booster Prelaunch Loads (Sheet 2 of 3)

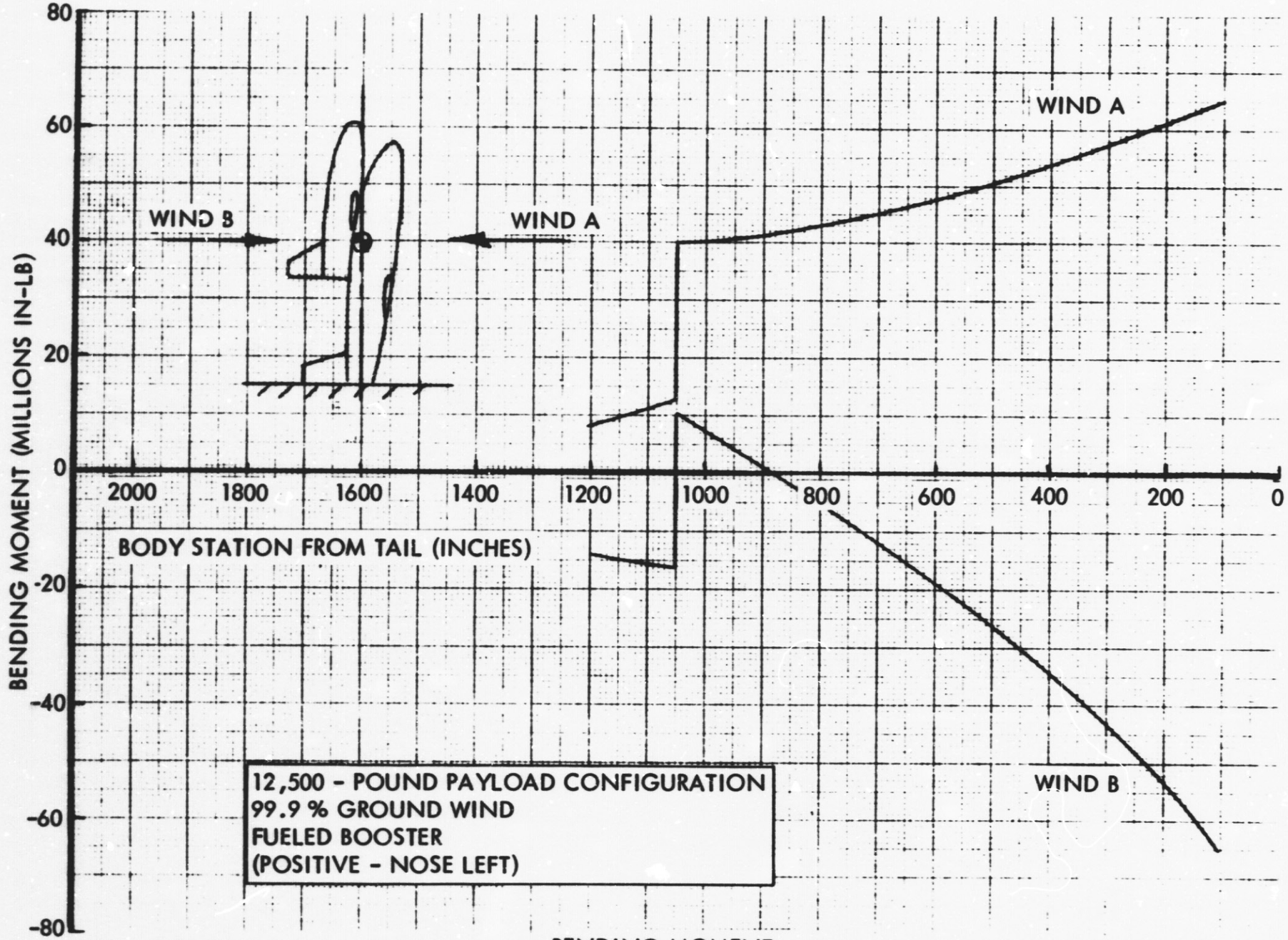

Figure 8.2-13. Booster Prelaunch Load (Sheet 3 of 3)

Space Division
North American Rockwell

12,500 - POUND PAYLOAD CLASS
BOOSTER LIMIT NET LOADS
MAXIMUM $q\alpha$ BOOST
M = 1.1 q = 420 PSF
α = 7° n_x = 1.46 G'S

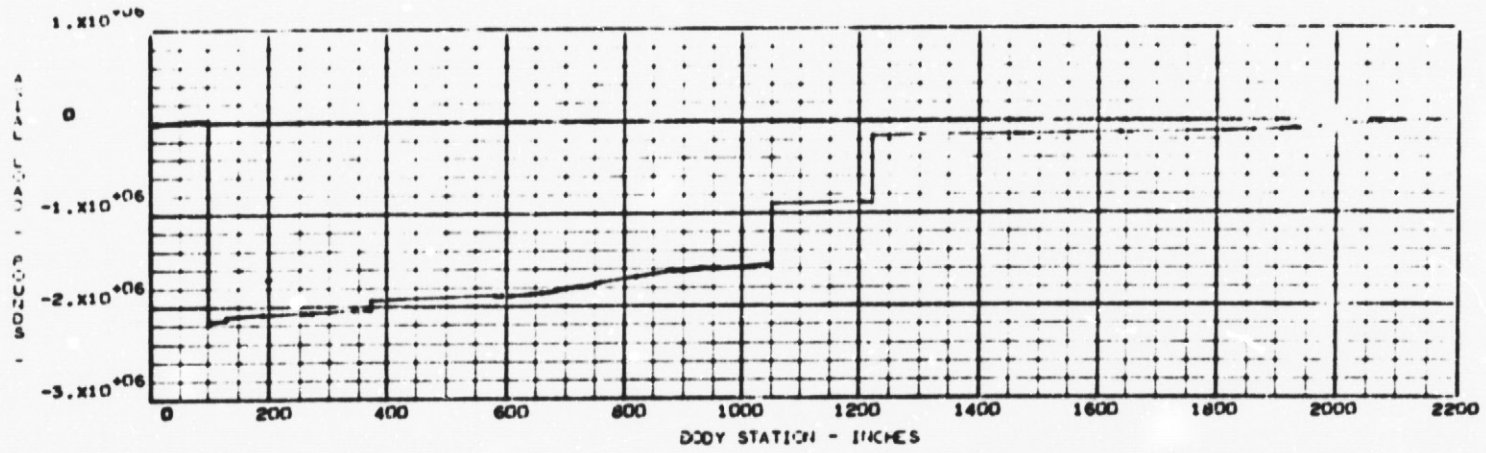

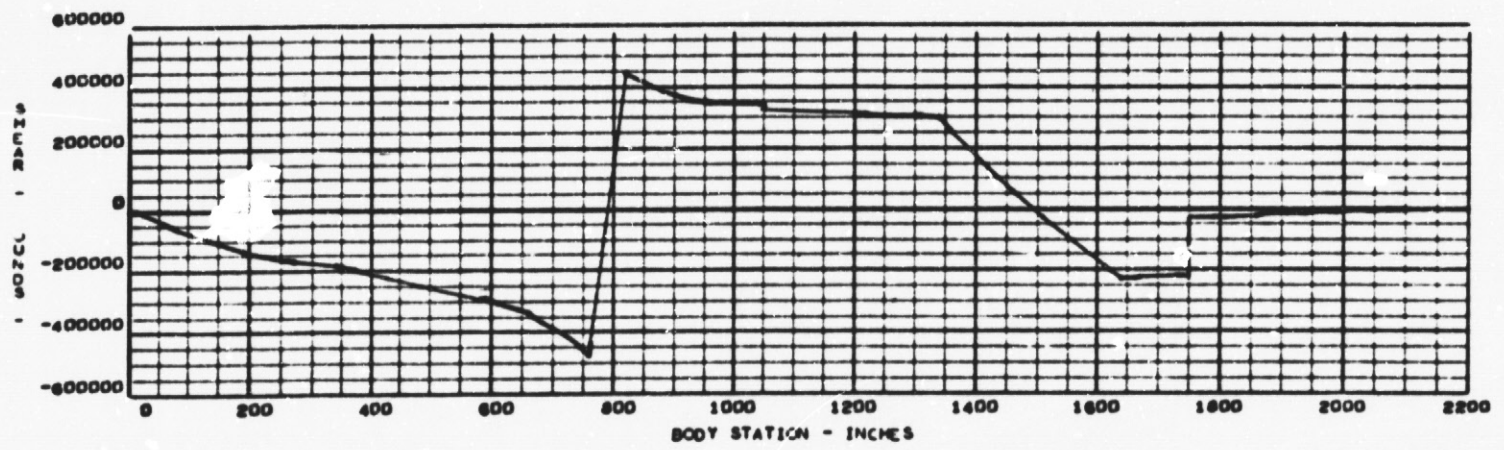

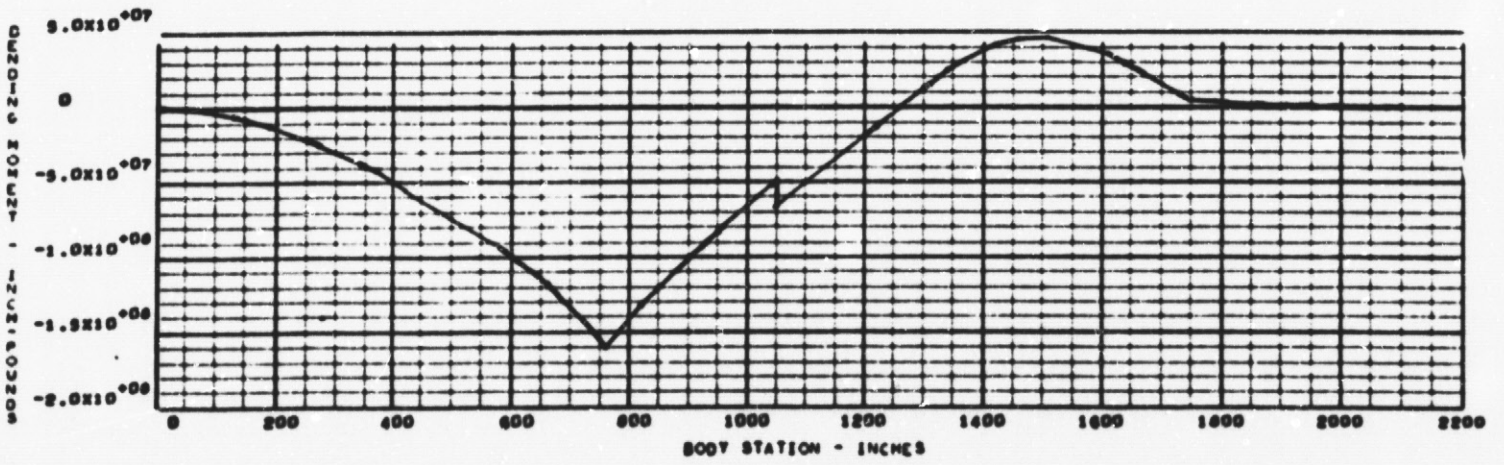

Figure 8.2-14. Booster Limit Net Loads During Maximum q Alpha

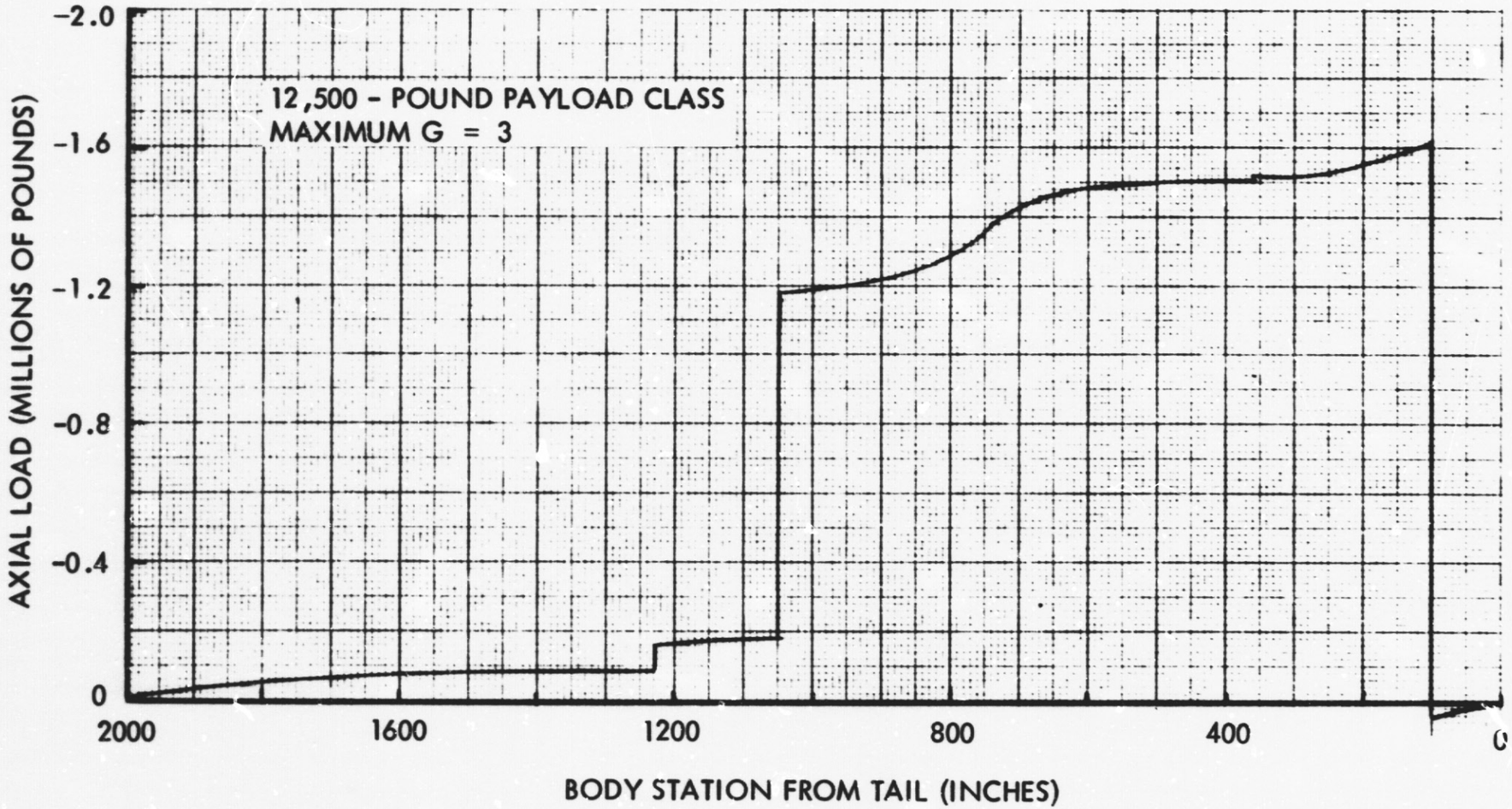

Figure 8.2-15. Booster Axial Load at Maximum Acceleration (End First Stage Boost)

Space Division
North American Rockwell

12,500 - POUND PAYLOAD CLASS
MAX G (FIRST STAGE END BOOST)
n_x = 3.0 G'S
BOOSTER SHEAR AND MOMENT

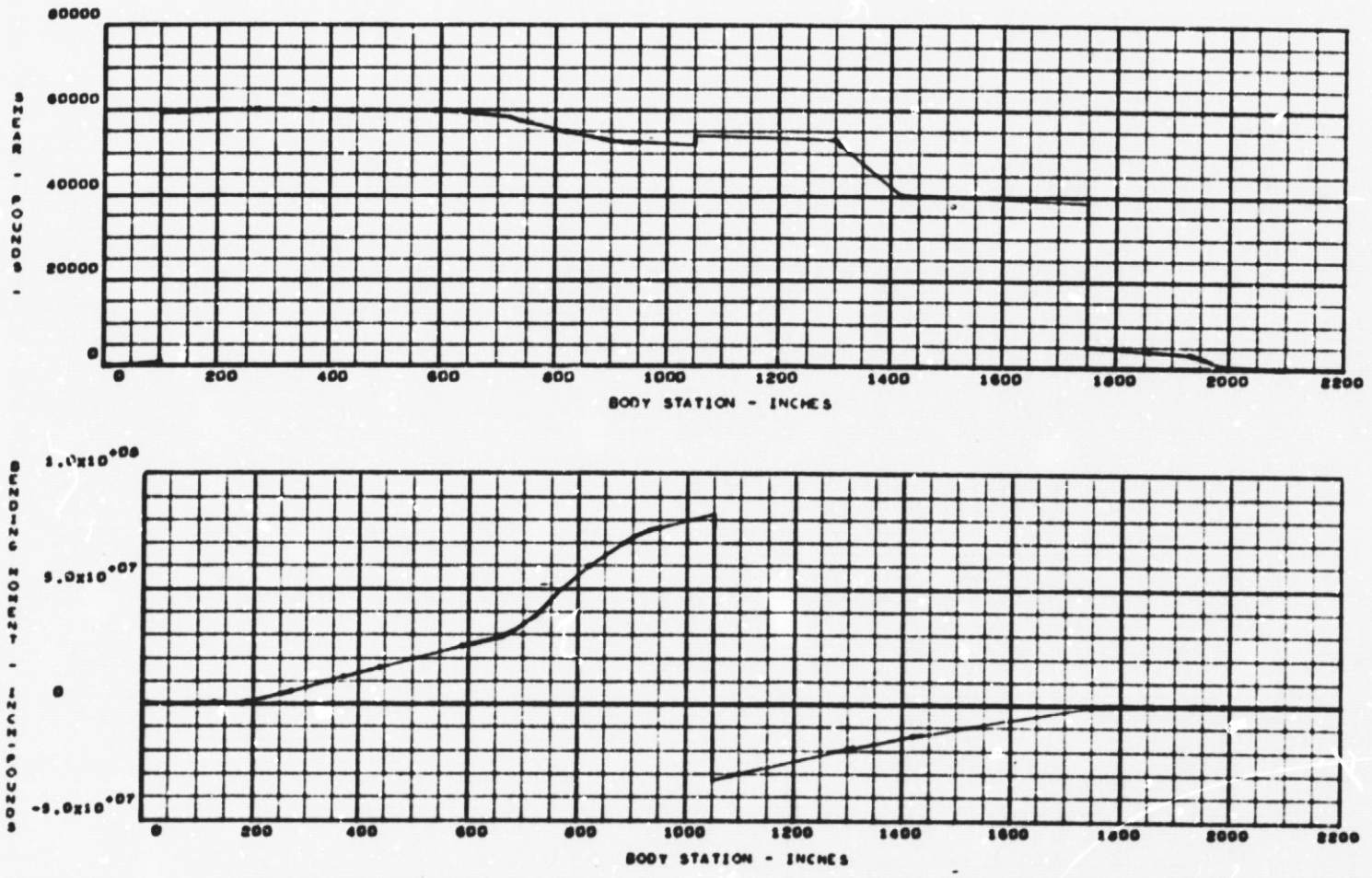

Figure 8.2-16. Booster Limit Net Loads at Maximum Acceleration

12,500 - POUND PAYLOAD CLASS
BOOSTER ENTRY CONDITION
M > 5 q = 85 PSF
α = 60° n_R = 4.0 G'S

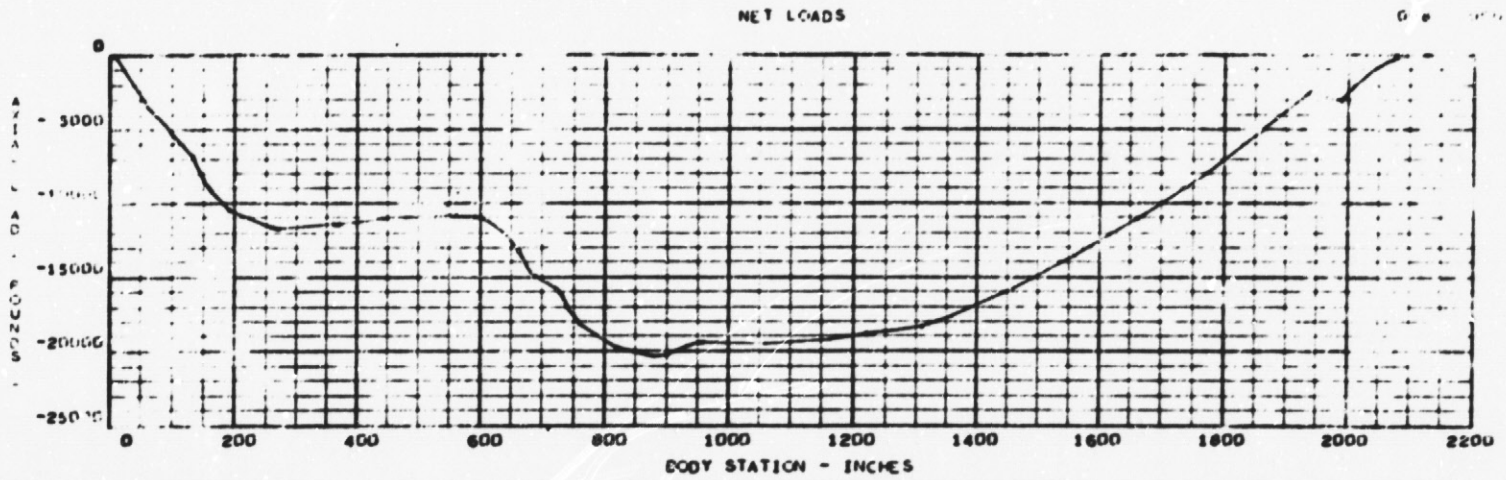

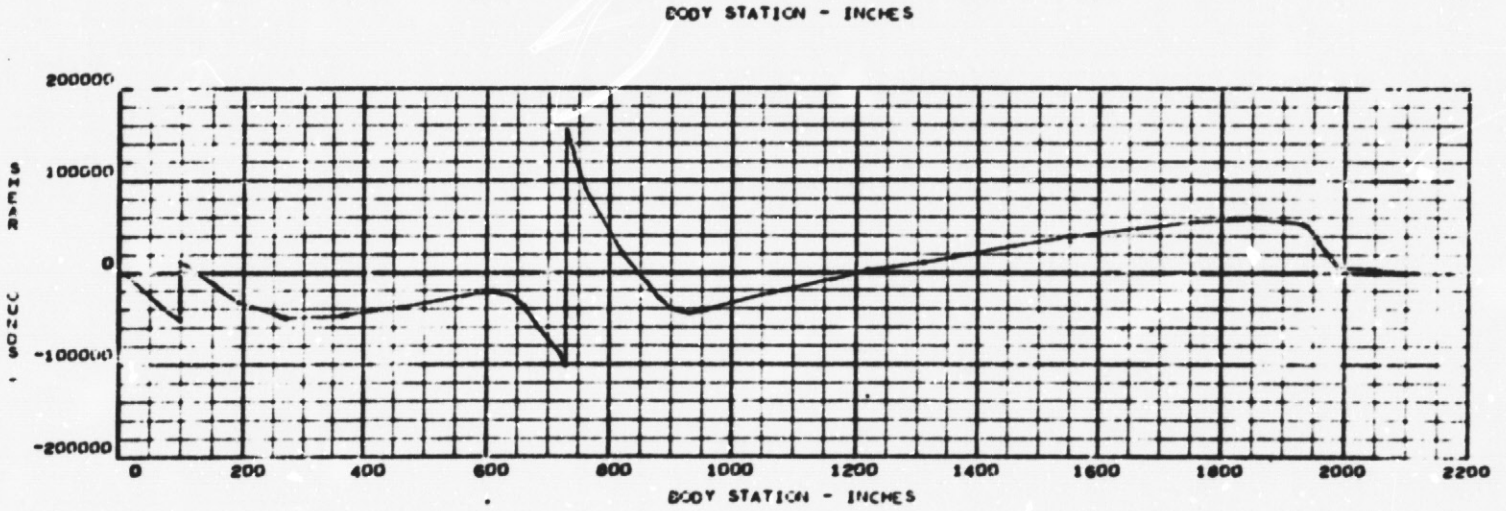

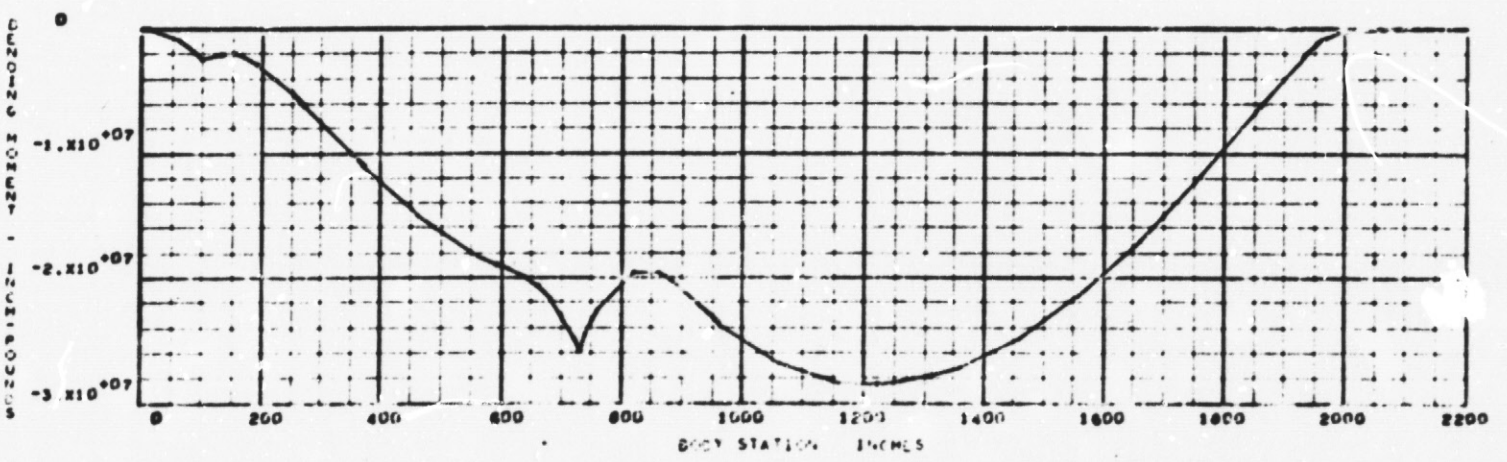

Figure 8.2-17. Booster Limit Net Loads During Entry

12,500 - POUND PAYLOAD CLASS
M = 0.66 q = 123 PSF
α = 16° n_z = 2.5 G

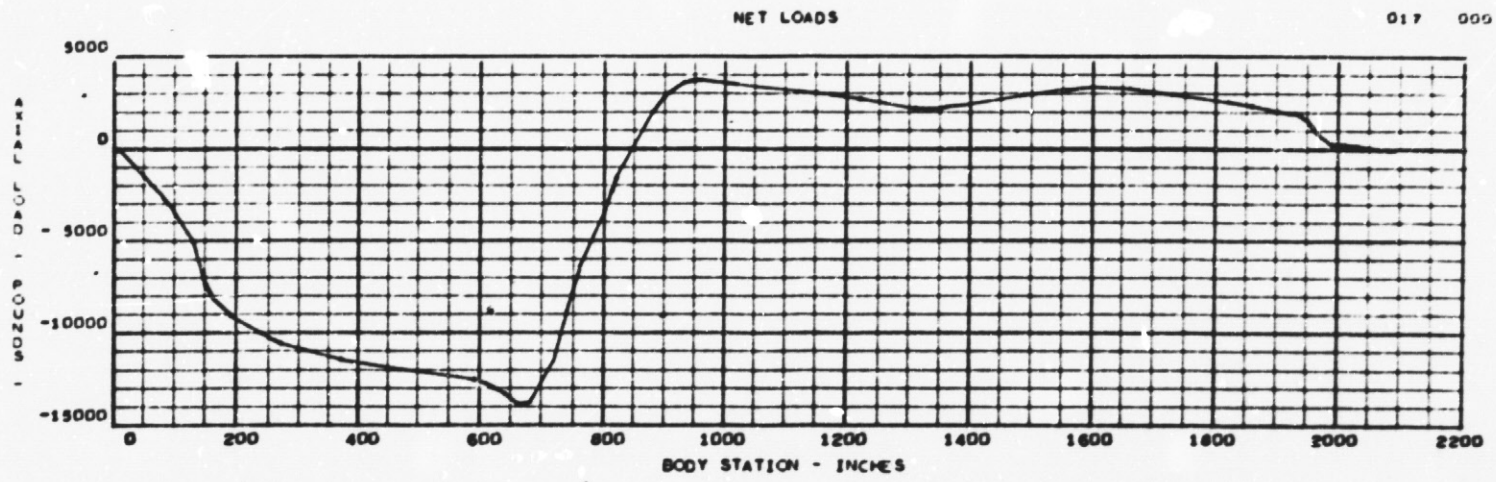

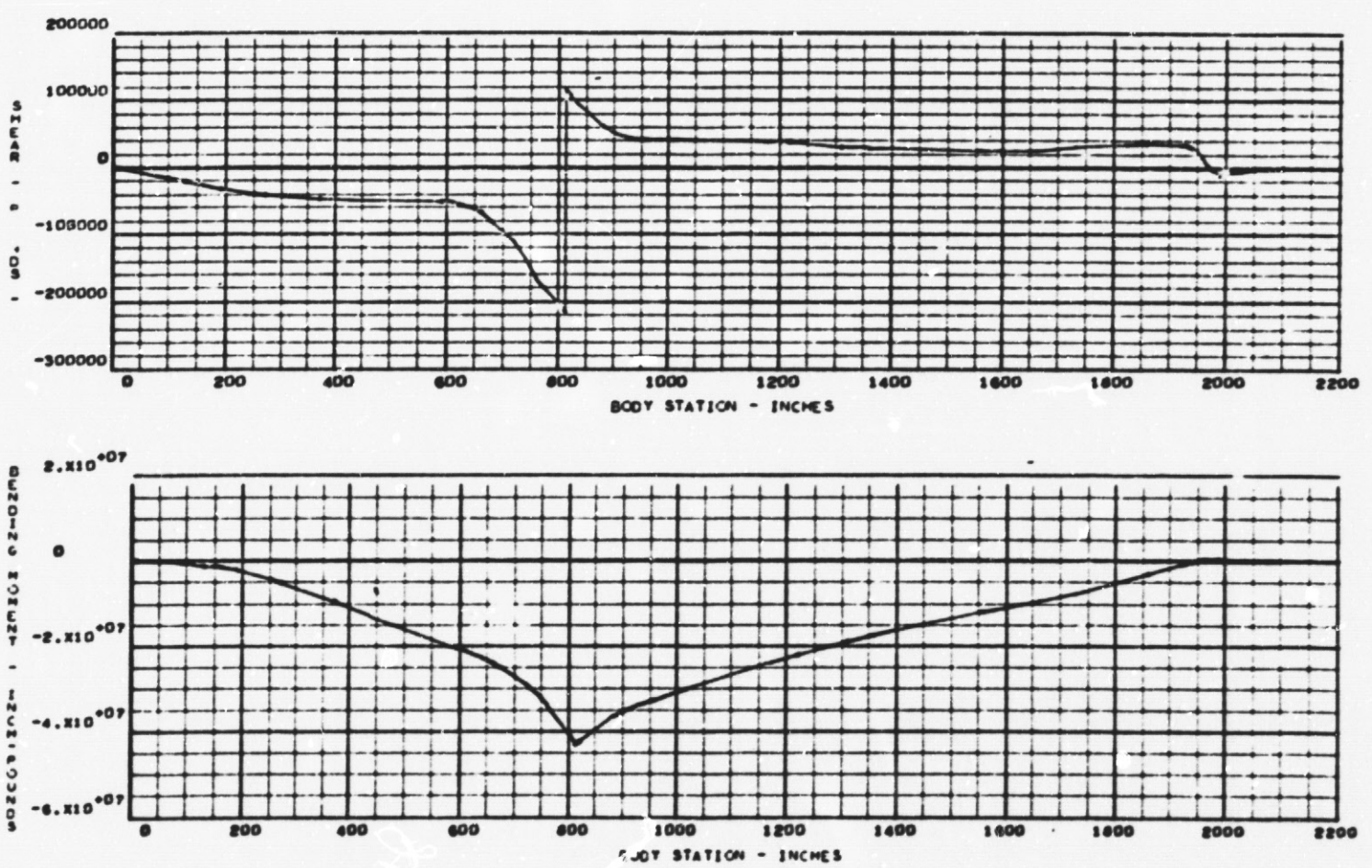

Figure 8.2-18. Booster Limit Net Loads During Subsonic Pitch-Down Maneuver

12,500 - POUND PAYLOAD CLASS
α = 10° V = 113 KTS

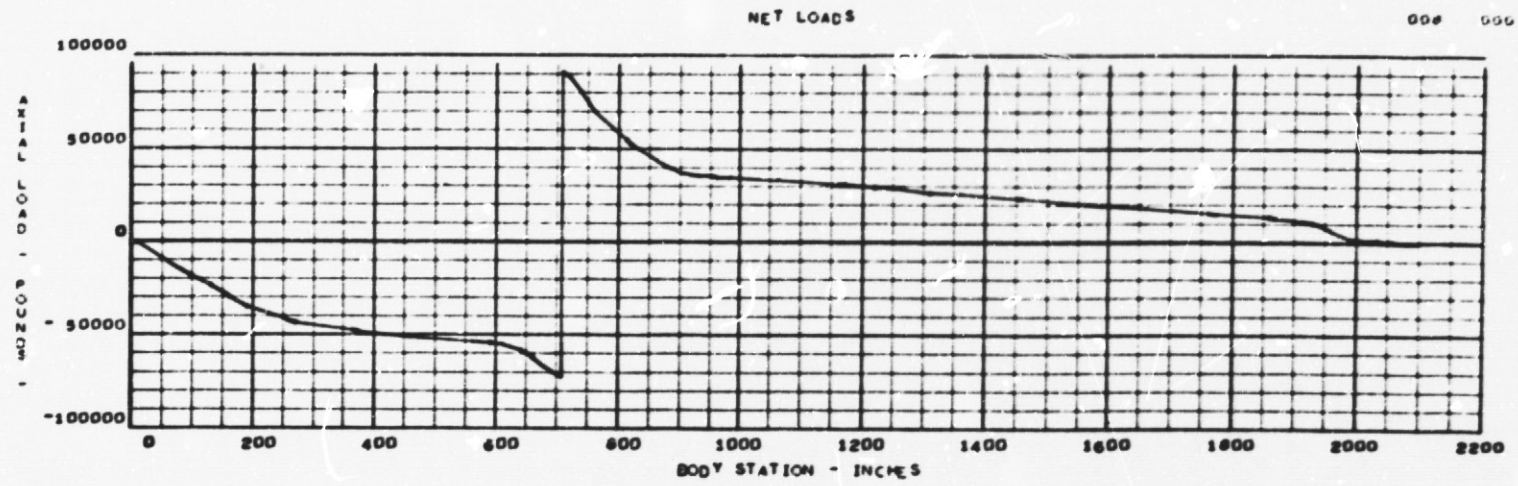

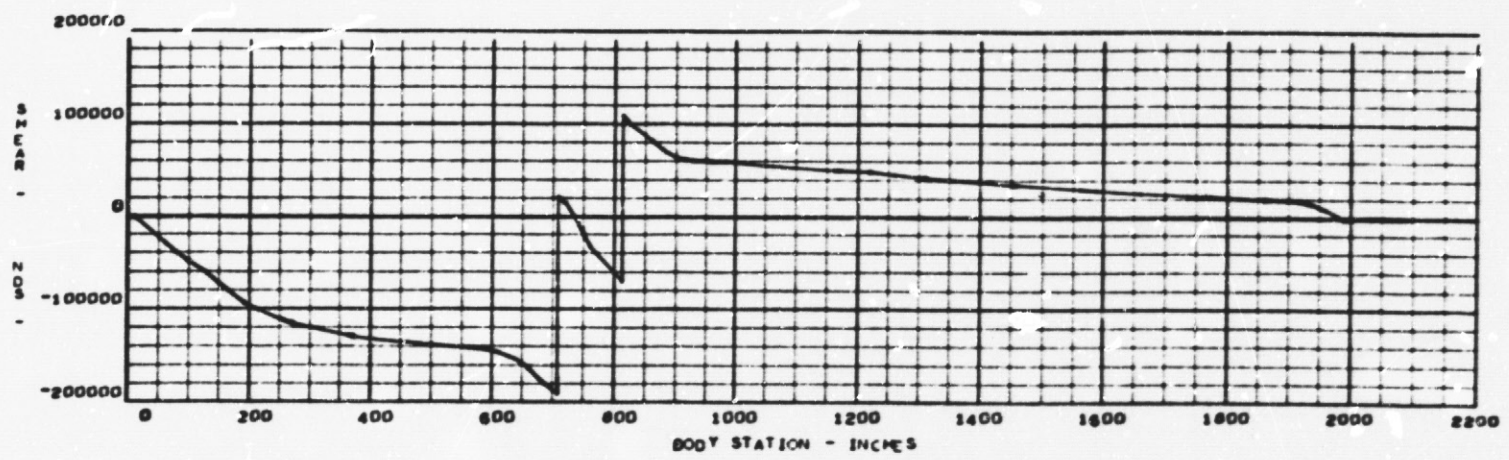

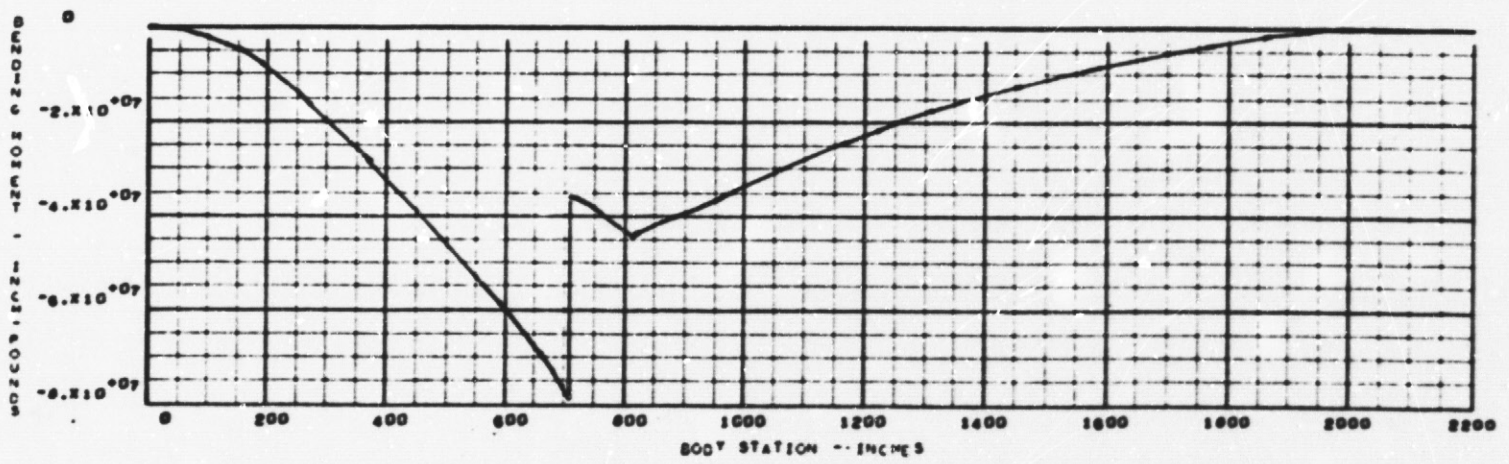

MAIN GEAR (SPIN-UP)

Figure 8.2-19. Booster Limit Net Loads During Landing (Sheet 1 of 2)

12,500 - POUND PAYLOAD CLASS
α = 10° V = 113 KTS

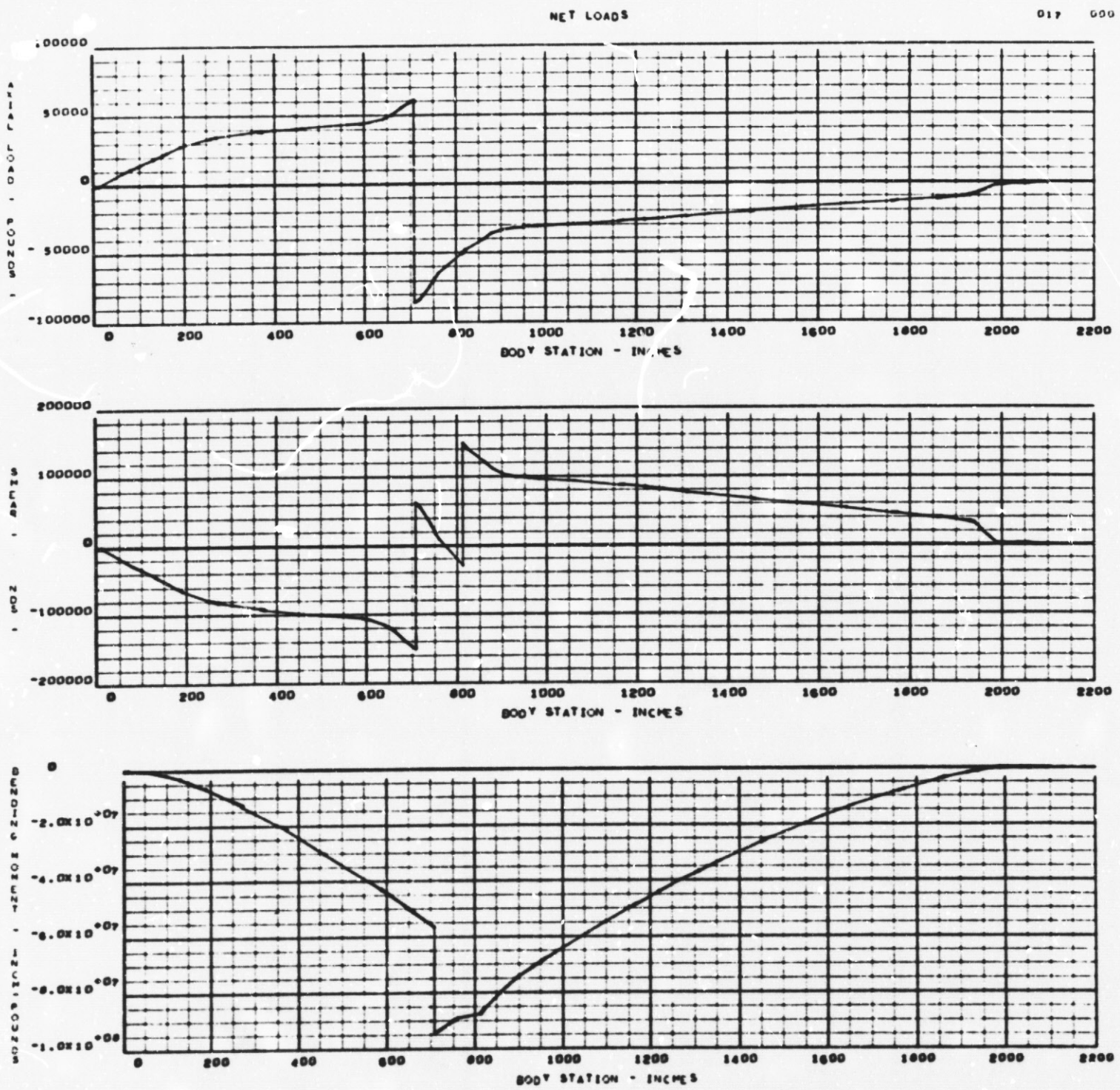

Figure 8.2-19. Booster Limit Net Loads During Landing (Sheet 2 of 2)

Figure 8.2-20. Orbiter Fuselage Bending Moments

Space Division
North American Rockwell

12,500 - POUND PAYLOAD CLASS
M = 1.1 q = 420 PSF
α = 7° n_X = 1.46 G'S

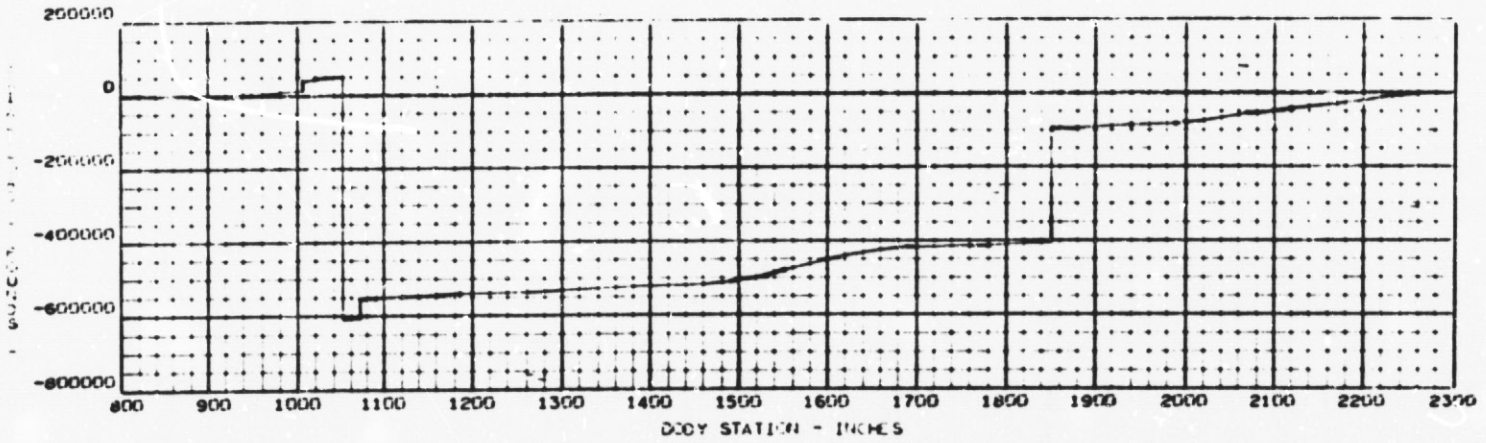

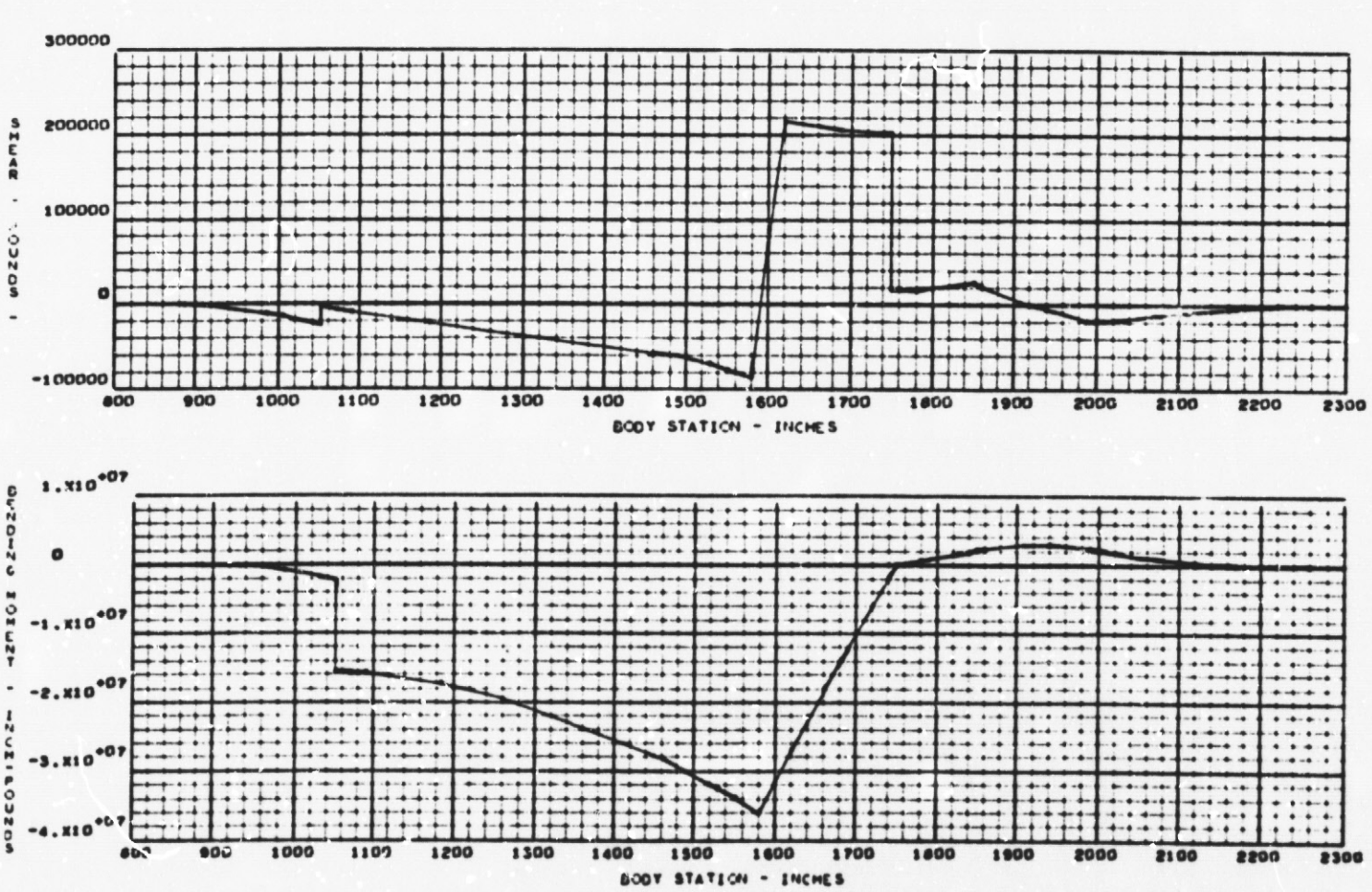

Figure 8.2-21. Orbiter Limit Net Loads During Maximum q Alpha

12,500 - POUND PAYLOAD CLASS
MAX G (FIRST STAGE END BOOST) 3 G

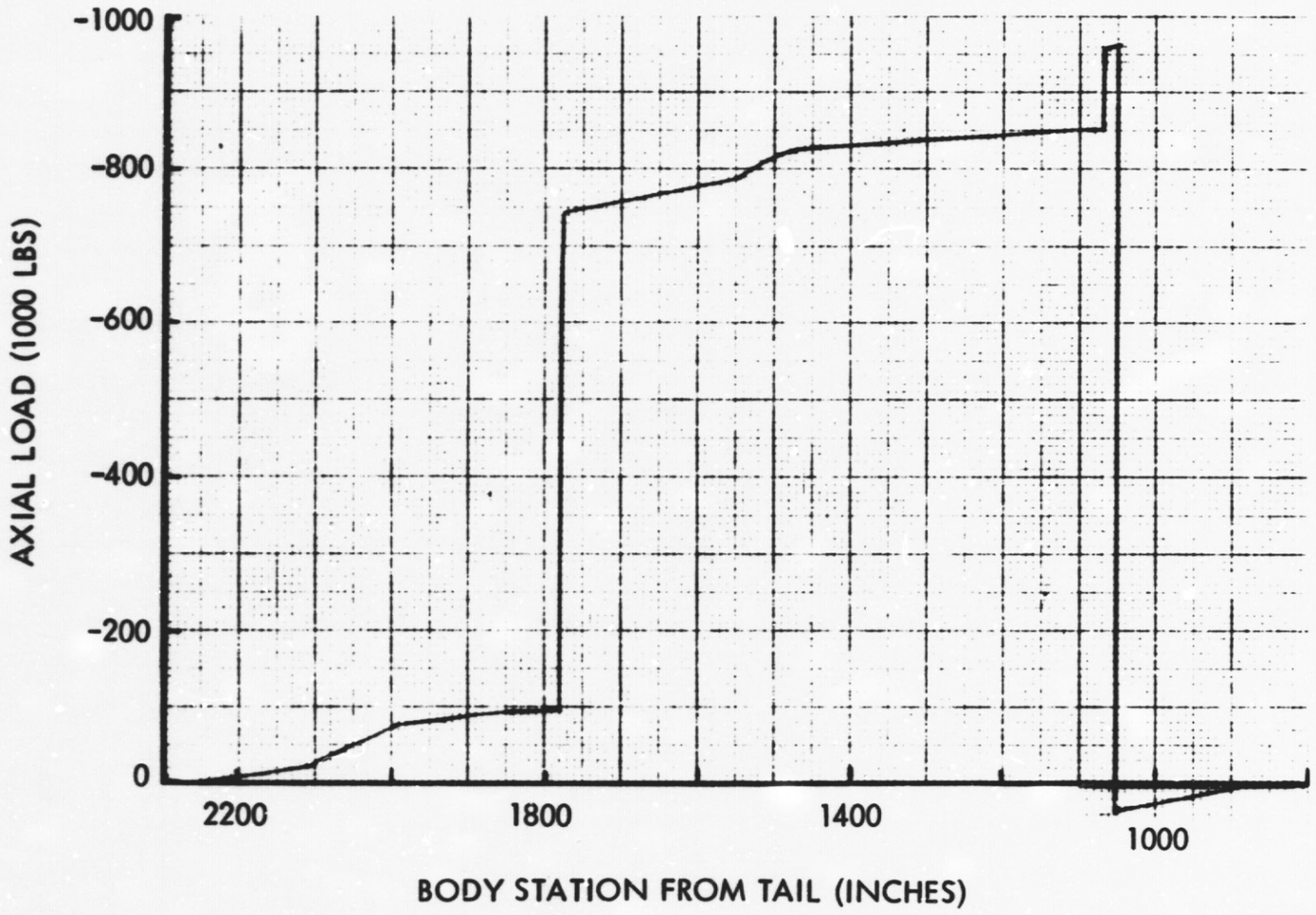

Figure 8.2-22. Orbiter Axial Load at Maximum Acceleration (End First Stage Boost)

12,500 - POUND PAYLOAD CLASS
FIRST STAGE END BOOST
n_x = 3.0 G'S

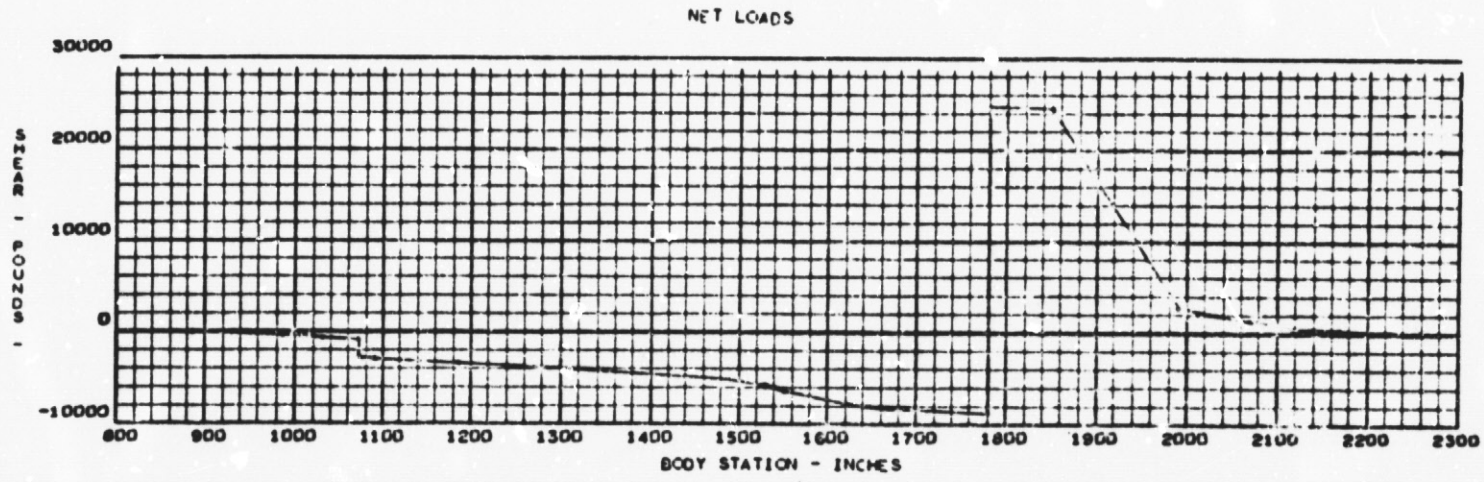

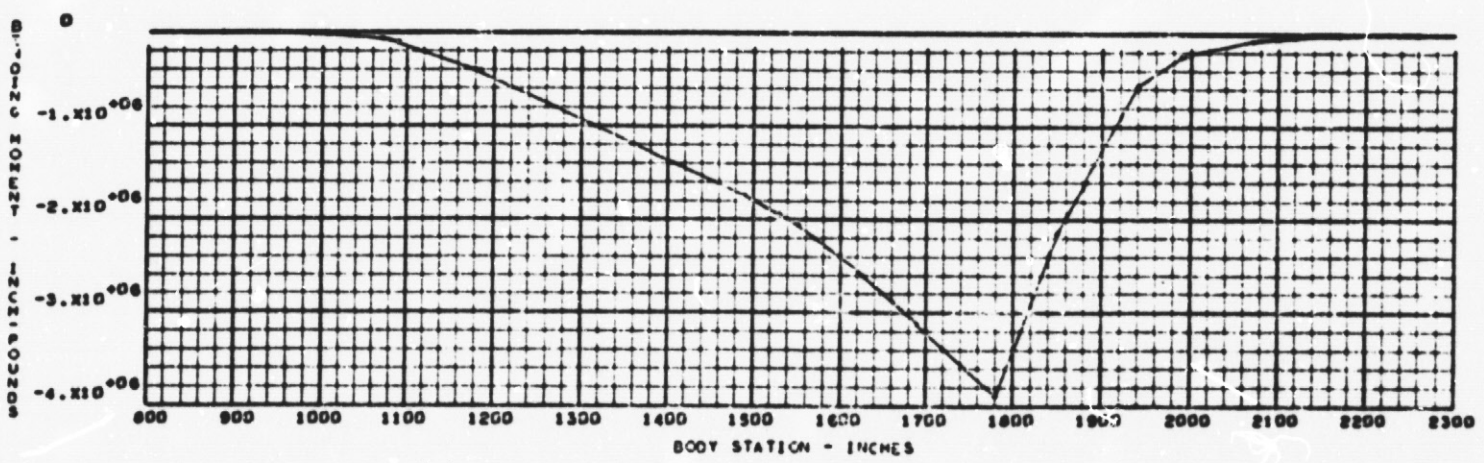

Figure 8.2-23. Orbiter Limit Shear and Moment Loads, Maximum Acceleration

12,500 - POUND PAYLOAD CLASS
n_x = 3.0 G'S

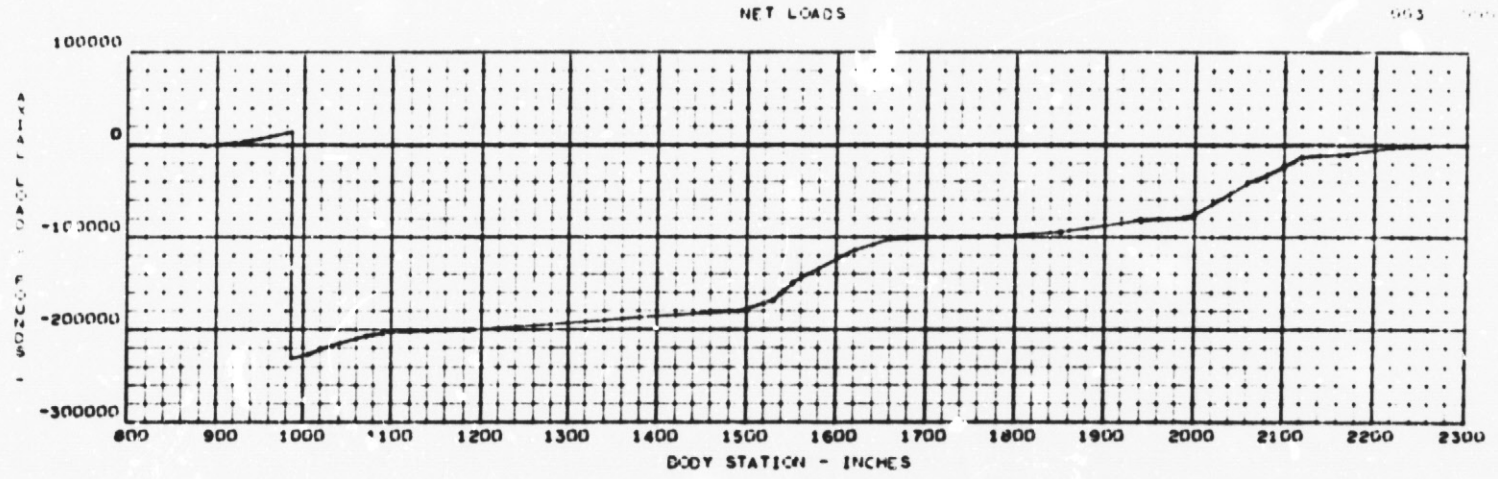

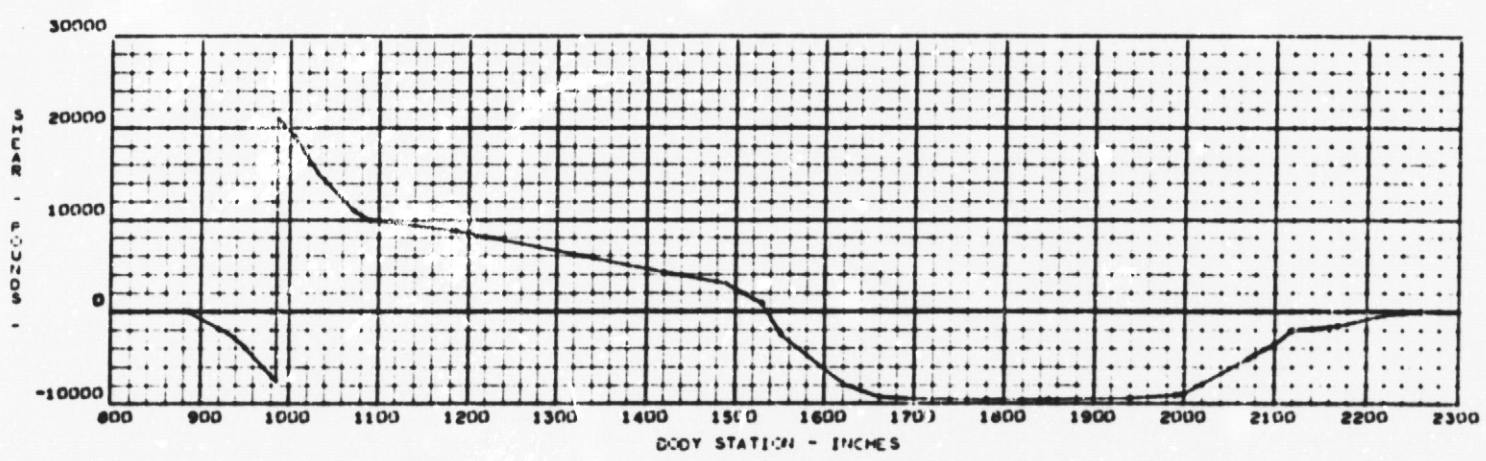

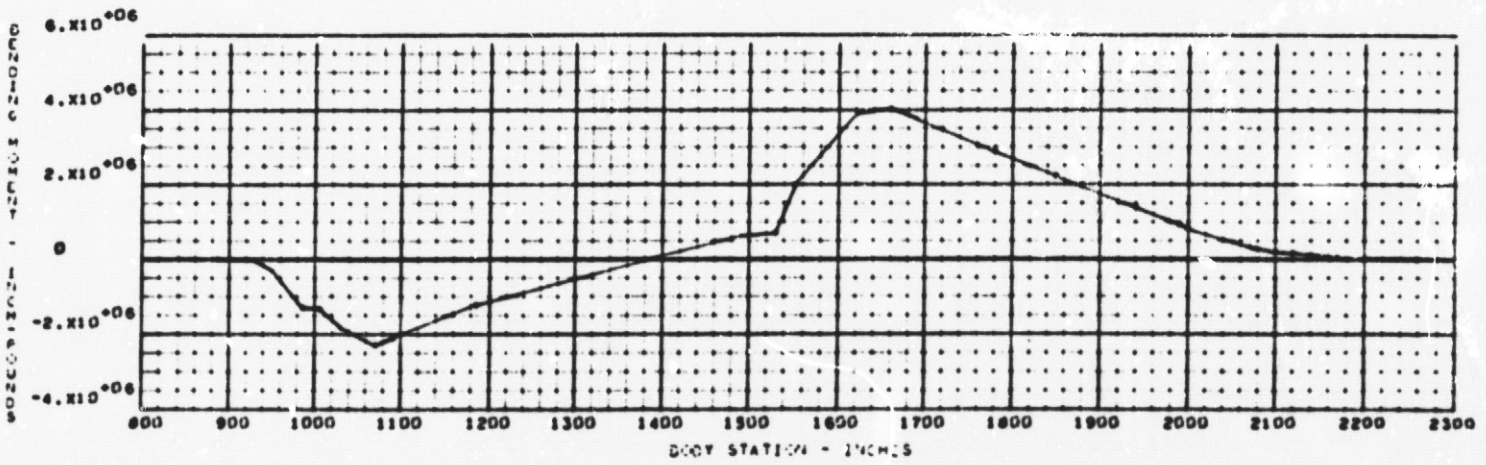

Figure 8.2-24. Orbiter Limit Net Loads, Second Stage End Boost

12,500 - POUND PAYLOAD CLASS
M > 5 α = 60° q = 40 PSF
n_r = 2.0 G'S

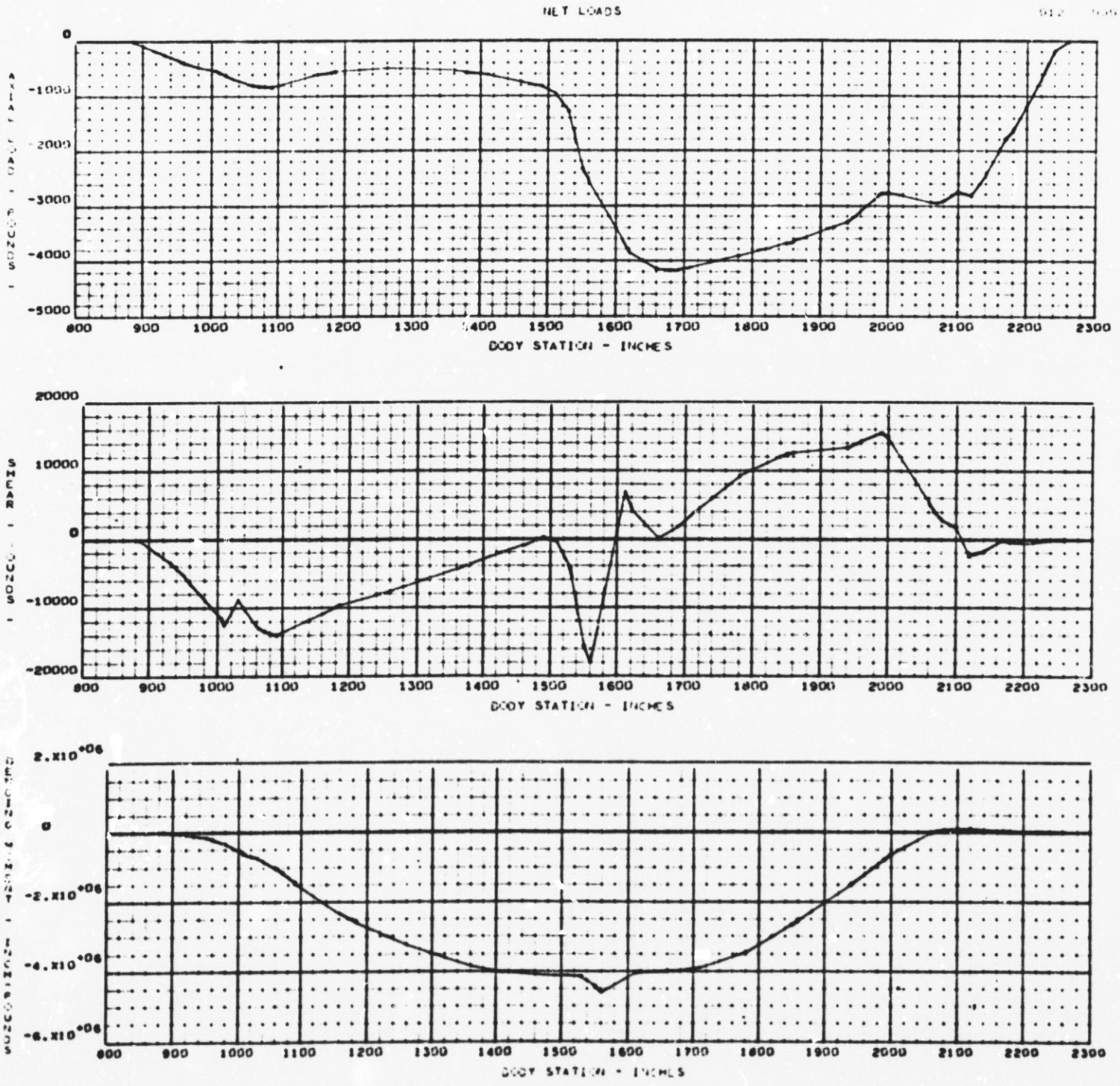

Figure 8.2-25. Orbiter Limit Net Loads During Entry

12,500 - POUND PAYLOAD CLASS
M = 0.66 q = 250 PSF
α = 16° n_z = 2.5 G

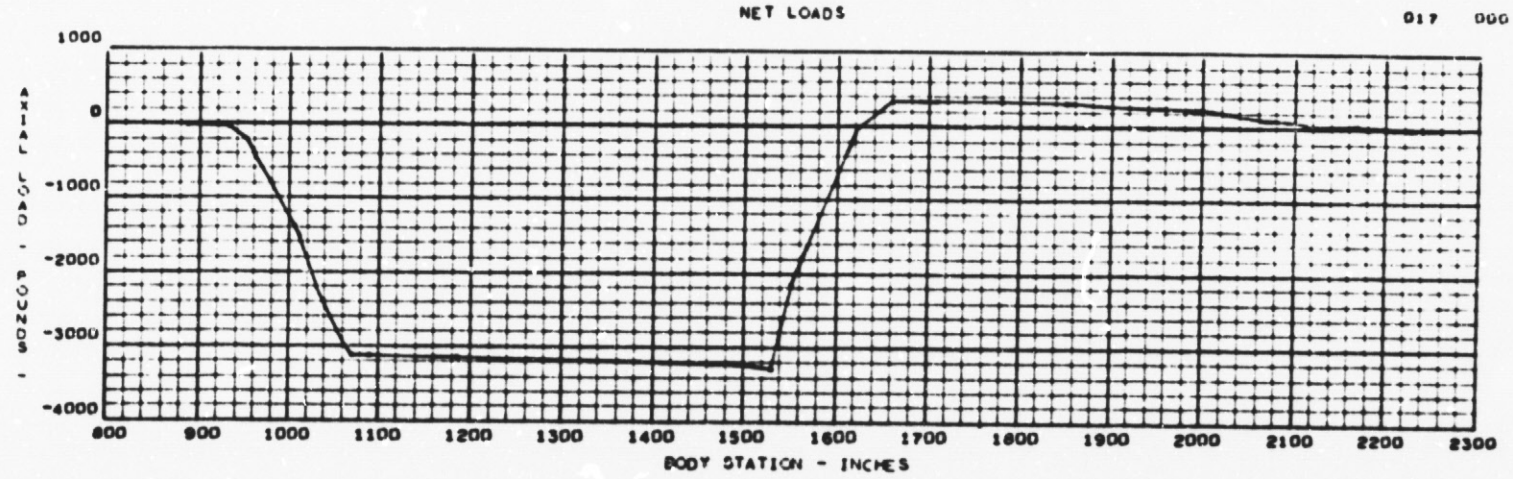

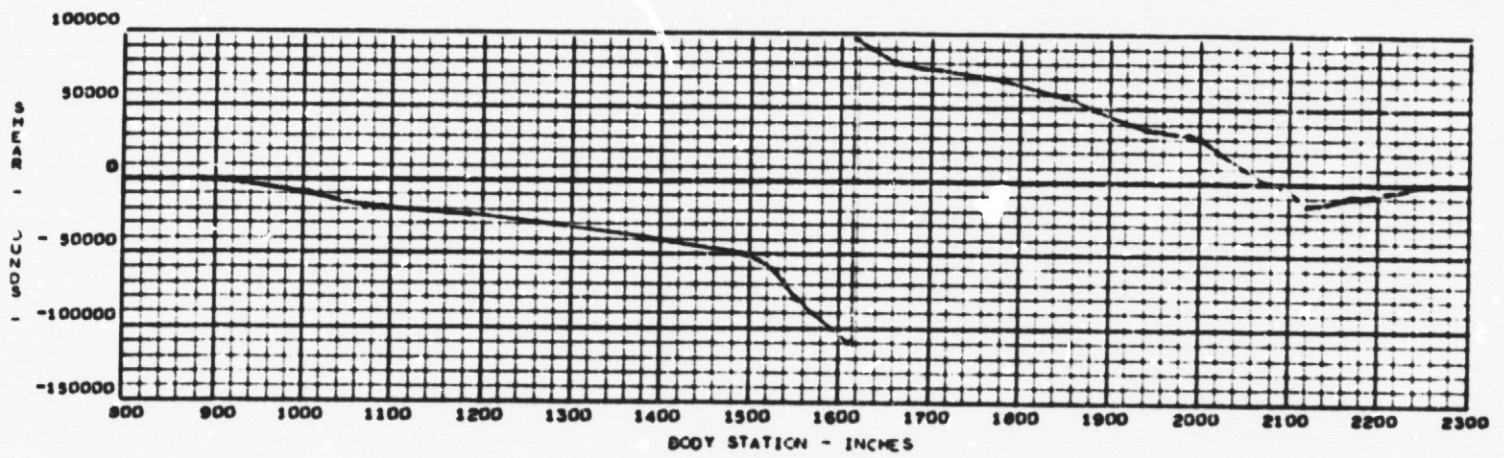

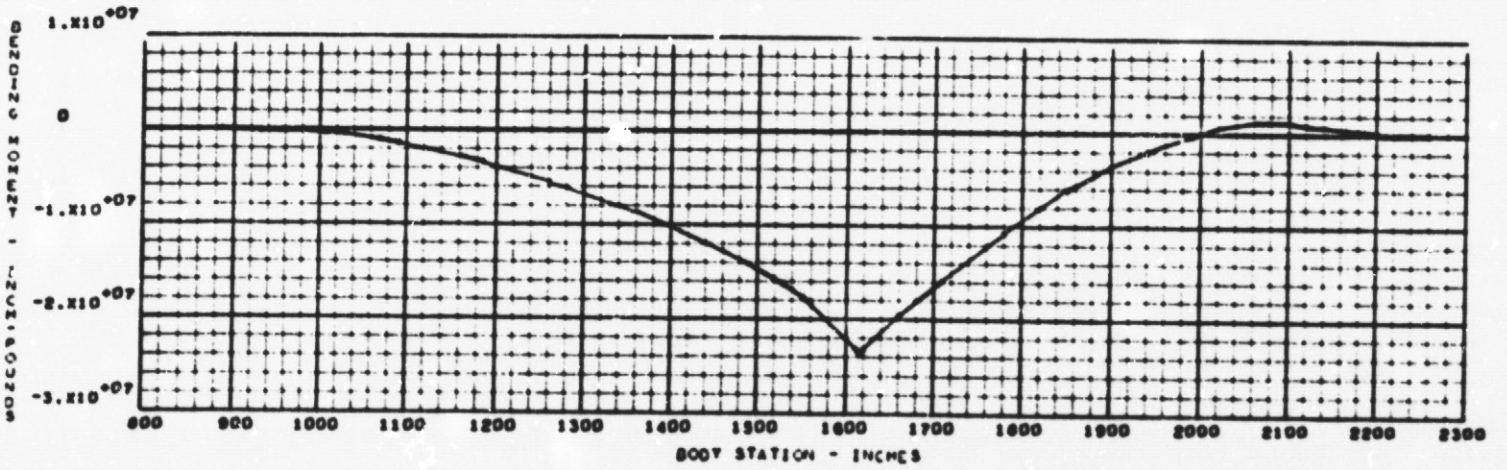

Figure 8.2-26. Orbiter Net Loads During Subsonic Pitch-Down Maneuver

12,500 - POUND PAYLOAD CLASS
α = 10° V = 125 KTS

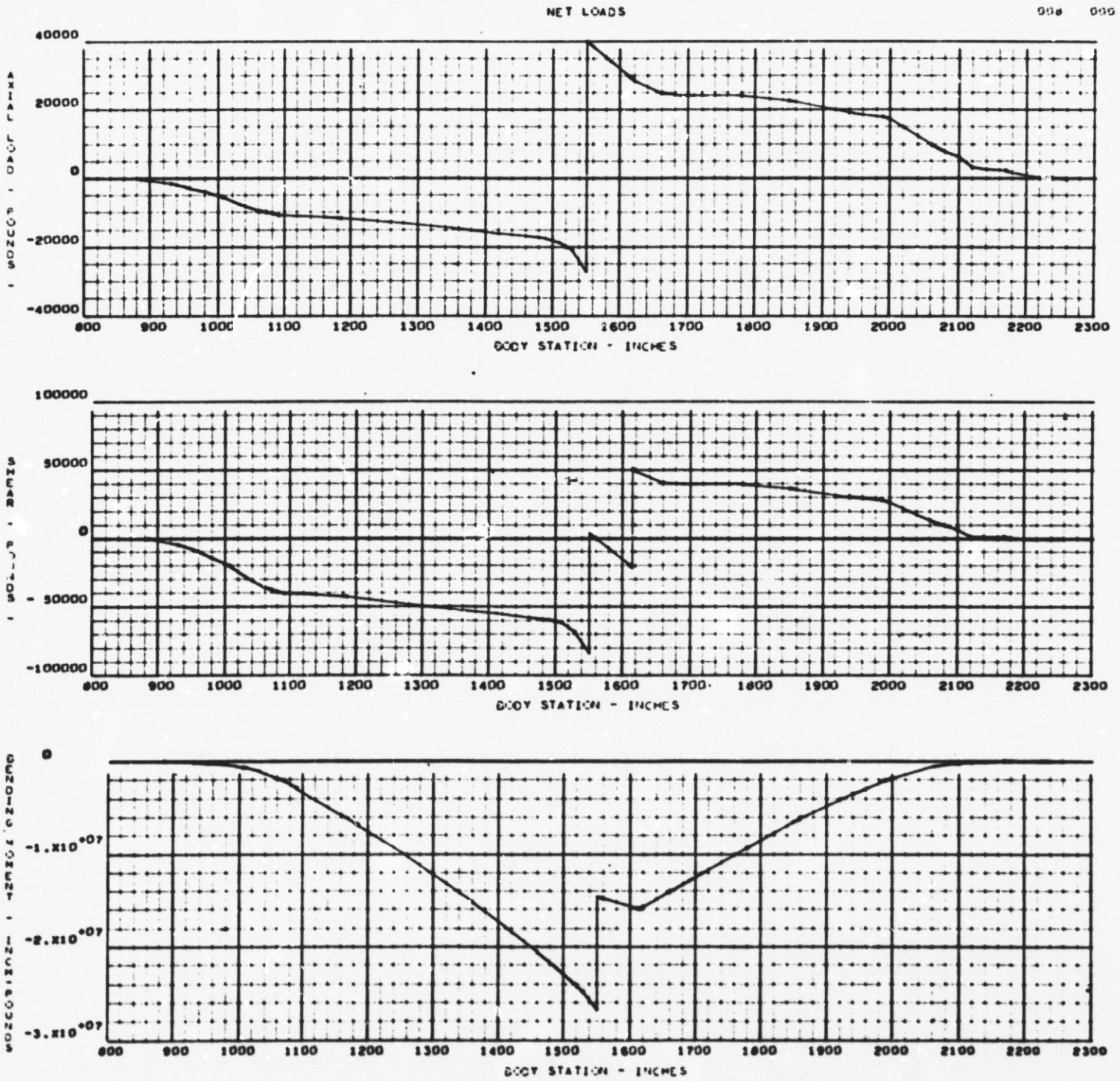

MAIN GEAR (SPIN-UP)

Figure 8.2-27. Orbiter Limit Loads During Landing (Sheet 1 of 2)

12,500 - POUND PAYLOAD CLASS
α = 10° V = 125 KTS

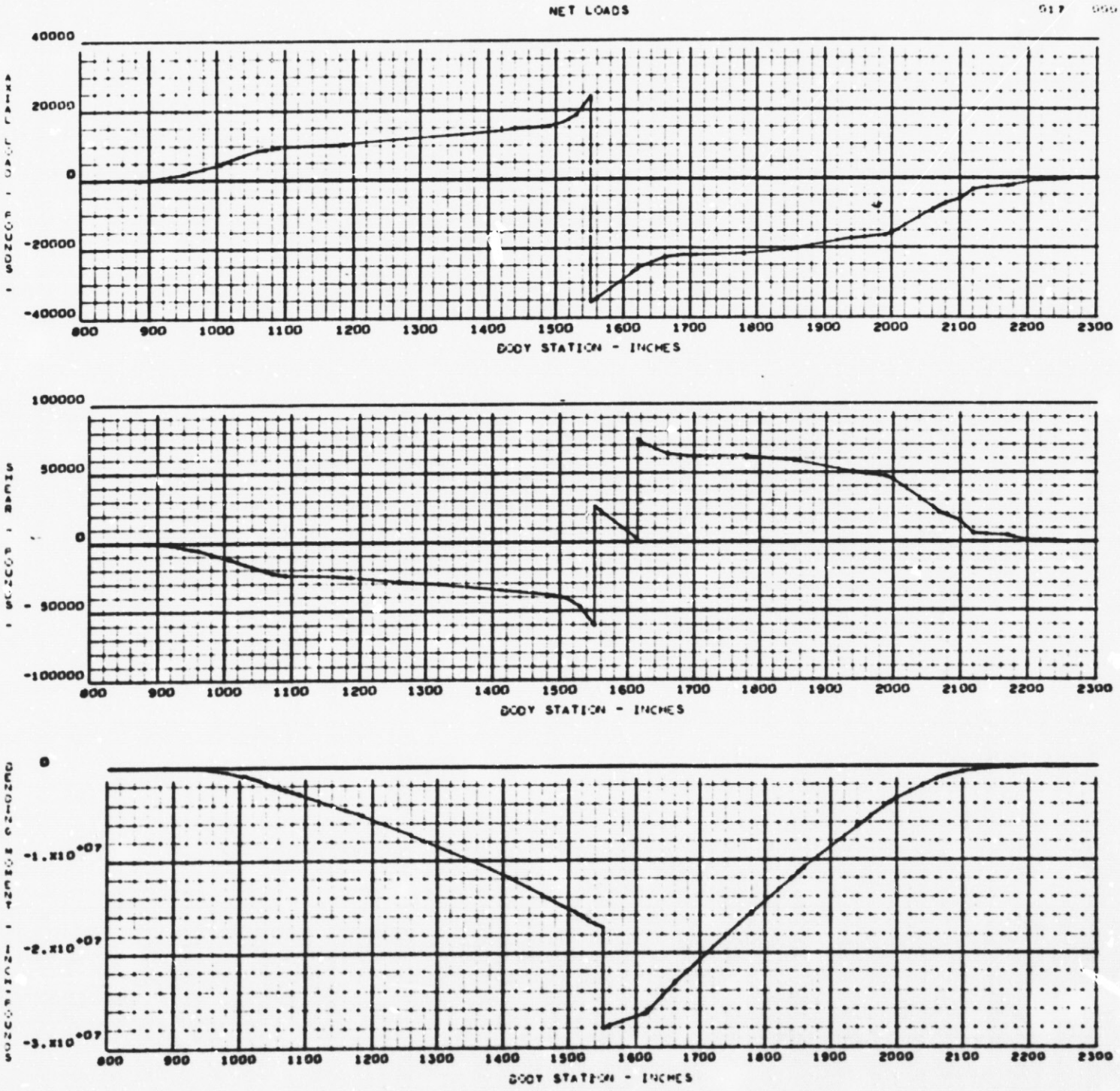

MAIN GEAR (SPRING-BACK)

Figure 8.2-27. Orbiter Limit Loads During Landing (Sheet 2 of 2)

CONDITION	ORBITER AT 103" FROM ℄		BOOSTER AT 156" FROM ℄	
	SHEAR $X10^{-3}$ (LB)	MOMENT $X10^{-6}$ (IN-LB)	SHEAR $X10^{-3}$ (LB)	MOMENT $X10^{-6}$ (IN-LB)
MAXIMUM $q\alpha$	-162.0	14.8	-487.0	86.2
2.5 G MANEUVER	-90.0	8.0	-120.0	19.1

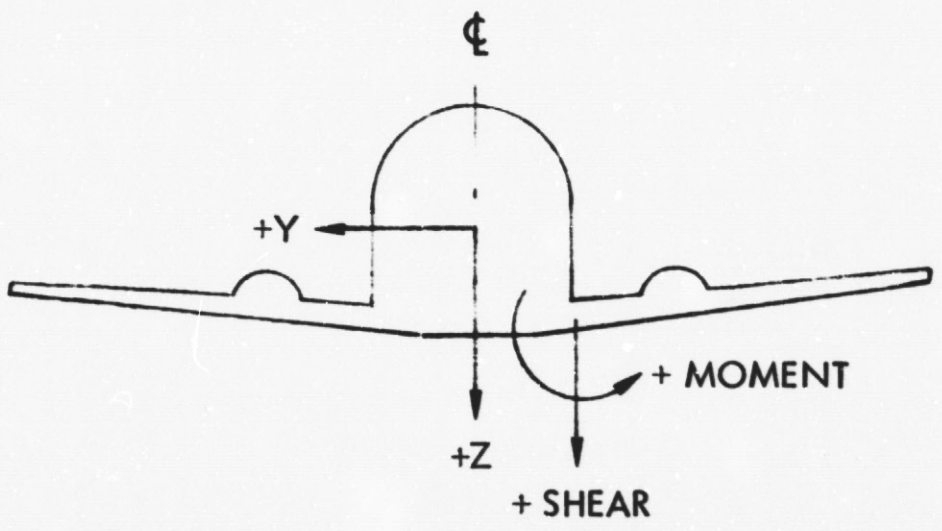

NOTE: LOADS INCLUDE DYNAMIC FACTOR
1.1 FOR MAX $q\alpha$
1.25 FOR 2.5 G MANEUVER

Figure 8.2-28. Wing Limit Loads, 12,500 - Pound Payload Class

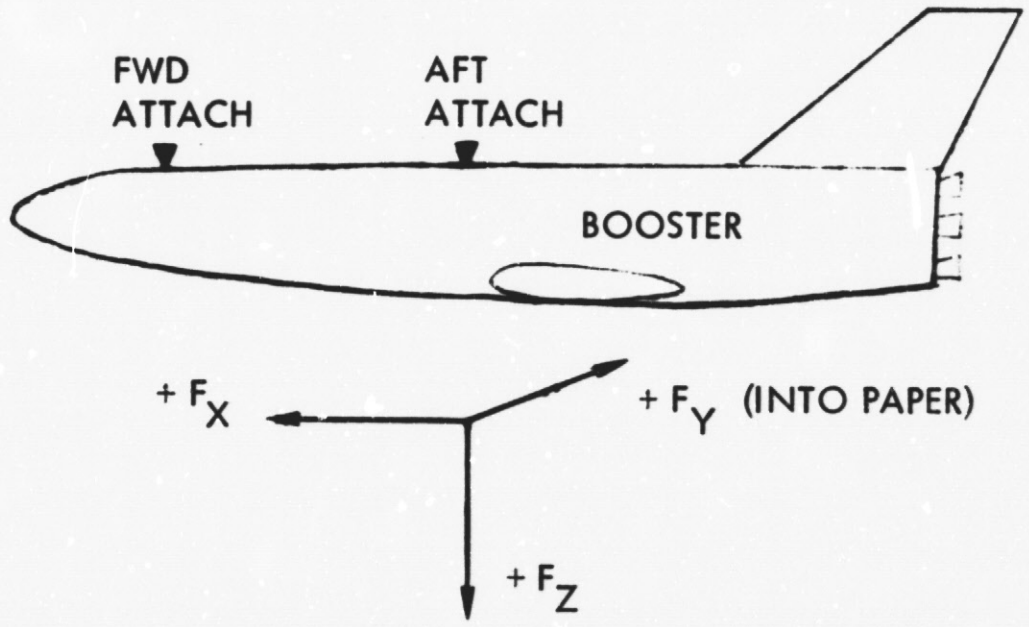

		F_X (LB)	F_Y (LB)	F_Z (LB)
FWD ATTACH	MAX $q\alpha$	———	± 81,100	+177,000 -187,000
	MAX ACCEL 1ST STAGE	———	± 5,310	33,600
AFT ATTACH	MAX $q\alpha$	-664,000	∓4,730	-18,700 +21,100
	MAX ACCEL 1ST STAGE	-995,000	∓310	-2,060

Figure 8.2-29. Booster/Orbiter Attachment Loads, 12,500 - Pound Payload Class

8.3 50,000-POUND-PAYLOAD BASELINE

Design structural and thermal environment were computed for the 50,000-pound-payload baseline booster and orbiter vehicle. Structural-load evaluation was based on the configuration of NR Drawings 2234-68 and -69..

8.3.1 Design Trajectories

The referenced boost trajectory used for definition of design environments is summarized in Figure 8.3-1. Launch was into an orbit of 50 by 100 nautical miles at a 55-degree inclination. Maximum dynamic pressure was 419 psf, which occurred 71.5 seconds after lift-off. Staging was 223 seconds after lift-off at an altitude of 230,300 feet and a velocity of 10,188 fps. After staging, the orbiter engines are ignited and burn for 194 seconds. Total boost time is 417 seconds. The orbiter is 623 nautical miles down-range at injection into the orbit of 50 by 100 nautical miles.

A banked entry/turnaround trajectory was used as the design entry trajectory for the 50,000-pound-payload booster. The initial conditions used were those for an early boost trajectory having an injection altitude of 50 nautical miles. The flight mode varied the pitch attitude of the booster to constrain the maximum normal load factor to 4.0. The roll attitude varied in the following manner: 90 degrees until the resultant load factor reached 0.5; 60 degrees until completion of the 180-degree turnaround; and zero degrees until the velocity was decreased to 400 fps. The flight conditions at significant points during the turnaround are given in Table 8.3-1. All quantities shown except time are referenced to the launch point. Time is referenced to the staging point.

A banked maximum-lateral-range entry trajectory was used as the design entry trajectory for the 50,000-pound-payload orbiter. The flight mode used maintained the pitch attitude of the orbiter at an angle of attack of 60 degrees (L/D of 0.5 and W/C_LS of 50.0 psf) throughout entry. The roll attitude varied in the following manner: 50 degrees until pullout, modulated roll after pullout to keep altitude constant until the equilibrium glide condition with roll attitude at 40 degrees is reached; and 40 degrees roll maintained until the velocity is decreased to 3000 fps. Although both right and left roll entries were computed, the right-roll entry trajectory was the one used as the design entry trajectory. The flight conditions at significant points during the entry are given in Table 8.3-2.

Table 8.3-1. Flight Conditions at Significant Points During Turnaround of Booster

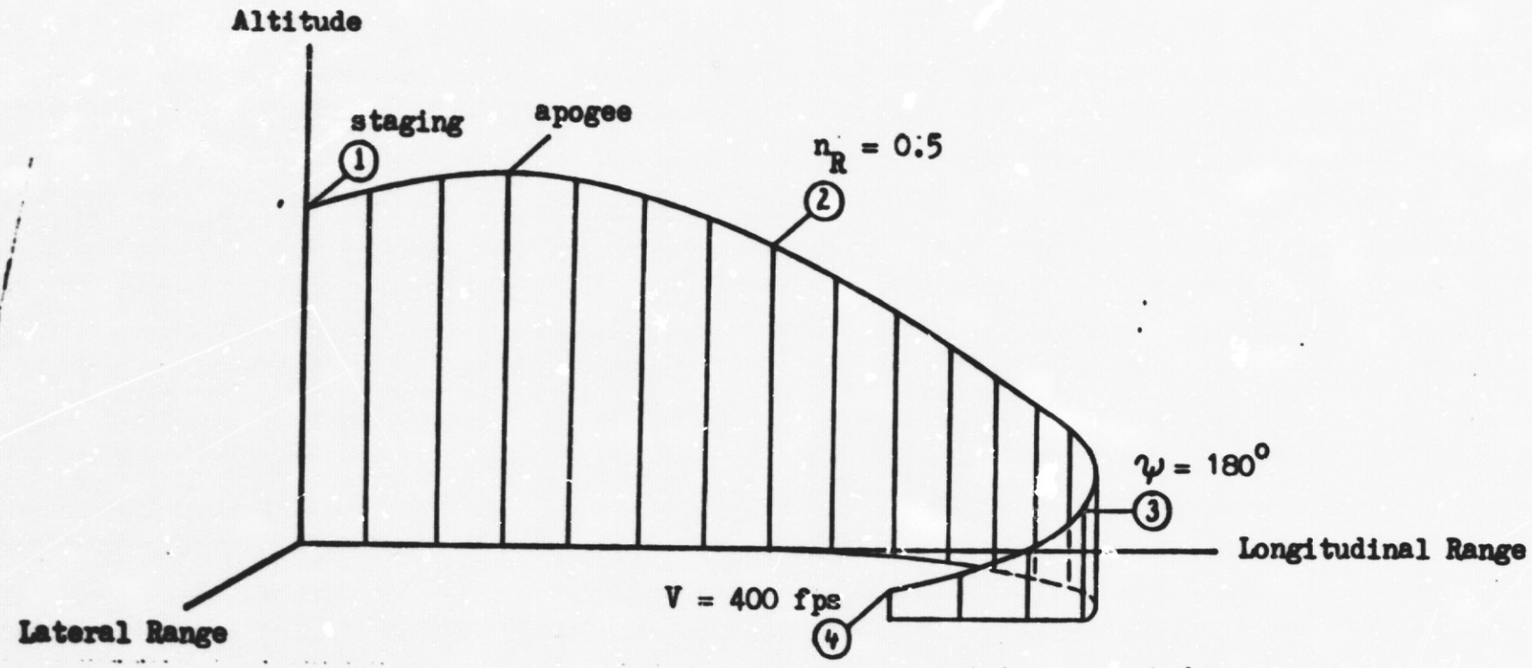

	①	②	③	④	MAX. LOAD
Bank angle, deg	90.0	90.0/60.0	60.0/0.0	0.0	60.0
Angle of attack, deg	52.5	52.5	52.5/4.5	4.5	32.7
Flight time, sec	0.0	105.36	292.12	947.42	176.0
Relative velocity, fps	10,082.0	9,763.2	720.4	400.0	5,457.1
Altitude, ft	242,000.	221,172.	78,425.	22,077.	120,362.
Flight-path angle, deg	6.68	-9.11	-53.20	-6.20	-5.96
Mach number	10.71	9.79	0.74	0.39	5.34
Dynamic pressure, psf	5.12	11.37	23.99	94.44	188.91
Resultant load factor	0.23	0.50	1.38	1.00	4.02
Longitudinal range, nau. mi.	97.8	266.5	369.0	310.4	355.9
Lateral range, nau. mi.	0.0	2.3	49.2	48.2	18.0
Heading angle, deg	0.0	2.00	180.00	182.39	32.85

Space Division
North American Rockwell

Table 8.3-2. Flight Conditions at Significant Points During Entry of Orbiter

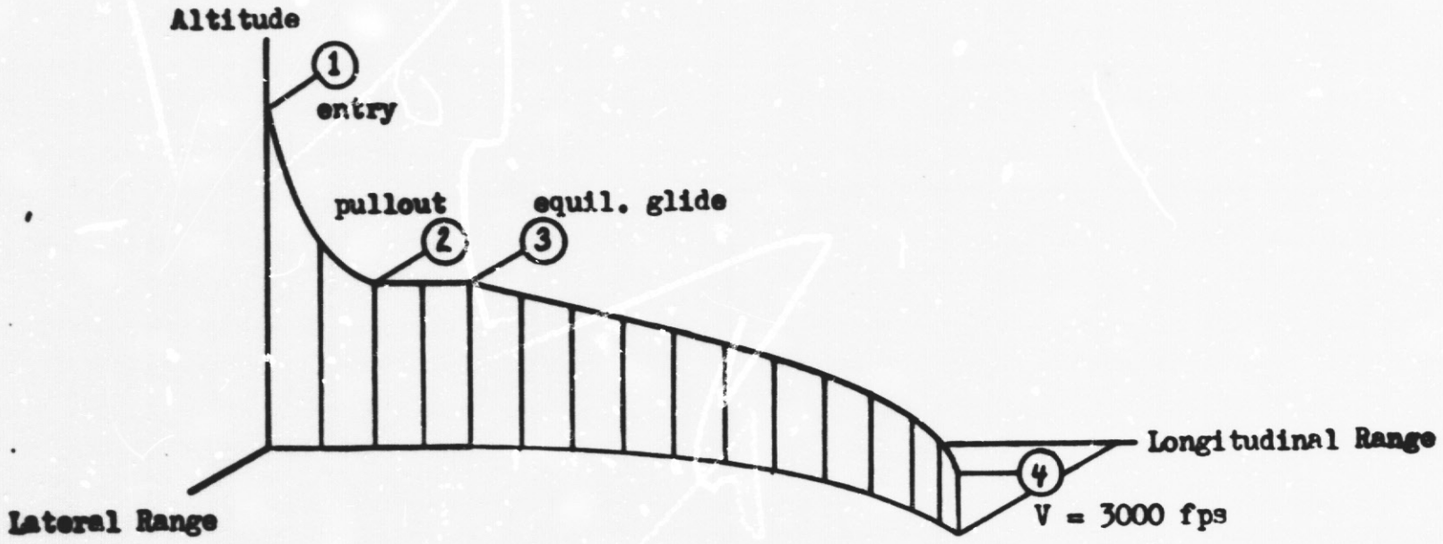

	1	2	3	4	MAX. LOAD
Bank angle, deg	50.0	50.0/69.6	40.0	40.0	40.0
Angle of attack, deg	60.0	60.0	60.0	60.0	60.0
Flight time, sec	0.0	314.89	392.72	839.55	776.0
Relative velocity, fps	25,134.1	23,200.2	21,541.1	3,000.0	6,425.8
Altitude, ft	400,000.	251,315.	251,315.	127,937.	160,775.
Flight-path angle, deg	-1.55	0.00	0.00	-10.80	-4.19
Mach number	19.13	25.33	23.52	2.90	5.94
Dynamic pressure, psf	0.01	17.82	15.36	40.43	46.56
Resultant load factor	~0	0.80	0.69	1.81	2.08
Longitudinal range, nau. mi.	0.0	1,269.4	1,551.7	2,545.4	2,505.7
Lateral range, nau. mi.	0.0	10.0	26.5	219.6	192.8
Heading angle, deg	0.0	2.35	4.29	43.56	28.12

Space Division
North American Rockwell

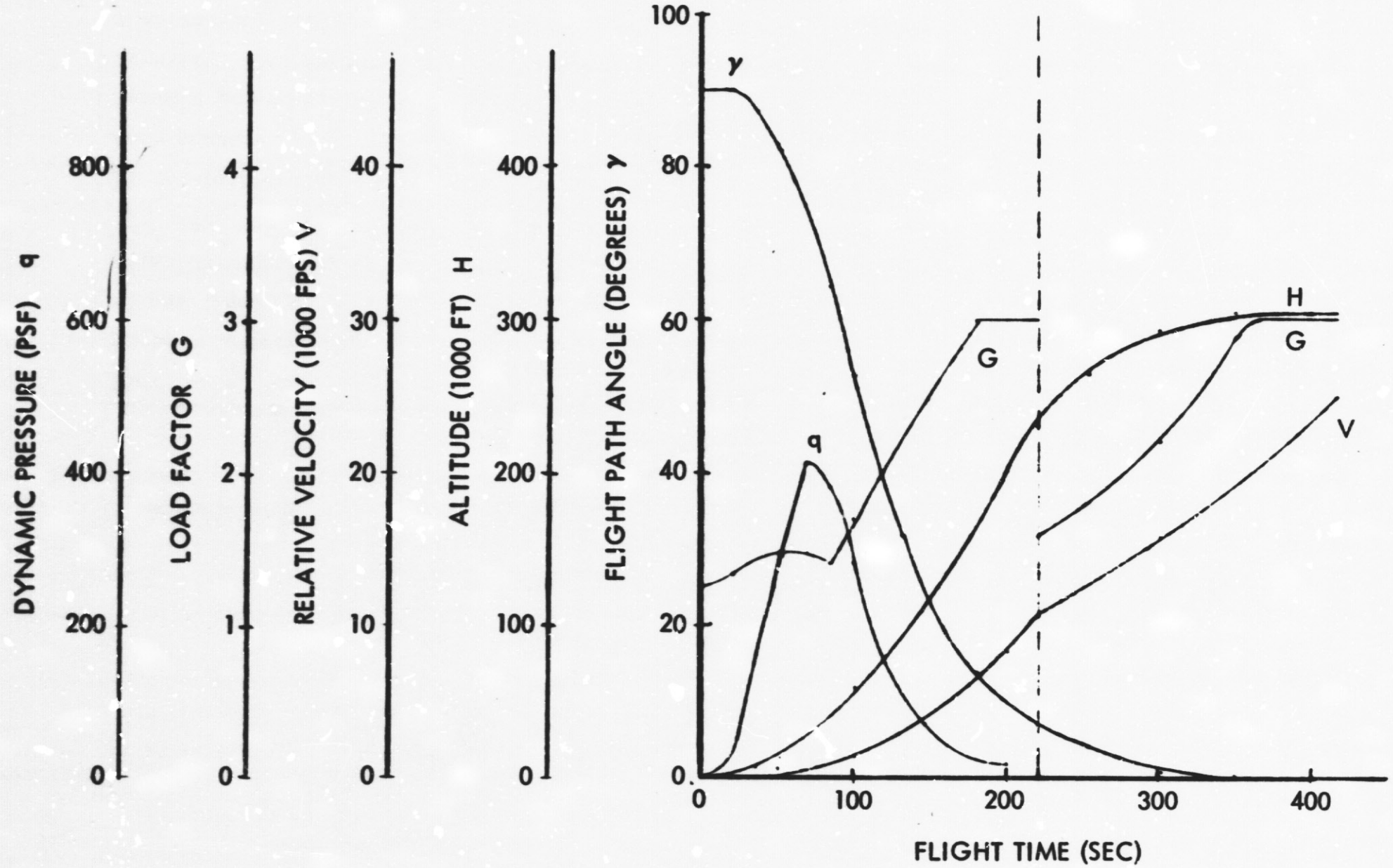

Figure 8.3-1. Nominal Ascent Trajectory Profile - 50,000 - Pound Payload Class, 50- by 100-Nautical-Mile Orbit

Space Division
North American Rockwell

8.3.2 Design Thermal Environment

Launch and entry design thermal environment for the 50,000-pound-payload orbiter and booster vehicles is summarized in Figure 8.3-2. Temperatures shown are radiation equilibrium temperatures for an emissivity of 0.8. Ascent, booster descent, and entry environments were based on the design trajectories described in the previous section. Temperatures for the worst case flight condition at each body location are listed. Temperatures for the wing do not include shock wave interference effects. It is estimated that the wing leading-edge temperature at the 20-percent span location could be as high as 4000 F. The design should be based on this value.

8.3.3 Air Loads (50,000-Pound-Payload Class)

Aerodynamic load distributions were estimated for four flight conditions:

1. Maximum $q\alpha$ during boost
2. Entry at 60-degree angle of attack
3. Subsonic transition
4. Landing

The methods used to estimate the load distributions are the same as for the 12,500-pound-payload baseline air loads.

The normal and axial load distributions during launch for the orbiter, booster, and composite configuration are presented in Figures 8.3-3 and 8.3-4.

Distributed air loads for the booster and orbiter vehicles are presented in Figures 8.3-5 and 8.3-6 for the transition maneuvers from high to cruise angle of attack. Body distributed loads were based on potential and cross flow theories. Wing and tail loads were determined from the results of the Langley wind tunnel tests. The entry normal load distribution evaluated at a 60-degree angle of attack is shown in Figures 8.3-7 and 8.3-8.

8.3.4 Structural Loads (50,000-Pound-Payload Class)

Presented in this section are results of the structural loads analyses of the 50,000-pound-payload class space shuttle concept. The analyses were based on the configuration drawings 2234-68 and 2234-69 for the orbiter and booster, respectively. The orbiter weight at launch was 835,000 pounds.

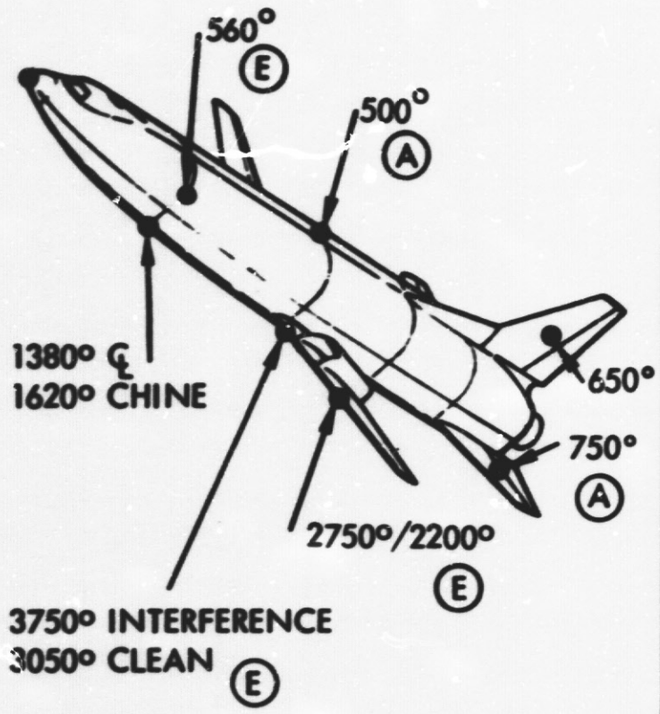

- ORBITER

  90% AREA < 1500°F

- BOOSTER

  90% AREA < 1400°F

LOCATION	CRITICAL FLIGHT CONDITIONS	RADIATION EQUILIBRIUM TEMPERATURE (°F)	
		BOOSTER	ORBITER
FUSELAGE			
NOSE	ENTRY	1275	1860
LOWER SURFACE 20%	ENTRY	1380	1420
LOWER SURFACE 80%	ENTRY	1220	1450
CHINE	ENTRY	1530	1620
SIDE	ENTRY	540	560
UPPER SURFACE	ASCENT	500	500
WING			
L.E. (NO INTERFERENCE)	ENTRY	2200	3000
LOWER SURFACE 20%	ENTRY	1400	1700
UPPER SURFACE 20%	ASCENT	650	700
HORIZONTAL SURFACE			
L.E.	ENTRY	2020	3450
LOWER SURFACE	ENTRY	1390	1500
UPPER SURFACE	ASCENT	600-650	700
VERTICAL SURFACE			
L.E.	ASCENT	1730	2320
SIDE	ASCENT	600-650	650

Figure 8.3-2. Thermal Environment Summary of 50,000-Pound Payload Class

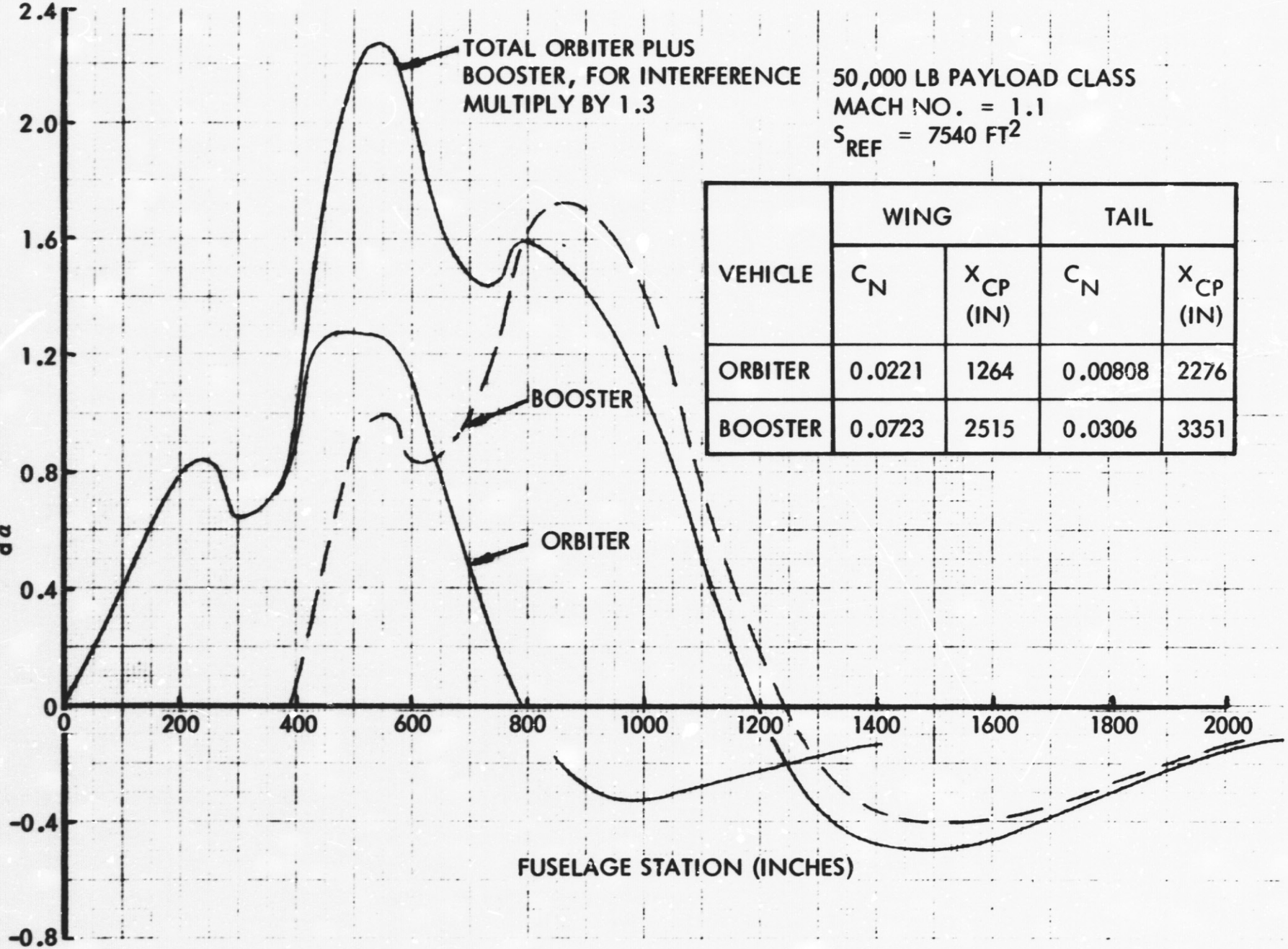

VEHICLE	WING		TAIL	
	C_N	X_{CP} (IN)	C_N	X_{CP} (IN)
ORBITER	0.0221	1264	0.00808	2276
BOOSTER	0.0723	2515	0.0306	3351

Figure 8.3-3. Normal Airload Distribution During Launch for Maximum q Alpha

Figure 8.3-4. Axial Load Distribution During Launch for Maximum q Alpha

Space Division
North American Rockwell

Figure 8.3-5. Booster and Orbiter Distributed Airload During Pitch-Down

Space Division
North American Rockwell

Figure 8.3-6. Booster and Orbiter Subsonic Wing and Tail Load

Figure 8.3-7. Orbiter Normal Load Distribution During Entry, 50,000 - Pound Payload Class

Space Division
North American Rockwell

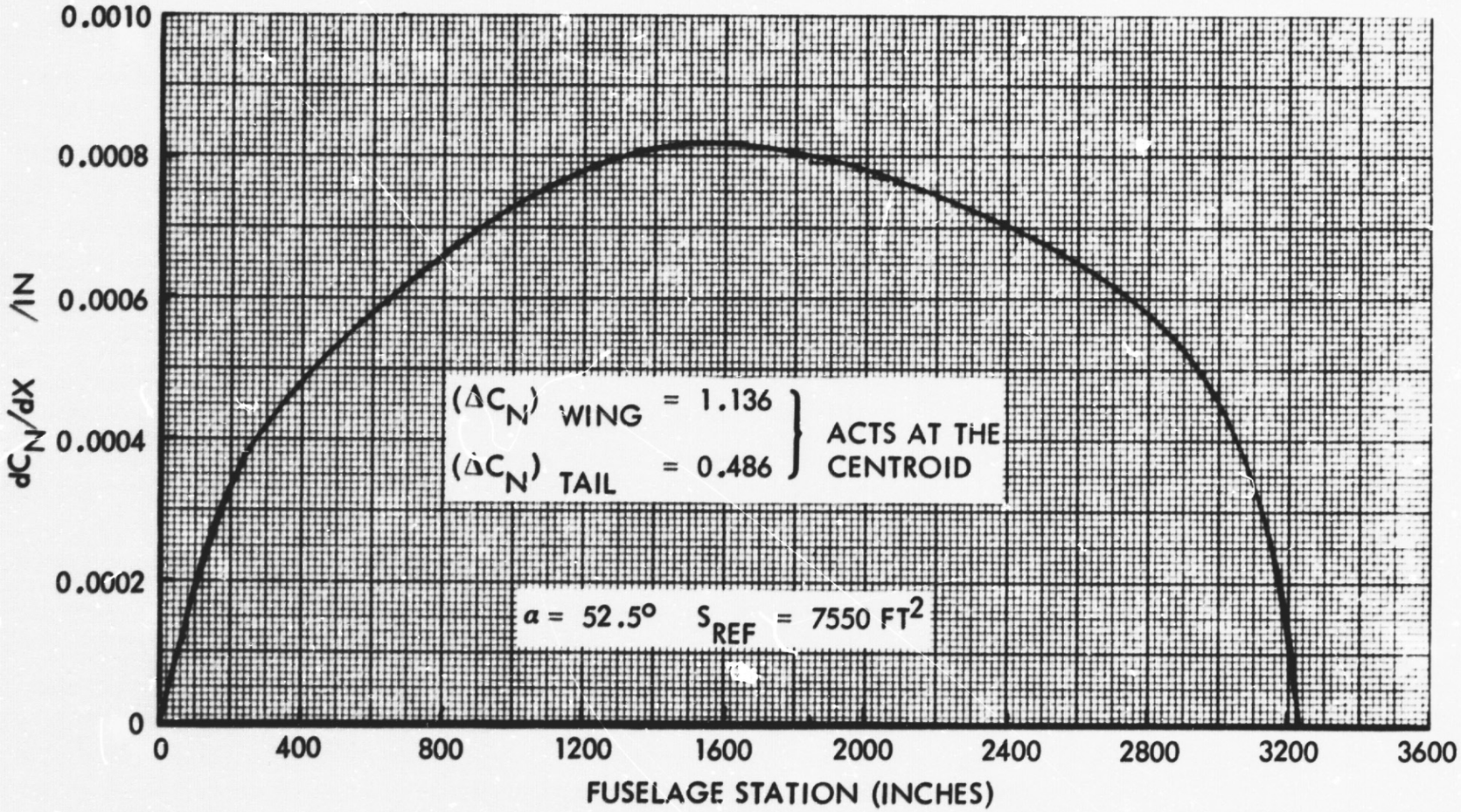

Figure 8.3-8. Booster Normal Load Distribution During Entry, 50,000 - Pound Payload Class

Space Division
North American Rockwell

Booster thrust at launch was approximately 5 million pounds, which resulted in a lift-off T/W of 1.25. Vehicle configurations and sign convention are presented in Figure 8.3-9. The booster and orbiter load conditions examined were prelaunch, maximum qα, maximum acceleration, entry, subsonic pitch-down, and landing.

Maximum body loads are summarized in Table 8.3-3. The loads are given for the indicated fuselage stations on the reference lines of the booster and orbiter respectively. Loads on the aerodynamic surfaces during boost and entry flight conditions are included in Tables 8.3-4 and -5, for the root and one-third panel length locations. Booster/orbiter attachment fitting loads for the orbiter are presented in Table 8.3-6 for the axial load taken out at the forward attachment and 8.3-7 at the aft attachment.

Prelaunch Loads

Prelaunch loads were calculated through use of wind criteria similar to those used for Apollo, since both vehicles are launched from the same area. The winds used are the 99.9-percent (ETR) winds taken from NASA TMX 53328. Standard features of this wind are 77.6 fps peak velocity at 60 feet above grade. Peak velocity equals 1.4 times the quasi-steady velocity. In addition. Von Karman vortex shedding loads equal to 1.25 times the quasi-steady loads were applied. The vortex shedding loads act perpendicular to the wind direction. Prelaunch loads were calculated for the vehicle tilted approximately two degrees in the plus Z direction. This tilt locates the total vehicle center of gravity vertically above the center of the hold-down station such that the base bending moment from dead weight is zero. Results are presented in Figure 8.3-10. The base bending moment of 520×10^6 in.-lb shown in Figure 8.3-10(C) is thus from air load only. Any tilt other than this will increase the base bending moment.

The rebound condition occurs during prelaunch, when engine thrust is cut off prior to release of the hold-down mechanism. Thrust is equal to or greater than weight at this time, and the structure aft of the engine supports is in tension. The response of the vehicle to the thrust decay and the resulting recontact with the compression pads will determine the maximum loads. Rebound analyses for the Saturn V provided a maximum longitudinal acceleration factor of 1.38 g's. Until dynamic analysis of the rebound acceleration has been made for the ILRV, the acceleration factor of 1.38 g's is recommended for use.

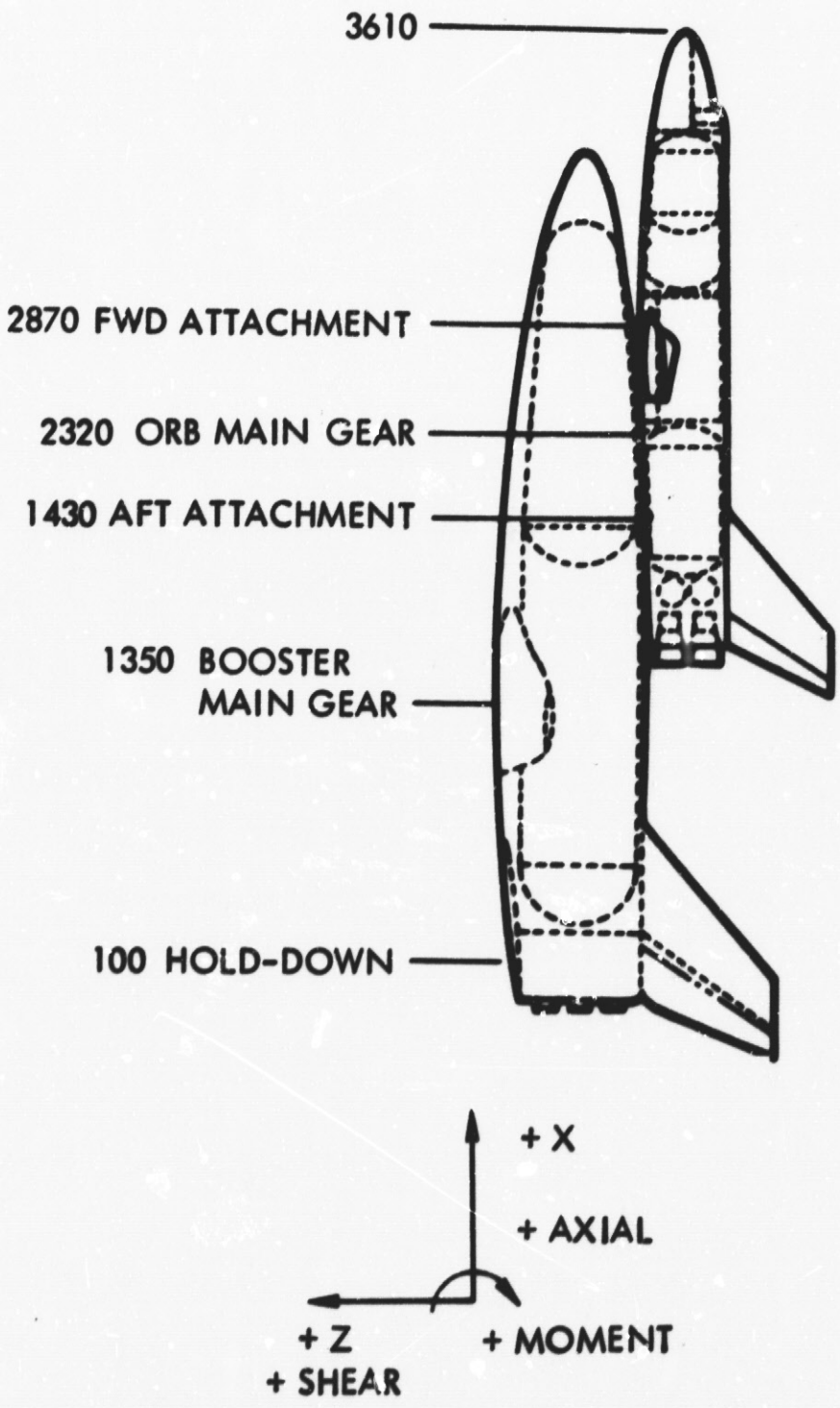

Figure 8.3-9. Loads Stations and Sign Conventions, 50,000-Pound Payload System

Table 8.3-3. Structural Design Loads Summary, 50,000-Pound-Payload System

	Load Station (Inches from booster tail with orbiter attached)	Limit Loads			
		Condition	Axial x 10^{-3} (lb)	Shear x 10^{-3} (lb)	Moment x 10^{-6} (in.-lb)
Booster	2870 (fwd attach)	Max q α	-1865	525	250
	2000 (LOX tank aft bulkhead)	Max q α	-4292	-207	-150
		Max accel	-3872	117	430
	1430 (aft attach)	Max q α	-4736	-311	-1.10
		Max accel	-4010	459	357
	1350 (main gear)	Landing	-185	500	-430
	100 (hold-down)	Prelaunch	-3985	-340	520 (Tilt) 740 (No Tilt)
Orbiter	2870 (fwd attach)	Max q α	848	484	215
		Max accel	-1552	254	488
	2320 (main gear)	Max accel	87[illegible]	270	344
		Landing	-195	-340	-96
	1430 (aft attach)	Max q α	140	-284	-29
		Max accel	80	334	-0.63

Space Division
North American Rockwell

Table 8.3-4. Aerodynamic Surface Limit Loads at the Root, 50,000-Pound-Payload System

Aero Surface	Orbiter		Booster	
	Shear x 10^{-3} (lb)	Moment x 10^{-6} (in.-lb)	Shear x 10^{-3} (lb)	Moment x 10^{-6} (in.-lb)
Max q α				
Wing	177 -89	-45.6 22.8	637 -319	-298 149
Horiz tail	86	-13	353	-94
Vert tail	211	32	474	95
Entry				
Wing	-41	10.5	-254	119
Horiz tail	-17	2.7	-91	24
Vert tail	Shielded		Shielded	

Table 8.3-5. Aerodynamic Surface Limit Loads at One-Third Panel Length From Root, 50,000-Pound-Payload System

Aero Surface	Orbiter		Booster	
	Shear x 10^{-3} (lb)	Moment x 10^{-6} (in.-lb)	Shear x 10^{-3} (lb)	Moment x 10^{-6} (in.-lb)
Max q α				
Wing	106 -53	-16.6 8.3	382 -191	-109 54.5
Horiz tail	51.5	-4.9	212	-35.4
Vert tail	127	118	284	35
Entry				
Wing	-25.4	4.0	-152.5	43.6
Horiz tail	-10.4	1.0	-54.4	9.1
Vert tail	Shielded		Shielded	

Table 8.3-6. Limit Attachment Loads
Axial Load at Forward Attachment

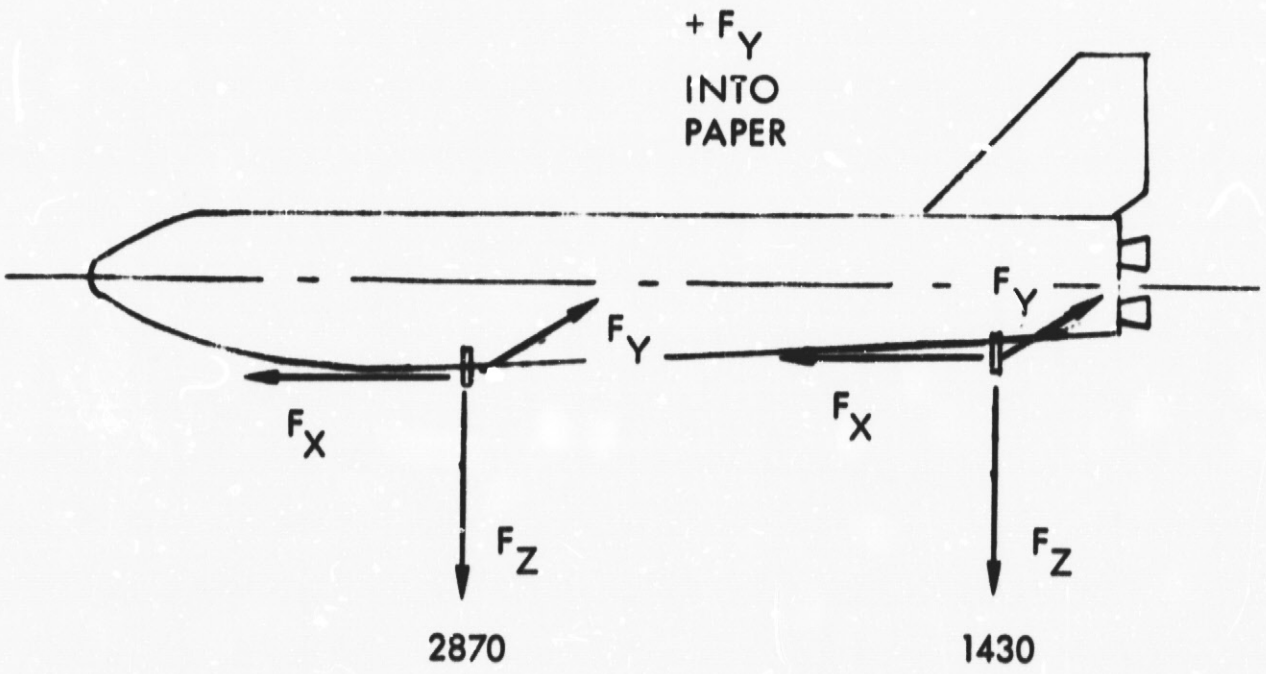

Limit Loads x 10^{-3} ~ lb

Load Condition	Fwd Attach. Sta 2870			Aft Attach. Sta 1430		
	F_X	F_Y	F_Z	F_X	F_Y	F_Z
Max q α	1608	±132	-383	-	±127	-295
Max axial acceleration	2630	-	130	-	-	-340

Table 8.3-7. Limit Attachment Loads, Axial Load at Aft Attachment

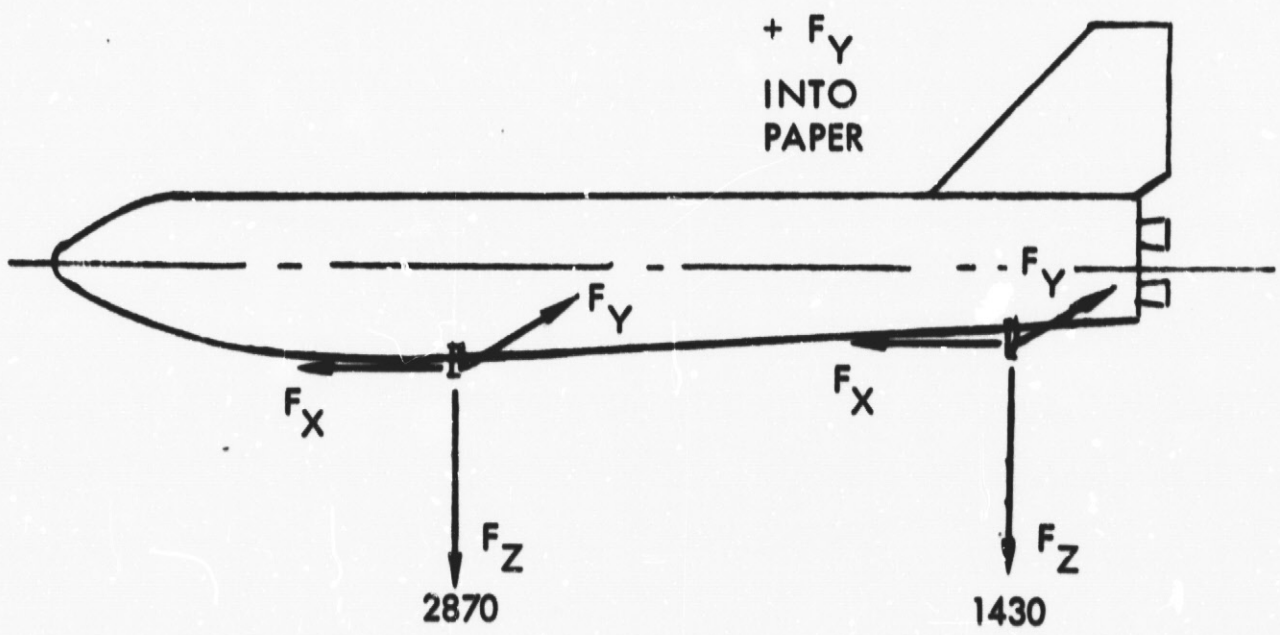

Limit Loads x 10^{-3} ~ lb

Load Condition	Fwd Attach. Sta 2870			Aft Attach. Sta 1430		
	F_X	F_Y	F_Z	F_X	F_Y	F_Z
Max q α	-	±132	-456	1608	±127	-222
Max axial acceleration	-	-	13	2630	-	-223

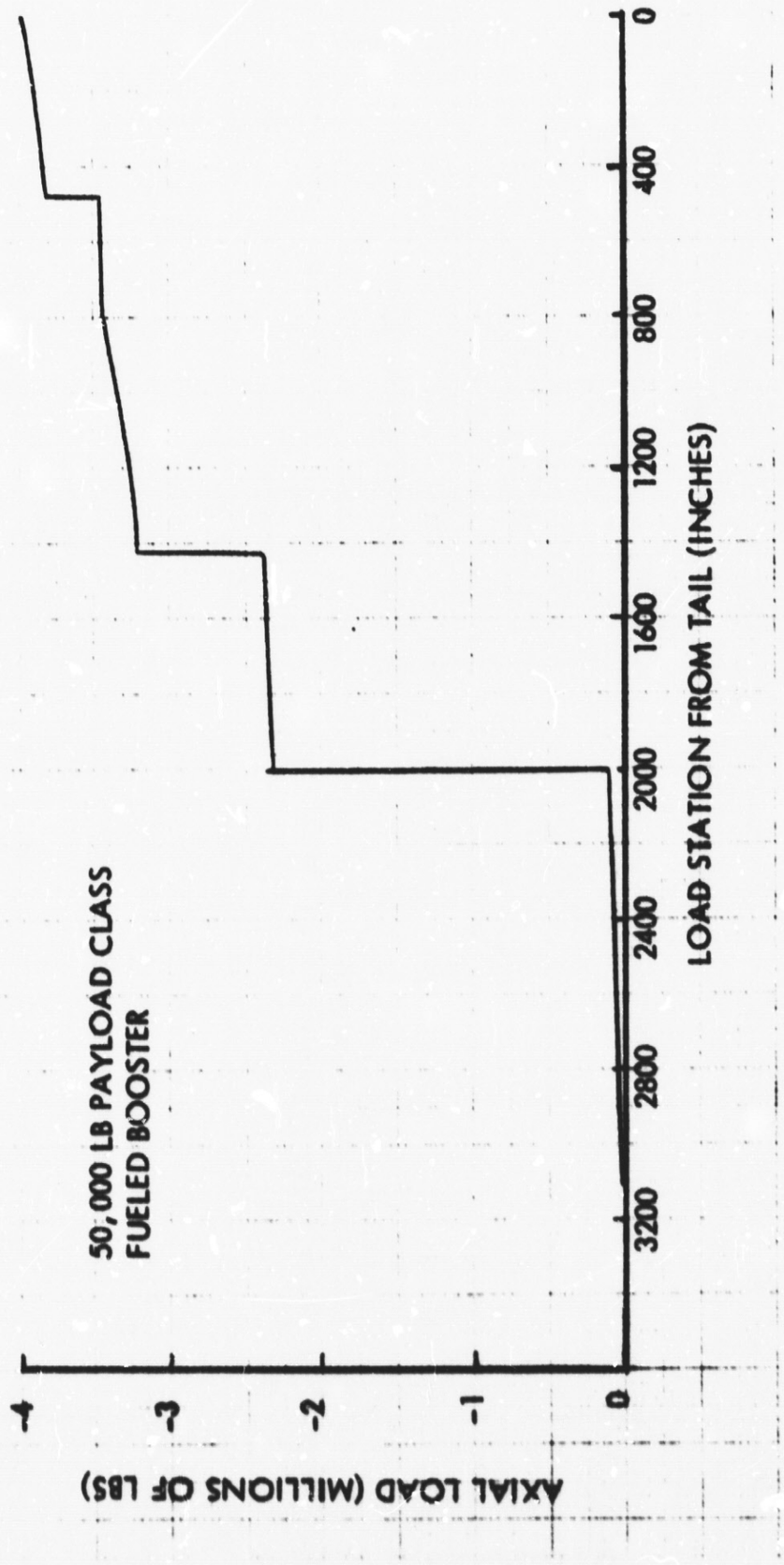

Figure 8.3-10(a). Prelaunch Loads, Booster Axial Load

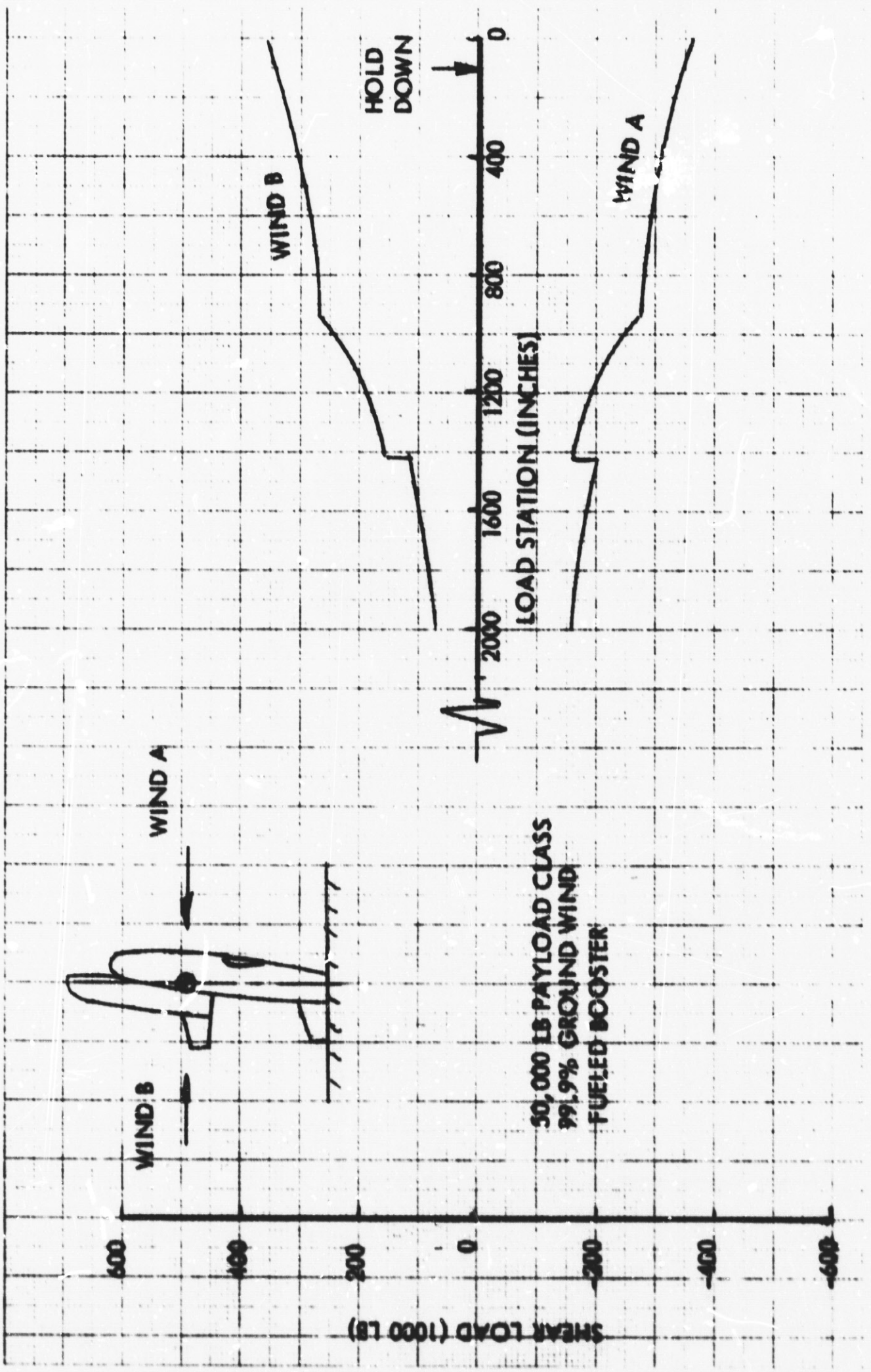

Figure 8.3-10(b). Prelaunch Loads, Booster Shear Load

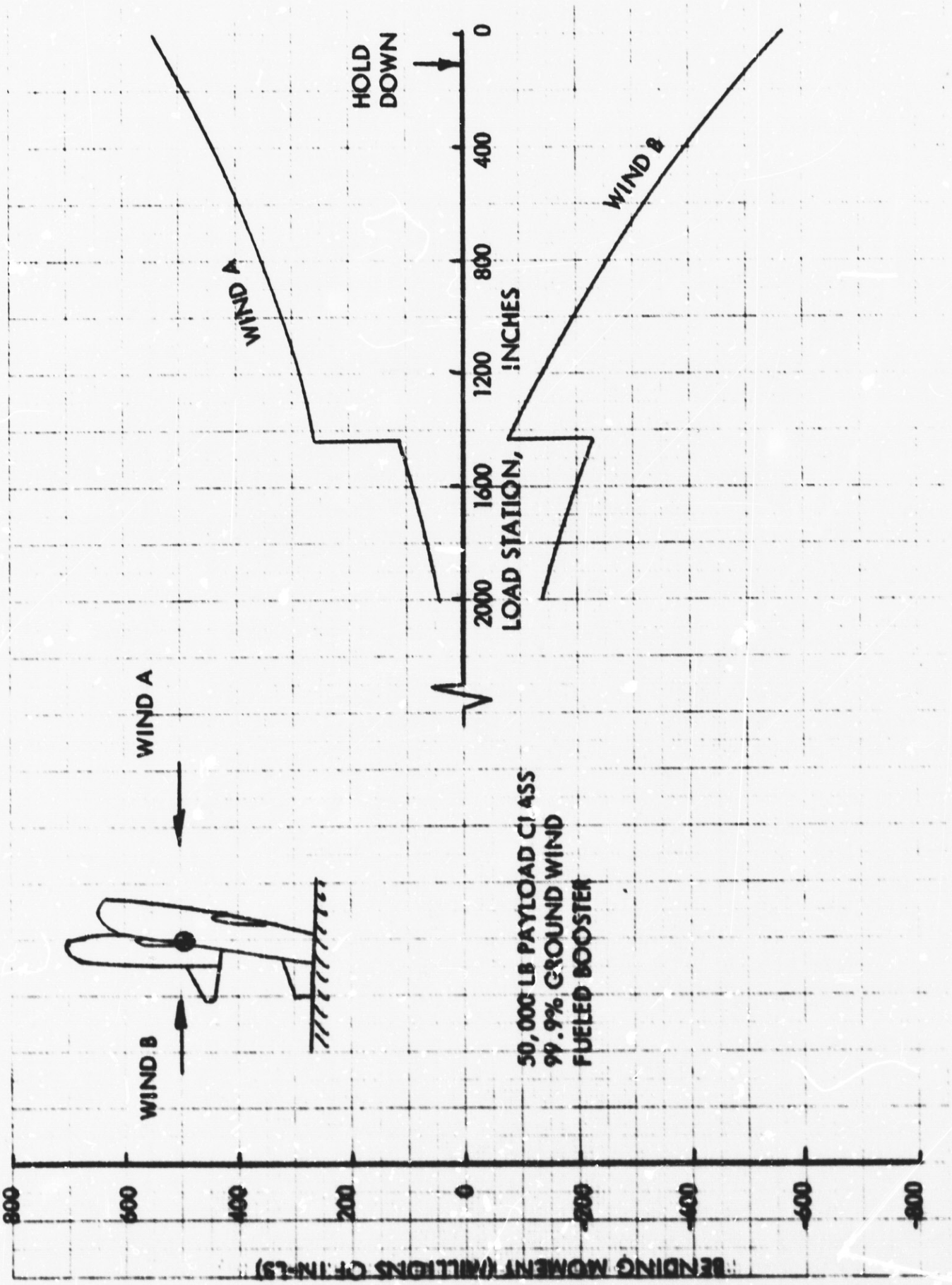

Figure 8.3-10(c). Prelaunch Loads, Booster, Bending Moment

Maximum q α Loads

The maximum q α condition was established for the design ascent tracjectory into an orbit of 50 by 100 nautical miles as discussed in Section 8.3.1. For loads definition, the maximum q α condition was defined as follows:

Mach No. = 1.1

Dynamic pressure, q = 420 psf

Angle of attack, α = -7°

Acceleration factor = n_x = 1.5 g's

Angle-of-attack (α) boost condition was given with respect to the booster reference line. A negative α indicates that the relative wind is from the orbiter to the booster. The launch trajectory is based on boosting the vehicle at zero lift. However, because of the effects of wind shear, α varies from approximately -1 to -7 degrees. Saturn V wind criteria were considered in estimating these angles of attack.

Results are presented in Figures 8.3-11 through 8.3-14. To support structural design trades, body loads were developed for -7 degree α for two booster/orbiter axial loading cases: load applied at the aft fitting (Figures 8.3-11 and 8.3-13) and load applied at the forward attach fittings (Figures 8.3-12 and -14).

Wing loads were computed for the α extremes, since the wings are mounted with positive incidence, and the wing load changes sign. Horizontal tail loads were computed only for α = -7 degrees, since they are mounted with negative incidence and the load does not change sign. The transverse maximum q α loads in Figures 8.3-11 through 8.3-14 should be multiplied by 1.1, as indicated, to account for dynamic effects of wind shear and gust.

Maximum Acceleration Loads

The maximum acceleration condition of 3.0 g's occurs at end of burn for the booster vehicle. Throttling of the booster engines may be required to limit acceleration to 3.0 g's, a specified design parameter. By the time this condition occurs, the dynamic pressure is practically zero, and the aerodynamic loads are negligible. The lateral loads for this condition result from the engine gimbal angle required to direct the thrust vector through the offset center of gravity of the total vehicle. A dynamic magnification factor of 1.05 was used for these loads to account for the transients resulting from unsteady thrust.

50,000-POUND PAYLOAD CLASS

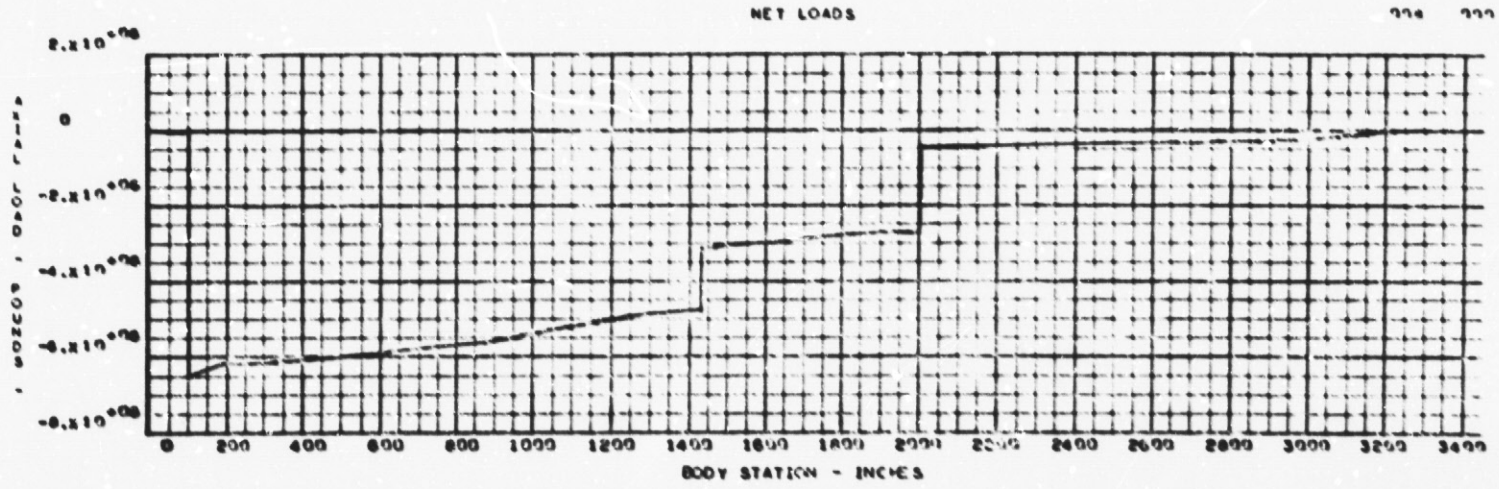

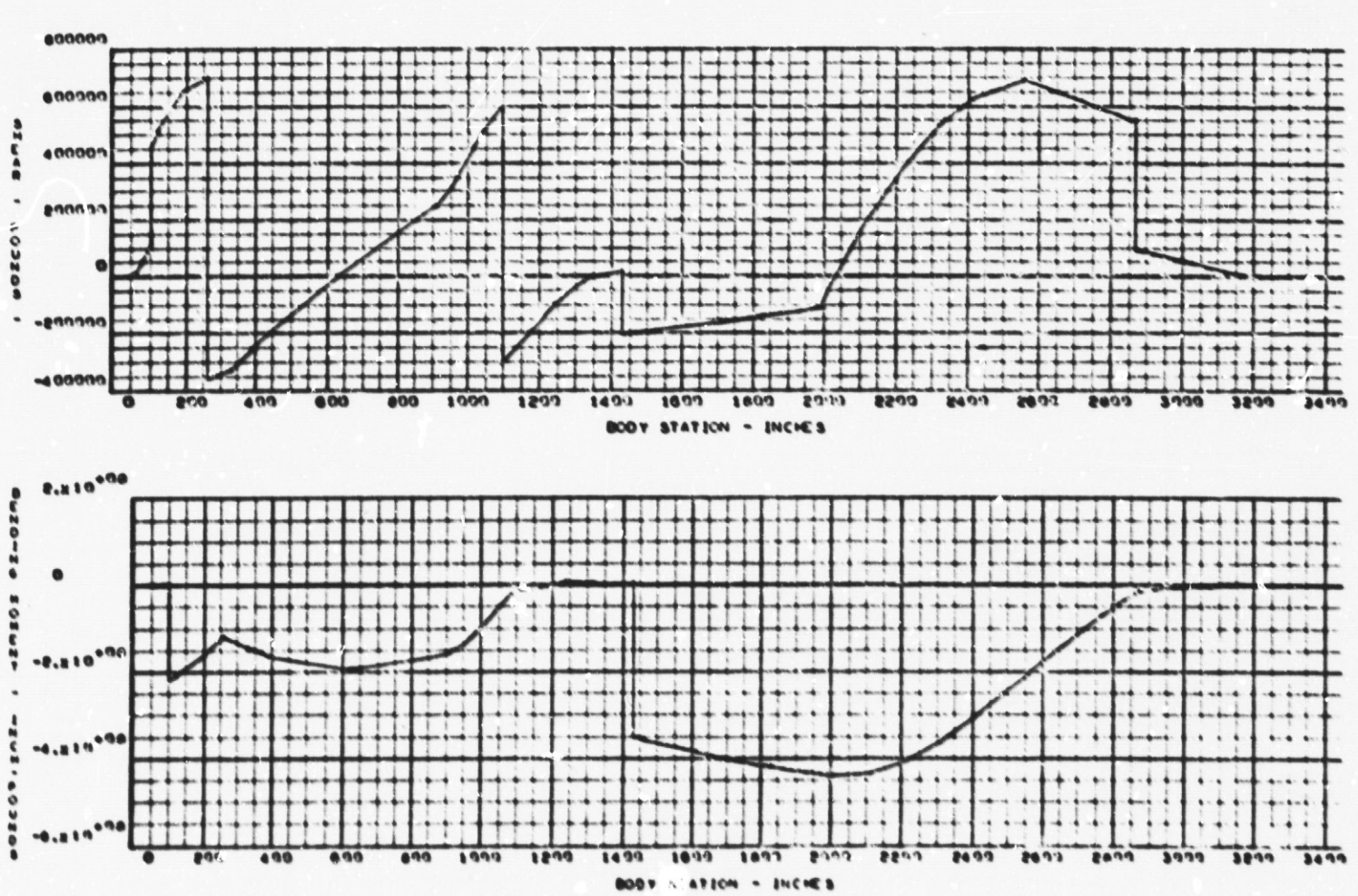

NOTE: MULTIPLY SHEAR AND MOMENT
BY 1.1 DYNAMIC FACTOR

Figure 8.3-11. Booster Loads for Maximum q Alpha (Axial Load at Aft Attachment)

50,000-POUND PAYLOAD CLASS

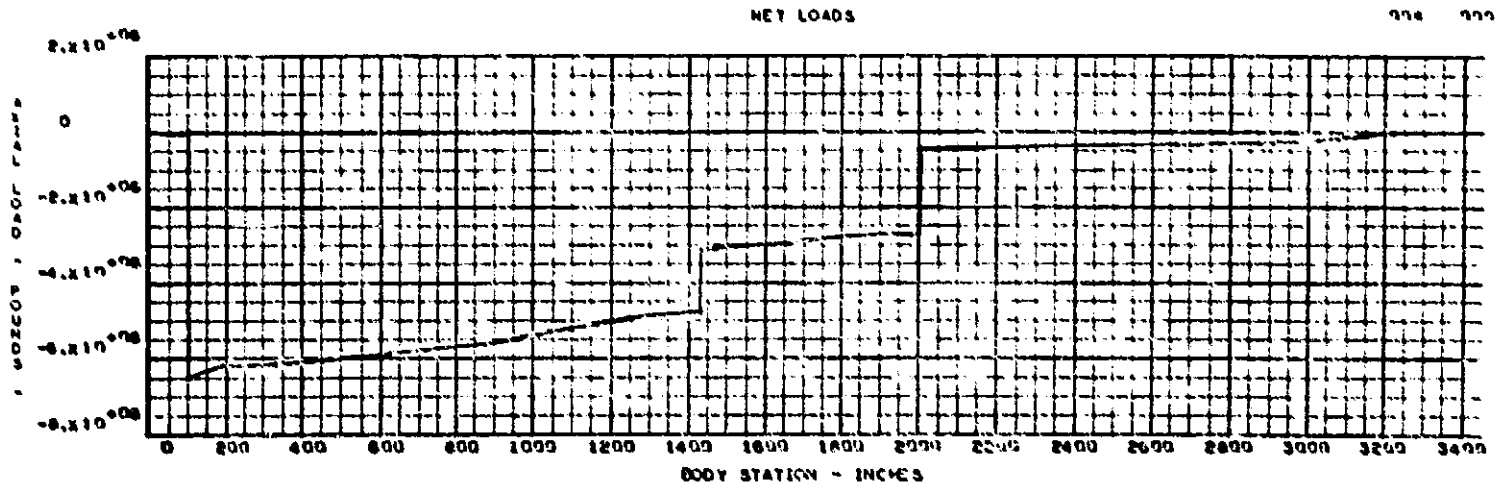

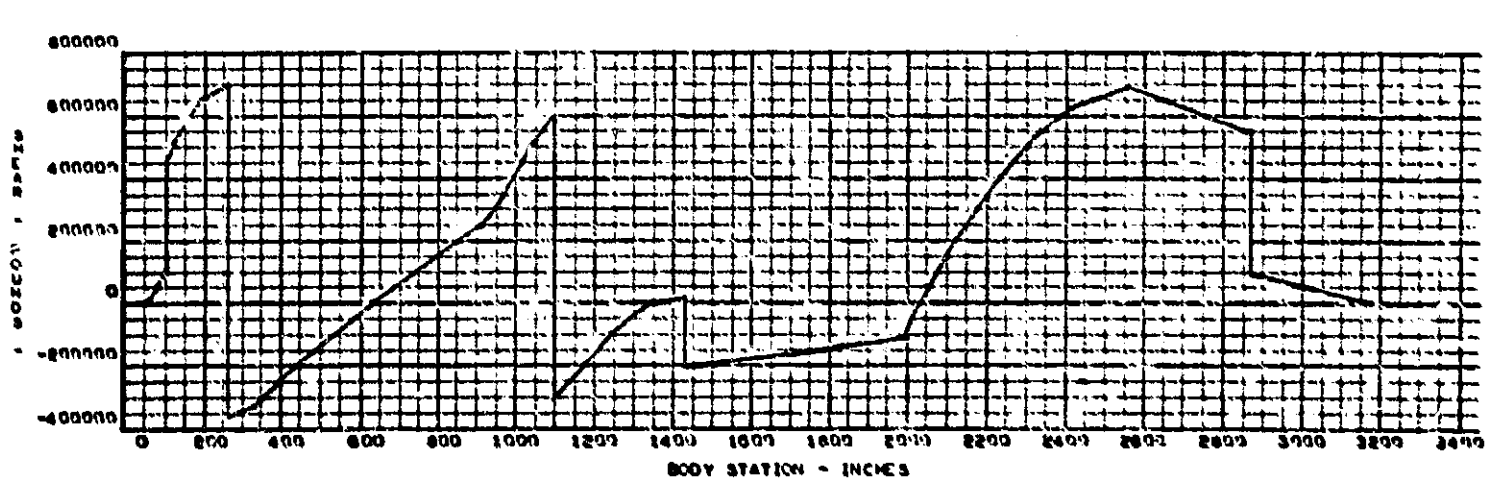

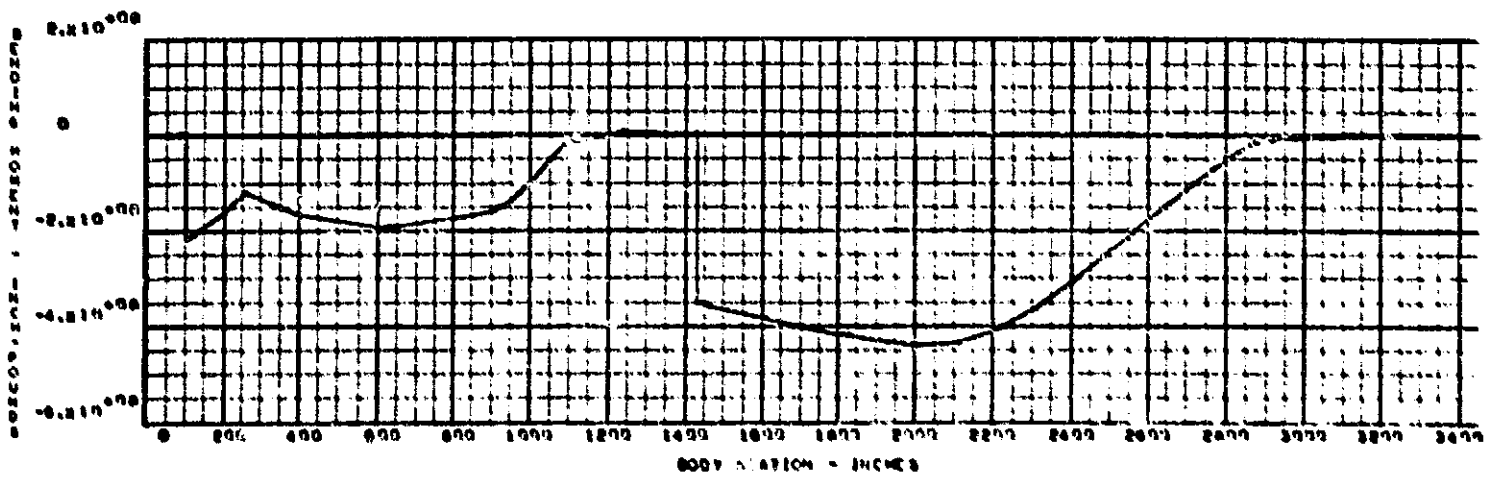

NOTE: MULTIPLY SHEAR AND MOMENT
BY 1.1 DYNAMIC FACTOR

Figure 8.3-11. Booster Loads for Maximum q Alpha (Axial Load at Aft Attachment)

50,000 - POUND PAYLOAD CLASS

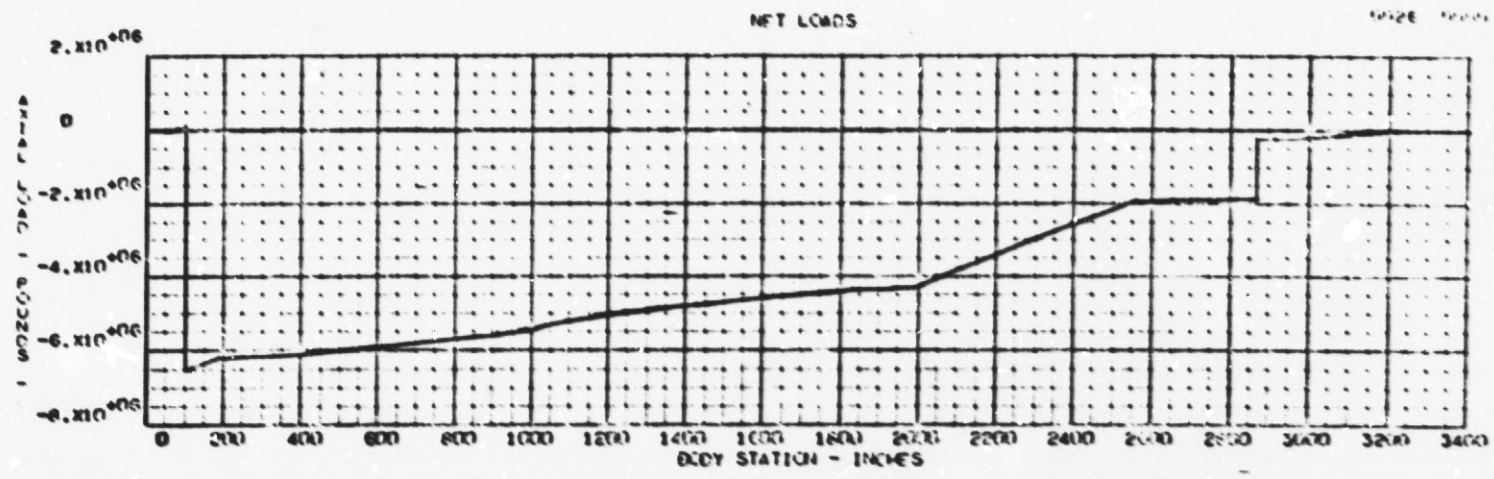

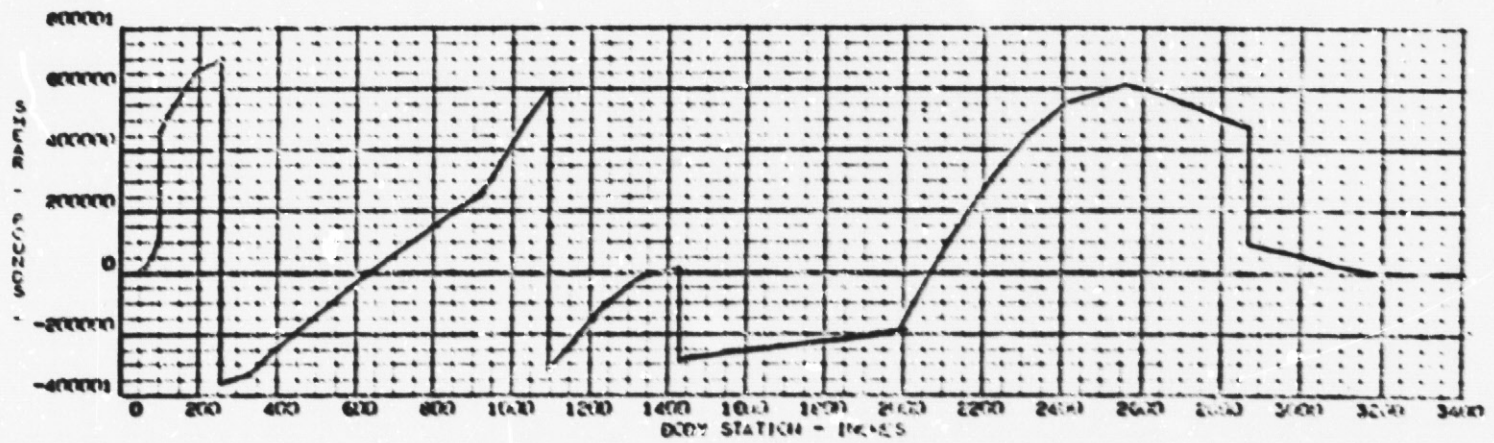

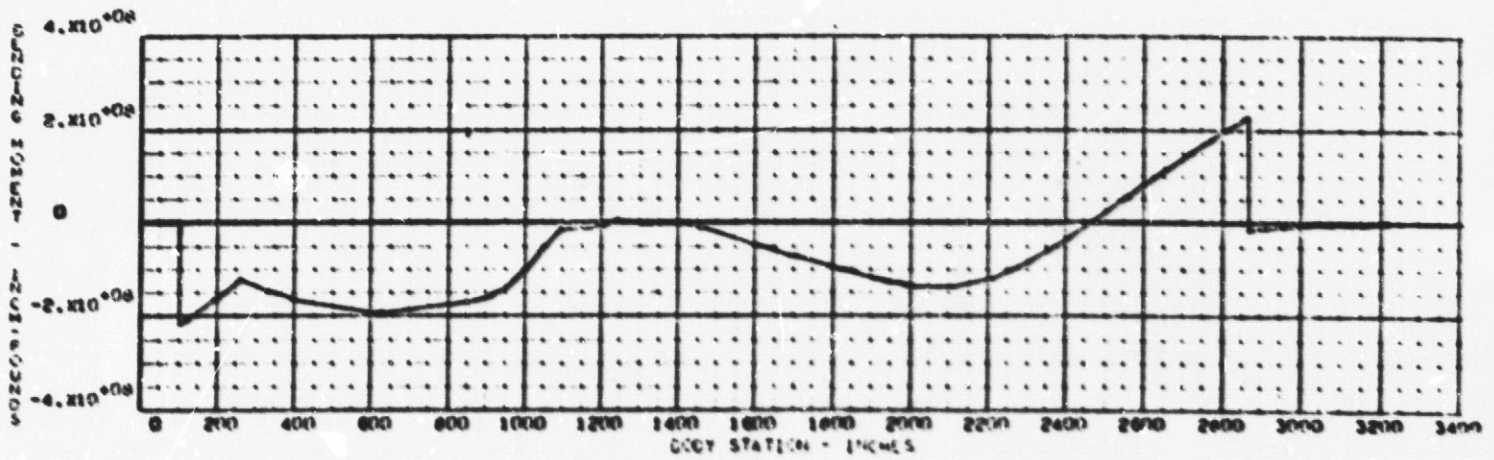

NOTE: MULTIPLY SHEAR AND MOMENT
BY 1.1 DYNAMIC FACTOR

Figure 8.3-12. Booster Limit Loads for Maximum q Alpha (Axial Load at Forward Attachment)

50,000 - POUND PAYLOAD CLASS

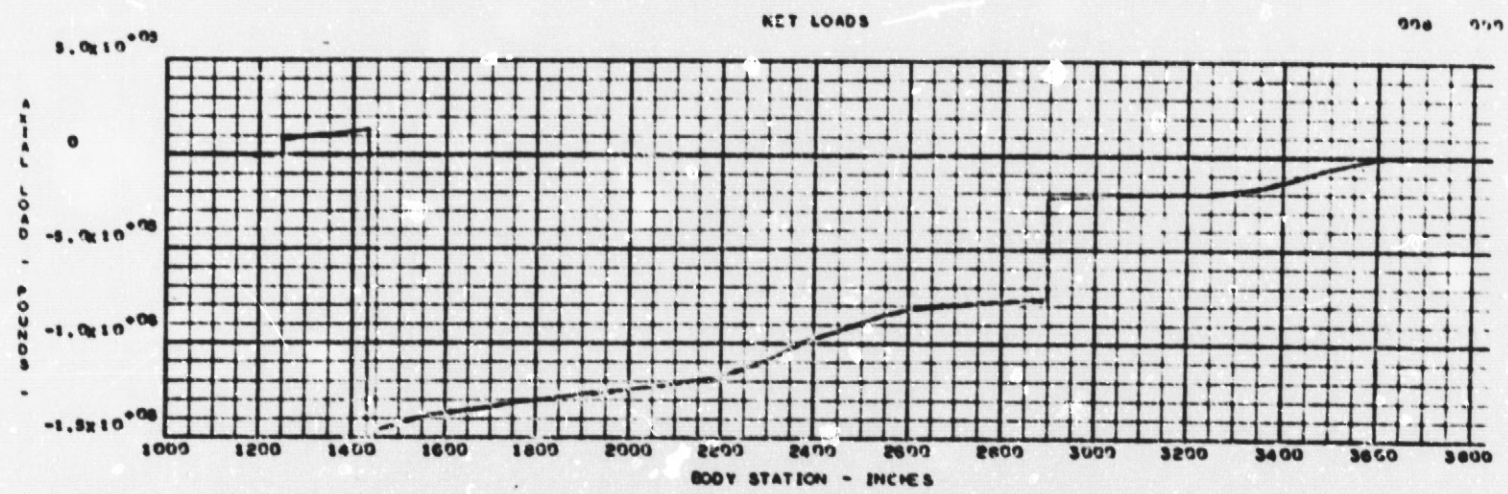

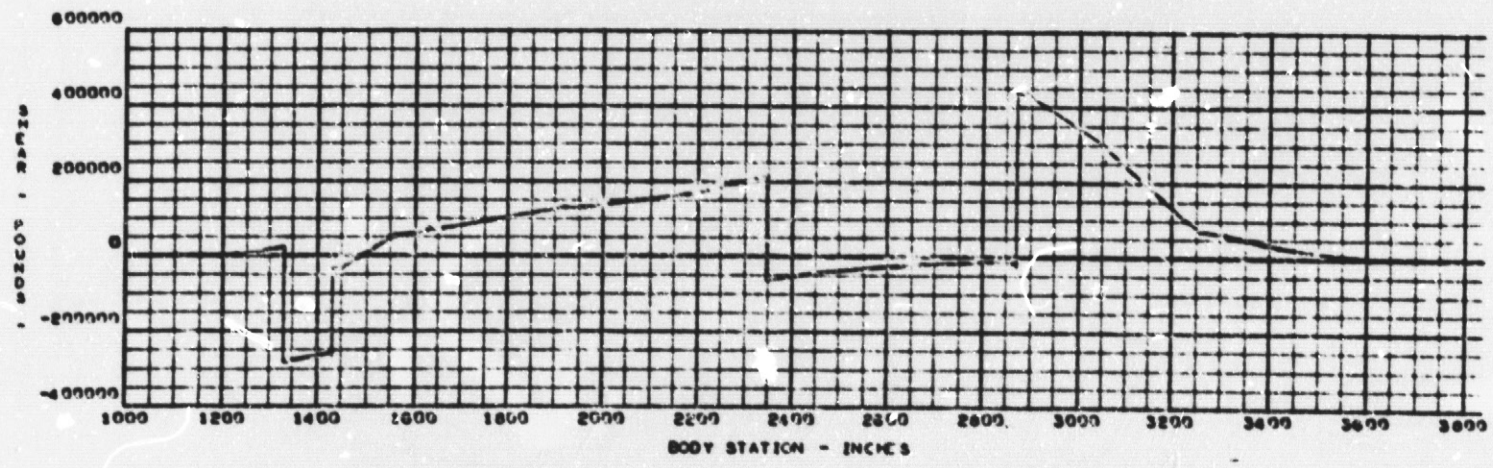

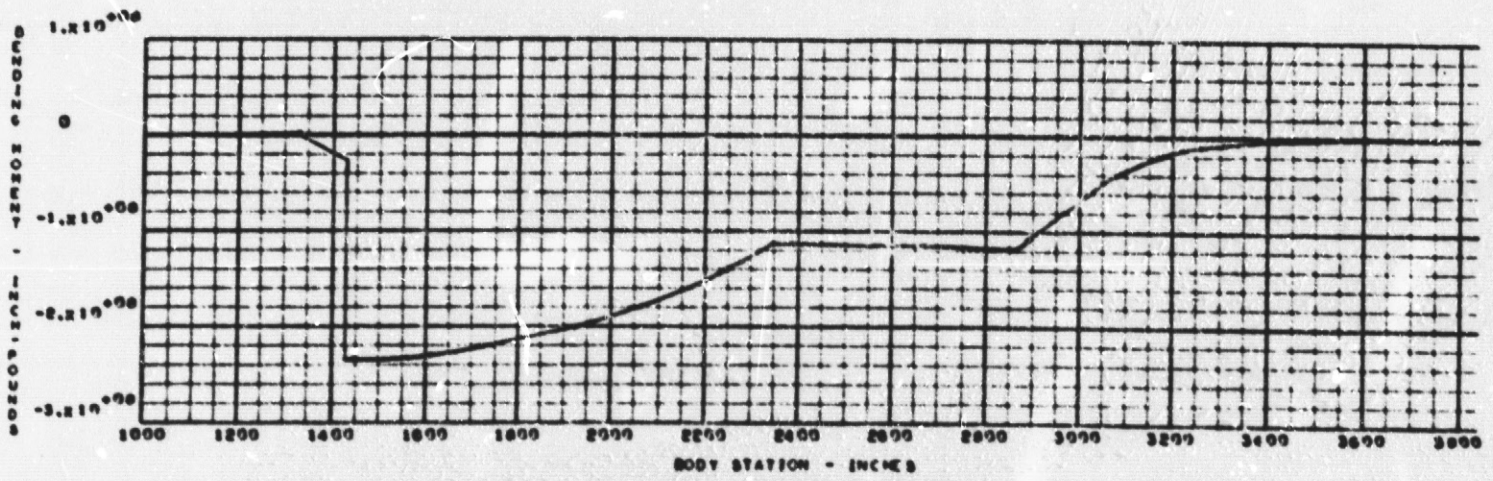

NOTE: MULTIPLY SHEAR AND MOMENT
BY 1.1 DYNAMIC FACTOR

Figure 8.3-13. Orbiter Loads for Maximum q Alpha (Axial Loads at Aft Attachment)

50,000 - POUND PAYLOAD CLASS

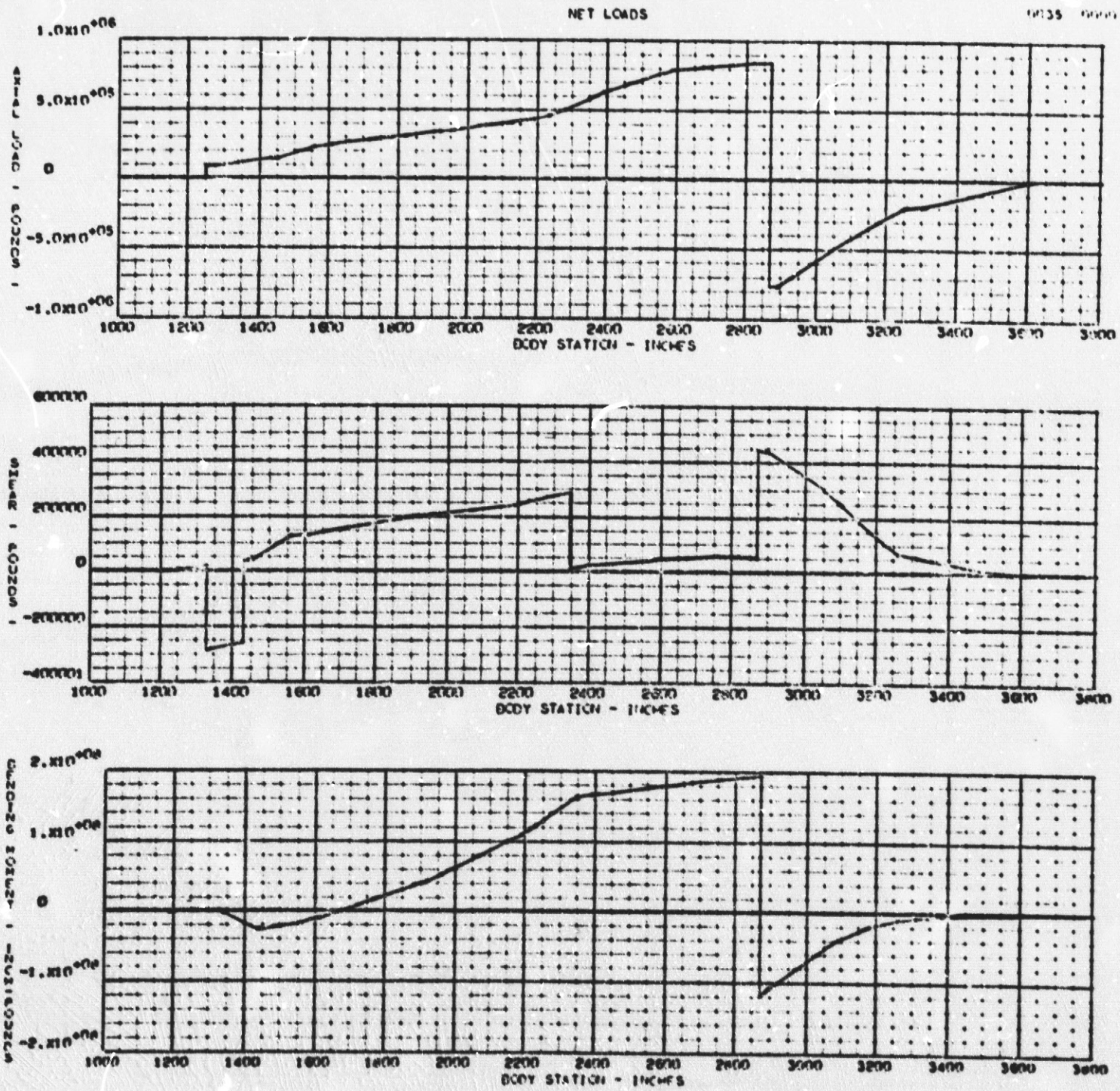

NOTE: MULTIPLY SHEAR AND MOMENT
BY 1.1 DYNAMIC FACTOR

Figure 8.3-14. Orbiter Loads at Maximum q Alpha (Axial Load at Forward Attachment)

Results are shown in Figures 8.3-15 through -18. Loads for the axial load applied at the aft attachment are given in Figures 8.3-15 and -17, while Figures 8.3-16 and -18 are for the axial load applied at the forward attachment.

Entry Loads

The body loads for booster and for orbiter at entry were based on the trajectory parameters shown in Section 8.3.1. The acceleration factor was 4.0 for the booster and 2.10 for the orbiter. The vehicle is in a power-off balanced condition where the weight of the vehicle is supported by the sum of aerodynamic lift and centrifugal forces. The acceleration factor acts in the direction of the resultant of the lift and drag forces.

Booster loads are shown in Figure 8.3-19. Orbiter loads are given in Figure 8.3-20.

Pitch-Down Maneuver and Landing Loads

Booster and orbiter body loads for the subsonic pitch-down maneuver condition after entry were computed for a 2.5-g symmetrical pull-up (Figure 8.3-21 and -22). The 2.5-g pull-up was considered to be the most severe maneuver that will be executed after entry. The parameters used for computation of pull-up loads were based on preliminary trajectory data for the smaller MSC baseline vehicle. Dynamic pressure (q) was taken as 102 psf for the booster and 142 psf for the orbiter. For this condition α was 16 degrees, and the acceleration factor was 2.5 g's. Subsequent trajectory and control studies indicated different flight conditions would exist for the 50,000-pound-payload vehicles, but time did not permit reevaluation of the loads.

Booster and orbiter body loads for main landing gear spin-up and spring-back conditions were computed for a gear acceleration factor of 1.4 based upon a sink speed of 10 fps and a gear stroke of 14 inches. Vertical and horizontal forces at the gear were computed as per military specification MIL-A-8862 (ASG). A dynamic magnification factor of 1.2 was included to cover contingencies such as runway roughness. Results are shown in Figures 8.3-23 and -24.

50,000 - POUND PAYLOAD CLASS

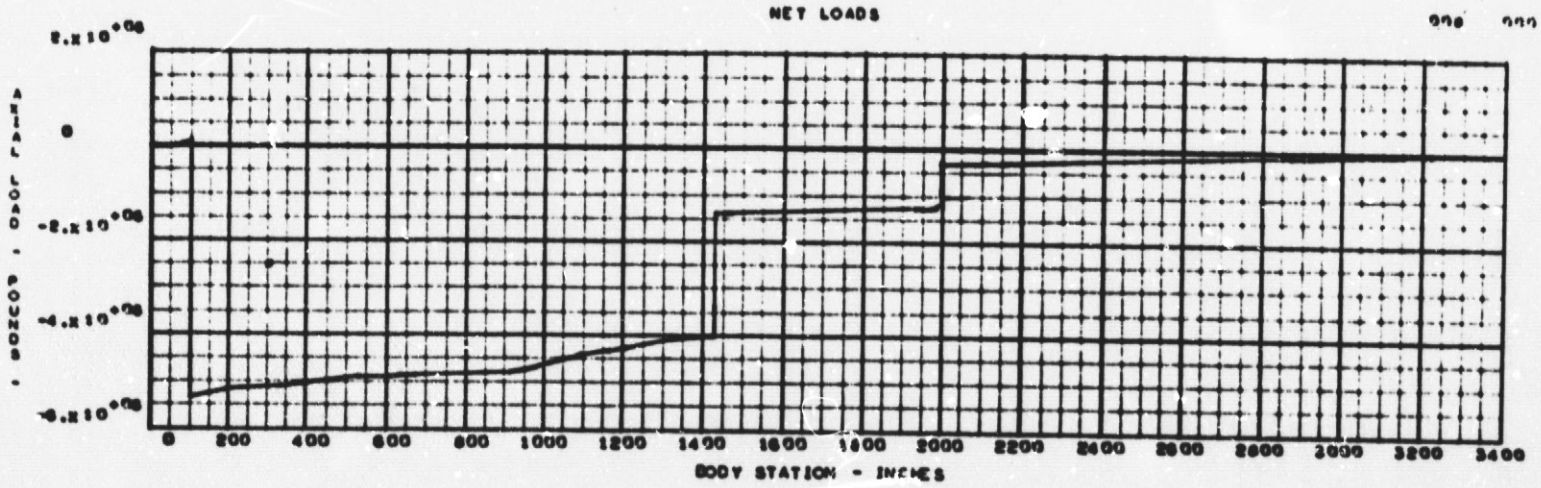

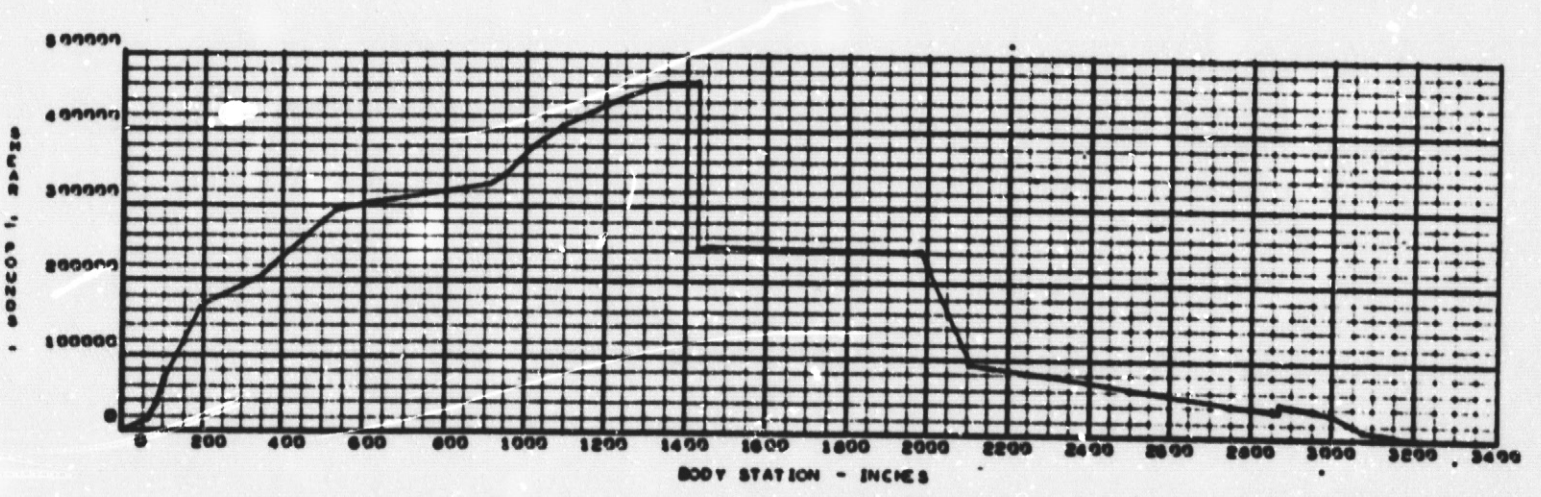

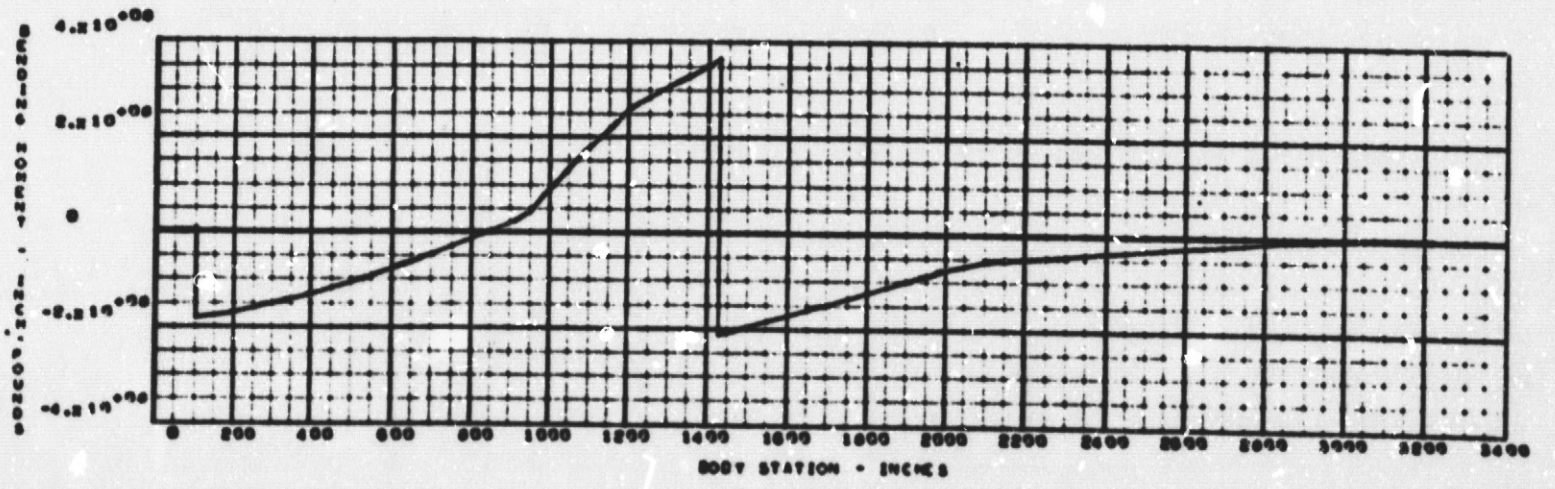

Figure 8.3-15. Booster Loads for Maximum Acceleration (Axial Load at Aft Attachment)

50,000 - POUND PAYLOAD CLASS

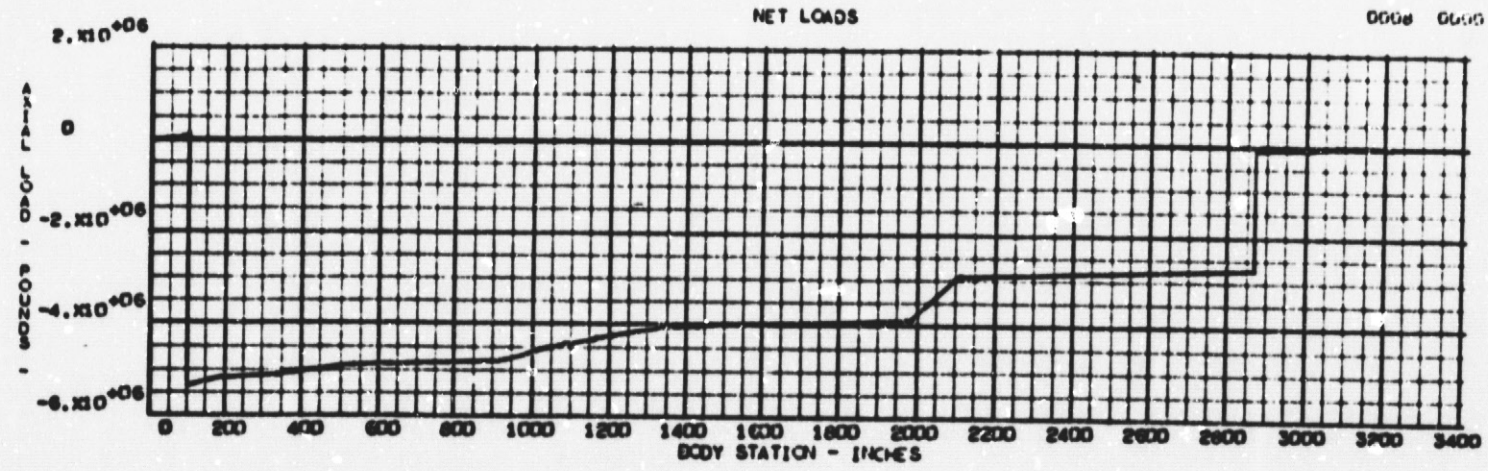

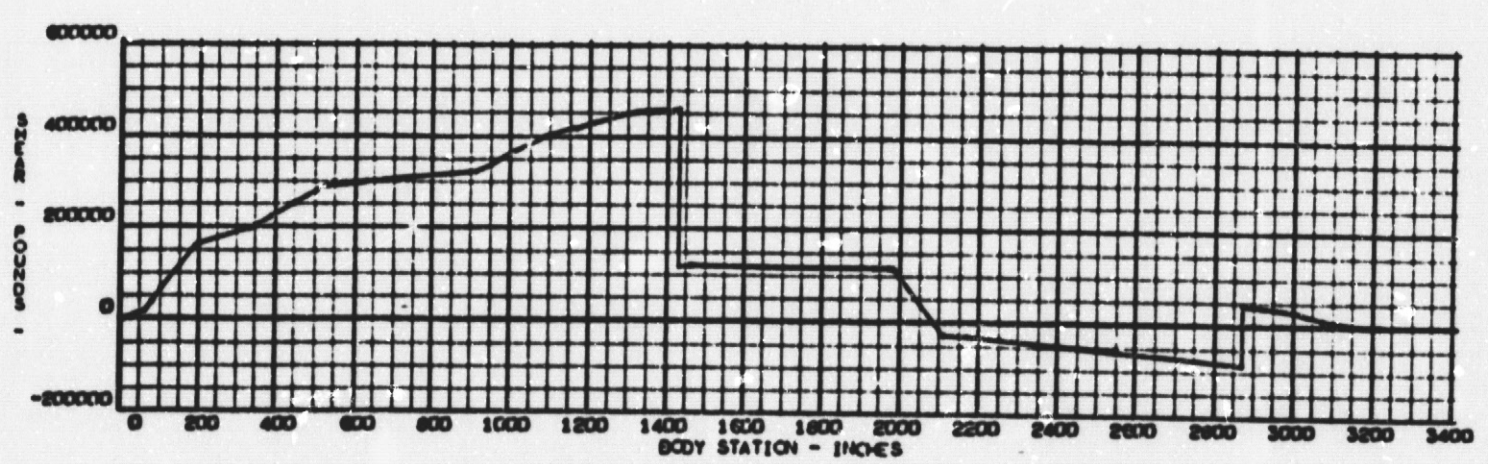

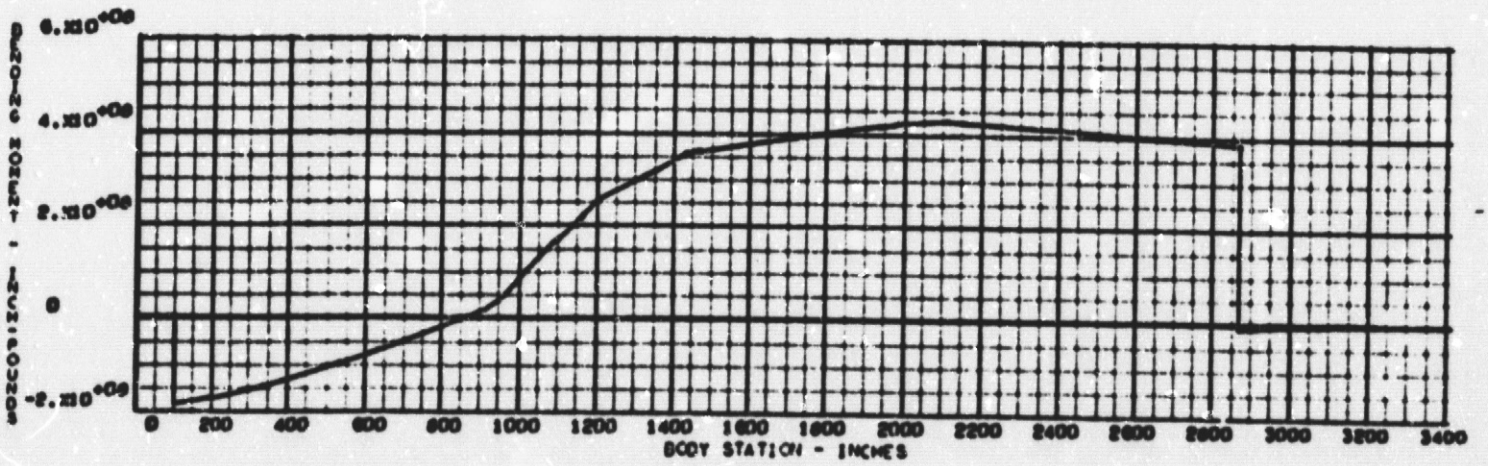

Figure 8.3-16. Booster Loads for Maximum Acceleration (Axial Load at Forward Attachment)

50,000 - POUND PAYLOAD CLASS

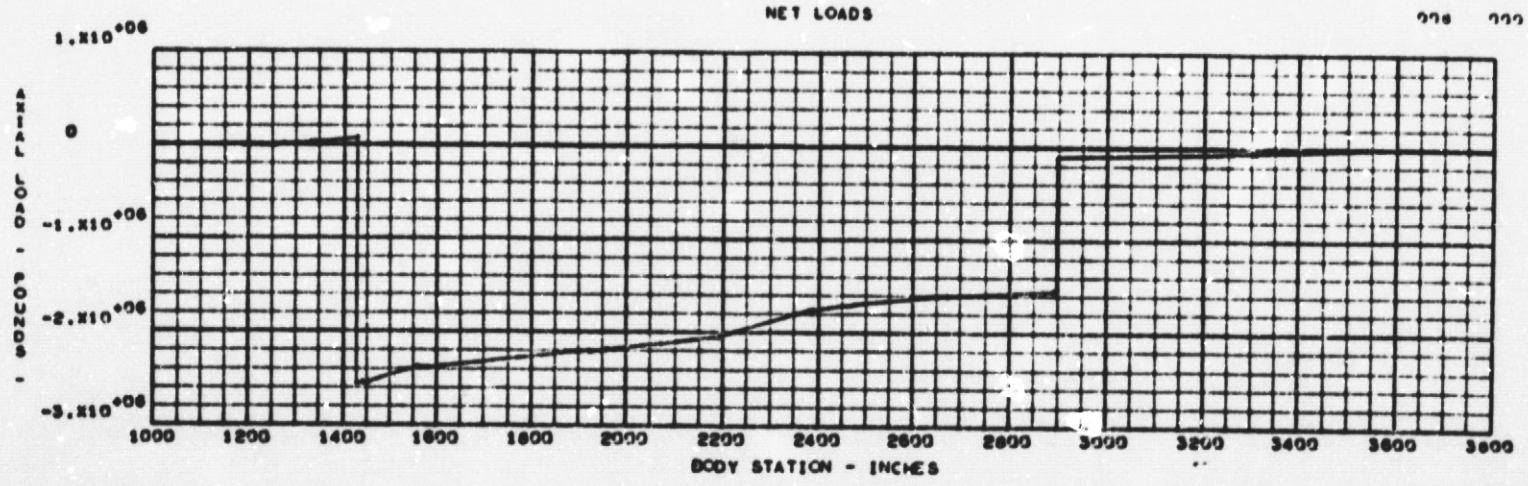

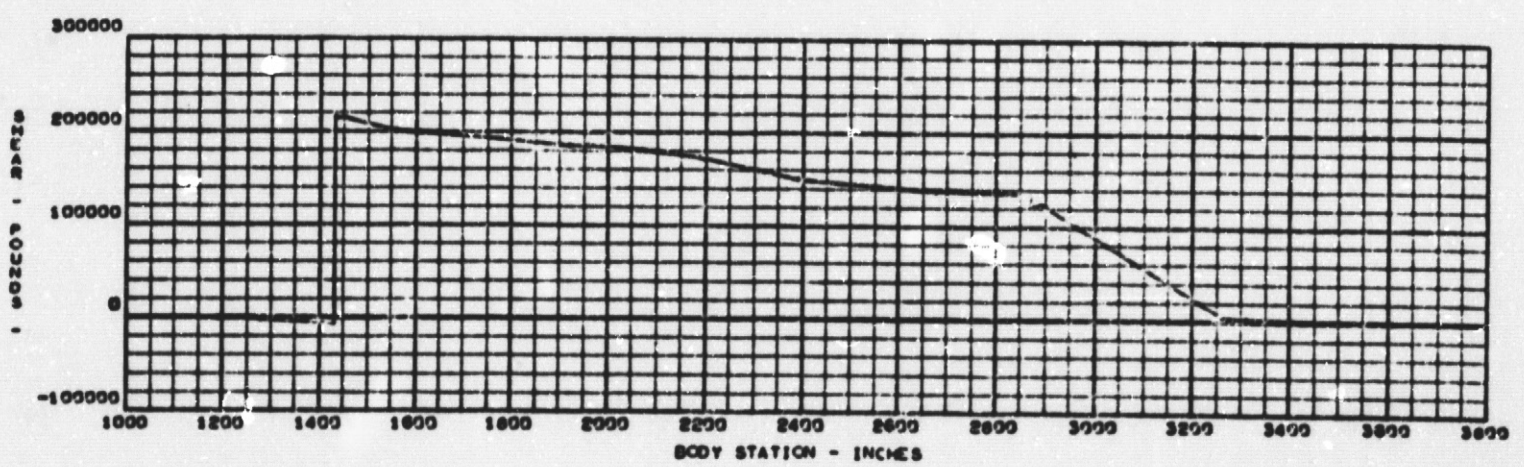

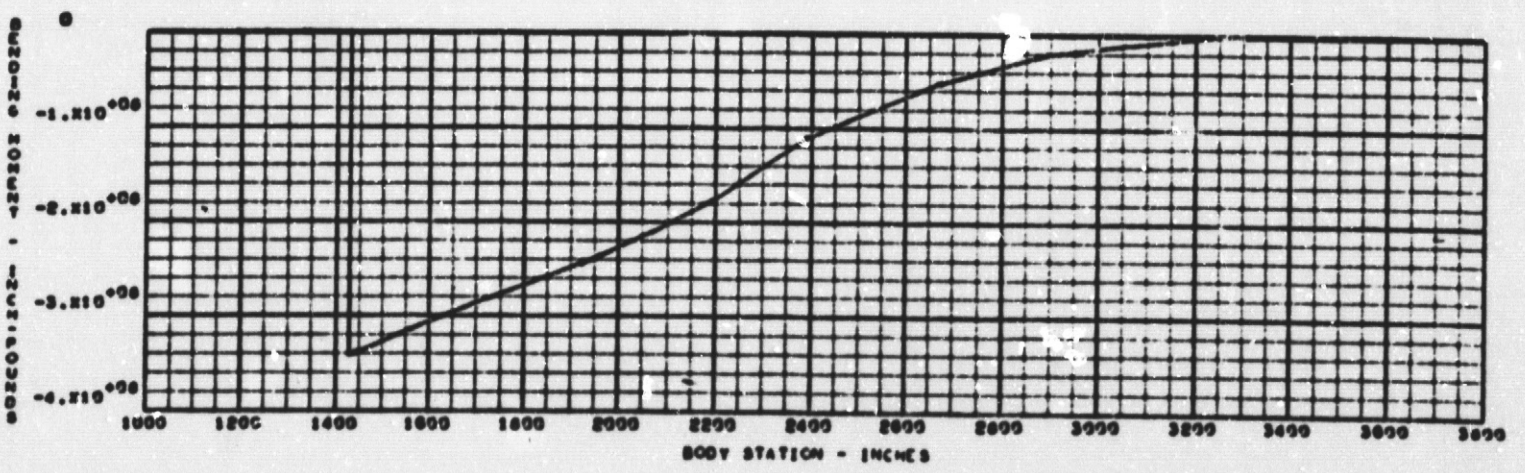

Figure 8.3-17. Orbiter Loads for Maximum Acceleration (Axial Load at Aft Attachment)

50,000 - POUND PAYLOAD CLASS

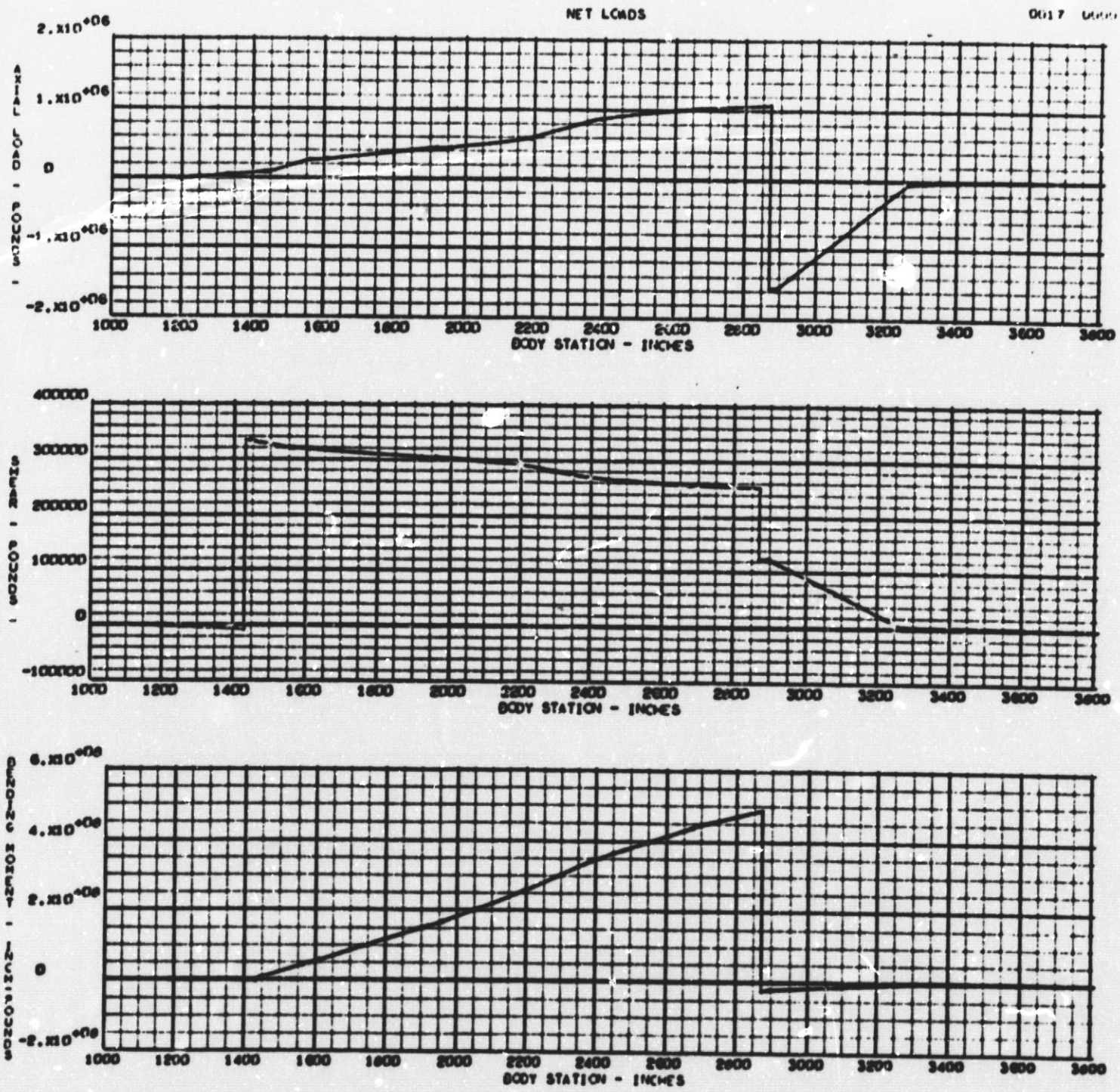

Figure 8.3-18. Orbiter Loads at Maximum Acceleration (Axial Load at Forward Attachment)

50,000 - POUND PAYLOAD CLASS
M = 5.9
α = 60° n_z = 4.0 G'S

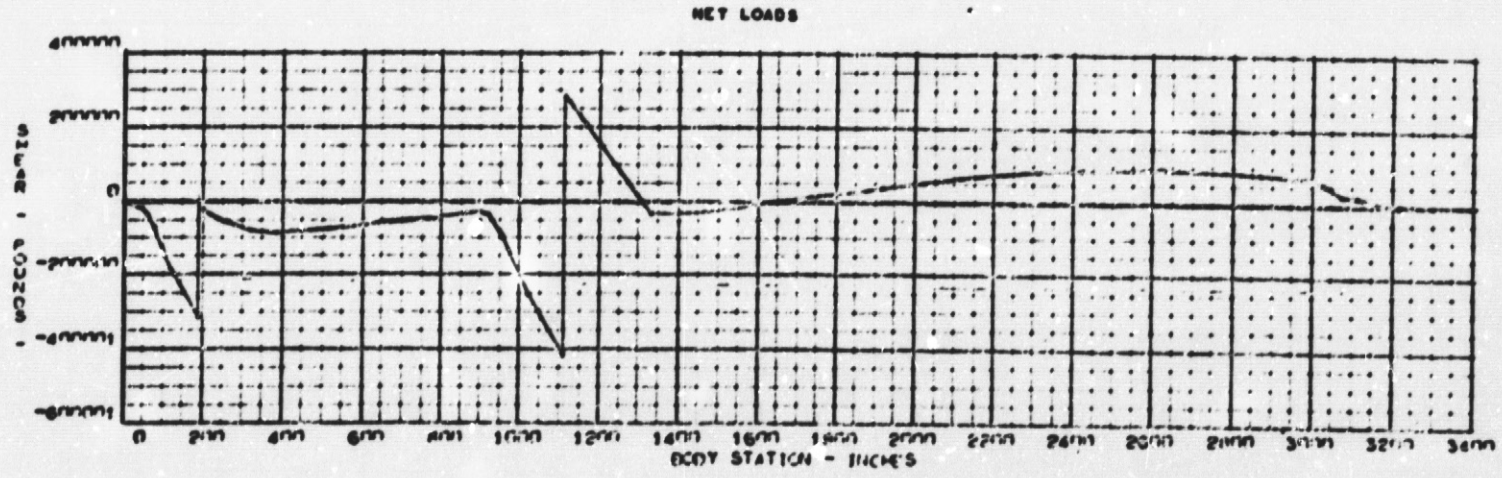

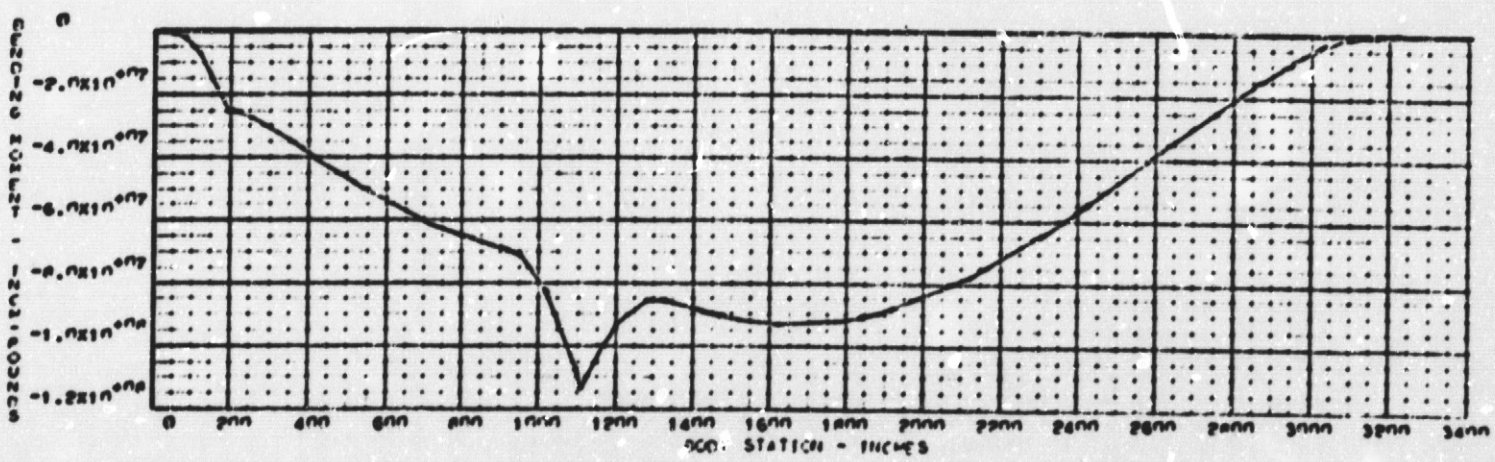

Figure 8.3-19. Booster Limit Loads During Entry

50,000 - POUND PAYLOAD CLASS
M = 5.9 n_z = 2.1 G'S
α = 60°

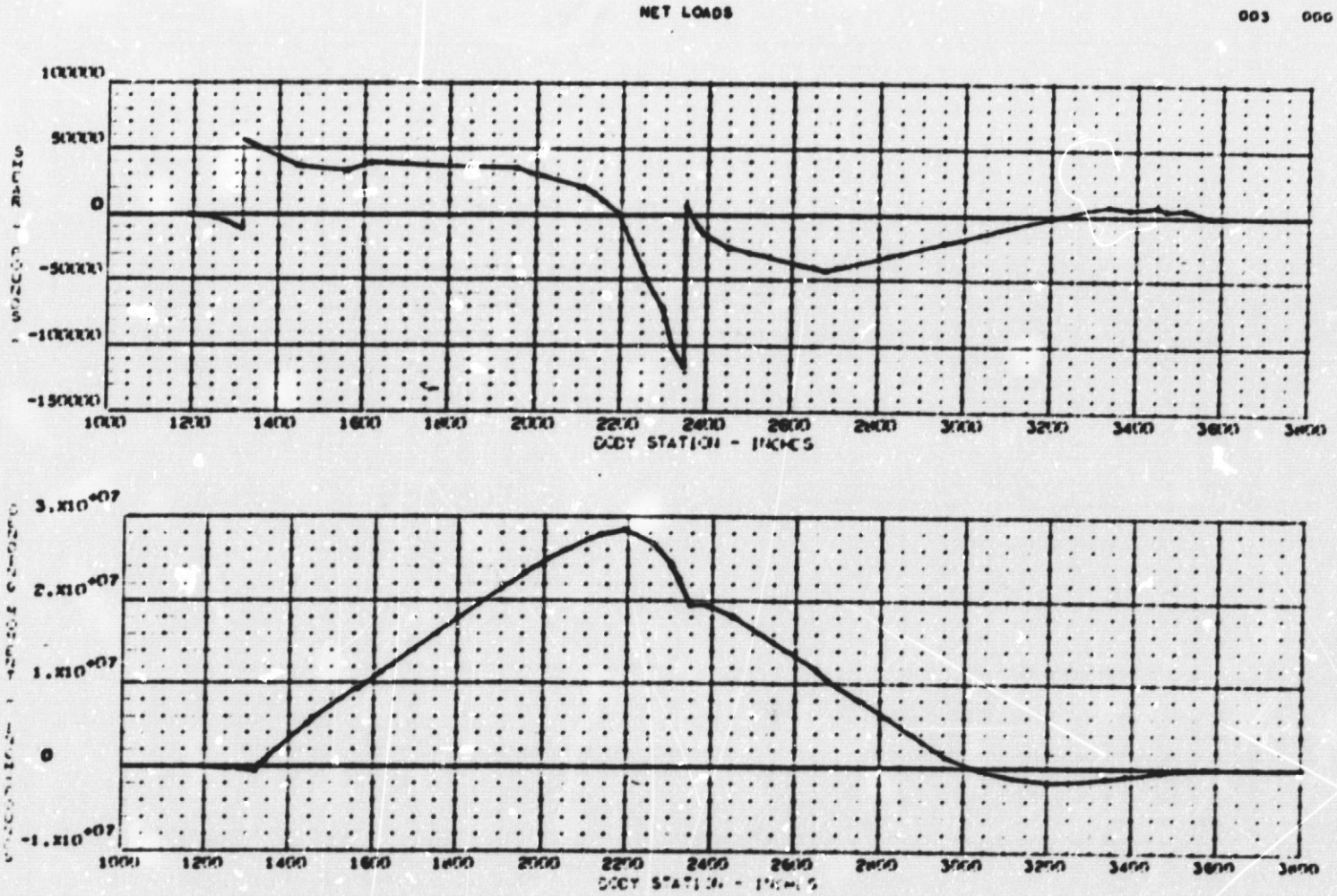

Figure 8.3-20. Orbiter Limit Loads During Entry

50,000 - POUND PAYLOAD CLASS
2.5 G MANEUVER
M = 0.4 q = 101.6 PSF
α = 16°

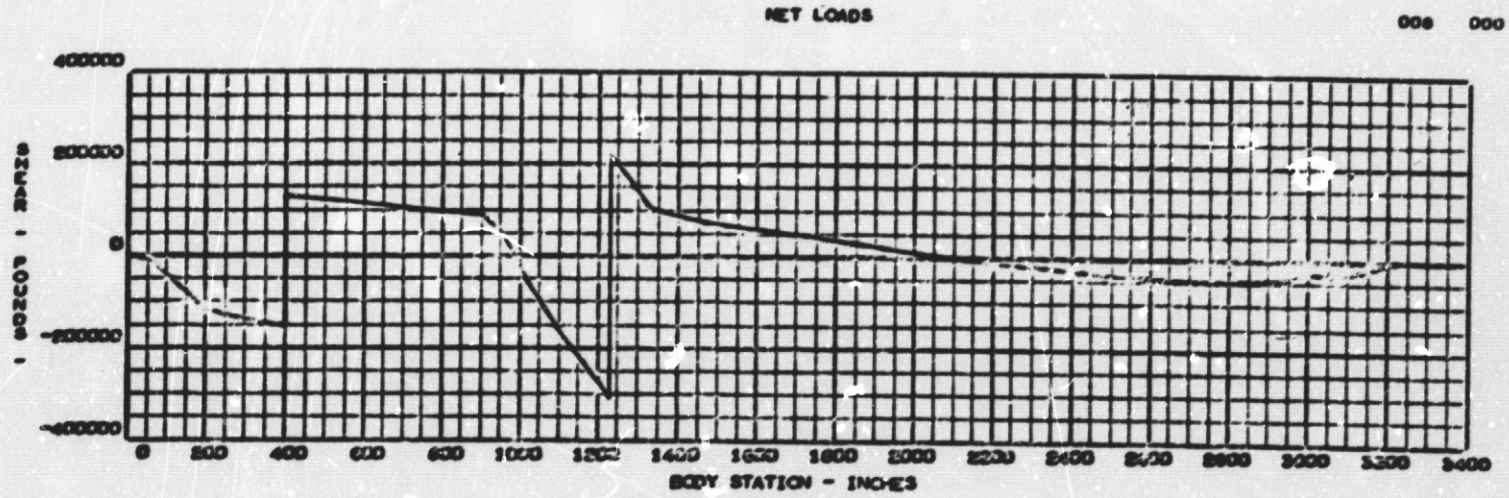

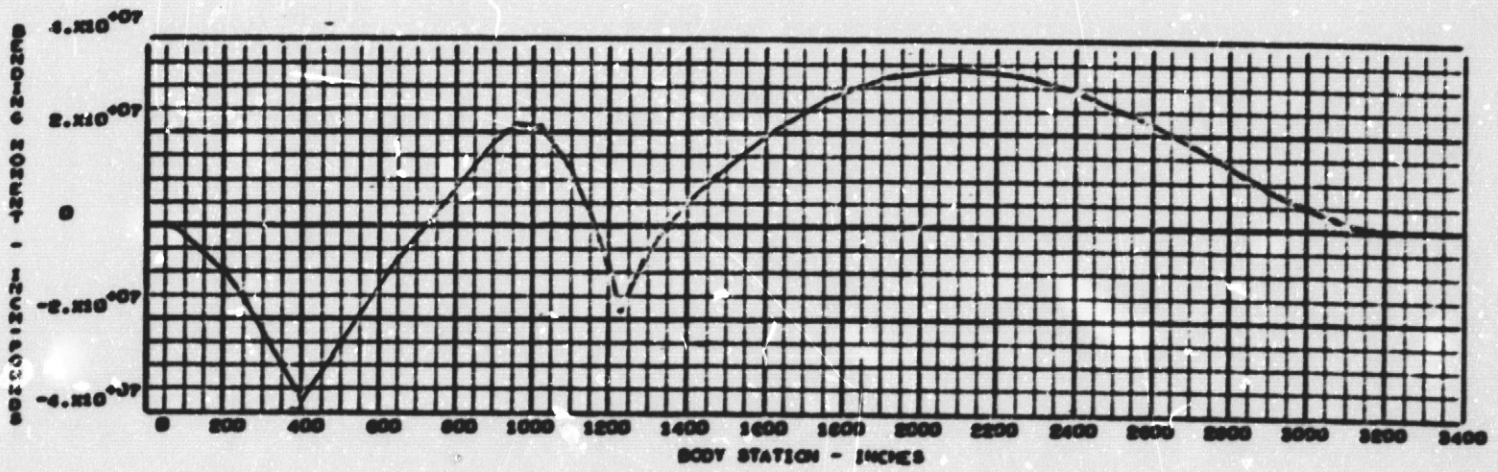

Figure 8.3-21. Booster Limit Loads During Transition to Cruise Maneuver

50,000 - POUND PAYLOAD CLASS
2.5 G MANEUVER
M = 0.4 q = 141.8 PSF
α = 16°

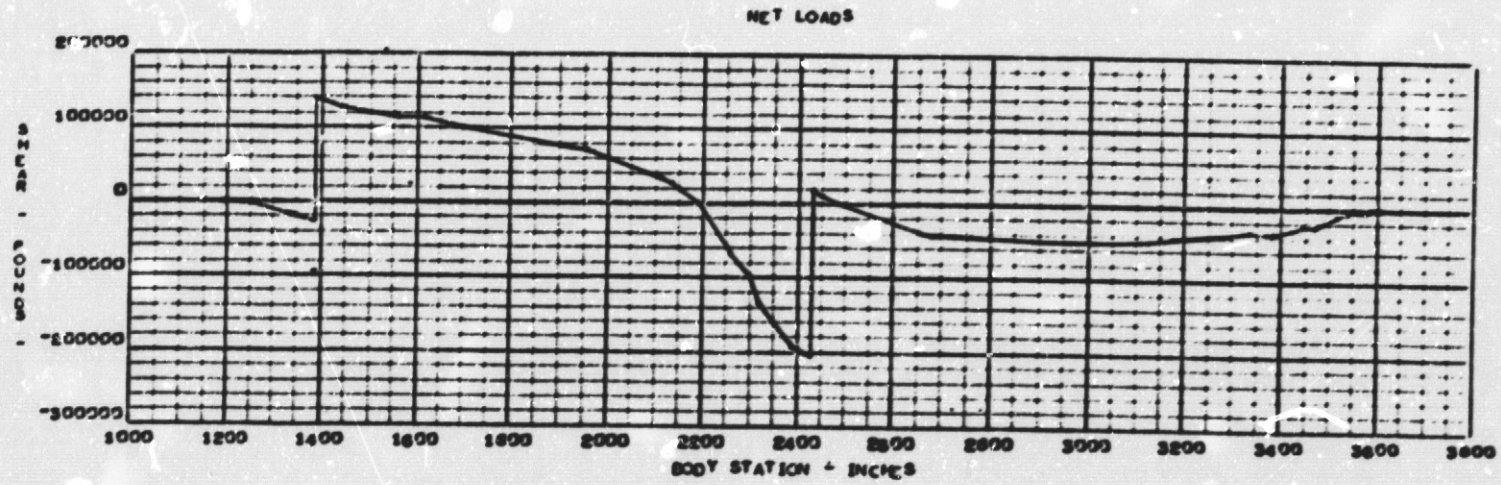

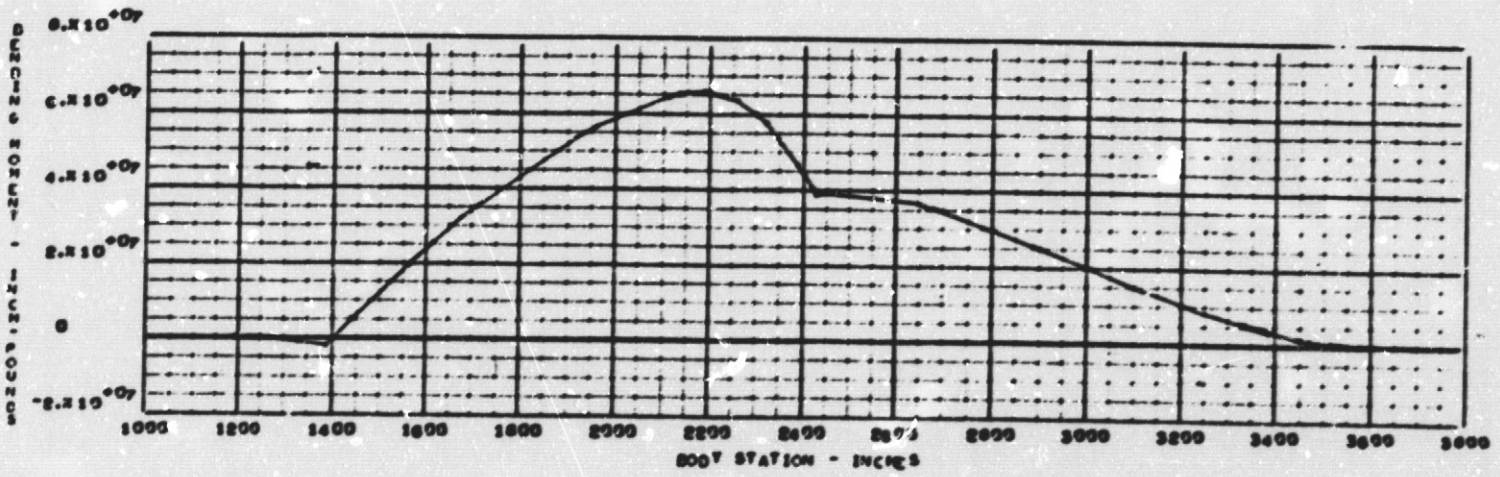

Figure 8.3-22. Orbiter Limit Loads During Transition to Cruise Maneuver

50,000 - POUND PAYLOAD CLASS
SINK SPEED = 10 FPS

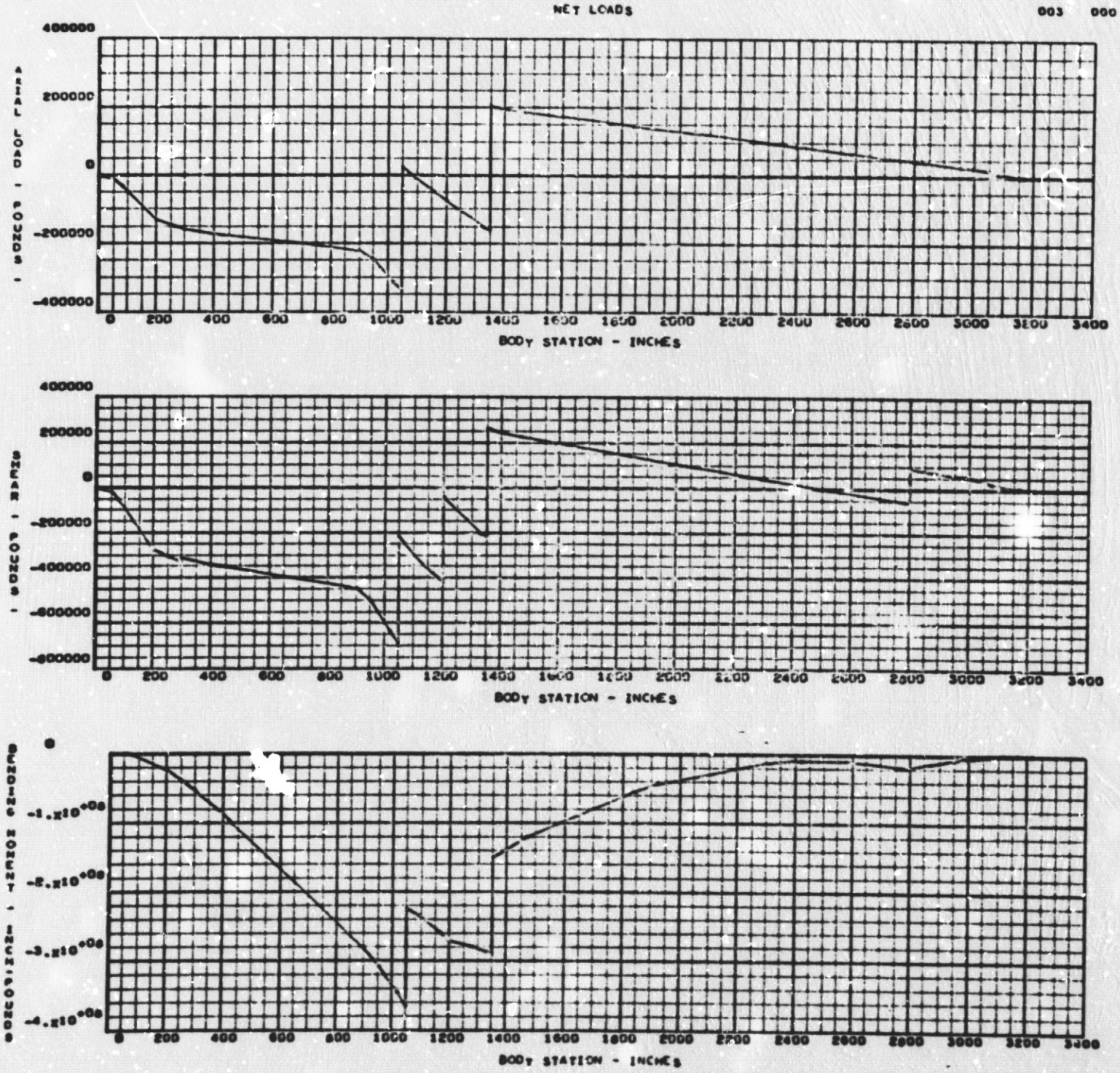

Figure 8.3-23(a). Booster Limit Loads During Landing, Main Gear (Spin-Up)

50,000 - POUND PAYLOAD CLASS
SINK SPEED = 10 FPS

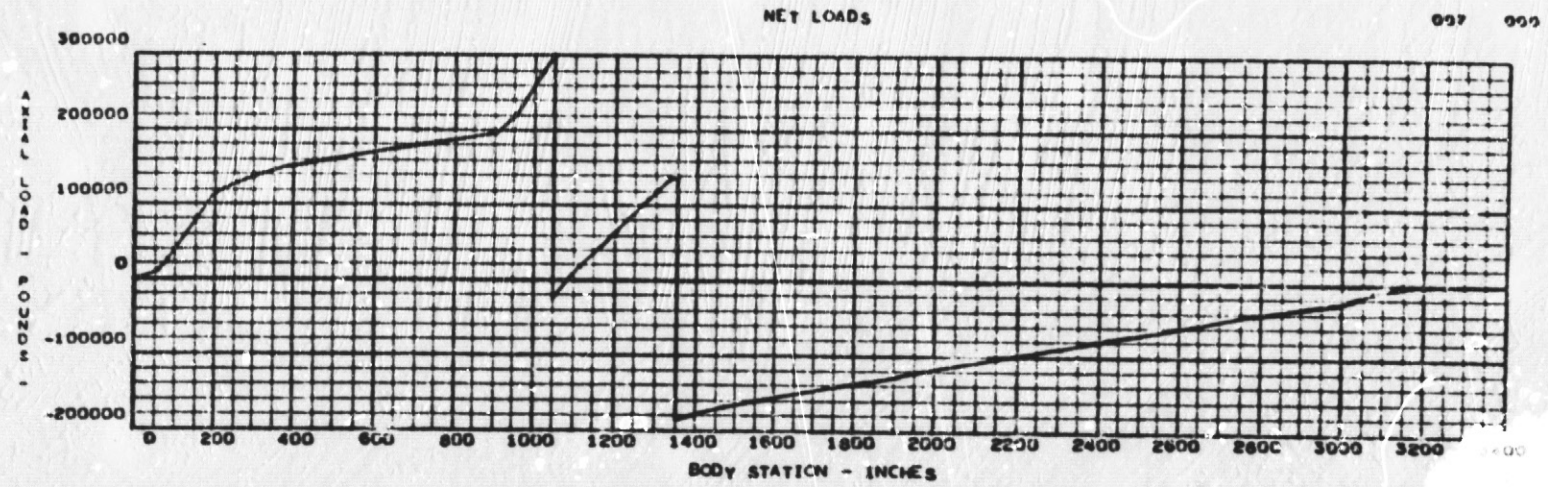

Figure 8.3-23(b). Booster Limit Loads During Landing, Main Gear (Spring Back)

50,000 - POUNDS PAYLOAD CLASS
SINK SPEED = 10 FPS

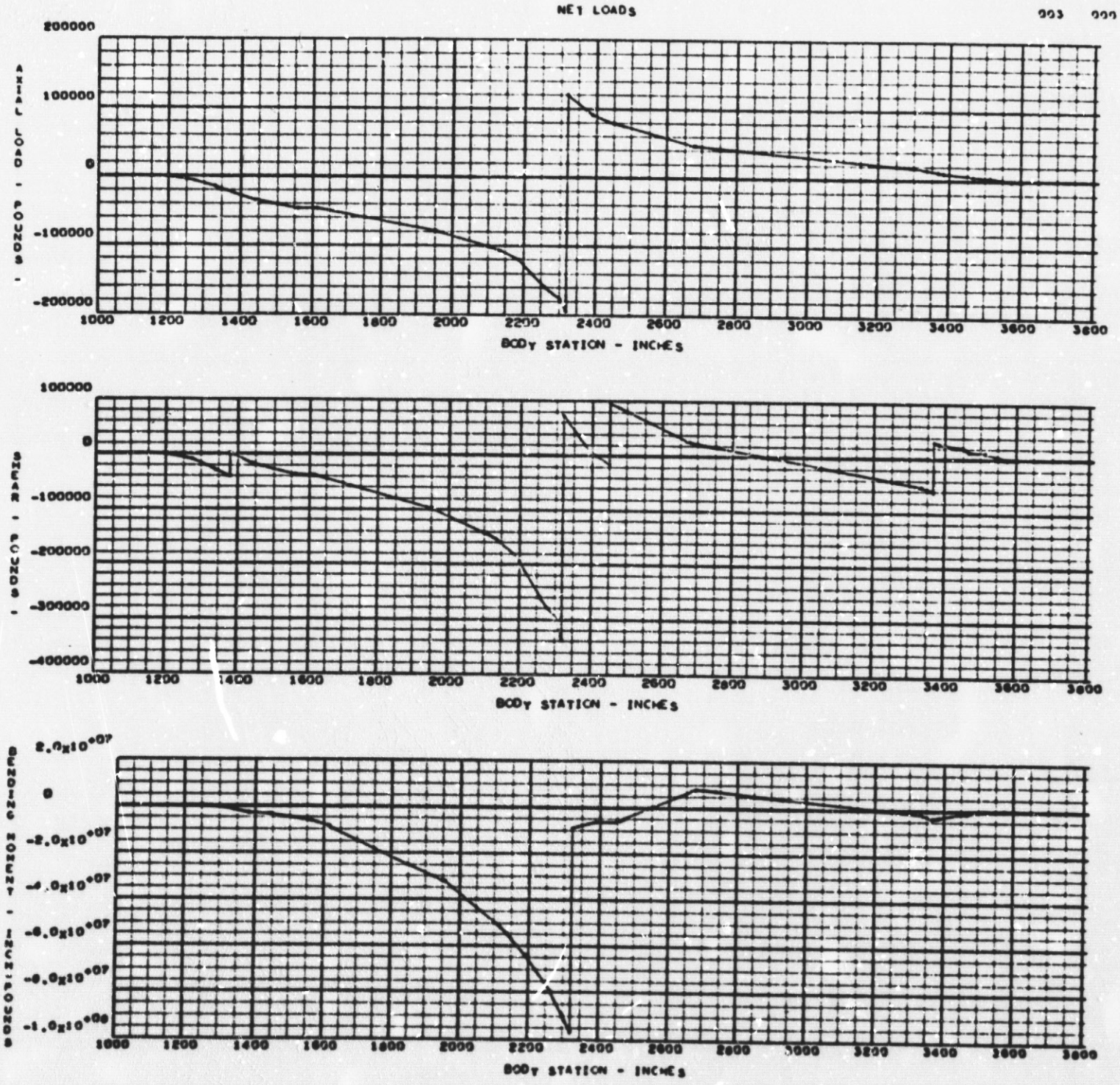

Figure 8.3-24(a). Orbiter Limit Loads During Landing, Main Gear (Spin-Up)

50,000 - POUND PAYLOAD CLASS
SINK SPEED = 10 FPS

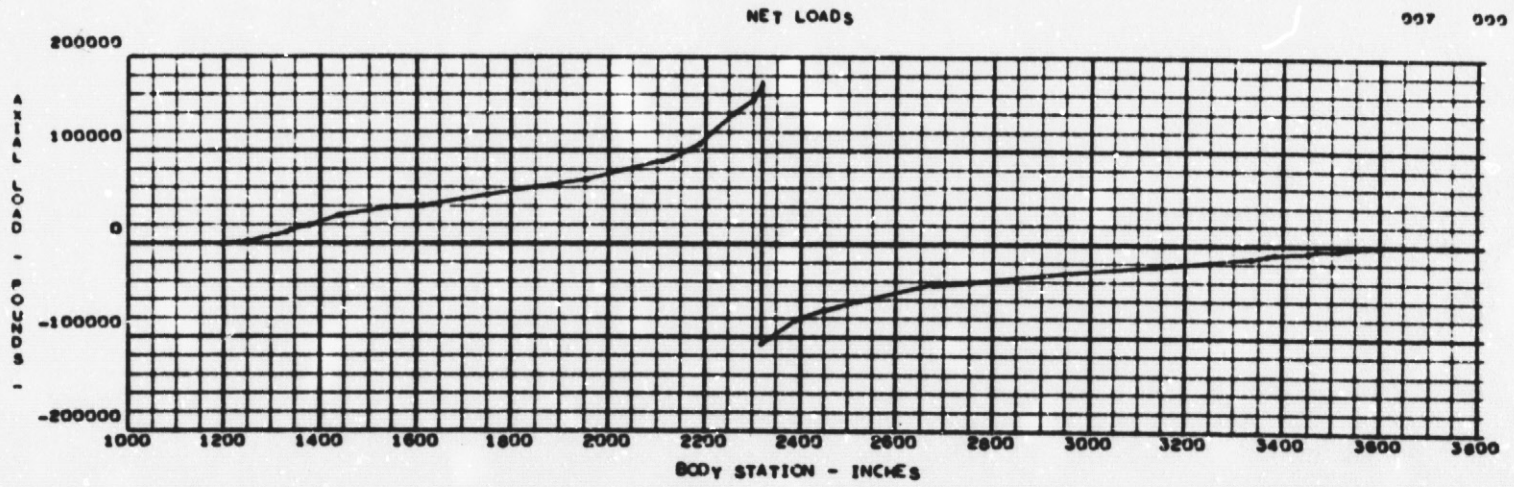

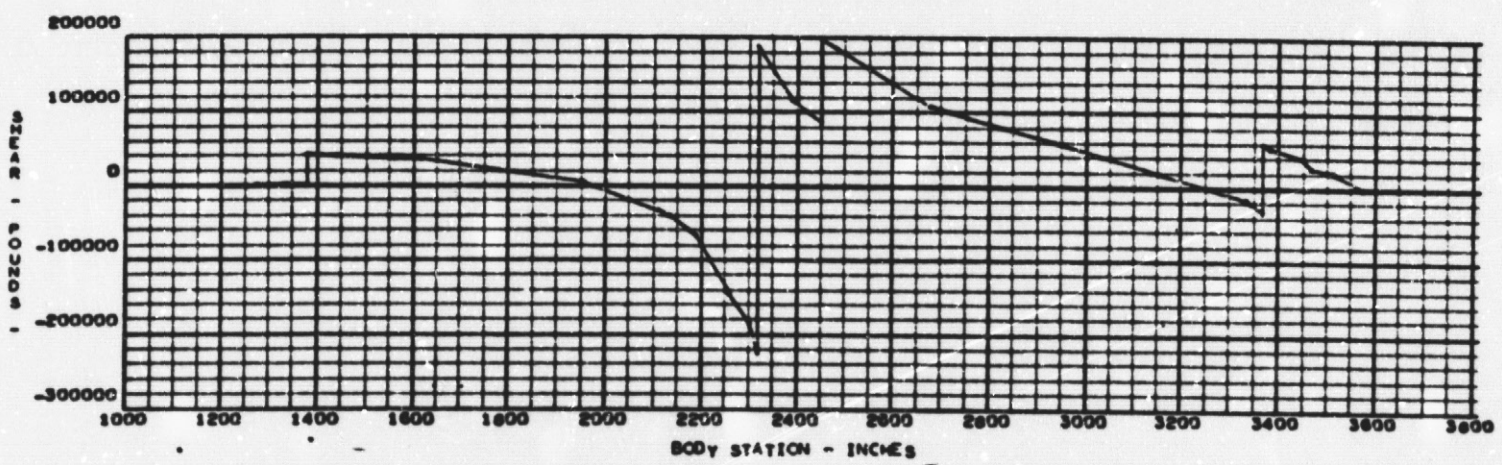

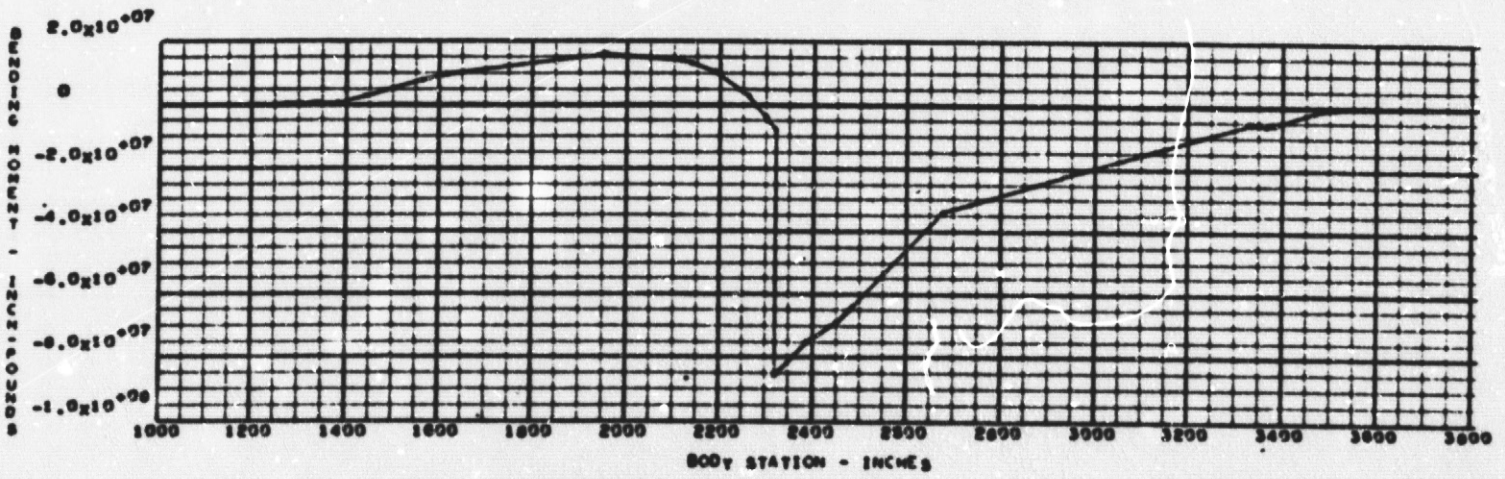

Figure 8.3-24(b). Orbiter Limit Loads During Landing, Main Gear (Spring Back)

9.0 CONCLUSIONS

Investigations to define shuttle vehicle design environment and performance characteristics have established the following conclusions:

1. The tandem launch configuration is statically stable from lift-off and throughout regions of flight where high aerodynamic loads can be developed. This results in low thrust-vector deflection angles, low angles of attack, and low aerodynamic loads.

2. The orbiter and booster vehicles will trim at high and low angles of attack. Therefore, the concept of entering at a high angle of attack to minimize temperature and subsequently pitching down to a low angle of attack for glide is a feasible operating mode. Establishment of the aerodynamic characteristics has been based on limited subsonic, transonic, and supersonic testing. This testing has not reflected Reynolds numbers that would be experienced in flight. Thus additional data are required.

3. Reentry of the vehicle at a high angle of attack in a stalled condition will minimize the lift loading and reduce temperatures experienced upon reentry. It is projected that temperatures on the orbiter vehicle will generally be less than 1500 F. Further efforts may be necessary to minimize heating effects of flow interference. The lateral-range capability of the orbiter obtained through banking with a 60-degree angle of attack is approximately 335 miles by entering into a phasing orbit. The capability exists for the orbiter to return to the selected landing site within 24 hours of recall without reducing payload. At a low angle of attack, the vehicle's lateral-range capability may be increased to 1500 nautical miles. This would require an increase of approximately 22,000 pounds in insulation weight, however. A portion of the 1500-mile ranging must also be obtained through subsonic cruise. This could be achieved by reducing payload and providing fuel for the turbojet operation.

4. Orbiter entry control simulation has shown that the RCS providing a 0.5 degree/sec^2 angular acceleration is adequate control authority. The vehicle is stable and well damped. Unstable directional derivatives ($C_{n_\beta} < 0$) are not significant to vehicle controllability, but can cause high RCS fuel consumption. Unstable dihedral effect ($C_{\ell_\beta} > 0$) could result in loss of vehicle control during entry.

5. A booster entry flight mode incorporating banked entry will reduce the flyback range by 24 percent over a straight-ahead entry. Flyback range is 310 nautical miles. Maximum temperatures during booster entry are not expected to exceed 1400 F for 90 percent of the vehicle.

6. Landing speeds for both the booster and orbiter elements will be under 130 knots, which is comparable to existing turbojet transport aircraft.

7. Failure of a single engine on either the booster or orbiter will not prevent completion of the primary mission. A system failure requiring premature staging will necessitate action to limit entry loads on the orbiter and propellant dumping. For mission termination at low altitude, the orbiter with two engines operating can abort to low altitude. With one or two engines operating on the orbiter, the engines may be used to shape the trajectory and prevent excessive loads. Failure of two orbiter engines, however, will cause excessive entry loads and possibly make a water landing necessary. Propellant dumping will be required in the event of failure of both orbiter engines.

8. For the shuttle vehicle configured to deliver a 50,000-pound payload, 11 engines on the booster provide a minimum gross weight system. This is based on the use of two main engines on the orbiter with the same basic engine design on both stages.

9. The studies show that sequential firing of booster and orbiter maximizes performance, and, with the two-stage system configured to deliver 50,000 pounds of payload, the gross weight is approximately 4-1/2 million pounds.

10. Ascent control simulations have shown that the vehicle can be controlled along a programmed flight path during boost and that the maximum $q\alpha$ does not exceed 2970 psf degrees when a 95-percentile wind with a gust is flown through.

11. The maximum $q\alpha$ condition during launch is the critical load case for the majority of the vehicle. Prelaunch with ground winds is the design condition for the hold down of the vehicle at the aft end of the booster. The establishment of loading environment has been based upon a rigid body analysis with factors applied to reflect magnification associated with a dynamic response. The effects of acoustic environment were not considered.

10.0 REFERENCES

7.2-1 Polhamus, E. Effect of Flow Incidence and Reynolds Number on Low Speed Aerodynamic Characteristics of Several Noncircular Cylinders With Applications to Directional Stability and Spinning. NASA, TR R-29 (1959).

7.2-2 USAF Stability and Control Handbook (DATCOM) (October 1960; rev. July 1963).

7.2-3 Lift and Center of Pressure of Wing-Body-Tail Combinations at Subsonic, Transonic, and Supersonic Speeds. NACA Report 1307 (1957).

7.2-4 Linear Aerodynamic Loads on Cone-Cylinders at Mach Numbers From 0.7 to 2.0. NASA CR-413.

7.2-5 Preliminary Data From Low Speed Static Free Tests in Langley Low Turbulence Pressure Tunnel on an 0.02 Scale Model of a Proposed MSC Orbiter Shuttle Configuration. MSC Internal Memorandum EX2416908-1716 (6 August 1969; informal revisions 11 August 1969).

7.2-6 Unpublished preliminary data from Ames Research Center Test No. 66-435 (Sept. 1 - Oct. 3, 1969).

7.2-7 A Method for Estimation of Aerodynamic Characteristics of Aircraft With Single Slotted or Double Slotted Trailing-Edge Flaps With or Without Leading Edge Slots of Flaps. North American Rockwell Report NA 68-414 (March 7, 1968).

7.2-8 A preliminary feasibility study of the separation at staging of a Piggyback Concept Space Shuttle, MSC Internal Memorandum EX22/6909-2146 (Sept. 4, 1969).

7.4-1 M. H. Bertram and P. E. Everhart. An Experimental Study of the Pressure and Heat Transfer Distribution on a 70° Sweep Slab Delta Wing in Hypersonic Flow. NASA TR R-153 (December 1963).

7.4-2 A. L. Nagel, H. D. Fitzsimmonds, and L. B. Doyle. Analysis of Hypersonic Pressure and Heat Transfer Tests on Delta Wings With Laminar and Turbulent Boundary Layer. NASA CR-535.

7.4-3 H. Hoshizaki. "Heat Transfer in Planetary Atmospheres at Super Satellite Speeds," ARS Journal (October 1962), pp. 1544-1552.

7.4-4 E.R. van Driest. "The Problem of Aerodynamic Heating," Aeronautical Engineering Review (October 1956).

7.4-5 N.S. Cohen. Similarity Solutions and Correlation Equations for Laminar Heat Transfer Distributions in Equilibrium Air at Velocities Up to 41,000 Feet per Second. NASA TR R-118 (1961).

7.4-6 E.R.G. Eckert. Survey of Boundary Layer Heat Transfer at High Velocities and High Temperatures. WADC TR 69-624 (April 1960).

7.4-7 J.G. Marvin and R. Sinclair. "Convective Heating in Regions of Large Favorable Pressure Gradient," AIAA V. 5 No. 11, pp. 1940-1948.

7.4-8 N.H. Kame, P.H. Rose, and R.W. Detra. "Laminar Heat Transfer Around Blunt Bodies in Dissociated Air," JAS (July 1959), pp. 421-430.

7.4-9 D.R. Chapman. A Theoretical Analysis of Heat Transfer in Regions of Separated Flow. NACA TN 3792.

7.4-10 B.E. Edney. "Effects of Shock Impingement on the Heat Transfer Arcund Blunt Bodies," AIAA V. 6, No. 1 (January 1968), pp. 15-21.

7.4-11 R.S. Hires and W.J. Lovesky. Effects of Shock Wave Impingement on the Heat Transfer on a Cylindrical Leading Edge. NASA TN D-3859 (February 1967).

7.4-12 E.H. Comfort. Experimental Investigation of Two Shock Wave - Boundary Layer Interaction Configurations. AIAA Paper 69-8.

7.4-13 E.A. Price and P.W. Howard. Heat Transfer Measurements on a Flat Plate and Attached Fins at Mach Numbers of 3.51 and 4.44. TN D-2340 (June 1964).

7.4-14 R.A. Jones. Heat-Transfer and Pressure Investigation of a Fin-Plate Interference Model at a Mach Number of 6. NASA TN D-2028 (July 1964).